



National Technical University of Athens
School of Mechanical Engineering
Department of Fluids
Laboratory of Hydraulic Turbomachines

**Simulation, development and experimental investigation of a
hybrid energy desalination system. Dimensioning and parameters
specification for optimum operation.**

Doctoral Dissertation

ERIKA N. NTAVOU

Mechanical Engineer, M.Sc.

PhD Supervisors:

D. Papantonis, NTUA Professor
I. Anagnostopoulos, NTUA Professor
D. Mathioulakis, NTUA Professor

Examination Committee:

D. Papantonis, NTUA Professor
I. Anagnostopoulos, NTUA Professor
D. Mathioulakis, NTUA Professor
G. Papadakis, AUA Professor
D. Manolakos, AUA Assistant Professor
D. Bouris, NTUA Assistant Professor
V. Riziotis, NTUA Assistant Professor

Athens, July 2018

Approval of the doctoral dissertation from the School of Mechanical Engineering of the National Technical University of Athens (NTUA) does not imply acceptance of the opinions of the author (Law 5343/1932, Article 202).



The investigated hybrid ORC- RO desalination system

"Extraordinary claims require extraordinary evidence"

Carl Sagan

Summary

A “hybrid energy desalination system” refers to a dynamical water treatment system that exhibits both continuous and discrete dynamic behavior, encompassing a larger class of systems within its structure, allowing more flexibility in modeling dynamic phenomena. In the current thesis, in order to contribute to the ongoing effort for promoting research in the area of reverse osmosis desalination combined to renewable energy sources, an investigation that addresses all the main aspects related to design, manufacturing and operation of a hybrid reverse osmosis desalination system is conducted. The investigated system is an integrated system that consists of three identical seawater reverse osmosis desalination units which intend to operate with energy from a designed, developed, installed and tested in the scope of the present thesis two- stage Organic Rankine Cycle heat-to-power engine. The main target of the present dissertation is to simulate and investigate experimentally the operation of the reverse osmosis units in variable power input, as the one deriving from solar collectors or other similar renewable energy source. The developed two- stage Organic Rankine Cycle engine uses heat to produce electrical power, based on the thermodynamic Rankine cycle and this electricity is intended to feed the reverse osmosis units.

The present work is the sequel of another research that referred to the design and experimental investigation of an autonomous reverse osmosis desalination system with solar Organic Rankine Cycle engine operating at a temperature range of 60 to 80°C. The present system intends to bring the research a step forward by increasing the operation temperature range up to 130°C, using a two- stage Organic Rankine Cycle engine, in order to investigate the efficiency amelioration and with the use of three reverse osmosis desalination units, in order to operate at a wide load range and produce fresh water even at low power input. The three main components of the integrated test- rig are: the electrical heater of a capacity of 100 kW_{th} used as the thermal source simulating for instance the solar collectors’ field (variable heat load), the designed and built two- stage Organic Rankine Cycle engine that convert the heat into electricity through the expansion of a previously compressed organic fluid and finally the three identical seawater reverse osmosis desalination units that will receive the electric power from the Organic Rankine Cycle engine and produce fresh potable water from water of high salinity in a wide operational range.

A thorough simulation of all the sub- units of the integrated system leads to the detailed and careful design of each sub- system. First, the two- stage most appropriate configuration of the Organic Rankine Cycle engine is analyzed and adopted and the most efficient organic fluid (refrigerant) is selected among several candidates. The scroll expanders for the current application are carefully designed as they will be manufactured by scroll compressors’ modification, and the whole Organic Rankine Cycle Engine design is finalized. The heat cycle simulation is selected to be an electric heater of appropriate capacity for the current application and the heat transfer fluid is thoroughly investigated resulting in Methylene Glycol (MEG) to be the most suitable and efficient. The reverse osmosis unit layout is then specified based on the expected power production of the Organic Rankine Cycle Engine.

Summary

All the components of each sub- system are then carefully selected and the construction and assembly of each one is realized. The reverse osmosis sub- units are market available desalination units of the same capacity and they are connected accordingly at the laboratory. The Organic Rankine Cycle engine is constructed from scratch on a common skid, including all the selected equipment (pump, evaporator, condenser etc.). Especially the scroll expanders are modified in a machine shop from market available scroll compressors in order to suit the current engine requirements. An electro- valve installed in between their connection, permits the by- pass of the first expander in order for the engine to operate at single- stage mode. When both sub- systems are installed at the laboratory, the test rig is ready for investigation.

The experimental evaluation starts with the experimental testing of the reverse osmosis desalination unit. The three sub- units operate connected to the grid, for different power input (by regulating the high-pressure pump's rotational speed), in different water salinities simulating brackish, heavy brackish and seawater quality and in different water temperatures. Case- studies of the operation of the developed reverse osmosis desalination unit consisting of several sub- units, powered by a PV system of different capacities in different locations for winter and summer and the comparison to a conventional single unit are also examined. The results of these studies intend to verify the offered flexibility of such a system.

The constructed Organic Rankine Cycle engine is then thoroughly tested in many different operation conditions in order to evaluate its performance and offered flexibility of the two- stage configuration. The engine is tested connected to the grid for low operating temperature (70 to 95°C) with water as the heat transfer fluid for single and two- stage operation in several thermal power input values, regulated by the pump's and expander(s)'s rotational speed. Then, an investigation for higher operating temperatures (110 to 130 °C) with MEG on the heat cycle is conducted. The power produced is driven to electric brakes and consumed on a thermal resistance. The two scroll expanders' operation is separately evaluated since these components are modified and require the plotting of operation curves for reference purposes. The results of multiple tests in different operation conditions provide a very clear and precise picture of the Organic Rankine Cycle engine performance.

Finally, a theoretical investigation of the integrated system operation based on the experimental results of the sub- systems is also presented. The net power production of the Organic Rankine Cycle engine both in single and two- stage operation at 120 and 130 °C (design point) is driven to the RO unit in order to examine the fresh water production from high feed water salinity and the sub- units' operation.

The complete design, construction and evaluation procedure of the sub- systems and the integrated system clearly defines the advantages of hybrid desalination systems. Moreover, the know- how gained permits the recognition and effective treatment of the technical aspects associated with such systems. Overall, the system developed is a very promising prototype which presents a sufficient and efficient operation under most of the operation conditions it is exposed to, and it is certainly an excellent springboard for further research in the field of water desalination through renewable energy sources. Recommendations for future research are provided as well as suggestions to further enhance the efficient operation of the hybrid desalination applications.

Περίληψη

Ένα «υβριδικό ενεργειακό σύστημα αφαλάτωσης» είναι ένα δυναμικό σύστημα επεξεργασίας νερού που επιδεικνύει τόσο συνεχή όσο και διακριτή δυναμική συμπεριφορά, περιλαμβάνοντας ένα ευρύτερο σύνολο συστημάτων εντός της δομής του, επιτρέποντας μεγαλύτερη ευελιξία στη μοντελοποίηση δυναμικών φαινομένων. Στην παρούσα διατριβή και με σκοπό τη συμβολή στην εξελισσόμενη προσπάθεια προώθησης της έρευνας στον τομέα της αφαλάτωσης με τη μέθοδο της αντίστροφης ώσμωσης συνδυασμένης με ανανεώσιμες πηγές ενέργειας, διεξάγεται μια εκτενής έρευνα που απευθύνεται σε όλες τις βασικές πτυχές που σχετίζονται με το σχεδιασμό, την κατασκευή και τη λειτουργία ενός υβριδικού συστήματος αφαλάτωσης με αντίστροφη ώσμωση. Το υπό έρευνα σύστημα είναι ένα ολοκληρωμένο σύστημα που αποτελείται από τρεις πανομοιότυπες μονάδες αφαλάτωσης θαλασσινού νερού με τη μέθοδο της αντίστροφης ώσμωσης οι οποίες θα λειτουργούν με την παραγόμενη ενέργεια από την σχεδιασμένη, κατασκευασμένη, εγκατεστημένη και ελεγμένη στα πλαίσια της παρούσας διατριβής διβάθμιας θερμικής μηχανής Οργανικού Κύκλου Rankine. Βασικός στόχος της παρούσας εργασίας είναι να προσομοιώσει και να ερευνησει πειραματικά τη λειτουργία της μονάδας αφαλάτωσης σε μεταβλητό ενεργειακό φορτίο, σαν αυτό που προκύπτει από ανανεώσιμες πηγές ενέργειας όπως για παράδειγμα οι ηλιακοί συλλέκτες. Η διβάθμια μηχανή Rankine που αναπτύχθηκε χρησιμοποιεί θερμότητα για να παράξει ηλεκτρική ενέργεια βασισμένη στο θερμοδυναμικό κύκλο Rankine και η ηλεκτρική αυτή ενέργεια θα τροφοδοτεί τις μονάδες της αφαλάτωσης.

Η παρούσα έρευνα αποτελεί συνέχεια προηγούμενης ερευνητικής εργασίας που σχετιζόταν με το σχεδιασμό και την πειραματική αξιολόγηση ενός αυτόνομου συστήματος αφαλάτωσης με ηλιακό Οργανικό Κύκλο Rankine για λειτουργία σε θερμοκρασιακό εύρος από 60 έως 80 °C. Το παρόν σύστημα έχει σκοπό να προχωρήσει την έρευνα ένα βήμα μπροστά αυξάνοντας το θερμοκρασιακό εύρος λειτουργίας στους 130 °C, με τη χρήση μιας διβάθμιας μηχανής Οργανικού Κύκλου Rankine, για τη διερεύνηση της βελτίωσης της απόδοσης και με τη χρήση πολυβάθμιας μονάδας αφαλάτωσης αντίστροφης ώσμωσης για λειτουργία σε ένα ευρύτερο πεδίο ενεργειακού φορτίου και την παραγωγή καθαρού νερού ακόμη και σε χαμηλό φορτίο. Οι τρεις βασικές συνιστώσες του πειραματικού συστήματος είναι: ο ηλεκτρικός θερμαντήρας ικανότητας 100 kW_{th} ο οποίος χρησιμοποιείται σαν πηγή θερμότητας προσομοιάζοντας το πεδίο των ηλιακών συλλεκτών για παράδειγμα (μεταβλητό φορτίο θερμότητας), η σχεδιασμένη και κατασκευασμένη διβάθμια μηχανή Οργανικού Κύκλου Rankine που μετατρέπει τη θερμότητα σε ηλεκτρική ενέργεια μέσω της εκτόνωσης ενός προηγούμενως συμπιεσμένου οργανικού ρευστού και τέλος οι τρεις όμοιες υπομονάδες αφαλάτωσης θαλασσινού νερού αντίστροφης ώσμωσης που θα δεχθούν την ηλεκτρική ενέργεια από τη μηχανή Οργανικού Κύκλου Rankine και θα παράξουν φρέσκο πόσιμο νερό από θαλασσινό για ένα ευρύ πεδίο λειτουργίας.

Η ενδεδειγμένη προσομοίωση όλων των υποσυστημάτων οδηγεί στο λεπτομερή και προσεκτικό σχεδιασμό τους. Κατ' αρχάς, η πλέον κατάλληλη διαμόρφωση διβάθμιου Οργανικού Κύκλου Rankine αναλύεται και υιοθετείται, και το πιο αποδοτικό οργανικό ρευστό (ψυκτικό) διαλέγεται ανάμεσα σε διάφορα υποψήφια. Οι ελικοειδείς εκτονωτές (τύπου scroll) της συγκεκριμένης εφαρμογής σχεδιάζονται με ιδιαίτερη έμφαση στα κατασκευαστικά τους χαρακτηριστικά καθώς θα προκύψουν από τροποποίηση ελικοειδών συμπιεστών. Με αυτά, ο τελικός σχεδιασμός της

μηχανής Οργανικού Κύκλου Rankine ολοκληρώνεται. Η προσομοίωση του θερμικού κυκλώματος επιλέγεται να γίνει με τη χρήση ενός ηλεκτρικού θερμαντήρα κατάλληλης δυναμικότητας για την εφαρμογή ενώ παράλληλα επιλέγεται και το κατάλληλο ρευστό για τη μετάδοση της θερμότητας που προκύπτει να είναι η μεθυλενογλυκόλη (MEG). Ακολουθεί ο σχεδιασμός της μονάδας αντίστροφης ώσμωσης βασισμένος στην αναμενόμενη παραγωγή ενέργειας από τη μηχανή Οργανικού Κύκλου Rankine.

Όλες οι συνιστώσες των υποσυστημάτων επιλέγονται κατόπιν ενδελεχούς έρευνας και εκτίμησης και πραγματοποιείται η κατασκευή και συναρμολόγησή τους. Οι υπομονάδες της μονάδας αντίστροφης ώσμωσης είναι μονάδες αφαλάτωσης ίδιας δυναμικότητας, διαθέσιμες στο εμπόριο οι οποίες εγκαθίστανται και συνδέονται στο εργαστήριο κατάλληλα μεταξύ τους. Η μηχανή Οργανικού Κύκλου Rankine κατασκευάζεται από το μηδέν, σε κοινό πλαίσιο που περιλαμβάνει όλο τον επιλεγμένο εξοπλισμό (αντλία, ατμοποιητή, συμπυκνωτή κτλ). Ειδικά οι ελικοειδείς εκτονωτές τροποποιούνται στο μηχανουργείο από διαθέσιμους στο εμπόριο ελικοειδείς συμπιεστές ώστε να ικανοποιήσουν τις απαιτήσεις της συγκεκριμένης εφαρμογής. Η εγκατάσταση ηλεκτροβάνας ανάμεσα στους δυο εκτονωτές επιτρέπει την πλήρη παράκαμψη του πρώτου εκτονωτή ώστε η μηχανή να τίθεται σε μονοβάθμια λειτουργία. Όταν και τα δυο υποσυστήματα τοποθετούνται στο εργαστήριο, το πρωτότυπο- δοκίμιο είναι έτοιμο προς διερεύνηση.

Η πειραματική αξιολόγηση ξεκινά με τον εργαστηριακό έλεγχο της μονάδας αντίστροφης ώσμωσης. Οι τρεις υπομονάδες συνδέονται στο ηλεκτρικό δίκτυο και λειτουργούν σε μεταβλητό φορτίο (ρυθμίζοντας την ταχύτητα περιστροφής της αντλίας υψηλής πίεσης της κάθε μιας), σε διάφορες αλατότητες νερού τροφοδοσίας προσομοιάζοντας υφάλμυρο, βαρύ υφάλμυρο και θαλασσινό νερό και σε διαφορετικές θερμοκρασίες νερού. Διεξήχθη επίσης, θεωρητική έρευνα σχετικά με τη λειτουργία της επιλεγμένης πολυβάθμιας διαμόρφωσης της μονάδας αφαλάτωσης, που τροφοδοτείται από ένα φωτοβολταϊκό σύστημα διαφόρων ικανοτήτων, σε διαφορετικές περιοχές του κόσμου για μια τυπική χειμερινή και καλοκαιρινή ημέρα και συγκρίνεται με μια συμβατική μονοβάθμια αφαλάτωσης. Τα αποτελέσματα αυτής της έρευνας σκοπεύουν να αποδείξουν την προσφερόμενη ευελιξία ενός τέτοιου συστήματος.

Η μηχανή Οργανικού Κύκλου Rankine που αναπτύχθηκε εξετάζεται σε ακόμη μεγαλύτερο βάθος σε διάφορες συνθήκες λειτουργίας με σκοπό να αξιολογηθεί η συμπεριφορά της και η προσφερόμενη ευελιξία από τη διβάθμια διαμόρφωση. Η μηχανή εξετάζεται με ρεύμα δικτύου για χαμηλή θερμοκρασία (70 με 95°C) με νερό σαν εργαζόμενο μέσο στο θερμικό κύκλωμα για μονοβάθμια και διβάθμια λειτουργία σε μεταβαλλόμενο θερμικό φορτίο ρυθμίζοντας τη συχνότητα της αντλίας και των εκτονωτών. Ακολουθεί η διερεύνηση για υψηλότερη θερμοκρασία λειτουργίας (110 με 130 °C), με μεθυλαιογλυκόλη ως εργαζόμενο μέσο στο θερμικό κύκλωμα. Η παραγόμενη ισχύς οδηγείται σε ηλεκτρικά φρένα και καταναλίσκεται σε μια θερμική αντίσταση. Η λειτουργία των δυο εκτονωτών εξετάζεται ξεχωριστά καθώς αυτές οι συνιστώσες του συστήματος είναι τροποποιημένες και απαιτούν χάραξη των καμπυλών λειτουργίας τους για να αξιολογηθεί η συμπεριφορά τους. Τα αποτελέσματα πολυάριθμων δοκιμών σε διάφορες συνθήκες λειτουργίας προσφέρουν μια πολύ ξεκάθαρη και ακριβή εικόνα της συμπεριφοράς της μηχανής Οργανικού Κύκλου Rankine.

Τέλος, παρουσιάζεται επίσης θεωρητική διερεύνηση του ολοκληρωμένου συστήματος της μηχανής Οργανικού Κύκλου Rankine με τη μονάδα αφαλάτωσης αντίστροφης ώσμωσης, που βασίζεται στα πειραματικά αποτελέσματα των ελέγχων

κάθε υποσυστήματος που διεξήχθησαν. Η καθαρή παραγόμενη ισχύς από τη μηχανή Οργανικού Κύκλου Rankine για λειτουργία στους 120 και 130 °C (σημείο σχεδιασμού) οδηγείται στη μονάδα αφαλάτωσης αντίστροφης ώσμωσης με σκοπό να εξεταστεί η παραγωγή καθαρού νερού υψηλής αλατότητας και η λειτουργία των υπομονάδων.

Η διαδικασία του πλήρους σχεδιασμού, της κατασκευής και αξιολόγησης των υποσυστημάτων και του ολοκληρωμένου συστήματος ορίζει ξεκάθαρα τα πλεονεκτήματα των υβριδικών συστημάτων αφαλάτωσης. Επίσης, η τεχνογνωσία που αποκτήθηκε επιτρέπει την αναγνώριση και την αποτελεσματική διαχείριση των τεχνικών θεμάτων που σχετίζονται με τέτοια συστήματα. Συμπερασματικά, το σύστημα που αναπτύχθηκε αποτελεί ένα πολλά υποσχόμενο πρωτότυπο που παρουσιάζει επαρκή και αποδοτική λειτουργία στις πλείστες των συνθηκών στις οποίες εκτέθηκε και ασφαλώς αποτελεί ένα εξαιρετικό εφαλτήριο για μελλοντική έρευνα στον τομέα της αφαλάτωσης νερού με χρήση ανανεώσιμων πηγών ενέργειας. Ολοκληρώνοντας την παρούσα διατριβή, προτείνονται συστάσεις για μελλοντική έρευνα καθώς και προτάσεις για περαιτέρω ενίσχυση της αποδοτικής λειτουργίας εφαρμογών υβριδικών συστημάτων αφαλάτωσης νερού.

Acknowledgments

The present doctoral dissertation was assigned by the Department of Fluids of the National Technical University of Athens.

First and foremost, I would like to express my gratitude to my Supervisor Professor D. Papantonis for the trust shown in me, his guidance, his patience and his support throughout this whole journey until the end. It is a great honor for me to have been his last PhD candidate before retirement and a pleasure to have collaborated with such a special individual.

Furthermore, I would also like to thank NTUA professors I. Anagnostopoulos and D. Mathioulakis for their supervision, support and patience throughout this work, as well as the examination committee for their presence at the finalization of this thesis. A special thank is addressed to the AUA Assistant Professor and precious friend D. Manolakos, thanks to whom the idea for the particular dissertation was formed. Moreover, thanks to him and AUA Professor G. Papadakis, the dissertation was supported under a European Program which was a great assistance for the realization of this effort. Cordial thanks are extended to an extraordinary scientist Dr. G. Kosmadakis, whose valuable guidance and comments have been vital throughout the whole process. Special thanks are addressed to a new friend of mine Dr. G. Caralis who acted as a catalyst with his support at a very sensitive moment for the completion of the current dissertation.

I wish to thank my parents and family with all my heart, since without them I would not be able to achieve any of the personal evolution achieved thanks to their support and the chances they have offered me.

I would like to thank my best friend Niki for always being there at the most important moments of my life and for her everlasting trust in me. Finally, nobody has been more important to me in the pursuit of this project than my husband Stergios, with his patience, his everyday support and encouraging smile and I owe him an apology for all the good things I have deprived of him on the altar of this feat.

Acknowledgments

Abbreviations

acc	Accuracy
AD	Adsorption Desalination
APM	Axial Piston Motor
APP	Axial Piston Pump
CA	Cellulose Acetate
CFCs	Chlorofluorocarbons
CHP	Combined Heat and Power
CIP	Clean In Place system
CSP	Concentrated Solar Power
DC/AC	Direct Current/ Alternative Current
E/M	Electromagnetic
ED	Electrodialysis Desalination
EDR	Energy Recovery Device
EES	Engineering Equation Solver
EU	European Union
FF	Feeling Factor
ff	Membranes Fouling Factor
GWP	Global Warming Potential
HBD	Hydrate- based desalination
HCFCs	Hydro-chlorofluorocarbons
HFCs	Hydrofluorocarbons
HP	High Pressure
HTF	Heat Transfer Fluid
IDA	International Desalination Association
LP	Low Pressure
MED	Multi- Effect Distillation
MEG	Monoethylene Glycol
MSF	Multi- stage Flash
MVC	Mechanical Vapor Compression
NTUA	National Technical University of Athens

Abbreviations

ODP	Ozone Deployment Potential
ORC	Organic Rankine Cycle
PRTs	Platinum resistance thermometers
PV	Photovoltaic System
RE	Renewable Energy
RO	Reverse Osmosis
RPM	Revolutions Per Minute
RTD	Resistance Temperature Detectors
SEC	Specific Energy Consumption
TDS	Total Dissolved Solids
TF	Thin Film
TVC	Thermal Vapor Compression
UAE	United Arab Emirates
UF	Ultrafiltration
Π	Osmotic Pressure

Nomenclature

$h_{ORCCONin}$	R245fa Condenser inlet enthalpy
$h_{ORCCONout}$	R245fa Condenser outlet enthalpy
$h_{ORCEVin}$	R245fa Evaporator inlet enthalpy
$h_{ORCEVout}$	R245fa Evaporator outlet enthalpy
$h_{ORCPoutis}$	R245fa Pump outlet isentropic enthalpy
h_{ORCPin}	R245fa Pump inlet enthalpy
$h_{ORCPout}$	R245fa Pump outlet enthalpy
$h_{ORCe1outis}$	First expander outlet isentropic enthalpy
$h_{ORCe1in}$	First expander inlet enthalpy
$h_{ORCe1out}$	First expander outlet enthalpy
$h_{ORCe2outis}$	Second expander outlet isentropic enthalpy
$h_{ORCe2in}$	Second expander inlet enthalpy
$h_{ORCe2out}$	Second expander outlet enthalpy
h_i	Specific enthalpy of each state
I_{hot}, V_{hot}	The current and voltage of the hot water pump
I_{cond}, V_{cond}	The current and voltage of the condenser pump
P_{hotp}	The power consumption of the hot water pump
$P_{ORCe1meas}$	First expander's power production
$P_{ORCe2meas}$	Second expander's power production
P_{ORCeid}	Total theoretical expanders' power production $P_{ORCeid} = P_{ORCe1} + P_{ORCe2}$
P_{ORCP}	Pump power consumption $P_{ORCP} = (h_{ORCPout} - h_{ORCPin}) * m_{ORCP}$
P_{ORCe}	Total expanders' power production $P_{ORCe} = P_{ORCe1meas} + P_{ORCe2meas}$
P_{ORCe1}	First expander theoretical power consumption $P_{ORCe1} = (h_{ORCe1in} - h_{ORCe1out}) * m_{ORCP}$
P_{ORCe2}	Second expander theoretical power consumption $P_{ORCe2} = (h_{ORCe2in} - h_{ORCe2out}) * m_{ORCP}$

Nomenclature

P_{condp}	The power consumption of the hot water pump
P_p	Pump power consumption $P_p = \frac{\rho * g * H * Q}{n_p}$
Q_{ORCCON}	Condenser thermal load $Q_{ORCCON} = (h_{ORCCONout} - h_{ORCCONin}) * m_{ORCP}$
Q_{ORCEV}	Evaporator thermal load $Q_{ORCEV} = (h_{ORCEVout} - h_{ORCEVin}) * m_{ORCP}$
Q_{HTF}	The thermal load of the heat transfer fluid $Q_{HTF} = \dot{m}_{HTF} * (h_{HTF,2} - h_{HTF,1}) = \dot{m}_{HTF} * c_{HTF} * (T_{HTF,2} - T_{HTF,1}) = Q_{ORC} = \dot{m}_{ORC} * (h_3 - h_2)$
Q_{ORC}	Thermal power at the evaporator $Q_{ORC} = \dot{m}_{ORC} * (h_3 - h_2)$
Q_{br}	Measured brine flow rate
Q_f	RO Feed water flow rate $Q_f = Q_{fr} + Q_{br}$
Q_{fr}	Measured fresh water flow rate
Q_{in}	Thermal Energy Input
Q_{out}	Work output
Q_{out}	Thermal power at the condenser $Q_{out} = \dot{m}_{ORC} * (h_5 - h_1)$
RPM_{ORCP}	ORC Pump's rotational speed $RPM_{ORCP} = \frac{f_{ORCP}}{50} * 960$
RPM_{ORCe1}	First expander's rotational speed $RPM_{ORCe1} = \frac{f_{ORCe1}}{50} * 2900$
RPM_{ORCe2}	Second expander's rotational speed $RPM_{ORCe2} = \frac{f_{ORCe2}}{50} * 2900$
$S_{ORCPout}$	R245fa Pump outlet entropy
$S_{ORCe1out}$	First expander outlet entropy
$S_{ORCe2out}$	Second expander outlet entropy
SEC_{tot}	Total specific energy consumption $salinity_{tot} = 0.627 * \frac{(con_1 * Q_{fr1} + con_2 * Q_{fr2} + con_3 * Q_{fr3})}{(Q_{fr1} + Q_{fr2} + Q_{fr3})}$
T_{hotin}	Electric heater inlet temperature
T_{hotout}	Electric heater outlet temperature
$T_{ORCCONin}$	Condenser's inlet temperature
$T_{ORCCONout}$	Condenser's outlet temperature
$T_{ORCEVin}$	Evaporator's inlet temperature

Nomenclature

$T_{ORCEV_{out}}$	Evaporator's outlet temperature
$T_{ORCP_{in}}$	Pump's inlet temperature
$T_{ORCP_{out}}$	Pump's outlet temperature
$T_{ORCe1_{in}}$	First expander's inlet temperature
$T_{ORCe1_{out}}$	First expander's outlet temperature
$T_{ORCe2_{in}}$	Second expander's inlet temperature
$T_{ORCe2_{out}}$	Second expander's outlet temperature
T_H	High Temperature
$T_{HTF,i}$	The temperature at the outlet and inlet of the heat source
T_L	Low Temperature
$T_{ex,in}$	the temperature of the evaporated organic fluid at the expander's inlet
U_{x_i}	The typical uncertainty of a measurement
U_R	The uncertainty in the calculated value
V_{condW}	The condenser water volume flow rate
\dot{V}	Volumetric flow rate of the pump $\dot{V} = c * (rpm)$
$V_{ex,in}$	The volumetric flow rate of the expander as a function of its rotational speed $V_{ex,in} = V_{swept} * FF * \frac{rpm_{ex}}{60}$
V_{swept}	The swept volume of the expander which is a geometric characteristic of the expander and remains constant during its operation
W_{ex}	Expanders' total power production $W_{ex} = W_{ex,1} + W_{ex,2} = \dot{m}_{ORC} * (h_3 - h_4) * n_{ex,m} + \dot{m}_{ORC} * (h_4 - h_5) * n_{ex,m}$
W_{ex}	Expander's work
W_p	Pump power consumption $W_p = \dot{m}_{ORC} * (h_2 - h_1) / n_{p,m}$
W_p	Pump's work
c_{HTF}	Specific heat capacity of the working fluid
f_{ORCe1}	First expander's frequency
f_{ORCe2}	Second expander's frequency
f_{ORCp}	Pump's frequency

Nomenclature

m_{ORCP}	ORC Pump mass flow rate $m_{ORCP} = \frac{v_{ORCP}}{60} * \frac{\rho_{R245fa}}{1000}$
m_{condW}	The mass flow rate of the condenser water circuit
\dot{m}	The ORC pump mass flow rate $\dot{m} = \frac{\dot{V}_p}{v_p} = \frac{10^{-6} * (rpm)}{v_p}$
m_{HTF}	The mass flow rate of the working fluid
m_{ORC}	The mass flow rate of the working fluid
n_{OPCPis}	Pump isentropic efficiency $n_{OPCPis} = \frac{h_{ORCPoutis} - h_{ORCPin}}{h_{ORCPout} - h_{ORCPin}} * 100$
$n_{OPCe1is}$	First expander isentropic efficiency $n_{OPCe1is} = \frac{h_{ORCe1out} - h_{ORCe1in}}{h_{ORCe1outis} - h_{ORCe1in}} * 100$
$n_{OPCe2is}$	Second expander isentropic efficiency $n_{OPCe2is} = \frac{h_{ORCe2out} - h_{ORCe2in}}{h_{ORCe2outis} - h_{ORCe2in}} * 100$
n_{OPCe1}	First expander actual efficiency $n_{OPCe1} = \frac{P_{ORCe1meas}}{m_{ORCP} * (h_{ORCe1in} - h_{ORCe1outis})} * 100$
n_{OPCe2}	Second expander actual efficiency $n_{OPCe2} = \frac{P_{ORCe2meas}}{m_{ORCP} * (h_{ORCe2in} - h_{ORCe2outis})} * 100$
$n_{ORCthid}$	ORC engine's ideal thermal efficiency $n_{ORCthid} = \frac{P_{ORCeid} - P_{ORCP}}{Q_{ORCEV}} * 100$
n_{ORCe}	Expander's efficiency $n_{ORCe} = 100 - \frac{P_{ORCeid} - P_{ORCe}}{P_{ORCeid}} * 100$
n_{ORCth}	ORC engine's thermal efficiency $n_{ORCth} = \frac{P_{ORCe} - P_{ORCP}}{Q_{ORCEV}} * 100$
$p_{ORCCONin}$	Condenser's inlet pressure
$p_{ORCCONout}$	Condenser's outlet pressure
$p_{ORCEVin}$	Evaporator's inlet pressure
$p_{ORCEVout}$	Evaporator's outlet pressure
p_{ORCPin}	Pump's inlet pressure
$p_{ORCPout}$	Pump's outlet pressure
$p_{ORCe1in}$	First expander's inlet pressure

Nomenclature

$p_{ORCe1out}$	First expander's outlet pressure
$p_{ORCe2in}$	Second expander's inlet pressure
$p_{ORCe2out}$	Second expander's outlet pressure
$p_{ex,in}$	The pressure of the evaporated organic fluid at the expander's inlet $p_{ex,in} = \rho_{ex,in} * R * (T_{ex,in} + 273.15)$
$p_{ex,in2}$	Inlet pressure at the second expander $p_{ex,in2} =$ $\frac{10^{-6} * (rpm_p)}{V_{swept} * FF * \frac{(rpm_{ex2})}{60}} * R * (T_{ex,in2} + 273.15)$
rpm_{ex}	Expander's rotational speed
$salinity_{tot}$	Total fresh water salinity $salinity_{tot} = 0.627 * \frac{(con_1 * Q_{fr1} + con_2 * Q_{fr2} + con_3 * Q_{fr3})}{(Q_{fr1} + Q_{fr2} + Q_{fr3})}$, con_i measured conductivity for each sub- unit, Q_{fr_i} measured fresh water flow rate for each sub- unit
v_{hotW}	The hot water volume flow rate
v_{ORCP}	ORC Pump volume flow rate $v_{ORCP} = 0.0205 * RPM_{ORCP}$
v_p	Specific volume
η_{th}	Heat cycle thermal efficiency $\eta_{th} = \frac{Q_{in} - Q_{out}}{Q_{in}}$
$\eta_{th_Rankine}$	Rankine cycle thermal efficiency $\eta_{th_Rankine} = 1 - \frac{h_4 - h_1}{h_3 - h_2}$
η_{th_carnot}	Carnot cycle thermal efficiency $\eta_{th_carnot} = 1 - \frac{T_L}{T_H}$
ρ_{R245fa}	R245fa density
$\rho_{ex,in}$	The density of the evaporated organic fluid at the expander's inlet $\rho_{ex,in} = \frac{m_{ex,in}}{V_{ex,in}}$
c	Proportionality factor $\sim 10^{-6} \text{ m}^3/\text{s}/\text{rpm}$
C_p	Specific heat capacity of the working fluid $c_p = 2329 + 4.819 T$
g	The gravitational acceleration (9.81 m/s ²)
H	The total head
I_1, I_2, I_3	Measured current

Nomenclature

k	Thermal conductivity of the working fluid $k = 0.3049 - 0.000771T$
$n_{ex,is}$	Expanders' isentropic efficiency
$n_{ex,m}$	Expanders' mechanical efficiency
n_{IHE}	Internal heat exchanger efficiency
$n_{p,is}$	Pump's isentropic efficiency
$n_{p,m}$	Pump's mechanical efficiency
P_{APM}	The power recovered by the ERD
P_{APP}	The total power given to the seawater from the HP pump
P_e	The net power fed to the RO unit motor from the ORC engine $P_e + P_{APM} = P_{APP}$
R	A quantity R calculated from a combination of measured quantities x_i , $R = R(x_1, x_2, x_3, \dots, x_i)$,
T_{fr}	Fresh water temperature
V	Voltage measured
μ	Dynamic viscosity of the working fluid $\mu = -0.001975 + \frac{0.4502}{T} - \frac{1.013}{T^2}$
ρ	Density of the working fluid $\rho = 1148 - 0.6755T - 0.000199T^2$
I	Current Input $I = I_1 + I_2 + I_3$
P	Power Input $P = \frac{I*V}{1000}$
P	Power consumed by the RO $P = \frac{(I_1+I_2+I_3)*V*cos\phi}{1000}$
<i>Pressure ratio</i>	First expander pressure ratio $Pressure\ ratio = \frac{P_{ORCe1in}}{P_{ORCe1out}}$
<i>Pressure ratio</i>	Second expander pressure ratio $Pressure\ ratio = \frac{P_{ORCe2in}}{P_{ORCe2out}}$
R	The specific gas constant ($R_{specific}$ is the ratio R/M , where R is the ideal gas constant equal to 8.314 J/mol.K and M is the molecular mass where for R245fa is equal to 134.05 kg/kmol)
SEC	RO Specific energy consumption $SEC = \frac{P}{Q_{fr}}$
con	Measured water conductivity
$cos\phi$	Power factor

Nomenclature

recovery

RO recovery rate $recovery = \frac{Q_{fr}}{Q_f}$

salinity

Fresh water salinity $salinity = 0.627 * 1.00114 * con$

Contents

CHAPTER 1 - Introduction

1.1 Problem description	27
1.2 Thesis delimitation	28
1.3 Literature Review & State of the Art	31
1.3.1 Water Desalination Technologies.....	32
1.3.1.1 Thermal desalination systems	32
1.3.1.2 Chemical desalination systems.....	39
1.3.1.3 Electrical desalination systems.....	41
1.3.1.4 Mechanical desalination systems.....	43
1.3.2 Reverse Osmosis desalination and Renewable Energy Sources.....	45
1.3.3 Organic Rankine Cycle Engines and applications	51
1.3.3.1 Heat engine definition	51
1.3.3.2 The ideal Carnot cycle	52
1.3.3.3 The Thermodynamic Rankine Cycle	53
1.3.3.4 Why the Organic Rankine Cycle?.....	58
1.3.3.5 ORC applications.....	60
1.4 Objective of the thesis.....	66
1.5 Thesis structure	67

CHAPTER 2 – Simulation model development analysis

2.1 Introduction.....	75
2.2 The Organic Rankine Cycle engine model	75
2.2.1 Organic fluid selection criteria and two- stages ORC configurations candidates	75
2.2.1.1 Organic fluid selection criteria	76
2.2.1.2 Two- stage ORC engine configurations candidates	79
2.2.2 Selected configuration investigation and organic fluid selection	81
2.2.3 Components design and ORC engine modeling	88
2.2.3.1 ORC organic fluid pump.....	89
2.2.3.2 ORC expanders	93
2.2.3.3 Heat exchangers of the ORC engine (evaporator & condenser)	100
2.2.3.4 Heat cycle pump (MEG pump)	104
2.3 The Reverse Osmosis Unit model.....	106
2.3.1 ORC engine and RO desalination unit coupling.....	108

Contents

2.3.2 Desalinated water production.....	108
2.3.3 Pump and ERD selection.....	114
2.3.4 Operation at variable load.....	115
2.3.5 HP pump and membranes cooperation	118
2.4 Conclusions.....	119

CHAPTER 3 – Prototype design and construction

3.1 Introduction.....	123
3.2 The integrated system and measurement instrumentation	123
3.2.1 Measurement locations.....	124
3.3 The Organic Rankine Cycle Engine and the heat source cycle	126
3.3.1 The heat source cycle	126
3.3.2 The Organic Rankine Engine	130
3.3.2.1 Organic fluid pump.....	130
3.3.2.2 Heat exchangers	133
3.3.2.3 Organic fluid receiver vessel and filter	137
3.4 Scroll expanders	138
3.4.1 Selection	138
3.4.2 Compressor conversion.....	147
3.5 ORC engine assembly and installation	154
3.6 Reverse Osmosis Desalination Unit.....	159
3.6.1 Water tank and filter	160
3.6.2 The RO sub- unit.....	160
3.6.2.1 Feed pump.....	161
3.6.2.2 Pretreatment filters.....	164
3.6.2.3 High pressure pump and ERD.....	164
3.6.2.4 Membranes and membrane vessels	166
3.6.2.5 Control panel.....	167
3.6.2.6 Switch board.....	168
3.7 RO assembly and installation	168
3.8 Conclusions.....	173

CHAPTER 4 – Experimental investigation and evaluation of the multi- skid RO unit

4.1 Introduction.....	175
4.2 Description of the test facilities.....	175

Contents

4.3 Test results	178
4.3.1 RO- unit evaluation for several water salinities	178
4.3.1.1 Low salinity (brackish water- 15150 ppm)	179
4.3.1.2 Medium salinity (30000 ppm)	187
4.3.1.3 High salinity (37500 ppm).....	192
4.3.1.4 Conclusions.....	198
4.3.2 RO sub- unit evaluation for high salinity in different water temperatures.....	199
4.3.2.1 Membranes operation characteristic curves for variable seawater temperature	199
4.3.2.2 HP pump operation characteristic curves for variable seawater temperature	201
4.4 Case study of a multi- skid RO unit operation in combination to PV fields of different capacities for three different areas on a winter and a summer day. Comparison to a conventional RO unit.....	204
4.5 Conclusions.....	210

CHAPTER 5 – Experimental investigation and evaluation of the ORC engine

5.1 Introduction.....	213
5.2 Tests at the Laboratory.....	213
5.2.1 ORC engine evaluation for several operating temperatures	219
5.2.1.1 ORC engine evaluation for operation at 70°C with water on the heat source cycle- single & two- stage operation	219
5.2.1.2 ORC engine evaluation for operation at 85°C with water on the heat source cycle- single & two- stage operation.....	222
5.2.1.3 ORC engine evaluation for operation at 95°C with water on the heat source cycle- single & two- stage operation.....	227
5.2.1.4 ORC engine evaluation for operation at 110°C with glycol on the heat source cycle- single & two- stage operation.....	231
5.2.1.5 ORC engine evaluation for operation at 120°C with glycol on the heat source cycle- single & two- stage operation.....	236
5.2.1.6 ORC engine evaluation for operation at 130°C with glycol on the heat source cycle- single & two- stage operation.....	239
5.2.2 Scroll expanders operation evaluation at single and two- stage operation	247
5.3 Conclusions.....	260

CHAPTER 6 – Theoretical investigation and evaluation of the integrated system

6.1 Introduction.....	263
6.2 Operation at 120°C: Single and two- stage operation, high water salinity	263

Contents

6.3 Operation at 130°C: Single and two- stage operation, high water salinity	268
6.4 Conclusions.....	271
CHAPTER 7 – Thesis appraisal- Future work suggestions	
7.1 Synopsis	273
7.2 Overall conclusions.....	274
7.2.1 Conclusions on the RO unit operation	274
7.2.2 Conclusions on the ORC engine operation.....	275
7.2.3 Conclusions on the integrated system theoretical operation evaluation.....	276
7.3 Innovative elements	276
7.4 Future work suggestions	277
7.5 Epilogue	278
7.6 Publications- Acknowledgement.....	278
APPENDIX I- RO unit design	281
APPENDIX II- Experimental uncertainty analysis.....	289
APPENDIX III – PV- RO Case study design.....	295
APPENDIX IV- ORC simulation in EES.....	315

CHAPTER 1 – Introduction

1.1 Problem description

The world's freshwater resources are renewed through a continuous cycle of evaporation, precipitation and outflow – known as the water cycle – that dictates their distribution and availability over time and place. The growing demand on fresh water in the developing countries has provoked an increase of global freshwater withdrawals of about 1% per year since 1980. Accelerated urbanization, rising living standards, increased demand for water, food and energy from an ever-growing global population will inevitably lead to significant variation of water availability, leaving countries “water scarce” for large periods, unless there is sufficient infrastructure to manage and store the water [1.1].

In order to get an overall view of modern world's water distribution, several ways have been developed to define and measure water scarcity or water stress (i.e. demand for water exceeds the available amount during a certain period or poor quality restricts its use). The best-known indicator of national water scarcity is per capita renewable water per year, where threshold values are used to distinguish between different levels of water stress [1.2]. A region or country is under regular water stress when renewable water supplies drop below 1,700 m³ per capita per year. Populations face chronic water scarcity when water supplies drop below 1,000 m³ per capita per year and absolute scarcity below 500 m³ per capita per year. Using these thresholds, significant disparities exist between countries. This rough approach to measuring water scarcity was primarily based on estimates of the number of people that can reasonably live with a certain unit of water resources [1.3]. Although useful, it oversimplifies the water situation of specific countries, ignoring local factors determining access to water, as well as the feasibility of solutions in different locations, among others [1.4].

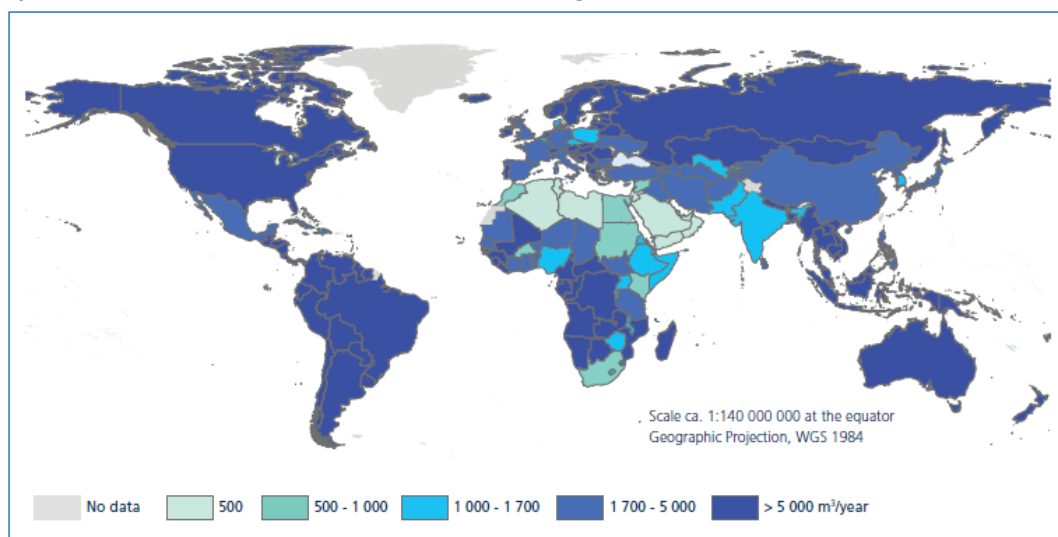


Figure 1.1 Total renewable water resources (m³/capita/year), 2014 [1.1]

Public health relies on safe and instantly available water, concerning either potable water and domestic use, or even food production and other purposes. Moreover, world's economy can improve and poverty can decrease through better water supply and quality and better management of water resources.

Freshwater consists a very small part of the total of water on our planet. While nearly 70% of the world is covered by water, just 2.5% of it is fresh and the

rest is saline and ocean-based. From this 2.5% of fresh water, only 1% is easily accessible, while much of it is trapped in glaciers and snowfields. Basically, only 0.007% of the planet's water is available to fuel and feed its 6.8 billion people.

The great inequalities of freshwater distribution around the world are mainly due to geography, climate, engineering, regulation and competition for resources. In much of the developing world, clean water is either hard to come by or a commodity that requires laborious work or significant currency to obtain [1.5].

The United Nations World Water Development Report published forecasts in 2015 noting that there will be 40% shortage of drinking water in the world by 2030 [1.6]. A sustainable way to obtain fresh potable water, suitable for human consumption and use, is to purify the highly saline ocean water that consist 97% of the total water present on earth [1.7] or even the medium- salinity ground water that is not already clean and consumable due to its chemical consistence.

1.2 Thesis delimitation

According to statistics released by the International Desalination Association (IDA), in 2016, the international desalination market continues to grow following a slowdown in the mid- 2000s. The 29th Worldwide Desalting Inventory, published by GWI DesalData in association with the IDA, indicates that desalination totals were up 14% in mid-2015 over the same time period in 2014, showing an increase in activity after a 13-year low in the desalination market. From 2015 to 2016, an increase of 3.7 million cubic meters per day (m^3/d) of desalination capacity added globally has been noticed, compared to 3.2 million m^3/d the previous year. The installed global capacity of the approximately 19,000 desalination plants considered to be online is 88.6 million m^3/d and it reached 95.6 million m^3/d in June 2016. Much of this added capacity came from large-scale seawater projects, especially in the Gulf region, as 2016 marked the third yearly increase in seawater capacity added 1.6 million m^3/d , surpassing 2015's total by 200,000 m^3/d . The brackish desalination market held steady in 2016. A resurgence of interest in reuse projects is occurring both in North America and also in India and China, according to the 2016 – 2017 IDA Desalination Yearbook, as the latter two markets experience continued industrialization and environmental control. Further global development of reuse solutions is expected as both industry and municipalities fully grasp the benefits of water reuse strategies. The 2016 – 2017 IDA Desalination Yearbook also shows that the largest gains in desalination capacity this year were in the Middle East and North Africa, driven by several new large projects and increased activity in Egypt and Oman. However, traditionally desalination-heavy Saudi Arabia saw mostly small projects this year as it deals with the maze of its national water policy and future desalination strategy as well as the effect of stubbornly low commodity prices. Commodity prices have also affected growth in Latin America but competition for resources and a predicted recovery in prices should spur activity in the region in the medium-term. New forays into desalination by the Philippines and Nigeria also demonstrate new opportunities in an expanding global market. The IDA Yearbook also explores a number of other interesting trends in 2016. For example, the adoption of membrane technologies over thermal technologies continues globally, including in the traditionally thermal Middle East, aided in part by the reduced capital costs and versatility of reverse osmosis. Private sector funding has also improved, surpassing 30% of total awarded capacity in 2015 for the first time in six years, and can also be attributed to the slew of new large-scale projects in the past year [1.8].

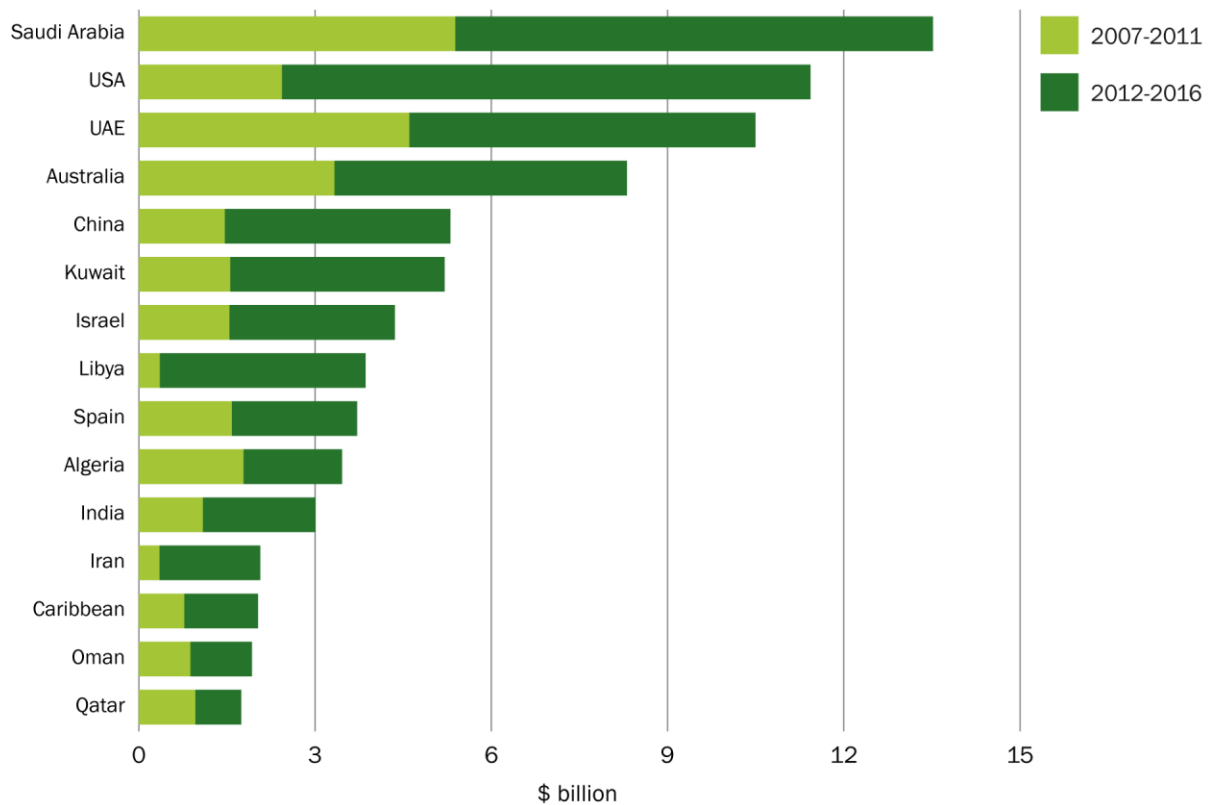


Figure 1.2 Top 15 country desalination markets (in billion \$ investment) [1.9]

Figure 1.2 demonstrates a comparative analysis of investment in desalination technologies throughout the world for two different quinquennium: 2007- 2011 and 2012- 2016. It is obvious that the investment has been more than doubled in most regions. In Figure 1.3 the new contracted capacity in million m³/day since 1980 is presented, as well as a projection until 2030. According to this data, since 2000 when desalination plants started expanding, the installed capacity has almost tripled and until 2030 it will be four times more.

GWI DesalData's long-range desalination market forecast

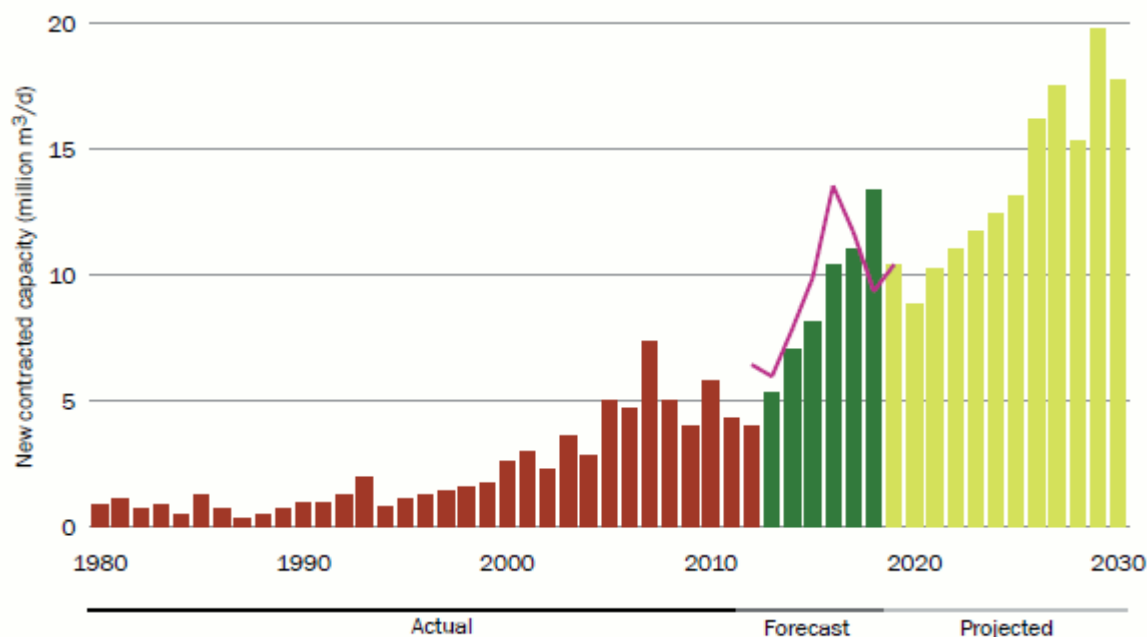


Figure 1.3 New contracted desalinated water capacity within 50 years.

In order to separate salts from water two basic technologies have been widely applied: thermal evaporation and membrane separation. The last decade desalination using semi-permeable seawater or brackish water reverse osmosis (RO) membranes has come to dominate desalination markets worldwide.

The cost of the produced fresh water has decreased throughout the last twenty years, thanks to RO desalination technology developments combined with a transition to large capacity plants, co-location with power plant generation and renewable energy sources exploitation. One of the key factors that contributed to the lower cost of water desalination is the development of the RO membrane technology. High-productivity membrane elements are designed with features to yield more fresh water per membrane element with a higher surface area and denser membrane packing. Increasing active membrane surface area allows for significant productivity gains using the same diameter membrane element. Advances in technology and equipment have resulted in a reduction of 80 percent of the energy used for water production over the last 20 years. Today, the energy needed to produce fresh water from seawater for one household per year (~2,000 kW/yr) is less than that used by the household's refrigerator.

Conventional technologies for water purification such as sedimentation and filtration, have seen modest advances since their initial use for water treatment several centuries ago; however new, more efficient desalination membranes, innovative thermal membranes or hybrid desalination technologies and equipment improvements are released every few years. It is not yet foreseen that major technology breakthroughs will dramatically lower the cost of water RO desalination in the next several years, however the steady reduction of production costs in combination with increasing costs of water treatment driven by more stringent regulatory requirements are expected to accelerate the current trend of increased reliance on the ocean as a water source. The trust in pure fresh water production from RO desalination systems will be increasing simultaneously. Technology progress is expected to reduce the cost of desalinated water by 20% in the next

five years and by up to 60% in the next 20 years making it a viable and cost-effective competitor for potable water production (Table 1) [1.10]:

Table 1 – Forecast of Desalination Costs for Medium and Large Size Projects

Parameter for Best-in Class Desalination Plants	Year 2016	Within 5 Years	Within 20 Years
Cost of Water (US\$/m³)	0.8 – 1.2	0.6 – 1.0	0.3 – 0.5
Construction Cost (US\$/MLD)	1.2 – 2.2	1.0 – 1.8	0.5 – 0.9
Electrical Energy Use (kWh/m³)	3.5 – 4.0	2.8 – 3.2	2.1 – 2.4
Membrane Productivity (m³/membrane)	28-47	35-55	95-120

1.3 Literature Review & State of the Art

A literature review of the desalination technologies currently applied for fresh potable water production is presented. The reverse osmosis (RO) desalination technology that is chosen for the current test-rig is extensively analyzed in order to present the advantages among other desalination methods. The combination with renewable and sustainable energy resources in order to decrease the carbon footprint and greenhouse emissions- the main reason of global warming and climate change- is also investigated for the potential of the RO technology to be integrated with renewable energy. Moreover, the engines based on the thermodynamic Organic Rankine Cycle for effective electricity production from a heat source and their several variations and applications are investigated. The review of the ORC engines will lead to the current ORC engine design which will be combined and feed the RO units in the current test-rig.

1.3.1 Water Desalination Technologies

Desalination systems can be classified according to the energy source they use such as; thermal systems, mechanical systems, electrical systems and chemical systems. Another classification depends on the process followed for the desalination: evaporation-condensation, filtration or crystallization. Figure 1.4 (a) illustrates the main desalination techniques around the world [1.11].

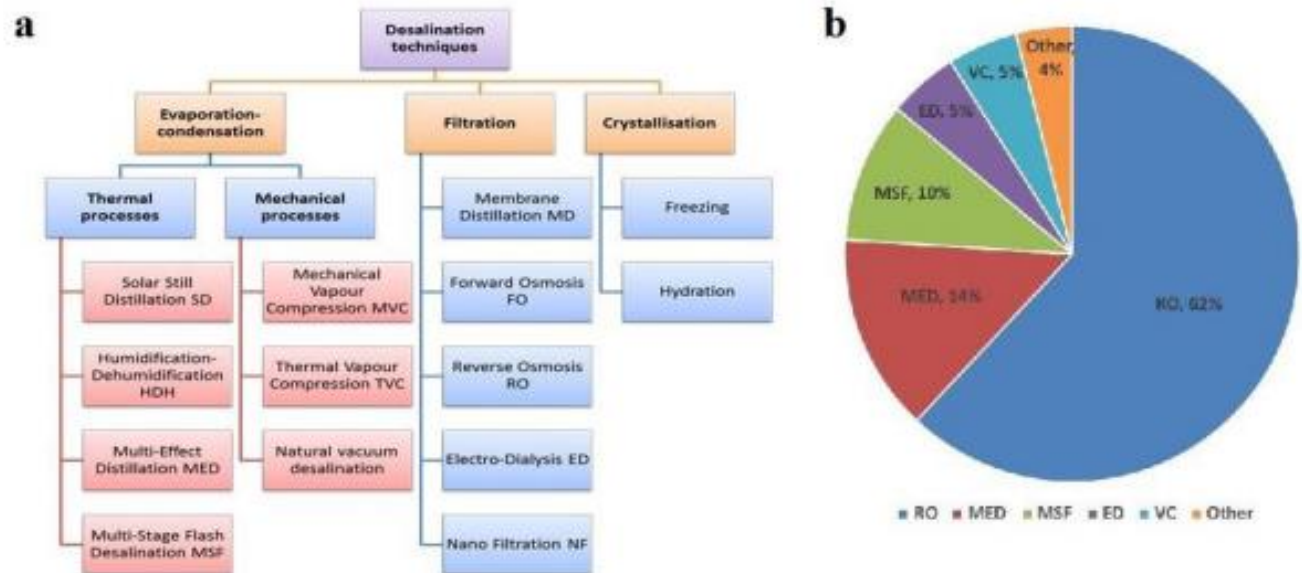


Figure 1.4 (a) the main desalination processes; (b) the contribution of each desalination process to the world water production.

1.3.1.1 Thermal desalination systems

The thermal desalination process uses energy to evaporate water and subsequently condense it again. When there is waste heat or sufficient electricity available, as is often the case with refineries and power plants, thermal desalination is an efficient and viable solution. The following thermal desalination technologies are the most prevailing nowadays;

- **Multi Effect Distillation (MED)**

Nowadays, MED technology obtains an increasing role in the desalination market. One major advantage of this technology is the use of low temperature heating steam between 60 and 90 °C. The absence of recirculation of brine masses reduces both pumping requirements and scaling tendencies. Moreover, MED process has great potential for solar applications since it is proven to be effective in part load operation. It also offers the same advantages as other thermal technologies such as high reliability and product safety [1.12].

MED process includes an asset of stages (called effects), a condenser, subsystems to feed the system with saline water and the heat source (usually hot liquid water or steam) and to collect and remove the distillate product and concentrated brine. An example of this system is shown in Figure 1.5 [1.13].

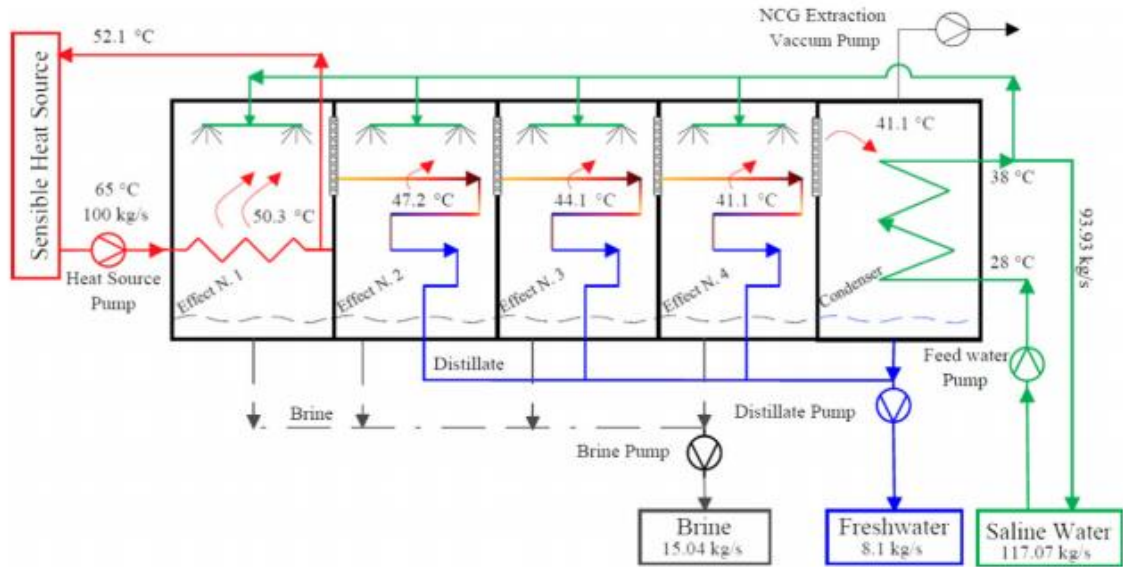


Figure 1.5 Schematics of an optimized conventional MED design (numbers for 65 °C simulation).

In the first effect, the heat transfer fluid (e.g. liquid water at 65 °C) is driven through the pump to the hot side of the evaporator, while saline feed water is pumped into the cold side. Due to the low pressure in the system, the feed water boils at 50.3 °C; the steam passes through a drainage and condenses on the hot side of the evaporator in the second effect. The remaining liquid from the first effect is drained off as brine. On the hot side of the evaporator of the second effect, the condensing vapor from the first effect becomes the pure distillate product; the heat lost from the distillate due to condensation boils more feedwater in the second effect at a lower pressure than in the first effect and steam from the second effect passes to the third etc. This sequence is repeated until the steam from the last effect reaches the condenser, which is usually cooled by the saline water source. The brine at the side product of each effect is collected and moved to the next step in disposal.

Conventional steam-driven MED systems are evaluated according to their production compared to the total heat input to the system or in several cases by the total amount of thermal energy available to the system. For different heat source temperatures, the MED configuration can be optimized to achieve a maximum waste heat performance ratio. The number of effects and the values given in Figure 1.5 are the result of such an optimization for a 65 °C heat source. Higher recovery ratio might give rise to scaling, while a lower figure would result in thermal inefficiency [1.13].

- **Thermal Vapor Compression (MED-TVC)**

The introduction of TVC makes MED more energy-efficient and competitive among desalination techniques. TVC is a kind of typical steam ejector which infuses low pressure steam using the force of supersonic flow, made by a small supersonic nozzle (maximum velocity in TVC reaches Mach 4–5) mounted in the center of a large converging-diverging duct [1.14].

The TVC plant remains a MED process which means it consists of several effects, each of which is equipped with heat exchanger beam tubes. The first stage is heated by steam from the thermo-compressor, where the TVC recompresses part

of the vapor produced in the last effect. The steam produced in each effect heats up the tubes in the next effect, while the condensate from the downstream effects and the final condenser is the source of the distillate water. The condensate from the first effect is recycled to the steam generation system. [1.15].

The main advantages of the MED-TVC process is that it operates at low temperatures with high thermal efficiency, which results in:

- ✓ small to large plant sizes
- ✓ low investment costs
- ✓ minimised corrosion risk
- ✓ reduced scaling risk
- ✓ lower thermal energy consumption
- ✓ low operating costs
- ✓ efficient use of plant volume

In Figure 1.6 a schematic of MED-TVC plant is presented [1.14].

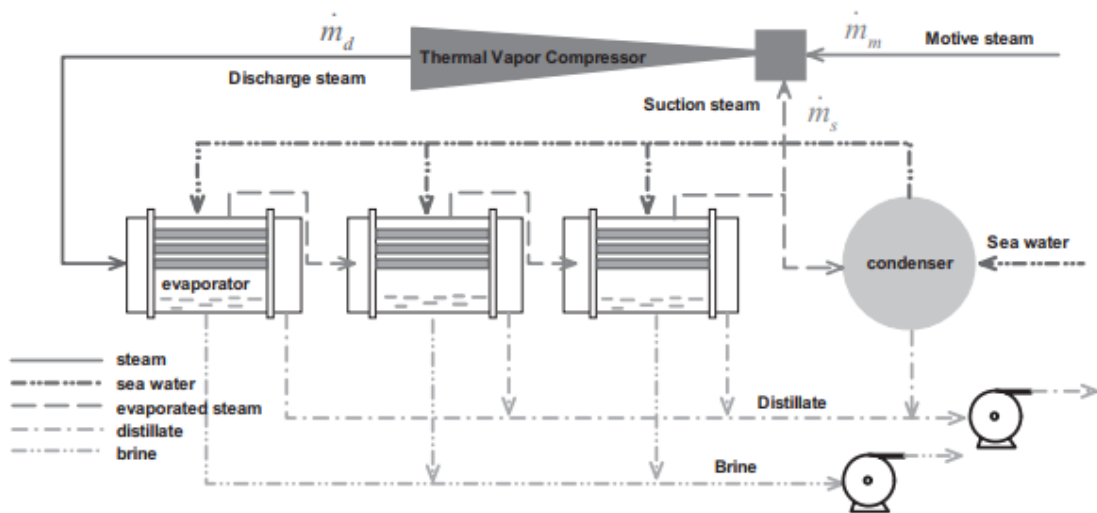


Figure 1.6 Schematics of MED plant with 3 evaporator effects and TVC sucking from 3rd effect.

- **Mechanical Vapor Compression (MED-MVC)**

The mechanical vapor compression (MVC) desalination system is another version of MED process and a very attractive and competitive solution for small and medium scale water production. The MVC process is one of the most promising, low temperature desalination methods due to advantages such as: compactness, efficient utilization of energy, easy integration with conventional desalination systems such as MSF or MED and other renewable systems such as solar, geothermal and waste thermal system, moderate civil work and construction requirements, low capital cost, high produced water quality, ease of operation and transportability. It is competitive for water production capacities less than 5000m³/d. Figure 1.7 presents a schematic of a single-effect MVC system which includes the basic equipment such as an evaporator/ condenser, a water-injected compressor, plate type feed preheaters and a non-condensable gases ejector.

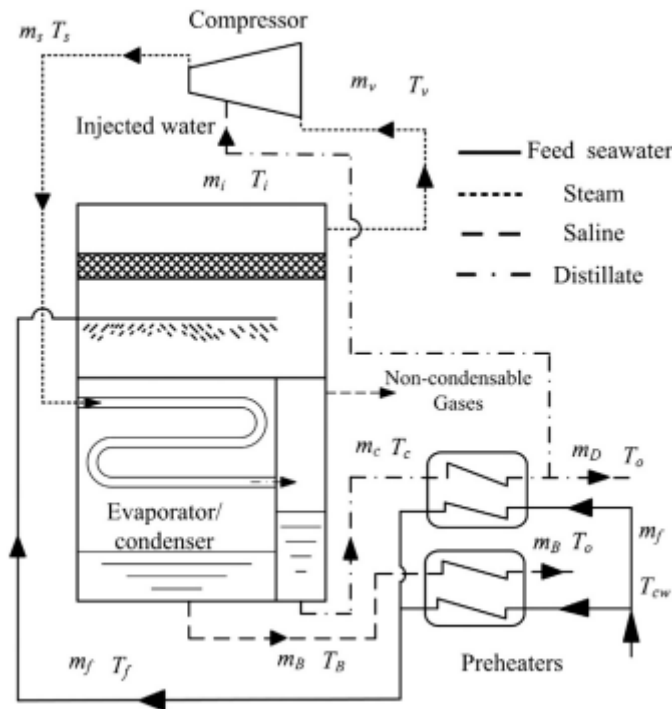


Figure 1.7 Schematics of a single- effect mechanical vapor compression system [1.16].

In the MVC desalination process, the feed seawater is heated in the distillate and brine plate preheaters. Most of the sensible thermal energy in distillate and brine stream is recovered by the feed stream which is then sprayed over the evaporator tubes. The feed temperature is further increased to the brine boiling temperature and then evaporation starts. The formed vapor flows through the demister into the water-injected compressor. A very small fraction of distillate is injected into the vapor during the compression process. The compressor increases the vapor saturation temperature to a higher pressure-temperature level. Due to the deliberate water injection, vapor in the compression process is always cooled by the injected water hence the compression process closely approximates to the isothermal process. In this way, specific power input is minimized. Furthermore, the water injection ensures that the vapor at the compressor exit is close to its saturation point. The compressed high temperature and pressure vapor flows inside the evaporator tubes where it condenses and exchanges its latent heat to the feed spray on the outer surface of the evaporator tubes. The condensed water product is collected at the side of the evaporator and the brine is at the bottom of the evaporator. The distillate and brine streams are then pumped through two plate type preheaters where the intake stream is pre-heated. It is worth noting that this system is solely operated by electricity, which is used to operate the twin screw compressor, pump, vacuum system and controllers. The MVC compressor represents the major component that consumes energy, and this is dependent upon the pressure difference. Industrial applications showed that operating the MVC at low temperatures is advisable, to minimize the formation of scaling and corrosion of materials. This is another motivation to use water-injected twin screw compressor, because the exit vapor temperature is normally lower than that from centrifugal compressors at the same pressure ratio.

- **Multi Stage Flash (MSF)**

In MSF desalination process the seawater is heated and allowed to evaporate in the so- called *flash* chambers and condense in the upper parts of these chambers, leaving the salts behind in the water component at the bottom of the chambers as concentrated brine. The feedwater needs to be heated rapidly in order to quickly reach the boiling point. The heated seawater is then fed to a cascade of chambers at pressure lower than the atmospheric so that boiling at pressure lower than the atmospheric pressure – called flashing- takes place in the flash chambers. In each stage, water vapor is collected and condensed to give fresh water. The produced clean water is tapped for drinking, irrigation or industrial usage. In Figure 1.8 the principle of MSF on a single flash stage is presented.

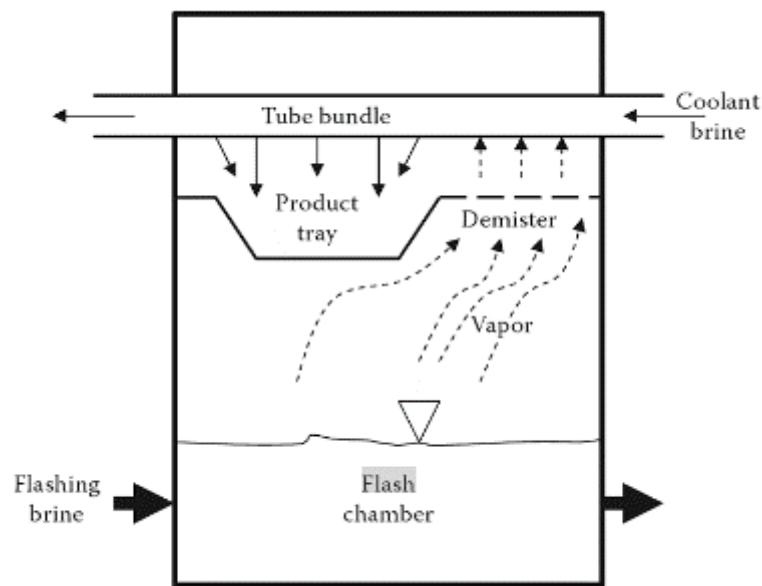


Figure 1.8 Schematics of a single- flash stage operation principle [1.17].

MSF desalination process is a major thermal desalination process since it represents around 90% of all thermal production and 42% of total world desalination production, thus it is among the most commonly used desalination technologies. It is robust and it can process water with a very high rate and relatively low maintenance. Moreover, it operates using a cascade of chambers, each with successively lower temperature and pressure in order to rapidly vaporize water which is condensed afterward from seawater. The number of chambers may be as high as 40. MSF operates at top brine temperatures (TBT) of 90- 120 °C and the recovery reached in high temperature recyclable MSF plants is 25- 50%. The produced fresh water reaches a quality of less than 50 ppm TDS and a minimal pretreatment of the feedwater is required. However, MSF desalination is an energy-intensive process, it requires a large capital investment and has a larger footprint in terms of land and materials. Moreover, its maintenance requires complete shutdown of the entire plant and it has slow start ups. Finally, high level technical knowledge is required and the recovery ratio is relatively low.

- **Solar distillation desalination**

The use of solar heat in order to purify impure water through evaporation and condensation is called solar distillation process. Solar desalination process comprises of two categories; *indirect systems*, where the solar energy is collected in a separate subsystem and produces fresh water in a conventional plant and *direct systems* where the heat collection and the solar purification take place in the same equipment, a solar still. Using the greenhouse effect, the still traps the solar radiation passing through the transparent cover and then it gets absorbed by the water and the absorber surface. This absorption results in a temperature and pressure increase to a point higher than that of the cover and the water evaporates. The lighter vapor rises to the upper part of the cover where it condenses and with gravity it gets collected into the collection tank.

One common still is a greenhouse type solar still. It is easy to build and its main parts are:

- ✓ The *transparent cover*, which may be symmetrical or asymmetrical and acts like the condenser of the vapor on its inside surface while reducing the heat losses by keeping the wind away.
- ✓ The *basin* where the saline water is kept for distillation and allows the drainage of the concentrated brine.
- ✓ The *collection trough* from where the distillate water is collected.

In Figure 1.9 a common greenhouse solar still is presented.

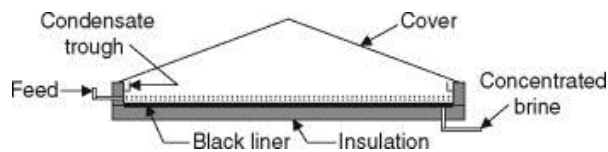


Figure 1.9 Schematic of a symmetrical greenhouse solar still [1.18].

Although solar distillation is an energy cost free and environmentally friendly desalination process, it presents high maintenance needs, since scaling and corrosion due to dissolved solids in raw water may occur. Moreover, if the still is left dry without water for a period of time it might suffer serious damage.

- **Freezing desalination**

Freezing desalination process is based on the fact that ice crystals essentially consist of pure water. More specifically, in desalination by freezing dissolved salts are extracted through the formation of ice crystals resulting in a separation of ice and brine. Although sea water ice is purer than seawater, it contains brine pockets therefore it is not pure fresh water. There are three main processes required in any freeze separation process: ice formation by heat removal, separation of ice from the brine and melting of the ice. In Figure 1.10, the basic components in freezing desalination process are presented.

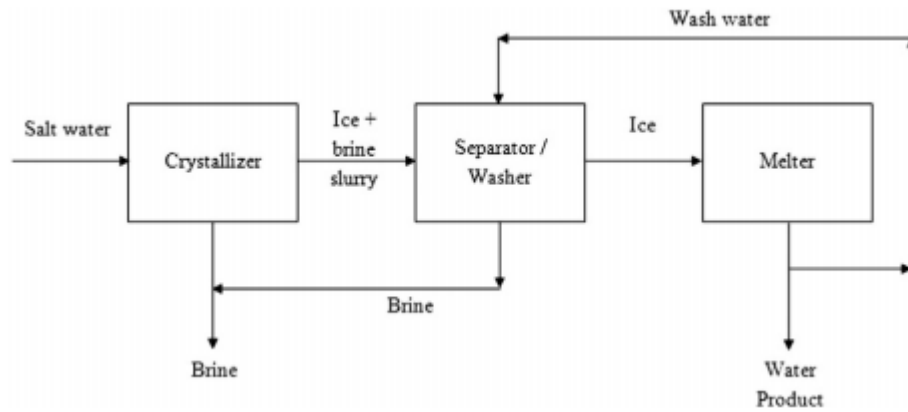


Figure 1.10 Schematic of basic freeze separation process [1.19].

A tank in which the ice crystals are formed is the freezer, the main part of the process which defines the type of the freezing process. This is the part of the process that defines its type. Once the ice crystals have been formed, the ice crystals and brine are separated in an ice separation unit. This unit might be a press, a gravity drainage, a centrifuge, a filter or a wash column and it usually acts as the wash unit as well, where clean water is used to wash the ice crystals and remove entrained brine. The melting unit is the final unit where the ice crystals are melted and the product water is selected and it is the part where energy can be recovered. The major types of freeze-melting units are based on the freezing process used, and include: (a) direct contact freezing, (b) vacuum freezing, (c) indirect contact freezing, and (d) eutectic separation.

The freeze-melting process has a number of important advantages:

- ✓ A very high separation factor.
- ✓ High energy efficiency as the latent heat of freezing is low compared to the latent heat of evaporation (lower energy requirement compared to other processes).
- ✓ Low operating temperature ensures resistivity towards biological fouling, scaling and corrosion problems, therefore less use of chemicals is required resulting in lower operating costs.
- ✓ No chemical pre-treatment is needed which means no discharge of toxic chemicals to the environment.
- ✓ Low operating temperature allows the use of inexpensive materials of construction resulting in lower capital cost.

Despite the significant advantages that the freezing desalination process presents (low energy and low temperature), it has only been used to a very limited point for fresh water production. This is mostly due to a very conservative approach to the adoption of new technology, the perception that such a process would be mechanically complex and the lack of appropriate test data. However, the recently rising urgent need for more effective solutions to water pollution problems and fresh water production, in combination to the development of simpler freezing technology lead to a better perception towards this process [1.19].

1.3.1.2 Chemical desalination systems

Chemical desalination processes are not widely used; however, they present a special interest as an alternative for different energy source desalination methods. Among them, the liquid- liquid extraction, the gas hydrate and the adsorption are the most common processes as presented below;

- **Liquid- liquid extraction desalination**

The liquid- liquid extraction desalination method's main parts are;

- ✓ a deaerator, where the dissolved gasses are mechanically removed from the feedwater,
- ✓ a heat transfer contractor, where the extraction takes place meaning that water and salt are transferred from the carrier to the solvent followed by a centrifugation that forces the mixture components of higher density to move away from the axis of the centrifuge, resulting in potable water
- ✓ a wash contractor, where the polymeric solvent is washed out in order to remove the dissolved salt in it and
- ✓ heat exchangers, which are used for heat recovery.

In Figure 1.11 the flowsheet of heat transfer contractor is presented where seawater (stream 5) mixes up with polymer solvent (stream 4) and through the extractor it leads to fresh water production [1.20].

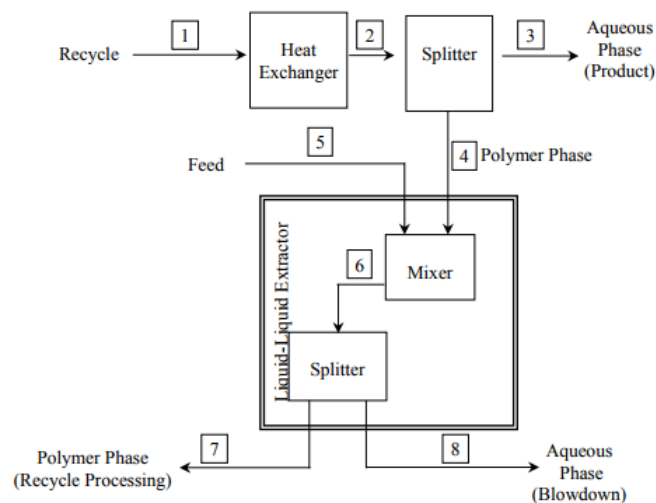


Figure 1.11 Flowsheet of heat transfer contractor [1.20].

- **Gas hydrate desalination**

In the scope of developing innovative desalination processes in order to process seawater at a large scale, considering energy costs minimizing, water recovery maximizing and becoming more environmentally friendly, recent research has been dedicated to a novel method called hydrate-based desalination (HBD) process.

Gas hydrates are nonstoichiometric crystalline ice-like compounds that are made of water (acting as host) and a number of gas molecules (acting as guests) at specific temperature and pressure conditions, which depend on hydrate-forming

gases. The hydrate-based desalination process lays on the phase change of water from liquid to solid (i.e. freezing method). In HBD a physical reaction coupled with an exclusion of ions by the hydrogen bonding of water molecules during hydrate formation compose the main idea of the process. After hydrate formation it is important to separate the solids (hydrates) from the remaining liquid phase (brines). Research has shown that 1m^3 hydrate, when dissociated, is able to produce up to 164m^3 of gas and 0.8 m^3 of pure water at standard temperature and pressure, a fact that makes the HBD process seem very promising [1.21].

Figure 1.12 presents the procedure of seawater desalination through gas hydrate-based technology. The heat content of seawater before entering the reactor is removed through the heat exchanger, in order to help the crystalline formation.

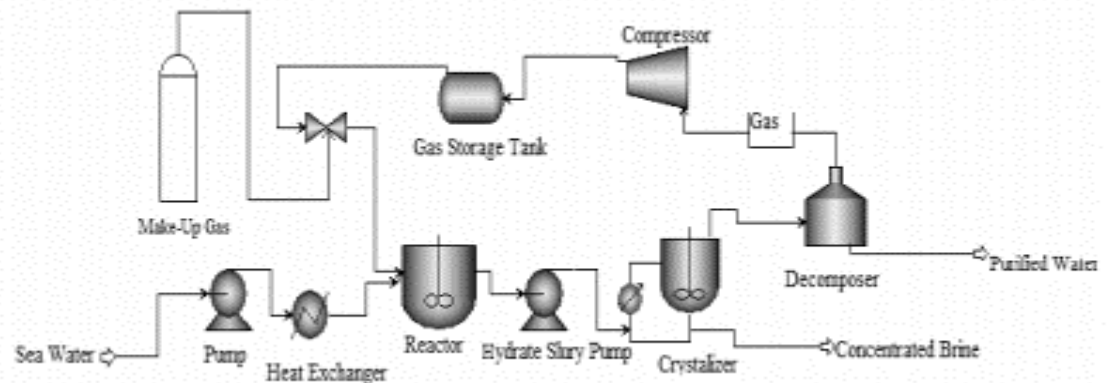


Figure 1.12 Typical process flowsheet of gas hydrate desalination system [1.22]

Inside the reactor, the seawater and the gas are thoroughly mixed with a stirrer. The stirrer turns at a desired rotational speed in order to assist the required pressure and temperature conditions by making a proper interface bonding between the water and gas molecules for the formation of gas hydrate. Low temperature and high-pressure conditions are desired in the reactor for given gas hydrate system. Gas is supplied to the reactor through a gas chamber connected to the reactor. A makeup gas cylinder is also provided for overcoming the gas losses during process flow. Once the hydrate slurry is produced, it is transferred to the crystallizer with the help of a transfer pump (hydrate slurry pump). This hydrate slurry is converted into a crystalline solid structure along with the concentrated brine. The brine is rejected from the crystallizer, while the crystalline solid structure is transferred to a decomposer. In the decomposer, the gas hydrate decomposes again into gas and water by the addition of heat and the gas flows into the gas storage tank and the remaining purified water is collected at the bottom of the decomposer. The purified water can then be used for the industrial and domestic purposes for daily routines [1.22].

- **Adsorption desalination**

Adsorption desalination (AD) is an energy efficient and environmentally friendly desalination method which produces high-quality potable water and at the same time it offers a cooling effect with just one heat source input. The process uses an adsorbent and an adsorbate, usually silica gel and water. The fundamentals of an adsorption desalination cycle lay on the efficient water vapor uptake by the chemical potential of an unsaturated adsorbent (silica gel) in one half-cycle, where

the same adsorbent could be then regenerated in the next half-cycle by heating at low temperature heat source (~ 50 to 85 °C).

During AD cycle the mesoporous surfaces of silica gel become polar and hydrophilic when they contain hydroxyl functional group (silanol group). However, at higher temperatures, silica gel rejects almost all water vapor and gives hydrophobic phenomena while regenerated. These hydrophilic and hydrophobic phenomena make silica gel a suitable adsorbent for water refrigerant-based cooling applications.

The vapor uptake by silica gel is realized with the help of the van der Waals forces and the electrostatic force between adsorbate molecules and the surface atoms. An adsorbent is always in contact with adsorbate. The adsorbent and adsorbate reach a maximum uptake at equilibrium state; however, the adsorbed phase depends on a given pressure and temperature as well as the pore surface diameter and area. The continuous production of vapor uptake is ensured through regeneration or reactivation of the adsorbent. The first is to restore the adsorption capacity of saturated adsorbent and the second is to recover valuable components present in the adsorbed phase [1.23].

In Figure 1.13, the schematic of a pilot plant of an AD system is presented.

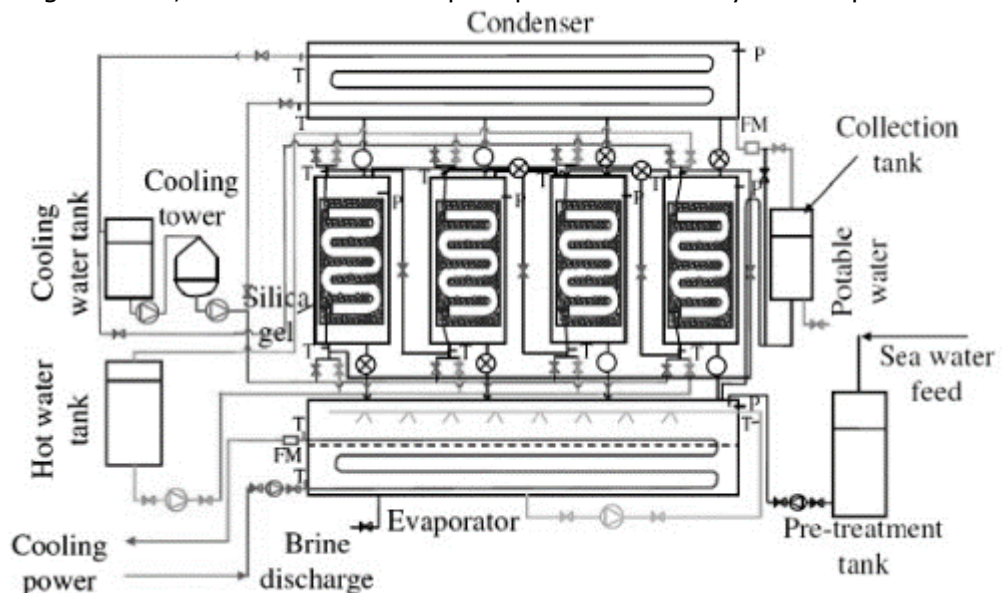


Figure 1.13 Schematic of an adsorption desalination system [1.23]

1.3.1.3 Electrical desalination systems

- **Electrodialysis desalination**

Electrodialysis (ED) is used to transport salt ions from one solution through ion-exchange membranes to another solution under the influence of an applied electric potential difference. When combined with necessary additional pre- and post-water treatment, ED becomes a cost-competitive, high recovery and low energy consumption desalination and water treatment system, especially for groundwater salinity range water sources. An ED system consists of two electrodes, a cathode and an anode and between them a series of anion (AEM) and cation exchange membranes (CEM) with spacers in between, that provide two isolated flow paths. The formed housing (stack) carries inlets and outlets for the feed,

desalinated and reject (concentrate) water. A voltage potential is applied across the membranes, in order to separate the feed solution to concentrate and product water streams [1.24].

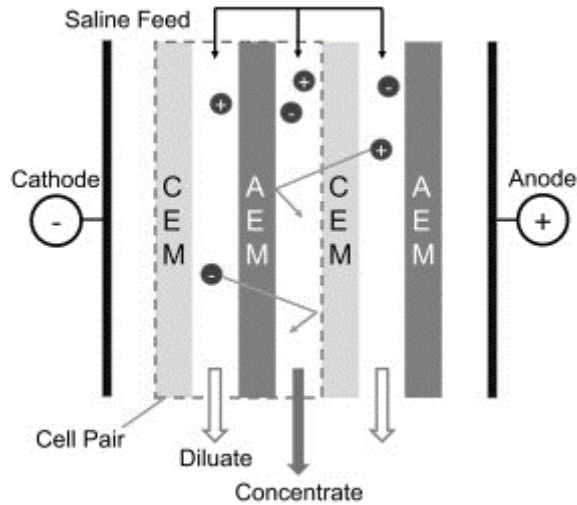


Figure 1.14 Schematic of the electro dialysis process for water desalination [1.24]

When a voltage potential is applied across the electrodes, water molecules dissociate at the cathode to produce hydroxide (OH^-) ion and hydrogen gas (H_2). At the anode, hydrogen ions (H^+), oxygen (O_2), and chlorine gas (Cl_2) are produced. Gas formation at the electrodes increases the electrical resistance of the stack and the acidic nature of the anode stream, which can produce scaling on that electrode. To prevent gas and Cl_2 formation on the electrodes that would increase the electrical resistance and would produce scaling phenomena on the electrode, a Na_2SO_4 solution is rinsed over the electrodes, which requires the use of an additional tank, pump and associated plumbing in order to be separated from the other streams.

ED systems can be formed in two different architectures: batch system and continuous system. The batch process involves recirculation of both the product and concentrate streams until the salt concentration in the product tank decreases to the desired level. In the continuous process, system parameters such as voltage and flow rate are set to produce the desired salinity in the product stream within a single pass, based upon the feed water salinity available in feed water.

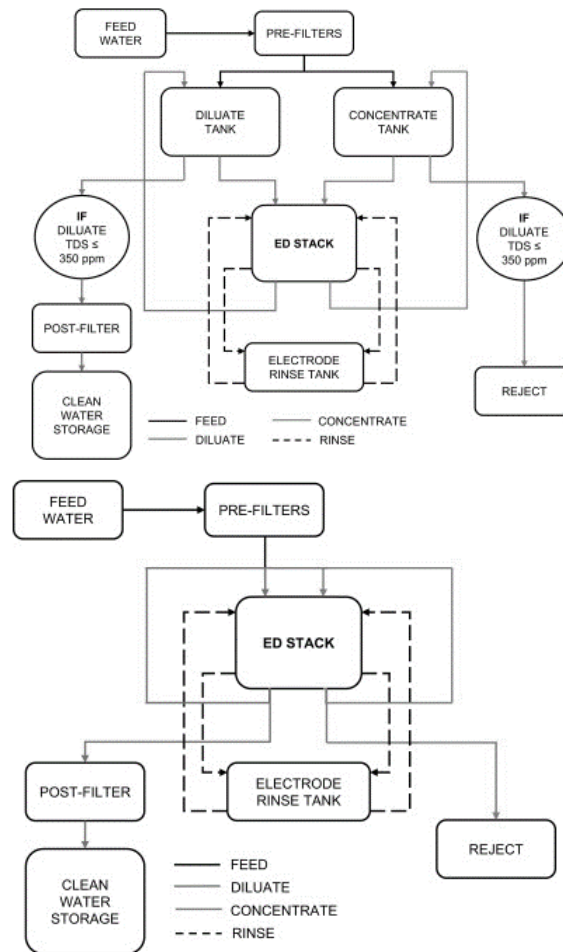


Figure 1.15 Schematic of the two electrodesialysis desalination system architectures: batch ED process(left) and continuous ED process (right) [1.24]

1.3.1.4 Mechanical desalination systems

- **Forward Osmosis desalination**

Osmosis is the phenomenon where water in a solution of higher water chemical potential (concentration), separated with a selectively permeable membrane from a solution of lower water chemical potential, passes through the membrane driven by a difference in solute concentrations across the membrane, which allows passage of water but rejects most solute molecules or ions. The pressure that if applied to the solution of higher concentration, would prevent the transfer of water across the membrane is called osmotic pressure. FO uses the osmotic pressure differential across the membrane as the driving force for water transportation. The process results in the formation of a concentrated feed stream on one side of the membrane and a dilution of a highly concentrated stream (referred to as the draw solution) on the other side of the membrane. The driving force of the FO process comes from the concentrated solution on the permeate side. The draw solution selection should ensure that it has a higher osmotic pressure than the feed solution, so that the re-concentration of the feed solution after it has been diluted in the FO process is simple [1.25]. In Figure 1.16 a schematic diagram of FO desalination process is presented.

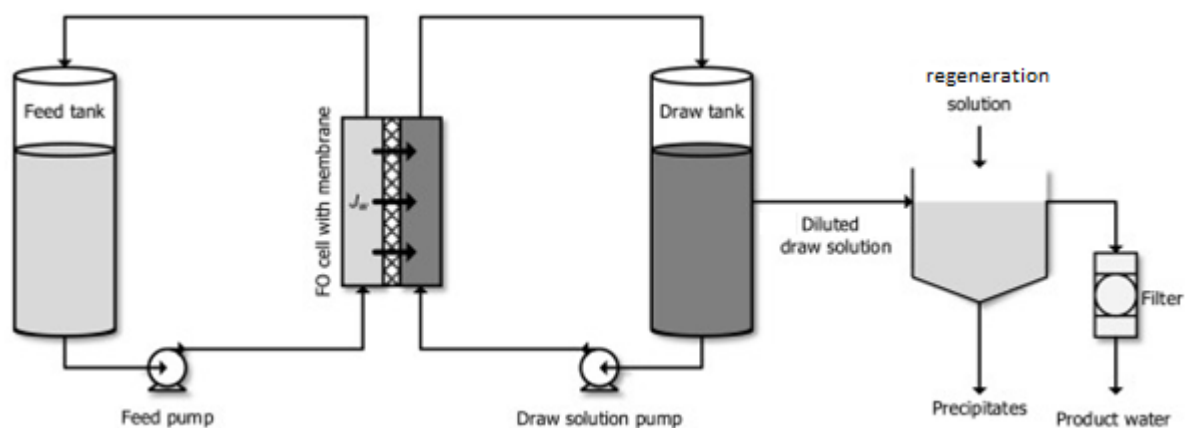


Figure 1.16 Schematic diagram of FO desalination process [1.26]

The recovery of draw solutes makes a significant energy cost in FO technology implementation. As explained previously, the draw solution is used to “attract” water from feed solution by osmotic pressure difference through a semi-permeable membrane, while most solutes are rejected by the FO membrane. Then, the diluted draw solution is being regenerated in order to produce clean water. Although some FO applications do not require draw solutes recovery (e.g. irrigation), most FO applications (e.g., desalination for drinking water, wastewater reclamation, etc.) do need draw solutes to separate water. The FO process efficiency and sustainability greatly depends on the selected draw solute. An ideal draw solute for water production through FO should be non-toxic, suitable for FO membranes, easily separated from water, economically feasible, environmentally friendly and of high osmotic pressure. The most used draw solutes may be generally classified into inorganic salts and organic compounds according to their properties. The inorganic salts have been proposed to reduce the energy cost for regeneration, however some inorganics may cause high reverse solute flux. The organic compounds are expected to have minimal reverse solute flux and require low energy cost for recovery. Some usual recovery methods used in FO process are; thermal separation, membrane separation including reverse osmosis (see below), Nano filtration, ultrafiltration, membrane distillation, electro dialysis, gas pressure, magnetic heating etc [1.27].

Even though forward osmosis process has been registered as a low energy consumption desalination process, the draw solution regeneration requires further steps in order to produce fresh potable water. Therefore, more energy could be required to extract the pure water from the draw solution than it does to extract it from the feed water, depending on the regeneration method. Moreover, there are a number of technical barriers that prevent forward osmosis from several applications. The most serious challenges to overcome are: the lack of an ideal draw solution of high osmotic pressure and easily regenerated to produce pure water and the lack of an optimized membrane of high water flux, low salt transmission and anti-fouling properties. A suitable module design is necessary in order to maintain long-term system performance for specific applications [1.28].

- **Ultra and nano- filtration**

Ultrafiltration (UF) is a process of membrane filtration where pressure or concentration gradients provoke separation through a semipermeable surface. Suspended solids and solutes' high molecules are blocked in the so-called retentate, while water and low molecular weight solutes pass through the membrane to the permeate. UF is usually used for potable water production, to either replace existing secondary (coagulation, flocculation, sedimentation) and tertiary filtration (sand filtration and chlorination) in reverse osmosis (RO) pre-treatment, in waste water treatment systems or as standalone systems in isolated regions with growing populations. Ultrafiltration process is preferred over traditional treatment methods as:

1. It requires no chemicals aside from cleaning
2. It provides constant product quality regardless of feed quality
3. The plant is compact
4. It is capable of exceeding regulatory standards of water quality, achieving 90-100% pathogen removal.

Recycled water can also be used for a number of industrial purposes such as boiler / cooling tower feed water, pH adjustment, washing equipment, fire extinguishing system, process rinse water or water for production lines in manufacturing industries etc [1.29]. UF membranes have originally been developed and tested in a wide range of much more difficult liquid environments than seawater, such as highly polluted municipal and industrial wastewaters. They are being increasingly considered for feed water pre-treatment in new RO desalination installations, especially when treating surface seawater and for retrofit upgrades to existing conventional RO pretreatment systems.

1.3.2 Reverse Osmosis desalination and Renewable Energy Sources

The Reverse Osmosis (RO) desalination process is currently considered the most reliable technique for brackish water and seawater desalination. Whereas osmosis occurs naturally without energy required between two solutions of different concentration, separated with a semi-permeable membrane as discussed previously, in order to reverse the process, energy should be applied to the solution of higher concentration. The reverse osmosis membrane allows the passage of water molecules but not the majority of dissolved salts, organics, bacteria etc. However, in order to desalinate water, it is necessary that pressure greater than the naturally occurring osmotic pressure is applied to feed water, allowing pure water through the membrane while holding back a majority of contaminants.

In Figure 1.17 the process of osmosis and Reverse Osmosis are schematically presented in order to clarify the difference between them. When pressure is applied to the concentrated solution, the water molecules are forced through the semi-permeable membrane and the contaminants are not allowed to pass through.

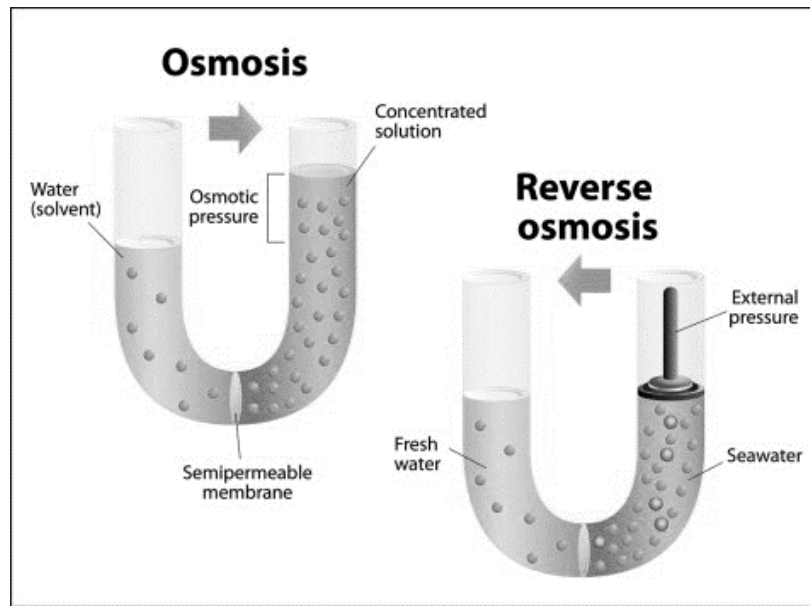


Figure 1.17 Schematic diagram of osmosis and reverse osmosis process [1.30]

Compared to the other technologies, RO process reveals a number of advantages which make it an attractive technology for seawater and brackish water desalination. Some of them are its reliability, high water recovery rate (up to 85% for brackish water and up to 50% for seawater) and salt rejection rate, and its ability to treat a wide range of seawater qualities. Nowadays, more than 50% of the world's desalination water is produced by RO process. Moreover, apart from water desalination, the RO membranes are being used in wastewater reuse and the production of ultra-pure water [1.31].

A schematic diagram of a typical RO desalination treatment plant is presented in Figure 1.18.

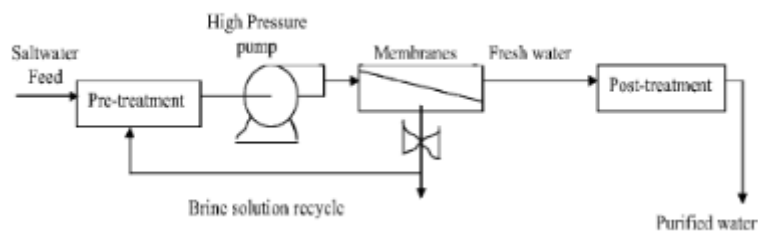


Figure 1.18 Schematic diagram of an RO desalination treatment plant [1.31]

The typical RO desalination treatment system includes three main processes; the pretreatment that prepares the feed water to enter the RO membranes, the RO desalination membranes and the post-treatment that makes the RO product water (permeate) suitable for human use and consumption.

By definition, the purpose of the pretreatment system is to remove foulants from the water source and to provide any chemical additives necessary to enable efficient desalination. Usually, the feed water (i.e. the water to be treated) is collected in a tank (called feed tank) where it is chlorinated in order to eliminate any contaminants. Depending on the water flow rate, the feed tank has sufficient volume so that water remains at least half an hour in it for an efficient chlorination. In some cases, the addition of a chemical to prevent coagulation/ flocculation is also predicted along with chlorination. The water is pumped to the main process

via a feed pump of appropriate capacity and material that endures pressure and corrosion. The water is then driven to a turbidity filter that withholds the turbidity caused by any suspended solids. The filter is filled with appropriate layers of filling that can remove up to approximately 25-micron size of solids. Moreover, the filter uses filtered water for its backwash with the help of the feed pump once or twice per day. After the turbidity filter(s) a de-chlorination of the water that will enter the RO membranes is necessary in order to protect the membranes from possible scaling. There are two ways to de-chlorinate the water: either use an active carbon filter (similar to the turbidity filter apart from the fact that in its fillings a layer of active carbon is included, capable to remove any organic load in the water) or dose a chemical called sodium metabisulphite (an inorganic compound of chemical formula $\text{Na}_2\text{S}_2\text{O}_5$ that reacts with Cl). The method chosen depends on several circumstances such as if the application is required to be free of chemicals (in this case an active carbon filter is used). A redox meter is usually used in order to check the neutralization of chlorine in the water.

The water is then dosed with antiscalant, a chemical added for the protection of the membranes from scaling and fouling (tendency of suspended solids to coagulate and coat the membrane surface). The pre-treated water, after passing through some cartridge filters of 5 and 1 micron accordingly, is then driven through the RO membranes with the help of the high-pressure pump (HPP) which increases the pressure to a pressure higher than the osmotic. Depending on the flow rate and the application different designs can be applied. For example, in brackish water applications, in order to reduce the HPP consumption a recirculation loop can be designed, leading the reject water back at the HPP inlet, exploiting its hydraulic energy in this way. In large seawater applications, an energy recovery device is usually applied, most commonly a pressure exchanger (PX) device. The philosophy of the PX is presented in Figure 1.19.

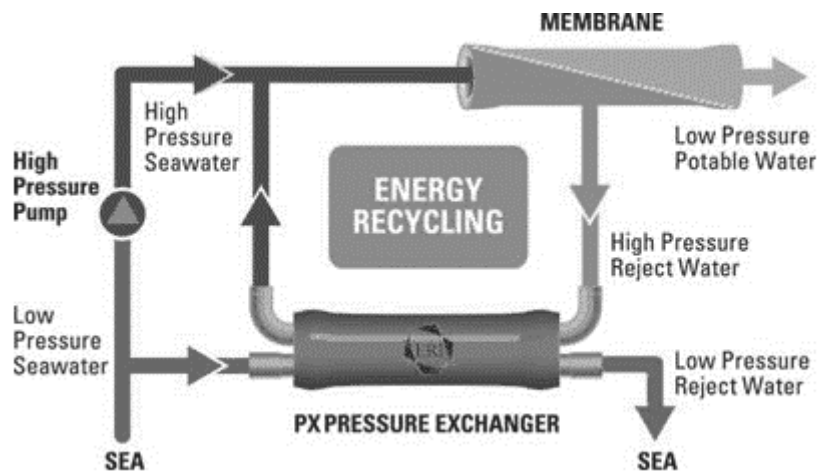


Figure 1.19 Schematic diagram of pressure exchanger (PX) energy recovery device [1.32]

A portion of the feed water will flow to the high-pressure pump after passing through a second stage of cartridge filtration with 1-micron porous size for the protection of the axial piston pump. The remaining feed water will be driven to the PX energy recovery system to gain the necessary pressure from the pressure exchanger. This configuration essentially minimizes the size of the high-pressure pump by 50% and hence the energy consumption by 50%. The water passing the RO is then fed to the high rejection/ low consumption membranes for maximum removal of salts at minimum energy consumption. Each RO desalination unit carries

a so called Clean In Place (CIP)/ flushing system for the flushing of the membranes with permeate water every time the RO stops and for the chemical cleaning when needed (usually once per year). Every time the plant stops operating, the cartridge filters, high pressure piping, high pressure pump as well as the membranes are flushed out with permeate water to remove any stagnant salt water and replace it with fresh water protecting the membranes and the high-pressure piping from corrosion. When chemical cleaning is necessary, the water follows the same route. The CIP system is composed by a CIP tank and a CIP transfer (booster) pump.

Concerning the post- treatment of the permeate and depending on the feed water quality, there are two main processes for potable water production; in brackish water, if the quality is acceptable (low TDS of the feed water) and if all of the important chemical parameters are within the potable water's limits, a mixing of the permeate with a portion of the feed water is possible. In heavy brackish and seawater, the most common way is to treat the permeate with a re- hardening filter: this is a filter of open or closed type that is able to enrich the permeate with calcium carbonate (CaCO_3), calcium and magnesium, ions that are necessary parameters of drinking water. Before the filter acid is added to the water in order to make the re- hardening more efficient and after the filter caustic soda is added in order to correct the product water's pH. A final chlorination of the class of 0.5 ppm is added to the product water tank for the disinfection of the water in the tank. Depending on the application many components could have a redundancy such as the feed pump (one operating- one stand by), the dosing pumps etc. Moreover, every RO plant has an electrical panel and a control panel of their own.

Besides the advantages that have promoted RO desalination process to the predominant water treatment process and the sustainable solution to the global fresh-water shortage, such as better control of produced water quality (for drinking water, irrigation, cooling towers, hemodialysis etc.), low cost of the produced fresh water (usually cents per euro), great ability to remove 95 to 99 percent of total dissolved solids (TDS) such as boron, chlorides and other impurities etc., there are some few disadvantages that the scientific and commercial community try to eliminate. Such disadvantages are the rejection of a thorough amount of water (reject water) which means low recovery and the high energy demand from the RO unit high pressure pump.

Concerning the energy consumption, energy is mostly supplied from conventional fuels which makes the installation of a desalination plant in developing countries challenging because of huge costs involved towards initial investments of operation and maintenance. It has been many years that fossil fuels such as coal, petroleum and natural gas have been used as the major sources of energy. However, the negative environmental impacts associated with the emission of the greenhouse gases from these sources forced to realize the importance of renewable energy sources. The Middle East countries that are rich in conventional fuel resources, encourage desalination technology but the huge consumption of energy in desalination results in greater emission of greenhouse gases, raising environmental pollution concerns. An estimate notes that for the production of 1 m^3 of fresh-water from sea water, the desalination plant consumes 3–10 kWh of energy, when a conventional drinking water plant consumes around 1 kWh/m^3 [1.33]. The combination of RO desalination process with renewable energy sources in order to make it an overall advantageous technology is vital.

The interest in renewable energy desalination systems is increasing worldwide. Solar, wind, geothermal, wave and tidal energy are the main sources of renewable energy, with solar energy being the most applicable source to be integrated with the desalination technology while it can produce the heat and electricity required by all desalination processes. Photovoltaic (PV), linear Fresnel,

parabolic trough and central receiver are the main solar harvesting technologies. Nowadays almost 70% of renewable desalination systems run by solar energy. Wind energy is applied mostly in coastal areas installations as well as wave and tidal energy, where wind and water are available. It is mostly combined with RO desalination systems because they require electricity rather than heat. Geothermal energy exploits the earth's underground high temperature to produce steam or to store the heat energy, however the underground temperature should be greater than 180° C to be efficient for the drilling works. There are two configurations of coupling desalination plant with renewable energy sources; either directly by connecting the plant to the energy source or by adding the produced power to the electricity grid to overcome the intermittency of the renewable energy [1.33].

Figure 1.20 presents an overview of the most common or promising RE - desalination technologies, including their typical capacities, their energy demand, the estimated water generation cost and the development stage. Most of them are already tested and the water generation costs are estimated based on operational experience and real data [1.34];

	TYPICAL CAPACITY	ENERGY DEMAND	WATER GENERATION COST	TECHNICAL DEVELOPMENT STAGE
SOLAR STILL	< 0.1 m ³ /d	solar passive	1–5 €/m ³	applications
SOLAR MEH	1–100 m ³ /d	thermal: 100 kWh/m ³ electrical: 1.5 kWh/m ³	2–5 €/m ³	applications/ advanced R&D
SOLAR MD	0.15–10 m ³ /d	thermal: 150–200 kWh/m ³	8–15 €/m ³	advanced R&D
SOLAR/CSP MED	> 5,000 m ³ /d	thermal: 60–70 kWh/m ³ electrical: 1.5–2 kWh/m ³	1.8–2.2 €/m ³ (prospective cost)	advanced R&D
PV-RO	< 100 m ³ /d	electrical: BW: 0.5–1.5 kWh/m ³ SW: 4–5 kWh/m ³	BW: 5–7 €/m ³ SW: 9–12 €/m ³	applications/ advanced R&D
PV-EDR	< 100 m ³ /d	electrical: only BW: 3–4 kWh/m ³	BW: 8–9 €/m ³	advanced R&D
WIND-RO	50–2,000 m ³ /d	electrical: BW: 0.5–1.5 kWh/m ³ SW: 4–5 kWh/m ³	units under 100 m ³ /d BW: 3–5 €/m ³ SW: 5–7 €/m ³ about 1,000 m ³ /d 1.5–4 €/m ³	applications/ advanced R&D
WIND-MVC	< 100 m ³ /d	electrical: only SW: 11–14 kWh/m ³	4–6 €/m ³	basic research
WAVE-RO	1,000–3,000 m ³ /d	pressurised water: 1.8–2.4 kWh/m ³ electrical: 2.2–2.8 kWh/m ³	0.5–1.0 €/m ³ (prospective cost)	basic research

Figure 1.20 Possible combinations of renewable energy with desalination technologies [1.34]

A photovoltaic- reverse osmosis (PV-RO) system includes a photovoltaic field which supplies electricity to a RO desalination unit through a DC / AC converter. For stand-alone operation, energy storage is accomplished with the use of a set of batteries. Therefore, it increases the daily operating hours. This technology is widely applied to supply water in rural areas in developing countries such as Tunisia, Morocco and other Mediterranean countries [1.34]. For systems with high capacity, investment costs are relatively high resulting in specific cost of drinking water in the range of 3.5 –7 €/m³ for brackish and 9 –12 €/m³ for seawater RO plants. However, this solution is economically feasible in remote

locations where the alternatives are limited and also expensive. Moreover, both PV and RO are mature technologies, with many suppliers worldwide and there are intensive efforts to increase the PV and RO efficiency. Thus, it is expected that costs of PV-RO systems will be significantly reduced in the future.

Wind energy is mostly combined with reverse osmosis desalination systems. In a wind-RO desalination system, a wind generator is coupled to a RO unit with a buffer and batteries as a back-up. The wind power is highly fluctuating; therefore, it requires a control system that fits the available wind to the energy requirements and achieves a stable operation. Interesting experimental research of mechanical and hydraulic coupling of a wind energy system and a RO desalination unit have been carried out at the Canary Islands Technological Institute, under the projects AERODESA I and AERODESA II. The first project concerns the mechanical connection of a wind turbine of 15 kW specifically designed for driving a reverse osmosis desalination plant of a capacity of 10 m³/d of a minimum maintenance for remote areas and developing countries. The second project combines a wind turbine of 15 kW, specifically designed for driving a two-modules reverse osmosis desalination plant of a total capacity of 15 m³/d. This system is hydraulically driven, which allows a very high automated system [1.35-1.36].

The geothermal energy sources are classified depending on the measured temperature as: 1) low (<100°C), 2) medium (100°C–150°C) and 3) high temperature (>150°C). Geothermal energy can be directly used with almost all thermal desalination processes. Moreover, thermal energy conversion into shaft power or electricity would permit the coupling with other desalination systems like RO. The first desalination system powered by geothermal energy was built in Holtville, USA in 1972 by the United States Department of the Interior, Bureau of Reclamation [1.34]. Loutatidou *et al.* provided a preliminary techno-economic evaluation of coupling a low-enthalpy geothermal resource, commonly found in regions such as the Arabian Gulf countries, with an appropriate desalination technology. The multiple effect distillation (MED) and reverse osmosis (RO) were chosen and designed as integrated energy–water systems. The two processes were compared in terms of their cost of water produced, taking into consideration some basic parameters including feed water quality, operational lifetime of both the geothermal and desalination systems, quality of the geothermal resource, cost of well-drilling etc. The results showed that geothermal RO could potentially be a more cost-effective option for seawater geothermal desalination in the Gulf countries [1.37].

In conclusion, most renewable energy sources can be coupled with RO desalination plants in order to form an efficient and autonomous desalination system. High enthalpy sources can be utilized via steam power cycles (single flash, double flash or dry steam) to generate the necessary electricity to feed the RO plant. Medium and low-enthalpy sources (i.e., hydrothermal fields of up to 150 °C) can also serve as a primary source of energy to produce electricity through an Organic Rankine Cycle (ORC) as an indirect utilization of any heat source, which can then be combined to a RO plant. In the next paragraph, an introduction to the Organic Rankine Cycle and its applications is presented, in order to highlight the utility of its application in RO desalination.

1.3.3 Organic Rankine Cycle Engines and applications

1.3.3.1 Heat engine definition

The Rankine cycle is a thermodynamic representation of a high-pressure or expansion type of steam engine cycle. A heat engine is simply a device that converts the thermal energy into mechanical work. The energy conversion is driven by the temperature gradient between a reservoir at a high temperature and a reservoir at a low temperature. Initially, heat engines simply produced mechanical work that was used directly (e.g., in manufacturing) or else they were connected to other engines, such as pumping engines (pumps) to move the water and later to electrical engines (generators) to generate electricity. Most heat engines use either a vapor or a gas as the internal energy transfer medium. As an essential component of the heat engine the working medium, thanks to its thermophysical properties transfers the heat received from the heat source to the sink, while part of it is turned into mechanical work. The device that actually produces the heat engine's output work is called the prime mover. A prime mover can be a reciprocating piston- cylinder steam engine, a steam turbine, an internal combustion engine and so forth [1.38]. In Figure 1.21 the basic concept of a heat engine operation is illustrated;

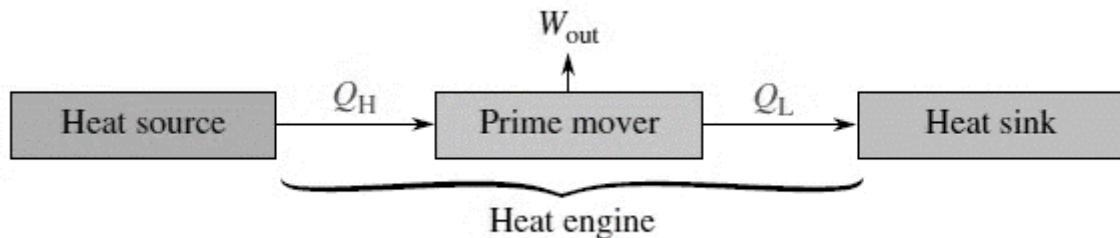


Figure 1.21 Heat engine terminology

Heat engines are very important to the study of thermodynamics while the history of heat engine technology is essentially the history of the Industrial Revolution. The heat engine whose prime mover was the reciprocating piston steam was the first large- scale source of portable mechanical power. It was a source of power that did not depend in wind or river and could therefore be located anywhere. The heat engine is still the primary source of power for travel and electricity today, and it is likely to remain so for the foreseeable future [1.39].

The power cycles on which the heat engines are based, are divided in two major categories based on the working medium: the *vapor power cycles* and the *gas power cycles*.

The vapor power cycle technology was the milestone of the Industrial Revolution that began in the mid18th century, which built the world as we know it today. The Carnot cycle, the Kalina cycle, the Maloney and Robertson cycle are some of the vapor power cycles examples.

On the other hand, the gas power cycles were originally developed as an alternative to the dangerous vapor cycle engines. The gas power cycles are divided into two types: the *external combustion cycles*, where the combustion process takes place outside the prime mover (e.i. Stirling cycle, Ericsson cycle, Brayton cycle etc) and the *internal combustion cycles* with the combustion process taking place inside the engine itself (e.i. Lenoir cycle, Otto cycle, Diesel Cycle etc.). Gas power cycle technology has also had a profound impact on our culture. Gas power have come to dominate portable power systems such as automobiles, ships, trains and airplanes [1.39].

1.3.3.2 The ideal Carnot cycle

The Carnot cycle is theoretically the power cycle with the highest thermal efficiency and sets the barrier for the thermal efficiency of any heat engine that operates between a reservoir of high temperature T_H and a low temperature reservoir T_L . The cycle (named by the French military engineer and physicist “father of thermodynamics” Sadi Carnot, 1796- 1832) is designed with the assumption that the reservoirs are large enough to accept and deliver heat without any change in their temperatures and all processes are completely reversible. The processes included are shown in the temperature- entropy diagram in Figure 1.22.

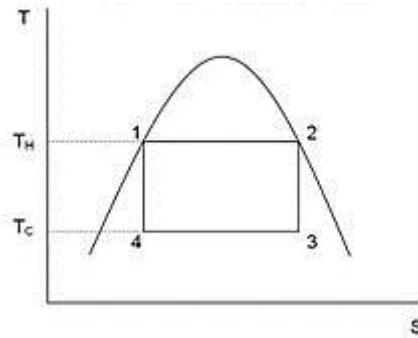


Figure 1.22 The Carnot cycle [1.40]

The processes as shown in Figure 1.22 are:

- Process 1-2: isothermal heating with heat addition to the working fluid from a heating medium on a boiler.
- Process 2-3: isentropic expansion in a turbine producing work by the working fluid
- Process 3-4: isothermal condensation with heat removal in a condenser from the working fluid to the cooling medium
- Process 4-1: isentropic compression while energy is given to the working fluid

The temperature of the heating and cooling medium is identical during heating and condensation. As the working fluid changes from state 1 to state 4 the heating medium changes from state 4 to state 1 and while the working fluid changes from state 2 to state 3 the cooling medium changes backwards. The area 12341 in Figure 1.22 represents the net useful work produced by the cycle (W_{net}). The cycle efficiency is defined as the proportion of the heat transformed to mechanical work, meaning the ratio of the heat input minus the heat output differential to the heat input as follows:

$$\eta_{th} = \frac{Q_{in} - Q_{out}}{Q_{in}} = 1 - \frac{Q_{out}}{Q_{in}} \quad (1.1)$$

Replacing Q_{in} with $T_H \cdot (s_1 - s_4)$ and Q_{out} with $T_L \cdot (s_2 - s_3)$ the Carnot efficiency can be expressed as follows:

$$\eta_{th_carnot} = 1 - \frac{T_L}{T_H} \quad (1.2)$$

where T_H and T_L are the absolute temperatures of the heat and cold reservoir accordingly. Therefore, as the temperature difference gets higher, the efficiency gets higher. The Carnot cycle is a theoretical cycle and the practical application of this cycle is impossible. First and foremost, irreversibilities are always generated

during work production and two- phase processes are not easy to manage during expansion or compression. Moreover, in order to succeed an isothermal heat transfer, the maximum temperature of the cycle should be kept far below the critical temperature of the working fluid, a fact that lowers the efficiency. However, real cycles will always have lower efficiency than the ideal Carnot cycle and the comparison provides how efficient a cycle is [1.38, 1.39].

1.3.3.3 The Thermodynamic Rankine Cycle

For thirty years since 1850, the subject of thermodynamics was formally developed in order to provide a scientific foundation for the empirical steam technology that had by then grown to dominate the economy of the Western World. By 1850, it had been determined that heat was a form of energy, and by 1860 the first and second laws of thermodynamics had been accurately formulated by Clausius, Kelvin, Joule and others. However, it was thanks to the Scottish engineer William John Macquorn Rankine (1820- 1872) that the thermodynamic cycle for a steam engine with an external condenser was developed. An adiabatic cylinder steam engine is any expansion engine or any atmospheric engine with an external condenser. The thermodynamic cycle for adiabatic cylinder engines is called the *Rankine cycle* since Rankine was the first to understand how this type of steam engine worked thermodynamically.

The Rankine cycle is the simplest vapor power cycle. It is composed of the four ideal processes shown on the temperature- entropy ($T-s$) diagram shown in Figure 1.23:

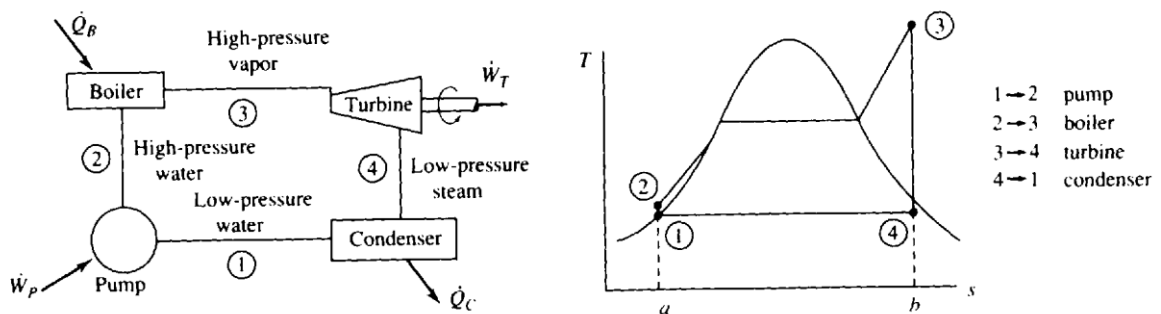


Figure 1.23 Graphic representation of main processes and the $T-s$ diagram of the Rankine cycle [1.40]

- 1 - 2: Isentropic compression in a pump
- 2 - 3: Heat addition in a boiler at constant-pressure
- 3 - 4: Isentropic expansion in a turbine
- 4 - 1: Heat extraction in a condenser at constant-pressure

An important feature of this cycle is that the pump requires little work to deliver high-pressure water to the boiler. A possible disadvantage is that the expansion process in the turbine could result in the formation of liquid droplets which might damage the turbine blades. The Rankine cycle is an idealized cycle where the working fluid passes through the various components without irreversibility, frictional pressure drops would be absent from the boiler and condenser, and the working fluid would flow through these components at constant pressure. Moreover, in the absence of irreversibility and heat transfer with the surroundings, the processes through the turbine and pump would be isentropic [1.40].

The cycle's thermal efficiency is the ratio of the produced work to the thermal power input:

$$\eta_{th_Rankine} = 1 - \frac{h_4 - h_1}{h_3 - h_2} \quad (1.3)$$

where h_i is the specific enthalpy of each state.

The efficiency of the Rankine cycle can be improved by *increasing the boiler pressure* while maintaining the cycle's maximum temperature and the minimum pressure. However, a raising of the boiler pressure could result in a very low quality of the steam exiting the turbine (less than 90 percent), causing severe water droplet damage to the turbine blades and lower turbine efficiency.

An increase of the maximum temperature also results in an improvement in thermal efficiency of the Rankine cycle, however material issues could occur concerning the maximum temperature that can be attained in the boiler. Moreover, the temperature raising at the boiler leads to an obviously increased quality of state 4 and this reduces water droplet formation in the turbine.

A decrease in condenser pressure would also result in an increased Rankine cycle efficiency. The net work would increase by a significant amount and the heat input would increase by a slight amount. The low pressure is limited by the heat transfer process that occurs in the condenser.

In order to improve the efficiency of a steam Rankine cycle, regeneration could be applied by integration of super heaters, by reheating and by increasing the boiler pressure in transcritical or supercritical cycles:

- *Superheating*: When transfer fluids with high boiling points such as water, methanol etc. are used in a Rankine cycle, the temperature at which heat is added to the cycle through the evaporator can be increased during the isobaric heating. The result is an increased net power output and a desirable decrease of moisture content of the working fluid after the expansion. In Figure 1.24 the effect of the superheating in the cycle efficiency is observed.

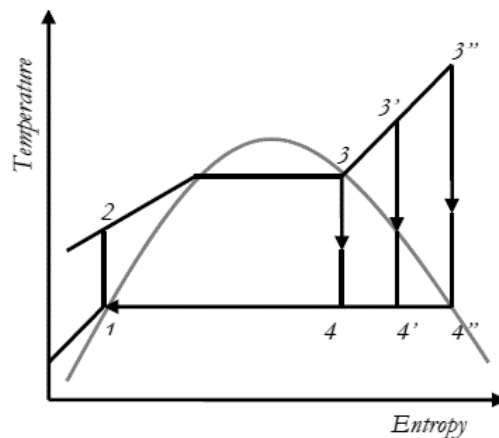


Figure 1.24 The T-s diagram of the superheated Rankine cycle [1.38]

The saturated vapor of state 3 is superheated to state 3' and this results in an increase of the power output presented by the area 33'4'4, state 4' being the end of the expansion process with less moisture. To prevent any droplet formation at the turbine during the expansion the saturated vapor fluid is superheated further to state 3''. The superheating is a good method to increase the cycle efficiency when wet fluids (see Chapter 2) are used as the working fluid. The case is different for dry fluids, since

their saturation vapor line in Mollier diagram is positive and the process takes place in the vapor region. For isentropic fluids on the other hand, the efficiency remains the same.

- *Reheating*: The formation of liquid droplets at the low side of the turbine is a major fear when operating a Rankine cycle with a high boiler pressure or a low condenser pressure. Considering that most metals cannot withstand temperatures above about 600 °C, the reheat cycle is often used to prevent liquid droplet formation: the steam passing through the turbine is reheated at some intermediate pressure, thereby raising the temperature to state 5 as presented in Figure 1.25.

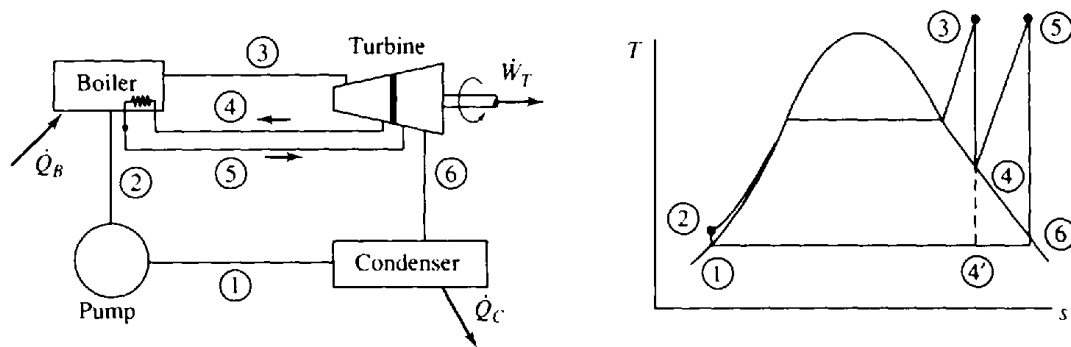


Figure 1.25 Graphic representation of main processes and the T-s diagram of the superheated Rankine cycle [1.40]

The steam then passes through the low-pressure side of the turbine and enters the condenser at state 6. In this way, the moisture problem in the turbine is controlled. Often the turbine is separated into a high-pressure turbine and a low-pressure turbine. The reheat cycle does not significantly influence the thermal efficiency of the cycle, but it does result in a significant additional work output, represented in the figure by area 4-5-6-4'-4. However, the reheat cycle demands a significant investment in additional equipment, the use of which must be economically justified by the increased work output.

- *Regeneration with open or close feedwater heater*: In the conventional and the reheated Rankine cycle, a considerable amount of the total energy input is used to heat the water from T_2 to its saturation temperature. A preheating of the water before it enters the boiler, with the help of some of the steam expanding in the turbine and mixing it with the water as it exits the pump would reduce this energy. In addition, this would avoid the necessity of condensing all the amount of steam, therefore reducing the energy lost from the condenser. A cycle that uses this type of heating is a *regenerative cycle*, and the process is referred to as *regeneration*. A schematic representation of the main elements of this cycle is shown in Figure 1.26.

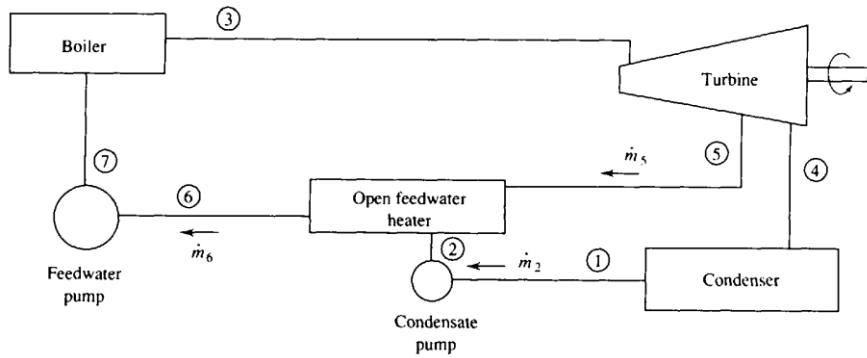


Figure 1.26 Graphic representation of main components of the regenerative Rankine cycle with open feedwater heater [1.40]

The component used to mix the extracted steam and the condenser water is called a *feedwater heater*. When the condensate is mixed directly with the steam, it is done so in an *open feedwater heater*. In order to define the amount of the extracted steam necessary for the preheating, the mass balance and energy balance equations in the open tank shall be applied as follows:

Considering m_2 the mass flow rate of the condensate and m_5 the mass flow rate of the extracted steam, then the feedwater flow rate would be:

$$m_6 = m_5 + m_2 \quad (1.3)$$

Moreover, the energy balance assuming an insulated heater and ignoring kinetic and potential energy changes gives:

$$m_6 h_6 = m_5 h_5 + m_2 h_2 \rightarrow$$

$$m_5 = [(h_6 - h_2) / (h_5 - h_2)] m_6 \quad (1.4)$$

Another possible design is the regeneration cycle with *close feedwater heater*. This is actually a heat exchanger where the water enters the tubes surrounded by the steam which condenses in the outer surfaces. The formed condensate is pumped with a small pump into the main feedwater line, as shown in Figure 1.27, or it passes through a device that permits only liquid to pass through and is fed back to the condenser or back to a lower-pressure feedwater heater. A mass and energy balance are also required when analyzing a closed feedwater heater; if pump energy requirement is neglected in the analysis, the same equation as (1.4) results.

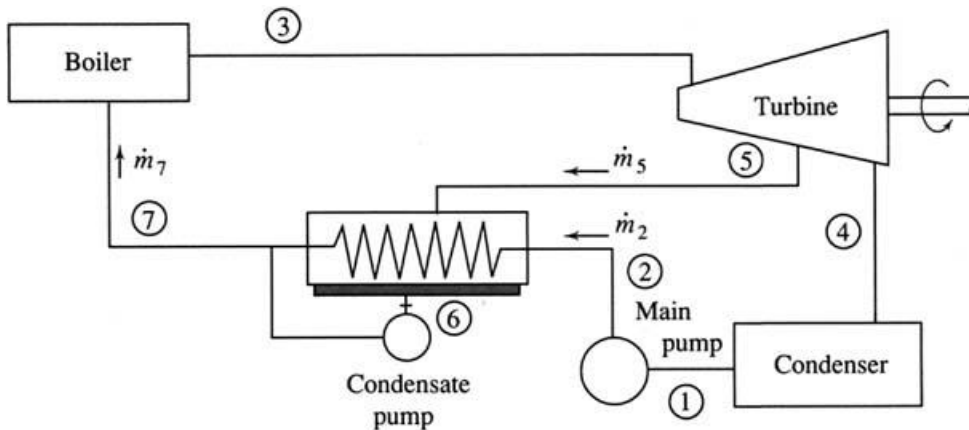


Figure 1.27 Graphic representation of main components of the regenerative Rankine cycle with closed feedwater heater [1.40]

However, this design requires a more expensive equipment and its heat transfer characteristics are less desirable than those where the steam and water are simply mixed, like in the open heater. Moreover, the more the number of the heaters the higher the cycle efficiency, however, the cost of the system gets unjustifiably high compared to the efficiency improvement.

- *Transcritical and supercritical Rankine cycle:* The subcritical Rankine cycle is defined by the fact that the heating in the boiler happens at a pressure below the critical point (i.e. the end point of a phase equilibrium curve). In the effort of increasing the cycle efficiency, the boiler's pressure can be set above the critical, creating transcritical and supercritical cycles, as shown in Figure 1.28. Transcritical cycle that uses steam presents high efficiency but requires special materials and high safety equipment due to very high pressure.

In recent research, many attempts have been made in order to replace steam in the Rankine cycle and different fluids of low boiling point and low critical temperature have been tested, such as organic fluids. When an organic fluid is used as the Rankine cycle working fluid, the Rankine cycle is called *an Organic Rankine Cycle*. While investigating the potentials of organic Rankine cycles, the supercritical cycles presented some interesting features since a better thermal match existed between the heat sources and the organic fluids. The supercritical cycle presented a better efficiency; however, some restrictions have been raised to the components selection due to the high-pressure operation [1.41]. Several research works have resulted in a few conclusions such as:

- The transcritical and subcritical organic Rankine cycles present similar efficiency.
- The heat exchangers present a better performance in transcritical and supercritical cycles due to better matching with the heat source.
- Transcritical and supercritical cycles require safety equipment due to higher pressures that increase the system's cost and slow down their implementation [1.38].

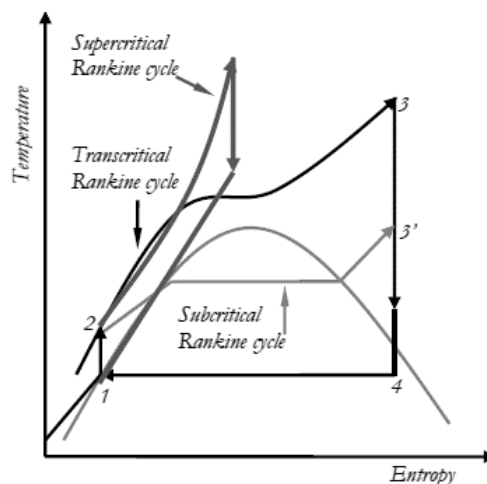


Figure 1.28 The T-s diagram of the transcritical and supercritical Rankine cycle [1.38]

1.3.3.4 Why the Organic Rankine Cycle?

According to their operating temperature the basic power cycles could be classified as shown in Figure 1.29.

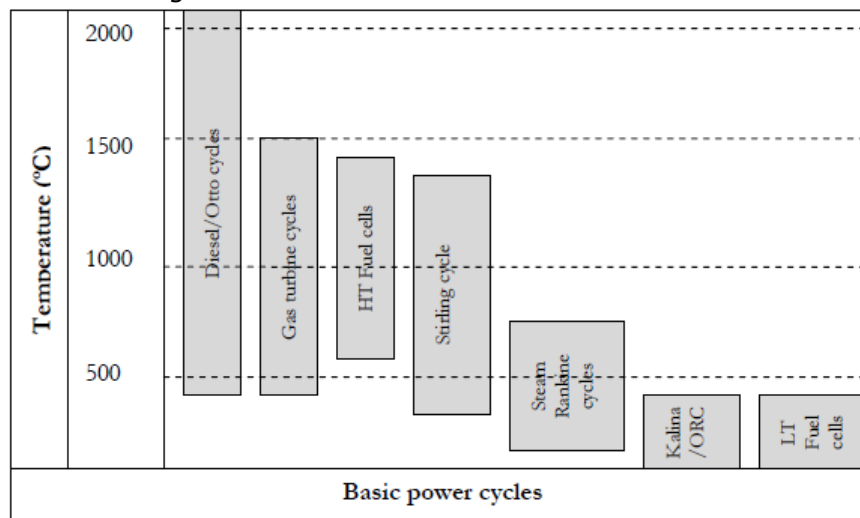


Figure 1.29 Basic power cycles classification according to the operating temperature [1.38]

Concerning the vapor cycles for low temperature applications, apart from the ORC technology, the candidates are the Kalina cycle, the Maloney and Robertson cycle and the low temperature fuel cells.

Maloney and Robertson used an ammonia- water mixture as a working fluid in an absorption power cycle in the early 1950s and integrated a flash tank in the usual Rankine cycle. In the Maloney and Robertson cycle, the heater delivers a vapor rich in ammonia which is then superheated. The expansion of the vapor produces the useful power and at the turbine's outlet the rich in ammonia vapor meets the weak solution from the distillation unit in order to be enriched. The regenerated basic solution is then pumped to a high pressure and heated before entering a flash tank to complete the cycle. Their thermodynamic analysis however, led them to the conclusion that the absorption power cycle in this configuration has no thermodynamic advantage over the Rankine cycle [1.42].

Almost thirty years later than Maloney and Robertson developed their cycle, Alexander I. Kalina presented a sequel of their idea, using an ammonia mixture and implementing new components in a Rankine cycle such as a separator, a recuperator and an absorber. In the Kalina cycle the ammonia- water mixture is heated in the evaporator and separated from the liquid phase in a separator, before entering the turbine. The rich- in- ammonia vapor enters the turbine producing useful work and then the vapor at the turbine's outlet is mixed with the liquid phase of the separator and condensed in the condenser. As the mixing ratio changes, the evaporation temperature increases continuously in the two- phase region, while it decreases during condensation. The recuperator is used for heat control in the cycle [1.43]. When first developed, there were several theoretical claims from researchers that the Kalina cycle presented a much better efficiency of around 30 to 50% than the Organic Rankine Cycle, however, experimental investigations have proved that it was only about 3% better than the ORC. On the contrary, the Kalina cycle required a very high maximum pressure in order to obtain high thermodynamic performance of the class of 100 bar when the corresponding ORC required only 10 bar. Moreover, experimental investigation has also shown that the adoption of Kalina cycle, at least for low power level and medium-high temperature thermal sources, is not justified, as the gain in performance with respect to a

properly optimized ORC is very small and must be obtained with a complicated plant scheme, large surface heat exchangers and particular high pressure resistant and non-corrosion materials [1.44].

Finally, besides conventional power generating cycles which depend on the thermal expansion of vapor/ gases to operate electro-mechanical generators, fuel cells lack moving parts, apart from controllers and blowers and form a different kind of electricity production technology. Due to the direct conversion, mechanical frictional losses are eliminated and an increased fuel conversion efficiency is obtained. Moreover, fuel cells are not limited by the thermodynamic barriers imposed by Carnot efficiency. The basic configuration of a low temperature fuel cell is presented in Figure 1.30.

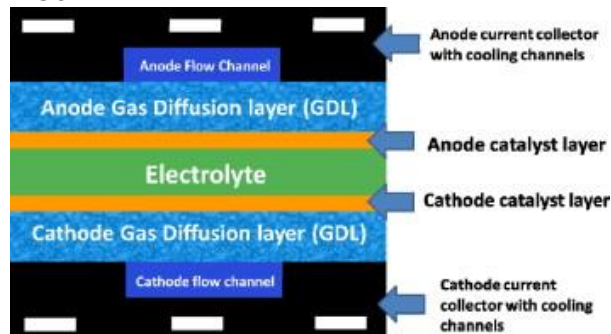


Figure 1.30 Schematic diagram of a fuel cell [1.45]

A fuel cell is basically a device that produces electricity through a chemical reaction. It has two electrodes, the anode and cathode. The reactions that produce electricity take place at the electrodes. It also carries an electrolyte, which drives electrically charged particles from one electrode to the other, and a catalyst, which speeds up the reactions. Hydrogen is the basic fuel, but oxygen is also required. A fuel cell is used to produce an electric current which can be directed outside the cell to produce work, such as powering an electric motor. Based on how electricity behaves, the current returns to the fuel cell completing an electrical circuit. In general, hydrogen enters a fuel cell at the anode where a chemical reaction separates the atoms of their electrons, ionizing the hydrogen atoms which now carry a positive electrical charge. The negatively charged electrons provide the current through wires to produce work. The current produced is direct current (DC). Oxygen atoms enter the fuel cell at the cathode and they combine with electrons returning from the electrical circuit as well as hydrogen ions that have traveled through the electrolyte from the anode. In some cell types the oxygen picks up electrons and then travels through the electrolyte to the anode, where it combines with hydrogen ions. The electrolyte permits only the appropriate ions to pass between the anode and cathode, since if free electrons travelled through the electrolyte, they would disrupt the chemical reaction. As long as a fuel cell is supplied with hydrogen and oxygen, it will generate electricity. Even if the low temperature fuel cells technology is a promising and a developing one, there are many obstacles yet to be overcome such as: their high cost due to expensive materials, the request of fuel and the fact that hydrogen fuel is not readily available, their controversial reliability and durability especially at high temperatures, their sensitivity in temperature and contamination etc. [1.46].

In conclusion, due to the nature of their operation, Rankine cycles and especially Organic Rankine cycles are the most efficient, cost-effective solution for low and medium temperature heat sources to transform thermal energy into mechanical work or electrical power.

1.3.3.5 ORC applications

As mentioned before, Organic Rankine Cycle (ORC) is a technology able to transform thermal energy to electricity at relatively low temperatures, in the range of 80 to 350 °C. The organic fluids that can be used in temperatures below 400 °C do not need to be superheated, a fact that leads to higher cycle efficiency. This makes it possible to exploit low-grade heat sources that otherwise would be wasted. It can play an important role to improve the energy efficiency of new or existing energy-intensive applications.

Nowadays, the ORC technology meets great development and has inserted in many applications, the most important being presented below.

1.3.3.5.1 ORC & concentrated solar power

Solar thermal electricity generation systems combine some kind of solar technology (i.e. solar collectors of parabolic trough design, linear Fresnel collectors, evacuated tube collectors etc.) with a thermal cycle for electricity production. Nowadays, the combination of ORC systems with solar technology is rapidly developing and widely investigated, since small scale ORC systems integrated to solar power systems, present a very good performance in cooperation with low and medium temperature collectors, producing clean water and clean electricity. The most applied solar technology in solar thermal ORC systems tends to be the concentrated solar power systems (CSP). Concentrated Solar Power systems are based on the concept of collecting solar radiation to produce steam or hot air that can be used for electricity generation using conventional power cycles. The collector collects the solar radiation rays and direct them to the absorber tubes where the fluid is heated, producing superheated steam. The steam thermal energy is then converted to electricity in a conventional steam power cycle or integrated into a combined steam and gas turbine cycle. [1.38, 1.47]. The basic principle is presented in Figure 1.31.

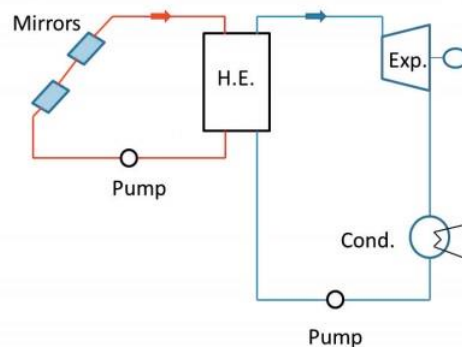


Figure 1.31 Schematic diagram of an ORC engine integrated to a concentrated solar power system [1.47]

A common heat exchanger exploits the heat from the concentrated solar collectors' system working fluid to heat the ORC organic fluid, in order to keep the cycle going.

There are several literature examples that prove the efficiency of such a combined technology; a small scale CSP of 630 kW plant coupled with an ORC system of a capacity of 629 kW with an efficiency of 20% installed in Ottana Solar facility (Sardinia, Italy) showed a sufficient performance even at partial load operation [1.48]. Recent research of a small-scale ORC system, operating at

supercritical conditions with a specially modified turbine, that operated in combination with a photovoltaic (PV) / thermal collectors field for the exploitation waste heat of the PVs and thus the improvement of their performance has shown that the ORC engine operated with good performance even at unsteady conditions, increasing the productivity of such a hybrid system during both a winter and a summer day [1.49]. Moreover, the on-site experimental evaluation of the performance of a low-temperature (around 80 °C) solar organic Rankine cycle system that uses evacuated tube solar collectors of a thermal capacity of 100 kW_{th} has resulted in an ORC thermal efficiency of around 4.3 % [1.50]. Even though it seems to be low, it bespeaks a promising technology, since the thermal efficiency is better than previous research at the same temperature range. Therefore, the combination of ORC technology with solar power systems is a promising technology at least for small and medium scale design and low to medium temperature.

1.3.3.5.2 ORC & biomass

In ORC systems combined to biomass combustion systems, the heat from biomass is transferred to the ORC working fluid by means of intermediate circuit. The media is usually thermal oil, saturated steam, pressurized water or directly the ORC working fluid. In a typical biomass- ORC cogeneration system the biomass fuel is burned in the boiler and the heat carried by the thermal oil is transferred to the ORC and converted to electricity. The basic idea is presented in Figure 1.32 [1.50].

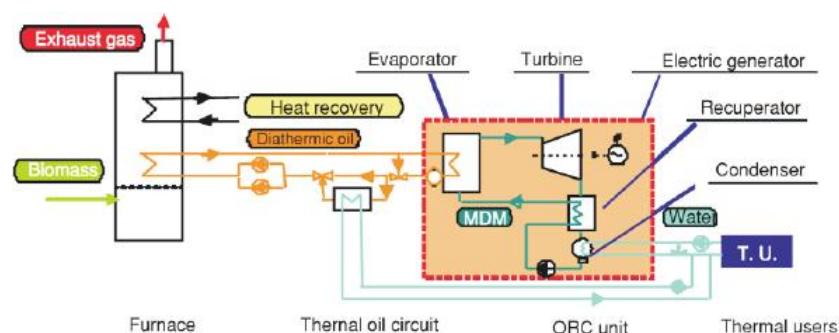


Figure 1.32 Schematic of a ORC biomass to energy co- generation plant [1.50]

According to recent statistics analysis, biomass power plants contribute to almost 12 % of all ORC installed capacity in the world. Germany and Italy are the most significant for biomass, mainly due to favorable policies, followed by Canada and Austria. Biomass development continues in Italy, Russia, Canada and the United Kingdom. However, the average size of biomass ORC installed in Italy is below 1 MW_{el}, while new plants in Canada and Russia have an average power output above 4 MW_{el}, mostly for saw mills [1.52].

Biomass- ORC integrated plants are a very promising technology for high temperature cycles. In February 2001, at Lienz, Austria, an ORC system with a nominal electric capacity of 1,000 kW was implemented in the biomass combined heat and power plant (CHP), in the framework of an EU demonstration project. The biomass CHP plant supplies the town of Lienz with district heat (about 60,000 MWh/a) and feeds the electricity produced (about 7,200 MWh/a) into the public grid. According to operational data, the net electrical efficiency of the ORC plant combined to the biomass CHP plant reached 18% at nominal load and about 16.5% at 50% partial load at feed water temperatures of 85°C. This result highlighted the excellent partial load behavior of this technology and its suitability for heat-

controlled operation. Moreover, taking under consideration the difference between the gross and the net electric power output of the plant and the fact that the internal electric power demand of the ORC for the feed pumps sums up to about 60 kW at nominal load, the gross electric efficiency of the ORC is about 19% at nominal load. The continuous operation experience of the integrated plant has concluded that the new biomass CHP technology based on the ORC process is an economically and technologically interesting solution for decentralized applications [1.53].

On the other hand, the biomass- ORC technology seems to be promising even at small- scale systems. A domestic CHP/ ORC prototype has been developed in 2014 in Poland, in order to investigate the operation in transient operating conditions, aiming to use it on single- family houses. The electric power of the system was 2.5 kW_e and the thermal power 25kW_{th}. The three- year operation of the prototype resulted that the system functions properly, while further laboratory tests conducted in 2017 showed that the ORC system operated under transient conditions with a maximum gross and net electric efficiency of 6.5 % and 4.5 % respectively. Even though these values seem to be low, the most important result has been the possibility to adjust the system settings to changing conditions as well as to maintain operational continuity of the machine. The system in question can function properly under broad changes in flow rate, temperature and pressure of the working medium and could serve as a basis for the development of a commercial domestic micro-CHP ORC power plant [1.54].

The biomass- ORC CHP systems are a very promising upcoming technology for both small and large-scale systems and research is recently being invested in the scope of efficiency increase.

1.3.3.5.3 ORC & geothermal

As mentioned above, the ORC technology is particularly suitable for the exploitation of medium-to-low enthalpy sources. It is a cost-effective solution with power outputs that can reach up to 40 MWe per single generator for sources with water temperature of 100°C to 200°C or higher. Heat from the earth is an excellent energy source since it is inexhaustible and renewable. Geothermal heat can be found in many regions especially at tectonic plate boundaries or at places where the crust is thin enough to let the heat through. The most common way of capturing the energy from geothermal resources is to tap into naturally occurring hydrothermal convection systems, where cooler water seeps into earth's crust and is heated up within a reservoir of water and/or steam. An ORC system, where a secondary fluid is heated up and vaporized by means of heat exchange with the geothermal fluid in order to drive a turbine and produce electricity while delivering wasted heat to a thermal user, is a very efficient way to exploit this kind of heat source.

The main idea of a geothermal – ORC integrated system is presented in Figure 1.33.

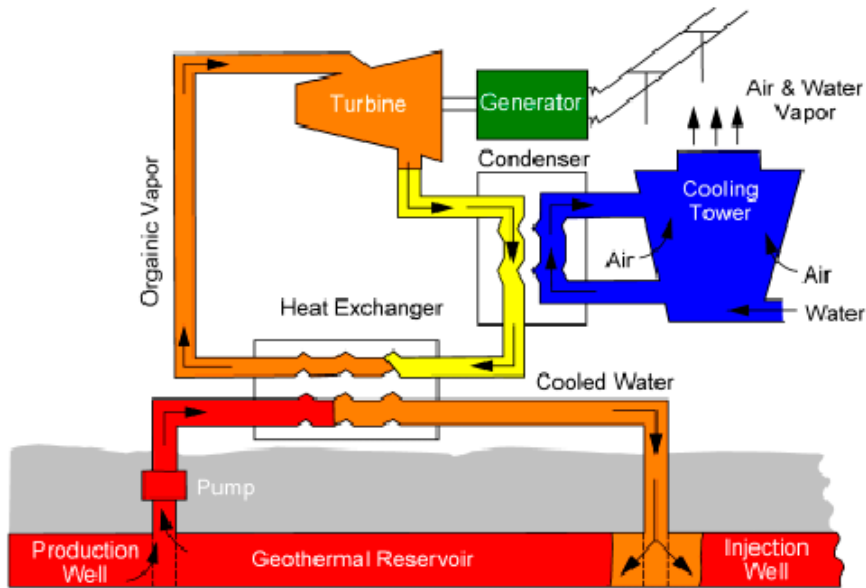


Figure 1.33 Schematic of a geothermal ORC to energy generation plant [1.55]

Usually a wet or dry cooling tower is used to condense the vapor after it leaves the turbine to maximize the temperature drop between the incoming and outgoing vapor and thus increase the efficiency of the operation.

Electric power has been produced from geothermal energy in 27 countries; however, Greece, Taiwan and Argentina have shut down their plants, due to environmental and economic reasons. Since 2000, additional plants have been installed in Costa Rica, France on Guadeloupe in the Caribbean, Iceland, Indonesia, Kenya, Mexico, and the Philippines. In 2004, Germany installed a 210-kWe binary plant at Neustadt Glewe and a 6-MWe plant has been installed on Papua New Guinea to generate electricity for a remote mine. Power generation from geothermal brines is the main field of application with 74.8% of all ORC installed capacity in the world; however, the total number of plant is relatively low with 337 installations as these applications require large investment and multi-MW plants. Figure 1.34 present in a schematic way the total installed capacity of ORC plants worldwide as formed in December 2016, where it becomes obvious that the geothermal exploitation has a dominant role [1.55,1.56].

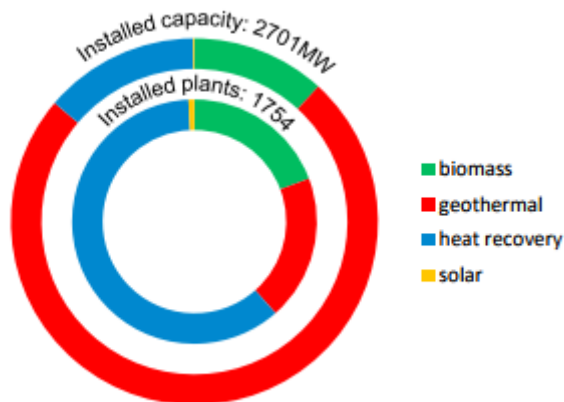


Figure 1.34 Schematic of total installed ORC capacity per application [1.56]

The latest update upon the use of geothermal technology in Greece has been in 2016. This update bespeaks some first steps in the utilization of geothermal sources. More specifically, geothermal energy in Greece is still being used only for direct uses, mainly in the agricultural, healing and recreation sectors (spa facilities, greenhouses, soil heating, aquaculture, and fish farming). In 2014, a new hydroponic geothermal greenhouse unit in Neo Erasmio (Xanthi, Northern Greece) became the most important investment in geothermal energy in the country, currently covering 8.2ha. Further exploitation of the low enthalpy geothermal potential is developing in the geothermal fields of Eratino-Chrysoupolis and Aristino in Northern Greece. Other regions such as Milos and Nisyros islands (>30 MWe confirmed through drilling, >200 MWe estimated) and other certain Aegean islands (e.g. Chios, Lesvos, Samothrace, Lemnos) but also Sidirokastro and Eastern Thessaly in Northern Greece have strong indications for the existence of medium enthalpy reservoirs. The planned geothermal power production includes at the moment the construction of small units (5-8 MWe) in six allocated concessions. However, the installation of the CHP plants in Greece has increased with approximately 3000 units in the last few years.

Heat recovery technology with ORC application, which is the second trend in Figure 1.34 will be discussed right below.

1.3.3.5.4 ORC & waste heat recovery

ORC units can produce electricity by recovering heat from industrial processes and in combined cycles with reciprocating engines and gas turbines. According to their temperature range, the waste heat sources can be divided into three main categories: high temperature (>650 °C), medium temperature (230–650 °C) and low temperature (<230 °C). Nevertheless, it has been noticed that more than 50% of industrial waste heat lays within the low-grade range. The use of appropriate thermodynamic power cycles such as ORC is a highly recommended strategy for recovering low-grade waste heat for power generation. The industrial sector accounts for one third of the total energy consumption in society. Of the energy consumed, almost 20 to 50% is rejected as a heat loss. However, this loss of energy could be exploited and usefully reused for "clean" power generation, by employing waste heat recovery systems. Waste heat recovery is a continuously growing concern of the industry in order to reduce energy consumption, operational costs and carbon emissions [1.57, 1.58].

Organic Rankine Cycle (ORC) is an ideal technology for industrial process heat recovery, since it operates with good efficiency for lower temperature applications. In Figure 1.35, the main concept of the use of ORC with an industrial waste heat source is presented.

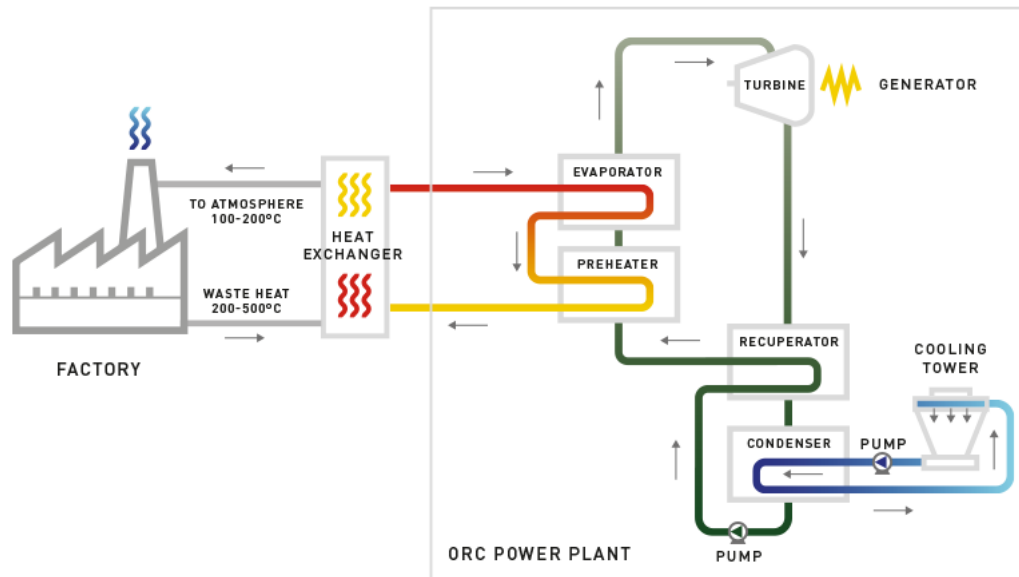


Figure 1.35 Schematic of an industrial waste heat- ORC to energy generation plant [1.58]

An experimental study of an ORC for low grade waste heat recovery in a ceramic industry in 2015 resulted in a gross ORC electrical efficiency of 12.47 %. The thermal power input ranged from 128.19 kW_{th} to 179.87 kW_{th}. The maximum gross and net electrical powers achieved were 21.79 kW and 18.51 kW, respectively, with maximum cycle gross electrical efficiency of 12.47% and a net electrical efficiency of 10.94% [1.59].

A comparative analysis of the waste heat exploitation among three different configurations (i.e. steam Rankine Cycle, ORC and solar ORC power generation) in medium- low heat source temperature has shown that under the condition of 150–210 °C heat source, ORC had the highest thermal efficiency of 9.60 %, exergy efficiency and power generation; while at 210–350 °C, the performance of the solar ORC had a distinct advantage [1.60].

Waste heat recovery is an emerging field for ORC with an interesting potential for all unit sizes: all the big players are active on that market with medium – large size plants recovering heat from gas turbines, internal combustion engines or industrial processes. Most of the other manufacturers are focused on small waste heat recovery applications with products ranging from 10 to 150 kW_{el}. Waste Heat recovery applications cover 13.9% of the total market with a relevant number of operating plants [1.57].

The ORC technology shows a great potential combined to other forms of heat sources such as the heat exploitation from the hot streams that can be found in the oil & gas downstream, midstream and upstream sectors, natural gas compression stations, steam & power CHP systems, wave power etc. However, these applications are in their infancy and in a primary research for the time being. The most important fact that derives from all the above-mentioned examples is that ORC technology is a very promising and widely applied technology for the conversion of low and medium temperature heat sources to electrical power.

1.3.3.5.5 ORC & RO application- prequel of thesis

Recently, an extended theoretical and experimental research has been carried out concerning the combined ORC- reverse osmosis (RO) desalination systems. Back in 2007, the Agricultural University of Athens simulated, designed, constructed and experimentally evaluated for operation in variable thermal input, an autonomous low- temperature solar ORC system for reverse osmosis desalination [1.50, 1.61- 1.65]. An evacuated solar collectors' field of a thermal capacity of 100 kW_{th} was coupled to a small- scale ORC cycle in order to produce mechanical power to the scroll expander of the ORC engine. Then, the ORC engine, mechanically coupled directly with the high-pressure pump of a RO unit (through a belt pulley), gave the RO unit the necessary energy to produce fresh desalinated water from feed sea- water. The specific system was chosen to be investigated due to some innovative advantages such as: low temperature thermal sources can be exploited efficiently for fresh water production; solar energy is used indirectly and does not heat seawater; the RO unit is driven by direct mechanical work produced from the process; such a system can be an alternative to PV-RO systems, while low temperature energy sources like thermal wastes may be used for RO desalination. Based on the design results, a prototype installation was built and evaluated, and the results concluded to an efficient solar ORC- RO plant with a production of 2.1 m³/d of fresh water and an ORC thermal efficiency of 7%, for operation at a temperature range between 70 and 80 °C. The system was also evaluated for partial load operation with an efficiency of 5% and a minimum mechanical energy consumption of 2 kWh/m³. An investigation of the operation with the ORC engine in transcritical and supercritical conditions has proven a better overall efficiency that could possibly reach 14%.

In the effort of increasing the ORC efficiency and the RO unit flexibility, a new ORC- RO configuration, based on the same heat source, has been designed and analyzed in the current thesis. The new configuration includes a two- stage ORC engine (meaning the expansion happens in two expanders) and a three identical RO units plant, in order to produce electricity and fresh desalinated water in a wide thermal input range and under variable input load. The temperature range that the new asset is tested lays between 80 and 130 °C [1.66- 1.69].

1.4 Objective of the thesis

In the scope of the above, in order to contribute to the ongoing effort for promoting research in the area of RO desalination combined to renewable energy sources, an investigation that addresses all the main aspects related to design, manufacturing and operation of a hybrid RO desalination system is conducted in the present thesis. The investigated system is an integrated system that consists of three identical seawater RO desalination units that operate with energy from a designed, developed, installed and tested in the scope of the present thesis two-stage Organic Rankine Cycle (ORC) engine. The main target of the present thesis is to simulate and investigate experimentally the operation of the RO units in variable power input, as the one deriving from solar collectors. The developed two-stage ORC engine uses heat to produce electrical power based on the thermodynamic Rankine cycle and this electricity feeds the RO units.

The present work is the sequel of another research of the design and experimental investigation of an autonomous RO desalination system with solar

ORC engine operating at a temperature range of 60 to 80°C [1.50, 1.61- 1.65]. The present system intends to bring the research a step forward by increasing the operation temperature range up to 130°C, using a two- stage ORC engine, in order to investigate the efficiency amelioration and with the use of three RO desalination units, in order to operate at a wide load range and produce fresh water even at low power input. The three main components of the integrated test-rig are: the electrical heater of a capacity of 100 kWth used as the thermal source simulating the solar collectors' field (variable heat load), the designed and built two- stage ORC engine that convert the heat into electricity through the expansion of a previously compressed organic fluid and finally the three identical seawater RO desalination units that receive the electric power from the ORC engine and produce fresh potable water from sea water in a wide operational range. The main objectives of the current work are the following:

- Simulation, design and construction of a two- stage ORC engine in order to investigate the operation in a wide load range up to 130 °C and the efficiency improvement in comparison to the single- stage one
- Sizing of the engine and selection of the appropriate consisting components (i.e. the pressure pump, the expanders, the evaporator, the condenser etc.)
- Selection of the appropriate organic fluid for the best ORC engine performance under the design conditions
- Expanders' modification in order to fulfill the research requirements
- Simulation, selection of the equipment and experimental test of a multi-skid desalination RO system in order to investigate the operation at a wide salinity (brackish to seawater) and temperature range
- Investigation on a case study of a multi- skid RO system connected to a Photovoltaic (PV) field in comparison to one conventional RO unit for a typical winter and a typical summer day, in order to ensure the flexibility of the selected asset for the current research
- Evaluation of the integrated system of the ORC engine with the multi- skid RO system

As will be thoroughly presented in the next chapters, the issues raised above are properly addressed within the framework of the current thesis. A prototype autonomous multi-skid RO desalination system connected to a two- stage ORC engine has been designed and experimentally tested and the results will be extensively discussed.

1.5 Thesis structure

The present work has been divided into seven chapters. Next to this introduction, where sovereign water desalination technologies and especially the reverse osmosis process are presented, along with a thorough presentation of the state of the art on the ORC technology, a simulation model development analysis of the ORC engine, the RO skid and the integrated system is analytically discussed in **Chapter 2**.

In **Chapter 3** the prototype design and construction of the integrated system is presented. The careful selection of every component based on the overall best efficiency of each sub- system and of the integrated system is discussed in detail. Special attention is paid on the scroll expanders' modification from market available scroll compressors in order to meet the current research requirements.

The experimental performance evaluation of the multi- skid RO unit is described in **Chapter 4**. The system is tested for operation in low, medium (brackish) and high (sea water) salinity, as well as in different water temperatures for high salinity. Moreover, a case study of a multi- skid RO unit operation in combination to PV fields of different capacities for three different areas on a typical winter and a typical summer day and a comparison to a single conventional RO unit is discussed in the same chapter in order to ensure the soundness of the multi- skid asset selection.

The experimental investigation and evaluation of the two- stage ORC engine is presented in **Chapter 5**, where the ORC engine is being tested for operation at several operation temperatures form 70 up to 130 °C. For each temperature, the system is being tested for single and two- stage operation in order to compare the two different configurations in aspects of efficiency and net produced power, according to the available heat load. Since the scroll expanders are modified scroll compressors in reverse operation and also the most important parameter of the ORC engine, a separate paragraph is dedicated to the scroll expanders operation evaluation at single and two- stage operation based on the test results.

Chapter 6 presents the evaluation of the integrated system based on the results of the separate investigation of the two main sub- systems; the multi- stage RO skid and the ORC engine. The two sub- systems have not finally been directly electrically connected due to the lack of time of the corresponding program, however the previous detailed investigation permits a safe forecast of the RO unit performance fed by the power of the ORC engine.

Overall conclusions and crucial comments on the parameters that could be optimized on the current work are being discussed in **Chapter 7**, among with future work that derives from the current research. The related publications that have already been published are also presented.

References:

- 1.1 The United Nations World Water Development Report 2016, Water and Jobs, Published in 2016 by the United Nations Educational, Scientific and Cultural Organization, ISBN 978-92-3-100146-8, available on <http://www.unwater.org/publications/publications-detail/en/c/396246/>
- 1.2 Falkenmark, M, and Widstrand, C. Population and Water Resources: A Delicate Balance. Population Bulletin No. 3. Washington, DC, Population Reference Bureau, (1992), available on <http://www.irwash.org/sites/default/files/276-92PO-10997.pdf>
- 1.3 Falkenmark, M. New Ecological Approach to the Water Cycle: Ticket to the Future. *Ambio*, 13(3), (1984), pp. 152–160.
- 1.4 Coping with Water Scarcity: An Action Framework for Agriculture and Food Security, (2012), FAO Water Reports No. 38. Rome, FAO, available on <http://www.fao.org/docrep/016/i3015e/i3015e.pdf>
- 1.5 [National Geographic “Fresh water crisis” report, available on http://www.nationalgeographic.com/freshwater/freshwater-crisis.html](http://www.nationalgeographic.com/freshwater/freshwater-crisis.html)
- 1.6 WWAP (United Nations World Water Assessment Programme). Water for a sustainable world. The United Nations World Water Development Report. Paris, UNESCO: 2015, available at <http://www.unesco.org/new/en/natural-sciences/environment/water/wwap/wwdr/2015-water-for-a-sustainable-world/>.
- 1.7 Manju S., Sagar N. Renewable energy integrated desalination: A sustainable solution to overcome future fresh-water scarcity in India. [Renewable and Sustainable Energy Reviews](#) (73), (2017), pp. 594–609.
- 1.8 International Desalination Association Releases Latest Statistics on Desalination Market, International Desalination Association, November 2016, available at: <http://idadesal.org/wp-content/uploads/2017/03/State-of-Desalination-Press-Release-IDA-and-GWI.pdf>
- 1.9 Global Water Intelligence, October 2010, available at: <https://www.prlog.org/10985677-desalination-market-in-egypt-to-reach-3938m-by-2016-new-gwi-report.html>
- 1.10 International Water Association, August 2016, Nikolay Voutchov, “Desalination – Past, Present and Future”, available at: <http://www.iwa-network.org/desalination-past-present-future/>
- 1.11 Alkaisia Ahmed, Mossad Ruth, Sharifian-Barforoush Ahmad, A review of the water desalination systems integrated with renewable energy. 1st International Conference on Energy and Power, ICEP2016, 14-16 December 2016, RMIT University, Melbourne, Australia. *Energy Procedia*, 110, (2017), pp. 268-274.
- 1.12 Frantz C., Seifert B., Thermal analysis of a multi effect distillation plant powered by a solar tower plant. International Conference on Concentrating Solar Power and Chemical Energy Systems, SolarPACES 2014. *Energy Procedia*, 69, (2015), pp.1928- 1937.
- 1.13 Rezvani Dastgerdi Hamid, B. Whittaker Peter, Tong Chua Hui, New MED based desalination process for low grade waste heat. *Desalination*, 395, (2016), pp. 57-71.

- 1.14 Park I.S., Park S.M., Ha J.S. Design and application of thermal vapor compressor for multi-effect desalination plant. *Desalination*, 182, (2005), pp.199-208.
- 1.15 Desalination technologies, Reverse Osmosis & Thermal Desalination for drinking water, industrial water & water recycling, Wabag 2016, available at: http://www.wabag.com/wp-content/uploads/2012/04/Desalination_2015_EN.pdf
- 1.16 Shen J., Xing Z., Wang X., He Z. Analysis of a single-effect mechanical vapor compression desalination system using water injected twin screw compressors. *Desalination*, 333, (2014), pp.146-153.
- 1.17 Abraha Woldai, Multi- Stage Flash Desalination; Modeling, Simulation, and Adaptive Control. CRC Press Taylor& Francis Group, 2016, ISBN: 13:978-1-4987-2170-7, pp. 8-10.
- 1.18 Al-Kharabsheh S., Goswami D.Y. Solar Distillation and Drying. *Encyclopedia of Energy*, (2004), pp. 597-606.
- 1.19 Williams P.M., Ahmad M., Connolly B.S., Oatley-Radcliffe D.L. Technology for freeze concentration in the desalination industry. *Desalination*, 356, (2015), pp. 314-327.
- 1.20 Polykarpou M. E., Dua V. Optimisation of a liquid-liquid extraction based sustainable water desalination process. *Proceedings of the 6th International Conference on Process Systems Engineering (PSE ASIA) 25 - 27 June 2013, Kuala Lumpur*.
- 1.21 Chan Kanga K., Linga P., Park K., Choi S.-J., Dong Lee J. Seawater desalination by gas hydrate process and removal characteristics of dissolved ions (Na^+ , K^+ , Mg^{2+} , Ca^{2+} , B^{3+} , Cl^- , SO_4^{2-}). *Desalination*, 353, (2014), pp. 84-90.
- 1.22 Sangwai J.S., Patel R.S., Mekala P., Mech D., Busch B. Desalination of seawater using gas hydrate technology – current status and future direction. *Proceedings of HYDRO 2013 INTERNATIONAL 4-6 Dec 2013, IIT Madras, Chennai, INDIA*.
- 1.23 Choon Ng K., Thu K., Kim Y., Chakraborty A., Amy G. Adsorption desalination: An emerging low-cost thermal desalination method. *Desalination*, 308, (2013), pp. 161- 179.
- 1.24 Nayar G.K., Sundararaman P., O'Connor L. C., Schacherl D.J., Heath L.M., Gabriel O.M., Shah R. S., Wright C. N., Winter G. A. Feasibility study of an electrodialysis system for in-home water desalination in urban India. *Development Engineering*, 2, (2017), pp. 38- 46.
- 1.25 Cath Y.T., Childress E.A., Elimelech M. Forward osmosis: Principles, applications, and recent developments. *Journal of Membrane Science*, 281, (2006), pp. 70- 87.
- 1.26 Qasim M., Mohammed F., Aidan A., Darwish A.N. Forward osmosis desalination using ferric sulfate draw solute. *Desalination*, 43, (2017), pp. 12- 20.
- 1.27 Luo H., Wang Q., Zhang C.T., Tao T., Zhou A., Chen L., Bie X. A review on the recovery methods of draw solutes in forward osmosis. *Journal of water process engineering*, 4, (2014), pp. 212- 223.

- 1.28 Wang R., Setiawan L., Fane G.A. Forward Osmosis: Current Status and Perspectives. *Journal of Membrane Science, Virtual Special Issue*, June 2012, available at; <https://www.journals.elsevier.com/journal-of-membrane-science/virtual-special-issues/forward-osmosis-current-status-and-perspectives>
- 1.29 Theobald D., What is ultrafiltration and what are ultrafiltration processes in wastewater. *Water technology magazine*, February 2015, available at: <https://www.watertechonline.com/what-is-ultrafiltration-and-what-are-ultrafiltration-processes-in-wastewater/>
- 1.30 Bennett A. Advances in desalination energy recovery. *World Pumps*, 7-8, (2015), pp. 30- 34.
- 1.31 Altaee A., Zaragoza G., Rost van Tonningen. Comparison between Forward Osmosis-Reverse Osmosis and Reverse Osmosis processes for seawater desalination. *Desalination*, 336, (2014), pp. 50- 57.
- 1.32 ERI pressure exchanger. ERI Energy Recovery INC. available at: http://www.cleantektv.com/companies2/showcase_detail.php?key=74&itemNumber=33
- 1.33 Manju S., Sagar N. Renewable energy integrated desalination: A sustainable solution to overcome future fresh-water scarcity in India. *Renewable and Sustainable Energy Reviews*, 73, (2017), pp. 594- 609.
- 1.34 Papapetrou M., Wieghaus M., Biercamp C. Roadmap for the development of desalination powered by renewable energy. *Intelligent Energy Europe PRODES program*. ISBN 978-3-8396-0147-1.
- 1.35 Desalination and water resources. *Renewable energy systems and desalination. Renewable Energy Systems and Desalination -. Volume 1*. ISBN: 978-1-84826-429-8
- 1.36 Afgan H.N, Carvalho G.M. *New and Renewable Technologies for Sustainable Development*, ISBN: 1402073410, 9781402073410.
- 1.37 Loutatidou S., Arafat A.H. Techno-economic analysis of MED and RO desalination powered by low-enthalpy geothermal energy. *Desalination*, 365, (2015), pp. 277- 292.
- 1.38 Tchanche F.B. *Low- Grade Heat Conversion into Power Using Small Scale Organic Rankine Cycles*. Doctoral Thesis, Agricultural University of Athens, Department of natural resources and agricultural engineering, 2010.
- 1.39 Balmer T.R., *Modern Engineering Thermodynamic*, ISBN:978-0-12-374996-3
- 1.40 Potter C.M., Somerton W.C. *Thermodynamics for engineers*, Schaum's outlines, ISBN: 0-07-050616-7
- 1.41 Kosmadakis G., Manolakos D., Papadakis G. Experimental investigation of a low-temperature organic Rankine cycle (ORC) engine under variable heat input operating at both subcritical and supercritical conditions. *Applied Thermal Engineering*, 92, (2016), pp. 1-7.
- 1.42 Maloney JD, Robertson RC. *Thermodynamic study of ammonia-water heat power cycles*. Oak Ridge National Laboratory Report.CF-53-8-43; 1953.

- 1.43 Kalina Al. Combined-cycle system with novel bottoming cycle. *ASME Journal of Engineering for Gas Turbines and Power*, 106 (1984), pp. 737-742.
- 1.44 Zhang X., He M., Zhang Y. A review of research on the Kalina cycle. *Renewable and Sustainable Energy Reviews*, 16, (2012), pp. 5309- 5318.
- 1.45 Vidnarooban K., Lin J., Arvay A., Kolli S., Kruusenberg I., Tammeveski K., Munukutla L., Kannan M.A. Nano-electrocatalyst materials for low temperature fuel cells: A review. *Chinese Journal of Catalysis*. 36, (2015), pp. 458- 472.
- 1.46 Uzunoglu M., Alam S.M. Fuel-Cell Systems for Transportations. *Power Electronics Handbook (Fourth Edition)*. (2018), pp. 1091- 1112.
- 1.47 Ferrara F., Gimelli A., Luongo A. Small- scale concentrated solar power (CSP) plant: ORCs comparison for different organic fluids. *Energy Procedia*, 45, (2014), pp. 217- 226.
- 1.48 Petrollese M., Cocco D., Cau G. Small-scale CSP plant coupled with an ORC system for providing dispatchable power: the Ottana Solar Facility. *Energy Procedia*, 129, (2017), pp. 708- 715.
- 1.49 Kosmadakis G., Landelle A., Lazova M., Manolakos D., Kaya A., Huisseune H., Karavas S.C., Tauveron N., Revellin R., Haberschill P., De Paepe M., Papadakis G. Experimental testing of a low-temperature organic Rankine cycle (ORC) engine coupled with concentrating PV/thermal collectors: Laboratory and field tests. *Energy*, 117, (2016), pp. 222- 236.
- 1.50 Manolakos D., Kosmadakis G., Kyritsis S., Papadakis G. On site experimental evaluation of a low-temperature solar organic Rankine cycle system for RO desalination. *Solar Energy*, 83, (2009), pp. 646- 656.
- 1.51 Moro R., Pinamonti P., Reini M. ORC technology for waste-wood to energy conversion in the furniture manufacturing industry. *Thermal Science*, 12, (2008), pp. 61- 73.
- 1.52 Tartiere T. ORC Market; A world overview. (2016), available at: <http://orc-world-map.org/analysis.html>
- 1.53 Obernberger I., Thonhofer P., Reisenhofer E. Description and evaluation of the new 1,000 kWel Organic Rankine Cycle process integrated in the biomass CHP plant in Lienz, Austria. *Euroheat & Power*, 10, (2002).
- 1.54 Zywica G., Kaczmarczyk Z. T., Ihnatowicz E., Turzynski T. Experimental investigation of the domestic CHP ORC system in transient operating conditions. *Energy Procedia*, 129, (2017), pp. 637- 643.
- 1.55 Lund J. Characteristics, development and utilization of geothermal resources. [Proceedings of ISES World Congress 2007 \(Vol. I – Vol. V\): Solar Energy and Human Settlement](#) (pp.87-95).
- 1.56 Tartiere T., Astolfi M. A world overview of the Organic Rankine Cycle market. *Energy Procedia*, 129, (2017), pp. 2-9 (IV International Seminar on ORC Power Systems, ORC2017 13-15 September 2017, Milano, Italy).
- 1.57 Li L., Ge T.Y., Luo X., Tassou A.S. Experimental investigations into power generation with low grade waste heat and R245fa Organic Rankine Cycles (ORCs). *Applied Thermal Engineering*, 115, (2017), pp. 815- 824.

- 1.58 Green power through innovation, ORC for heat recovery industrial process, available at <http://exergy-orc.com/applications/heat-recovery-from-industrial-process>.
- 1.59 Peris B., Navarro- Esbri J., Moles F., Mota- Babiloni A. Experimental study of an ORC (organic Rankine cycle) for low grade waste heat recovery in a ceramic industry. *Energy*, 85, (2015), pp. 534- 542.
- 1.60 Zhang X., Wu L., Wang X., Lu G. Comparative study of waste heat steam SRC, ORC and S-ORC power generation systems in medium-low temperature. *Applied thermal engineering*. 106, (2016), pp. 1427- 1439.
- 1.61 Manolakos D. Papadakis G., Mohamed Sh. E., Kyritsis S., Bouzianas K. Design of an autonomous low-temperature solar Rankine cycle system for reverse osmosis desalination. *Desalination*, 183, (2005), pp. 73- 80.
- 1.62 Manolakos D. Papadakis G., Kyritsis S., Bouzianas K. Experimental evaluation of an autonomous low-temperature solar Rankine cycle system for reverse osmosis desalination. *Desalination*, 203, (2007), pp. 366- 374.
- 1.63 Manolakos D., Kosmadakis G., Kyritsis S., Papadakis G. Identification of behaviour and evaluation of performance of small scale, low-temperature Organic Rankine Cycle system coupled with a RO desalination unit. *Energy*, 34, (2009), pp. 767- 774.
- 1.64 Li C., Kosmadakis G., Manolakos D., Stefanakos E., Papadakis G., Goswami Y.D. Performance investigation of concentrating solar collectors coupled with a transcritical organic Rankine cycle for power and seawater desalination co-generation. *Desalination*, 318, (2013), pp. 107- 117.
- 1.65 Manolakos D., Mohamed Sh. E., Karagiannis I., Papadakis G. Technical and economic comparison between PV-RO system and RO-Solar Rankine system. Case study: Thirasia island. *Desalination*, 221, (2008), pp. 37- 46.
- 1.66 Kosmadakis G., Manolakos D., Kyritsis S., Papadakis G. Economic assessment of a two-stage solar organic Rankine cycle for reverse osmosis desalination. *Renewable Energy*, 34, (2009), pp. 1579- 1586.
- 1.67 Kosmadakis G., Manolakos D., Papadakis G. Parametric theoretical study of a two-stage solar organic Rankine cycle for RO desalination. *Renewable Energy*, 35, (2010), pp. 989- 996.
- 1.68 Kosmadakis G., Manolakos D., Kyritsis S., Papadakis G. Design of a two stage Organic Rankine Cycle system for reverse osmosis desalination supplied from a steady thermal source. *Desalination*, 250, (2010), pp. 323- 328.
- 1.69 Ntavou E., Kosmadakis G., Manolakos D., Papadakis G., Papantonis D. Experimental evaluation of a multi-skid reverse osmosis unit operating at fluctuating power input. *Desalination*, 398, (2016), pp. 77- 86.

CHAPTER 2 – Simulation model development analysis

2.1 Introduction

In the current chapter the modeling of the system is presented. The major scope is the connection of all three sub- systems (heat source- ORC engine and RO unit) to one integrated system and the evaluation of its operation. Each sub- system is optimized and simulated separately.

Since the heat source simulates renewable energy sources which depend on current conditions and provide variable and fluctuating thermal load, the ORC engine is designed to operate efficiently at a variable power input. First, the optimum two- stage ORC configuration is examined in order to ameliorate the engine efficiency. Meanwhile, the optimum refrigerant in terms of environmental criteria and thermodynamic properties is selected. The ORC engine is designed based on the thermodynamic characteristics of the theoretical organic Rankine cycle in order to determine the engine operation characteristics for efficiency and net power production maximization throughout the whole operation load range (0-100%).

The RO unit is to be electrically connected to the ORC engine; therefore, it should be able to follow the power input fluctuation. Since flexibility is the most important feature required from the RO unit, it is designed in order to maximize the fresh water production as a function of the power input. Even at low thermal load, the RO unit should be able to produce water of acceptable quality and quantity.

The simulation model of the integrated system is realized with the use of appropriate commercial software which will be presented in this chapter, and it is constructed for unsteady conditions. Moreover, in order to better understand the design parameters especially for the ORC engine, a series of parametric analysis takes place to combine the efficiency to each component of the engine (i.e. heat exchanger).

2.2 The Organic Rankine Cycle engine model

2.2.1 Organic fluid selection criteria and two- stages ORC configurations candidates

The main scope of the current section is the selection of the most appropriate working fluid for the ORC engine, based on environmental and energy parameters. Simultaneously, the selection of the most efficient configuration of the ORC engine is examined. Both research tasks (the selection of the most appropriate working fluid and two- stages configuration) focus on the operation at partial and full load (nominal operation/ design point), since the current engine is supposed to operate with thermal load from renewable energy sources, where the power input often strongly fluctuates. The main goal of the research is the maximization of the ORC engine efficiency and net power production [kW], throughout the whole operation load range (0- 100%).

2.2.1.1 Organic fluid selection criteria

All processes of the ORC engine and important operation factors such as the thermal efficiency, the net power production etc., strongly depend on the properties of the organic working fluid of the ORC engine. For the current engine, the organic fluid must possess some physical properties, of which the most important are presented below [2.1, 2.2]:

- ✓ Appropriate high critical temperature and pressure, in order to remain in subcritical conditions throughout the whole cycle, otherwise a larger and more expensive heat exchanger would be needed and the thermal efficiency would decrease (note: critical point is the temperature and pressure above which the gaseous and liquid phase of a pure substance no longer have distinguishable limits and share similar properties)
- ✓ Low specific volume [m^3/kg] at the expander's inlet, as well as small specific volume ratio at the inlet and outlet of the expander, in order to use an expander of lower size and cost
- ✓ High thermal conductivity, in order to transfer an important amount of thermal energy to the heat exchangers, reducing their heat exchange area at the same time
- ✓ High adiabatic enthalpy drop at the expander for obtaining large power output
- ✓ High specific heat (c_p) for enlarging heat capacity
- ✓ High chemical and thermal stability, especially at high temperature
- ✓ Low viscosity for lowering the pressure losses due to the fluid friction in the return pipe and for increasing the heat exchange at the heat exchangers
- ✓ Low cost and easy purchasing
- ✓ Nonflammable and non-toxic
- ✓ Compatibility with engineering material, which means that it should be non-corrosive, nontoxic and compatible with both materials and lubricating oil (if used)
- ✓ Self-lubricity for the smooth rotation of the turbine
- ✓ A near-vertical saturated vapor line is desirable so that, on one hand, little moisture occurs during expansion and, on the other, it is unnecessary to condense a superheated gas
- ✓ Acceptable according to the environmental limitations set for the refrigerants. More specifically, it should have a zero ODP (Ozone Deployment Potential) and a low GWP (Global Warming Potential) and also, it should not be under a withdrawal regime (phase out), according to Montreal and Kyoto protocols [2.3] and EU directive No. 2006/4/EC.

The decision parameters that were mentioned before include thermal efficiency, which is one of the most important and reliable criteria that can be used. It depends on the specific temperature limits that have been set, as well the lower/higher operational pressure. It also depends on and is limited by the irreversibility due to the entropy changes of the working fluid during various stages of the cycle. All the above conditions affect each other, and it is a difficult task to optimize a thermodynamic system and maximize the thermal efficiency, even in operation of a system at constant conditions and at full load. Another crucial parameter is the specific range of applicability of each organic fluid, meaning that there is a temperature range, in which the fluid is stable and does not suffer any significant decomposition. For this range there is an upper limit, which is the critical

temperature. The behavior that a fluid can have while it is being saturated is another criterion that working fluids should meet and significantly affects their behavior. Fluids show three different types of slope on their saturation vapor curves (ds/dT) and can be categorized into three groups, according to their temperature-entropy (T - s) diagrams [2.4, 2.5]:

- Dry fluids: they have a positive slope and are (in general) of high molecular numbers
- Wet fluids: they have a negative slope and are (in general) of low molecular numbers
- Isentropic fluids: they have nearly vertical saturated vapor curves

In Figure 2.1 the schematic presentation of the three categories in T - s diagrams is observed:

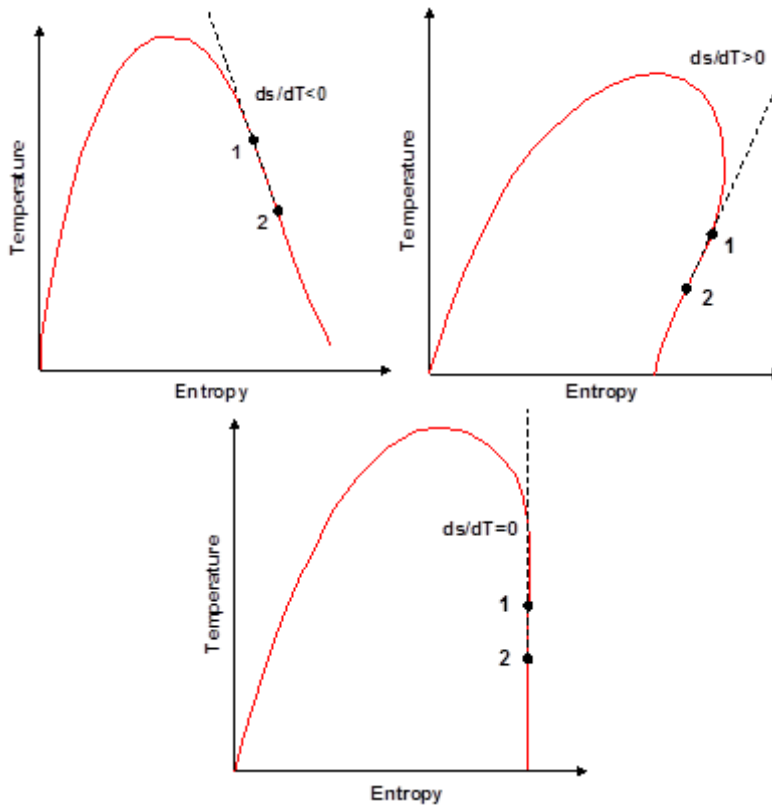


Figure 2.1 Characteristic T - s charts for wet (a), dry (b) and isentropic (c) fluids.

In the ORC it is preferred to use dry or isentropic fluids. This is because these fluids do not become saturated once they produce work in the turbine after a large enthalpy drop, so the fear of coming under the two-phase area during expansion is limited. This leads to the increase of the thermal efficiency and leaves the possibility of a partial condensation heat recovery open.

The organic fluids' pre-screening is mainly based on their environmental characteristics, their critical temperature and the experience that derives from their use. More specifically, this pre-screening is based on the criteria presented below:

- As mentioned before, their ODP factor must be equal to zero. Therefore, all CFC's (chlorofluorocarbons) are excluded, such as CFC- 11 (R11) which may present good efficiency for similar applications, however it is rejected due to environmental reasons.

- These fluids must not subject to any international protocol on EU directive for future phase out, such as HCFC- 123 (hydro-chlorofluorocarbon) which has almost zero ODP, however its use has been limited in order to completely phase out in the near future, therefore its cost is significantly high.
- The examined organic fluids must have a high critical temperature, close to the maximum operation temperature (110- 130 °C). There are several organic fluids with a critical temperature close to 50 and 70 °C, however, for operation at high temperature they present low thermal efficiency (such as hydrofluorocarbon HFC- 143a). Therefore, these fluids are not further examined, since there are others of similar thermal properties and better efficiency.
- The experience of their use and their cost are two major selection factors. For example, the HFC- 245ca presents good efficiency under conditions of the current application and fulfills all the environmental barriers, however its cost is prohibitive.

According to the above discussed criteria and with the help of the REFPROP software [2.6] for the organic fluids properties, the organic fluid candidates that will be further examined are presented in Table 2.1, where their critical temperature, critical pressure and some environmental information can be observed.

Table 2.1 Organic fluids candidates

Organic fluid	Properties			Environmental data		
	Molecular weight (kg/kmol)	Critical temperature (°C)	Critical pressure (bar)	ALT ¹	GWP ² (100 years)	ODP ³
Propane (R-290)	44.10	96.68	42.47	0.04	~20	0
HFC-134a	102.03	101.06	40.59	14	1430	0
HFC-227ea	170.03	101.65	29.26	42	3220	0
HFC-236ea	152.04	139.29	35.02	8	710	0
HFC-245fa	134.05	154.05	36.40	7.6	1030	0
Butane (R-600)	58.12	151.98	37.96	0.02	~20	0

¹ALT: Atmospheric life time

²GWP: Global Warming Potential

³ODP: Ozone deployment Potential

The organic Rankine cycle on which the designed engine is based, is a two-stage cycle and the nominal thermal load varies between 110° and 130°C. The heat source simulates any renewable energy source of this temperature range; thus, the thermal load fluctuates and the organic Rankine cycle performance shall be examined throughout the whole range (0-100%). These characteristics are directly related to the organic fluid selection, therefore a detailed research before this selection is considered desirable.

2.2.1.2 Two- stage ORC engine configurations candidates

The use of a two- stage ORC grounds on the fact that when the maximum operation temperature is high (such as the current application, where the operation temperature varies around 120 °C), the pressure ratio (pressure ratio= P_{in}/P_{out}) during the expansion results to be high (around 10). High pressure ratios during the expansion cannot be supported by existing scroll type expanders, thus the type selected to be used in the current system and present high efficiency for pressure ratios of 3 to 4. Therefore, the separation of the expansion in several steps, where the pressure ratio of each step will be around 3, is necessary. The advantages of such a system are several:

- Thermal efficiency increase at each expansion stage
- Thermodynamic optimization of the cycle with potential use of different working fluids
- Increased thermal efficiency in partial load operation, due to the expanders' operation near the nominal pressure ratio
- Possible use of a by- pass branch, in order to operate only one expander in low load
- Better control of the organic fluid condition at the expander's outlet in order to avoid an expansion at the two- phase area which would lead to a net power production decrease.

However, there are some disadvantages from the two- stages configuration cycle:

- Installation cost increase due to several sub- systems
- Higher monitor complexity, since the operation control (practically the rotational speed control) is applied upon two expanders
- In case that two organic fluid pumps are used, the monitoring is even more complicated, since the control of both pumps would be necessary.

According to literature, there are two basic two- stages ORC configurations. In the first one, two separate thermodynamic cycles called the (high temperature) "upper stage" and the (low temperature) "lower stage" are used (cascade system). The heat is provided to the upper stage where the expander produces the desired mechanical work. During the condensation of the organic fluid at this stage, the condensation heat is transferred to the lower stage in order to evaporate the compressed organic fluid of this stage [2.7-2.10]. In this configuration, two different organic fluids are used, in order to increase the total cycle efficiency. What is also observed for this configuration is the fact that thermal losses take place at the intermediate heat exchanger and also because of the use of two fluid pumps. In partial load (indicatively: lower than 50%) the first stage is by- passed and only the second (lower) stage operates (at low temperature and low thermal load input).

Such a configuration is presented in Figure 2.2 below:

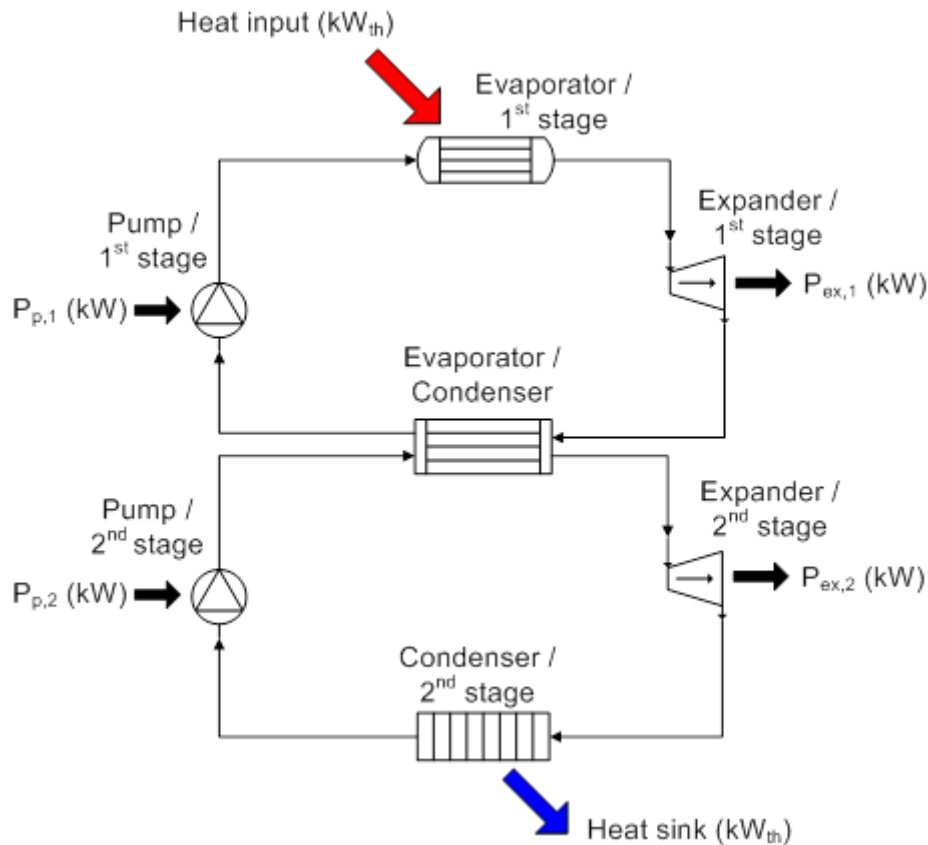


Figure 2.2 Cascade ORC system

Crucial design and control parameters in such a system are:

- Condensation temperature of the upper stage which depends on the evaporation temperature of the lower stage
- Evaporation temperature of the upper stage
- Mass flow rates at both stages, as well as the ratio of the mass flow rates of the two stages which strongly determines the participation of each stage in the power production
- Maximum pressure of each stage
- Condensation temperature of the lower stage

The second possible two- stages ORC configuration resembles the configuration of several conventional power production systems which are based on the typical vapor "Clausius- Rankine" cycle. This configuration includes a single thermodynamic cycle, while the expansion is divided in two expanders connected in series [2.11, 2.12]. The application of such a configuration can result to the increase of the maximum temperature of the cycle, as well as to the total pressure ratio increase. The expansion is divided into two steps with an intermediate expansion pressure. In this way, the control in low thermal load is easy and the expanders operate with high efficiency throughout a wide load range. For operation at a thermal load lower than 50- 60% of the nominal one, the first expander is completely by- passed with the use of one electro- valve (by- pass valve), thus the evaporated organic fluid's expansion is realized only in the second expander. In this way, the pressure ratio fluctuation is kept low throughout the whole thermal load range. The expander's efficiency is widely dependent upon this ratio [2.13, 2.14].

Such a configuration is depicted in Figure 2.3 below:

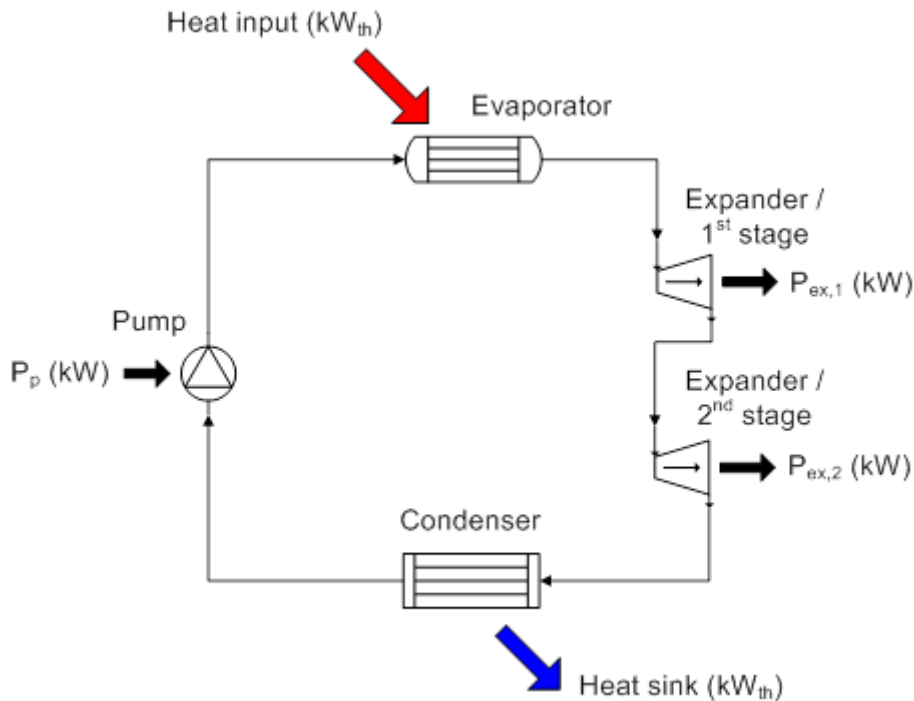


Figure 2.3 Two- stages series expander ORC system

The crucial design and control parameters for this configuration are:

- The organic fluid evaporation temperature
- The thermodynamic cycle high pressure
- The intermediate expansion pressure of the two expanders
- The organic fluid mass flow rate
- The condensation temperature

The selected configuration is the second one, with one single thermodynamic cycle and two expanders connected in series. According to an extended analysis that has been carried out within the scope of the corresponding project (see Acknowledgements), it presents great advantage in terms of efficiency throughout the whole load range [2.32]. The efficiency was proved to be even 1% higher than the one of the first configuration and at medium and low thermal load the increase of the efficiency is even more intense. Counting in the use of less sub- systems (lack of second pump and heat exchanger) which reduces the total building cost, as well as the application of a much simpler control system (mass flow rate, rotational speed and pressure monitoring in one cycle than in two), it is obvious that the use of the second configuration with two expanders connected in series is more appropriate than the first one.

2.2.2 Selected configuration investigation and organic fluid selection

In the current section, the selected ORC engine configuration with two expanders connected in series is investigated. More specifically, the cycle efficiency and some crucial operational parameters are examined, as well as some additional characteristics such as:

- The organic fluid mass flow rate and its control
- The appropriate organic fluid selection

- The recovery of a part of the condensation heat for use either for seawater preheating (RO unit recovery increase) or for ORC engine efficiency increase (organic fluid preheating after compression)

The current investigation is carried out for both full and partial load operation, thus another parameter is added, that of the thermal load variation. The operation at partial load is dictated by the variation of heat input (heat source: any kind of low temperature renewable energy source such as solar thermal energy) and it influences both the operation temperature and the organic fluid mass flow rate [2.15]. In table 2.2, all the coefficients used for the expanders and the pump, as they derived from experimental research and from manufacturers' manuals are presented [2.13, 2.15-2.17]:

Table 2.2 Component coefficients

Expanders' isentropic efficiency ($n_{ex,is}$)	85 %
Pump's isentropic efficiency ($n_{p,is}$)	85 %
Expanders' mechanical efficiency ($n_{ex,m}$)	85 %
Pump's mechanical efficiency ($n_{p,m}$)	75 %
Internal heat exchanger efficiency (n_{IHE})	60 %

In order to better understand the process taking place in the ORC engine, the thermodynamic diagrams of the selected cycle (Mollier diagram and temperature/entropy diagram) are presented below (Figures 2.4 and 2.5), where the conditions of the organic fluid in each point can be observed:

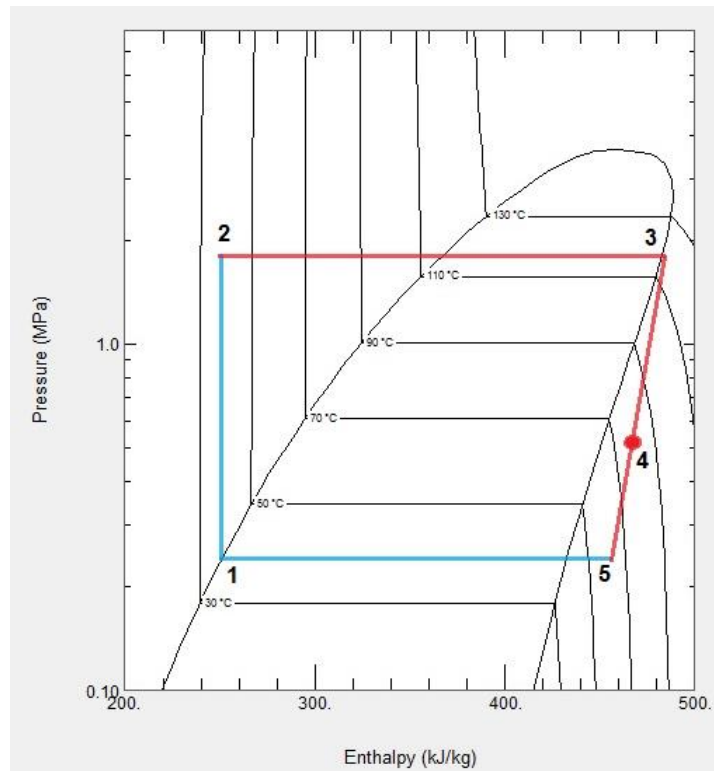


Figure 2.4 Pressure- enthalpy diagram of two- stages ORC with two expanders in series

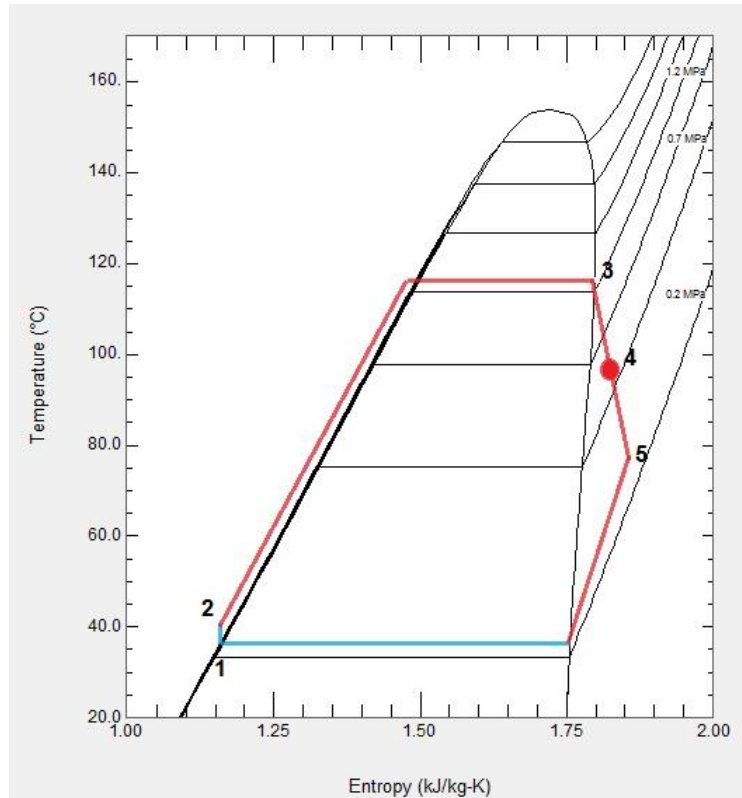


Figure 2.5 Temperature- entropy diagram of two- stages ORC with two expanders in series

During process 2-3, heat is transferred to the organic fluid from the heat cycle (through the evaporator) in order to preheat and evaporate the organic fluid. At point 3, the organic fluid is saturated vapor, or even slightly superheated vapor (almost for 5 K, as it will be explained later on). Then, the organic fluid enters the first expander in order to produce mechanical work and exits in condition 4, where for dry organic fluids this condition is the superheated area and for the isentropic fluids it is almost on the saturation line. However, for the wet organic fluids, this area corresponds to two- phases area and this is the reason that wet organic fluids are avoided in such an engine. The organic fluid then enters the second expander and exits at point 5 where it enters the condenser, loses more heat and results at the pump input (point 1) as a subcooled liquid. Then the pump compresses the fluid up to the maximum cycle pressure and the cycle goes on.

The equations that govern the efficiency and power of each component of the engine are:

Expanders' total power production:

$$W_{ex} = W_{ex,1} + W_{ex,2} = \dot{m}_{ORC} * (h_3 - h_4) * \eta_{ex,m} + \dot{m}_{ORC} * (h_4 - h_5) * \eta_{ex,m} \quad (2.1)$$

Pump power consumption:

$$W_p = \dot{m}_{ORC} * (h_2 - h_1) / \eta_{p,m} \quad (2.2)$$

Thermal power at the evaporator:

$$Q_{ORC} = \dot{m}_{ORC} * (h_3 - h_2) \quad (2.3)$$

Thermal power at the condenser:

$$Q_{out} = m_{ORC} \cdot (h_5 - h_1) \quad (2.4)$$

Thermal efficiency:

$$n_{th} = \frac{W_{ex} - W_p}{Q_{ORC}} \quad (2.5)$$

where m_{ORC} the mass flow rate of the working fluid and h_i the enthalpy at each point.

In case that condensation heat recovery is included (from point 5 of superheated vapor in diagrams 2.4 and 2.5, to the point of saturated vapor) for the preheating of the subcooled compressed liquid organic fluid (point 2 of the Figures) with the use of an internal heat exchanger (recuperator), one more coefficient of exploitation of this heat is inserted, the coefficient n_{IHE} equal to 0.60. Then, the equations 2.3 and 2.4 are alternated as:

$$Q_{ORC} = m_{ORC} \cdot (h_3 - h_{2a}) \quad \text{and}$$

$$Q_{out} = m_{ORC} \cdot (h_{5a} - h_1)$$

Where h_{2a} and h_{5a} are the enthalpy values at the inlet (second expander's outlet) and outlet (pump's inlet) of the preheater.

In order to investigate the cycle and select the most appropriate organic fluid, the ORC engine is modeled with the use of the EES software [2.18]. Apart from the above-mentioned equations for the engine's components, another parameter shall be considered; the heat source cycle which simulates the heat source of any low temperature renewable energy and provides the ORC engine with heat. The mass flow rate of the working fluid in the heat cycle which controls the temperature at this side can change, simulating the thermal input fluctuation that would occur of any variable renewable energy source. At this point, for the investigation of the ORC engine it is assumed that the mass flow rate of the working fluid on the heat cycle is kept constant and the variation of the heat load (variation of the available thermal input) implies uniquely variation of the working fluid temperature, therefore a direct change in the evaporation temperature of the organic fluid. The equation that couples the two sides (heat cycle and ORC engine) and expresses the thermal load is the following:

$$Q_{HTF} = \dot{m}_{HTF} \cdot (h_{HTF,2} - h_{HTF,1}) = \dot{m}_{HTF} \cdot c_{HTF} \cdot (T_{HTF,2} - T_{HTF,1}) = Q_{ORC} = m_{ORC} \cdot (h_3 - h_2) \quad (2.6)$$

where Q_{HTF} the thermal load of the heat transfer fluid, m_{HTF} the mass flow rate of the working fluid and $T_{HTF,I}$ the temperature at the outlet and inlet of the heat source (in the current experiment of an electric heater). The specific heat capacity (c_{HTF}) can be used since the working fluid at the heat cycle remains at the liquid phase and the temperature difference (from $T_{HTF,1}$ to $T_{HTF,2}$) is relatively small.

Concerning the heat transfer fluid of the heat cycle, the parameters that determine its selection are the operation temperature and pressure. The operation temperature of the current engine, as it was mentioned before, is around 110°-130°C. For safety reasons and in order to simulate heating systems that operate at such temperatures (like evacuated tube solar collectors) the maximum operation pressure of the heat cycle has been set to 5 bar [2.8]. In case that the heat transfer working fluid was water under pressure, in order to avoid its vaporization at such high temperature (110°- 130°C), the requested pressure would be greater of around 3 bar. This pressure barrier drastically increases with a temperature increase, since at 150°C it already becomes almost 5 bar. Therefore, for security

reasons, the use of water as a heat transfer working fluid on the heat source side is avoided. On the contrary, the use of a working fluid which would remain at the liquid phase for high temperature values and low pressure (close to the atmospheric) while maintaining good thermal properties (similar to those of water) is encouraged. In chemistry, glycols are proven to be good candidates since they present high boiling points (over 190°C). Between them, two are the most prevalent: monoethylene glycol- MEG and propylene glycol- PEG. Finally, the working fluid that has been chosen is MEG [2.11], which has lower cost, better thermal properties (which leads to a smaller heat exchanger surface) and lower viscosity (fewer pressure losses at the heat cycle, therefore lower power consumption from the heat cycle pump). MEG's boiling point is at around 197°C and its thermal properties as a function of the temperature (°C) are briefly reported below:

$$\text{Dynamic viscosity [kg/m/s]: } \mu = -0.001975 + \frac{0.4502}{T} - \frac{1.013}{T^2}$$

$$\text{Density [kg/m}^3\text{]: } \rho = 1148 - 0.6755 T - 0.000199 T^2$$

$$\text{Specific heat capacity [J/kg/K]: } c_p = 2329 + 4.819 T$$

$$\text{Thermal conductivity [W/m/K]: } k = 0.3049 - 0.000771 T$$

When the thermal load decreases the temperature at the heat cycle decreases as well. Since there is a temperature difference between the heat transfer working fluid at the heat cycle and the evaporation temperature of the organic fluid at the ORC engine (of around 5- 15K/ pinch point), the load variation causes a change of the evaporation temperature (T_3). In the current study, the heat cycle represents a thermal source of 110° to 130 °C that gives a thermal capacity of around 100 kW_{th} (i.e. solar thermal collectors, geothermal heat source etc). The ORC engine design is therefore based on a heat cycle of a capacity of 100 kW_{th}. The investigation starts for operation at full load and then the operation at partial load will also be presented (20 and 60 kW_{th}). For the organic fluids' properties, the commercial software REFPROP is used, mostly due to its connectivity to the EES software [2.6]. For the design of the organic Rankine cycle a slight sub- cooling (equal to 5 K) of the working fluid at the pump's inlet is considered, in order to avoid cavitation phenomena. For similar reasons, a slight superheating of the organic fluid is considered before the entrance at the expander (equal to 5 K), in order to avoid the expansion within the two- phase area (which would endanger the expander's condition and would decrease the power production). In all cases the condensation temperature is considered equal to 40°C (condensation temperature almost equal to the evaporation temperature of the organic fluid).

In the organic fluid selection process, all the possible candidates of Table 2.1 are examined. With the use of the aforementioned equations (2.1 -2.6) in the EES software, the organic fluids are tested in terms of mass flow rate, ORC thermal efficiency, thermal efficiency with heat recovery and specific volume ratio. The intermediate pressure of the two expanders is calculated as follows: according to the literature, in a two- stages expansion the maximum power production is realized when each expansion step has the same pressure ratio and this criterion was selected to the current configuration [2.8]. Based on that and from Figure 2.4, the intermediate pressure (P_4) is given: $\frac{P_3}{P_4} = \frac{P_4}{P_5} \Rightarrow P_4 = \sqrt{P_3 * P_5}$ (2.7).

In case of full load operation (100kW_{th}) the evaporation temperature is considered at 115°C and with 5 K superheating the maximum temperature of the organic fluid is 120 °C (a linear interpolation of the evaporation temperature with

the heat power input is assumed). For thermal load 60kW_{th} , the evaporation temperature is 90°C and for 20 kW_{th} the evaporation temperature is 60°C .

The results of the organic fluids investigation for operation at full and partial load are presented in Tables 2.3-2.5 below. It should be noticed that in the cases of propane, R134a and R227ea, whose critical temperature is lower than 120°C , the organic fluid is superheated up to that temperature with pressure lower than the critical one. This explains the great difference in specific volume ratios.

Table 2.3 Organic fluid results for operation at 100 kW_{th}

Organic fluid	Mass flow rate (kg/s)	Total specific volume ratio of the two expanders (-)	ORC thermal efficiency (%)	ORC thermal efficiency with heat recovery (%)
Propane	0.23	2.96	7.71	8.58
R-134a	0.44	3.41	7.85	8.71
R-227ea	0.59	3.72	6.89	8.33
R-236ea	0.51	7.89	9.91	10.77
R-245fa	0.43	7.93	10.50	11.34
Butane-R600	0.23	5.75	10.44	11.28

Table 2.4 Organic fluid results for operation at 60 kW_{th}

Organic fluid	Mass flow rate (kg/s)	Total specific volume ratio of the two expanders (-)	ORC thermal efficiency (%)	ORC thermal efficiency with heat recovery (%)
Propane	0.17	2.91	6.69	6.70
R-134a	0.32	3.31	6.87	6.91
R-227ea	0.44	3.68	6.45	6.94
R-236ea	0.36	3.62	7.17	8.10
R-245fa	0.30	3.72	7.50	8.44
Butane-R600	0.16	3.12	7.45	8.38

Table 2.5 Organic fluid results for operation at 20 kW_{th}

Organic fluid	Mass flow rate (kg/s)	Total specific volume ratio of the two expanders (-)	ORC thermal efficiency (%)	ORC thermal efficiency with heat recovery (%)
Propane	0.06	1.43	2.85	2.90
R-134a	0.11	1.50	2.89	2.95
R-227ea	0.16	1.56	2.77	2.90
R-236ea	0.20	1.58	2.93	3.50
R-245fa	0.16	1.60	3.00	3.59
Butane-R600	0.08	1.50	2.99	3.57

One of the criteria for the organic fluid selection is the mass flow rate. The mass flow rate is preferably small in order to use smaller pump and expanders for lower installation cost. In terms of the mass flow rate, in all cases of Tables 2.3-2.5, it is obvious that the propane and the butane present the lowest values. However, the propane presents low thermal efficiency (with or without heat recovery) in all cases. In terms of thermal efficiency, in all cases the best thermal efficiency presents the R245fa and right after that the butane- R600. In Table 2.3, it is also observed that the three refrigerants whose critical temperature is below 120°C (i.e. propane, R134a and R227ea) present significantly low thermal efficiency, compared to the other three organic fluids, due to their extended superheating. However, the condensation heat recovery provides better thermal efficiency in these cases. Among the two more adequate organic fluids (Butane R600 and R245fa), it should be underlined that butane R600 is a flammable fluid and even though its ignition temperature is high (at around 420°C), special safety measures should be taken during its use. On the contrary, R245fa is not flammable and its cost is much lower than that of Butane R600. Therefore, from the examined and presented above organic fluids, *R245fa* is the most suitable for the current application.

The thermodynamic properties of the selected organic fluid throughout the ORC engine cycle, as well as the state in each point are presented in Table 2.6 below:

Table 2.6 Thermodynamic properties of R245fa throughout the Organic Rankine cycle

Point	State	Temperature (°C)	Pressure (bar)	Enthalpy (kJ/kg)	Entropy (kJ/kg/K)	Specific volume (m ³ /kg)
1	Subcooled liquid	35.00	2.49	245.80	1.157	0.000762
2	Subcooled liquid	35.43	17.45	246.80	1.157	0.000760
3	Superheat vapor	120.00	17.45	489.60	1.817	0.009937
4	Superheat vapor	88.11	6.59	474.30	1.824	0.02955
5	Superheat vapor	64.29	2.49	458.10	1.183	0.07879

2.2.3 Components design and ORC engine modeling

The most important control and design parameters of the ORC engine are:

- The evaporation temperature of the organic fluid HFC- R245fa, which depends on the organic fluid pump's monitoring (change of the rotational speed), on the available thermal load input and on the mass flow rate of the working fluid on the heat cycle
- The high pressure of the thermodynamic cycle (points 2 and 3)
- The intermediate expansion pressure of the two expanders (related to the efficiency of each expander) at point 4
- The condensation temperature (related to the cooling system operation)

The result of these parameters' research is the optimized design of the organic cycle and the quantification of their influence. As mentioned in the previous paragraph, for the sake of design, in this research the mass flow rate of the working fluid on the heat cycle (MEG) is considered to remain constant and the thermal power input at the ORC engine is equal to the capacity of the electric heater (i.e. 100 kW_{th}). Therefore, for the current analysis, the variation of the thermal input is a linear function of the heat cycle's working fluid temperature, thus the organic fluid's evaporation temperature. The ORC engine investigation starts with the operation at full load (100kW_{th}) and consequently the operation at partial load is also examined.

2.2.3.1 ORC organic fluid pump

The organic fluid pump increases the pressure and controls the mass flow rate of the organic fluid. Indicative suction pressure values are 2-5 bar and discharge values are 10-35 bar (also see Table 2.6), depending on the organic fluid selected and the evaporation temperature [2.7, 2.8, 2.11, 2.15, 2.19- 2.24]. Therefore, the organic fluid pump must be able to transport the fluid through high pressures, while providing the required mass flow rate ($\sim 0.5-1$ kg/s) [2.1, 2.2, 2.7, 2.19]. Moreover, the organic fluids have low viscosity, thus lubrication issues with the pump's moving parts occur. A possible solution is the adding of lubricating oil to the system alongside with the organic fluid, which amplifies the heat transfer in the heat exchanger [2.16]. The lubrication oil may separate before the expander's entrance in order to increase the efficiency of this component, even though it would help its lubrication as well as the possible leakage decrease from its clearances, which would decrease the produced power. However, the use of lubricant oils separator in such small-scale ORC systems – as the one currently developed- is avoided, therefore the selection of a special pump, which can operate efficiently under these conditions and with the lowest possible number of components that would increase the system's and the monitoring's complexity, is required.

In such systems, a piston- diaphragm pump is usually selected, which is suitable for all applications [2.1, 2.2, 2.7, 2.19]. These pumps are industrial positive replacement pumps. They consist of a diaphragm and a vessel, as well as of suction and depression valves in order to block the organic fluid's return to the vessel. The pistons may be directly connected to the diaphragm or impel hydraulic oil, which pulsate the diaphragm. The diaphragm pumps are very credible since they do not include internal moving parts which would cause friction between them. There are two types: with one or two diaphragms. Moreover, there are no internal leakages during their operation that would cause a decrease at the system's efficiency. The diaphragm pumps have high mechanical efficiency throughout a wide operation range (rotational speed, mass flow rate, pressure), while they can operate under high pressure (of 30 bar) with low volume flow rate (of 100 l/min). The ORC engine operation conditions lay within those limits.

Another possible candidate would be a centrifugal pump, similar to those used for water transportation [2.19]. These pumps decrease the pressure at the depression line with the increase of the mass flow rate. They are suitable for the transport of liquids with very high mass flow rates (of several m^3/min), however with low pressure (of several bar).

The final selection of the most adequate type of pump will be presented in the next chapter, where the prototype design and construction will be observed. The monitor of this pump in the current application is realized with control of the rotational speed, thus change of the power consumption. The variation of the rotational speed provokes a change of the mass flow rate of the organic fluid, which strongly influences the evaporation temperature when the thermal power input is constant. As presented before, the available thermal input provided to the organic Rankine cycle in any moment is equal to:

$$Q_{ORC} = \dot{m}_{ORC} * (h_3 - h_2) \quad (2.3)$$

Therefore, by alternating the mass flow rate \dot{m}_{ORC} , the enthalpy h_3 - which is the maximum enthalpy of the organic fluid during its evaporation (assuming steady state of the organic fluid at the pump inlet) is influenced.

With the assumption that the thermal power input corresponds to the electric heater's thermal capacity (100 kW_{th}), that the expanders' rotational speed is constant in order to alternate the maximum cycle pressure and that the slight sub cooling and superheating are maintained as explained previously, Figure 2.6

below presents the maximum temperature of the ORC engine and the power consumption change during mass flow rate variation at maximum load:

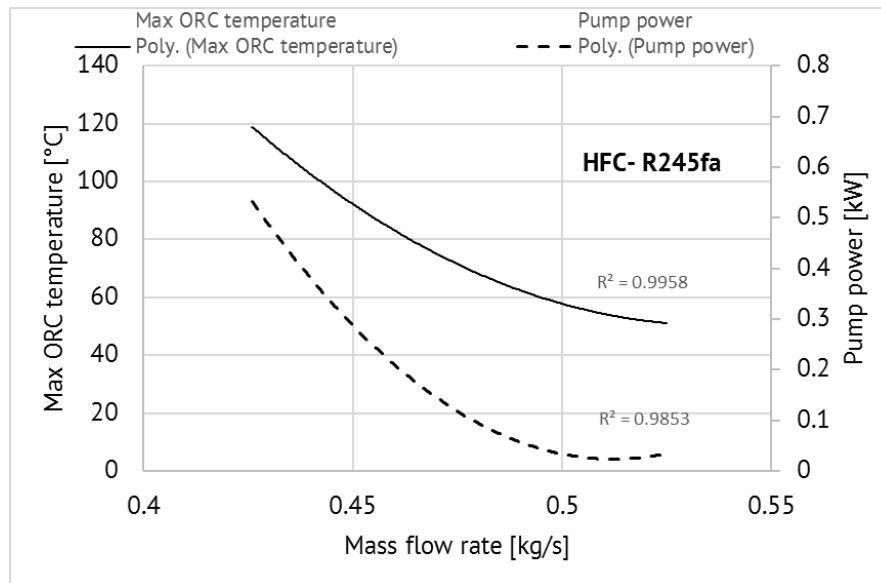


Figure 2.6 Organic fluid maximum temperature and pump's power consumption variation during the mass flow rate change at 100kW_{th} power input

As it is observed in Figure 2.6, for a small mass flow rate variation of less than 20% which is caused by a change of the pump's rotational speed, the maximum temperature of the cycle shows an important decrease (from 120 °C to 50°C) alongside with a change of the maximum pressure (from 17.5 to 3.5 bar). This strongly affects the cycle's efficiency which drastically decreases, as well as the produced power from the expanders, even though the mass flow rate increases. The pump's power consumption decreases since the organic fluid is compressed to a lower evaporation temperature. Figure 2.6 shows the great importance of the pump's rotational speed control in order to result in the desirable mass flow rate of the organic fluid for the increase of the operating temperature which influences the ORC engine efficiency.

In Figure 2.7, the same diagram is presented for operation at partial load (60 and 20 kW_{th}):

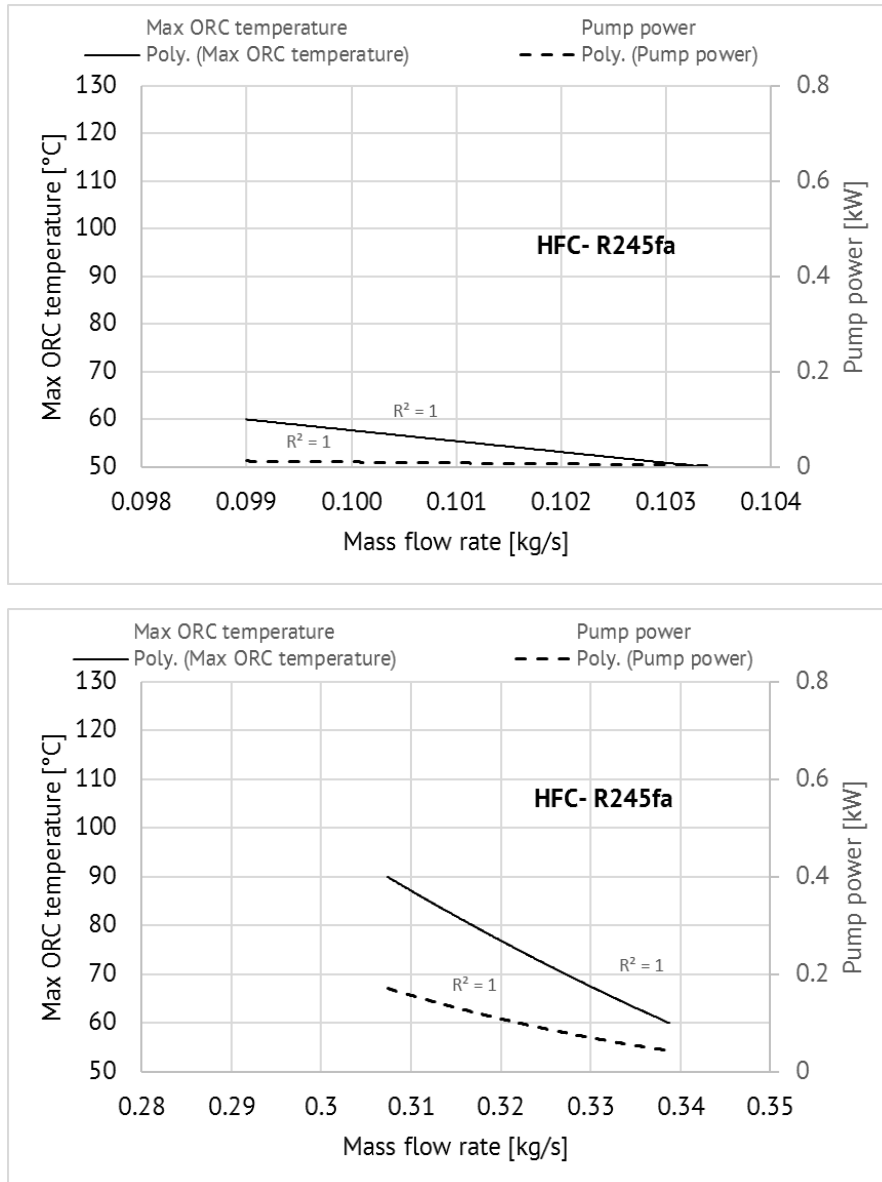


Figure 2.7 Organic fluid maximum temperature and pump's power consumption variation during the mass flow rate change at 20 kW_{th} and 60 kW_{th} power input respectively

In Figure 2.7, it is obvious that in partial load operation a more detailed control of the mass flow rate is required in order for the ORC engine to operate close to the optimized operation point each time. During the thermal load variation throughout the whole operation range (0-100%) the operation points that maximize the thermal efficiency of the ORC engine and depend on the mass flow rate of the organic fluid were calculated. These points correspond to the design points of the thermodynamic cycle which has been previously presented. In Figure 2.8 the optimized mass flow rate and the optimized pump power consumption with the thermal load variation are presented:

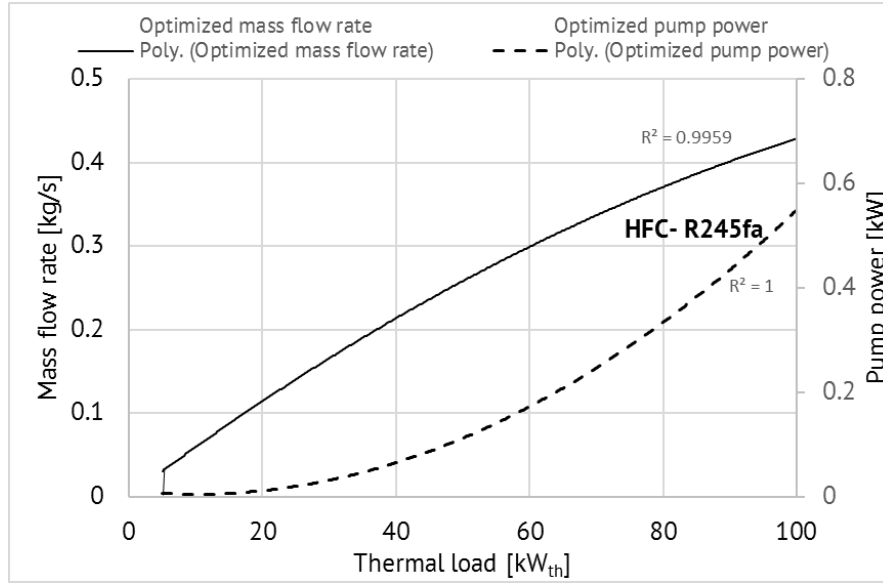


Figure 2.8 Optimum organic fluid mass flow rate and pump power during the thermal load change

The detailed control of the mass flow rate is presented in the next chapter of the prototype construction. A way to control the pump is to assume that the volumetric flow rate of the pump (\dot{V}_p [m³/s]) changes linearly with the pump's rotational speed (rpm) through a proportionality factor "c", as follows:

$$\dot{V} = c * (rpm) \quad (2.8).$$

A common value for factor "c" and for the kind of pumps examined here, is around 10⁻⁶ m³/s/rpm [2.25]. The mass flow rate is related to the specific volume (v_p [m³/kg]) of the working fluid by the relation:

$$\dot{m} = \frac{\dot{V}_p}{v_p} = \frac{10^{-6} * (rpm)}{v_p} \quad (2.9).$$

For the selected organic fluid R245fa, the change of the specific volume inside the pump is neglected, since the fluid remains in the liquid phase and its optimum value is slightly influenced by the thermal load. As derived from the previous analysis, for each load tested, the specific volume of the fluid at the pump inlet is around 0.000763 m³/kg and at the outlet 0.000760 m³/kg for high thermal load and 0.000763 m³/h for low thermal load. The optimum regulation of the pump rotational speed during the thermal load variation is presented in Figure 2.9 below.

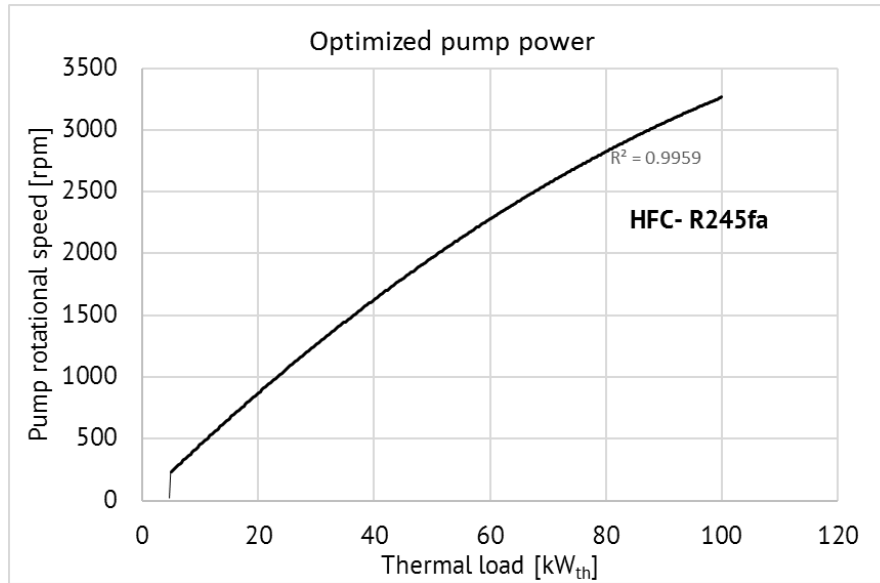


Figure 2.9 Optimum pump speed during thermal load variation

The maximum value of the rotational speed that derives from Figure 2.9 remains within the operation limits of most of the pumps that can be used in the current application.

2.2.3.2 ORC expanders

As mentioned before during the system simulation in EES, from the literature it is known that the maximum power production in a two- stage expansion is realized when the two expansions have the same pressure ratio [2.8]. Based on this criterion, in the current application two expanders have been selected in order to increase the system's flexibility (operation at low thermal load). The intermediate pressure is given from equation (2.7): $\frac{P_3}{P_4} = \frac{P_4}{P_5} \Rightarrow P_4 = \sqrt{P_3 * P_5}$. With the thermal load decrease, the maximum temperature of the ORC cycle decreases as well, therefore the total pressure ratio of the expanders (P_3/P_5) decreases. With the further increase of this ratio, a range of values occurs, where the isentropic efficiency of these components is significantly low [2.21, 2.16, 2.26]. Therefore, from a crucial thermal load and below, it is more efficient to completely by- pass the first expander and operate only one expander with higher pressure ratio and higher isentropic efficiency. In this way, those volumetric machines operate with high efficiency (of 60%) throughout the most of the thermal load, increasing simultaneously almost proportionally the total efficiency of the integrated system [2.14, 2.22, 2.23, 2.27]. The first expander by- pass is realized with the use of an electro- valve, as presented in Figure 2.10:

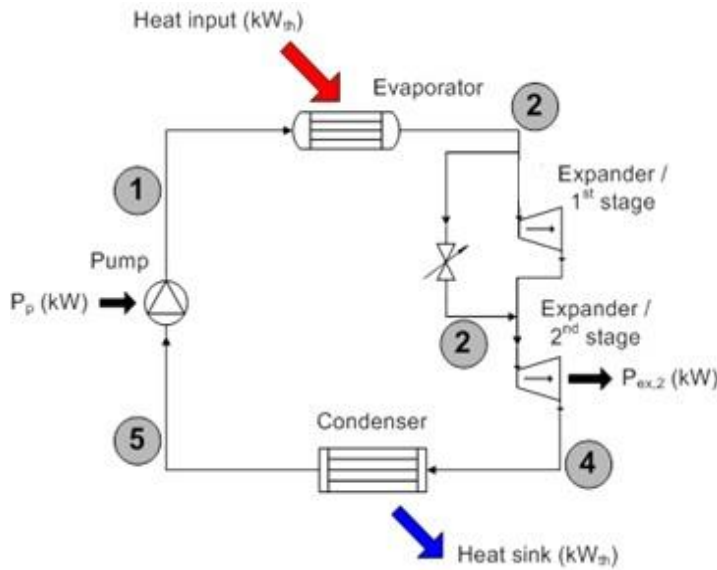


Figure 2.10 Organic Rankine cycle configuration with first expander by-pass in low thermal load operation

During the thermal load variation, the mass flow rate of the organic fluid—thus the pump's rotational speed, should be monitored in order to increase the ORC engine efficiency. Therefore, the rotational speed of the expanders should be simultaneously controlled in order to control the evaporation temperature, thus the expanders' inlet pressure [2.28, 2.29]. At the same time, a slight superheating is set (5 K). The optimum evaporation pressure for the best ORC efficiency, throughout the whole operation range, as well as the intermediate pressure of the expanders are presented in Figure 2.11 below:

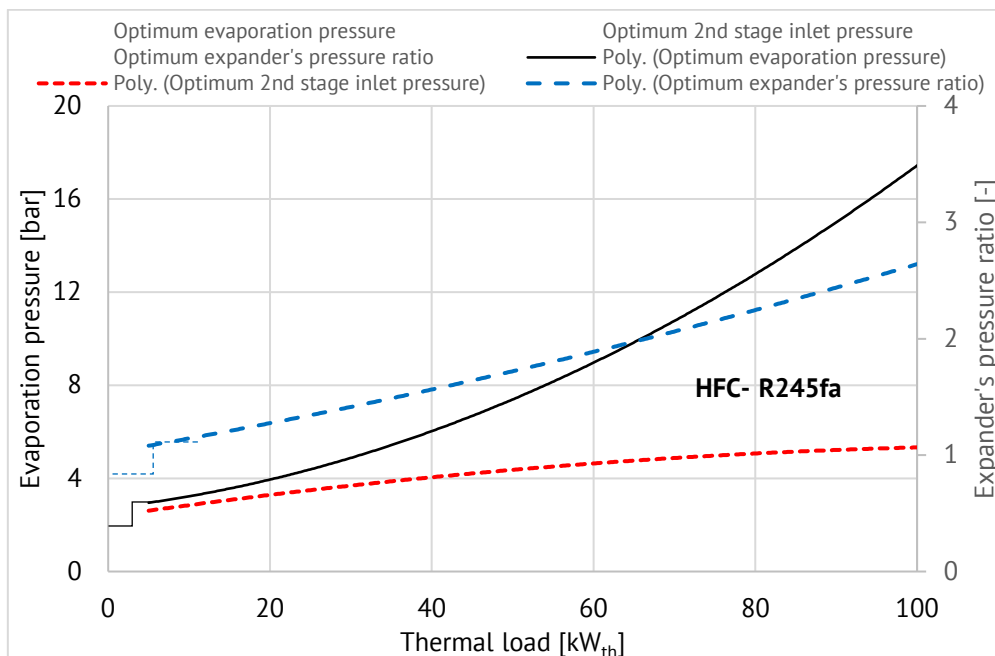


Figure 2.11 Optimum evaporation and expanders' inlet pressures and expanders' pressure ratio for ORC efficiency optimization

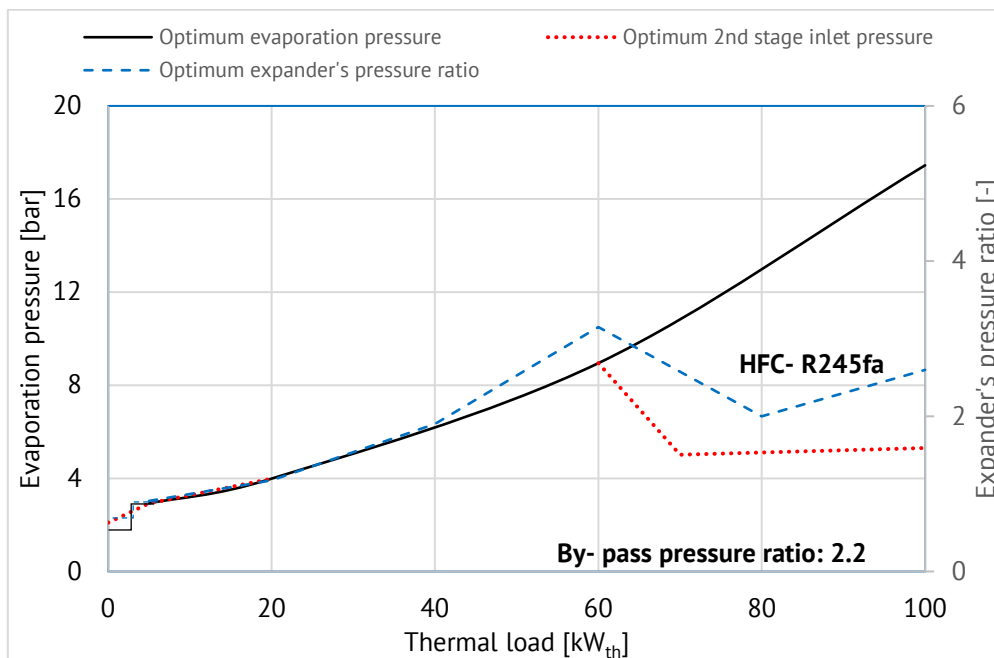
In Figure 2.11, it is observed that the optimum inlet pressure at the first expander drastically decreases with the thermal load decrease. At full load

operation, it is close to 17 bar, while at the 50% of the thermal load this value decreases to almost 7.5 bar. The inlet pressure at the second expander depends less on the thermal load and its total variation is from almost 6 bar to 2.5 bar. Moreover, the pressure ratio of each expander widely varies with the decrease of the thermal load and it reaches the value 1 when the thermal load is less than 5 kW_{th} and the system operation stops.

At this point, an initial detection of the monitoring of the ORC engine can be discussed. The pressure ratio in Figure 2.11 at full load operation is near 3, when for operation at 60% of the thermal load it decreases to 2. Most of the expanders that can operate at the power range examined for the current application, present efficient operation at pressure ratio from around 2 to 4 [2.13]. Therefore, when the pressure ratio is less than 2, the two expanders will present an efficiency decrease, since their isentropic efficiency drops. When the pressure ratio falls to less than 1.5 (almost 30% of the thermal load input), both expanders will start to present problems during their operation [2.13, 2.21], such as instability and high cyclic dispersion. Therefore, the by-pass of the first expander is then required and only the second one operates in higher pressure ratio.

An optimization factor deals with the appropriate operation point where the first expander should be by-passed. In Figure 2.12 below, the characteristic curves with the by-pass of the first expander are presented, for two extreme pressure ratio values. In the first case, the by-pass of the first expander is realized for high pressure ratio and in the second case for low pressure ratio.

It should be noted that the pressure ratio which appears when the first expander has been by-passed (for pressure ratio equal to 2.2 or 1.5 in each case) is the pressure ratio that corresponds only to the second expander, since the first one does not operate.



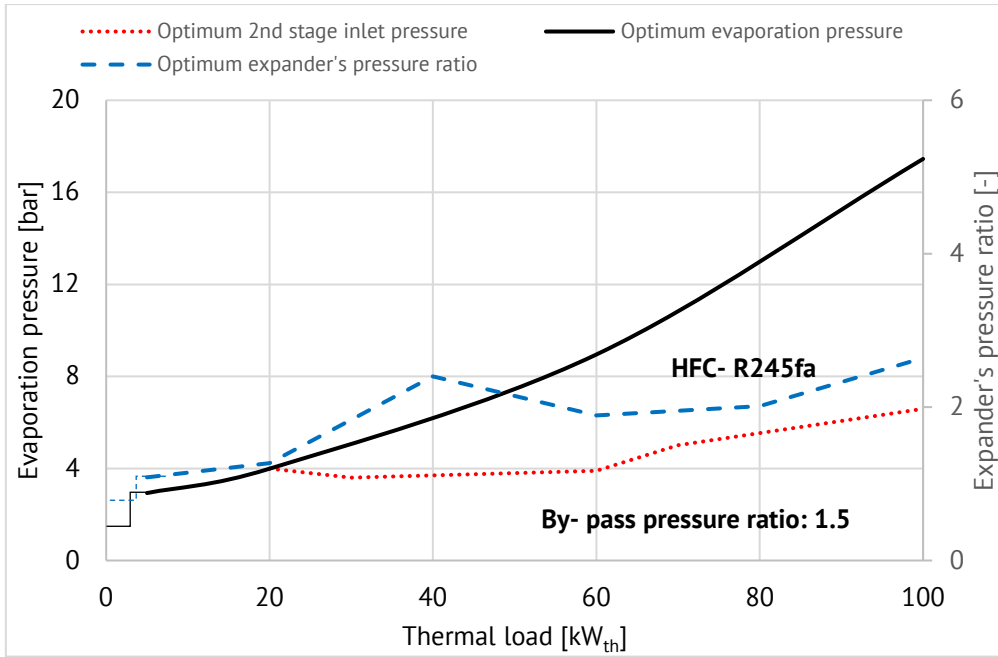


Figure 2.12 Optimum inlet pressure and pressure ratio of each expander during the by- pass of the first expander with two different strategies (by- pass pressure ratio 2.2 and 1.5)

As mentioned previously, the control of the pump's rotational speed changes the mass flow rate of the organic fluid, as well as the pump's power consumption. This mass flow rate is provided to the expander- after evaporation at the evaporator- and the expander as any volumetric machine can support a specific volumetric rate. Since the mass flow rate is controlled by the pump and the volumetric flow rate from the expander, the organic fluid's pressure at the expander's inlet will change with the change of the rotational speed of the expander, according to the equation:

$$p_{ex,in} = \rho_{ex,in} * R * (T_{ex,in} + 273.15) \quad (2.10),$$

where $p_{ex,in}$, $\rho_{ex,in}$ and $T_{ex,in}$ are the pressure, the density and the temperature of the evaporated organic fluid at the expander's inlet and R is the specific gas constant ($R_{specific}$ is the ratio R/M , where R is the ideal gas constant equal to 8.314 J/mol.K and M is the molecular mass where for R245fa is equal to 134.05 kg/kmol, [2.31]). The density is directly related to the mass flow rate (pump control) and the volumetric flow rate of the expander (expander control). The volumetric flow rate of the expander as a function of its rotational speed (in [rpm]) is given as:

$$V_{ex,in} = V_{swept} * FF * \frac{rpm_{ex}}{60} \quad (2.11),$$

where V_{swept} is the swept volume of the expander which is a geometric characteristic of the expander and remains constant during its operation. Typical values for this volume for expanders of low power production (several kW) are around 100- 150 cm³. The filling factor FF has an almost constant value throughout the whole operation range of the expander which relates to its characteristics. Usual values for the FF factor are 0.6- 1.0 [2.15, 2.21], and it also relates to the volumetric efficiency of the expander during its operation in a scroll compressor mode.

In Figure 2.13 below, the volumetric flow rate of the expander during its rotational speed variation within a typical limit of 500 to 5000 rpm for several swept volumes (100 and 150 cm³) and filling factors (0.6 and 1.0) is presented:

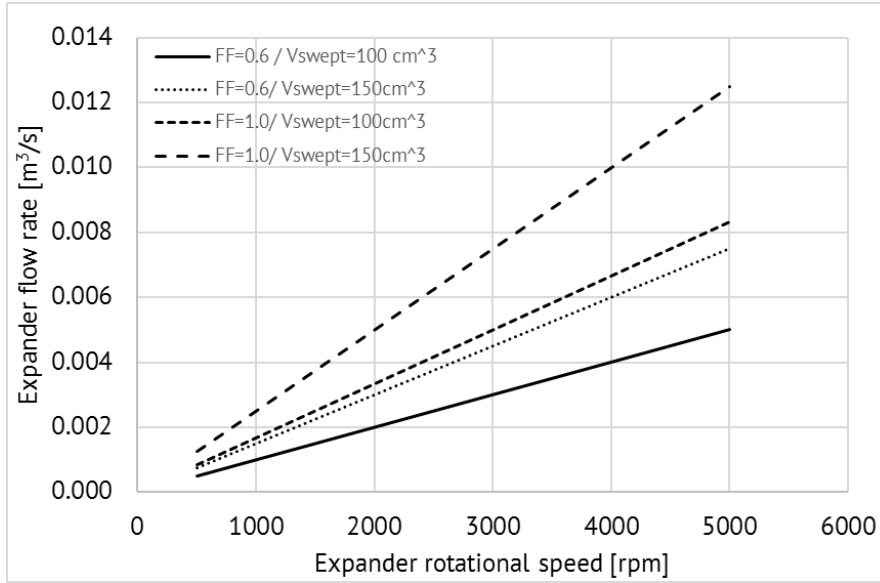


Figure 2.13 Expander flow rate variation with the rotational speed for two filling factors and two swept volumes

The density is calculated by the equation: $\rho_{ex,in} = \frac{\dot{m}_{ex,in}}{\dot{V}_{ex,in}}$ (2.12)

With the use of equations (2.10, 2.12 and 2.5), the relation between the pressure of the organic fluid with the rotational speed of the expander and the pump (since $\dot{m}_{ex,in} = \dot{m}_p$) occurs:

$$p_{ex,in} = \rho_{ex,in} * R * (T_{ex,in} + 273.15) \Rightarrow p_{ex,in} = \frac{10^{-6} * (rpm_p) * v_p}{V_{swept} * FF * \frac{(rpm_{ex})}{60}} * R * (T_{ex,in} + 273.15) \quad (2.13)$$

In case the pump rotational speed is kept steady for steady thermal load, the expander's rotational speed determines the evaporation pressure. Little influence does it have in the evaporation temperature, which mainly depends on the thermal load. The correlation of the pressure with the rotational speed is presented in Figure 2.16, where the expander's characteristics have been chosen based on representative values and the optimum rotational speed of the pump is assumed to be 1000 rpm (load equal to 30% based on Figure 2.11):

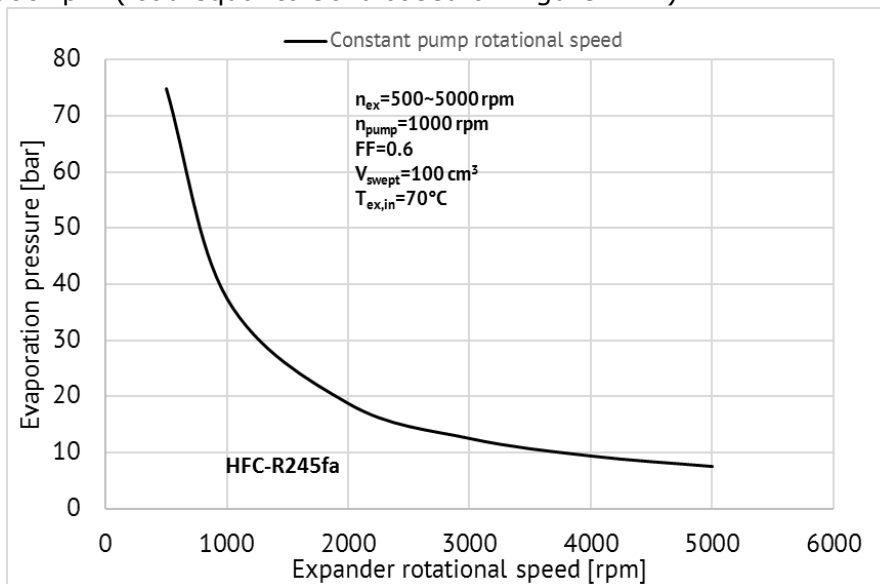


Figure 2.14 Evaporation pressure during the first expander's rotational speed variation

In Figure 2.14, it is observed that in low rotational speed the pressure increases dramatically. However, throughout the most of the whole expander's operation range the values of the evaporation pressure lay within acceptable limits [2.30], for 1500 rpm and above.

The organic fluid conditions (temperature and pressure) at the inlet of the second expander greatly depend on the expansion at the first expander. The isentropic efficiency of the expansion plays a major role at the condition of the organic fluid at the first expander's outlet (which is the second expander's inlet since they are connected in series). The inlet pressure at the second expander also influences the efficiency of the first expander. Therefore, a careful control of the rotational speed of the second expander is required since it is related to the first expander's efficiency. Using the expander's operation curves, the organic fluid conditions can be determined at the first expander's outlet (since the outlet temperature is known). Therefore, the equation (2.13) can be used for the calculation of the inlet pressure at the second expander:

$$p_{ex,in2} = \frac{10^{-6} * (rpm_p)}{V_{swept} * FF * \frac{(rpm_{ex2})}{60}} * R * (T_{ex,in2} + 273.15)$$

The second expander's inlet pressure variation is presented in Figure 2.15 below. This expander should have a larger swept volume than the first one, since it deals with greater volumetric flow rate, due to lower pressure and the volumetric flow rate at the inlet.

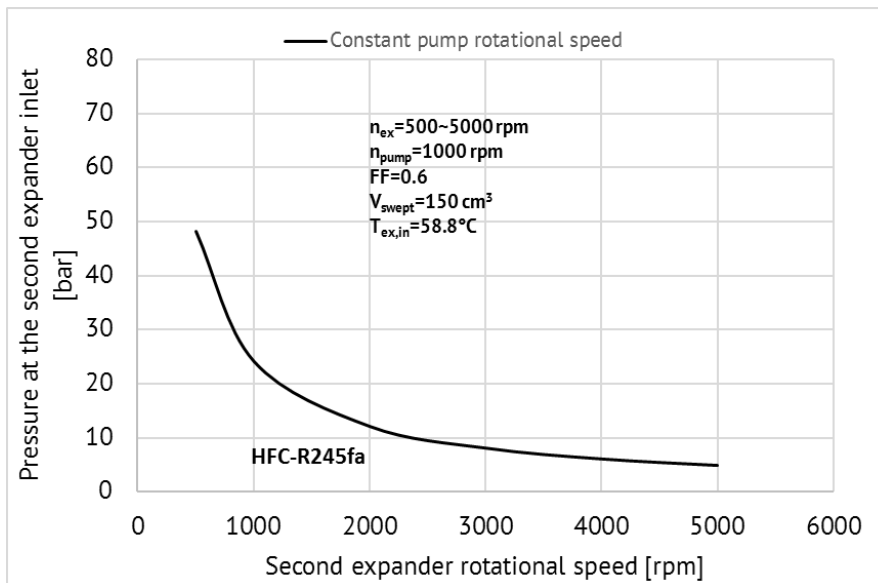


Figure 2.15 Inlet pressure at the second expander during the second expander's rotational speed variation

The pump's rotational speed varies as a function of the thermal load input according to Figure 2.9. In this case, for the optimum operation of the ORC engine, the rotational speed of the two expanders should vary simultaneously. In Figure 2.16, such a variation is presented for the whole operation range (0-100 kW_{th}). The results presented in Figure 2.16 take under consideration the thermal load, the mass flow rate variation and the operation temperature of the HFC- R245fa. It should also be noticed that for the calculations, the first expander's by- pass at low load has not been considered.

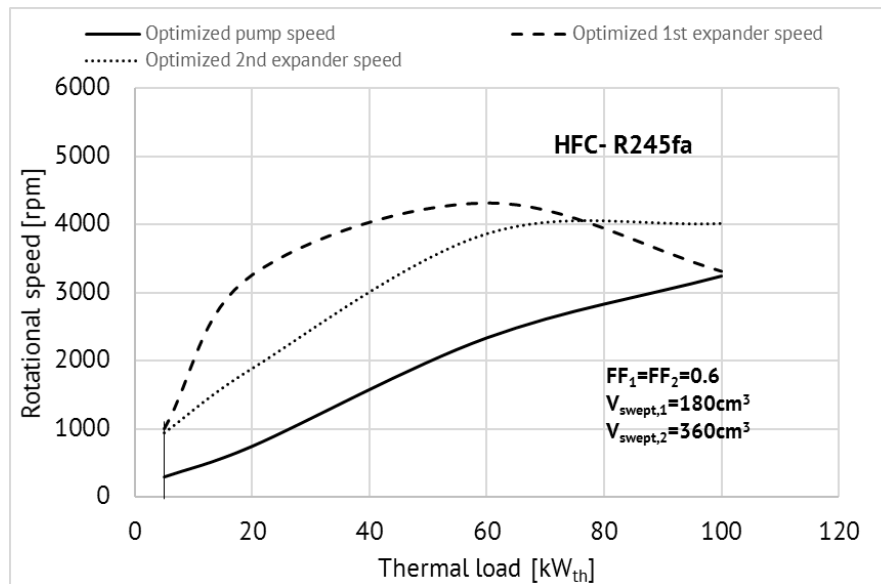


Figure 2.16 Optimum rotational speed of the pump and the two expanders during the thermal load variation

In Figure 2.16, it is observed that in low thermal load the rotational speed of the first expander is higher than the one of the second expander. The opposite seems to happen in higher thermal load operation. The second expander's swept volume is significantly higher than the first one (360 cm^3 rather than 180 cm^3 of the first expander) in order to avoid an excess increase of the rotational speed that would consequently cause a radical increase of the mechanical losses [2.11]. However, the rotational speed of the second expander shows significantly high values especially in high thermal load input.

A crucial result of the above expanders investigation is that the rotational speed can hardly relate to the rest of the properties that have been taken under consideration during the optimization of the ORC engine. Moreover, the expanders used in the current application are scroll expanders which are practically scroll compressors in reverse operation. Therefore, their characteristic curves are not available from their manufacturer and they need to be approached through the experimental investigation that will be presented in Chapter 5.

According to manufacturers of scroll compressors, each expander is capable to operate through a wide range of rotational speed which is related to the electric current frequency of their asynchronous generator, and it varies between 500 and 5000rpm [2.32]. However, the operation at such a wide range should be avoided in order for the expanders to operate more efficiently. Since the current designed system will operate in a fluctuated power input the expanders should alternate their rotational speed according to their operation point in order to optimize their operation. This variation should happen within the manufacturers limits, avoiding possible operation problems such as metal friction, poor lubrication etc. With low swept volumes the rotational speed of the expanders increases, since the same expander is supposed to manage the same volumetric flow rate, therefore it increases the rotational speed in order to keep the evaporation pressure at the optimum value. Moreover, the rotational speed of the one expander does not depend on the swept volume of the other expander. Therefore, the selection of the appropriate first expander can be realized separately of the selection of the second expander, which facilitates the final system design.

Finally, in Figure 2.17, the optimum power production of each expander during the power input variation is presented:

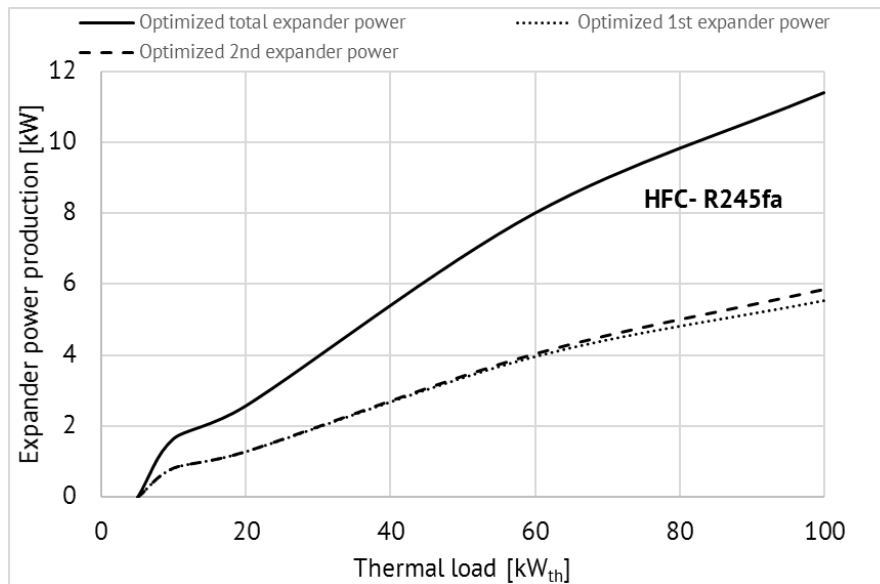


Figure 2.17 Optimum power production of the two expanders during the thermal load input variation

The mass flow rate of the two expanders is the same, since they are connected in series, however an important observation of Figure 2.17 is that the power production of the second expander is slightly higher than the one of the first expander especially for high thermal load, due to the difference of the specific volume of the organic fluid at the inlet of each expander. Moreover, with the thermal load input increase, the total power production of both expanders drastically and non-linearly increases, while at the maximum thermal load input it gets the value of almost 11 kW.

2.2.3.3 Heat exchangers of the ORC engine (evaporator & condenser)

As previously mentioned, the organic fluid, should be slightly superheated at the expander's inlet and slightly subcooled at the pumps inlet, in order to avoid a two-phase condition in those components.

The heat exchangers that are used in the current application are counter-flow plate heat exchangers, since they present the optimum heat exchange properties and have a higher total heat exchange coefficient in comparison to other shell and tube exchangers [2.33- 2.36]. This means that a smaller total heat exchange area is used, a fact that significantly decreases the system cost. Since the maximum operation pressure is kept within low values (lower than 20 bar), the use of these heat exchangers is permitted, since they have maximum pressure limit equal to almost 35 bar.

At the beginning, the superheating (temperature difference from the temperature of the saturated vapor: dT_{sh}) of the organic fluid at the evaporator's outlet is investigated, as well as its sub cooling (temperature difference from the saturated liquid: dT_{sc}) at the condenser outlet. This investigation relies on the thermal efficiency of the cycle.

The superheating of the organic fluid depends on the evaporator's operation, since in low grade ORC engines there is no super-heater and all the heat exchange is realized within the evaporator [2.22]. In the current application the superheating variation results in thermal efficiency variation. In general, the more the superheating (for constant thermal input) the less the thermal efficiency [2.37], in case that there is no heat recovery [2.38]. Therefore, the thermal efficiency during the superheating temperature is investigated. In order to do that, all the other

properties are assumed to remain constant. The investigation takes place for three different values of thermal load input that correspond to high load (100 kW_{th}), to medium load (60 kW_{th}) and low load (20 kW_{th}). During the superheating temperature variation, the maximum organic fluid temperature in any load remains constant, therefore in each case the evaporation pressure and temperature vary. In Figure 2.18, the influence of the superheating at the thermal efficiency of the ORC engine for the three different values of the thermal load input is presented:

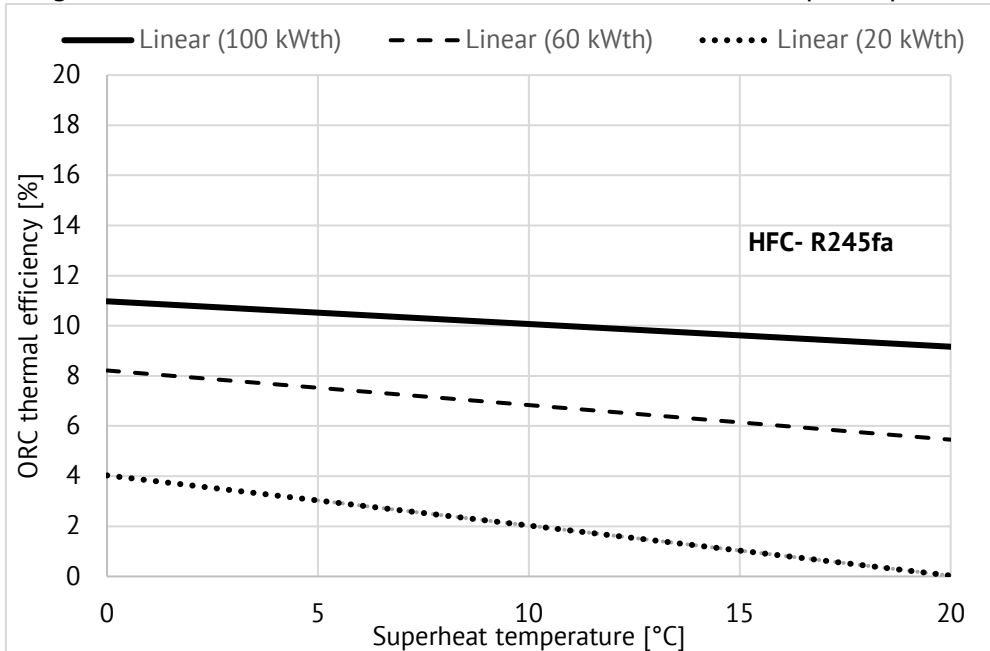


Figure 2.18 Thermal efficiency during the superheat temperature variation for three thermal load operation points

As observed in Figure 2.18, in case that no superheating is applied, the thermal efficiency is increased. Moreover, during the thermal load increase, the superheating seems to affect less the thermal efficiency. However, a slight superheating is necessary in order to avoid a two-phase mixture of the organic fluid at the inlet and outlet of the expander. The expander's operation at the two-phase area significantly decreases the capacity of the expander to produce power, since the liquid part of the mixture does not participate in the power production. Therefore, a slight superheating of 5 K (as it has been assumed in the previous system simulation) is considered necessary for the efficient operation of the ORC engine throughout the whole operation range, as well as during its sudden change.

The evaporation pressure variation with the superheat temperature for several thermal load inputs is presented in Figure 2.19:

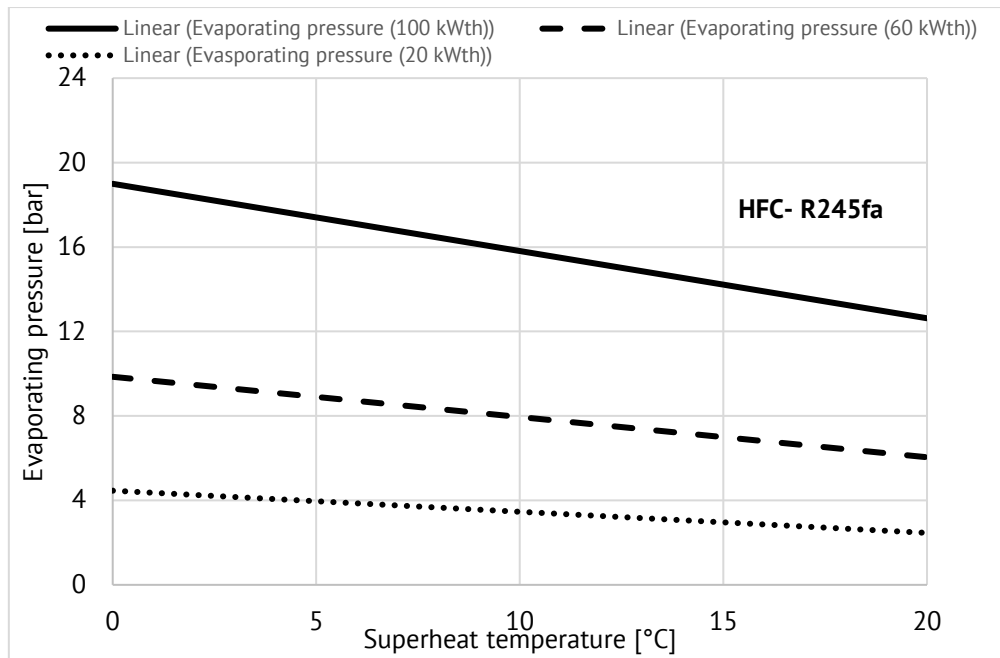


Figure 2.19 Evaporating pressure during the superheat temperature variation for three thermal load operation points

As the superheat temperature increases, the evaporating pressure significantly decreases. Therefore, the organic fluid pump power consumption decreases as well. This fact though, does not provoke a thermal efficiency increase since simultaneously the power production from the expanders also decreases.

The influence of the subcooling of the organic fluid at the thermal efficiency is examined next. The subcooling depends on the condensation temperature and on the organic fluid total mass in the closed system [2.16]. The minimum temperature of the organic fluid is assumed to be constant (constant condenser efficiency and temperature difference), therefore the sub-cooling variation provokes condensation pressure and temperature variation as well. In Figure 2.20 below, the effect of the sub-cooling in the thermal efficiency is presented and in Figure 2.21 the effect on the condensation pressure is shown. Once again, the investigation takes place for three different thermal load input values (100, 60 and 20 kW_{th}).

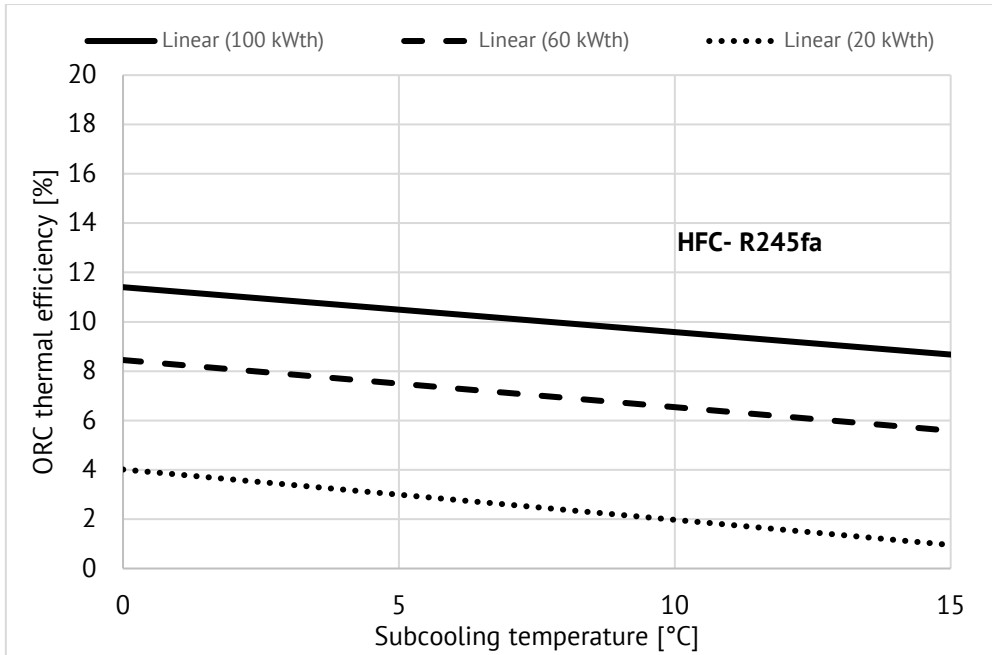


Figure 2.20 Thermal efficiency during the subcooling temperature variation for three thermal load operation points

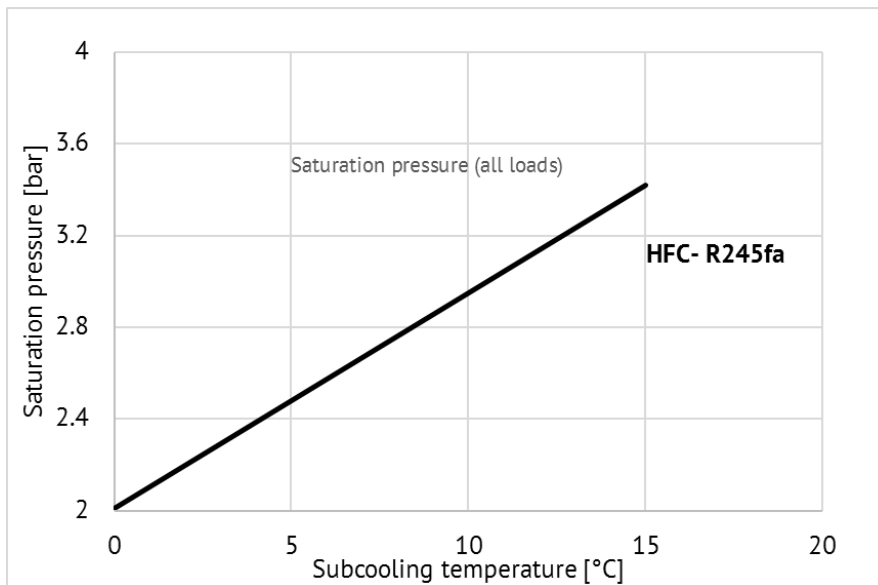


Figure 2.21 Saturation pressure during the subcooling temperature variation for three thermal load operation points

The saturation pressure in Figure 2.21 is the same for all three thermal load input values and is only influenced by the subcooling temperature. During the subcooling temperature increase, the saturation pressure increases as well and this provokes the following consequences:

- Pump power consumption decrease, since the maximum pressure (evaporation pressure) is kept constant
- Expanders' power production decrease, due to the operation in lower pressure ratio, since the organic fluid outlet from the second expander is under high pressure and temperature.

Especially the second consequence plays a major role from a thermodynamic point of view, since with the subcooling temperature increase the thermal efficiency decreases (as presented in Figure 2.22) and more intensively in comparison to the superheating temperature (see Figure 2.21). Therefore, from a thermodynamic point of view, the conservation of the subcooling temperature in low values is desirable. The slight subcooling is necessary in order to avoid the cavitation phenomena inside the pump, especially in high load operation where the pressure ratio of the pump is high (around 8~9). Moreover, the pump does not pump- off organic fluid that remains in the gas phase (two- phase mixture) during the thermal load variation. Therefore, a slight subcooling of 5 K, as selected during the simulation, is necessary [2.38] and this value will be used for the ORC engine design.

2.2.3.4 Heat cycle pump (MEG pump)

For the heat cycle pump's consumption estimation, the power calculation equation is used as shown below:

$$P_p = \frac{\rho * g * H * Q}{n_p} \quad (2.15)$$

where ρ is the MEG density, g the gravitational acceleration (9.81 m/s^2), H the total head (with maximum value equal to around 10 m, proportional to the square power of the mass flow rate: $H \sim Q^2$), Q the mass flow rate in $[\text{m}^3/\text{s}]$ (and a maximum value equal to around $7 \text{ m}^3/\text{h}$) and n_p the pump efficiency equal to 75% (see Table 2.2) [2.26]. The equation (2.15) results in a maximum power of the pump of around 0.3 kW. During the mass flow rate variation (and volume), the power variation is presented in Figure 2.22 below, keeping the efficiency value constant (equal to 75%):

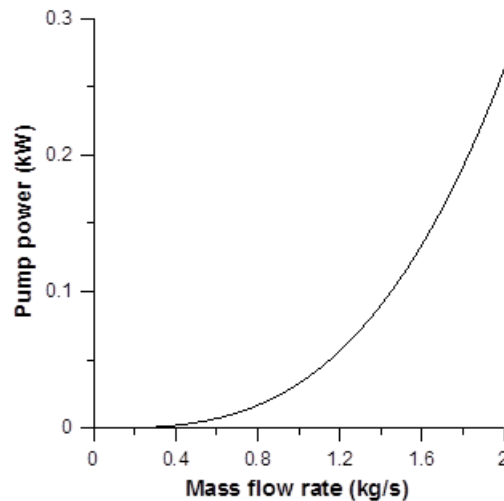


Figure 2.22 Heat cycle pump's power with the MEG mass flow rate variation

This pump will operate under varying rotational speed, in order for the mass flow rate to vary in every operation point, according to the thermal load input variation simulation. The final selection of this pump will be realized in the next chapter.

According to the previous analysis for the organic fluid selection, in full and partial load, the thermal efficiency of the ORC engine during the thermal load fluctuation is presented in Figure 2.23:

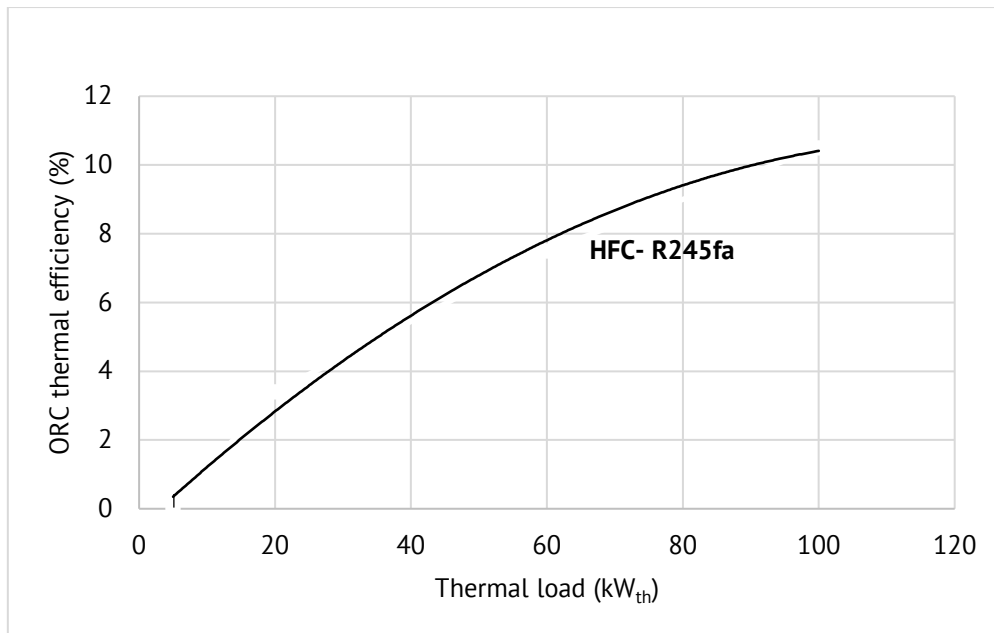


Figure 2.23 ORC engine thermal efficiency during thermal load fluctuation (0-100 kW_{th})

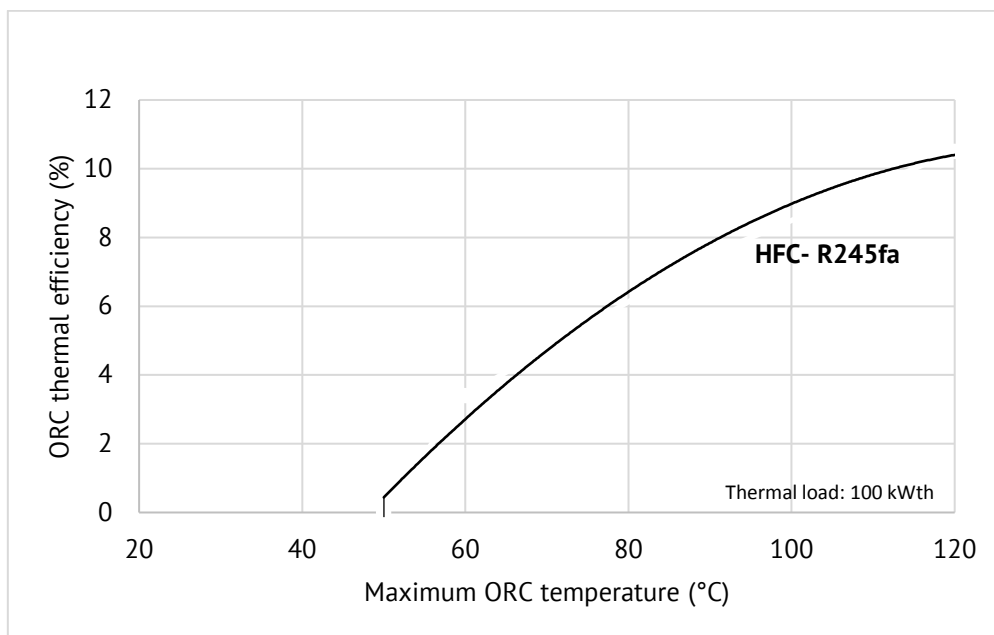


Figure 2.24 ORC engine thermal efficiency during the variation of the maximum temperature of the organic fluid (50- 120°C) for 100 kW_{th}

In Figure 2.24, the ORC engine thermal efficiency as a function of the maximum temperature of the organic fluid is presented. Once the thermal load input falls under the critical value of 5 kW_{th}, it is assumed that the system stops operating since it is not able to cover its own- consumptions (pump consumptions) and especially the required power consumption of the pump on the heat cycle. This operation point corresponds to the organic fluid's temperature of 50 °C (at the evaporator).

2.3 The Reverse Osmosis Unit model

The reverse osmosis process, as mentioned before, is a consequence of the application of an external pressure (P) greater than the osmotic pressure (Π) on a high-density liquid mixture which is separated from a low-density liquid mixture with semipermeable barrier or membrane. In case that no pressure is applied in any of the mixtures, diffusion of solvent (water) is observed from the low-density mixture to the high-density pressure until the concentrations of the two mixtures become equal. Consequently, the two mixtures in equilibrium state will have a different surface level. However, if an external pressure higher than the osmotic pressure is applied on the high-density mixture surface, the flow is reversed and water molecules are diffused from the high-density mixture (e.g. seawater) to the low-density mixture (e.g. permeate). In the end of the process, the result is a high-density mixture (drain) and a low-density mixture (processed/ desalinated water). The flow rate velocity of the water through the membrane is proportional of the difference of the applied pressure ΔP on the high-density mixture and of the osmotic pressure $\Delta \Pi$.

There are four membrane types that are used in reverse osmosis process:

- Spiral wound
- Hollow fiber
- Tubular
- Plate and frame

The main components of a RO desalination unit are presented below:

- ✓ Feed tank and feed pump
- ✓ Pretreatment system
- ✓ High- pressure pump
- ✓ Membranes and membrane vessels
- ✓ Energy recovery device (ERD) (if applied)
- ✓ After- treatment system
- ✓ Piping & fittings
- ✓ Pump and rinsing container of the Clean In Place system (CIP)
- ✓ Control panel and instrumentation (e.g. switch board, flowmeters, pH meters etc.)

In Figure 2.25 a typical low capacity RO desalination unit is presented:



Figure 2.25 Commercial RO desalination unit of a capacity of 2.4 m³/d desalinated water, of a nominal power of 1.8 kW, company TEMAK S.A. (type TSW03 MARINE) [2.40]

Lately, almost all RO seawater desalination units have an ERD system. These systems take advantage of the hydraulic energy of the drain flow (in the range of 40- 80 bar), producing power through a turbine or a pressure exchanger. The produced power is driven to the high-pressure pump of the RO unit and part of the power demand that is necessary for the RO process (i.e. practically the high-pressure pump) is offered by the ERD, decreasing the specific mechanical energy consumption to values of 3 kWh/m³. There are several ERD systems and their use depends on the RO unit capacity [2.39].

For the RO desalination unit efficiency calculation and performance during the load input variation, the commercial software ROSA 7.2.7 (Reverse Osmosis System Analysis) has been used [2.41]. The RO power input is equal to the net power production of the ORC engine, meaning the power produced by the expanders minus the pump power consumption and the heat cycle pump power consumption of the ORC engine. The net power production from the ORC engine is presented in Figure 2.26:

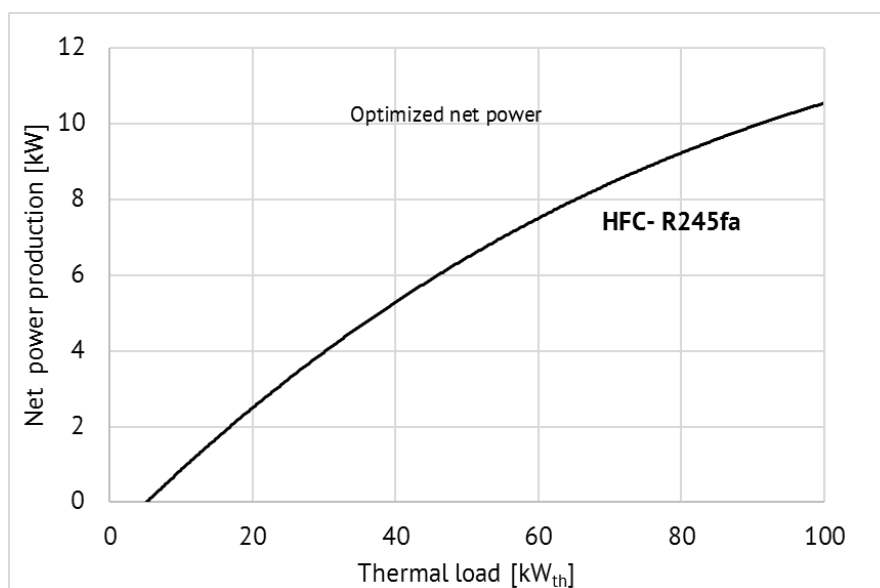


Figure 2.26 Net power production driven to the RO desalination unit

As observed in Figure 2.26, there is a strong fluctuation of the available power. At maximum load operation (100 kW_{th}) around 10 kW are available, when at 50% of the load (around 50 kW_{th}) the available power decreases to around 6 kW. The RO unit design starts with the assumption of operation at full load (100 kW_{th}) where the available power input is 10 kW. This power feeds mostly the high-pressure pump, in order for the RO unit to operate, and a small part of it is consumed in the feed pumps as presented below.

2.3.1 ORC engine and RO desalination unit coupling

There are two possible ways to connect the expanders of the ORC engine with the RO desalination unit: the mechanical way and the electrical way. The first one is more direct, since a system of pulley- belt can be used and a direct engagement of the expanders and the high-pressure pump can be realized [2.8, 2.14]. The disadvantage of this method is that the high-pressure pump will rotate with the same rotational speed as the expanders, therefore at some operation points it may have a very small rotational speed which decreases the volumetric efficiency of the pump. Moreover, this solution should foresee the power feed of the other pumps and consumptions of the system (heat cycle pump, organic fluid pump, etc.) which makes its selection practically inevitable. In addition, the expanders used in the current application are sealed scroll compressors in reverse osmosis and the direct mechanical connection is practically unattainable.

The electrical coupling, on the other hand, presents the disadvantage of the losses due to the transformation of the mechanical power on the expanders' shafts to electrical power through the small generator (transformation efficiency around 90- 95%) and a similar loss due to the consequent transformation of the electrical power to mechanical power with the use of a motor (transformation efficiency around 90- 95%) for the pumps' operation. The total power loss of these transformations is around 15%, which can decrease when all the RO unit pumps operate at their optimum operation point during the load variation (thermal load variation).

In the current system, the second solution has been selected, since it offers greater flexibility at every sub- system operation and higher RO efficiency. All the aforementioned power values are expressed in electrical power.

2.3.2 Desalinated water production

A typical composition of the seawater is presented in Table 2.7 where the feed water temperature is 25 °C:

Table 2.7 Typical seawater composition

Water type: Seawater (Open Intake) SDI<5				
Ions	mg/l	ppm CaCO ₃	meq/l	Total Conc. (mg/l)
Ammonium (NH ₄)	0	0	0	0
Potassium (K)	32.01	40.931	0.819	32.01
Sodium (Na)	12850.82	27948.72	558.974	12850.82
Magnesium (Mg)	1506.49	6196.487	123.930	1506.49
Calcium (Ca)	383.13	955.913	19.118	383.13
Strontium (Sr)	0	0	0	0
Barium (Ba)	0	0	0	0
Carbonate (CO ₃)	7.472	12.452	0.249	7.47
Bicarbonate (HCO ₃)	129.93	106.491	2.130	129.93
Nitrate (NO ₃)	0	0	0	0
Chloride (Cl)	20404.05	28776.200	575.524	20404.05
Fluoride (F)	0	0	0	0
Sulfate (SO ₄)	5997.05	6246.927	124.939	5997.05
Silica (SiO ₂)	0.2	n.a.	n.a.	0.2
Boron (B)	0	n.a.	n.a.	n.a.
Total dissolved solids: 41311.2 mg/l				
Cations: 702.84, Anions: 702.84, pH: 7.6				

Due to the great variation of the available power, the feed mass flow rate with seawater and the desalinated water production also present a great variation. Therefore, flexibility in terms of RO unit operation is necessary in order to efficiently operate on any level and also the fresh water (permeate) quality to be sufficient (low salinity). The RO unit flexibility has some similar characteristics with the ORC engine, since several stages are used according to the available load. More specifically, the RO unit consists of three identical RO sub- units, each of them consisting of the following equipment:

- Feed pump
- Cartridge filters
- High pressure pump (APP- axial piston pump)
- Energy recovery device (APM- axial piston motor)
- Four RO membranes FILMTEC SW30-4040 (operation at the load range of the current application) (Appendix I)
- Two membrane vessels placed in series (each one includes two membranes places in series)

This configuration is used in order to offer flexibility during the load variation. The three sub- units, which constitute the RO unit, pump the seawater from the

same water tank through a small feed pump as shown in the flow diagram of Figure 2.27. The seawater is then driven through the cartridge filters and ends up in the high-pressure pump (APP), where it is compressed to a pressure higher than the osmotic in order to pass through the membranes. Part of the feed water is desalinated and the rest (drain) which remains in high pressure, is driven to the ERD system (APM) for the specific consumption decrease (kWh/m^3).

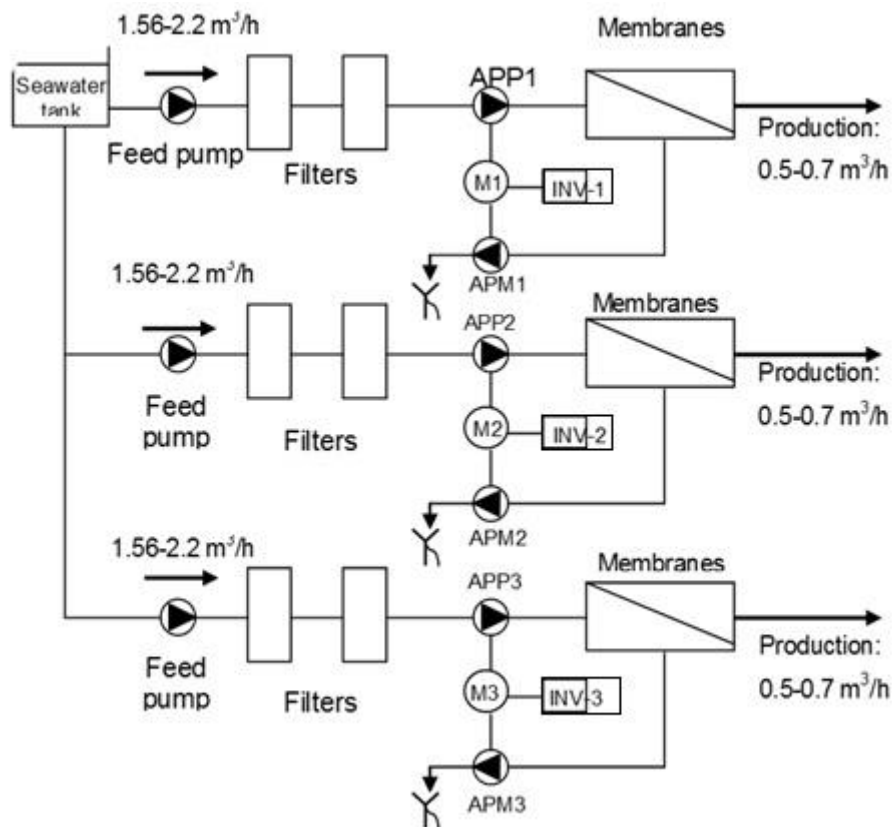


Figure 2.27 Flow diagram of the RO unit

The available power for the RO unit feeding depends on the thermal power input (driven to the ORC engine) almost linearly as presented in Figure 2.26, previously. For the RO unit control a variable should be connected to the operation point of the three sub- units. This variable could be for example the expanders' rotational speed.

Since the high-pressure pumps' motors of each sub- unit are controlled by an inverter, each sub- unit can operate producing fresh water of 0.5 to 0.7 m³/h, depending on the available power. The operation at variable operation point is realized with high efficiency. Since the RO unit consists of three identical, independent sub- units, which start up and stop are set from the available power, the total fresh water production will vary from 0.5 up to 2.1 m³/h, depending on the number of operating sub- units. In case that only one sub- unit operates (when the thermal load, thus the available power is low) the system production is the minimum (0.5 m³/h) and the basic flow characteristics are presented in Table 2.8, for seawater temperature of 20°C, as resulted from ROSA software:

Table 2.8 Water properties at every inlet and outlet of every sub- unit component in low load

Flow string	Flow rate (m ³ /h)	Pressure (bar)	TDS (mg/l)
HP pump inlet pressure (feed)	1.56	2	41309
Membranes inlet (feed)	1.56	51.94	42710
Concentrate (drain)	1.06	51.04	62655
Desalinated water (permeate)	0.5	-	325

At full load operation, the maximum feed seawater flow rate is equal to 6.6 m³/h and the water recovery equal to 32% (permeate to feed seawater ratio), which is kept constant throughout the load variation. Therefore, the maximum fresh water production is almost 2.1 m³/h.

With the help of the previously presented data and the typical configuration of the number of membranes in every membrane vessel (two membranes connected in series in each vessel) the ROSA software is used once again to determine the basic design characteristics of the whole RO unit. The maximum inlet flow rate, equal to 6.6 m³/h, results from the introduction of the specific energy consumption in case that an ERD is used, therefore in the current case it is more than 3~ 4 kWh/m³ especially if the feed pump consumption is added. Moreover, the water recovery has been assumed constant and equal to 32%. Consequently, the maximum permeate flow rate (operation at full load of all the three sub- units) is equal to 2.1 m³/h (maximum feed power from the ORC engine equal to almost 10 kW). The water properties in this case are presented in Table 2.9:

Table 2.9 Inlet/ outlet water properties

Flow string	Flow rate (m ³ /h)	Pressure (bar)	TDS (mg/l)
Inlet (before the HP pump)	6.6	2	41309
Inlet (after the HP pump)	6.6	56.60	42710
Concentrate (drain)	4.5	55.55	62697
Permeate	2.1	-	235
	% Recovery	32	

The basic characteristics of the RO unit and its operation properties are presented In Table 2.10. In case that no ERD is included, the specific energy consumption is equal to 6.64 kWh/m³.

Table 2.10 RO unit details

Feed Flow, m ³ /h	6.6
Raw Water Flow to System, m ³ /h	6.6
Feed Pressure, bar	56.60
Fouling Factor	0.85
Chem. Dose	None
Total Active Area, m ²	3 x 44.03
Water Classification	Seawater (Open Intake) SDI < 5
Permeate Flow, m ³ /h	2.1
Recovery, %	32
Feed Temperature, °C	20
Feed TDS, mg/l	42710
Number of Elements	3 x 4
Average Flux, l/mh	3 x 23.98
Osmotic Feed Pressure, bar	29.88
Osmotic Concentrate Pressure, bar	44.74
Osmotic Average Pressure, bar	37.31
Average NDP, bar	18.85
Power, kW	3 x 3.84
Specific Energy, kWh/m ³	5.46

Each RO sub- unit and membranes characteristics are presented in Table 2.11:

Table 2.11 Flow characteristics in the membranes

Membrane vessel	Membrane	Recovery	Permeate (m ³ /h)	Conductivity (mg/l)	Feed flow (m ³ /h)	Seawater conductivity (mg/l)	Seawater pressure (bar)
1	1	0.14	0.15	165.59	1.10	42710.43	56.26
	2	0.12	0.11	248.87	0.95	49655.58	56.19
2	1	0.06	0.09	304.23	1.67	56318.28	55.79
	2	0.05	0.08	391.37	1.57	59685.69	55.67

It is observed that the permeate exiting the first membrane vessel has the lowest salinity, since the inlet pressure is the highest one. The permeate at the outlet of the other membranes shows higher salinity, however within the acceptable limits, in such a way that the sum of the fresh water of the RO unit is potable (TDS<500 mg/l).

In Table 2.12, the chemical consistence (quality) of the water flows is presented. The product water quality occurs equal to almost 235 mg/l, which indicates produced fresh potable water of a good quality.

Table 2.12 Chemical composition of the water flow

Pass Streams (mg/l as Ion)				
Name	Feed	Adjusted Feed	Concentrate	Permeate
NH ₄	0.00	0.00	0.00	0.00
K	32.01	32.01	46.82	0.18
Na	12850.82	16139.39	23691.91	65.93
Mg	1506.49	0.00	0.00	0.00
Ca	383.13	0.10	0.15	0.00
Sr	0.00	0.00	0.00	0.00
Ba	0.00	0.00	0.00	0.00
CO ₃	7.47	7.47	10.17	0.00
HCO ₃	129.93	129.93	187.65	1.78
NO ₃	0.00	0.00	0.00	0.00
Cl	20404.05	20404.05	29962.26	97.78
F	0.00	0.00	0.00	0.00
SO ₄	5997.05	5997.05	8816.51	5.68
SiO ₂	0.20	0.20	0.25	0.00
Boron	0.00	0.00	0.00	0.00
CO ₂	1.78	1.79	2.58	1.84
TDS	41309	42710	62697	172
pH	7.60	7.60	7.62	6.17

Throughout the load variation, the permeate flow rate can relate to the thermal load input at the ORC engine as presented in Figure 2.28:

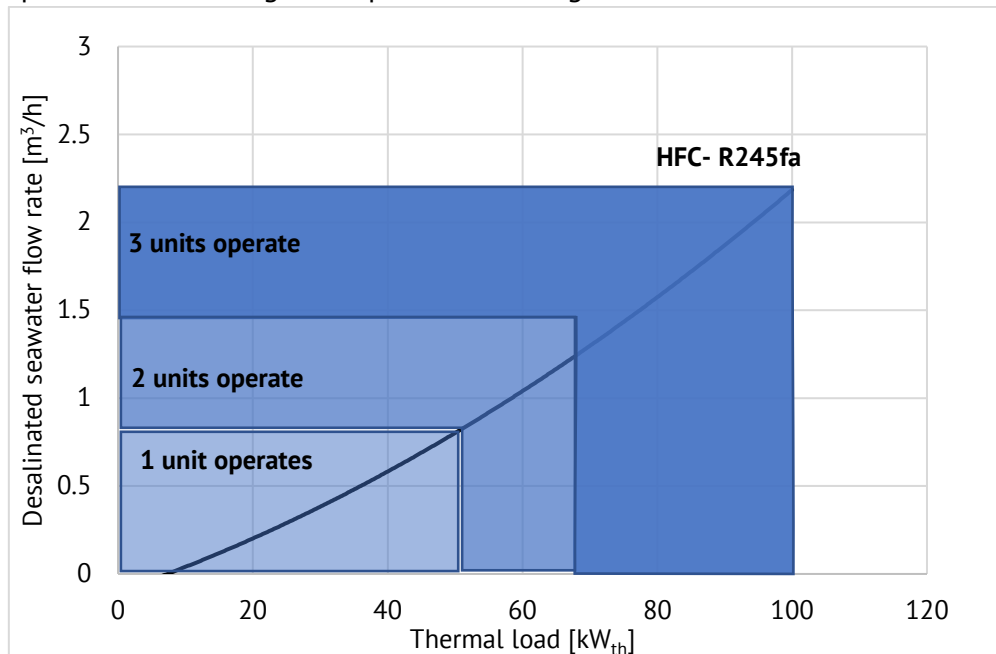


Figure 2.28 Fresh water flow rate during the load variation and operation of the three sub- systems

As expected, the desalinated water curve follows the shape of the net produced power curve from the ORC engine, since it has been assumed that the RO unit operates with constant efficiency. For operation at a load lower than 50 kW_{th}, the desalinated water flow rate significantly decreases, getting values lower than 1 m³/h. It is obvious that the RO unit should operate efficiently throughout the whole operation range (even at low load levels) in order to obtain a sufficient fresh water production throughout a day or year. Moreover, in Figure 2.28, it is observed that in low load operation (up to 50 kW_{th}) only the first sub- unit operates, from 50 up to almost 65 kW_{th} the two sub- units operate and for load over than 65 kW_{th} all three sub- units operate.

2.3.3 Pump and ERD selection

The basic characteristics of the pump and the ERD are presented subsequently. The basic sub- systems of a RO unit are the motor, the high-pressure pump and the ERD, which are connected on the same shaft. The motor converts the available electric power to hydraulic power on the high-pressure pump (APP), which is then driven to the seawater and increases its pressure. The seawater is then fed to the membranes, where a part is desalinated and the rest (concentrate), remaining at high pressure, is driven to a similar but smaller piston pump in reverse operation (APM- operation like a turbine), for mechanical work production. Such a system is presented in Figure 2.29 below. The motor can be observed in the middle, on the right the high-pressure pump and on the left the piston pump in reverse operation. It should be noted that the motor obtains an inverter for operation frequency variation, thus rotational speed variation. This configuration's coupling is presented in Figure 2.29 and 2.30 [2.44].



Figure 2.29 Coupled HP pump with motor and ERD system (APP-APM)

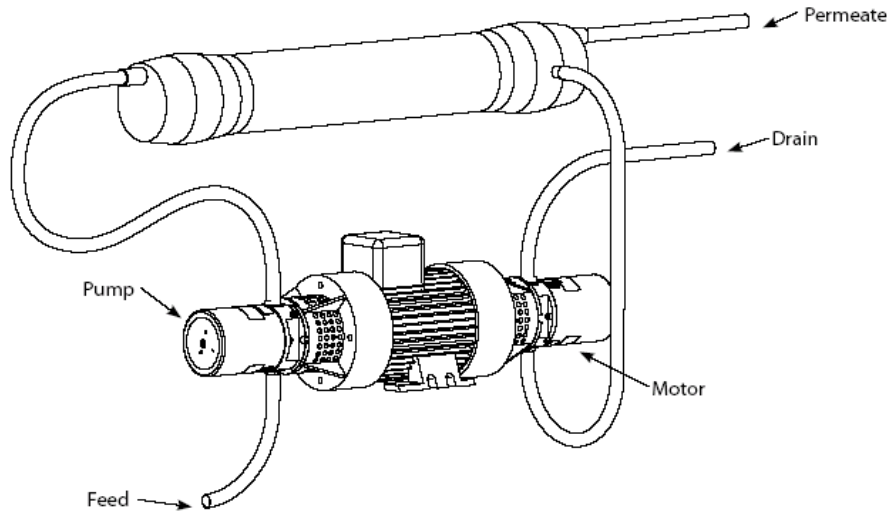


Figure 2.30 Motor/ HP pump/ ERD coupling

Since the three sub- systems are coupled on the same shaft, they share the same rotational speed. The power balance is given:

$$P_e + P_{APM} = P_{APP} \quad (2.16)$$

where P_e is the net power fed to the RO unit motor from the ORC engine (maximum value around 10 kW), P_{APM} the power recovered by the ERD and P_{APP} the total power given to the seawater from the HP pump.

The specific energy consumption [kWh/m^3] is a factor of great interest, since it indicates the RO unit efficiency and expresses the power that should be consumed on the motor in order to desalinate one cubic meter of water. In large- scale RO units which operate at constant conditions, the specific energy consumption gets values of around 2 to 3 kWh/m^3 . However, in small- scale systems which operate at variable conditions, this value increases to 4 to 5 kWh/m^3 [2.42]. It should be high lightened that in these values, the required power for the feed pump is also included, which however is very low and usually neglected. Since the RO unit obtains an ERD, only a part of the required total power is covered by the ORC engine (around 50 %). This fact does not affect the operation point (membranes' pressure/ volumetric flow rate), however it influences the specific energy consumption.

2.3.4 Operation at variable load

Until now, focus has been given to the relation of the available power with the fresh water production, without operation details of the pumps and membranes operation. Therefore, there has been no discussion over the effect of the operation at partial load on the permeate salinity. Indeed, with the decrease of the available power, the membrane pressure decreases, as well as the seawater mass flow rate. This causes the increase of fresh water salinity and the decrease of the specific energy consumption.

In order to investigate the RO unit operation at partial load, the operation characteristic curves of the pumps, the ERD and the membranes are necessary. With the combination of the aforementioned variables, the operation point can be determined and other ways of coupling could be investigated, in order to make the system more flexible in the load variation and switch it on at the first available excess power.

In Figure 2.31 the inlet seawater volumetric flow rate in relation to the pressure and the salinity of the permeate is presented.

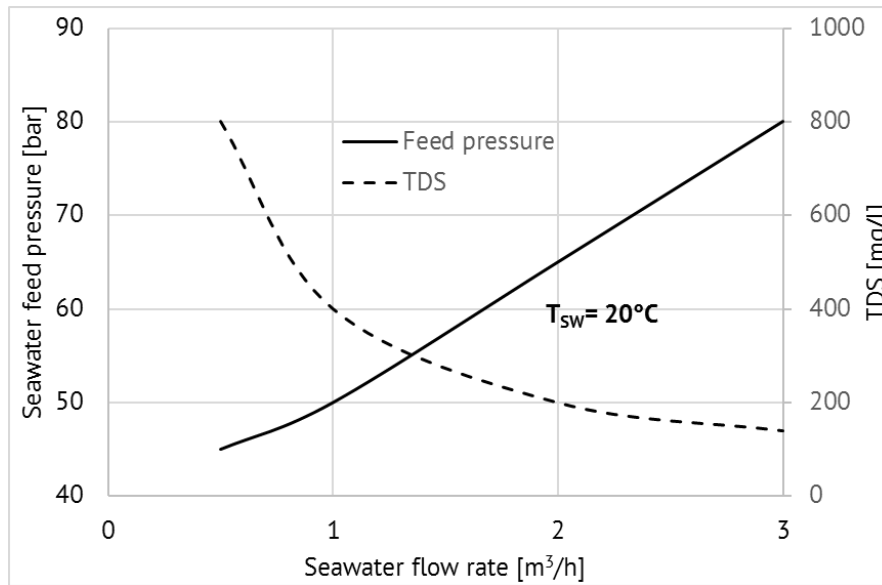


Figure 2.31 Membrane pressure and permeate salinity as a function of the seawater volumetric rate

As it is observed in Figure 2.31, the membrane pressure is related almost linearly with the seawater volumetric flow rate. On the contrary, the permeate salinity is reversely proportional of the volumetric flow rate [2.26]. For seawater volumetric flow rate greater than 0.9 m³/h, acceptable values of permeate salinity occur.

The high-pressure pump and ERD operation characteristic curve in partial load present more complexity since it depends on the volumetric efficiencies of each of those volumetric machines in non- stable conditions. These data are not available from the pump manufacturers. Therefore, at this point, they can only be approximately estimated and they will be further examined during the experimental investigation.

In a typical APP- APM- ERD configuration, the rotational speed of the system (since all three components are connected on the same shaft) and the volumetric flow rate of the seawater can be related, as well as the motor power consumption, which depends on the operation pressure [2.39]. These data are presented in Figure 2.32:

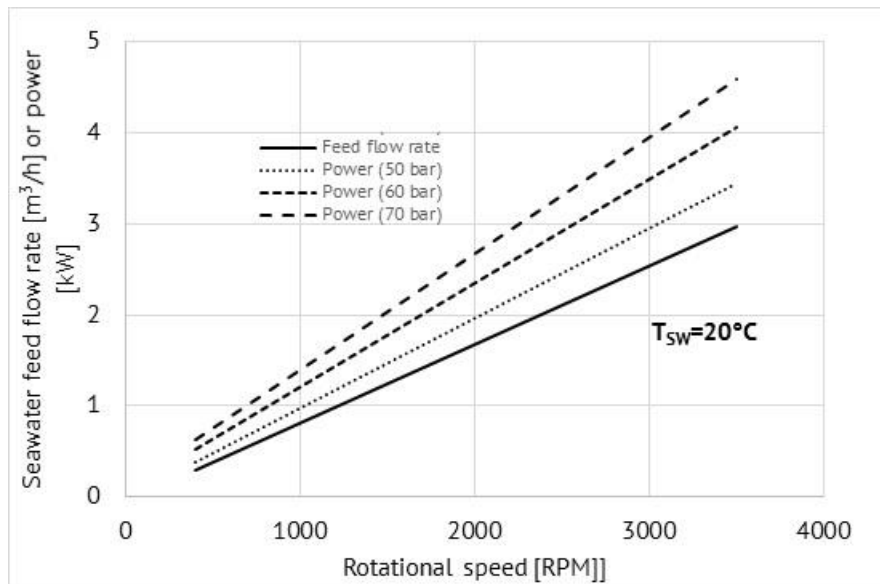


Figure 2.32 Seawater flow rate and power consumption for several pressure values as a function of the HP pump rotational speed

The HP pump power for several pressure values presents a linear relation to the rotational speed, therefore with the volumetric flow rate as well, and it increases with the pressure increase. The specific energy consumption and the power demand in relation to the seawater pressure at the HP pump outlet are presented in Figure 2.33:

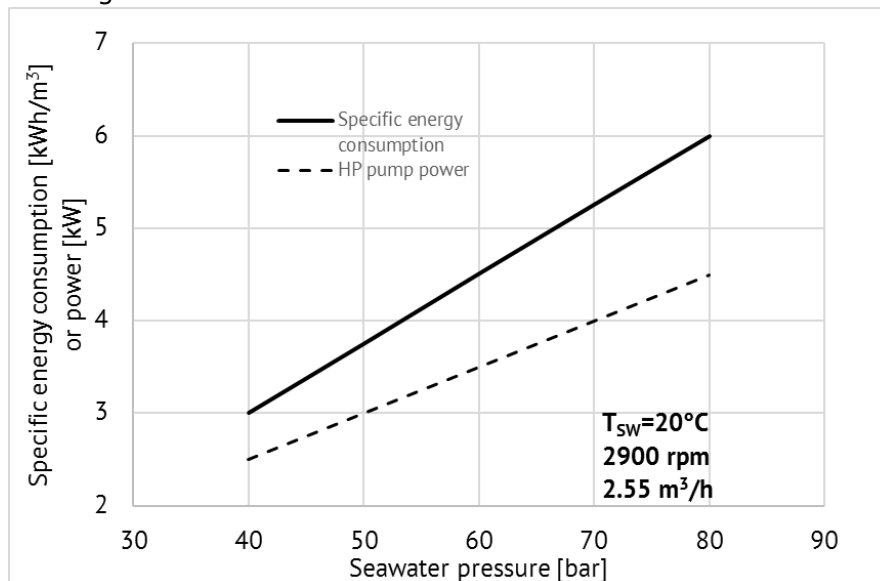


Figure 2.33 Specific energy consumption and HP pump power as a function of the seawater pressure at the HP pump outlet (membrane inlet)

It should be noticed that in low operation pressure, regardless the volumetric flow rate the energy consumption significantly decreases as well as the power demand. However, under those conditions, the fresh water salinity is increased and, in some cases, it might be higher than the maximum acceptable value (500 mg/l) as presented in Figure 2.31. Therefore, the HP pump operation optimization is related to the desired quality of the fresh water. For permeate of a salinity close to the acceptable limits, the RO unit can efficiently operate and with low specific energy consumption (around 3.5 kWh/m³), however if the desired

quality is higher and the salinity lower than 200 mg/l, the specific energy consumption increases to values around 4~5 kWh/m³.

2.3.5 HP pump and membranes cooperation

The power produced from the ORC engine is driven to the RO unit. Therefore, its value is pre-determined and based on this value, the rest of the variables can be determined. In order to calculate the volumetric flow rate and the membranes' pressure, a system of two equations and two unknown variables should be solved. Once these two variables are determined, the rest of variables can easily be determined as well.

The current analysis is based on the graphic method since basic values of efficiency and the characteristic curves are unknown. For a specific value of available power (2 and 4 kW accordingly, in Figure 2.34) the diagrams of Figure 2.34 present the relation between the operation pressure, the volumetric flow rate and the power. This characteristic curve corresponds to only one of the three sub-units of the RO unit.

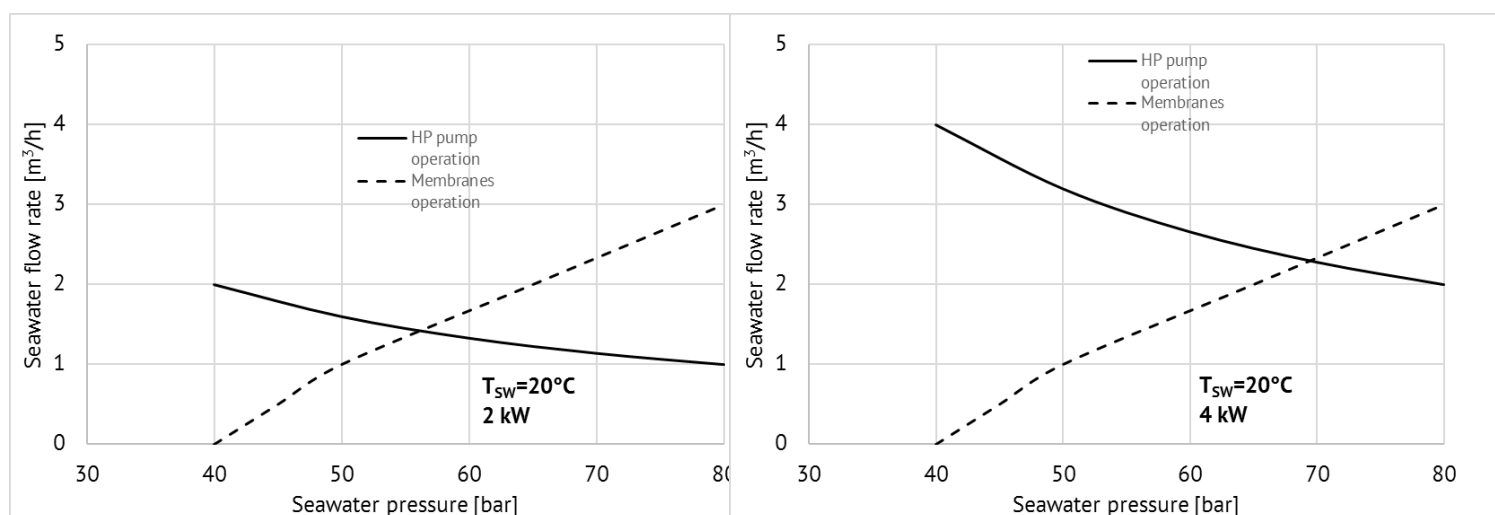


Figure 2.34 Characteristic curves of membranes and HP pump for two values of available power on the HP pump (2 and 4 kW)

The membranes characteristic curve does not change with the power availability, as it was expected. Therefore, from the cross section of these two curves, the desired values occur as presented in Table 2.13:

Table 2.13 Operation characteristics for two available power values (2 and 4 kW)

HP pump power (kW)	2	4
Power input from ORC engine (kW)	~2	~4
Membranes' pressure (bar)	52	62
Seawater volumetric flow rate (m ³ /h)	1.6	2.9
Permeate volumetric flow rate (m ³ /h)	0.51	0.93
Salinity (mg/l)	317	180
Specific energy consumption (kWh/m ³)	5.04	5.9

According to Table 2.13, when the ORC engine operates at high load and the net power production is increased, the RO unit will operate at high membranes' pressure, producing desalinated water of low salinity and high quality. However, the specific energy consumption will be increased due to the high membranes' pressure.

2.4 Conclusions

In the current chapter, a detailed analysis of the simulation model development, both for the ORC engine and the RO unit, has been presented. The organic fluid selection has been extensively justified as well as the chosen two-stage ORC configuration.

All the components of the ORC engine have then been outlined in order to specify their properties and conclude to a specific design that will help their selection in the next step.

The RO unit and its three sub- units have also been carefully designed, based on the power available from the ORC engine that will feed this system. Both ORC and RO systems have been tested as per their design in partial and full load operation, where full load is the barrier set as the maximum heat power input to the system from a low temperature heat source (equal to $100 \text{ kW}_{\text{th}}$).

Based on the detailed design of this chapter, the next step is the selection of the components that will be combined to construct the prototype of the thesis, which will be experimentally evaluated in order to validate or cancel the accuracy of the current design.

References:

- 2.1 Kosmadakis G, Manolakos D, Kyritsis S, Papadakis G. Comparative thermodynamic study of refrigerants to select the best for use in the high-temperature stage of a two stage organic Rankine cycle for RO desalination. *Desalination* 243 (1-3), (2009), pp. 74–94.
- 2.2 Tchanche BF, Papadakis G, Lambrinos G, Frangoudakis A. Fluid selection for a low temperature solar organic Rankine cycle. *Appl Thermal Engin* 29(11-12), (2009), pp. 2468– 76.
- 2.3 Montreal Protocol on substances that deplete the Ozone layer. Report of the Refrigeration, Air-Conditioning and Heat Pumps Technical Options Committee, 2010.
- 2.4 Badr O., Probert S.D. and O’Callaghan P.W. Selecting a working fluid for a Rankine-cycle engine. *Appl. Energy*, 21(1) (1985), pp. 1–42.
- 2.5 Morrison G. The shape of the temperature-entropy saturation boundary. *Inter. J. Refrig.*, 17(7) (1994), pp. 494–504.
- 2.6 Lemmon EW, Huber ML, McLinden MO. NIST Standard Reference Database 23: Reference Fluid Thermodynamic and Transport Properties-REFPROP, Version 8.0, National Institute of Standards and Technology, Standard Reference Data Program, Gaithersburg, 2007 (<http://www.nist.gov/srd/nist23.cfm>).
- 2.7 Kosmadakis G, Manolakos D, Kyritsis S, Papadakis G. Design of an autonomous, two stage solar organic Rankine cycle system for reverse osmosis desalination. *Desalination and Water Treatment*, 1(1-3), (2009), pp. 114–27.
- 2.8 Kosmadakis G, Manolakos D, Papadakis G. Parametric theoretical study of a two-stage solar organic Rankine cycle for RO desalination. *Renewable Energy* 35(5), (2009), pp. 989– 96.
- 2.9 Kane M, Larrain D, Favrat D, Allani Y. Small hybrid solar power system. *Energy* 28(14), (2003), pp. 1427–43.
- 2.10 Delgado-Torres AM, García-Rodríguez L. Double cascade organic Rankine cycle for solar-driven reverse osmosis desalination. *Desalination* 216(1-3), (2007), pp. 306–13.
- 2.11 Quoilin S, Orosz M, Hemond H, Lemort V. Performance and design optimization of a low-cost solar organic Rankine cycle for remote power generation. *Solar Energy* 85(5), (2011), pp. 955–66.
- 2.12 Hung TC, Shai TY, Wang SK. A review of organic Rankine cycle (ORCs) for the recovery of low grade waste heat. *Energy* 22(7), (1997), pp. 661–67.
- 2.13 Manolakos D, Kosmadakis G, Kyritsis S, Papadakis G. Identification of behavior and evaluation of performance of small scale, low-temperature Organic Rankine Cycle system coupled with a RO desalination unit. *Energy* 34(6), (2009), pp. 767–74.
- 2.14 Manolakos D, Kosmadakis G, Kyritsis S, Papadakis G. On site experimental evaluation of a low-temperature solar organic Rankine cycle system for RO desalination. *Solar Energy* 83(5), (2009), pp. 646–56.
- 2.15 Quoilin S, Aumann R, Grill A, Schuster A, Lemort V, Spliethoff H. Dynamic modeling and optimal control strategy of waste heat recovery Organic Rankine Cycles. *Appl Energy* ,88(6), (2011), pp.2183–90.
- 2.16 Quoilin S, Lemort V, Lebrun J. Experimental study and modeling of an Organic Rankine Cycle using scroll expander. *Appl Energy*, 87(4), (2010), pp.1260–68.
- 2.17 Manolakos D, Papadakis G, Kyritsis S, Bouzianas K. Experimental evaluation of an autonomous low-temperature solar Rankine cycle system for reverse osmosis desalination. *Desalination*, 203(1-3), (2007), pp.366–74.

- 2.18 Klein SA. Engineering Equation Solver (EES), Academic Professional version; 2010.
- 2.19 Pei G, Li J, Li Y, Wang D, Ji J. Construction and dynamic test of a small-scale organic rankine cycle. *Energy* 36(5), (2011), pp.3215–23.
- 2.20 Wang XD, Zhao L, Wang JL, Zhang WZ, Zhao XZ, Wu W. Performance evaluation of a low-temperature solar Rankine cycle system utilizing R245fa. *Solar Energy* 84(3), (2010), pp.353–64.
- 2.21 Lemort V, Quoilin S, Cuevas C, Lebrun J. Testing and modeling a scroll expander integrated into an Organic Rankine Cycle. *Appl Thermal Engin*, 29(14-15), (2009), pp.3094–102.
- 2.22 Schuster A, Karellas S, Aumann R. Efficiency optimization potential in supercritical Organic Rankine Cycles. *Energy*, 35(2), (2010), pp.1033–39.
- 2.23 Saleh B, Koglbauer G, Wendland M, Fischer J. Working fluids for low-temperature organic Rankine cycles. *Energy*, 32(7), (2007), pp.1210–21.
- 2.24 Manolakos M, Papadakis G, Mohamed Essam Sh, Kyritsis S, Bouzianas K. Design of an autonomous low-temperature solar Rankine cycle system for reverse osmosis desalination. *Desalination*, 183(1-3), (2005), pp.73–80.
- 2.25 Naunheimer H., Bertsche B., Ryborz J., Novak W. Automotive transmissions, Fundamentals, Selection, Design and Application. Second edition, Springer, 1994, 2011.
- 2.26 Μανωλάκος Δ. Ανάπτυξη αυτόνομου ηλιακού οργανικού κύκλου Rankine χαμηλής θερμοκρασίας για ασφαλάτωση νερού με αντίστροφη όσμωση. Διδακτορική Διατριβή, Γεωπονικό Πανεπιστήμιο Αθηνών, 2006.
- 2.27 Schuster A, Karellas S, Kakaras E, Spliethoff H. Energetic and economic investigation of Organic Rankine Cycle applications. *Appl Thermal Engin*, 29(8-9), (2009), pp. 1809–17.
- 2.28 Zanelli R, Favrat D. Experimental Investigation of a Hermetic Scroll Expander-Generator. In: Proceedings of the International Compressor Engineering Conference at Purdue, USA, 1994, pp. 459–64.
- 2.29 Kane M, Larrain D, Favrat Dm Allani Y. Small hybrid solar power system. *Energy* 28(14), (2003), pp. 1427–43.
- 2.30 Guangbin L, Yuanyang Z, Yunxia L, Liansheng L. Simulation of the dynamic processes in a scroll expander-generator used for small-scale organic Rankine cycle system. *Proc Inst Mech Engrs, Part A, J Power Energy*, 225(1), (2011), pp. 141–49.
- 2.31 Musbaudeen O.B. Modeling and performance evaluation of an Organic Rankine Cycle (ORC) with R245fa as working fluid. A thesis submitted to the board of Campus graduate programs of middle east technical university, Northern Cyprus Campus, May 2012.
- 2.32 Lemort V, Declaye S, Quoilin, S. Experimental characterization of a hermetic scroll expander for use in a micro-scale Rankine cycle. *Proc of Instit of Mech Eng, Part A: J Power Energy*;226(1), (2012), pp. 126–36.
- 2.33 Hettiarachchi HDM, Golubovic M, Worek WM, Ikegami Y. Optimum design criteria for an Organic Rankine cycle using low-temperature geothermal heat sources. *Energy*, 32(9), (2007), pp. 1698–706.
- 2.34 Guo T, Wang HX, Zhang SJ. Fluids and parameters optimization for a novel cogeneration system driven by low-temperature geothermal sources. *Energy*, 36(5), (2011), pp. 2639–49.
- 2.35 Nakaoka T, Uehara H. Performance test of a shell-and-plate-type condenser for OTEC. *Exp Thermal Fluid Sci*, 1(3), (1988), pp. 275–81.
- 2.36 Nakaoka T, Uehara H. Performance test of a shell-and-plate-type evaporator for OTEC. *Exp Thermal Fluid Sci*, 1(3), (1988), pp. 283–91.

- 2.37 Roy JP, Mishra MK, Misra A. Performance analysis of an Organic Rankine Cycle with superheating under different heat source temperature conditions. *Appl Energy*, 88(9), (2011), pp. 2995–3004.
- 2.38 Delgado-Torres AM, García-Rodríguez L. Analysis and optimization of the low-temperature solar organic Rankine cycle (ORC). *Energy Convers Management*, 51(12), (2010), pp. 2846–56.
- 2.39 Valbjorn A. ERD for small SWRO plants. *Desalination*, 248, (2009), pp. 636–641.
- 2.40 <http://www.temak.gr/site/>
- 2.41 <http://www.dow.com/en-us/water-and-process-solutions/resources/design-software/rosa-software>
- 2.42 Mohamed ES, Papadakis G, Mathioulakis E, Belessiotis V. The effect of hydraulic energy recovery in a small sea water reverse osmosis desalination system; experimental and economical evaluation. *Desalination*, 184(1–3), (2005), pp. 241–6.
- 2.43 Kosmadakis G, Manolakos D, Papadakis G. An investigation of design concepts and control strategies of a double-stage expansion solar organic Rankine cycle. *International Journal of Sustainable Energy*, 34(7), (2015), pp.446- 467
- 2.44 http://files.danfoss.com/documents/521B0889_DKCFN.PD.010.GA2.02_Sea%20Water%20Pump%20with%20Energy%20Recovery%20SWPE_GB.pdf

CHAPTER 3 – Prototype design and construction

3.1 Introduction

In Chapter 3, the design and construction of the integrated system that is installed and tested in the laboratory is being presented. The appropriate measurement instrumentation as well as the locations of measurement on the system are determined. The heat source cycle with the electric heater and MEG as working fluid and the ORC engine design and component selection are subsequently presented. A special paragraph is devoted to the construction of the scroll expanders, since they are the most important components of the ORC engine. They are commercial scroll compressors which have been modified in order to be used in reverse operation. Then the RO unit of a capacity of 2.1 m³/d of seawater desalination is presented as it has been assembled and installed in the laboratory. Finally, the step-by-step construction and installation of the integrated system in the laboratory is presented.

3.2 The integrated system and measurement instrumentation

The installation of the integrated system at the laboratory is hereby presented, based on the design analysis presented in Chapter 2. In Figure 3.1, a schematic diagram of the ORC engine connected to the heat source is presented. In the same diagram, the appropriate instrumentation that will be used in the experimental evaluation of the system is being shown [3.1- 3.3].

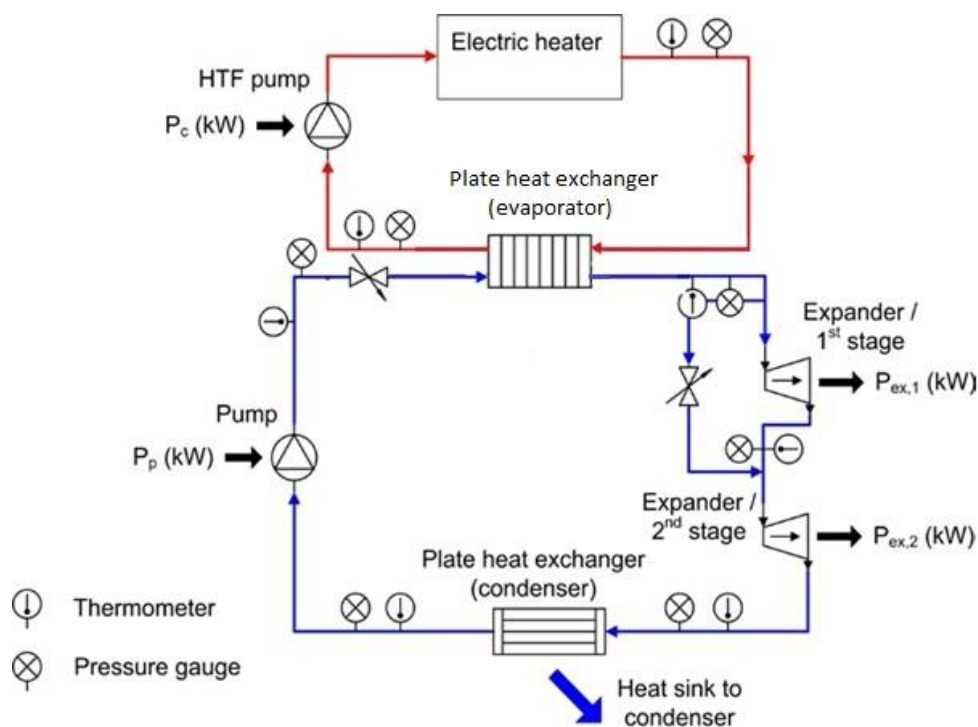


Figure 3.1 ORC engine and heat source cycle diagram with appropriate instrumentation

3.2.1 Measurement locations

The measurement points have been selected in order to systematically measure the characteristic operation values, necessary for the system evaluation. The measurement instrumentation of the ORC engine as well as their measurement range is presented in Table 3.1;

Table 3.1 ORC engine instrumentation, location and measurement range

Temperature sensor Pt 100		Measurement range	Accuracy (%)
1	After the pump	0-80 °C	±0.05
2	After the evaporator	0-200 °C	±0.05
3	Between the scroll expanders	0-200 °C	±0.05
4	After the second expander	0-150 °C	±0.05
5	After the condenser	0-80 °C	±0.05
Pressure sensors			
1	After the pump	0-35 bar	±1.6
2	After the evaporator	0-35 bar	±1.6
3	Between the scroll expanders	0-35 bar	±1.6
4	After the second expander	0-35 bar	±1.6
5	After the condenser	0-35 bar	±1.6

On the heat source side only two Pt100 thermometer sensors are being used in order to measure the working fluid temperature at the inlet and the outlet of the electric heater.

Resistance thermometers (also called resistance temperature detectors- RTDs) are sensors used to measure temperature by correlating the resistance of the RTD element with temperature. Most RTD elements consist of a length of fine coiled wire wrapped around a ceramic or glass core. The element is usually quite fragile, so it is often placed inside a sheathed probe to protect it. The RTD element is made of a pure material, typically platinum, nickel or copper. The material has a predictable change in resistance as the temperature changes and it is this predictable change that is used to determine temperature. They are slowly replacing the use of thermocouples in many industrial applications below 600 °C, due to higher accuracy and repeatability. By far the most common devices used in industry have a nominal resistance of 100 ohms at 0 °C and are called Pt100 sensors ('Pt' is the symbol for platinum, 100 for the resistance in ohm at 0 °C.). Furthermore, platinum resistance thermometers (PRTs) offer excellent accuracy over a wide temperature range (from -200 to +850 °C). Standard sensors are available from many manufacturers with various accuracy specifications and numerous packaging options to suit most applications. Unlike thermocouples, it is not necessary to use special cables to connect to the sensor. The principle of operation is to measure the resistance of a platinum element. The relationship between temperature and resistance is approximately linear over a small temperature range [3.5].

In Figure 3.2, a schematic diagram of the RO desalination unit with the three identical sub- units is presented;

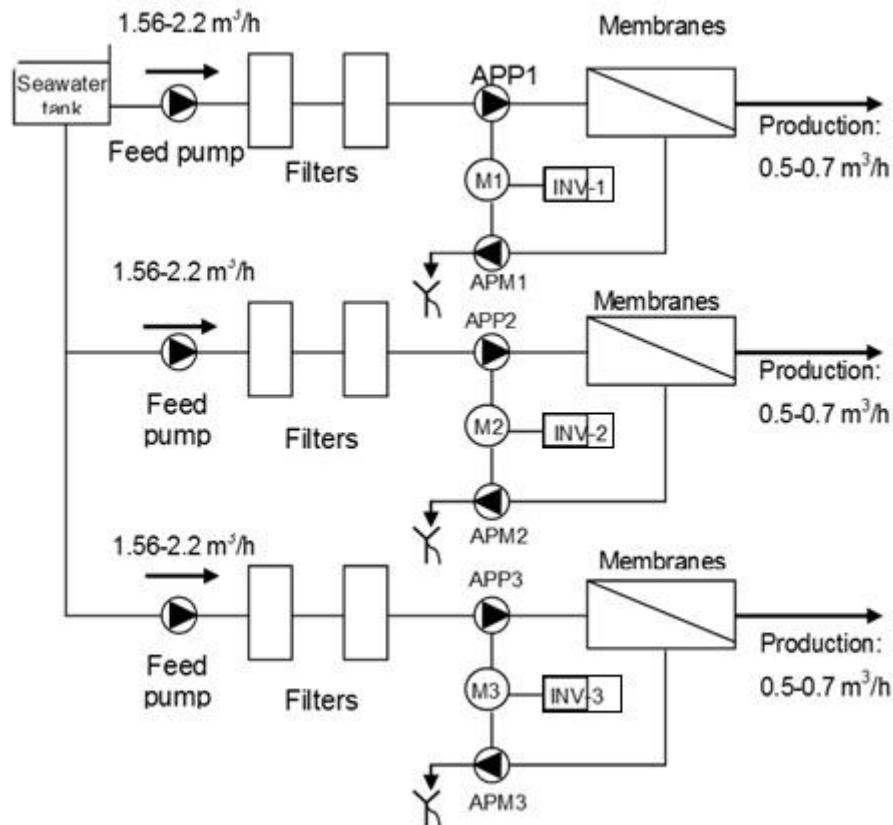


Figure 3.2 RO desalination unit with three identical sub- units

In Table 3.2 the measurement instrumentation of each sub- unit is presented. Each sub- unit is separately tested in order to evaluate the efficient operation of each one and of the RO desalination unit as a whole [3.4].

Table 3.2 RO sub-unit instrumentation and location and measurement range

Temperature thermometers		Measurement range	Accuracy (%)
1	After the membranes	0-60 °C	±0.15
Pressure gauges			
1	After the feed pump and before the filters	0-10 bar	±0.1
2	Between the two filters	0-10 bar	±0.1
3	After the filters and before the high-pressure pump	0-10 bar	
4	After the high-pressure pump and before the membranes	0-100 bar	±1.0
5	At the brine's membranes outlet	0-100 bar	±1.0
Pressure switches			
1	Low- pressure switch after the filters and before the high-pressure pump (protects the high-pressure pump from no water operation)	2 bar	≤ ±1.0 % of span ± 1 digit
2	High-pressure switch after the high-pressure pump and before the membranes (protects the membranes and membrane vessels under high pressure)	70 bar	≤ ±1.0 % of span ± 1 digit
Water flow rate (mechanical flow meter)			

1	At the membranes' outlet on the fresh water side (on each sub- unit)	0.1 – 1 m ³ /h	±0.05
2	At membranes' outlet on the brine's side	0.25 – 2.5 m ³ /h	±0.125
Water conductivity			
1	At the membranes' outlet on the fresh water side (digital indication)	0-2000 mS/cm	±2

High pressure pump rotational speed is monitored at each sub- unit by a frequency inverter, while current and voltage of the motors are also measured in order to calculate their power consumption.

3.3 The Organic Rankine Cycle Engine and the heat source cycle

3.3.1 The heat source cycle

The heat source cycle simulates any heat source of low/ medium temperature (up to 120~ 130°C) with thermal load variation and maximum capacity 100 kW_{th} (e.i. renewable energy sources). In the laboratory, the heat cycle consists of an electric heater and a circulation pump.

The electric heater provides heat to a working fluid (in current application monoethylene glycol- MEG, see chapter 2) by increasing its temperature up to 130 °C and this heat is then provided to the organic fluid of the ORC engine through the evaporator. The electric heater selected for the current application is commercially available from the company CIAT [3.6], its maximum operation pressure is 6 bar and it is presented in Figure 3.3:



Figure 3.3 The electric heater of the heat cycle

The circulation pump provides the heat transfer fluid with the necessary hydraulic power. The maximum power of this pump is around 0.3 kW (see Chapter 2). The circulation pump operates in constant speed. The MEG operating conditions are shown below:

Mass flow rate (kg/s): $0 \leq \dot{m}_c \leq 2 \text{ kg/s}$

Cold string temperature (°C): $30 \leq T_{in} \leq 120 \text{ } ^\circ\text{C}$

Hot string temperature (°C): $40 \leq T_{out} \leq 150 \text{ } ^\circ\text{C}$

Viscosity (kg/m/s): $0.00098 \leq \mu_{gl} \leq 0.0119 \text{ kg/m/s}$

Especially in low operation temperature, there might be some difficulty in the pump's start due to low viscosity which leads to higher friction and pump's power consumption. Therefore, this fact should be taken under consideration during the pump's selection. Another characteristic of the feed pump is the high maximum temperature, which dictates the use of stainless steel and special materials for the pump shaft sealing with tolerance to such temperatures. This leads to a cost increase. Moreover, the presence of glycol affects the performance of a pump; it reduces the flow, decreases the head capability, and increases the horsepower requirements. Therefore, the simple centrifugal pumps used in water applications are not suitable, since their guaranteed temperature limits vary between 80 and 90 °C. The use of a gear pump on the other hand is suitable, however with some cost increase, since these pumps are destined for special applications (industrial applications). For the heat source cycle, an industrial centrifugal pump that can circulate fluid of high temperature, commercially available by Packo company has been selected. Its type is ICP2. These pumps are sufficiently robust and can circulate high temperature fluids, as well as light chemical fluids like MEG. It should be noted that this kind of pumps are also commercially available by Salmson company, however Packo has been preferred, since the cost is almost half the one of Salmson, with similar tolerance and reliability. In Figure 3.4, the selected circulation pump for the heat cycle is presented.



Figure 3.4 Centrifugal circulation pump of the heat cycle, Packo company, ICP2

The technical characteristics of the selected circulation pump of the heat cycle and its motor are presented in Table 3.3:

Table 3.3 Circulation pump and motor characteristics, Packo ICP2/32-125/112 (O-05)

Pump's general features	
Company	Packo
Type	ICP2
Series	ICP2/32-125/112(O-05)
Maximum volumetric flow rate (@2900 rpm)	7 m ³ /h
Maximum operation temperature	130 °C
Pump shell	Stainless steel 316L
Elastomers	Viton
Impeller	Stainless steel 316L
Sealing	Mechanical ring SHJ SIC/SIC/VITON
Nozzles dimensions	Nozzle DN50 X DN32 Flanges loose, EN1092-1/02
Maximum power demand	~0.7 kW
Motor's general features	
Type	3-phase bipolar electric motor
Power capacity/ frequency/ rotational speed	1.1 kW/50 Hz/2900 rpm
Electric voltage	380 V

Finally, on the heat source cycle, an open-type expansion tank is necessary for handling the temperature difference of MEG during operation. The basic selection parameters of the expansion tank are the maximum pressure in the cycle (equal to almost 2 bar) and the total volume which is related to the operating conditions variation and the total volume of the heat transfer fluid. The selected expansion tank is open- type (since the maximum pressure is low and the cost is lower than the closed type) and it is placed above the ORC engine metallic frame structure. It is shown in Figure 3.5:



Figure 3.5 The heat source cycle expansion vessel

A schematic presentation of the heat cycle is presented on the left of Figure 3.6 and the constructed heat cycle (as it was installed in the laboratory) on the right of Figure 3.6:

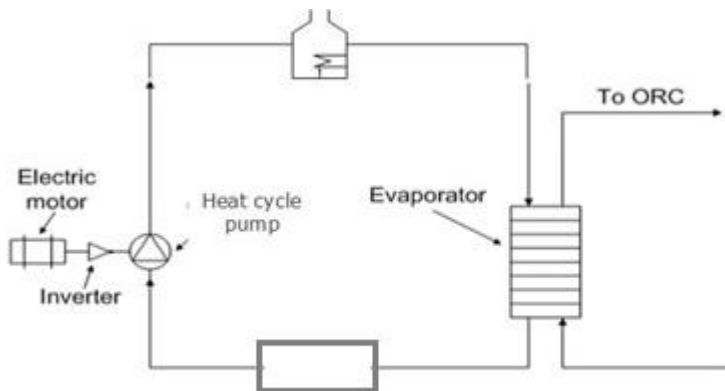


Figure 3.6 The heat source cycle

3.3.2 The Organic Rankine Engine

3.3.2.1 Organic fluid pump

The first element of the ORC engine that will be selected is the organic fluid pump. This pump is intended to circulate the organic fluid in the engine. According to the analysis of Chapter 2, the maximum pressure of the organic fluid in the cycle is almost 20 bar and the maximum temperature of the fluid at the inlet and outlet of the pump is low and does not exceed 40 to 45 °C (depending on the condensation temperature). The maximum mass flow rate of the organic fluid (R245fa) at full load operation is 0.42 kg/s and the corresponding volumetric flow rate is around 1.16 m³/h (~19.3 l/min). The maximum power consumption is around 0.7 kW, which certainly depends on the motor features (efficiency assumed equal to 92%) and the inverter. With the maximum volumetric flow rate known, the swept volume and the rotational speed can be related as discussed in Chapter 2, as follows:

$$\dot{m}_{orc} = \frac{\dot{V}_p}{v_p} = \frac{c(rpm)}{v_p}, \quad (3.1)$$

where c is related to the swept volume [cm³]. The ORC engine pump selected is a diaphragm pump [3.1, 3.6- 3.8] which ensures the sealing of this volumetric machine in order to eliminate organic fluid leakage. Moreover, these pumps operate at high pressure and low mass flow rate, which are the conditions of the current application.

Some companies constructing high quality piston- diaphragm pumps are Doseuro, Wanner, McFarland- Tritan and Garco. In most cases, a gear unit is also used in order to obtain the desired mass flow rate of the organic fluid within the technical features of the pump, since these pumps operate in low rotational speed (600- 1000 rpm) and within a small range. The company that was finally selected is Wanner and more specifically the type "Hydra Cell" which present high efficiency and low maintenance necessity. For the selection of the current type, the diagram of Figure 3.7 which is provided by the manufacturer, is useful. As mentioned before, the maximum volumetric flow rate is around 20 l/min and the maximum discharge pressure is around 20 bar (maximum inlet pressure almost 2.5 bar which depends on the pressure/ temperature of condensation).

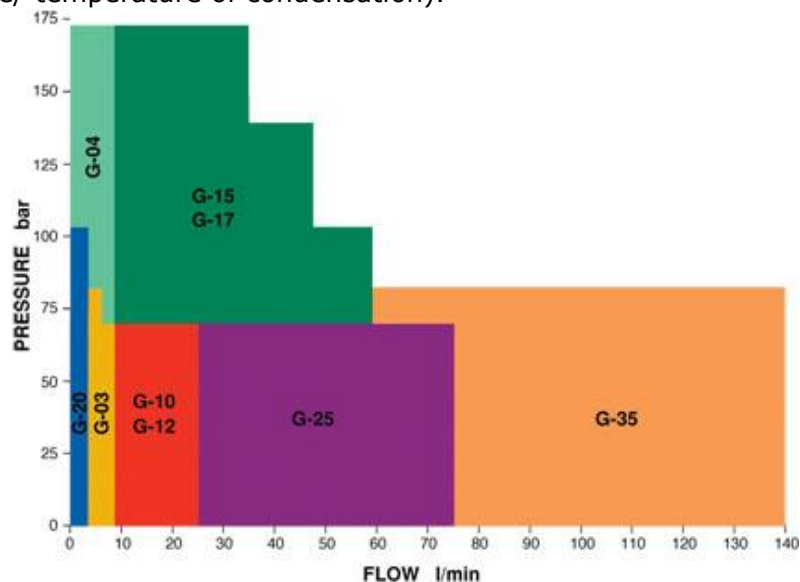


Figure 3.7 Piston- diaphragm pump selection map

It is observed that the pump type that satisfies the whole operation range of the application here is "G-10", while "G-12" could also be used, since the only difference is that the second is appropriate for vertical operation.

This pump has maximum volumetric flow rate equal to almost 30 l/min, a value which is higher than the calculated one. The minimum volumetric flow rate in which it can operate is around 2 to 3 l/min, as presented in Figure 3.8 where the operation range of this specific pump is given in more detail (200- 1000 rpm). Moreover, these pumps operate in low pressures. For example, the metallic head from stainless steel 316 has a maximum discharge pressure limit at 70 bar, while the maximum suction pressure is 17 bar, which are greater than the expected values in the current system.

D/G-10 Series Performance

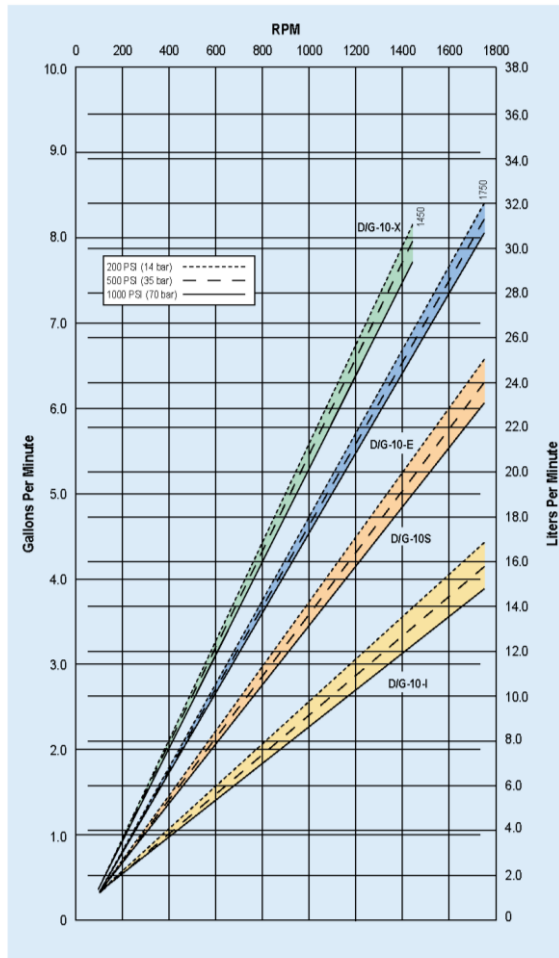


Figure 3.8 Piston- diaphragm pump G-10 operation range, Wanner company

The net weight of the selected pump is around 22 kg, while the maximum motor power (which operates the pump) is equal to 2.2 kW at 960 rpm (50 Hz).

Some design features of the pump with metallic head are presented in Figure 3.9 below. The numbers in parenthesis correspond to dimensions in [mm], and it derives that the maximum pump dimensions are almost 30x20 cm.

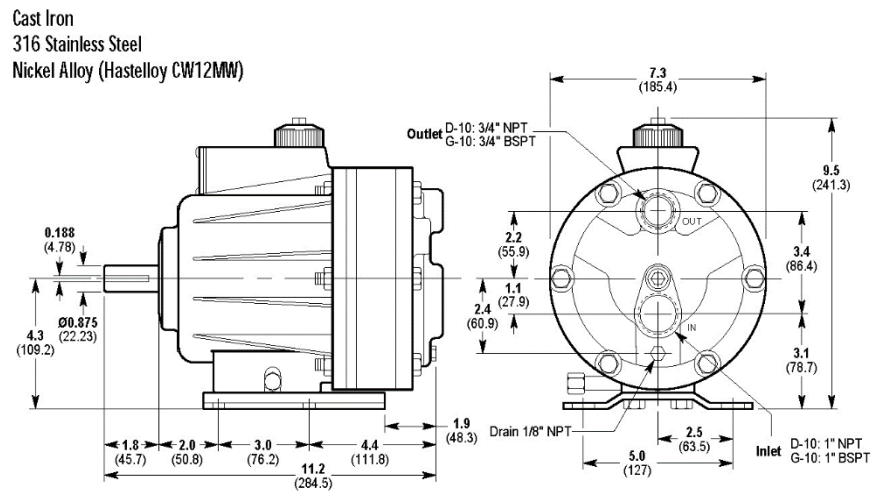


Figure 3.9 Design features of the organic fluid pump Wanner G-10

Moreover, this pump has a maximum temperature limit at 121 °C, which is significantly high, and minimum at -10 °C, while the rotational speed is not kept constant in order to maximize the produced power at every moment, as it has been presented in the analysis of Chapter 2. A frequency inverter controls the rotational speed. The motor of the pump is placed on the same shaft with the pump through a flexible coaxial coupler and it is aligned on a heavy-duty steel base, according to the common practice. Moreover, a cooling fan coaxially connected to the motor and electrically independent (3-phase), which rotates with constant rotational speed is used, in order to ensure the adequate motor's cooling especially when its rotational speed is very low (low frequency).

The selected pump is shown in Figure 3.10, where on the left the (polypropylene) pump is observed with and without the (brass) metallic head, and on the right the installed pump in the laboratory is presented.

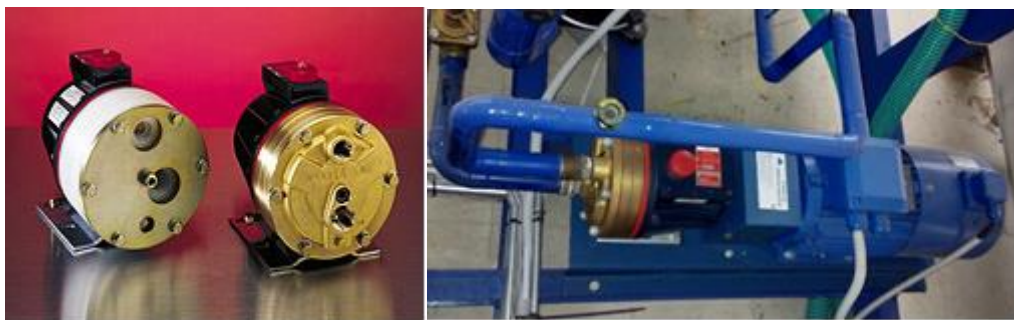


Figure 3.10 The organic fluid pump selected (without and with the metallic head) and installed in the laboratory

The detailed features of the selected pump are presented in Table 3.4:

Table 3.4 Technical features of the organic fluid pump Wanner G-10

General features of the piston- diaphragm pump	
Company	Wanner
Type	Hydra-cell
Series	G10XKBTHFEHB
Maximum volumetric flow rate (@1450 rpm)	29 l/min
Metallic head	Brass
Diaphragms	Buna-N-XS
Valves	Stainless steel 316
Valve seat	Stainless steel 316
Valve spring	Elgiloy
Springs	Elgiloy
Pump body	Aluminum
Lubricant	10W30

3.3.2.2 Heat exchangers

The heat exchangers used for the heat transfer from and to the organic fluid are counter- flow plate heat exchanger [3.3, 3.6]. These heat exchangers are compact with good efficiency, low cold/ hot temperature difference, they can operate at high pressures (up to 35- 40 bar) and they are commercially available especially for low thermal power (from few kW_{th} up to few MW_{th}) with low cost. As presented in the analysis of Chapter 2, the capacity of the evaporator is 100 kW_{th}. On its hot side, MEG is circulated while the minimum temperature difference to the organic fluid (pinch point) is 10 K. Some manufacturers of high-quality plate heat exchangers are Alfa Laval, CIAT and Danfoss. All three companies have products of high efficiency and tolerance in high pressures, while offering a wide range of heat exchangers according to their heat capacity (low to medium and high capacity). In the current system, the evaporator selected is a CIAT product. Such a heat exchanger is presented in Figure 3.11 where the inlet and outlet piping is observed.



Figure 3.11 Counter- flow plate heat exchanger, CIAT

As observed in Figure 3.11, on the up and left side and low right side the organic fluid inlet and outlet are observed, when on the up and right and low and left side the MEG inlet and outlet are shown (counter- flow).

In Figure 3.12, the inner part of this heat exchanger is shown where the plates and the heat exchanging area between the two flows are shown, as well as the way they are placed. On the connection points brazing has been placed in order to avoid the high-pressure losses and the possible mixture of the two flows.

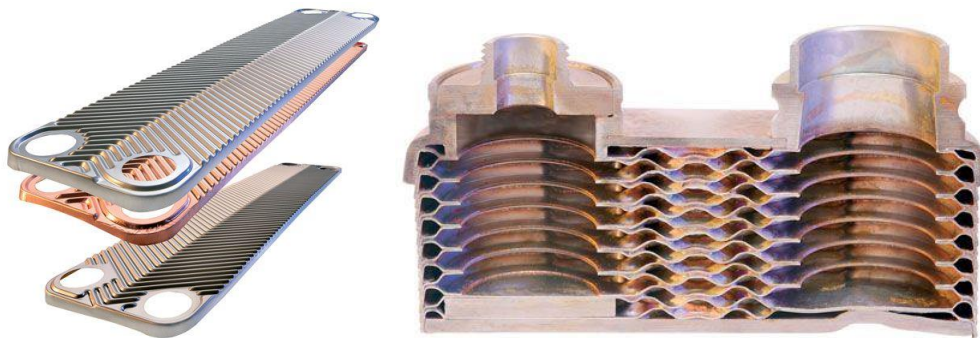
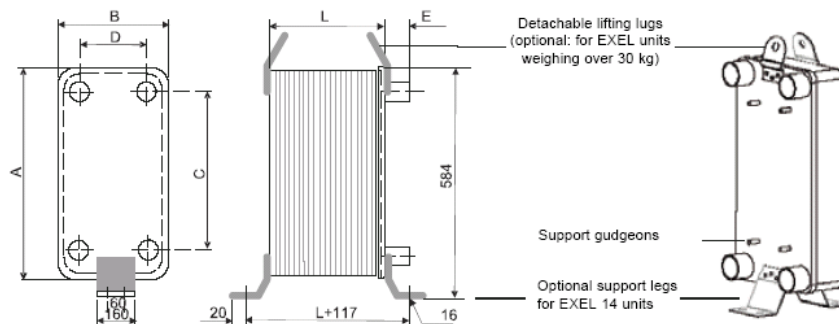



Figure 3.12 Heat exchanger's plates

Usual dimensions of such a heat exchanger of a capacity of 100 kW_{th} are: height around 0.5 m and width around 0.25 m. The number of plates of the current heat exchanger is 70 plates and the data sheet as well as the drawing of the heat exchanger are presented in Figure 3.13:





Project references :
Two-stage Rankine-RO

Date : 24/02/2012
Page : 1 / 1

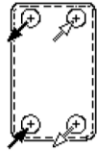
Client : AUA
Contact : SYNERGASIA
Your reference : SYNERGASIA

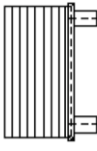
AUA
Your contact :
Phone : Fax : e-mail :

EXEL HEAT EXCHANGER
EXL 14 70 fig. 511

Very economic heat exchanger for its basic cost, easy installation and maintenance. Very light and compact it is easy to install. EXEL has a very high pressure withstand because it is entirely brased.

	R245fa	Pure MEG
Evaporating temperature (*)	115 °C	
Inlet / outlet temperature		130 / 110 °C
Superheat	5 °C	
Liquid temperature before evaporation	35 °C	
Flow	0.494 kg/s	1.84 kg/s
Pressure drop	7.72 mbar	44 mbar
Fouling		0.000005 m ² K/W
Working pressure / design	19.5 / 2.5 bar	1.96 / 30 bar
Inlet/outlet piping	With groove	Without groove
Heat exchange coefficient :	4,490 W/m ² /K	2,180 W/m ² /K
Speed :		0.0875 m/s
Reynolds :		321
Dtm / Dtmc :	18.2 / 18.2 °C	
Installed area / IA/RA :	8.80 m ² / 6.79	





Dimensions (L x w x h) 206 x 265 x 528 mm

Empty weight 37 kg

Total volume : 15.6 l

Plates Stainless 316

Brazings Copper

Connections st. steel 316

By brazing 54 or 53.98 mm

Fluids circulation counter flow

Construction in accordance with CIAT standard PED 97/23/EC hot/cold : Article 3.3 / Category II CIAT approval

Our units are guaranteed against all manufacturing faults but we are not responsible in case of corrosion
Performances validated for use with an oil miscible with the frigorigen fluid
(*) Value of the dew point temperature corresponding to the pressure measured at the outlet connection of the unit

Description	Quantity
EXL 14 70 fig. 511	1
- Distribution system for EXL14 (evaporation) - 7007076	1
Options in extra :	
- Insulation (25 mm glass wool + aluminium sheet)	1
- Flanges DN50/PN40 on 1 circuit	1
- Supporting with studbolts fixed on rear face (non insulated unit)	1

As per CIAT general sales conditions in your possession

C:\PROGRAM FILES\CIAT\TU\DELESA1.ECH - 002
ELSAV 1.02.17 - EO 05/2003

Figure 3.13 Data sheet of the used heat exchanger, CIAT

As presented in Figure 3.13, the heat exchanger that has been used is of type EXL 1470, with 70 plates in total, plate dimensions 206 x 265 x 528 mm, total heat exchange area 8.8 m² and heat capacity 100 kW_{th}. The exact same heat exchanger has been used on the condensation part of the ORC engine where the two flows are the organic fluid on the hot side and water from the laboratory tank on the cold side. The two heat exchangers are shown in Figure 3.14:

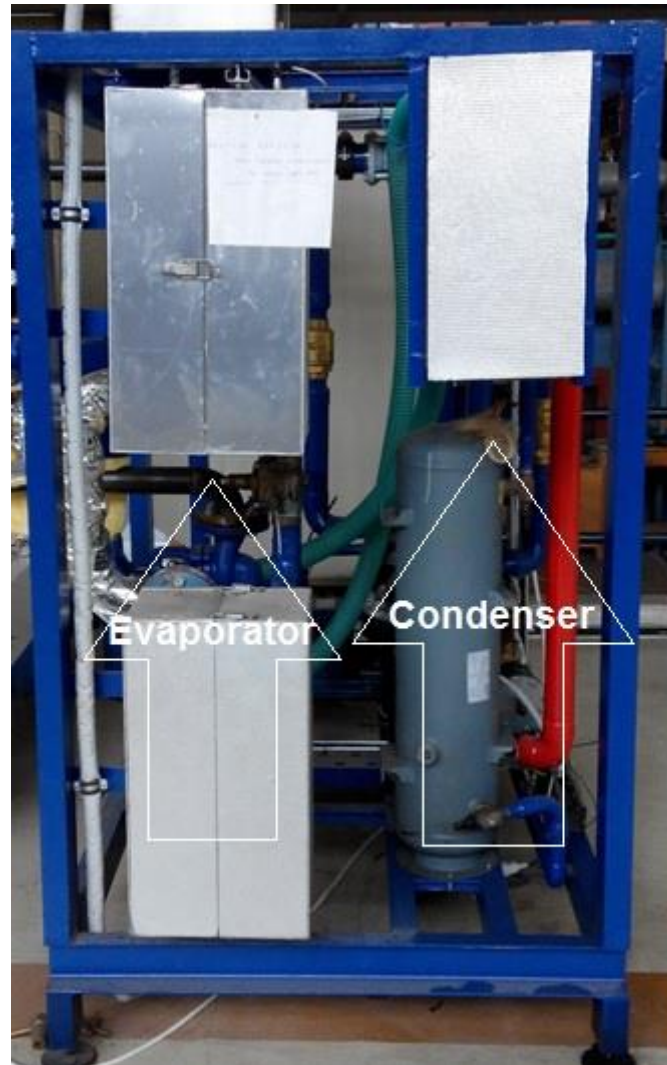


Figure 3.14 Counter- flow heat exchangers (evaporator- condenser) installed on the ORC engine

For the condensation, the water from the laboratory water tank must circulate on the cold side of the condenser in order to reduce the organic fluid temperature at the expander's outlet and before the pump's inlet. Therefore, a small pump is used for the water circulation. This pump was also available from the previous project [3.5]. It is a single stage centrifugal pump of DAB company, model 18/500T, presented in Figure 3.15:



Figure 3.15 Centrifugal pump K 18/500 T, DAB company

Its operation features at the typical operating point are:

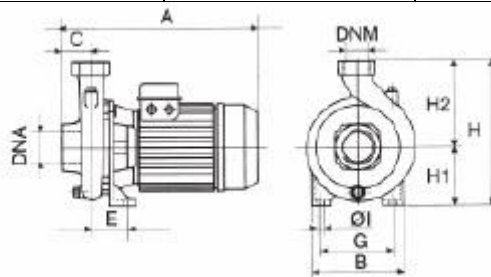
Total head: 27 m

Mass flow rate: 20 m³/h

In Table 3.5, the electrical and dimensional features of this pump are presented:

Table 3.5 Electrical and dimensional features of K18/500T, DAB pump

Model	Voltage at 50Hz	Maximum power	Nominal power	Current
K18/500T	3x230- 400 V AC	3.4 kW	3 kW	10.2- 5.9 A
	A B C	E G ΦI	H H1 DNA	DNM Weight
K18/500T	440 240 62	100 155 14	312 132 2 ^{1/2} "G	2" 35.6kg



3.3.2.3 Organic fluid receiver vessel and filter

The receiver vessel of the HFC- R245fa is placed before the pump on the ORC engine in order to ensure the smooth operation of the pump, since the organic fluid will always be available and ready on the suction line. The most important design parameters are:

- Maximum operation pressure which is equal to the maximum organic fluid pressure in the cycle (20 bar)
- Vessel volume, which depends on the operation point variations and with the sub- cooling of the organic fluid at the pump inlet, since the initial filling of the cycle with HFC- R245fa has a direct effect on the sub- cooling and the operation of the system in general.

The organic fluid filter is placed after the receiver vessel and before the pump, in order to protect the pump and the rest of the ORC components from possible dirt, which has entered the organic fluid or oil excess.

The receiver vessel used in the current system is presented in Figure 3.16:



Figure 3.16 Receiver vessel and filter of the organic fluid

3.4 Scroll expanders

3.4.1 Selection

The expander holds a vital role in the overall system performance since it is a core component of the ORC engine. There are two main types of expanders usually applied in ORC technology: the velocity type, such as axial turbines and radial-flow turbines and the positive displacement type, such as scroll expanders, screw expanders, piston expanders and rotary vane expanders. Turbine expanders are mostly used in relatively large-scale systems with an output power above 50 kW. Some experimental and modeling researches have recently employed turbine expanders in small-scale ORC systems, however, turbine expanders are not suitable for small-scale units, mainly because their rotational speed increases exponentially with the decrease of turbine output power. Moreover, a small-scale turbine expander is expensive and not commercially viable. Recent research has resulted in that the positive displacement expanders are more suitable for small-scale units. Scroll machines have been widely used in the fields of air conditioning and refrigeration. The scroll machine technology has become more matured in the residential and commercial markets ever since the continuous development and improvements of manufacturing technologies. The majority of scroll expanders integrated in low-grade energy utilization systems are modified from scroll compressors. Some commercial and in-house designed scroll expanders have also been manufactured, however, great performance differences have resulted between practical applications and theoretical researches, because of several loss factors such as under- and over-expansion, friction losses, internal leakage, supply pressure drop and heat transfer. Several types of commercial scroll machines can be modified into expanders which can be integrated into ORC systems for low grade heat recovery, such as hermetic refrigeration scroll compressor, automotive air-conditioning compressor and open drive scroll air compressor as shown in Figure 3.17, [3.6].

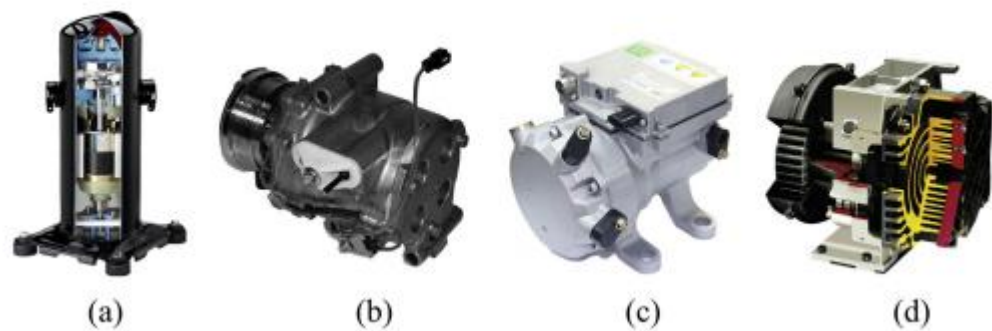


Figure 3.17 Types of scroll compressors: (a) hermetic refrigeration compressor, (b) open- drive automotive A/C compressor, (c) Semi- hermetic automotive A/C compressor and (d) air compressor [3.6]

In the current application, a hermetic refrigeration compressor has been selected to be modified to a hermetic scroll expander, as the compressor and the motor are a single compact and portable unit that can easily be handled. No coupling, belt and pulley arrangement is involved thus the maintenance is lesser. The lubrication system is inherent and no external lubrication is required, while the suction and discharge connections and the electrical connections are available externally. Finally, hermetically sealed compressors have very long life and the manufacturers offer warranty period of up to seven years for these compressors.

The general characteristics and requirements of the two expanders of the ORC engine have been presented in the optimization analysis of Chapter 2. Their most important feature is that since they operate in a pressure ratio equal to 3 the inner pressure ratio is almost 3 and due to the great rotational speed variation, there is a limit concerning the swept volume of these expanders.

During the optimization analysis of Chapter 2, the swept volumes of the two expanders and their effect on the rotational speed have been examined. The result was that the swept volume of the first expander varies between 120- 240 cm³ and of the second expander 240- 360 cm³ (where an even smaller expander could be used in order to decrease the cost, operating at the maximum load close to the permitted limit of its rotational speed). However, it is favorable to use a larger expander in lower rotational speed in order to avoid a mechanical efficiency decrease due to increased friction losses. It should also be noted that the maximum power production of each expander is almost 6 kW, in order to produce almost 12 kW from both expanders at full load operation (net power production equal to 9 kW).

The expanders that will be used in the current system are market available scroll compressors in reverse operation. Some reliable and highly efficient scroll compressors are manufactured by the companies Sanden, Copeland and Hitachi. In previous research studies [3.11, 3.12] a hermetic scroll expander of the Copeland company has been used, while in more previous studies [3.1- 3.3., 3.8] an open- type expander of the company Sanden has been used, where its mediocre efficiency due to the lack of an efficient lubrication system has been observed. Moreover, the scroll compressors of the companies Sander and Hitachi are intended especially for smaller range applications, since the larger compressors they obtain, have a swept volume of 120 cm³, a limit significantly low for the current application (the second expander has almost double swept volume than the first one, in order to manage the large volumetric flow rate caused by the lower temperatures at its inlet).

With the use of a special selection software (Product Selection Software), provided by Copeland (redeemed by Emerson Climate Technologies), the adequate scroll compressors for the current application are being selected. In Figure 3.18 the home page of the aforementioned software that has been used is presented:

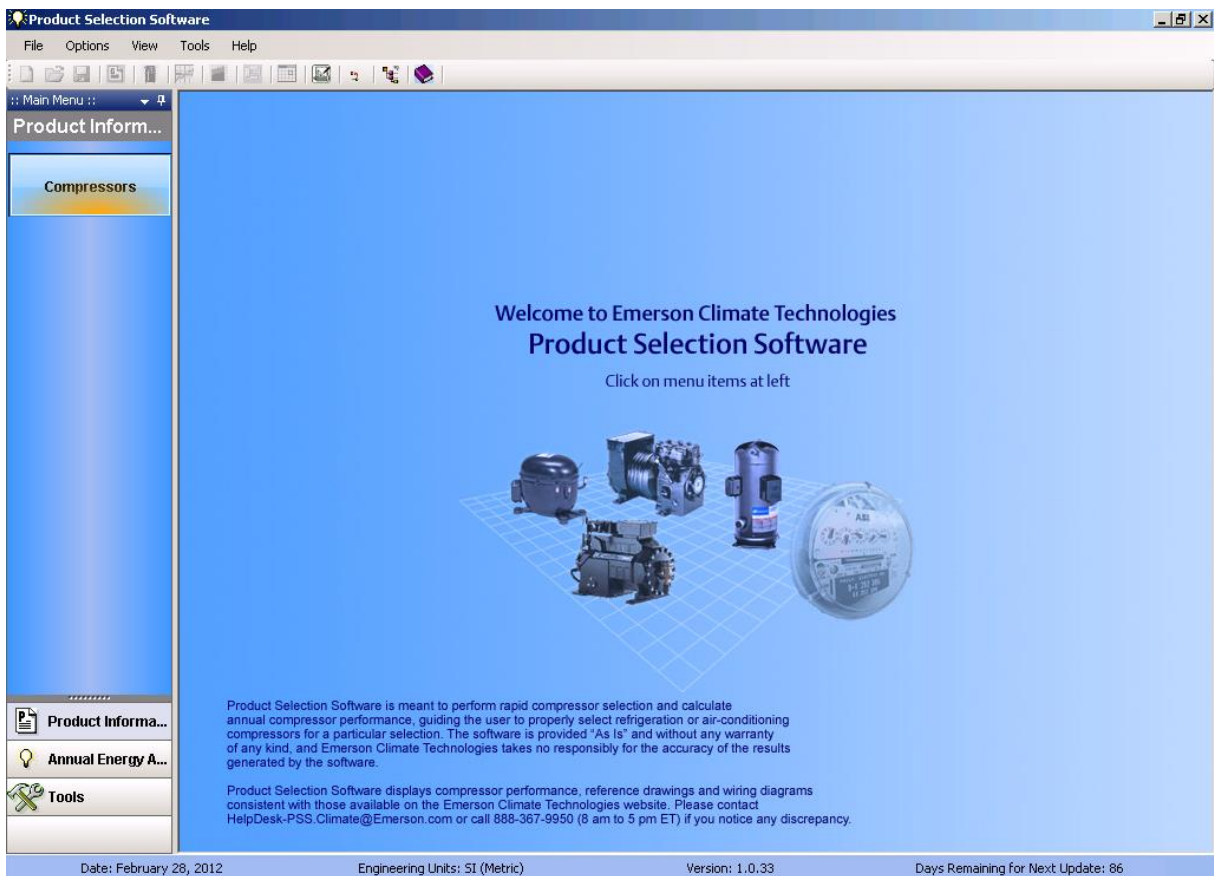


Figure 3.18 Product (scroll compressors) selection software home page

In Figure 3.19, the selection process of the adequate scroll expander (compressor) for the two stages of the ORC engine is shown. This selection is based on the data that have been previously calculated, while the scroll compressors operation knowledge is necessary, since the available data concern these volumetric machines. The data input are the basic design data, like operation temperatures, the selected organic fluid, sub-cooling and superheating temperatures etc. From the expanders available, the one that satisfies all the criteria related to the power (maximum almost 6 kW), to the maximum volumetric flow rate (in m^3/h) and the swept volume related to the rotational speed can be selected.

The screenshot shows the 'Product Selection Software - [Compressor]' interface. The search criteria are set to: Application: Air-Conditioning, Voltage: 380-460, Refrigerant: All, Phase: Three, Temp. Range: Air-Conditioning, Frequency: 50, Product Type: Scroll, Modulation: All, Availability: All. The search results table is as follows:

Select	Model	Refrig.	HP	Compressor Capacity (W)	Compressor COP	Evaporator Capacity (W)	Evaporator COP	Return Gas Temp. (°C)	Compressor Superheat (K)
<input type="checkbox"/>	ZR125KC-TFD	R-22	10.00	31,000	3.44	31,000	3.44	18.3	11.1
<input checked="" type="checkbox"/>	ZR125KCE-TFD	R-134a	10.00	20,500	3.33	20,500	3.33	18.3	11.1
<input type="checkbox"/>	ZR125KCE-TFD	R-407C	10.00	30,200	3.38	30,200	3.38	18.3	11.1
<input type="checkbox"/>	ZR11M3-TWD	R-22	9.00	26,300	3.31	26,300	3.31	18.3	11.1
<input type="checkbox"/>	ZR11M3E-TWD	R-22	9.00	26,300	3.31	26,300	3.31	18.3	11.1
<input type="checkbox"/>	ZR11M3E-TWD	R-407C	9.00	25,600	3.24	25,600	3.24	18.3	11.1
<input type="checkbox"/>	ZR108KT-TFD	R-22	9.00	26,400	3.52	26,400	3.52	18.3	11.1
<input type="checkbox"/>	ZR108KTE-TFD	R-407C	9.00	25,800	3.40	25,800	3.40	18.3	11.1

The interface also shows search criteria, conditions (Temperature, Pressure), and various settings like Economizer Settings, Temp. Range Info, Definitions, Search, and Reset. The status bar at the bottom indicates 'Date: May 15, 2012', 'Engineering Units: SI (Metric)', 'Version: 1.0.33', and 'Days Remaining for Next Update: 9'.

Figure 3.19 Data input and scroll expanders (compressors) selection

With the use of this software, the two scroll compressors are selected, taking under consideration all the technical parameters presented in previous analysis. The selected scroll compressors are presented in Tables 3.6 and 3.7. They are used in applications related to heat pumps, while they include a self-lubrication system in order to minimize friction losses (leading to volumetric efficiency increase with simultaneous increase of the mechanical efficiency due to friction losses decrease [3.11]). Another advantage of the scroll compressors is that they include in one unit the motor and generator which operate efficiently and there is no need of any added component. Additionally, any organic fluid leakage is eliminated and their cost is relatively small.

Table 3.6 First expander's specifications


General features		
Company	Copeland	
Type	Scroll	
Series	ZR125KCE-TFD	
Swept volume	167.15 cm ³ /rev	
Maximum volumetric flow rate (@2900 rpm)	29.08 m ³ /h	
Maximum pressure	32 bar	
Net weight	61.23 kg	
Inner volume ratio	~3	
Electrical features		
Maximum electric current	19.6 A	
Operation frequency	50-60 Hz	
Phases	3	
Voltage	380-460 V	
Maximum electric power	9.02 kW	
Efficiency		
Maximum isentropic efficiency (compressor operation with R- 134a)	70.9%	
Power at the nominal pressure ratio	6.15 kW	

Table 3.7 Second expander's specifications

General features		
Company	Copeland	
Type	Scroll	
Series	ZR190KCE-TFD	
Swept volume	249.16 cm ³ /rev	
Maximum volumetric flow rate (@2900 rpm)	43.35 m ³ /h	
Maximum pressure	32 bar	
Net weight	66.22 kg	
Inner volume ratio	~3	
Electrical features		
Maximum electric current	34 A	
Operation frequency	50-60 Hz	
Phases	3	
Voltage	380-460 V	
Maximum electric power	15.64 kW	
Efficiency		
Maximum isentropic efficiency (compressor operation with R- 134a)	69.2%	
Power at the nominal pressure ratio	9.2 kW	

In Figure 3.20, the scroll compressor design is shown, where the inlets/ outlets of the organic fluid and the necessary oil for the lubrication of the expander, are observed. In Figure 3.21, the design of the second compressor is presented.

CHAPTER 3 – Prototype design and construction

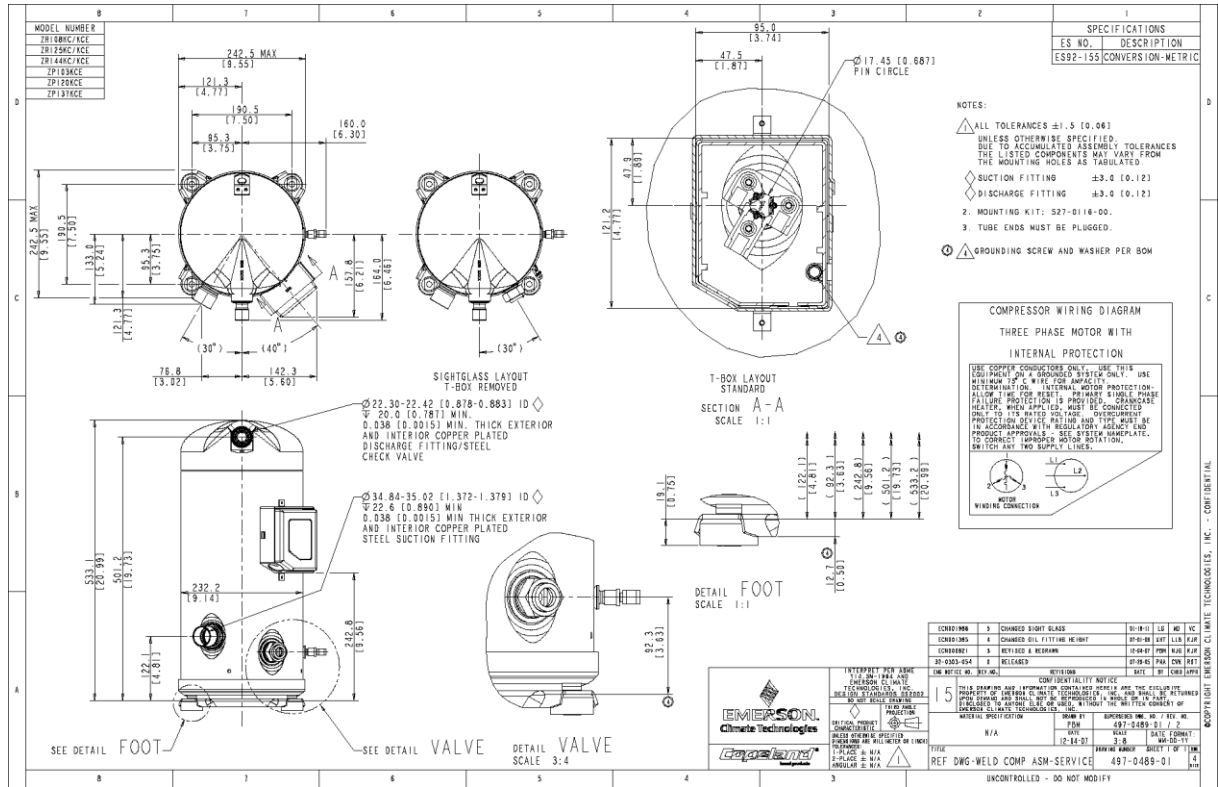


Figure 3.20 First expander's detailed drawing

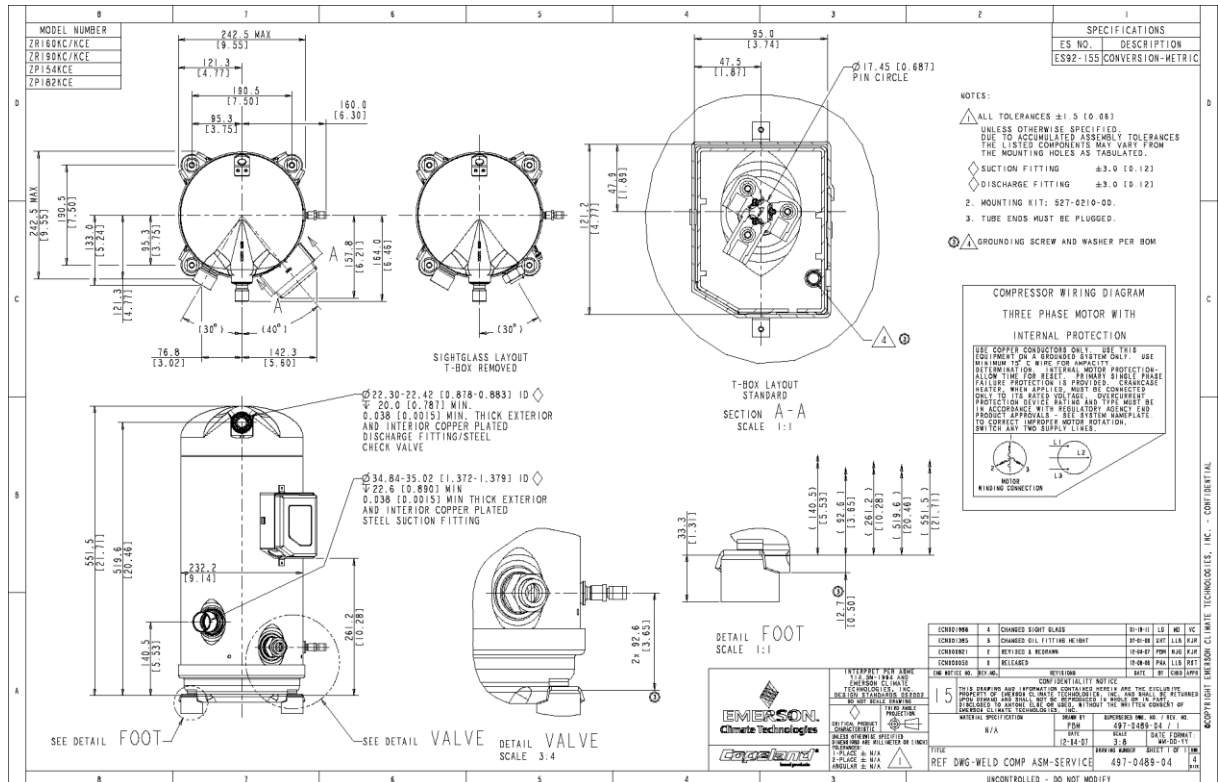


Figure 3.21 Second compressor's detailed design

It is observed that the external dimensions of the two expanders are identical. This is the reason that their weight is similar, even though the second expander includes a larger scroll geometry and motor/ generator.

CHAPTER 3 – Prototype design and construction

The efficiency data which are given by the manufacturer correspond to the scroll compressors and are not valid when they operate reversely (as expanders). Therefore, during the experimental investigation (Chapter 5) their operation will be examined in detail in several operating conditions. For completeness, the efficiency data of these expanders in compression mode (normal operation) as provided by Copeland are given in Figures 3.22 and 3.23 for several inlet and outlet conditions.

		AIR CONDITIONING								
		RATING CONDITIONS		ZR125KCE-TFD		HFC-134A COPELAND SCROLL® TFD 380/420-3-50				
		11.1 K Superheat 8.3 K Subcooling 35 C Ambient Air Over								
		50 Hz Operation								
		Evaporating Temperature C (Sat Dew Pt Pressure, bar)								
		-23(1.2)	-20(1.3)	-15(1.6)	-10(2)	-5(2.4)	0(2.9)	5(3.5)	10(4.1)	15(4.9)
Condensing Temperature C (Sat Dew Pt Pressure, bar)	65 (19)	C						15900	19500	
	P							7550	7550	
	A							14.7	14.7	
	M							444	530	
	E							2.1	2.6	
	%							60.7	65.3	
	60 (17)	C						13900	17300	21100
	P							6800	6850	6850
	A							13.4	13.4	13.5
	M							376	455	545
E							2	2.5	3.1	
%							59.2	63.7	67.9	
55 (15)	C					12050	15100	18600	22700	
P						6100	6150	6200	6200	
A						12.3	12.3	12.3	12.4	
M						315	384	465	555	
E						2	2.5	3	3.7	
%						57.5	62.1	66.2	69.8	
50 (13)	C				10350	13000	16200	19900	24200	
P					5450	5500	5550	5600	5600	
A					11.2	11.2	11.3	11.3	11.4	
M					261	321	391	470	560	
E					1.9	2.4	2.9	3.5	4.3	
%					55.4	60.3	64.6	68.1	70.9	
45 (12)	C			8750	11100	13950	17300	21200	25700	
P				4870	4900	4970	5050	5100	5050	
A				10.3	10.3	10.4	10.4	10.5	10.6	
M				214.5	266	327	398	480	570	
E				1.8	2.3	2.8	3.4	4.2	5.1	
%				52.7	58.2	62.9	66.5	69.1	70.6	
40 (10)	C		7350	9350	11850	14850	18400	22500	27100	
P			4420	4390	4420	4480	4540	4590	4590	
A			9.4	9.5	9.6	9.6	9.7	9.8	9.9	
M			175.5	218	271	333	404	485	575	
E			1.7	2.1	2.7	3.3	4	4.9	5.9	
%			49.2	55.4	60.7	64.9	67.6	68.8	68.6	
30 (8)	C	7150	8300	10550	13300	16600	20500	24800	29800	
P		3640	3570	3520	3540	3610	3700	3770	3800	
A		8.2	8.3	8.3	8.4	8.5	8.6	8.7	8.8	
M		158	180.5	225.5	279	341	413	495	580	
E		2	2.3	3	3.8	4.6	5.5	6.6	7.8	
%		49.8	54.1	60.2	64.4	66.2	65.7	62.9	57.8	
25 (7)	C									
P										
A										
M										
E										
%										

Nominal Performance Values (±5%) based on 72 hours run-in. Subject to change without notice. Current @ 380 V

C:Capacity(Watts), P:Power(W), A:Current(Amps), M:Mass Flow(kg/hr), E:COP(W/W), %:Isentropic Efficiency%)

Figure 3.22 Efficiency data of the first compressor in several conditions

RATING CONDITIONS
 11.1 K Superheat
 8.3 K Subcooling
 35 C Ambient Air Over

50 Hz Operation

AIR CONDITIONING

ZR190KCE-TFD
 HFC-134A
 COPELAND SCROLL®
 TFD 380/420-3-50

Evaporating Temperature C (Sat Dew Pt Pressure, bar)

		-23(1.2)	-20(1.3)	-15(1.6)	-10(2)	-5(2.4)	0(2.9)	5(3.5)	10(4.1)	15(4.9)
Condensing Temperature C (Sat Dew Pt Pressure, bar)	65 (19)							23200	28700	
	C							11500	11500	
	P							24.3	24.4	
	A							650	780	
	M							2	2.5	
	E							58.2	62.9	
	%									
	60 (17)						20600	25700	31000	
	C						10300	10300	10300	
	P						22.3	22.4	22.5	
A						555	675	805		
M						2	2.5	3		
E						57.7	62.8	66.3		
%										
55 (15)					18000	22700	27800	33500		
C					9200	9250	9300	9350		
P					20.5	20.6	20.7	20.8		
A					470	580	695	820		
M					2	2.5	3	3.6		
E					56.6	62.3	66.2	68.5		
%										
50 (13)				15500	19800	24500	29700	35500		
C				8200	8250	8300	8350	8400		
P				18.9	19	19.1	19.2	19.3		
A				391	490	595	705	825		
M				1.9	2.4	3	3.6	4.2		
E				55	61.3	65.7	68.3	69.2		
%										
45 (12)			13050	17000	21400	26200	31500	37500		
C			7300	7350	7400	7500	7550	7650		
P			17.4	17.6	17.7	17.8	17.9	18		
A			320	409	500	600	710	830		
M			1.8	2.3	2.9	3.5	4.2	4.9		
E			52.6	59.7	64.7	67.7	68.9	68.2		
%										
40 (10)		10700	14400	18400	22800	27600	33000	39000		
C		6450	6550	6600	6700	6750	6850	6950		
P		16.2	16.4	16.5	16.6	16.7	16.8	17		
A		256	337	421	510	605	710	830		
M		1.7	2.2	2.8	3.4	4.1	4.8	5.7		
E		49.2	57.5	63.2	66.7	68.3	67.8	65.5		
%										
30 (8)		11000	13100	16700	20700	25200	30000	36000	42500	
C		5100	5150	5250	5350	5450	5550	5650	5750	
P		14.5	14.6	14.7	14.8	14.9	15	15.2	15.4	
A		243	285	358	435	520	610	710	825	
M		2.1	2.5	3.2	3.9	4.6	5.4	6.3	7.3	
E		54.4	58.8	63.9	66.4	66.6	64.6	60.5	54.1	
%										
25 (7)										
C										
P										
A										
M										
E										
%										

Nominal Performance Values (±5%) based on 72 hours run-in. Subject to change without notice. Current @ 380 V

C:Capacity(Watts), P:Power(W), A:Current(Amps), M:Mass Flow(kg/hr), E:COP(W/W), %:Isentropic Efficiency(%)

Figure 3.23 Efficiency data of the second compressor in several conditions

It should be noted that the use of electric brake is not necessary for the compressors' electric features determination, since they include asynchronous induction generator. The consideration of the use of a frequency inverter however is necessary for the regulation of the expanders' rotational speed. The compressors' rotational speed can be calculated through their frequency (in Hz converted to

rpm). However, as it will be presented later, electric brakes have been used for both expanders.

3.4.2 Compressor conversion

As previously mentioned, the most important component of the ORC engine is the scroll expander. The conversion includes several processes which mostly concern the modification of the scroll compressors to scroll expanders. The internal side of such a compressor is presented in Figure 3.24:



Figure 3.24 Internal part of a scroll compressor, Copeland company, series ZR

The basic steps of the modification are described below. It should be noted that a similar process took place for both expanders, by installing different connection components (flanges) since the inlet and outlet pressures are significantly different. The modification steps are:

1. Perimetric cutting of the upper part of the inlet chamber (lower than the organic fluid inlet, but higher than the steady scroll geometry), in order to get access to the internal part of the compressor, since they are hermetically sealed in metallic cage, in order to avoid refrigerant leakage. The cut of the upper part of the compressor is shown in Figure 3.25, while in Figure 3.26 the compressor's internal part is observed:



Figure 3.25 Cutting and removal of the scroll compressor's upper part



Figure 3.26 Scroll compressor's internal part

2. Flanges installation for connecting the compressor's head, which are dimensioned depending on the expected pressure range of the organic fluid (especially the maximum pressure) in order to avoid their failure and fluid leakage and to ensure the smooth expander's operation. At the first expander's inlet, the maximum pressure is around 20 bar and at the second 10 bar (second expander operates only in low load). In this way, the expander can open easily and quickly for inspection and maintenance purposes, offering flexibility. The flanges placement is presented in Figure 3.27:



Figure 3.27 flanges placement at both expanders

3. Check valves and non-return valves removal from the inner part of the scroll compressor, which ensure the operation of this component as a compressor. With the removal of these valves the operation as an expander is released. Such a check valve is placed at the compressor's outlet (expander's inlet in reverse operation) at the upper part of the steady scroll (middle picture in Figure 3.25).
4. Concerning the lubrication system, there is no need to interfere. The specific expander has two bearings on its shaft. One of them is placed inside the oil tank and is constantly lubricated, while the second one is placed directly under the moving and the steady scroll (right over the asynchronous generator/ motor). Its lubrication is feasible even in reverse operation as an expander, since the shaft of the expander has an eccentric helical configuration internally and during its rotation the centrifugal forces pump the lubricant oil up at the second bearing (acting like a centrifugal pump), as shown in Figure 3.28. The scroll elements are lubricated and ensure the

decrease of leakages, since the organic fluid contains a small portion of oil (around 1%), which also ameliorates the heat exchange in the evaporator.

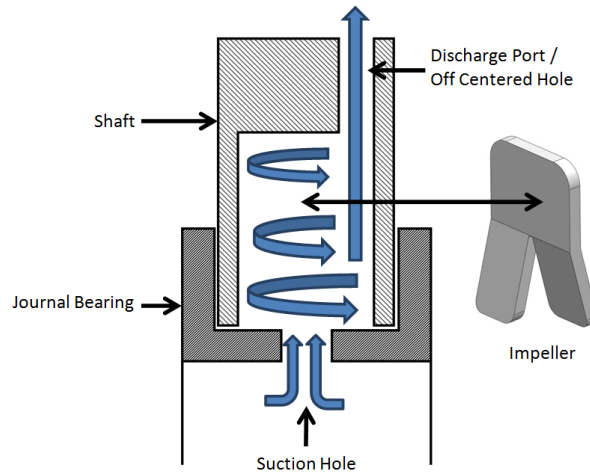


Figure 3.28 Shaft which operates as a centrifugal pump, lubricating the two bearings [3.12]

5. The initial scroll compressor includes an induction motor which can be used in reverse operation like an induction generator [3.13].
6. For securing the sealing and isolation of the two vessels of low and high pressure inside the expander (before and after the scrolls), no spring has been placed which allows the escape of the organic fluid during the initial operation as a common practice [3.12, 3.13]. This method is followed in order to avoid the superheating of the generator during the starting. On the contrary, a thread is placed which can be controlled even from the outside of the expander's cage with the tightening of a screw. This monitored way of control and isolation of the two areas is better than the use of a spring, since it offers better reliability and it is expected to stay indestructible for a long time operation of the expander. During the starting of operation, where the pressure difference is significantly low, the most organic fluid escapes without producing any power. For the initiating of the power production, the piston chamber pressurization is necessary, which is realized through a small hole (of a diameter of 3 mm), which connects the two areas and has been opened during the expander's modification, as presented in Figure 3.29. In Figure 3.30 the aforementioned process and the thread in one of the two modified expanders is observed:

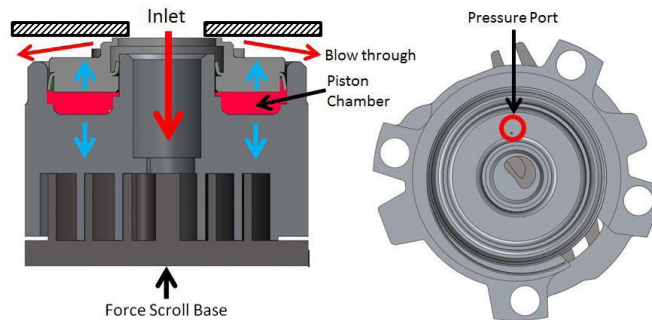


Figure 3.29 Middle piston chamber for pressure counterbalance (left) and small hole (right) [3.12]



Figure 3.30 Small hole (left) and adjustable thread on the cap of the scroll compressor (right)

In Figure 3.31, the internal part of a similar scroll compressor is presented, which has undergone interventions in order to operate as an expander [3.13]. The flange which connects the expander's cap with the main body, as well as the inlet and outlet of the organic fluid are observed.

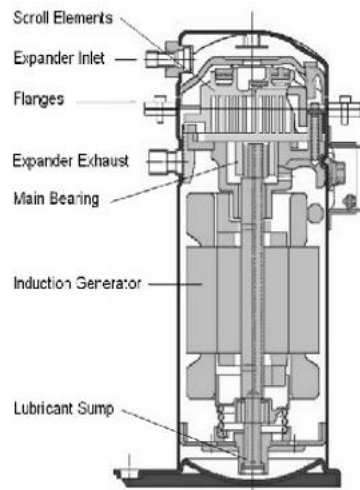


Figure 3.31 Internal design of a scroll expander [3.13]

The modified scroll expanders, installed on the current ORC engine are shown in Figure 3.32.



Figure 3.32 Scroll expanders of the two- stages ORC engine

The two expanders include an analog manometer, however, their inlet and outlet pressure are also measured with pressure sensors, giving a digital signal on the electric panel of the ORC engine.

The switching of single to two- stages operation is realized with the use of an electro vane which is closed during the two- stages operation and opens when the available thermal load is low, thus the first expander is completely by- passed (single stage operation). Moreover, two manually controlled valves are used for the complete isolation (and also for maintenance reasons) of the circuit of the first expander. The electro valve is presented in Figure 3.33.



Figure 3.33 Electro valve for the single and two- stages interval

The electric panel of the ORC engine includes all the electric components such as switches, fuses, cables and the circuit breakers (in case of failure). The inverters are also placed in the electric panel. Two dynamic brake transistors (one for each expander) drive the produced power (AC) and

convert it to direct current (DC) in order to be dissipated in the electric resistances. The resistances are used for the produced power production in the lab, in order to examine the ORC engine alone. The electric brakes selected for the current application are manufactured by Bonitron company and their type is M3452-E75B7-A. These brakes are heavy duty brakes and they can apply braking for 100 % of the time (100% duty cycle). In Figure 3.34 the selected brakes are presented:



Figure 3.34 Bonitron M3452 brakes

The ORC engine electric panel is presented in Figure 3.35, where all the aforementioned electric components are shown.

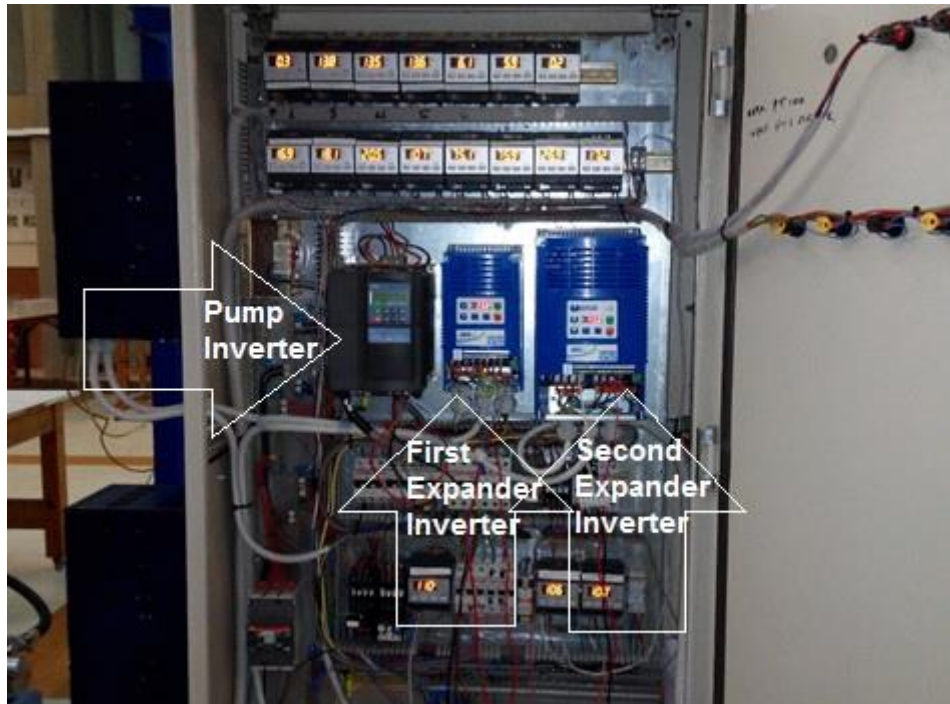


Figure 3.35 ORC engine electric panel

In Figure 3.35, all the digital indicators (LAE company) of all the measurement instrumentation at every location (inlet/ outlet) of each component of the engine are observed. In the middle, the three inverters of the pump (the grey on the left), of the first expander (middle) and the second expander (right) are shown, as well as the two brakes (on the left of the panel) and their connection to the corresponding expander's inverter. The digital meters on the bottom of the panel set the desired temperature of the heat cycle (thermal load input) each time.

3.5 ORC engine assembly and installation

The ORC engine components assembly includes their placement on a common frame, the piping construction, the measurement instrumentation placement in the appropriate place and the organic fluid filling with lubricant oil where needed (i.e. diaphragm pump, expanders). Before the filling with organic fluid, nitrogen under pressure is inserted in the piping (the air pressurizing is avoided in order to eliminate the possibility of humidity existence in the pipes) for the construction monitoring and the identification of any possible leakage. The ORC engine framing and its components are designed as presented in Figure 3.36, where the necessary height difference in order to avoid pump caving is observed. The avoidance of cavitation can also be ensured by the condensation of the organic fluid in order for the pump to manage a slightly sub- cooled organic fluid.

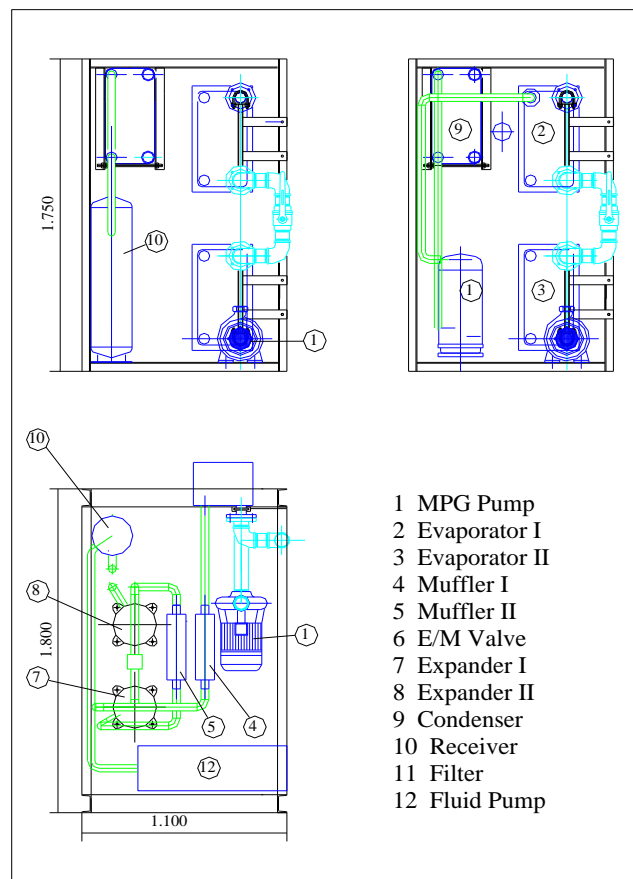
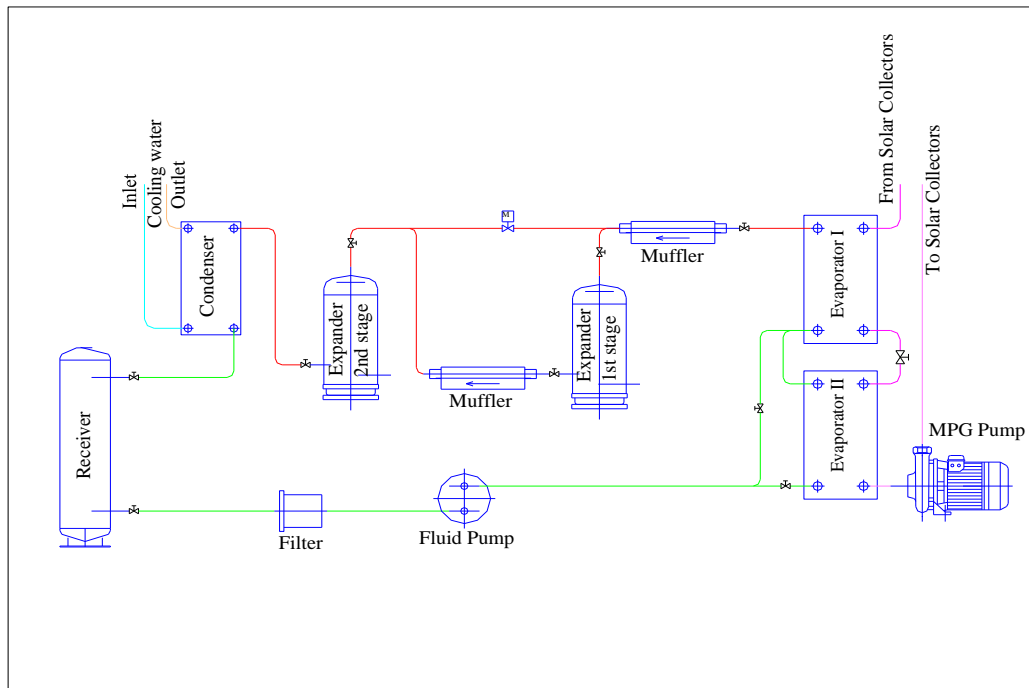


Figure 3.36 Two- stage ORC engine drawings

The frame construction with the basic components of the ORC engine is presented in Figure 3.37.



Figure 3.37 Several views of the ORC engine where the frame and several components (heat exchangers, organic fluid pump, scroll expander, receiver, heat cycle pump) are observed

The finalized ORC engine as well as a detail picture of the modified expanders on the engine are presented in Figure 3.38.





Figure 3.38 The finalized ORC engine and the modified expanders

After the assemblage, the ORC engine is installed in the NTUA Laboratory of Hydraulic Turbomachines, and the electric heater is then connected to the heat source cycle pump as presented in Figure 3.39.



Figure 3.39 The ORC engine and the electric heater connection on the heat source cycle pump

The design of Figure 3.40 presents the electric heater connection to the pump. The heat exchangers are also observed.

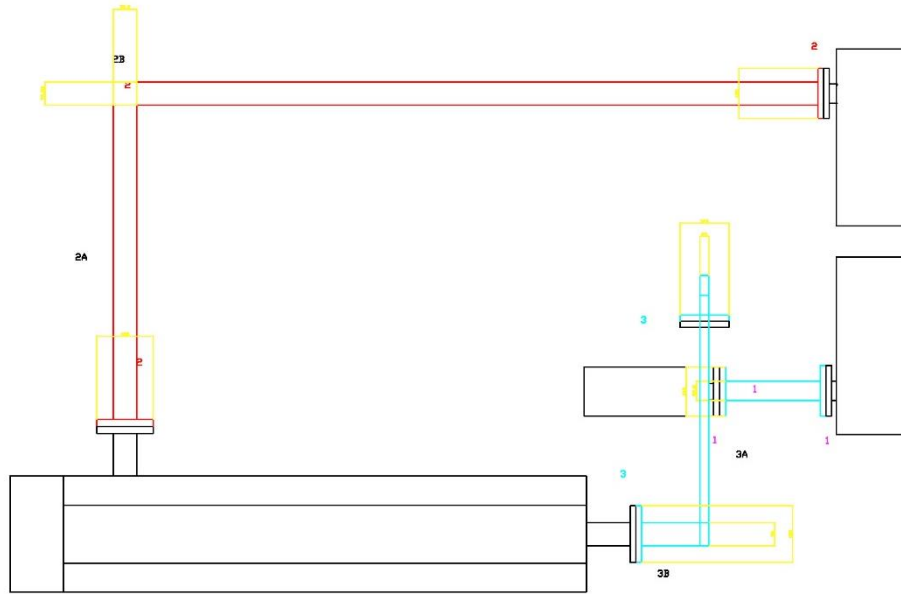


Figure 3.40 The electric heater connection to the heat cycle pump

3.6 Reverse Osmosis Desalination Unit

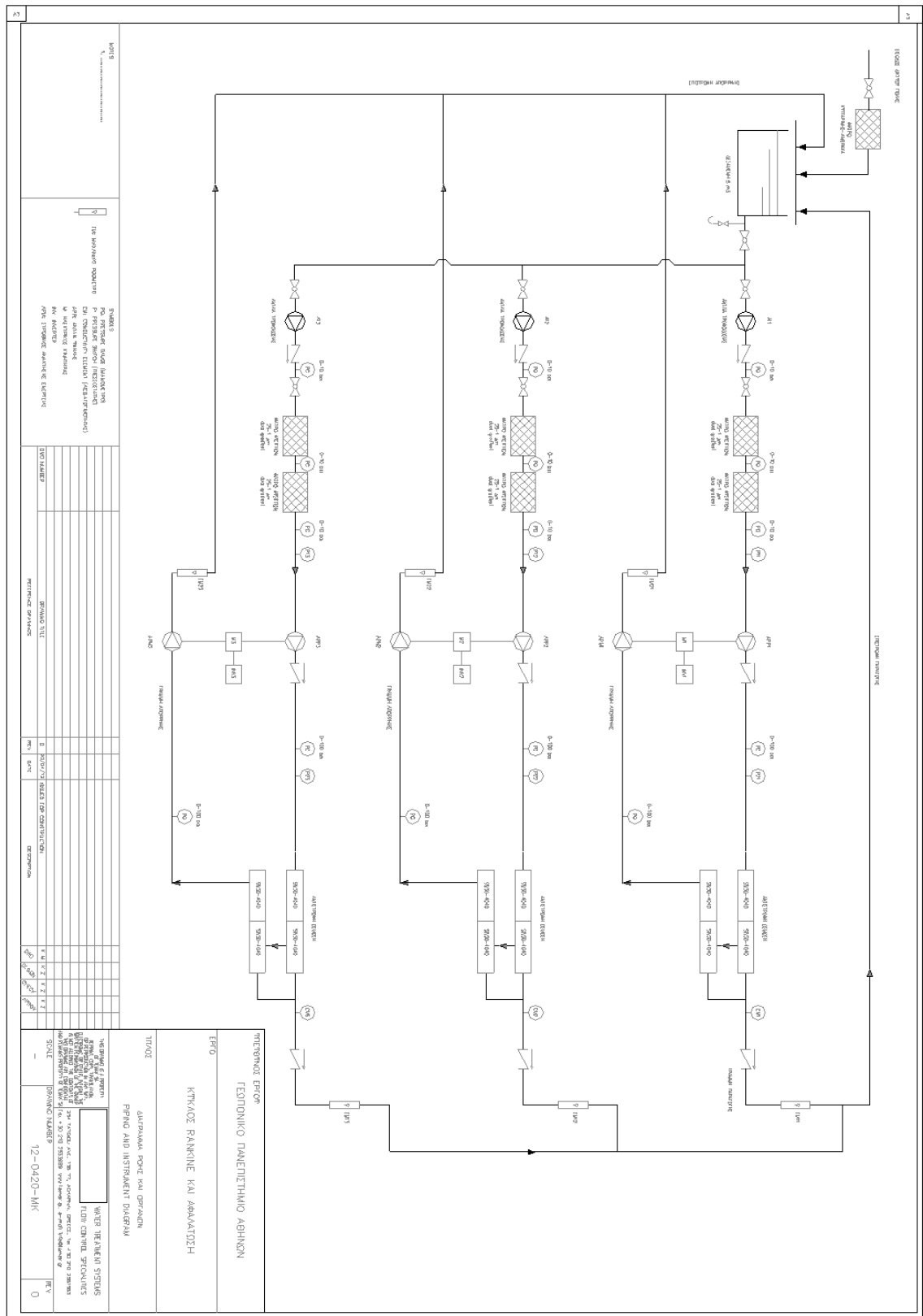


Figure 3.41 Mechanical drawing of the RO unit

The RO unit is designed next, according to the simulation results of Chapter 2. Before the dimensioning of the RO unit, a Piping and Instrumentation Diagram of the RO unit where the three sub- units as well as the feed water tank (same for all three sub- units) are observed. This drawing is presented in Figure 3.41.

3.6.1 Water tank and filter

In the laboratory, tap water passes through a cellulose- carbon filter for a primary filtration and enters the feed water polyethylene tank (of a volume of 5 m³). Then, salt is added in order to create the necessary amount of seawater. The water tank as well as the filter are presented in Figure 3.42.

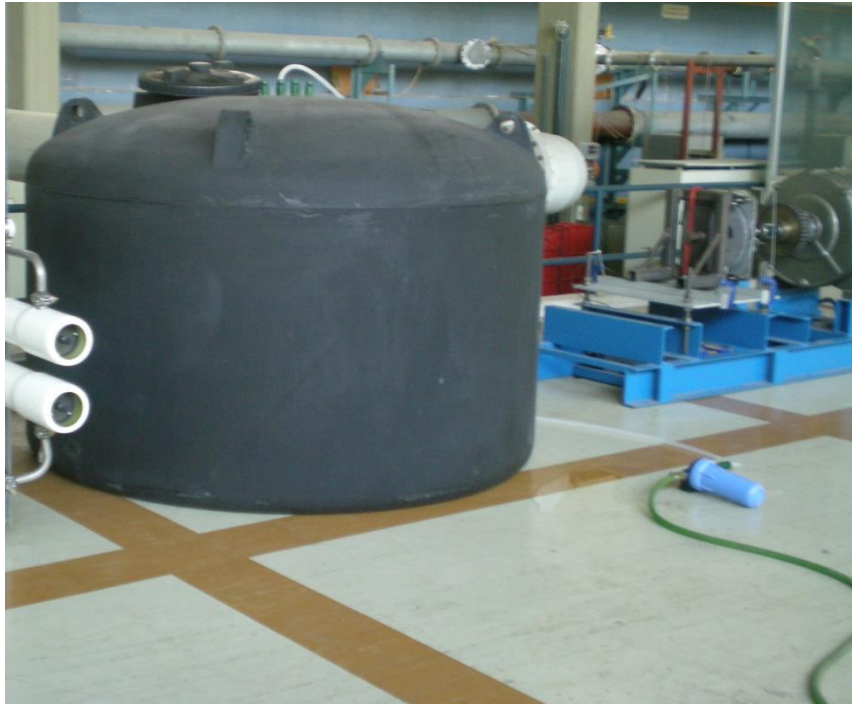


Figure 3.42 The water tank and the cellulose- carbon filter

3.6.2 The RO sub- unit

From the feed water tank, three identical sub- units consisting the RO unit system are fed with seawater. The design and dimensioning of one of those sub- units is subsequently described. The sub- unit selected is of series TSW24 (see Appendix I) and has been manufactured by TEMAK company. A schematic representation of the RO sub- unit is presented in Figure 3.43:

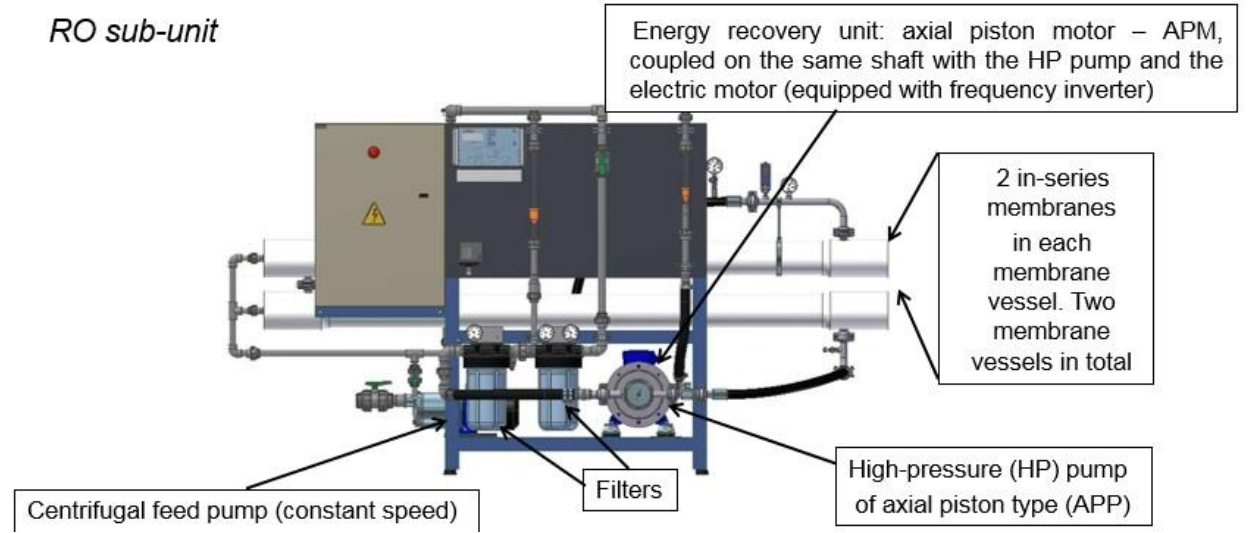


Figure 3.43 RO sub- unit schematic representation, series TSW24, TEMAK company

3.6.2.1 Feed pump

At the inlet of each RO sub- unit there is a feed pump which circulates the seawater in the hydraulic system. This pump is manufactured by the company LOWARA, type 2HMS4 (see Figure 3.46), with a three-phase motor of power capacity of 0.45 kW (bipolar, with constant rotational speed equal to 2900 rpm), made of stainless steel 316L, with special passivation in order to tolerate corrosion from the seawater contact. The mechanical design of this pump is shown in Figure 3.44 and a picture of the pump with its motor is presented in Figure 3.45.

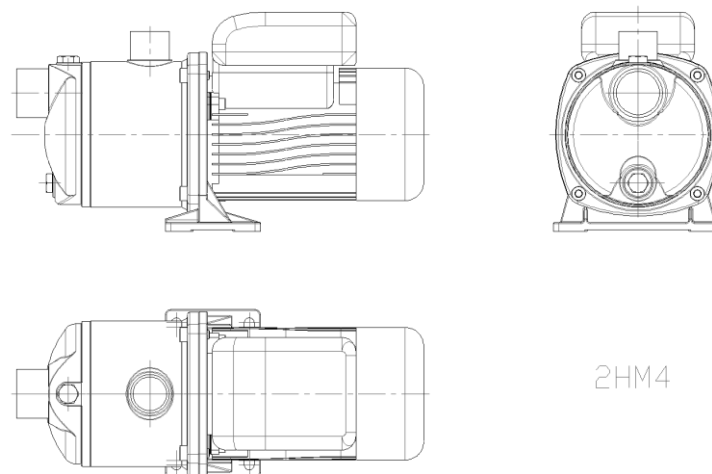


Figure 3.44 Mechanical drawing of the RO sub- unit feed pump



Figure 3.45 The RO feed pump (LOWARA company)

This pump is carefully selected in terms of materials, in order to avoid corrosion due to the contact with the seawater. In Table 3.8, the materials of each part of the pump are observed.

Table 3.8 Feed pump parts' materials

PART	MATERIAL			
		UNI	ASTM - AISI	EN - DIN
Pump body	Stainless steel	X2 CrNiMo 17-12-2	316L	1.4404
Seal housing disk	Stainless steel	X2 CrNiMo 17-12-2	316L	1.4404
Diffusers	Stainless steel	X2 CrNiMo 17-12-2	316L	1.4404
First stage case	Stainless steel	X2 CrNiMo 17-12-2	316L	1.4404
Spacers	Stainless steel	X2 CrNiMo 17-12-2	316L	1.4404
Impellers	Stainless steel	X2 CrNiMo 17-12-2	316L	1.4404
Shaft extension	Stainless steel	X5 CrNiMo 17-12-2	316	1.4401
Impeller lockscrew and washer	Stainless steel	X5 CrNiMo 17-12-2	316	1.4401
Fill/drain plugs	Stainless steel	X5 CrNiMo 17-12-2	316	1.4401
Fill/drain plug gaskets	EPDM			
Mechanical seal	Ceramic/Carbon/ EPDM			
Seal shoulder washer	Stainless steel	X5 CrNiMo 17-12-2	316	1.4401
O-rings	EPDM			
Pump/motor support	Aluminium			
Pump body fastening screws	Zinc plated steel			

Most of the parts of the pump are made of stainless steel and the material of its mechanical sealing is constructed of ceramics on the most part.

Concerning the operation of the feed pump, the characteristic curve on the nominal operation point is presented in Figure 3.46 (rotational speed equal to 2900 rpm). The mass flow rate that this pump manages on the nominal operation point is 2.2 m³/h and the pressure at the RO sub- unit inlet must be around 3 bar (H= 30 m) in order for the membranes to receive water at a minimum pressure of 2 bar (~1 bar considered in pressure drop at the filters).

**2HMS SERIES
OPERATING CHARACTERISTICS AT 2850 rpm 50 Hz**

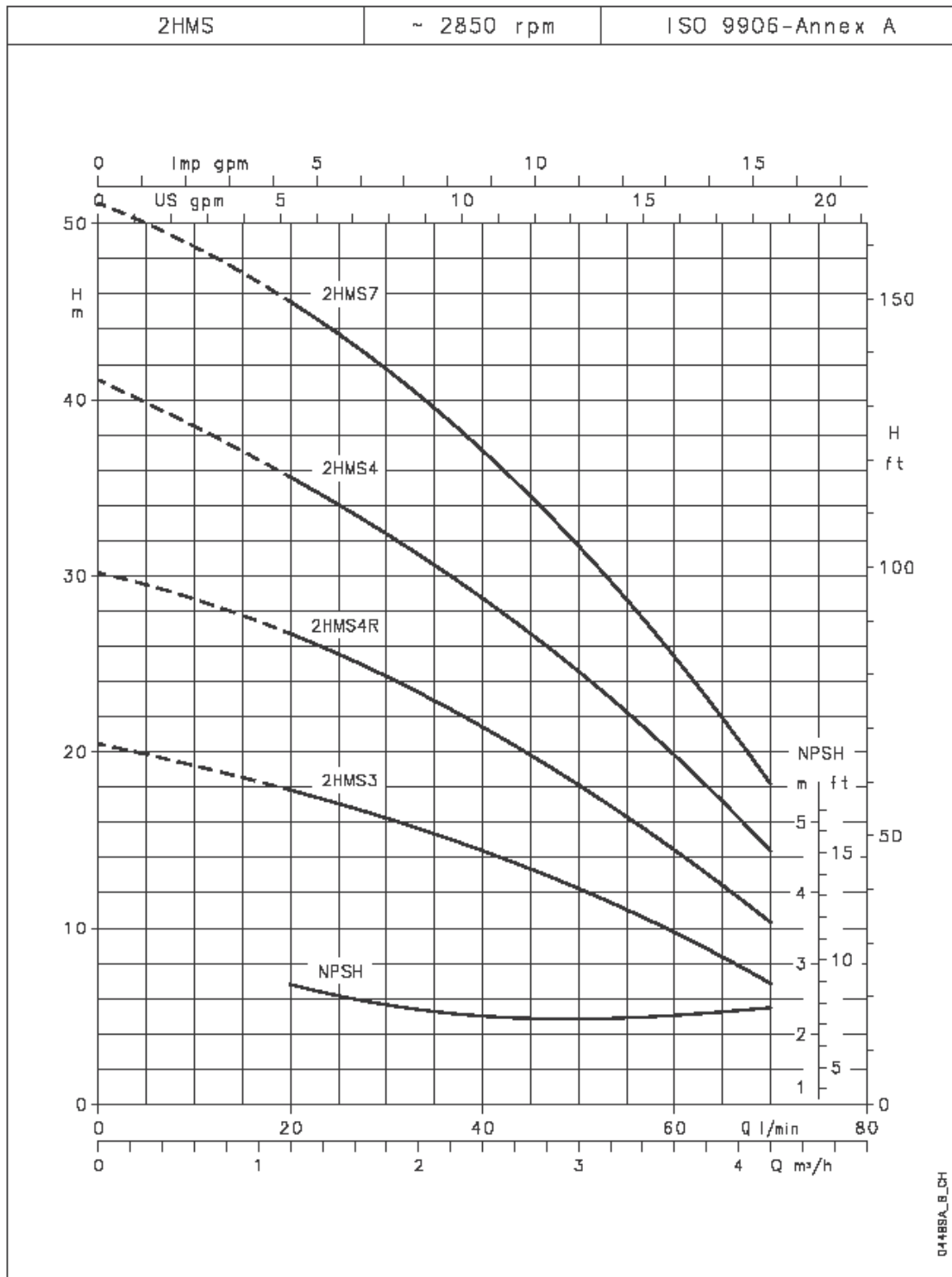


Figure 3.46 Characteristic operation curve of the feed pump at the nominal operation point

It should be noted that this pump operates at constant rotational speed (no use of inverter) since it can adjust its mass flow rate (and outlet pressure) according to the required mass flow rate from the HP pump, which operates at variable rotational speed. Therefore, at the outlet of the feed pump the seawater has variable pressure that varies between 2 and 3 bar.

3.6.2.2 Pretreatment filters

Double filtration filters are placed on the hydraulic circuit after the feed pump. Every sub- unit includes two filter housings of 10" with orifices 1^{1/2}" and a cartridge filter of a dual gradient 25-1 µm in each housing (manufacturer Pentair). These two filters are placed in series, where a slight pressure drop is noticed (replaced by the feed pump). The filter housings on the installed sub- unit are shown in Figure 3.47.



Figure 3.47 Filter housings on the sub- unit

3.6.2.3 High pressure pump and ERD

After passing through the two filters, the seawater is driven to the high-pressure pump which is equipped with an energy recovery device. The pump that has been selected is APP2.5/APM1.8 by Danfoss company, which is the most appropriate for the mass flow rate range of the current system. The pumping system is driven by an electric motor of a capacity of 4 kW (bipolar at 2900 rpm) which is monitored by a frequency inverter. The water recovery rate of the sub-unit is equal to 32% which remains almost constant during the operation point variation. In Figure 3.48 a schematic picture of the pumping system is presented, when in Figure 3.49 a picture of the installed APP- APM system is shown.

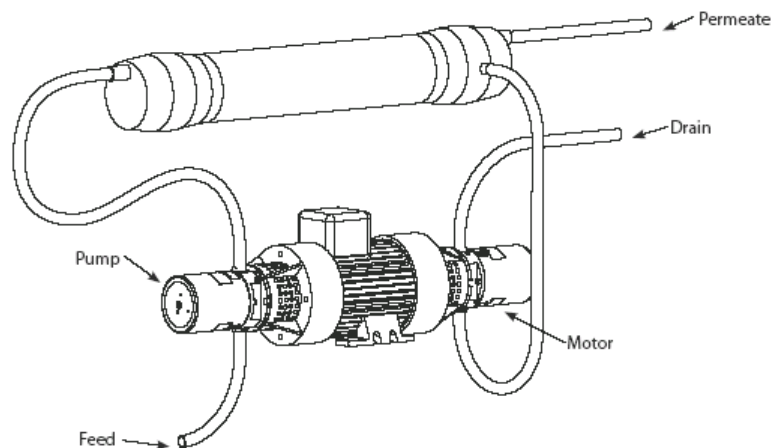


Figure 3.48 Schematic drawing of the hydraulic system (HP pump- ERD)

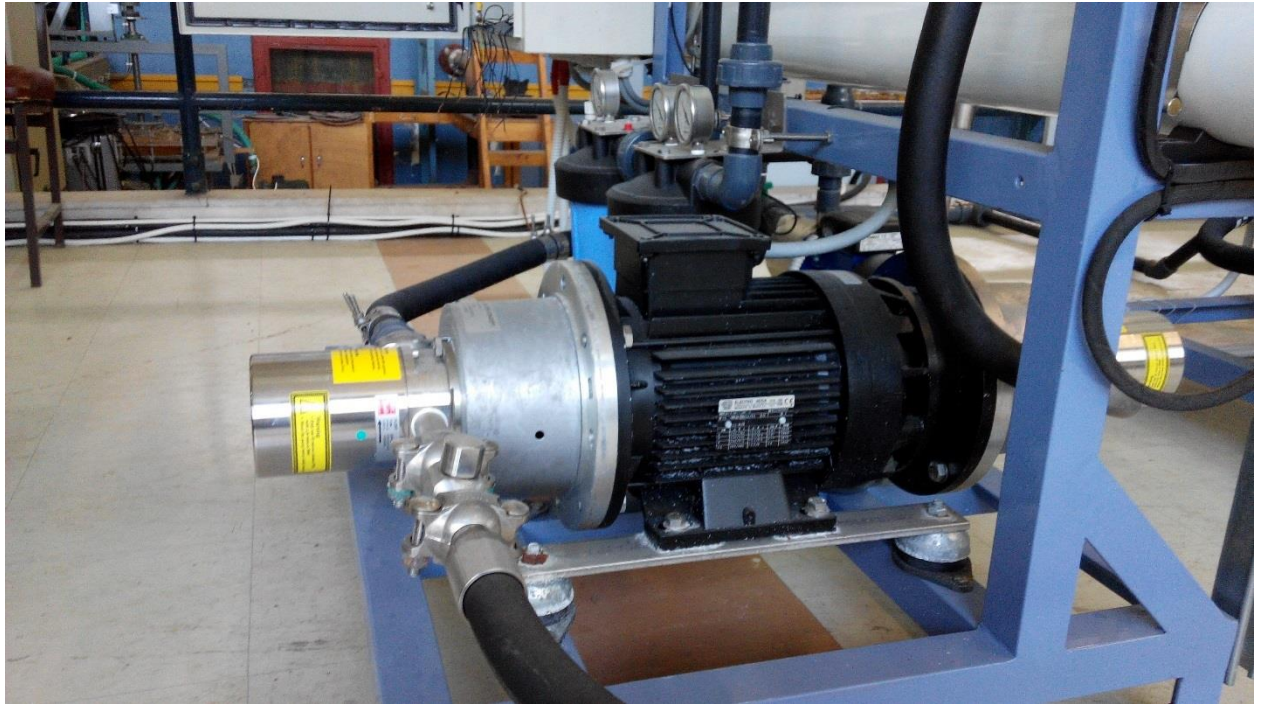
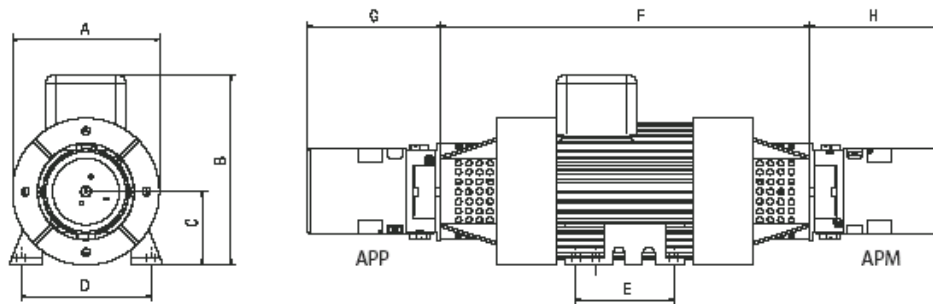


Figure 3.49 Installed hydraulic system on the RO sub- unit (Danfoss company)

In Figure 3.50, the mechanical design of the HP pump is presented along with its dimensions. It should be noted that the HP pump (APP pump) is an axial-piston pump which presents a high volumetric efficiency (maximum $\sim 98\%$), while it also presents a high mechanical efficiency. The turbine used (APM) is basically a pump in reverse operation and has similar efficiency compared to its normal operation.



Pump/motor	rpm	A (mm)	B (mm)	C (mm)	D (mm)	E (mm)	F (mm)	G (mm)	H (mm)	IEC Electric motor
APP1.0/APM0.8	1450	190	220	90	140	100	460	131	131	1.1 kW, IEC 90-4
APP1.5/APM1.2	1450	190	220	90	140	125	460	166	131	1.5 kW, IEC 90-4
APP1.8/APM1.2	1450	190	220	90	140	125	460	166	131	1.5 kW, IEC 90-4
APP2.5/APM2.0	1450	210	240	100	160	140	560	166	166	2.2 kW, IEC 100-4
APP2.5/APM1.8	1450	210	240	100	160	140	560	166	166	2.2 kW, IEC 100-4
APP1.0/APM0.8	2900	190	220	90	140	125	460	131	131	2.2 kW, IEC 90-2
APP1.5/APM1.2	2900	210	240	100	160	140	560	166	131	3 kW, IEC 100-2
APP1.8/APM1.2	2900	210	240	100	160	140	560	166	131	3 kW, IEC 100-2

Figure 3.50 Mechanical drawing and dimensions of the APP system (Danfoss company)

Concerning the HP pump operation, the rotational speed varies with the operation frequency variation, thus with the mass flow rate, according to the diagram of Figure 3.51:

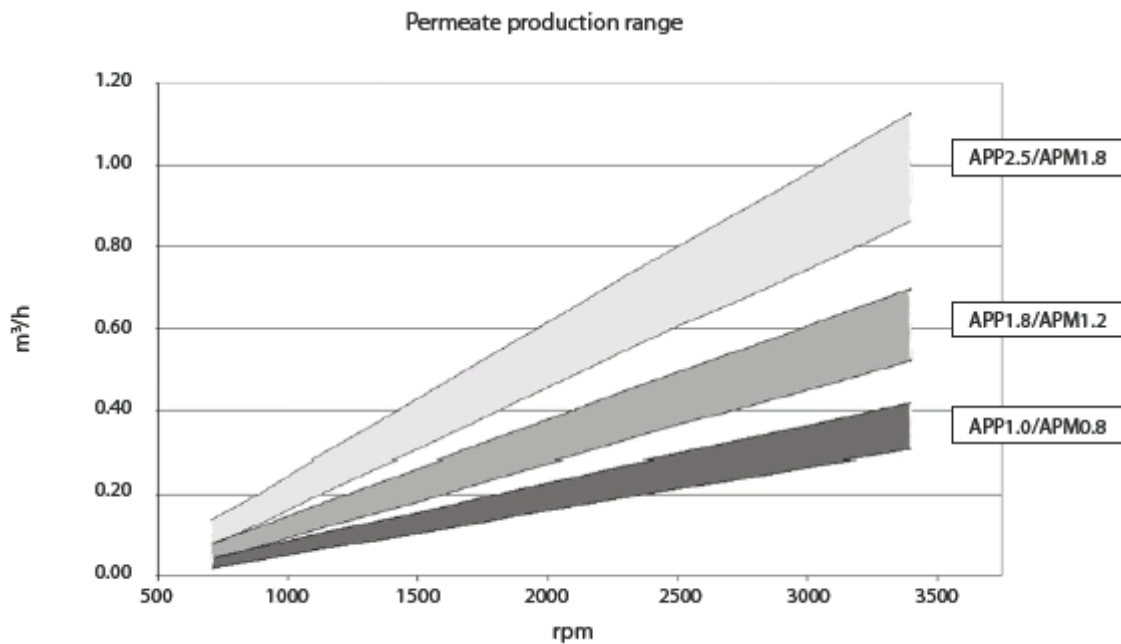


Figure 3.51 Rotational speed and permeate flow rate relation

As observed in Figure 3.51, the maximum flow rate of the permeate at every sub- unit is almost equal to 0.7 m³/h at 2900 rpm.

3.6.2.4 Membranes and membrane vessels

Right after the HP pump, the seawater at a high enough pressure of around 60 bar is driven to the membranes of the sub- unit. The membranes are put in membrane vessels. According to the simulation of Chapter 2, in order to produce the desired quantity of desalinated water and with the recovery ratio that was chosen (typical for the Mediterranean water quality), two membranes are placed in series in every membrane vessel, which are also installed in series. All the membranes that are used in the current system are identical (a total of 4 membranes per sub- unit) and their manufacturer is Filmtec DOW company, their type is SW30-4040 (4"x40) and the two membrane vessels have maximum operation pressure of 1200 psi (82.74 bar) and diameter 4", made of fiber- glass. The two membrane vessels of the sub- unit are shown in Figure 3.52.



Figure 3.52 the sub- unit membrane vessels (membranes manufacturer Filmtec DOW company)

3.6.2.5 Control panel

Every sub- unit obtains a control panel of type RO-T4 (TEMAK Company) and communicates with the switch board. This panel is responsible for the sub- unit control and is equipped with a microprocessor with embedded digital conductivity meter and thermometer. The input/ output signal from the panel is 4 to 20 mA. The control panel is able to stop the RO unit when the salinity of the permeate exceeds a specific non- acceptable value (e.g. set point at 2000 $\mu\text{S}/\text{cm}$) or in case that high pressure values at the membranes are detected (~ 80 bar). The control panel of the sub- unit is presented in Figure 3.53.



Figure 3.53 The sub- unit RO-T4 control panel (TEMAK company)

3.6.2.6 Switch board

The switch board consists of the electric circuit of all the RO sub- unit pumps and is able to communicate with the control panel. This switch board is common for all three sub- units of the RO unit. On this board, the inverters that control the three high pressure pumping systems as well as the power circuits of the feed pumps are placed. On the outside of the switch board there is a START/STOP switch for the operation control and also an "emergency stop" button in case of failure. For the reporting of the power consumption there are Ampere and Voltage meters embedded. The nominal power of the switch panel is 5 kW. The switch board of the RO sub- unit is presented in Figure 3.54.



Figure 3.54 The switch board of the RO sub- unit (outside and inside view)

3.7 RO assembly and installation

The first component constructed of each RO sub- unit is the metallic frame with four plastic footholds for pump vibration absorption. The frame is presented in Figure 3.55.

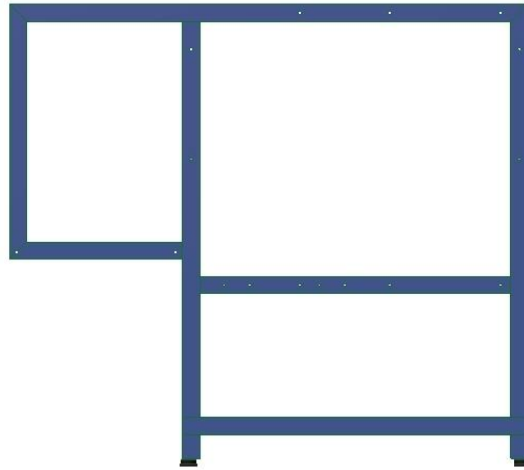


Figure 3.55 Metallic frame of the RO sub- unit

The two membrane vessels are put on the frame along with the basic equipment, such as the feed pump, the HP pump with the ERD, the filters, the measurements instrumentation etc., as presented in Figure 3.56 and 3.57.

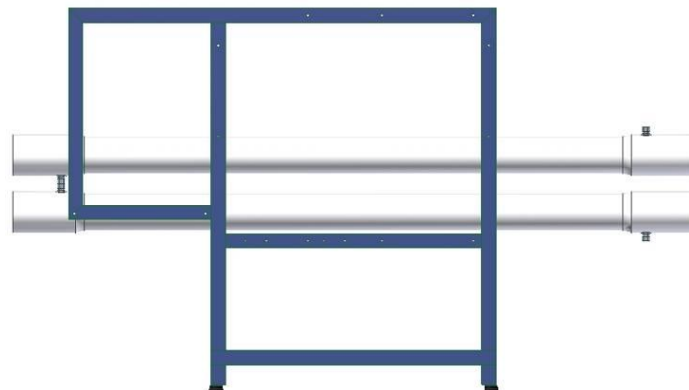


Figure 3.56 The membrane vessels placement



Figure 3.57 Basic equipment placement

The pumping systems and the two membrane vessels are connected with hydraulic piping according to the pressure that dominates each part (e.g. PVC pipes for low pressure branches, stainless steel pipes for high pressure branches). The piping connections are presented in Figure 3.58.

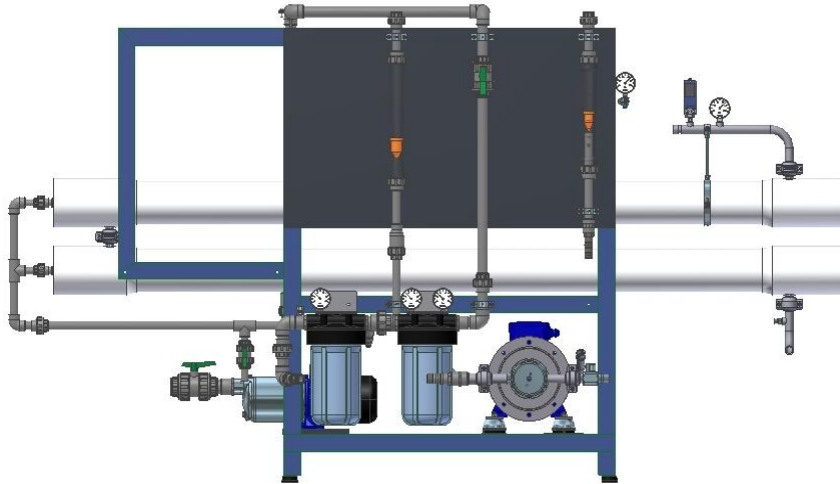


Figure 3.58 Piping connections

Especially at the inlet and outlet of the HP pump with the ERD, flexible pipes are used in order to facilitate construction, since their length is short. Their placement on the RO sub- unit is presented in Figure 3.59.



Figure 3.59 Flexible pipes at the inlet and outlet of the HP pump

Once all the components are put on the RO sub- unit frame and their hydraulic connection has finished, the RO sub- unit construction is finalized with the placement and electric connection of the switch board as presented in Figure 3.60.



Figure 3.60 The switch board installation

The finalized RO sub- unit in front and back view is presented in Figure 3.61.



Figure 3.61 Back and front view of the RO sub- unit to be installed in the laboratory

Three identical sub- units, as the one presented previously, are connected in parallel and with the water tank. Their installation in the Laboratory of Hydraulic Turbomachines of NTUA is presented in Figure 3.62.



Figure 3.62 The installed RO unit system in the NTUA Laboratory of Hydraulic Turbomachines

Finally, the integrated system installed in the Laboratory is presented in Figure 3.63.



Figure 3.63 The integrated system installed in the laboratory

3.8 Conclusions

In Chapter 3 the prototype design and construction have been developed. The measurement instrumentation and the measurement locations on the system were mentioned and the heat source cycle setting has been presented. Moreover, the ORC components' selection is justified and presented in detail. Special care was given to the explanation of the scroll expanders' modification, presenting step- by- step the scroll compressors' transformation into expanders. The RO unit and each sub- unit are also presented, based on the design analysis of Appendix I. Finally, the ORC assembly and the RO unit assembly have also been shown, resulting in the integrated prototype at the laboratory.

References

- 3.1 Manolakos D, Kosmadakis G, Kyritsis S, Papadakis G. Identification of behavior and evaluation of performance of small scale, low-temperature Organic Rankine Cycle system coupled with a RO desalination unit. *Energy*,34(6), (2009), pp. 767– 74.
- 3.2 Manolakos D, Kosmadakis G, Kyritsis S, Papadakis G. On site experimental evaluation of a low-temperature solar organic Rankine cycle system for RO desalination. *Solar Energy*, 83(5), (2009), pp. 646– 56.
- 3.3 Manolakos D, Papadakis G, Kyritsis S, Bouzianas K. Experimental evaluation of an autonomous low-temperature solar Rankine cycle system for reverse osmosis desalination. *Desalination*, 203(1-3), (2007), pp. 366– 374.
- 3.4 Ntavou E., Kosmadakis G., Manolakos D., Papadakis G., Papantonis D. Experimental evaluation of multi- skid reverse osmosis unit operating at fluctuating power input. *Desalination*, 398, (2016), pp. 77-86.
- 3.5 Jones D.P. Sensors technology series, Biomedical sensors. Technology & Engineering, Momentum Press, 2010.
- 3.6 Song P., Wei M., Shi L., Danish N.S., Ma C. A review of scroll expanders for organic Rankine cycle systems. *Applied Thermal Engineering*, 75, (2015), pp. 54- 64.
- 3.7 Μανωλάκος Δ. Ανάπτυξη αυτόνομου ηλιακού οργανικού κύκλου Rankine χαμηλής θερμοκρασίας για αφαλάτωση νερού με αντίστροφη όσμωση. Διδακτορική Διατριβή, Γεωπονικό Πανεπιστήμιο Αθηνών, 2006.
- 3.8 Wang XD, Zhao L, Wang JL, Zhang WZ, Zhao XZ, Wu W. Performance evaluation of a low-temperature solar Rankine cycle system utilizing R245fa. *Solar Energy*, 84(3), (2010), pp. 353–64.
- 3.9 Lemort V, Quoilin S, Cuevas C, Lebrun J. Testing and modeling a scroll expander integrated into an Organic Rankine Cycle. *Appl Thermal Engin*, 29(14-15), (2009), pp. 3094–102.
- 3.10 Quoilin S, Orosz M, Hemond H, Lemort V. Performance and design optimization of a low-cost solar organic Rankine cycle for remote power generation. *Solar Energy*, 85(5), (2011), pp. 955–966.
- 3.11 Lemort V, Declaye S, Quoilin S. Experimental characterization of a hermetic scroll expander for use in a micro-scale Rankine cycle. *Proc of Instit of Mech Eng, Part A: J Power Energy*, 226(1), (2012), pp. 126–136.
- 3.12 Harada KJ. Development of a small-scale scroll expander. Master Thesis, Oregon State University, USA, 2010 [<http://ir.library.oregonstate.edu/xmlui/handle/1957/18837>].
- 3.13 Quoilin S. Sustainable energy conversion through the use of organic Rankine cycles for waste heat recovery and solar applications. Ph.D. Thesis, University of Liege, Belgium, 2011 [<http://orbi.ulg.ac.be/handle/2268/96436>].

CHAPTER 4 – Experimental investigation and evaluation of the multi- skid RO unit

4.1 Introduction

In the current chapter the experimental investigation in the laboratory with electricity from the grid and the evaluation of the multi- skid reverse osmosis (RO) unit is being presented. As mentioned in Chapter 3, a RO desalination unit, composed of three identical skids connected in parallel and using an energy recovery system, has been designed and manufactured for operation and testing at variable conditions. The main goal of the current experimental investigation is the evaluation of such a system for operation at variable power input and the increase of fresh water production as a function of the power input conditions.

A RO desalination unit can be powered by renewable energy sources such as wind and solar energy. However, the power that derives from these sources can strongly fluctuate, since it depends on the weather conditions and/or available solar radiation. As the available power production fluctuates, the water feed and the production of permeate also fluctuate. Therefore, flexibility concerning the RO unit is required, in order to operate efficiently, ensuring the good quality (low salinity) of the produced fresh water. A configuration of three identical sub-systems using an energy recovery unit of axial piston motor – APM type seems enticing, in order to ensure flexibility at variable load operation. The number of the sub-units that operate depends on the available power. The total chosen RO unit capacity is 2.1 m³/h of fresh water. All the components have been equipped with the appropriate instrumentation for detailed experimental testing.

An efficient performance of the RO unit is expected to be achieved due to the on/off switching of the three sub-units, keeping an acceptable fresh water quality at both part and full load operation.

4.2 Description of the test facilities

The laboratory experimental testing at this stage uses grid electricity to simulate the power input from the ORC unit. Thus, the available power varies from very low values (around 1 kW, which corresponds to just around 10% of the full load) up to the maximum one equal to 10 kW. The laboratory experimental testing uses frequency inverters in order to simulate the variable power input. The power input has been monitored through the control of the high-pressure pump frequency. The operation of each sub- unit and of the RO unit as a whole are being tested for three different water salinity levels – 15150 ppm, 30000 ppm and 37500 ppm, simulating low, medium and high salinity water (from brackish up to seawater). Thereafter, the operation of the first sub- unit at 37500 ppm and for three different seawater temperatures is being evaluated in order to test the temperature effect on the operation. The application of such a flexible RO unit has been then examined and demonstrated in three different case studies, using local weather data. The power input originated from photovoltaics (PV) of capacity ranging from 10 up to 20 kWp, showing that it is suitable to combine RO with renewable energy sources with strong intermittent power production.

In the laboratory three different tests for *three different water salinities* took place, in order to test the RO unit performance in low, medium and high load range. In all three tests the power input to the RO unit was 50 Hz, while in each sub-unit

three frequencies were tested, those of 25, 30 and 35 Hz for different high-pressure pump’s rotational speed. The water tank has been filled with 3.3 m³ of water. Salt has been added consecutively: a total of 50 kg, 100 kg and 125 kg of salt have been used in order to obtain the desired salinity (i.e. 15150 ppm, 30000 ppm and 37500 ppm) for each case.

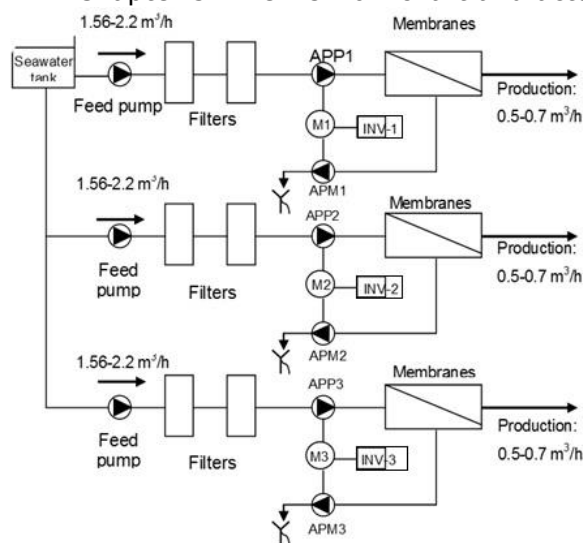
Thereafter, tests for *three different seawater temperatures* took place, for the same water salinity in order to examine the effect of the temperature on the operation. Once again, three HPP frequencies were tested, those of 25, 30 and 35 Hz for different high-pressure pump’s rotational speed to test the RO unit operation in variable power input (50%, 60% and 70% of its nominal operation). In the current test for simplicity reasons, only the first sub- unit operation has been presented since the three sub- units are identical and their operation and measured parameters were the same. In these tests, the water tank remained full with 3.3 m³ of water and 125 kg of salt consisting the desired salinity of 37500 ppm.

In Table 4.1. a briefing on the following experiments is presented.

Table 4.1 Experimental evaluation tests of the RO unit at the laboratory

Test No.	Salinity [ppm]	Feed water temperature [°C]	HPP frequency [Hz]
1	15150	12.5	25, 30, 35
2	30000	12.5	25, 30, 35
3	37500	12.5	25, 30, 35
4	37500	17.0	25, 30, 35
5	37500	19.0	25, 30, 35
6	37500	23.0	25, 30, 35

A detailed description of the laboratory set- up has been presented in Chapter 3. The RO flow chart and actual test rig are presented below.



Adequate instrumentation has been used in order to measure some crucial operation values, which are shown in Table 4.2.

Table 4.2. RO sub-unit instrumentation and measurement range

Temperature thermometers		Measurement range	Accuracy (%)
1	After the membranes	0-60 °C	±0.15
Pressure gauges			
1	After the feed pump and before the filters	0-10 bar	±0.1
2	Between the two filters	0-10 bar	±0.1
3	After the filters and before the high-pressure pump	0-10 bar	±0.1
4	After the high-pressure pump and before the membranes	0-100 bar	±1.0
5	At the brine's membranes outlet	0-100 bar	±1.0
Pressure switches			
1	Low- pressure switch after the filters and before the high-pressure pump (protects the high-pressure pump from no water operation)	2 bar	≤ ±1.0 % of span ± 1 digit
2	High-pressure switch after the high-pressure pump and before the membranes (protects the membranes and membrane vessels under high pressure)	70 bar	≤ ±1.0 % of span ± 1 digit
Water flow rate (mechanical flow meter)			
1	At the membranes' outlet on the fresh water side (on each sub- unit)	0.1 – 1 m ³ /h	±0.05
2	At membranes' outlet on the brine's side	0.25 – 2.5 m ³ /h	±0.125
Water conductivity			
1	At the membranes' outlet on the fresh water side (digital indication)	0-2000 mS/cm	±2

The values recorded for each sub-unit are; the input power (current and voltage), the pressure of the feed pump, the high- pressure pump pressure, the pressure after the membranes, the drain flow rate, the fresh water flow rate, the fresh water conductivity (in $\mu\text{S}/\text{cm}$), the fresh water temperature and the RO sub-unit electrical characteristics (current, voltage and frequency). It should be noted that the feed water temperature can safely be considered equal to the measured fresh water temperature since the temperature increase through the pumps is insignificant and can be neglected [4.1].

The most important values in an RO unit are the power consumption, the specific energy consumption (power consumed per cubic meter of fresh water per hour, kWh/m^3), the membranes' pressure, the seawater flow rate, the water recovery ratio (the fraction of seawater that is desalinated) and the quality (salinity) of the fresh water [TDS in mg/l]. These values are greatly related and lead to the identification of the RO performance and its evaluation. The water recovery ratio based on the design of the RO unit is around 32% and is almost constant throughout the test-rig operation. The main request in the specific system is the evaluation of the efficiency at variable load, which is a critical issue in the operation of these units, since at low load the membrane pressure decreases and the quality of the fresh water deteriorates (higher salinity).

The equations that govern the calculated properties are presented in Table 4.3:

Table 4.3 Equations governing the RO unit calculated properties (also see Appendix II)

Calculated Property	Equation	Unit	Symbols
Power Input	$P = \frac{I * V}{1000}$	kW	I= current measured [A], V= Voltage measured [V]
Current Input	$I = I_1 + I_2 + I_3$	A	I ₁ , I ₂ , I ₃ measured current [A]
Feed water flow rate	$Q_f = Q_{fr} + Q_{br}$	m ³ /h	Q _{fr} = measured fresh water flow rate Q _{br} = measured brine flow rate, [m ³ /h]
Power consumed	$P = \frac{(I_1 + I_2 + I_3) * V * \cos\phi}{1000}$	kW	I ₁ , I ₂ , I ₃ measured current [A] V= Voltage measured [V] cosφ=power factor*
Recovery rate	$recovery = \frac{Q_{fr}}{Q_f}$	%	Q _{fr} = measured fresh water flow rate Q _{br} = measured brine flow rate, [m ³ /h]
Specific energy consumption	$SEC = \frac{P}{Q_{fr}}$	kWh/m ³	P=power consumed [kW] Q _{fr} = measured fresh water flow rate [m ³ /h]
Fresh water salinity	$salinity = 0.627 * 1.00114 * con$	mg/l	con=measured conductivity [μS/cm]
Total fresh water salinity	$salinity_{tot} = 0.627 * \frac{(con_1 * Q_{fr_1} + con_2 * Q_{fr_2} + con_3 * Q_{fr_3})}{(Q_{fr_1} + Q_{fr_2} + Q_{fr_3})}$	ppm	con=measured conductivity for each sub- unit [μS/cm] Q _{fr} = measured fresh water flow rate for each sub- unit [m ³ /h]
Total specific energy consumption	$SEC_{tot} = \frac{P_1 + P_2 + P_3}{Q_{fr_1} + Q_{fr_2} + Q_{fr_3}}$	kWh/m ³	P=power consumed for each sub- unit [kW] Q _{fr} = measured fresh water flow rate for each sub- unit[m ³ /h]

*Power factor: considering the power consumption of the feed pump and the HP pump, the power factor gets the value 0.7 for HP pump operation at 25 Hz, 0.75 for operation at 30 Hz and 0.80 for operation at 35 Hz [4.14]

4.3 Test results

4.3.1 RO- unit evaluation for several water salinities

In the current tests, the effect of the seawater salinity on the RO unit operation at partial and full load is being evaluated. The investigation of the high-pressure pump and the membranes operation curves is necessary for the RO unit operation research.

4.3.1.1 Low salinity (brackish water- 15150 ppm)

Membranes operation characteristic curves

The main factors that affect the RO membrane performance are; the feed water pressure, the water temperature, the salt concentration, the water recovery ratio and the water pH [4.2]. In the current test, the recovery ratio is constantly around 32% (based on the design, however as resulted from the experimental evaluation the recovery ratio reached about 38%). Concerning the pH tolerance, different types of RO membranes can vary widely. Thin-film composite (TF) membranes are typically stable over a broader pH range than cellulose acetate (CA) membranes and, therefore, offer greater operating latitude. Membrane salt rejection performance depends on pH and water flux may also be affected. The stability of TF membrane over a broad pH range permits stronger, faster, and more effective cleaning procedures to be used compared to CA membranes [4.2]. In the examined setup, the DOW Filmtec SW30-4040 membranes chosen, are of Polyamide Thin-Film Composite type, therefore the pH influence is negligible in the membranes operation and has not been examined. Moreover, in the current test, the water salinity is kept constant to 15150 ppm and the water temperature is kept constant at around 12.5 °C.

The feed water pressure effect on the permeate (fresh water) flow rate and salinity is being observed for each sub- unit of the RO unit. In Figure 4.1, the relation between the feed water pressure and the permeate flow rate is presented:

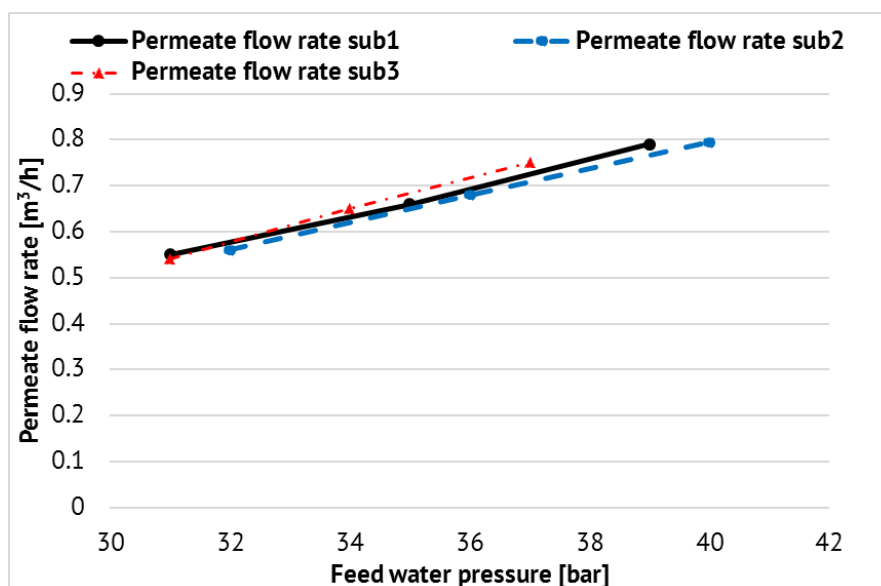


Figure 4.1 Feed water pressure effect on the permeate flow rate for the three sub- units

Feed water pressure affects both the water flow rate and salt rejection (fresh water salinity) of RO membranes. As explained before, reverse osmosis technology involves application of pressure to the feed water stream in excess of the osmotic pressure and a portion of the feed water (concentrated solution) is forced through the membrane to emerge as purified product water of the dilute solution side. As shown in Figure 4.1, permeate flux (the rate of permeate transported per unit of membrane area across the membrane) increases in direct relationship to the increase of feed water pressure. This was expected since the permeate flux is directly proportional to the feed pressure when the temperature,

the recovery ratio and the feed water salt concentration remain constant [4.3-4.4]. In Figure 4.1 it is observed that the permeate flow rate for the first and the second sub- units varies between 0.55 to ~0.80 m³/h, while for the third sub- unit it reaches a lower value at around 0.75 m³/h. This is due to the fact that there were some slight differences in pressure range as shown in Figure 4.1: at the first and second unit the pressure range was from 31 up to 39 or 40 bar, when at the third unit reached a lower value of 37 bar. This slight difference could be due to some uncertainty of the measurement instrumentation or slight different operation conditions (e.g. slight difference in membranes' construction, different pipe length in each sub- unit etc.) since all three sub- units are identical and connected in parallel. Moreover, in Figure 4.1 it is observed that the fresh water production reached a slightly higher value than the designed one. According to the design, the RO sub- unit capacity at nominal rotational speed of the HP pump was 0.70 m³/h of permeate. However, the experiment has shown that the maximum fresh water production has been near 0.80 m³/h, which has been observed at lower HP pump's rotational speed than the nominal one. Nevertheless, it has also been noticed that the recovery ratio resulted to be slightly higher than the designed one (38% rather than 32%). This could be due to the fact that the produced feed sea- water in the laboratory might be of a slightly better quality (lower salinity) than the calculated one (therefore the feed water was slightly "easier" to manage) or because the experimental temperature is slightly different than the design temperature (design temperature 20 °C, water temperature in the laboratory 12.5 °C), a fact that also affects the quality of water as will be presented in the next paragraph.

In Figure 4.2, the relation between the permeate salinity and the feed water pressure is presented:

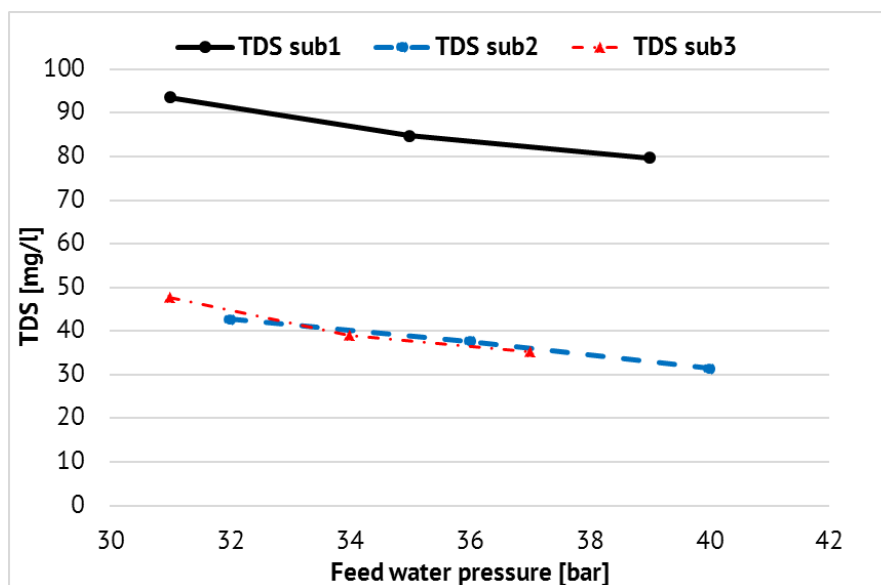


Figure 4.2 Feed water pressure effect on the permeate salinity for the three sub-units

Increased feed water pressure also results in decreased fresh water salinity but, as Figure 4.2 demonstrates, the relationship is less direct than for water flux. The fresh water salinity is almost inversely proportional to the seawater flow rate. Since RO membranes are imperfect barriers to dissolved salts in feed water, there is always some salt passage through the membrane. As feed water pressure increases, this salt passage is increasingly overcome as water is pushed through the membrane at a faster rate than salt can be transported. Therefore, the

permeate salinity curve decreases with the pressure increase [4.1]. As observed in Figure 4.2, the fresh water quality is within acceptable limits, in fact it is of very good quality (since the water used in the laboratory is tap water mixed with pure salt, water quality in the current tests is determined only by the salt concentration) [4.5]. What is interesting in Figure 4.2 is the observation that the first sub- unit presents a lower salt rejection than the other two sub- units, which present similar operation (45- 30 mg/l). Once again, this could be due to some instrumentation uncertainty or difference in operational conditions, since the three sub- units are identical and connected in parallel. However, even the first sub- unit produces water of very good quality, since the salinity varies from 95 to 80 mg/l.

HP pump operation characteristic curves

The HP pump operation curve in variable load as well as the energy recovery unit operation show greater complexity since they depend on the partial efficiency of those volumetric machines in non- stable operational conditions. However, in the current system, the HP pump, the energy recovery unit and the motor are connected on the same shaft, therefore their rotational speed can be related to the feed water flow and the motor power consumption that depends on the operational pressure [4.7]. Frequency inverters are used for the control of the HP pump rotational speed which defines the operational points of the sub- unit. The rotational speed change results in a variation of the seawater flow rate as presented in Figure 4.3:

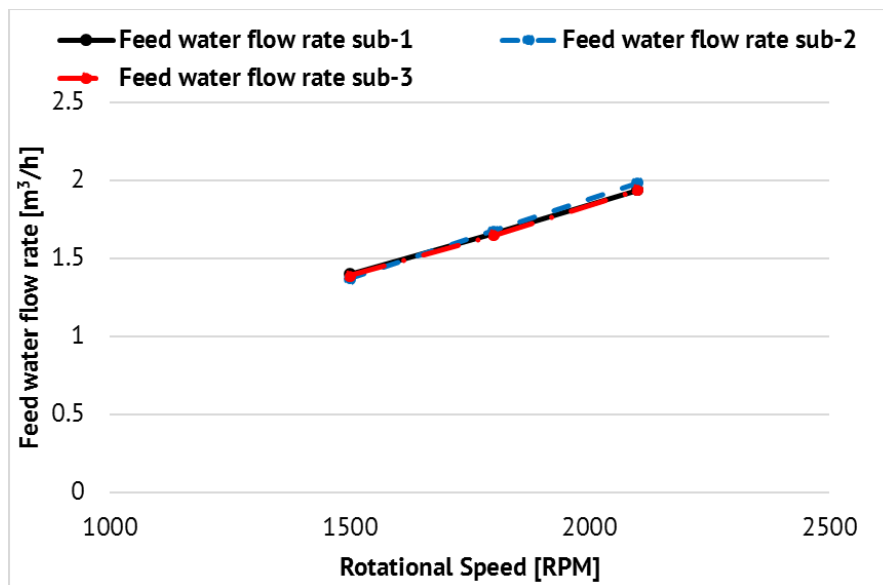


Figure 4.3 Feed water flow rate as a function of HP pump rotational speed for the three sub- units

In Figure 4.3 it is noticed that the feed water flow rate curves as a function to the motor rotational speed almost coincide for all sub- units which was expected since the three sub- units are identical. When all sub- units operate at 2100 RPM (35 Hz) their operation reaches a feed water flow rate of 2 m³/h, resulting in about 6 m³/h of feed water at the whole RO unit.

In the reverse osmosis (RO) process, a key figure of merit is the specific energy consumption (SEC), generally defined as the total energy consumed to produce a unit volume of permeate. Currently, nearly all seawater RO plants do use some form of energy recovery device in order to minimize SEC, but energy still

remains the largest single operating and maintenance item for a desalting plant, exceeding in most cases 50% of the total cost. The specific energy consumption of RO plants is largely dominated by two factors: the amount of transmembrane pressure difference required in order to achieve the necessary permeate flow rate at various mass transfer conditions, and the design and efficiency of the feed water pump in combination with the respective energy recovery system. For a given recovery rate, the required feed pressure is determined by the feed water properties, mostly temperature and feed salinity, which may vary significantly throughout the year due to seasonal influences. Feed water properties together with hydraulic losses from feed to brine also determine the outlet pressure of the membrane array, i.e. the inlet pressure for the energy recovery device. For the reasons outlined above, real-life operation of an RO plant will always be determined by variations in feed water conditions, actual plant state, and actual permeate requirements [4.6]. This means that the plant is operated within a certain range of each of the following operational parameters:

- feed, brine, and permeate flow rate (governed by the desired recovery rate)
- feed and brine pressure (governed by salinity, temperature, membrane condition, and recovery rate)

In Figure 4.4 the SEC and the power demand by the HP pump as a function of the feed water pressure are presented for the three sub- units:

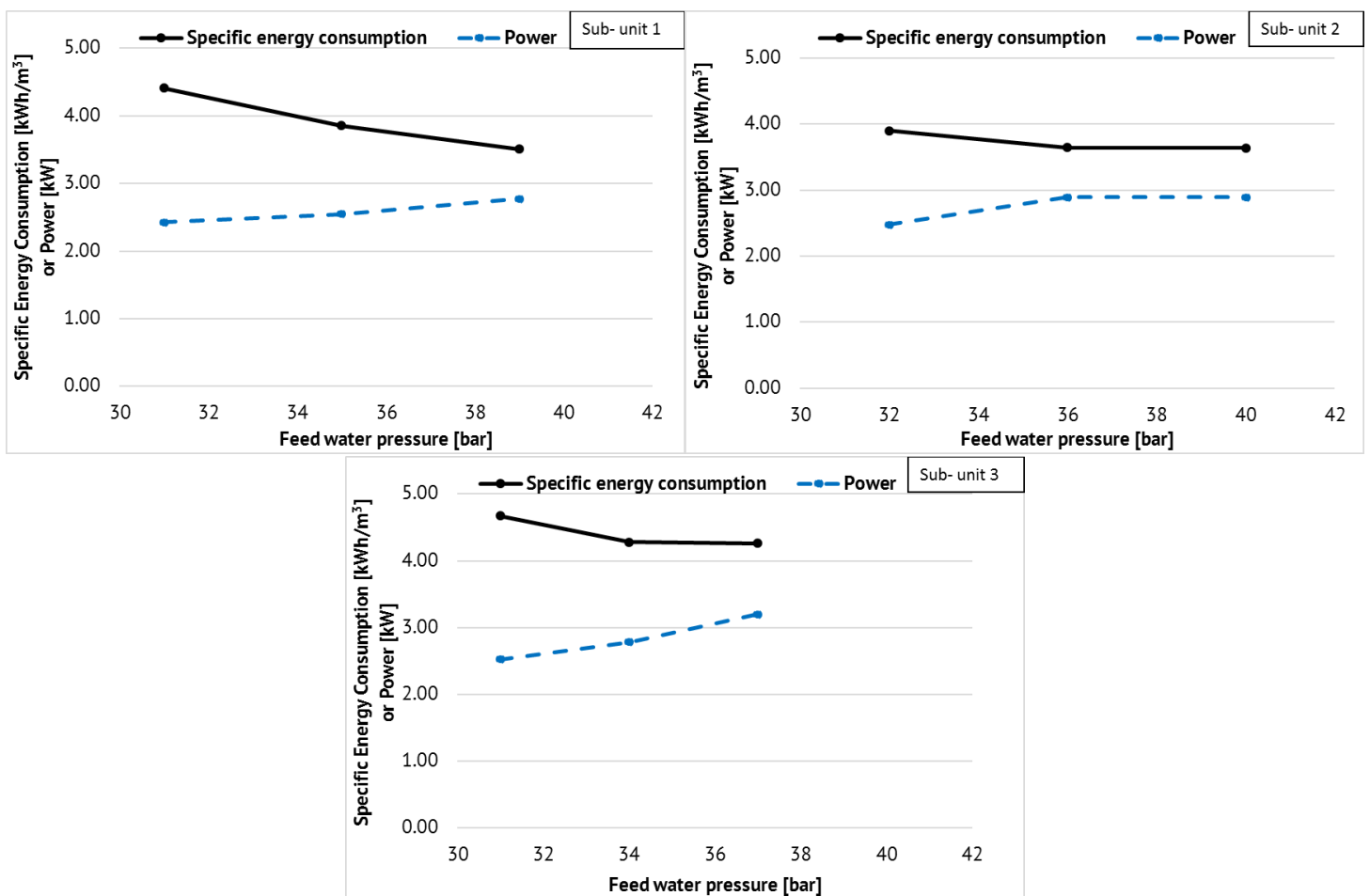


Figure 4.4 Specific energy consumption and power as a function of the feed water pressure for the three sub- units

As observed in the three charts of Figure 4.4, the specific energy consumption is decreasing with the increase of the feed water pressure. The

pressure at the membranes inlet increases with the increase of the HP pump's rotational speed which results in an increase of the permeate production as discussed in Figure 4.1, so the fresh water production is also high. This results in a decrease in the specific energy consumption. Figure 4.4 reveals the relationship between sub- unit energy consumption, energy expenditure per m³ of product water and feed water pressure. It can be noticed that at low pressure, total plant consumption is lower but the energy expenditure required to obtain 1 m³ of product water is higher. As pressure rises, so does the total plant consumption but the energy required to obtain 1m³ of product water falls. In other words, when operating pressure rises, kilowatt consumption per cubic meter of permeate falls. For this reason, the energy cost to obtain 1 m³ of product falls with rising membrane operating pressure. It can clearly be seen in Figure 4.4 how, with increasing pressure, product or permeate production rises and energy consumption per cubic meter of product water falls.

In Figure 4.4 it is also noticed that the SEC for the first sub- unit varies between 4.5 and 3.5 kWh/m³ for a pressure range from 31 to 39 bar, the SEC of the second sub- unit varies between 3.9 and 3.5 kWh/m³ for pressure 32 to 40 bar and the SEC of the third sub- unit varies between 4.8 and 4.2 kWh/m³ for pressure from 31 to 37 bar. The third sub- unit presents a slightly higher SEC than the other two sub- units which is justified by the fact that its HP pump power reached slightly higher values than the other two sub- units, as shown in Figure 4.4, and also that with the pressure decrease the SEC is higher. It should also be noticed that in the specific energy consumption measured, the feed pump energy consumption is also included. This pump operates at constant speed and requires around 0.6 kW.

Concerning the HP pump power demand, as it is observed in Figure 4.4, as feed water pressure increases the power demand increases almost linearly, varying from 2.5 to 2.9 kW for the first two sub- units and from 2.7 to 3.1 kW for the third sub- unit. The slight difference could be due to uncertainty of the measurement instrumentation or a difference in operational conditions since the three sub- units are identical and connected in parallel.

The relation between the SEC, the fresh water salinity and the power input gives a good picture of the sub- unit operation in order to estimate the expected results from the operation of the integrated system (ORC engine coupled to the RO unit). In Figure 4.5 this relation is presented for the three sub- units:

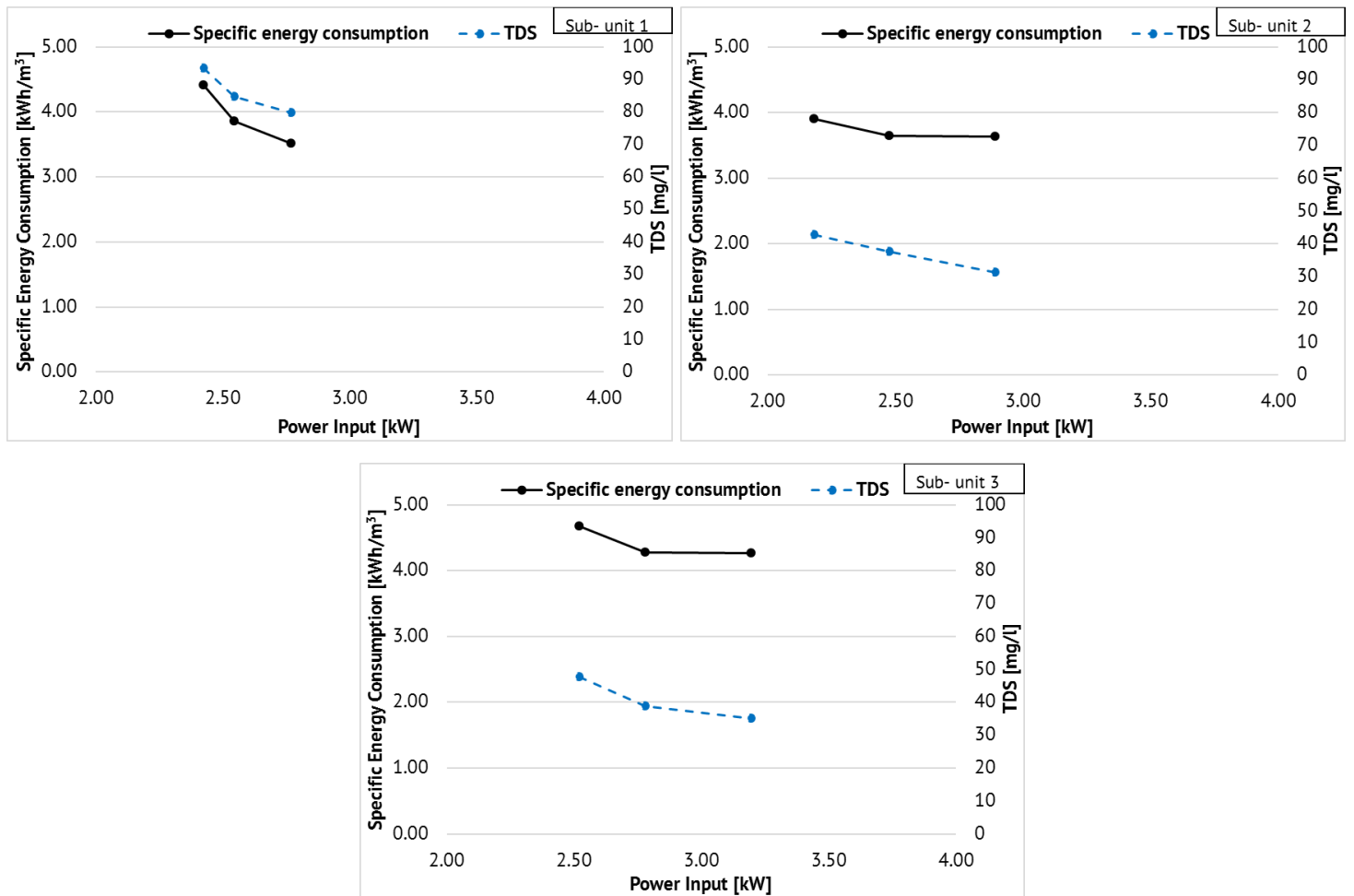


Figure 4.5 Specific energy consumption and fresh water salinity as a function of the power input for the three sub- units

In Figure 4.5 the power input that every sub- unit uses to operate varies between 2.2 and 3.2 kW, with slight differences due to momentary difference of current measured on each sub- unit. Concerning the SEC of the first sub- unit it varies between 4.5 and 3.5 kWh/m³ for power input from 2.4 to 2.8 kW. The SEC of the second sub- unit has been 3.9 to 3.5 kWh/m³ for power input from 2.2 to 2.9 kW and the SEC of the third sub- unit was 4.8 to 4.2 kWh/m³ for power input between 2.52 and 3.20 kW. The fresh water salinity varies for the same power inputs between 93.5 and 79.7 mg/l for the first sub- unit, 42.7 to 31.4 mg/l for the second sub- unit and 47.7 to 35.2 mg/l for the third sub- unit. Since the fresh water temperature was the same in all sub-units (measurements taken at the same day) and the three sub- units are identical, the small differences of the conductivity of the produced water (especially between the first and the two other sub units) is due to some measurement error or uncertainty of instrumentation. As the power input increases, the membrane pressure increases and since the recovery ratio is constant (the pump and motor are volumetric machines), the fresh water salinity decreases.

The relation between the power input and the fresh water production of the three sub- units is presented in Figure 4.6:

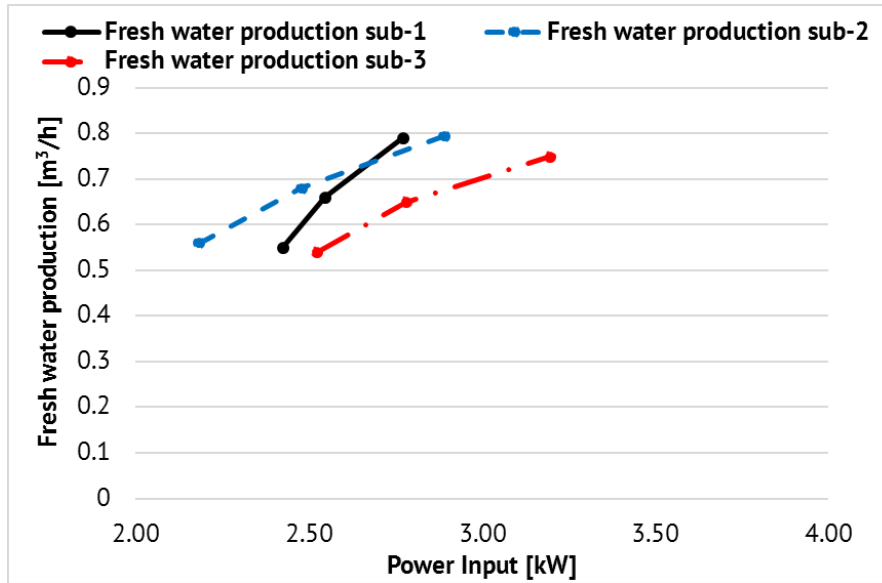


Figure 4.6 Fresh water production as a function of the power input for the three sub- units

As it is observed in Figure 4.6, the first and second sub- unit produce 0.55 to 0.80 m³ of fresh water for power input between 2.2 and 2.9 kW, while the third sub- unit reached a lower value of around 0.75 m³ for a slightly higher power input, varying from 2.5 to 3.2 kW. This slight difference could be due to some uncertainty of the measurement instrumentation since all three sub- units are identical and connected in parallel.

The overall operation of the whole RO unit could be presented through the presentation of the specific energy consumption, the fresh water salinity and the fresh water production as a function of the power input. In Figure 4.7 the SEC and the fresh water salinity for the total power input is presented for the RO unit:

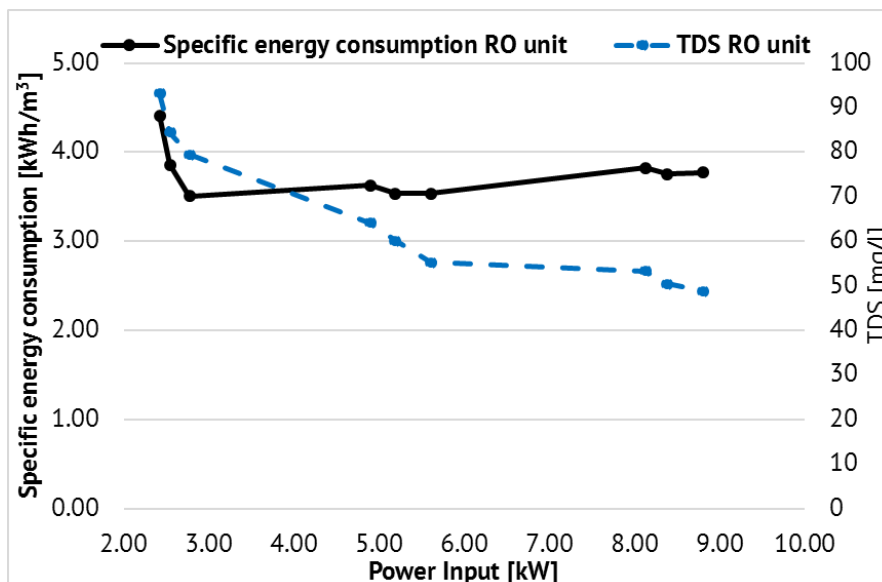


Figure 4.7 Specific energy consumption and fresh water salinity as a function of the total power input for the whole RO unit

As presented in Figure 4.7, the salinity presents a fluctuation especially at low available power values. As the power input decreases, the membrane pressure and the water feed flow decrease as well, and in consequence the fresh water salinity increases as well as the specific energy consumption increases. This is the reason that a small fluctuation in the specific energy consumption curve is noticed. The SEC of the whole RO unit operation varied between 4.5 and 3.5 for the overall operation which indicates an efficient operation. The power input range varied from around 2.2 kW up to 9 kW and as presented in Figure 4.7 the second unit started operating at 4.9 kW and the third at 8 kW. It can be noticed that with the second and third sub- unit in operation the SEC of the RO unit tends to get a constant value. The fresh water salinity fluctuated between 93 and 50 mg/l which indicates fresh water of very good quality throughout the whole operation. At very low loads, when only the first sub unit operates, the salinity of the produced fresh water is higher, although still of very good quality.

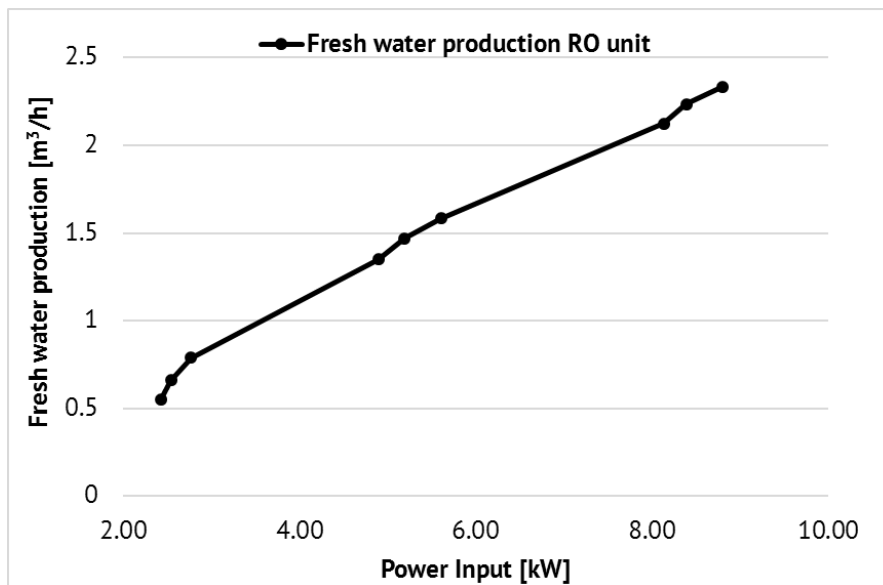


Figure 4.8 Fresh water production as a function of the total power input for the whole RO unit

The fresh water production of the whole RO unit was from 0.5 m³ with the operation of just the first sub- unit at low HP pump rotational speed, to almost 2.4 m³ for the full operation of all three sub- units at 2900 RPM. The maximum permeate production was slightly higher than the expected from the design and for lower HP pump rotational speed than the nominal one, a fact that leads to the assumption that the RO unit may be slightly oversized. Once again, in Figure 4.8 it is obvious that the second sub unit starts operating at around 4.8 kW and the third at almost 8 kW.

4.3.1.2 Medium salinity (30000 ppm)

In the second test of the RO unit another 50 kg have been added to the feed water in order to evaluate the operation of the RO unit in medium salinity. The same properties have been investigated and are presented below.

Membranes operation characteristic curves

In Figure 4.9 the effect of the feed water pressure on the permeate production on each sub- unit is presented:

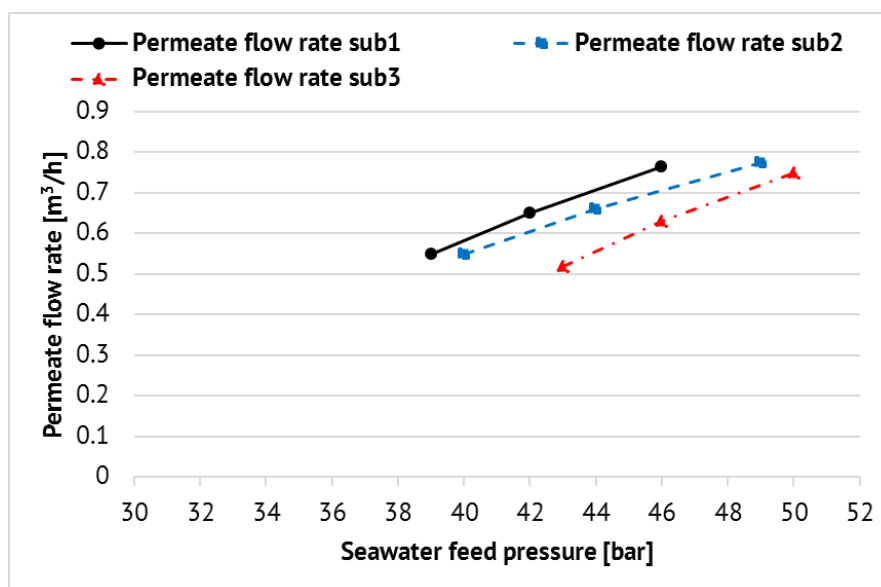


Figure 4.9 Feed water pressure effect on the permeate flow rate for the three sub- units

As observed in Figure 4.9 the permeate flux is once again directly proportional to the feed pressure since the temperature, the recovery ratio and the feed water salt concentration remain constant. The permeate flow rate for the first and the second sub- units varies between 0.55 to ~ 0.78 m³/h, while for the third sub- unit it starts from a lower value at around 0.50 m³/h. It is noticed that there is a slight difference in pressure range as shown in Figure 4.9: the first sub- unit operates between 39 and 46 bar, the second sub- unit between 39 and 49 and the third sub- unit between 43 and 50 bar. As mentioned in Figure 4.1 though, this slight difference could be due to some uncertainty of the measurement instrumentation or slight different operation conditions (e.g. slight difference in membranes' construction, different pipe length in each sub- unit etc.) since all three sub- units are identical and connected in parallel. Once again, a slightly higher permeate production of 0.08m³ is noticed possibly due to the slightly different recovery ratio noticed in the experiment. Compared to the low salinity operation, it is noticed that the feed water pressure range is higher, since for the low salinity it was around 31 to 40 bar and in the current test it varies between 38 and 50 bar. This was expected since higher salinity signifies higher pressure on the membranes in order to produce the permeate through reverse osmosis.

In Figure 4.10 below, effect of feed water pressure on the permeate salinity is presented:

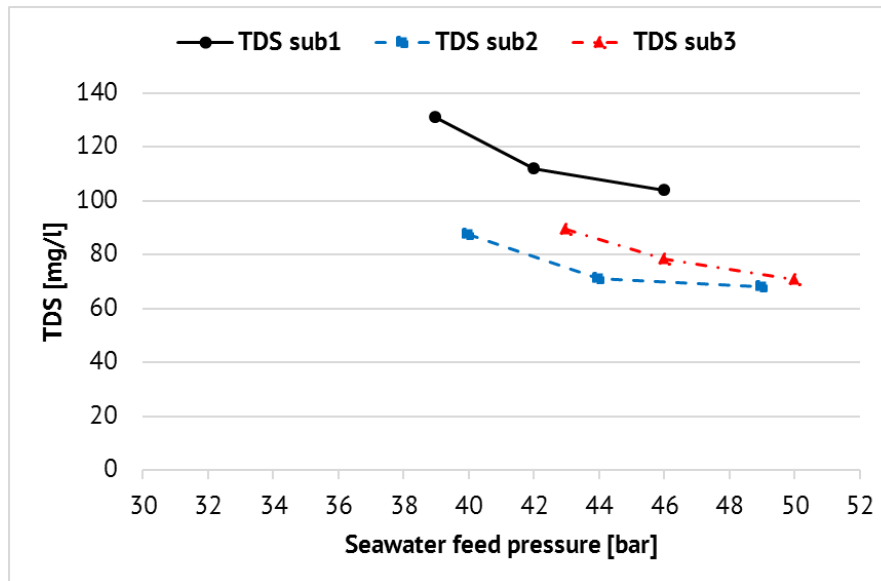


Figure 4.10 Feed water pressure effect on the permeate salinity for the three sub-units

The permeate salinity varies between 130 and 70 mg/l which assures fresh water of good quality. The first sub- unit presents a lower salt rejection which leads to the assumption that some uncertainty of the measurement instrumentation or some difference in operational conditions such as a slight difference in membranes' construction, different pipe length in each sub- unit etc. take place, rather than random error, since all three sub- units are designed identical and are connected in parallel. However, the permeate varies within acceptable limits throughout the whole operation and moreover it is of good quality. Moreover, the produced water salinity is slightly higher than the one of the produced water of the previous experiment (lower feed water salinity), since the fed water salinity is higher in the current test.

HP pump operation characteristic curves

The HP pump operation is being evaluated for operation with medium salinity. The variation of the seawater flow rate as a function of the rotational speed is presented in Figure 4.11.

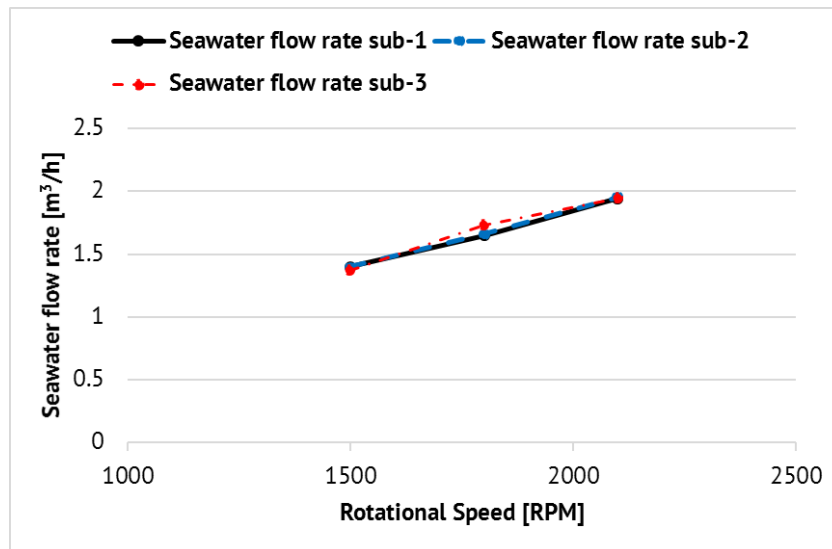


Figure 4.11 Feed water flow rate as a function of HP pump rotational speed for the three sub- units

Figure 4.11 is similar to Figure 4.3 showing that in operation with medium salinity the feed water flow rate has not been affected throughout the HP pump operation range. Over again, when all three sub- units' HP pumps operate at 2900 RPM the feed flow rate is almost 2 m³/h (total of 6 m³/h). The specific energy consumption and power demand related to the feed water pressure are presented for each sub- unit in Figure 4.12:

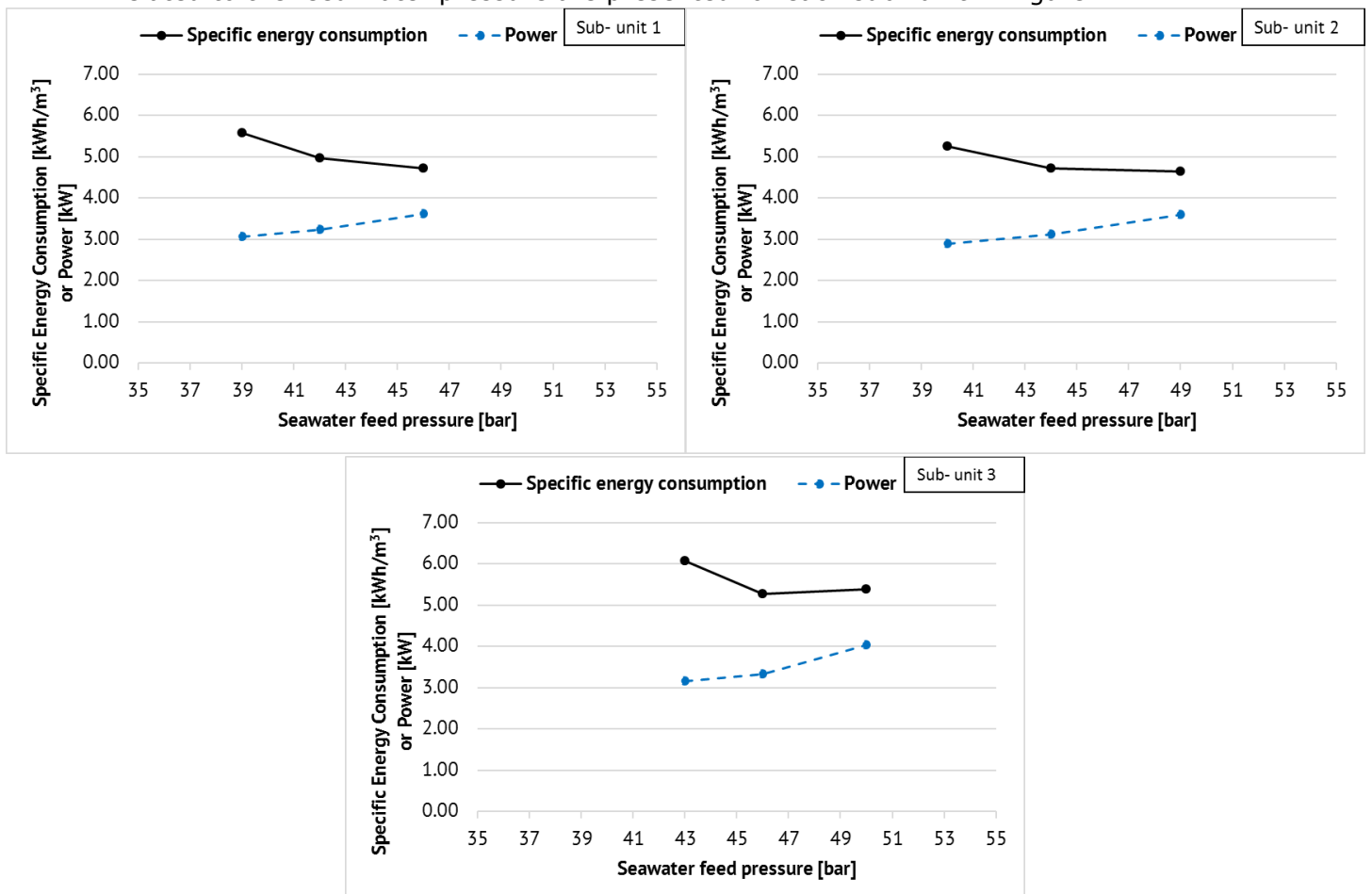


Figure 4.12 Specific energy consumption and power as a function of the feed water pressure for the three sub- units

The SEC in the current test varies between a higher range of values. The SEC of the first sub- unit varies from 5.6 to 4.7 kWh/m³ for feed water pressure from 39 to 46 bar, the SEC of the second sub- unit varies from 5.3 to 4.6 kWh/m³ for feed water pressure from 40 to 49 bar and the SEC of the third sub- unit varies between 6.1 and 5.4 kWh/m³ for feed water pressure from 43 to 50 bar. The first and second sub- unit present similar operation while the third one presents a higher SEC. However, a closer look at the power consumption curves reveals that the first and second sub- unit consume 3.1 to 3.6 kW and 2.9 to 3.6 kW respectively, while the third sub- unit uses 3.2 to 4 kW. This fact in combination to Figure 4.9 where it is shown that the permeate flow rate is almost equal for all three sub- units, explains the fact that the SEC of the third sub- unit is higher. The higher power need of the third sub- unit could be due to some measurement instrumentation uncertainty, however the difference is almost 0.4 kW which can be acceptable.

The relation between the SEC, the permeate salinity and the power input for each sub- unit is examined next:

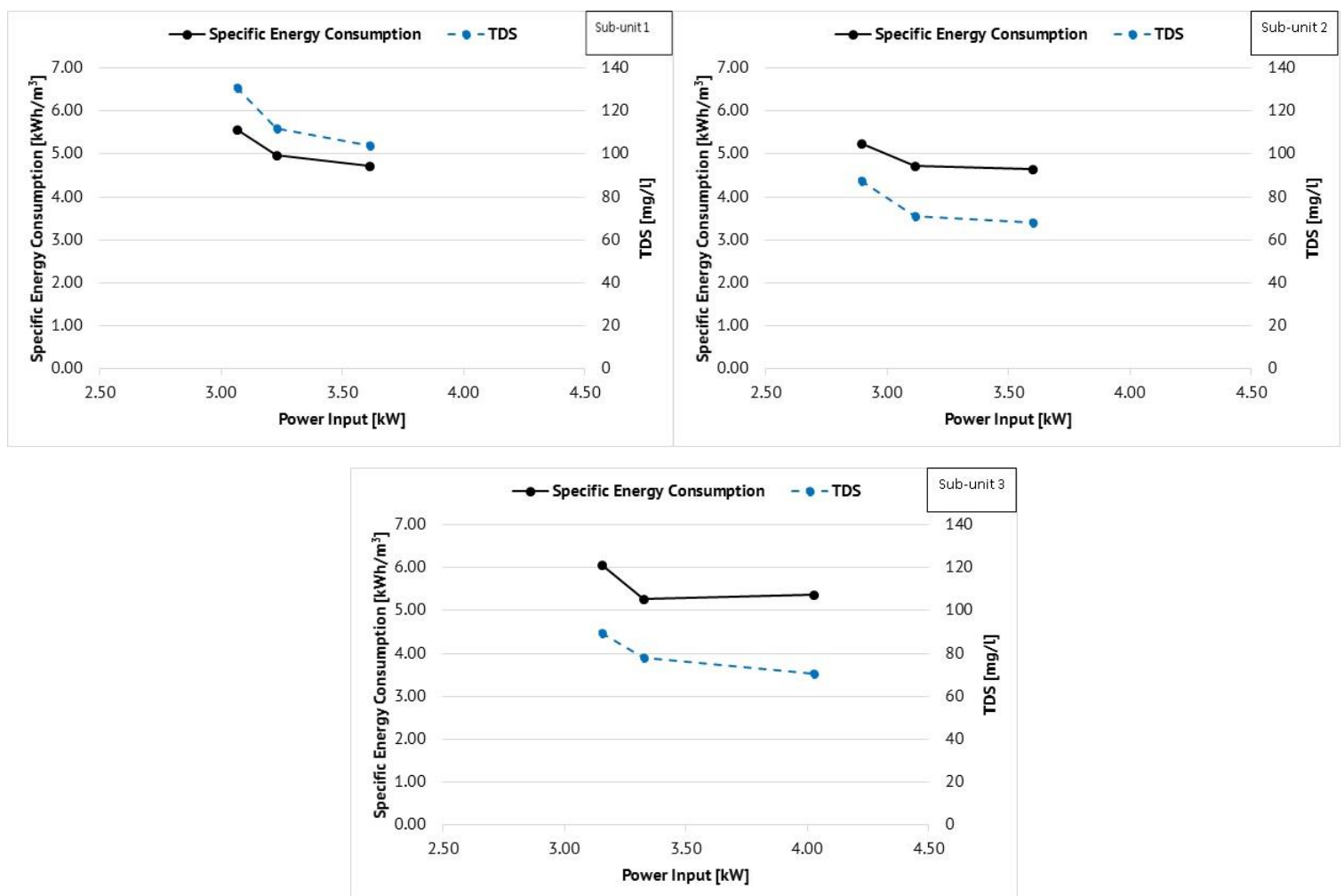


Figure 4.13 Specific energy consumption and fresh water salinity as a function of the power input for the three sub- units

In Figure 4.13, the difference in SEC and power for the third sub- unit is more clearly observed. Concerning the fresh water salinity, the first sub- unit produces water of a salinity of 130.8 to 130.9 mg/l for operation with 3.1 to 3.6 kW, the second sub- unit produces water of a salinity of 87.6 to 68.2 mg/l for operation between 2.9 and 3.6 kW, while the salinity of fresh water for the third

sub- unit is 89.5 to 70.7 mg/l for operation at 3.2 to 4 kW. For a similar power input range, the first sub- unit produces water of higher salinity, due to some measurement uncertainty. The second and third sub- unit produce water of very similar quality, while in the previous test of lower feed water salinity it was the first and second unit that presented similar produced water salinity. However, all of the sub- units produce water of good quality. The effect of power input to the fresh water production is presented in Figure 4.14 below:

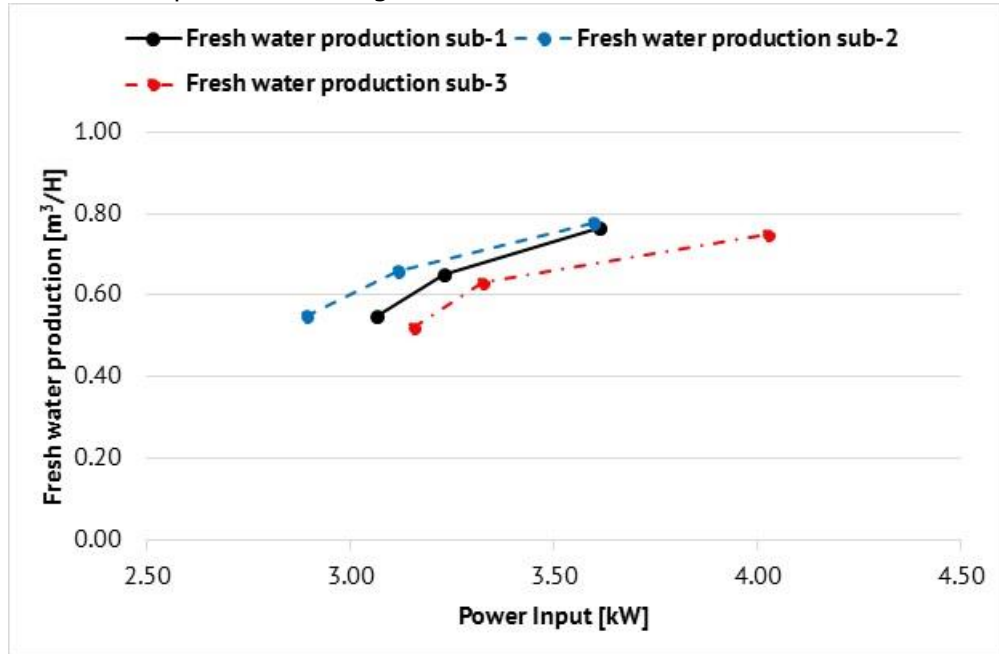


Figure 4.14 Fresh water production as a function of the power input for the three sub- units

The water production of the three sub- units varies between 0.55 and 0.75 m³/h throughout the whole power input range, as presented in Figure 4.14. However, the power input of each sub- unit presents a slight difference, as discussed previously. The examination of the whole RO unit through the relation between the SEC, the permeate salinity and the power input is presented in Figure 4.15:

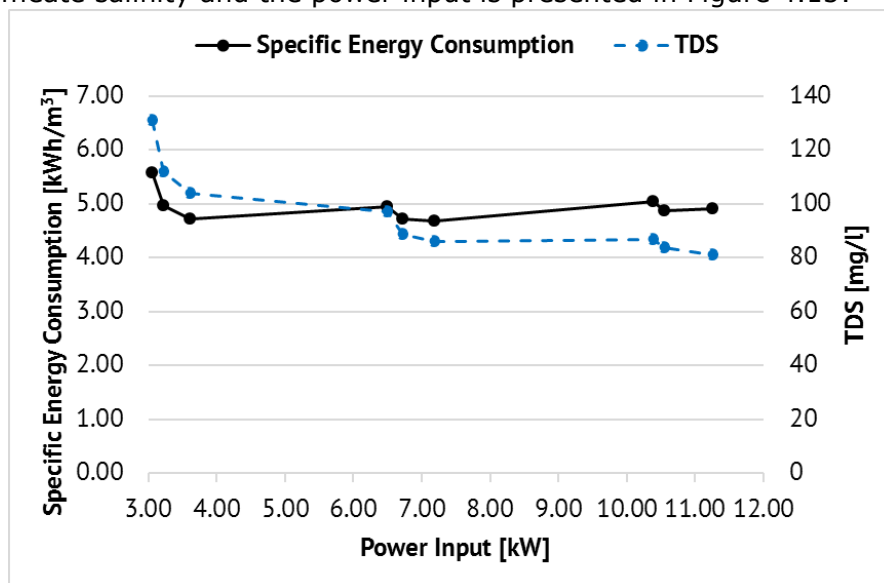


Figure 4.15 Specific energy consumption and fresh water salinity as a function of the total power input for the whole RO unit

The RO unit, based on Figure 4.15, operates at a power input range from 3.1 kW when only the first sub- unit operates at low HP pump rotational speed, up to 11.3 kW where all three sub- units operate at full HP hump rotational speed. The second sub- unit starts operating at 6.5 kW and the third sub- unit at a power input of 10.4 kW. The SEC varies between 5.6 and 4.6 kWh/m³ which indicates an efficient operation throughout the whole power input range. The fresh water salinity varies between 130.6 and 80.9 mg/l which shows fresh water production of good quality throughout the whole power input range. Concerning the fresh water production as a function of the power input, Figure 4.16 below shows that it varies between 0.55 m³/h when only the first sub- unit operates at low speed, and 2.3 m³/h when all three sub- units operate at full speed.

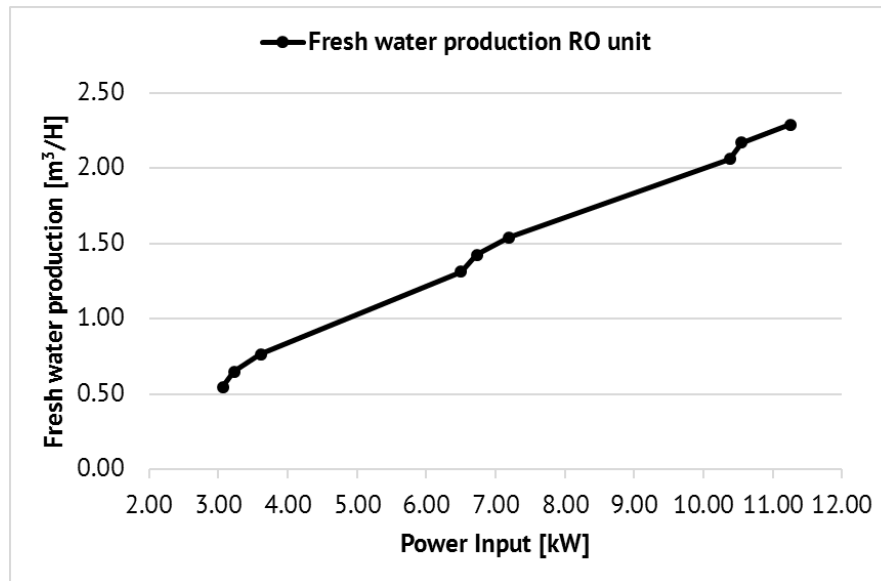


Figure 4.16 Fresh water production as a function of the total power input for the whole RO unit

The maximum production of 2.3 m³/h is very close to the design expected one (2.1 m³/h) however at this operation point, each of the three sub- units operates at 70% of its total capacity. A slight oversizing of the RO unit may be assumed.

4.3.1.3 High salinity (37500 ppm)

For the third test another 25kg of salt has been added (total of 125 kg in 3.3 m³ of water in the tank) representing seawater of high salinity. This test is significant for the area of the Mediterranean, since it represents its salinity, as well as the salinity of some other sea areas such as the Arabic sea in the Indian Ocean and some parts of the Atlantic Ocean [4.15]. The same properties that define the sub- units' operation are examined below.

Membranes operation characteristic curves

In Figure 4.17 the effect of the feed water pressure on the permeate flow rate is presented:

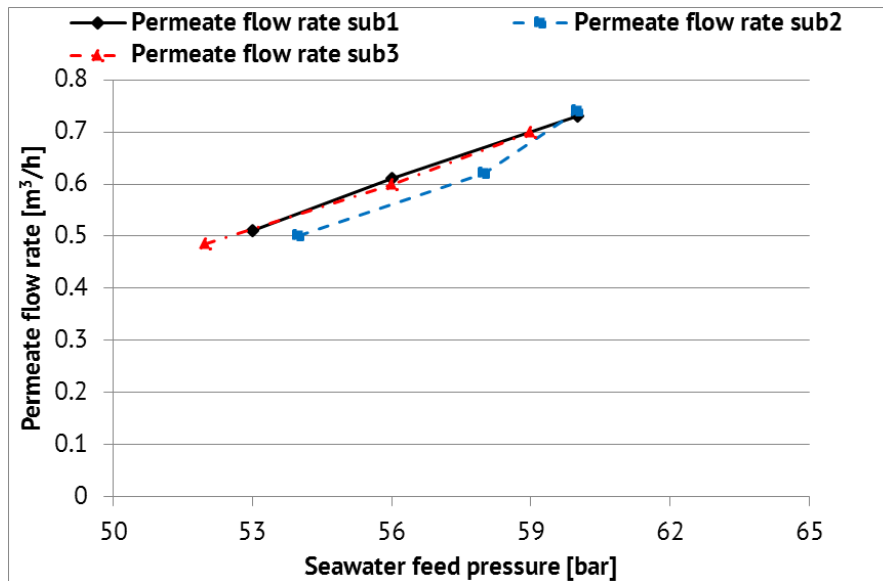


Figure 4.17 Feed water pressure effect on the permeate flow rate for the three sub- units

In Figure 4.17 it is obvious that the higher salinity leads to higher feed water pressure. As explained before, reverse osmosis technology involves application of pressure to the feed water stream in excess of the osmotic pressure and for constant temperature the osmotic pressure is directly proportional to the molar concentration of the solutes. The range of the seawater pressure throughout the RO unit operation varies between 52 and 60 bar and more specifically: for the first sub- unit varies between 53 and 60 bar with permeate production from 0.53 to 0.73 m³/h, for the second sub- unit varies between 54 and 60 bar with permeate production from 0.50 to 0.74 m³/h and for the third sub- unit varies between 52 and 59 bar with permeate production 0.49 to 0.70 m³/h. The maximum permeate production of each sub- unit reaches the maximum expected from the design, however, the maximum is reached on 70% of the maximum capacity. The effect of the feed water pressure on the permeate salinity is presented in Figure 4.18 below:

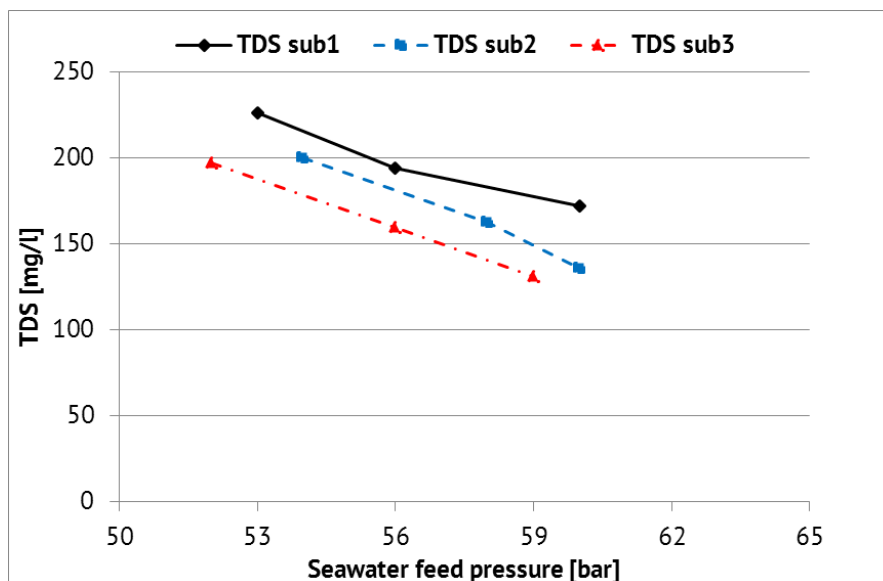


Figure 4.18 Feed water pressure effect on the permeate salinity for the three sub- units

As observed in Figure 4.18 the permeate salinity produced by the first sub-unit varies between 226.5 and 172.1 mg/l, by the second sub- unit varies between 200.2 and 135.8 mg/l and by the third sub- unit varies between 197.1 and 137.4 mg/l, throughout the whole operation range. Even though there are slight differences in the permeate salinity due to some measurement instrumentation uncertainty, all three sub- units produce water of good quality during the whole operation.

HP pump operation characteristic curves

The HP pump operation investigation starts again with the effect of the rotational speed on the feed water flow rate, presented in Figure 4.19:

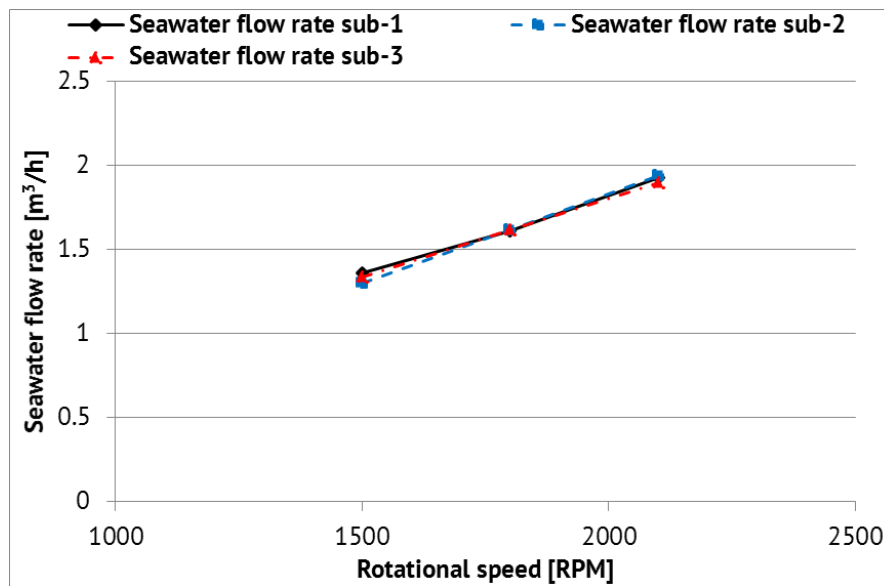


Figure 4.19 Feed water flow rate as a function of HP pump rotational speed for the three sub- units

In Figure 4.19, afresh the feed water flow rate varies between 1.3 to 2 m³/h for all HP pump operation speed, reaching a maximum of 2 m³/h (a total of 6 m³/h). Again, the feed water flow rate is proportional to the HP pump rotational speed and all three operational curves almost coincide.

The relation between the feed water pressure and the SEC and power for each sub- unit is presented in Figure 4.20 below:

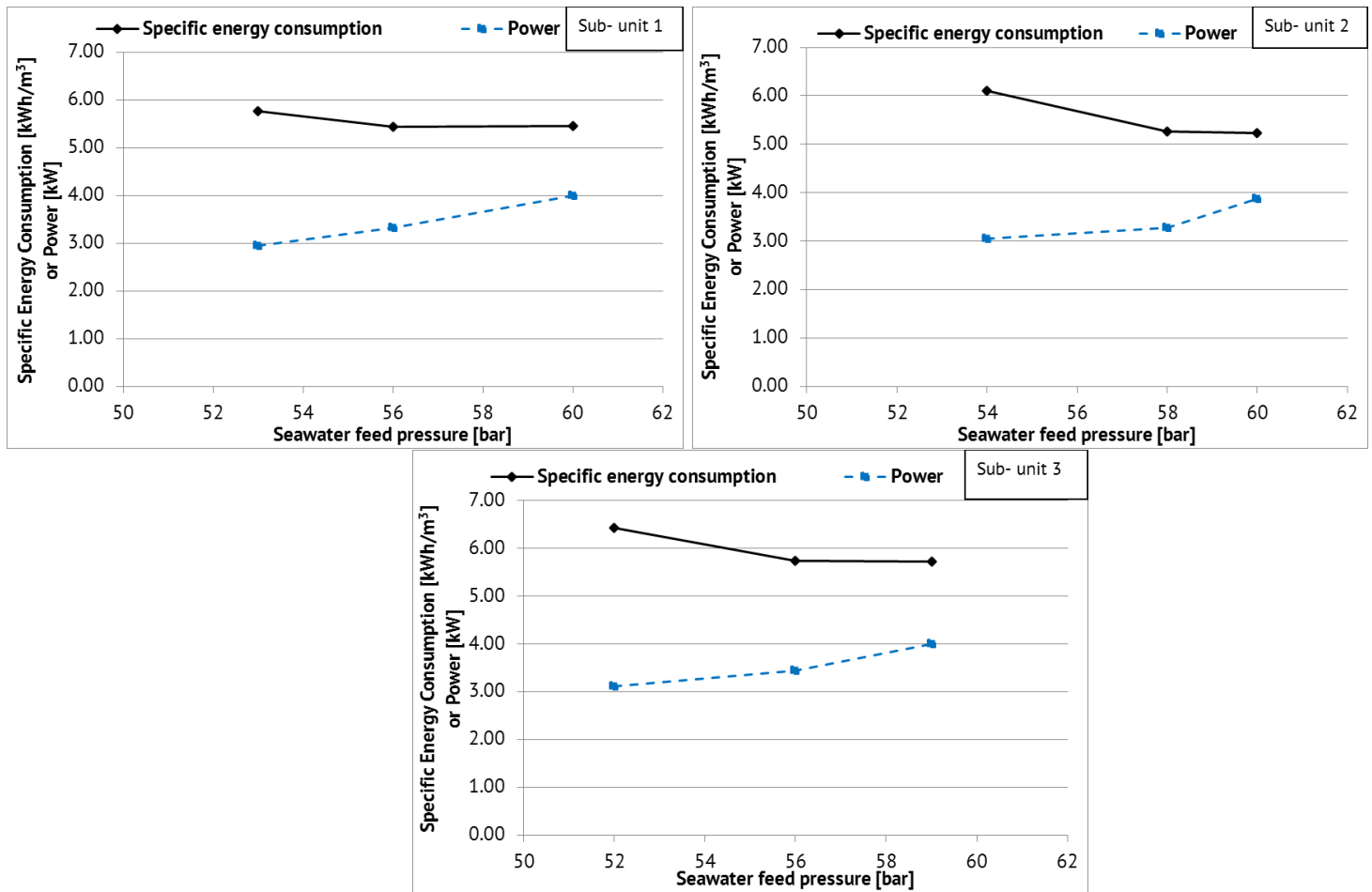


Figure 4.20 Specific energy consumption and power as a function of the feed water pressure for the three sub- units

In the current test the SEC of each sub- unit is increased, varying between 5.8 and 5.5 kWh/m³ for the first sub- unit, between 6.1 and 5.2 kWh/m³ for the second sub- unit and between 6.4 and 5.7 kWh/m³ for the third sub- unit, as presented in Figure 4.20. Higher feed water salinity results in higher power demand in order to increase the feed water pressure to limits overpassing the osmotic pressure. The power demand of every sub- unit varies between 3 to 4 kW, as it is observed in the chart of Figure 4.20. The SEC of each sub- unit remains within limits of efficient operation, considering the fact that SEC includes the consumption of the feed pump as it has been mentioned previously.

A clearer relation between the SEC and the power consumed by each sub- unit as well as the relation of the power with the permeate salinity is presented in Figure 4.21:

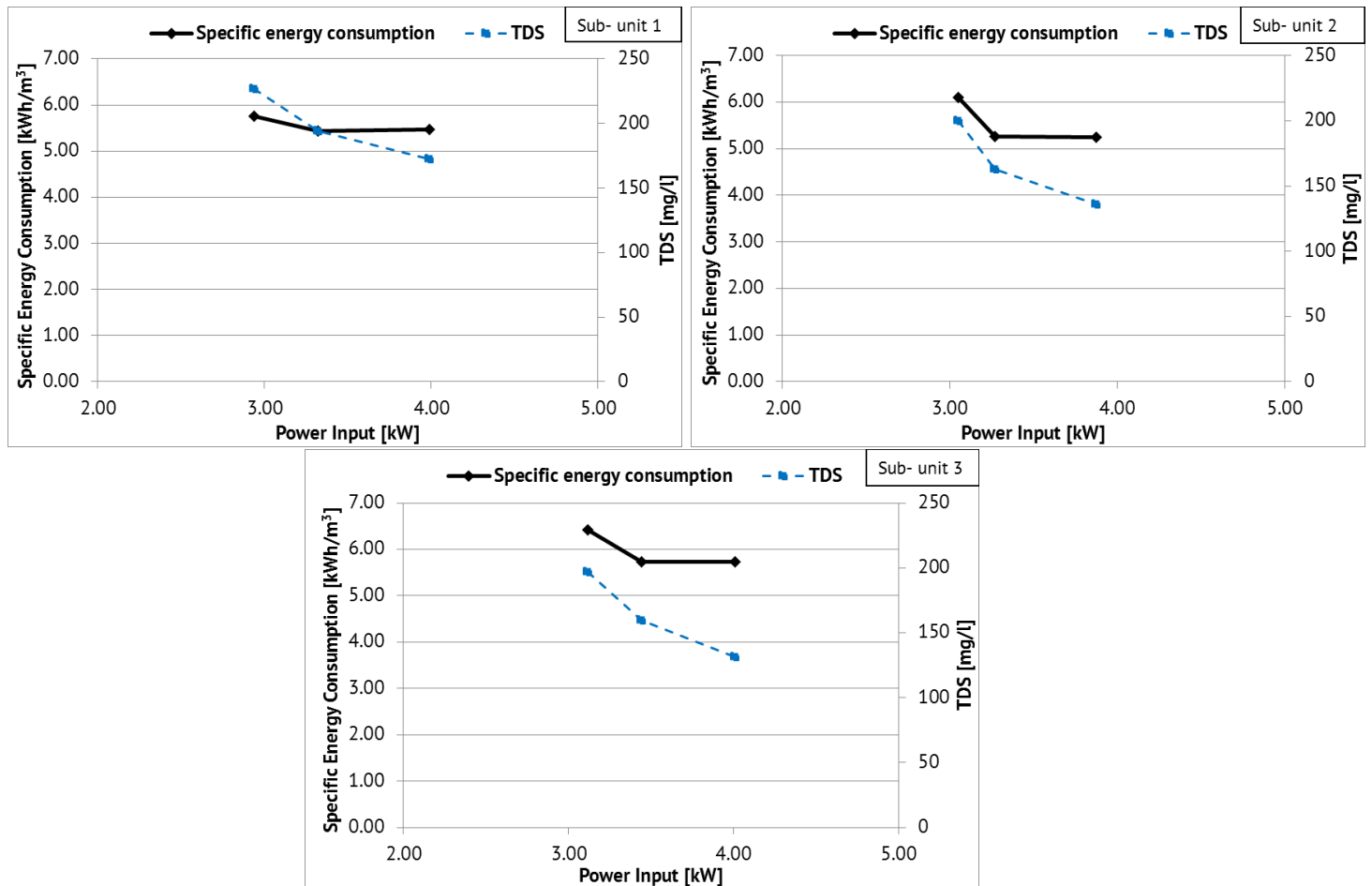


Figure 4.21 Specific energy consumption and fresh water salinity as a function of the power input for the three sub- units

For operation between 3 and 4 kW of power input, the SEC for each sub-unit is presented in Figure 4.21. The slight differences in SEC and permeate salinity between the three identical sub- units are due to some measurement instrumentation uncertainty, though within acceptable limits (see Appendix II).

The HP pump evaluation of each sub- unit for the current test concludes with the examination of the relation between the power input and the permeate production, shown in Figure 4.22:

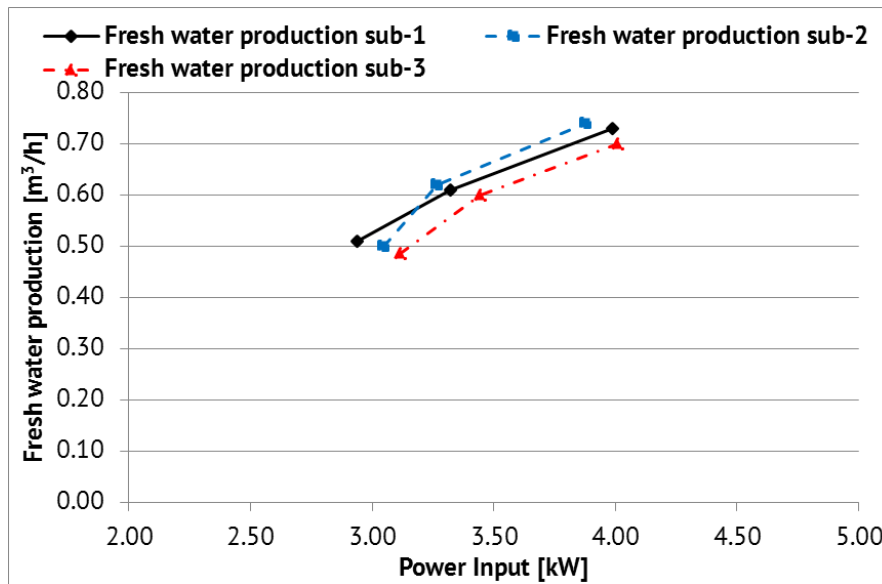


Figure 4.22 Fresh water production as a function of the power input for the three sub- units

For 3 kW power input each sub- unit produces almost 0.50 m³/h of fresh water and for the maximum power input of 4 kW each sub- unit produces almost 0.72 m³/h, which is close to the value expected from the sub- unit design, however it reaches the maximum value for operation at the 70% of its maximum capacity.

An evaluation of the whole RO unit operation is presented in Figure 4.23, connecting the power input to the SEC and the fresh water salinity.

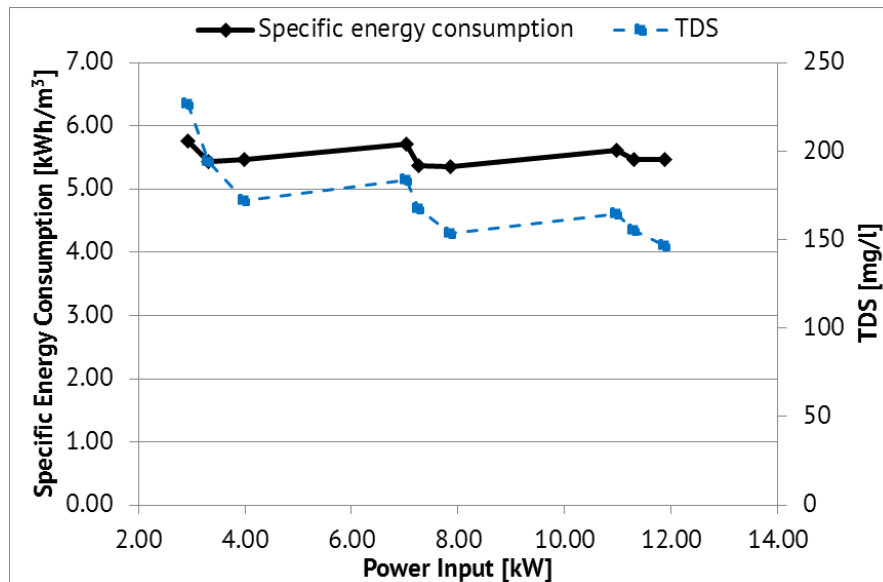


Figure 4.23 Specific energy consumption and fresh water salinity as a function of the total power input for the whole RO unit

According to Figure 4.23 the SEC of the RO unit throughout the whole power input range varies between 5.8 and 5.3 kWh/m³ proving an efficient operation, considering the fact that the RO unit operates at lower pump rotational speed than the nominal. The fresh water salinity varies between acceptable limits throughout the whole operation range, getting values from 226.5 to 146.6 mg/l, reassuring fresh water of good quality.

Finally, the fresh water production as a function of the power input for the whole RO unit is presented in Figure 4.24 below:

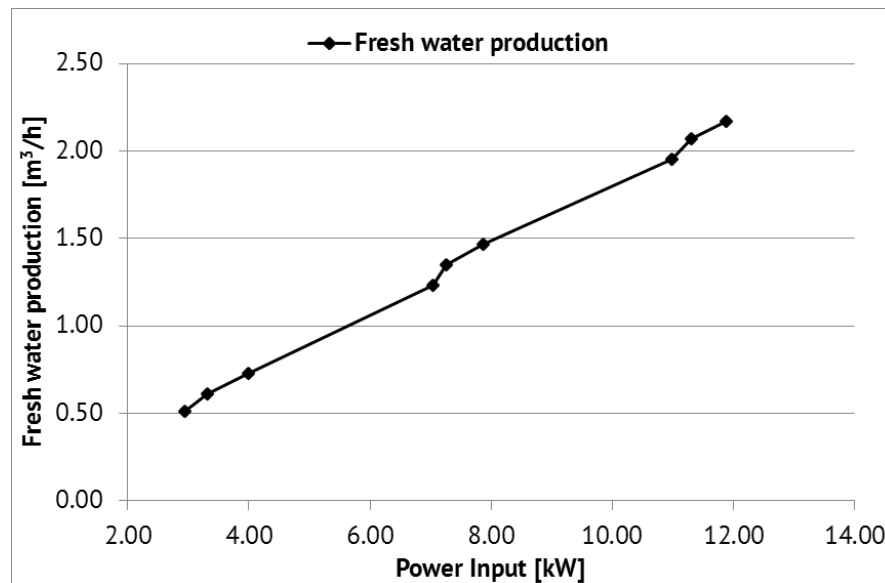


Figure 4.24 Fresh water production as a function of the total power input for the whole RO unit

The fresh water production starts from 0.50 m³/h for operation of only the first sub- unit and at low HP pump rotational speed (1500 RPM) and reaches a maximum of 2.3 m³/h for full operation of all three sub- units at high HP pump rotational speed (2900 RPM, at 70% of maximum capacity). The second sub- unit starts operating at 7 kW input and the third at 10.9 kW input. The RO unit has been designed for production of 2.1 m³/h at 10 kW power input, so the current results could be considered as a slight oversize of the RO unit or a result of the current test conditions or construction reasons.

4.3.1.4 Conclusions

The tests of the RO unit operation in three different feed water salinities that were presented in the current paragraph have all proved an efficient operation of the RO unit throughout the whole power input range. Each test took place at a different day with different temperature at the laboratory (different temperature of feed water), however, since in each test a different salinity was examined, a direct comparison of the RO unit in order to present the effect of temperature in its operation is not possible. However, in all three cases, the RO unit produced fresh water of good quality (<500 mg/l, [4.5]), over 2.1 m³/h at full operation (at 70% of its maximum capacity) and with acceptable specific energy consumption values. It should be noticed that the SEC has been a little high considering the fact that the sub- units obtain an energy recovery system, however the fact that the HP pumps operated at lower rotational speed than their nominal, for the same fresh water production they needed more power which led to a slightly increased specific energy consumption. The seawater flow rate was the same in all cases and proportional to the HP pump rotational speed. Finally, the fact that the fresh water production was a little higher than the expected from the design and for operation at 70% of the nominal and for a power input higher than the maximum of 10 kW (expected from the ORC engine) leads to the conclusion that in practice and in current tests' conditions the RO unit resulted to be more efficient than expected,

due to construction or test conditions reasons (i.e. temperature, feed water salinity etc.).

4.3.2 RO sub- unit evaluation for high salinity in different water temperatures

In the laboratory three different tests for three different seawater temperatures took place, for the same water salinity in order to examine the effect of the temperature on the operation as well. In each sub-unit three frequencies were tested, those of 25, 30 and 35 Hz for different high-pressure pump's rotational speed to test the RO unit operation in variable power input (50%, 60% and 70% of its nominal operation). In the current test for simplicity reasons, only the first sub- unit operation has been presented since the three sub- units are identical and their operation and measured parameters were the same. The water tank has been filled with 3.3 m³ of water and 125 kg of salt, consisting the desired salinity of 37500 ppm.

Once again, the same parameters as the previous tests have been recorded. It should be noted that the feed water temperature can safely be considered equal to the measured fresh water temperature since the temperature increase through the pumps is insignificant and can be neglected [4.1].

As mentioned before, the most important values in an RO Unit are the power consumption, the specific energy consumption [in kWh/m³], the membranes' pressure, the seawater flow rate, the water recovery ratio (the fraction of seawater that is desalinated) and the quality of fresh water [TDS in mg/l]. These values are greatly related and lead to the identification of the RO performance and its evaluation. The water recovery ratio based on the design of the RO unit is around 32% and is almost constant throughout the test-rig operation. The main request in the specific system is the evaluation of the efficiency at variable load, which is a critical issue in the operation of these units, since at low load the membrane pressure decreases and the quality of the fresh water deteriorates (higher salinity).

4.3.2.1 Membranes operation characteristic curves for variable seawater temperature

In the current tests, the effect of the variable power input on the fresh water salinity is being evaluated. The main details of the membranes and the high-pressure pump operation will be observed, since with the decrease of the available power and the consequent decrease of the membranes' pressure, the permeate quality is reduced. The investigation of the high-pressure pump and the membranes operation curves is necessary for the RO unit operation research. The effect of the feed water temperature is also examined.

As mentioned previously in paragraph 4.2.1, the main factors that affect the RO membrane performance are; the feed water pressure, the water temperature, the salt concentration, the water recovery ratio and the water pH [4.2]. Here, the feed water salinity is kept constant to 37500 ppm and the recovery ratio is around 32%, as resulted from the experimental evaluation. Concerning the pH tolerance, as analyzed in 4.2.1, thin-film composite (TF) membranes like the ones used in the current test rig, are typically stable over a wide pH range and, therefore the pH influence is negligible in the membranes operation and has not been examined [4.2]. In Figure 4.25, the feed water pressure effect on the permeate (fresh water) flow rate and salinity is being observed for three different water temperatures.

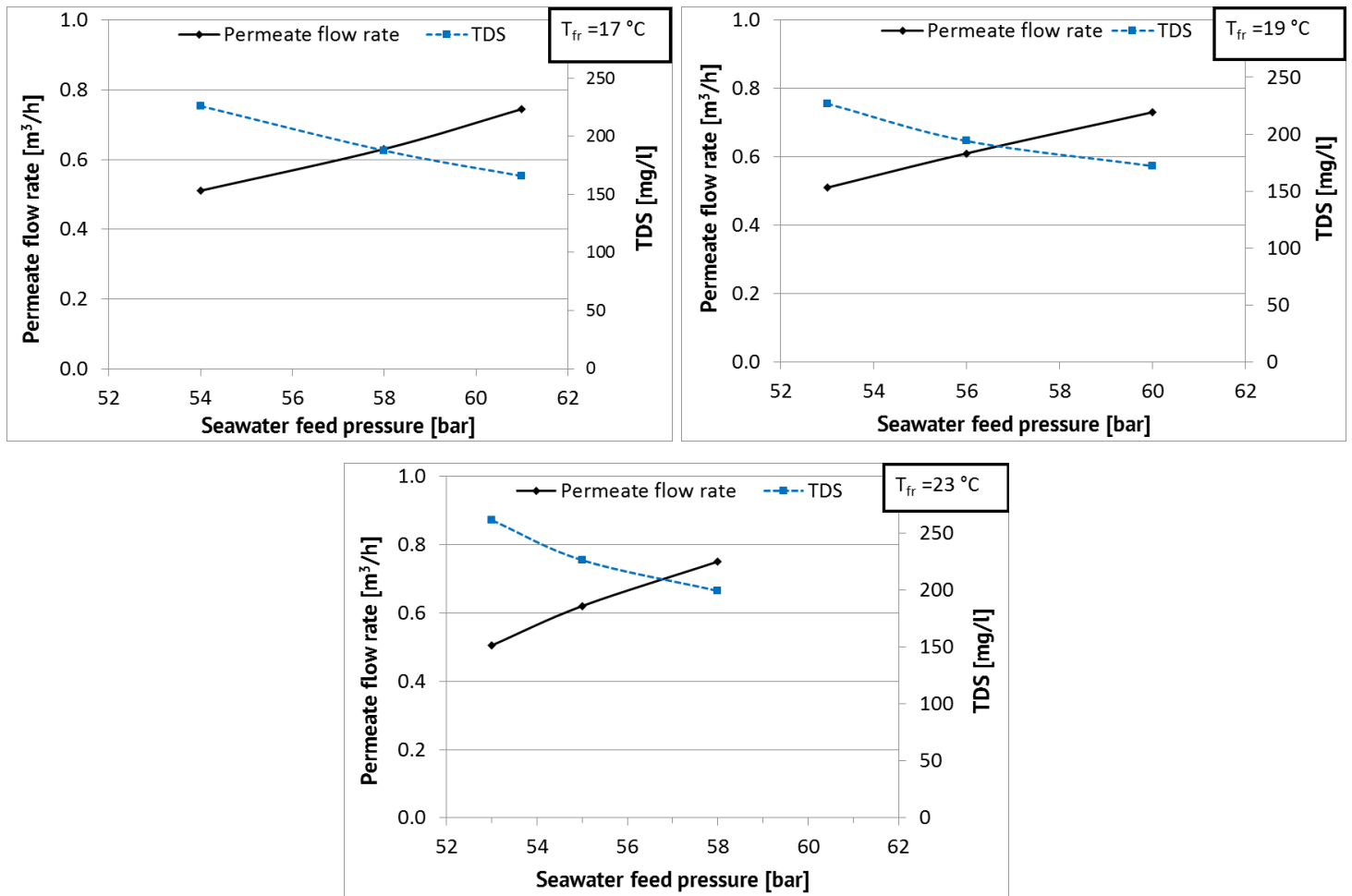


Figure 4.25 Feed water pressure effect on the permeate flow rate and permeate water salinity for different water temperatures (T_{fr})

Feed water pressure affects both the water flux and salt rejection (fresh water salinity) of RO membranes. As explained before, reverse osmosis technology involves application of pressure to the feed water stream in excess of the osmotic pressure and a portion of the feed water (concentrated solution) is forced through the membrane to emerge as purified product water of the dilute solution side. As shown in Figure 4.25, water flux across the membrane increases in direct relationship to the increase of feed water pressure. Increased feed water pressure also results in decreased fresh water salinity but, as Figure 4.25 demonstrates, the relationship is less direct than for water flux. For low water temperature the fresh water production varies between 0.5 and 0.75 m^3/h for feed water pressure from 53 to 61 bar, when for higher temperature at 23°C the fresh water production varies within the same values but for maximum pressure at 58 bar. This was expected, since when the temperature of feed water is increased for constant product flow, the required applied pressure decreases and the product water salinity increases [4.8]. Membrane productivity is very sensitive to changes in feed water temperature [4.2]. As water temperature increases, water flux increases linearly, due primarily to the higher diffusion rate of water through the membrane. In other words, as the temperature increases, the amount of energy available for diffusion is increased, which means that a given particle will move faster at a higher temperature. Thus, the rate of diffusion will be faster as the temperature increases. Higher diffusion rate however, also results in lower salt rejection or higher salt passage through the membrane. This explains the salinity increase from low to high

water temperature. Since RO membranes are imperfect barriers to dissolved salts in feed water, there is always some salt passage through the membrane. As feed water pressure increases, this salt passage is increasingly overcome as water is pushed through the membrane at a faster rate than salt can be transported. Therefore, the permeate salinity curve decreases with the pressure increase. As observed in Figure 4.25, in low water temperature the salinity varies from 230 to 160 mg/L while at 23 °C the salinity range is higher from 260 to 200 mg/L. However, in all cases the fresh water is of good quality (<500 mg/L) [4.5].

Moreover, in Figure 4.25 it is observed that the fresh water production reached a slightly higher value than the designed one. According to the design, the RO unit capacity at nominal rotational speed of the HP pump was 0.70 m³/h of permeate. However, the experiment has shown that the maximum fresh water production has been 0.75 m³/h, which has been observed at lower HP pump’s rotational speed than the nominal one. Nevertheless, it has also been noticed that the recovery ratio resulted to be slightly higher than the designed one (38% rather than 32%), due to reasons mentioned in the previous paragraph 4.3.1.4.

4.3.2.2 HP pump operation characteristic curves for variable seawater temperature

The RO- unit operation control is achieved with the use of frequency inverters on each sub- unit in order to monitor the HP pump rotational speed. The rotational speed change provokes a variation of the seawater flow rate and the HP pump pressure, as presented in Figure 4.26:

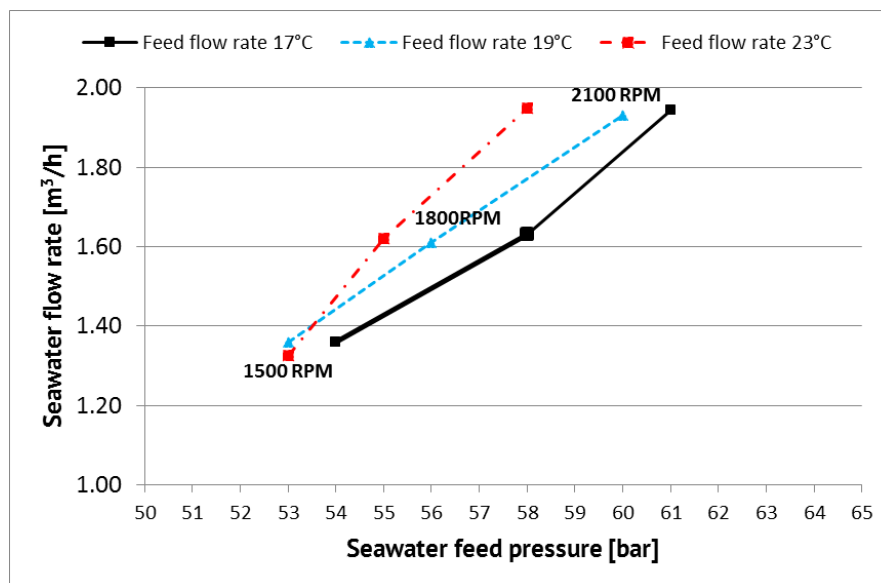


Figure 4.26 Seawater flow rate as a function of HP pump pressure for different rotational speed and different water temperatures

In Figure 4.26, the almost linear correlation of the seawater flow rate and the HP pump pressure for each rotational speed is noted, so the seawater flow rate is almost proportional to the HP pump pressure, and the HP pump operates for a wide speed range since the available power input varies. It is also noticed that as the temperature increases, for the same rotational speed, the seawater flow rate almost remains the same, when the HP pump pressure decreases, due to lower water viscosity in higher temperatures. The viscosity of water varies with

temperature. Water’s viscosity decreases as temperature increases and vice versa. For every 12°C decrease of the feed water temperature, the feed water pressure is increased by 15%. In other words, the water permeability of the membranes increases with temperature. Therefore, as the seawater temperature increases, for the same pump rotational speed and the same flow rate, the pressure needed to pump the water is lower thus the HP pressure decreases [4.2, 4.3, 4.9].

In Figure 4.27, the specific energy consumption and the HP pump electric power (since the motor is connected on the same shaft to the axial piston pump and the energy recovery system) as a function of the seawater feed pressure are presented.

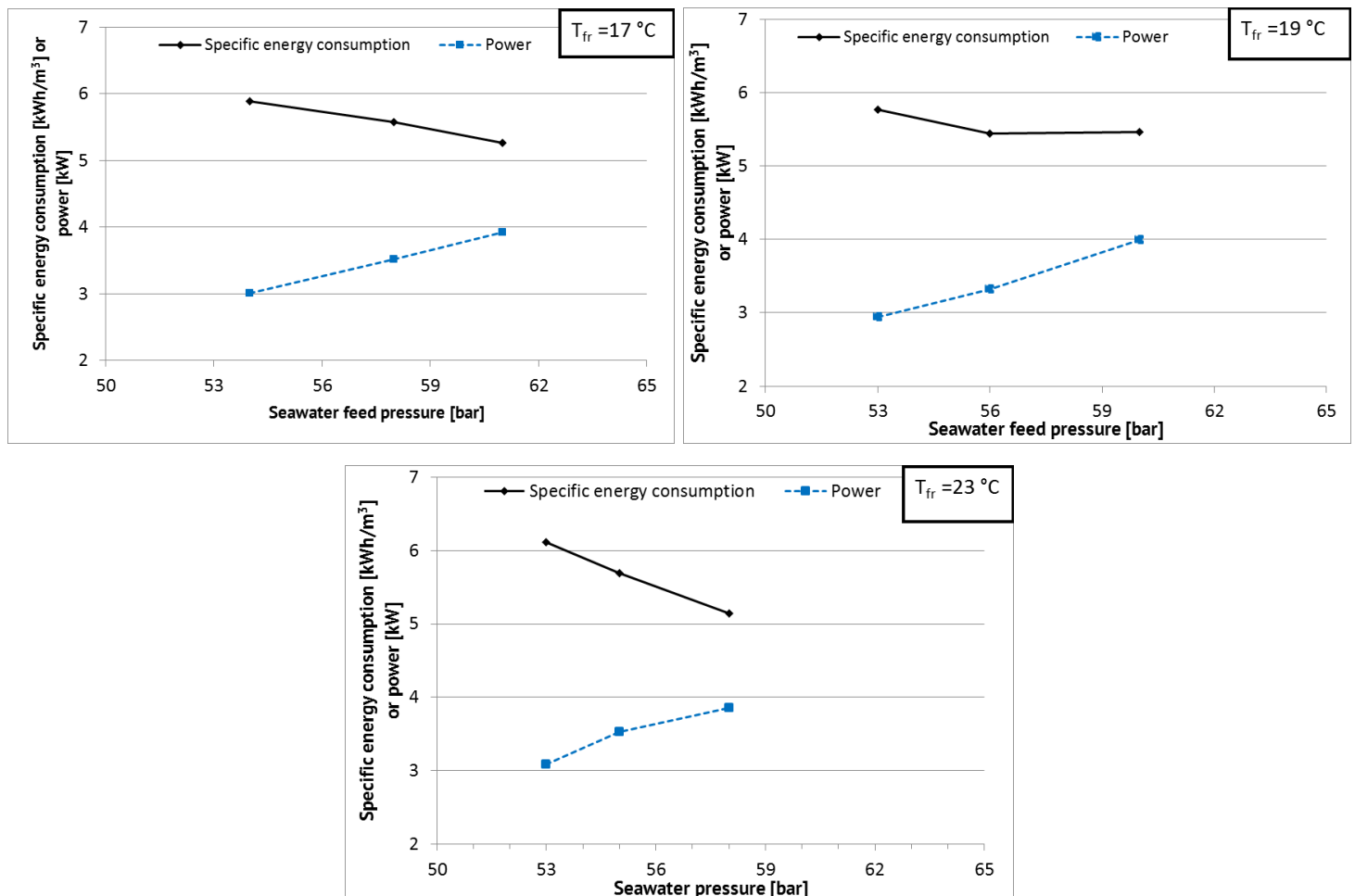


Figure 4.27 Specific energy consumption and HPP power as a function of the seawater feed pressure at the membranes inlet at different water temperatures (T_{fr})

The specific energy consumption is the ratio of the HPP pump power consumption to the fresh water production. As observed in the three charts of Figure 4.27, the specific energy consumption is decreasing with the increase of the seawater feed pressure. As the high-pressure pump speed increases, the pressure at the membranes inlet increases and the fresh water production is also high. This results in a decrease in the specific energy consumption. The high-pressure pump power on the other side increases with the augmentation of the seawater feed pressure. What is also noticed in Figure 4.27 is that the specific energy consumption varies between 5.2 and 5.8 kWh/m³ but for operation at 23 °C it reaches a slightly higher value of 6.1 kWh/m³. This is due to the fact that as it is observed in the third chart

of Figure 4.27 ($T_{fr}=23\text{ }^{\circ}\text{C}$), the power reaches a slightly higher value at the same operation point, than in the lower temperature (of $T_{fr}=17\text{ }^{\circ}\text{C}$ and $T_{fr}=19\text{ }^{\circ}\text{C}$). However, the difference in power is small, 0.1 kW and this could be due to measurement uncertainty. According to literature, for a range of membrane pressures between 40 and 70 bar, an energy of around 4.1 and 4.8 kWh is required for each m^3 of product water obtained [4.10]. However, in the present case the specific energy consumption values were found to be a little higher. This could be due to the operation of the unit at lower rotational speeds than the nominal, since for the same fresh water production it needs more power which leads to a slightly increased specific energy consumption. In Figure 4.28, the specific energy consumption and the fresh water salinity are presented as a function of the power input.

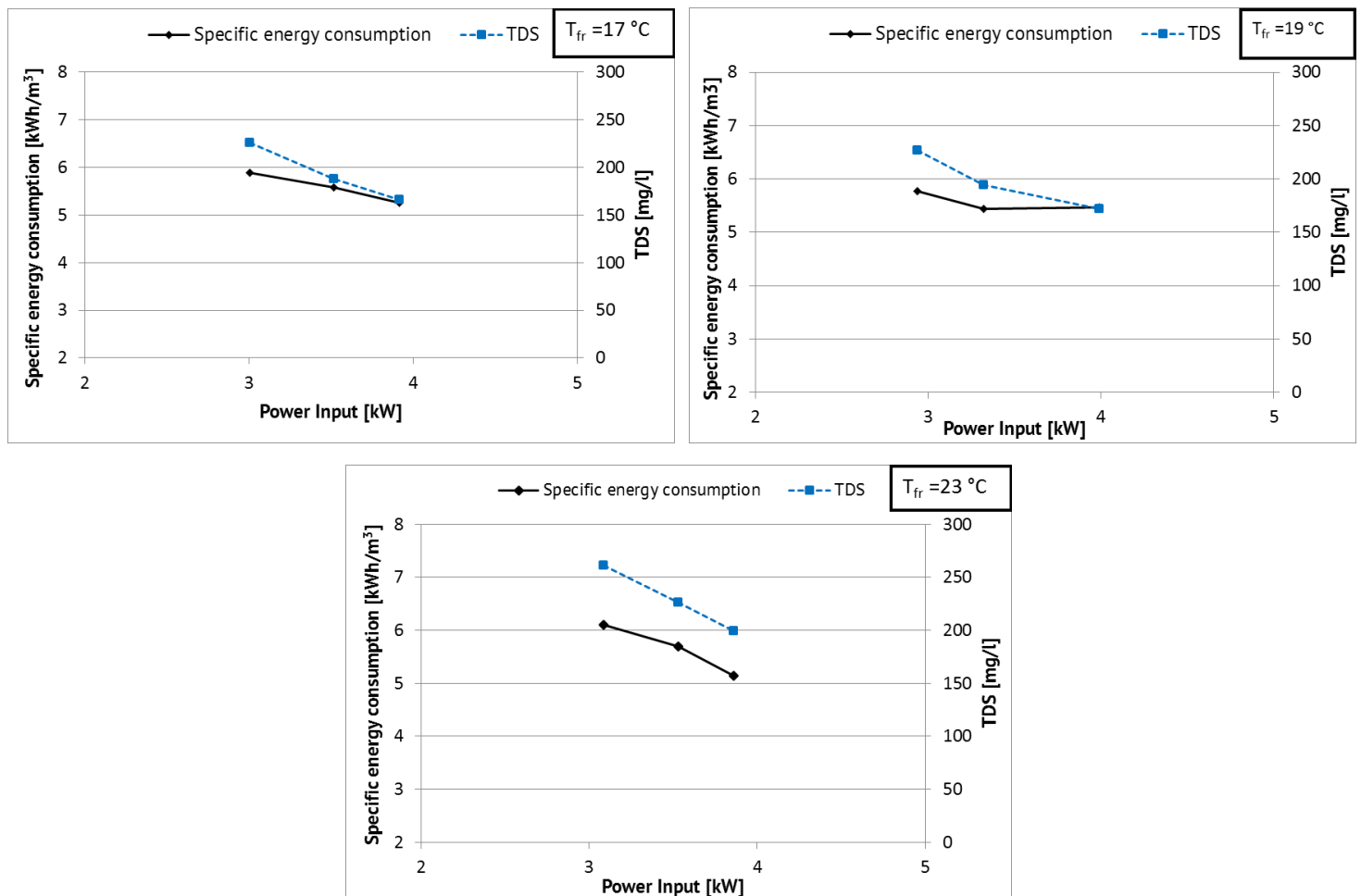


Figure 4.28 Specific energy consumption and fresh water salinity as a function of the power input at different water temperatures (T_{fr})

The specific energy consumption in all three cases remains between the values of 6.1 to 5.2 kWh/m³ for a power input of 3 to 4 kW. Concerning the fresh water salinity however, in lower operation temperature it varies between 240 and 160 mg/L for a power input from 3 to 4 kW, when for higher operation temperature it gets higher values from 260 to 200 mg/L for the same power input. However, in all three cases the fresh water produced is of very good quality.

Finally, in Figure 4.29, the fresh water production is presented as a function of the power input.

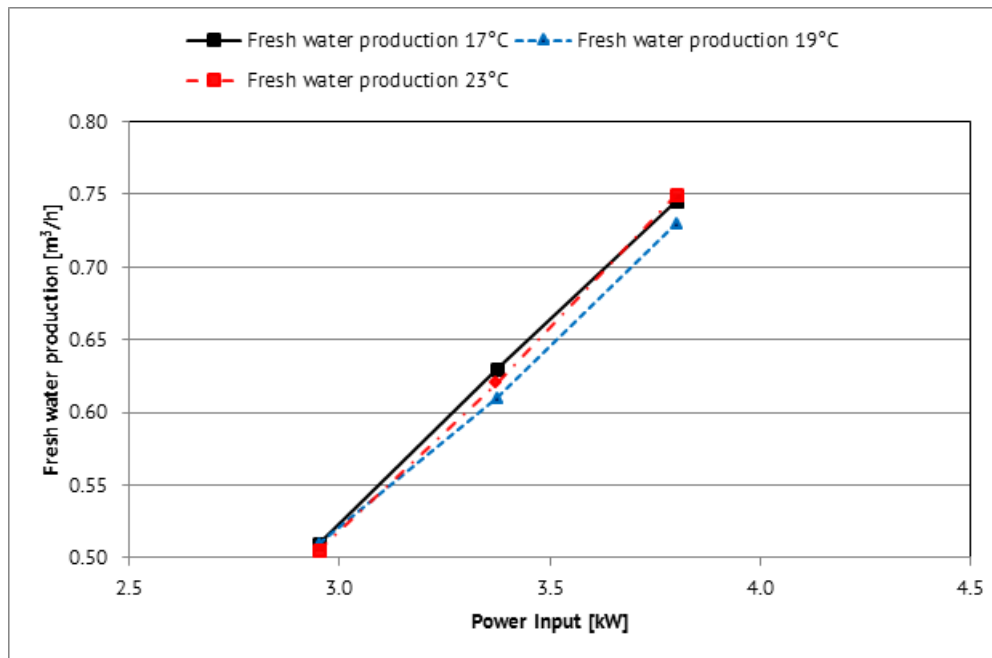


Figure 4.29 Fresh water production as a function of the power input

In Figure 4.29, it is observed that the fresh water production for operation at 17 °C and 23 °C the operation curves almost coincide while at 19 °C there is a slightly lower maximum production which reaches 0.73 m³/h rather than 0.75 m³/h at the lower temperature operation for the same power input. However, this difference is small and it may be concluded that the HP pump operation is not considerably affected by the temperature. The maximum fresh water production has been expected to be around 0.70 m³/h but as mentioned in Figure 4.27, the recovery ratio resulted to be a little higher than expected from the design.

4.4 Case study of a multi- skid RO unit operation in combination to PV fields of different capacities for three different areas on a winter and a summer day. Comparison to a conventional RO unit.

In order to prove the flexibility offered by the use of a multi- skid RO desalination unit in combination to renewable energy sources, different case studies of RO desalination powered by a photovoltaic field is hereby presented. For this analysis, it is assumed that the solar-powered reverse osmosis system does not incorporate any energy storage and would only operate when the solar power is available. Three different locations have been selected where the system could be installed; Athens- Greece, Palma- Spain and Abu Dhabi- United Arab Emirates (UAE). For all cases, the mono- crystalline silicon photovoltaic (PV) technology has been chosen. The orientation has been determined to be South and the slope degree has been set at 32° for Greece, 37° for Spain and 22° for UAE [4.11, 4.12]. The PV panels have been chosen to apply fixed mounting position. Three different cases of installed peak PV power are being observed for each case with the help of the appropriate software [4.12]; 10 kWp, 15 kWp and 20 kWp. The scenarios examined are for a typical summer day (July 21st) and a typical winter day (December 21st). Based on the daily solar irradiance profile for the 21st of July and with the use of the appropriate software [4.13], the PV daily power production occurs, presented in Figure 4.30;

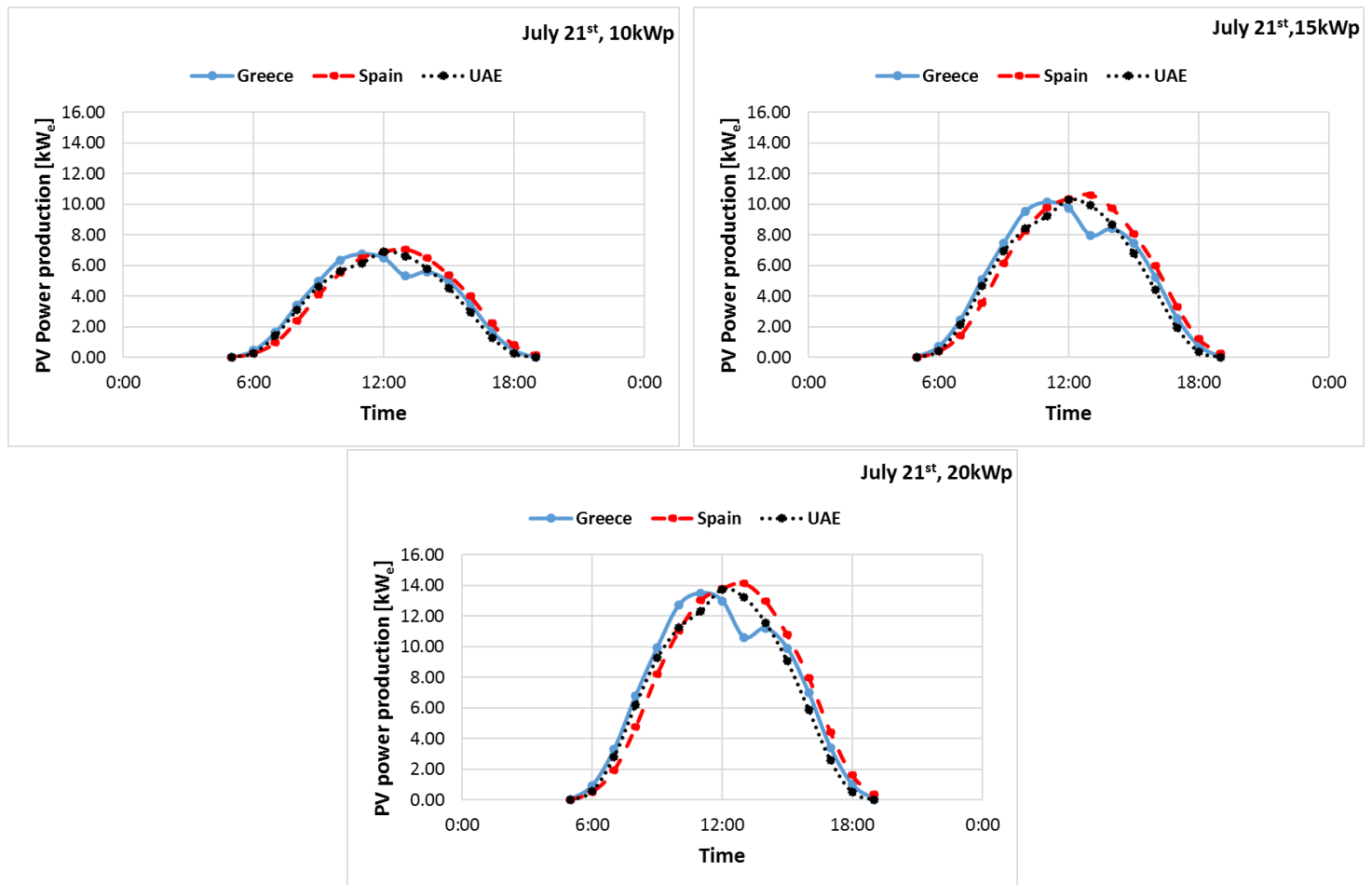


Figure 4.30 PV power production for different capacity for the three locations (Athens- Greece, Palma- Spain and Abu Dhabi- United Arab Emirates), July 21st

As observed in Figure 4.30, the PV power production profiles for all three areas are similar, even in UAE, because of the higher ambient temperature in the summer decreasing PV efficiency.

Taking into account the minimum power that a tested sub- unit needs to operate at the corresponding temperature (Figure 4.29), Figure 4.31 presents the number of sub- units that would operate in the three examined areas throughout a typical summer day, July 21st;

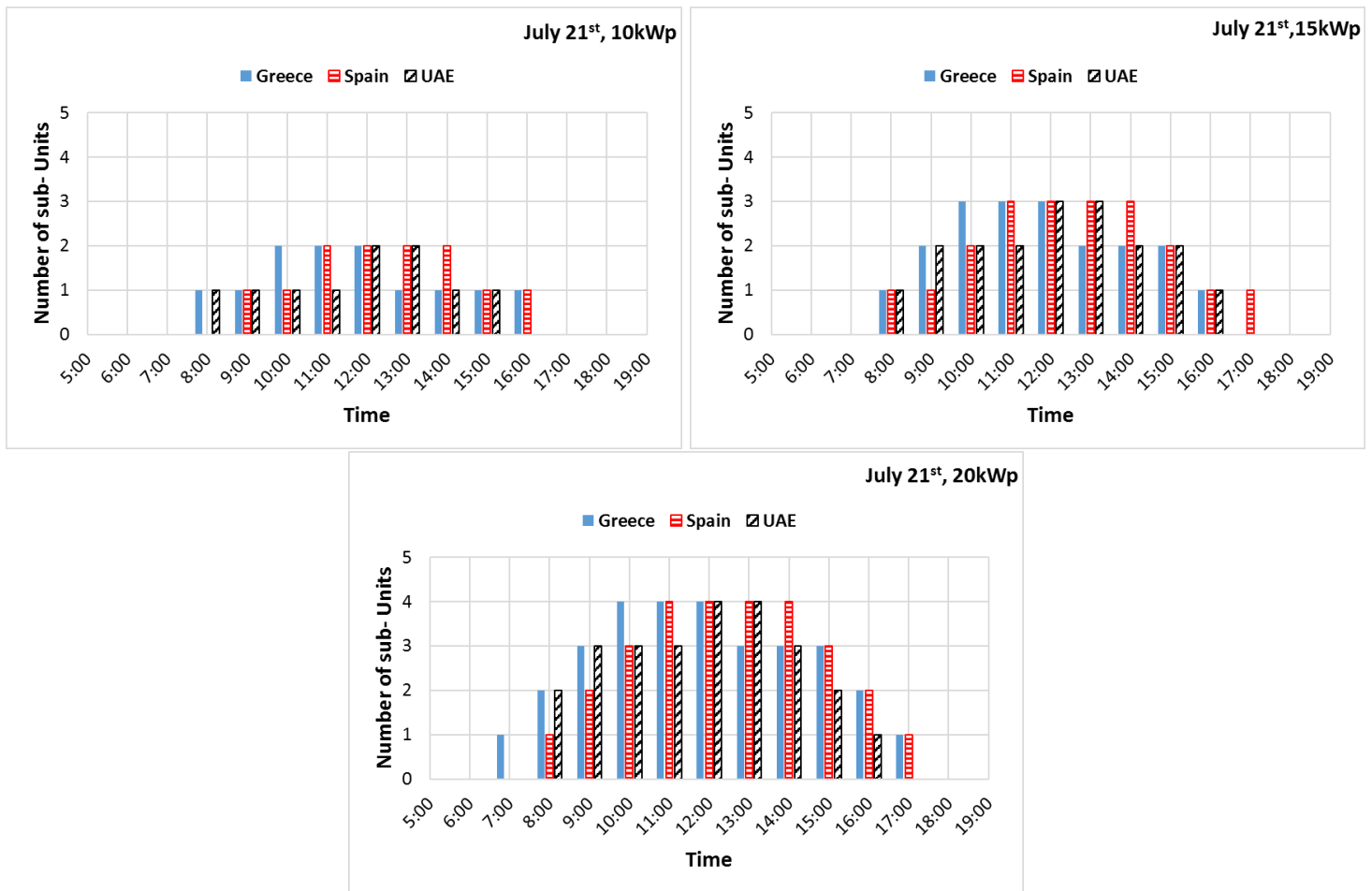


Figure 4.31 Number of operating sub- units throughout the day of July 21st for different PV capacity.

As it is observed in Figure 4.31, a PV system of 10 kWp will provide enough power for one or two sub- units to operate at each area, in different time of the day. There are some differences in time profiles, therefore different number of sub- units operate at different time of the day. For the system of 10 kWp, the unit operation lasts from 8:00 to 16:00, when in Spain the fresh water production starts one hour later. For higher PV system capacity, similar observations are noticed, however the number of sub- units in use increases, reaching the number of 3 for 15 kWp and 4 for 20 kWp for all areas. The operation time also increases and for the system of 15 kWp operation starts at 8:00 and lasts until 16:00 for Greece and UAE and until 17:00 for Spain. Finally, for the system of 20 kWp it is noticed that in Greece the production starts an hour earlier than in the other two areas and in UAE the fresh water production stops an hour earlier than in the other two areas and four units operate only for two hours of the day, when in Spain they operate for four hours and in Greece for three.

For a typical winter day, December 21st, a similar methodology is followed. The daily power production based on the daily solar irradiance profile for the 21st of December, for the three selected areas and different PV capacity is shown in Figure 4.32;

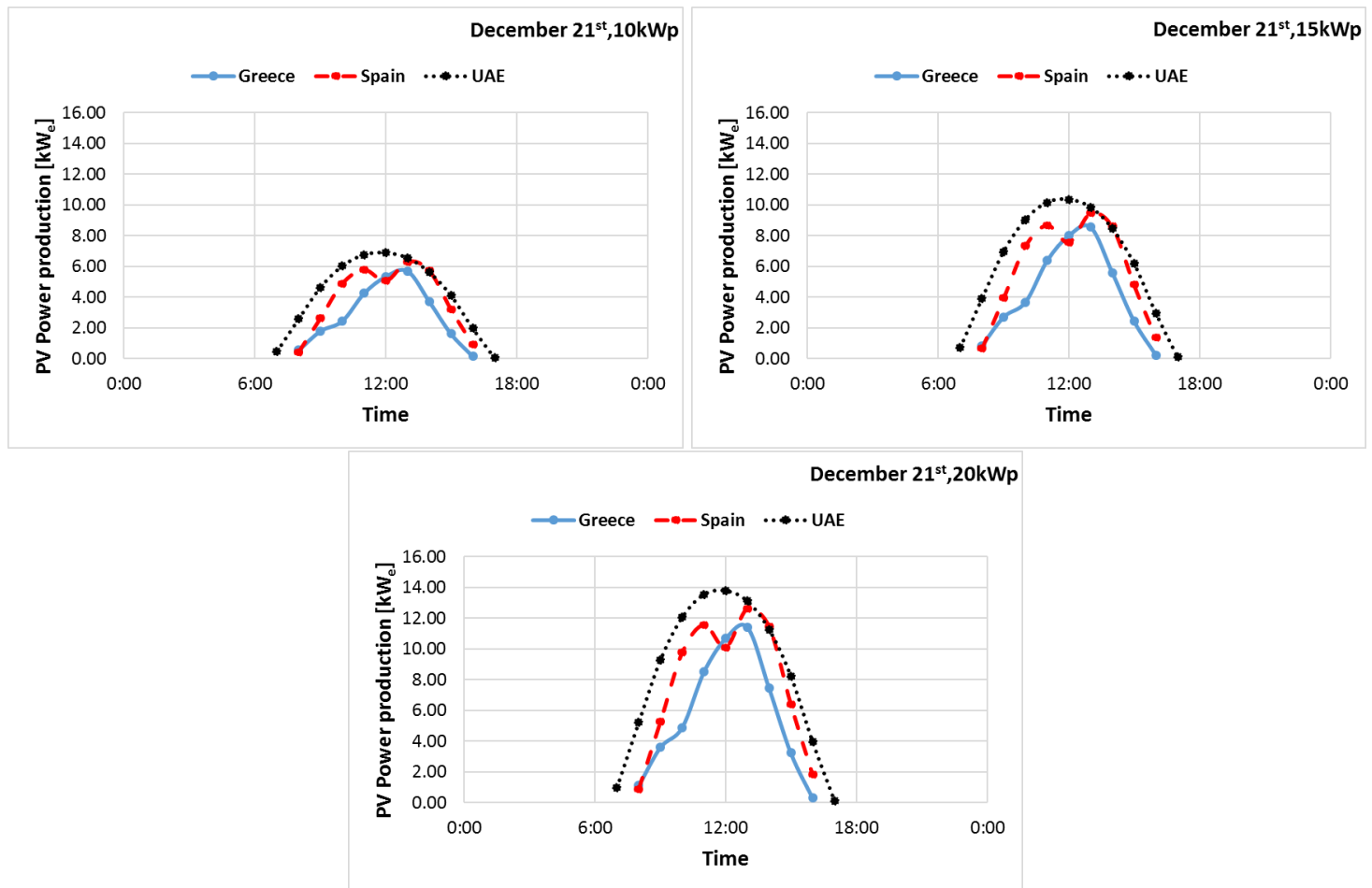


Figure 4.32 PV power production for different capacity for the three locations (Athens- Greece, Palma- Spain and Abu Dhabi- United Arab Emirates), December 21st

As observed in Figure 4.32, a PV installation in Athens and Palma shows similar production, with the one in Palma reaching a maximum of 13 kW and in Athens 11.5 kW for a PV system of 20 kWp. The PV in Abu Dhabi produces more power reaching a maximum of almost 14 kW for the 20 kWp case. Moreover, Abu Dhabi presents a much smoother profile than the other two countries. Based on these power production profiles, the RO sub- units number that will operate during this winter day are presented in Figure 4.33 below;

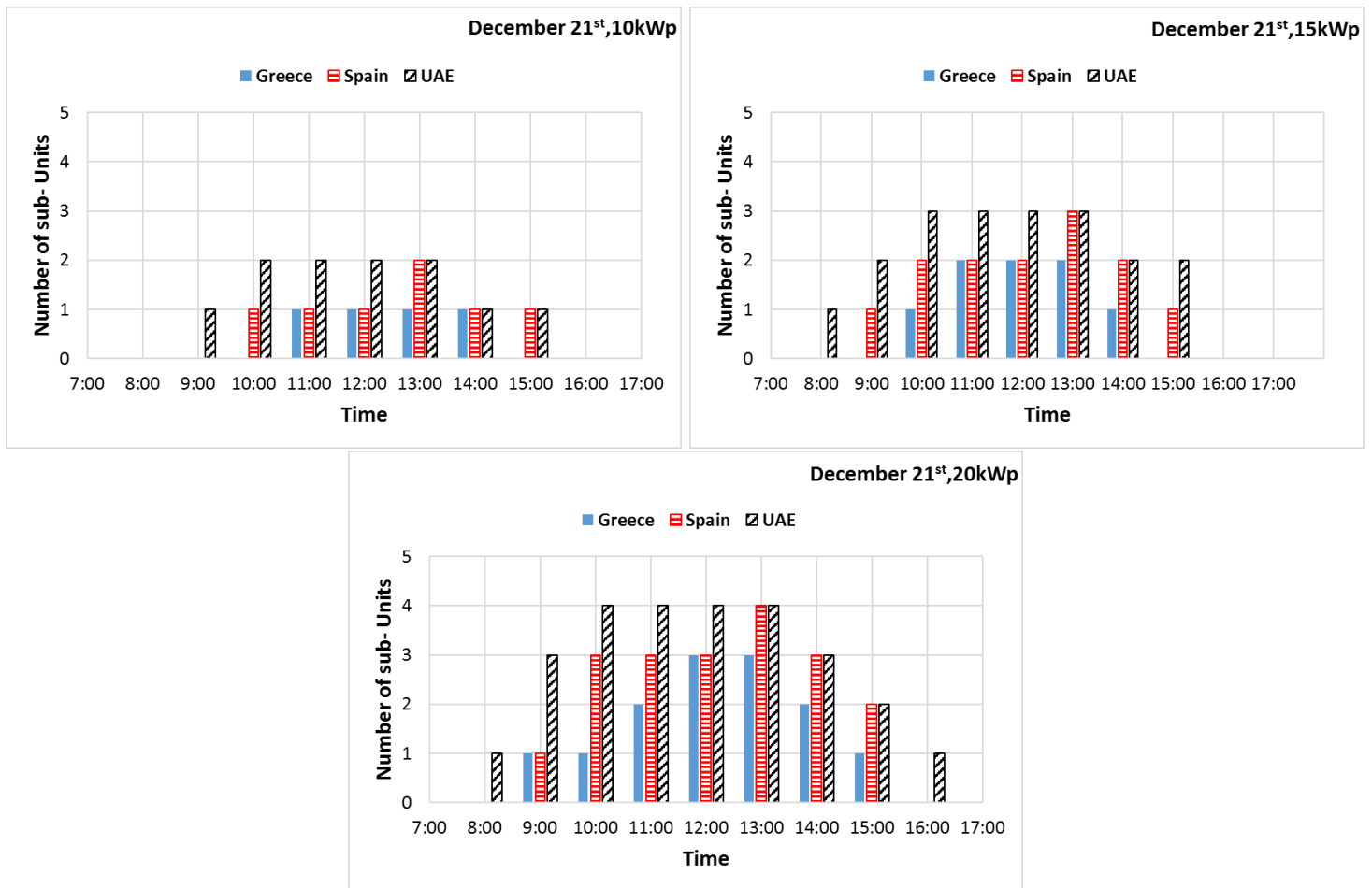


Figure 4.33 Number of operating sub- units throughout the day of December 21st for different PV capacity

It is obvious that in UAE more units will operate for each installed PV capacity and for a longer time period during the day. All three systems operate with at least one sub- unit even for low PV power input for a sufficient amount of time during the day. The system in UAE presents the best operation with the maximum operation of two, three or even four sub- units for 10 kWp, 15 kWp and 20 kWp accordingly. The system in Spain also shows good operation reaching the number of three or four sub- units for higher PV capacity, while the system in Greece reaches a maximum of three sub- units operation. These facts could be justified by the location and solar irradiance in each case. However, even at a winter day of low solar irradiance, the flexibility of the system is proved, since there will be fresh water production from the operation of one sub- unit.

In order to better realize the benefit of the multi- skid RO system, in Table 4.4, the fresh water production of the previously examined systems for each examined day and location is presented and compared to the operation of a large conventional unit instead;

Table 4.4 Daily fresh water production for the different case studies

	Greece			Spain			UAE		
PV capacity (kWp)	10	15	20	10	15	20	10	15	20
Fresh water production (21 st of December) – multi-skid RO (m ³ /day)	3.60	6.08	9.20	5.78	9.54	12.44	7.46	11.99	17.15
Fresh water production (21 st of December) – conventional RO (m ³ /day)	3.36	4.95	6.80	4.93	7.62	10.10	7.22	11.38	15.40
Fresh water production (21 st of July) – multi-skid RO (m ³ /day)	8.71	13.36	19.02	8.46	14.03	19.16	7.92	12.88	17.35
Fresh water production (21 st of July) – conventional RO (m ³ /day)	7.18	13.32	15.21	8.17	12.88	17.05	7.14	11.19	15.15

According to the maximum power input from the PV system, in each case a conventional RO unit of the appropriate capacity has been chosen for the comparison. For example, for the PV system of 10 kWp, for all areas, a conventional unit of 7 kW has been chosen. For the system of 15 kWp for Greece a unit of 10 kW- when for Spain and UAE one of 11 kW, have been chosen and for the system of 20 kWp for Greece and UAE a unit of 14 kW and for Spain one of 15 kW have been chosen. (For the calculation analysis see Appendix III). Based on the maximum fresh water production of the previously tested RO unit and taking into account that the conventional unit stops operating for power load below 50% of its capacity (the RO HPP operation is limited to around 25 Hz, [4.16]), it is observed that the multi- skid RO unit presents a much better operation profile than the conventional unit, since the fresh water production is higher in all cases. For the multi-skid RO system, the fresh water production for each case occurs knowing the SEC and the power production of the experimental results and with linear interpolation (since the SEC is the ratio of the power consumption to the freshwater

production, as mentioned before). For the conventional unit, a similar way for the freshwater production calculation occurs, taking into account that the conventional unit will stop operating when the power input falls below 50% of each capacity and assuming that the SEC at 100% of the capacity is 5 kWh and at 50% of the capacity is 6 kWh.

The flexibility of the multi- skid RO system is confirmed, since in some cases the multi- skid system produces even more than 4 m³/ day fresh water than the conventional unit system. Such flexibility and higher water production is demonstrated especially for the 20 kWp case, as shown in Figure 4.34, where the increase of water production is shown for all cases.

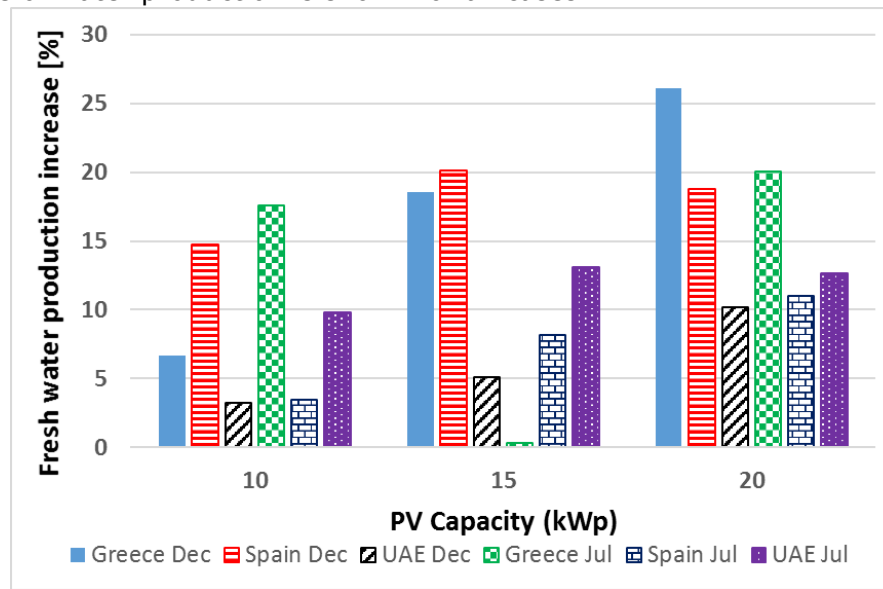


Figure 4.34 Increase of fresh water production with the multi-skid RO unit for different PV capacity

As observed in Figure 4.34, the fresh water production increase, occurring with the use of the multi- skid RO desalination system, reaches as high as 26% for Greece in December for 20 kWp PV capacity. Similar increase is noticed in every system in all areas for summer and winter day and it proves the better operation of the multi- skid system in comparison to the conventional unit system.

4.5 Conclusions

In the present analysis, an RO unit implemented to operate in a wide load range at the laboratory with variable power input, has been investigated. At first, all three sub- units of the system were examined in switchable operation according to the available load and for three different feed water salinities. Focus was given on the performance values, when the membrane pressure, the feed flow range and the motor rotational speed change, due to the variable power input. Each sub- unit operation as well as the whole RO unit investigation has shown that such a system is able to produce fresh water of good quality throughout the whole available power input range, due to the fact that it consists of three identical sub- units. The specific energy consumption has been also kept low, even though that for high salinity it reaches a slightly higher value due to the fact that the sub- units' HP pumps operate at lower rotational speed than the nominal one, so the power needed for the production of a cubic meter of fresh water is higher. Moreover, it has been noticed that for high feed water salinities (>30.000 ppm) the total power demand exceeded

the available power of 10 kW, expected to be fed from the ORC engine that will be electrically connected in the immediate next research steps. This leads to the assumption that the RO unit operated in slightly different test conditions (i.e. feed water quality, temperatures etc.) in comparison to the design that preceded. Membranes' and HP pump's operation for all three sub- units was proven to be efficient and the slight differences that occurred were due to some measurement instrumentation uncertainty. However, these differences laid within acceptable limits throughout the whole operation. The fresh water production slightly exceeded the maximum value of 2.1 m³/h and for lower HP pumps' rotational speed than the nominal one, as well as the power demand exceeded the expected of 10 kW in comparison to the design.

Since the investigation of the RO unit operation took place in different days (therefore different water temperature) and the salinity of each test was different, the previous testing did not allow the examination of the RO operation in different temperature. Therefore, the next step of the current investigation has been the temperature effect on the RO unit operation for a constant feed water salinity of 37500 ppm. Since all three sub- units of the system are identical, only one sub- unit has been examined in switchable operation according to the available load and for three different feed water temperatures. Once again, focus was given on the performance values, when the membrane pressure, the feed flow range and the motor rotational speed changed, due to the variable power input. At low temperature the RO unit operation resulted to be relatively steady. At high temperature of 23 °C the SEC and the fresh water salinity of the RO unit resulted to be slightly poorer, however, the RO unit investigation has shown that such a system is able to produce fresh water of acceptable quality throughout the whole available power input range. The membranes operation, as well as the HP pump operation, were proven to operate efficiently at any water temperature.

Case- studies of the operation of the RO desalination unit consisting of several sub- units, powered by a PV system in different locations for different installed capacity has been also presented. The results of this case study verify the offered flexibility of such a system. Moreover, the comparison on the fresh water production to a conventional RO unit of similar capacity has shown that the multi- skid system operates within a larger load range, producing more fresh water in some cases than the conventional unit system.

The configuration tested, undoubtedly offers flexibility and can secure an acceptable fresh water quality at all operating conditions from very low load up to the maximum one. These results are remarkable in order to further improve such integrated systems with increased performance, while at the same time they show promising improvement for future commercialized systems, powered by renewable energy sources.

References

- 4.1 Dhawan G. K, Webb R. Development of Reverse Osmosis Membranes and Systems. Report on 3-year development program, National Research Council of Canada, IRAP Contract ROPE-184, completed September, 1976.
- 4.2 FILMTEC Membranes, Factors Affecting RO membrane performance, DOW, Published April 1998.
- 4.3 FILMTEC Membranes Basics of RO and NF: Principle of Reverse Omosis and Nanofiltration, DOW, Published April 1998.
- 4.4 Anil K. Pabby, Syed S.H. Rizvi, Ana Maria Sastre Requena, Handbook of Membrane Separations: Chemical, Pharmaceutical, Food, and Biotechnological Applications, Second Edition, April 9, 2015 by CRC Press.
- 4.5 Guidelines for drinking-water quality, fourth edition 2011, World Health Organization, Chapter 10 - Acceptability aspects: Taste, odor and appearance. ISBN 9789241548151, http://www.who.int/water_sanitation_health/publications/2011/dwq_chapters/en/
- 4.6 Thomas Manth, Michael Gabor, Eli Oklejas, Jr. Minimizing RO energy consumption under variable conditions of operation. Desalination, Presented at the European Conference on Desalination and the Environment: Fresh Water for All, Malta, 4–8 May 2003. European Desalination Society, International Water Association.
- 4.7 Valbjørn A. ERD for small SWRO plants. Desalination, 248 (2009), pp. 636–641
- 4.8 Ibrahim S. Al-Mutaz, Mohammad A. Al-Ghunaimi. Performance of Reverse Osmosis Units at High Temperatures. Presented at the IDA World Congress on desalination and water reuse, Bahrain, October 26 – 31, 2001.
- 4.9 Jesus "henry" Avina. Combating the effects of cold water on RO system performance. Water quality products magazine, (2006) <https://www.wqpmag.com/combating-effects-cold-water-ro-system-performance>
- 4.10 F.J. Garcia Latorre, S.O.Perez Baez, A.Gomez Gotor, Energy performance of a reverse osmosis desalination plant operating with variable pressure and flow. Desalination, 366 (2015), 146-153.
- 4.11 Hassane Darhmaoui, Driss Lahjouji. Latitude Based Model for Tilt Angle Optimization for Solar Collectors in the Mediterranean Region. Energy Procedia, 42 (2013), pp. 426–435, Mediterranean Green Energy Forum 2013: Proceedings of an International Conference MGEF-13.
- 4.12 Jafarkazemi Farzad, Saadabadi S. Ali. Optimum tilt angle and orientation of solar surfaces in Abu Dhabi, UAE. Renewable Energy, 56 (2013), pp. 44-49.
- 4.13 NREL System Advisor Model (SAM), <https://sam.nrel.gov/download>
- 4.14 ABB, Motor Guide. Low Voltage motors, February 2014
- 4.15 <https://www.sciencelearn.org.nz/resources/686-ocean-salinity>
- 4.16 Manning D.N., Mehta S.V. Physical Limitations for the Bandwidth Frequency of a Pressure Controlled, Axial-Piston Pump. Journal of Dynamic Systems, Measurement, and Control, 133 (2011), DOI: 10.1115/1.4004056.

CHAPTER 5 – Experimental investigation and evaluation of the ORC engine

5.1 Introduction

As previously discussed in Chapter 2, the two- stage ORC configuration to which the current tests correspond, is based on the use of an integrated system with an organic working fluid and two expanders connected in series. The selected organic fluid is the R245fa. This configuration resulted to be the best solution, concerning not just the efficiency for the whole load range, but also the cost and the simplicity of the monitor system. At a lower load than the 50- 60 % of its nominal, the first expander is completely by- passed with the use of an electro vane, therefore the evaporated organic fluid expansion is realized only in the second expander. In that way, the pressure ratio fluctuation on which the expander efficiency is depended, is kept low throughout the whole load range [5.1, 5.2].

The basic components of the ORC engine that have already been analyzed are the organic fluid pump, the evaporator, the scroll expanders and the condenser. For the simulation of the thermal source that feeds the ORC engine with heat, an electric heater of a capacity of 100 kW_{th} is used. In every inlet and every outlet of each component, special temperature and pressure measurement instrumentation is used and their digital indications are shown on the engine's electric panel. More specifically, a temperature sensor Pt100 and a pressure gauge with a range from - 0.5 – 35 bar are placed at the fluid pump's inlet, at the fluid pump's outlet (which is also the evaporator inlet), at the evaporator's outlet (which is also the inlet of the first expander), at the first expander's outlet (second expander's inlet) and at the second expander's outlet (condenser's inlet).

The shift between one and two- stage operation is realized through an electro vane which permits the complete by- pass of the first expander, for operation at low/ medium thermal load. Two smaller vanes that isolate the first expander's branch for maintenance purposes are manually monitored for more safety during the switch from two to one- stage operation.

In the current tests that took place in the Laboratory of Hydraulic Turbomachines of the National Technical University of Athens, the engine's operation has been tested in different operation conditions and temperatures and the pressure and temperature indications have been recorded in order to be processed and determine the organic fluid condition at each point of the engine. Therefore, the efficiency is calculated and the characteristic curves for each operation point are drawn. Moreover, the most important components of the engine- the scroll expanders- are separately investigated in order to evaluate their operation after their modification from market available scroll compressors.

5.2 Tests at the Laboratory

At the laboratory several tests took place in order to investigate the system operation in many operation points, therefore in many different environmental conditions. The electric heater simulated the operation for days with low thermal load (temperature and solar irradiation), as well as for days with very high thermal load, conditions that consist the main part of the investigation of the current system (the main scope is the operation at a temperature between 120 and 130 °C).

The ORC engine has been tested in low operating temperature at 70°C, at 85°C and at 95°C and for high operating temperature at 110°C, 120°C and 130°C correspondingly. At low temperature the working fluid on the electrical heater's cycle was water, as these conditions are permissible for its use, when for high temperature MEG has replaced water for the reasons explained in Chapter 3 which prove that MEG is the most appropriate choice for the current system operation in high temperature. The selected organic fluid of the ORC engine was R245fa and the ORC engine was tested in single and two-stage operation. Frequency inverters for the organic fluid pump and for each expander contribute in changing operation points with the control of the rotational speed of these components.

During the tests, appropriate measurement instrumentation was used in order to record some properties which were then used to calculate other properties, necessary for the evaluation of the system's operation. More specifically, the temperature and pressure at each inlet and outlet of every component of the ORC engine were measured with the help of temperature and pressure sensors. Therefore, the fluid condition at each point is known. Moreover, the rotational speed of the pump and expanders is set with the use of the inverters and the power production of the expanders is measured with the use of a multimeter. Finally, electric brakes and a heater are used as the produced energy consumption sink. In Table 5.1 the measured properties and their symbols are presented:

Table 5.1 Measured properties

Measured Property	Symbol	Unit
Electric heater inlet temperature	$T_{hot_{in}}$	°C
Electric heater outlet temperature	$T_{hot_{out}}$	°C
Pump's frequency	f_{ORC_p}	Hz
Pump's inlet temperature	$T_{ORC_{P_{in}}}$	°C
Pump's outlet temperature	$T_{ORC_{P_{out}}}$	°C
Pump's inlet pressure	$p_{ORC_{P_{in}}}$	bar
Pump's outlet pressure	$p_{ORC_{P_{out}}}$	bar
Evaporator's inlet temperature	$T_{ORC_{EV_{in}}}$	°C
Evaporator's outlet temperature	$T_{ORC_{EV_{out}}}$	°C
Evaporator's inlet pressure	$p_{ORC_{EV_{in}}}$	bar
Evaporator's outlet pressure	$p_{ORC_{EV_{out}}}$	bar
First expander's frequency	$f_{ORC_{e1}}$	Hz
First expander's inlet temperature	$T_{ORC_{e1_{in}}}$	°C

First expander's outlet temperature	$T_{ORCe1out}$	$^{\circ}C$
First expander's inlet pressure	$p_{ORCe1in}$	bar
First expander's outlet pressure	$p_{ORCe1out}$	bar
First expander's power production	$P_{ORCe1meas}$	kW
Second expander's frequency	f_{ORCe2}	Hz
Second expander's inlet temperature	$T_{ORCe2in}$	$^{\circ}C$
Second expander's outlet temperature	$T_{ORCe2out}$	$^{\circ}C$
Second expander's inlet pressure	$p_{ORCe2in}$	bar
Second expander's outlet pressure	$p_{ORCe2out}$	bar
Second expander's power production	$P_{ORCe2meas}$	kW
Condenser's inlet temperature	$T_{ORCCONin}$	$^{\circ}C$
Condenser's outlet temperature	$T_{ORCCONout}$	$^{\circ}C$
Condenser's inlet pressure	$p_{ORCCONin}$	bar
Condenser's outlet pressure	$p_{ORCCONout}$	bar

Some other properties concerning the hot water pump and circuit as well as the condenser water circuit and pump are also known by default;

The hot water volume flow rate is determined by the hot water pump capacity and is equal to $v_{hotW} = 7 \left[\frac{m^3}{h} \right]$. The current and voltage of the hot water pump are also known: $I_{hot} = 2.55 [A]$, and $V_{hot} = 380 [V]$. The power consumption of the hot water pump is $P_{hotp} = 1.10 [kW]$. The same properties are known for the condenser water circuit: $I_{cond} = 5.90 [A]$, $V_{cond} = 400 [V]$, $P_{condp} = 3 [kW]$. The mass flow rate of the condenser water circuit is $m_{condW} = 3.33 \left[\frac{kg}{s} \right]$, and the inlet and outlet temperature of the water is $T_{condin} = 16.5^{\circ}C$ and $T_{condout} = 20^{\circ}C$ correspondingly. Finally, the water volume flow rate is $V_{condW} = 12 \left[\frac{m^3}{h} \right]$.

With the use of the recorded properties that have been presented in Table 7.1, other properties can be calculated in order to determine the system's operation. The calculated properties are presented in Table 5.2 below:

Table 5.2 Calculated properties

Calculated property	Equation	Unit	Symbols
Pump's rotational speed	$RPM_{ORCP} = \frac{f_{ORCP}}{50} * 960$	RPM	f_{ORCP} =pump frequency [Hz]
Pump volume flow rate	$v_{ORCP} = 0.0205 * RPM_{ORCP}$	l/min	RPM_{ORCP} =pump's rotational speed [RPM]
Pump mass flow rate	$m_{ORCP} = \frac{v_{ORCP}}{60} * \frac{\rho_{R245fa}}{1000}$	kg/s	v_{ORCP} =pump volume flow rate, ρ_{R245fa} =R245fa density at the current temperature and pressure, liquid phase
R245fa Pump inlet enthalpy	h_{ORCPin}	kJ/kg	Derives from the R245fa h-T diagram for the corresponding temperature T_{ORCPin} and pressure p_{ORCPin} each time
R245fa Pump outlet enthalpy	$h_{ORCPout}$	kJ/kg	Derives from the R245fa h-T diagram for the corresponding temperature $T_{ORCPout}$ and pressure $p_{ORCPout}$ each time
R245fa Pump outlet entropy	$S_{ORCPout}$	kJ/kg/K	Derives from the R245fa T-s diagram for the corresponding temperature $T_{ORCPout}$ and pressure $p_{ORCPout}$ each time
R245fa Pump outlet isentropic enthalpy	$h_{ORCPoutis}$	kJ/kg	Derives from the R245fa h-T diagram for the corresponding outlet entropy $S_{ORCPout}$ and pressure $p_{ORCPout}$ each time, for saturated vapor condition
Pump isentropic efficiency	$n_{OPCPis} = \frac{h_{ORCPoutis} - h_{ORCPin}}{h_{ORCPout} - h_{ORCPin}} * 100$	%	$h_{ORCPoutis}$, h_{ORCPin} , $h_{ORCPout}$ as explained before
Pump power consumption	$P_{ORCP} = (h_{ORCPout} - h_{ORCPin}) * m_{ORCP}$	kW	$h_{ORCPout}$, h_{ORCPin} , m_{ORCP} as explained before
R245fa Evaporator inlet enthalpy	$h_{ORCEVin}$	kJ/kg	Derives from the R245fa h-T diagram for the corresponding temperature $T_{ORCEVin}$ and pressure $p_{ORCEVin}$ each time
R245fa Evaporator outlet enthalpy	$h_{ORCEVout}$	kJ/kg	Derives from the R245fa h-T diagram for the corresponding temperature $T_{ORCEVout}$ and pressure $p_{ORCEVout}$ each time

CHAPTER 5 – Experimental investigation and evaluation of the ORC engine

Evaporator thermal load	$Q_{ORCEV} = (h_{ORCEVout} - h_{ORCEVin}) * m_{ORCP}$	<i>kW_{th}</i>	$h_{ORCEVout}$, h_{ORCEV} , m_{ORCP} as explained before
First expander's rotational speed	$RPM_{ORCe1} = \frac{f_{ORCe1}}{50} * 2900$	<i>RPM</i>	f_{ORCe1} =first expander's frequency [Hz]
First expander pressure ratio	$Pressure\ ratio = \frac{P_{ORCe1in}}{P_{ORCe1out}}$	-	$P_{ORCe1in}$, $P_{ORCe1out}$ as explained before
First expander inlet enthalpy	$h_{ORCe1in}$	<i>kJ/kg</i>	Derives from the R245fa h-T diagram for the corresponding temperature $T_{ORCe1in}$ and pressure $p_{ORCe1in}$ each time
First expander outlet enthalpy	$h_{ORCe1out}$	<i>kJ/kg</i>	Derives from the R245fa h-T diagram for the corresponding temperature $T_{ORCe1out}$ and pressure $p_{ORCe1out}$ each time
First expander outlet entropy	$S_{ORCe1out}$	<i>kJ/kg/K</i>	Derives from the R245fa T-s diagram for the corresponding temperature $T_{ORCe1out}$ and pressure $p_{ORCe1out}$ each time
First expander outlet isentropic enthalpy	$h_{ORCe1outis}$	<i>kJ/kg</i>	Derives from the R245fa h-T diagram for the corresponding outlet entropy $S_{ORCe1out}$ and pressure $p_{ORCe1out}$ each time, for saturated vapor condition
First expander isentropic efficiency	$n_{OPCe1is} = \frac{h_{ORCe1out} - h_{ORCe1in}}{h_{ORCe1outis} - h_{ORCe1in}} * 100$	%	$h_{ORCe1outis}$, $h_{ORCe1in}$, $h_{ORCe1out}$ as explained before
First expander actual efficiency	$n_{OPCe1} = \frac{P_{ORCe1meas}}{m_{ORCP} * (h_{ORCe1in} - h_{ORCe1out})} * 100$	%	$P_{ORCe1meas}$, m_{ORCP} , $h_{ORCe1outis}$, $h_{ORCe1in}$ as explained before
First expander theoretical power consumption	$P_{ORCe1} = (h_{ORCe1in} - h_{ORCe1out}) * m_{ORCP}$	<i>kW</i>	$h_{ORCe1out}$, $h_{ORCe1in}$, m_{ORCP} as explained before
Second expander's rotational speed	$RPM_{ORCe2} = \frac{f_{ORCe2}}{50} * 2900$	<i>RPM</i>	f_{ORCe2} =first expander's frequency [Hz]

CHAPTER 5 – Experimental investigation and evaluation of the ORC engine

Second expander pressure ratio	$Pressure\ ratio = \frac{P_{ORCe2in}}{P_{ORCe2out}}$	-	$P_{ORCe2in}, P_{ORCe2out}$ as explained before
Second expander inlet enthalpy	$h_{ORCe2in}$	kJ/kg	Derives from the R245fa h-T diagram for the corresponding temperature $T_{ORCe2in}$ and pressure $p_{ORCe2in}$ each time
Second expander outlet enthalpy	$h_{ORCe2out}$	kJ/kg	Derives from the R245fa h-T diagram for the corresponding temperature $T_{ORCe2out}$ and pressure $p_{ORCe2out}$ each time
Second expander outlet entropy	$S_{ORCe2out}$	$kJ/kg/K$	Derives from the R245fa T-s diagram for the corresponding temperature $T_{ORCe2out}$ and pressure $p_{ORCe2out}$ each time
Second expander outlet isentropic enthalpy	$h_{ORCe2outis}$	kJ/kg	Derives from the R245fa h-T diagram for the corresponding outlet entropy $S_{ORCe2out}$ and pressure $p_{ORCe2out}$ each time, for saturated vapor condition
Second expander isentropic efficiency	$n_{OPCe2is} = \frac{h_{ORCe2out} - h_{ORCe2in}}{h_{ORCe2outis} - h_{ORCe2in}} * 100$	%	$h_{ORCe2outis}, h_{ORCe2in}, h_{ORCe2out}$ as explained before
Second expander actual efficiency	$n_{OPCe2} = \frac{P_{ORCe2meas}}{m_{ORCP} * (h_{ORCe2in} - h_{ORCe2out})} * 100$	%	$P_{ORCe2meas}, m_{ORCP}, h_{ORCe2outis}, h_{ORCe2in}$ as explained before
Second expander theoretical power consumption	$P_{ORCe2} = (h_{ORCe2in} - h_{ORCe2out}) * m_{ORCP}$	kW	$h_{ORCe2out}, h_{ORCe2in}, m_{ORCP}$ as explained before
R245fa Condenser inlet enthalpy	$h_{ORCCONin}$	kJ/kg	Derives from the R245fa h-T diagram for the corresponding temperature $T_{ORCCONin}$ and pressure $p_{ORCCONin}$ each time
R245fa Condenser outlet enthalpy	$h_{ORCCONout}$	kJ/kg	Derives from the R245fa h-T diagram for the corresponding temperature $T_{ORCCONout}$ and pressure $p_{ORCCONout}$ each time
Condenser thermal load	$Q_{ORCCON} = (h_{ORCCONout} - h_{ORCCONin}) * m_{ORCP}$	kW_{th}	$h_{ORCCONout}, h_{ORCCONin}, m_{ORCP}$ as explained before

Total theoretical expanders' power production	$P_{ORC_{e_{id}}} = P_{ORC_{e1}} + P_{ORC_{e2}}$	<i>kW</i>	$P_{ORC_{e1}}, P_{ORC_{e2}}$ as explained before
Total expanders' power production	$P_{ORC_e} = P_{ORC_{e1meas}} + P_{ORC_{e2meas}}$	<i>kW</i>	$P_{ORC_{e1meas}}, P_{ORC_{e2meas}}$ as explained before
Expander's efficiency	$n_{ORC_e} = 100 - \frac{P_{ORC_{e_{id}}} - P_{ORC_e}}{P_{ORC_{e_{id}}}} * 100$	%	$P_{ORC_{e_{id}}}, P_{ORC_e}$ as explained before
ORC engine's ideal thermal efficiency	$n_{ORC_{th_{id}}} = \frac{P_{ORC_{e_{id}}} - P_{ORC_P}}{Q_{ORC_{EV}}} * 100$	%	$P_{ORC_{e_{id}}}, P_{ORC_P}, Q_{ORC_{EV}}$ as explained before
ORC engine's thermal efficiency	$n_{ORC_{th}} = \frac{P_{ORC_e} - P_{ORC_P}}{Q_{ORC_{EV}}} * 100$	%	$P_{ORC_e}, P_{ORC_P}, Q_{ORC_{EV}}$ as explained before

5.2.1 ORC engine evaluation for several operating temperatures

In the current section, the results that derived from the experimental investigation of the ORC engine towards best operation are presented. The best operation points are defined by the combination of the pump and expander(s) rotational speeds (one or two expanders for single and two-stage operation) that provides the best values of each variable of interest (i.e. power production, thermal efficiency). In this way, a thorough comprehension overview of the ORC engine operation can be acquired.

5.2.1.1 ORC engine evaluation for operation at 70°C with water on the heat source cycle- single & two- stage operation

The ORC unit was first tested for single stage operation at a water temperature of 70°C. The ORC engine operated only for single stage operation, since at 70 °C the power input is significantly lower than the design point of the engine, where the pressure ratio is high. However, the efficiency of the single stage operation is evaluated below. The working fluid of the heat source cycle is water.

In Figure 5.1, the maximum power production as a function of the heat input at 70 °C for variable ORC pump speed is presented.

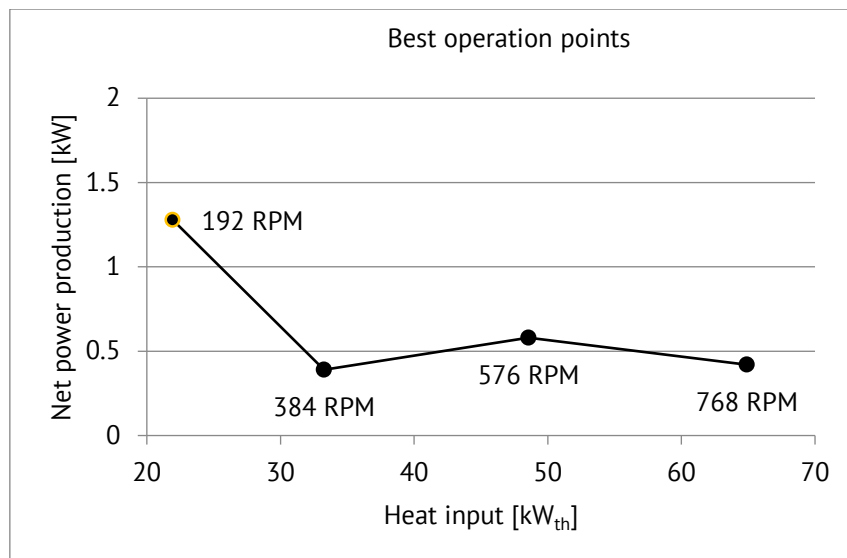


Figure 5.1 Net power production as a function of the heat input, single-stage operation, 70°C.

As explained above, the “best operational points” are determined by the pairs of expander's and pump's rotational speed (RPM points on diagram) that result to maximum power production for each heat input.

From 384 to 768 RPM, as the pump rotation speed increases, the organic fluid mass that can absorb the transferred heat increases and as a result the power production increases accordingly. However, in high pump rotation speed, the expander is not capable of expanding the fluid so efficiently, and the power production starts to decrease. The best operation was noticed for low pump rotational speed for power input of around 22 kW_{th} . For pump rotational speed at 384 RPM the engine operated only at one operational point with expander rotational speed at 580 RPM and produced power of 0.40 kW. As pump's rotational speed increases, the pump power consumption increases and the power production of the expander decreases, so the net power production decreases. In addition, the expander's inverter sets a maximum current value over which the expander does not operate efficiently expanding the fluid correctly and the current is cut. The best operational point was noticed for pump rotational speed at 192 RPM and expander rotational speed at 1740 RPM, when the thermal power input was ~22 kW_{th} and the power produced from the expander was around 1.30 kW. In higher pump rotational speed and power input the engine operates producing about 0.40 to 0.50 kW for a wide power input. It should be high lightened though, that the operating temperature (70 °C) is low in comparison to the design temperature of the engine (120°~ 130°C), therefore the expander operates at a significantly lower point than the designed one.

The total thermal efficiency for the best operation points as a function to the thermal power input is presented in Figure 5.2:

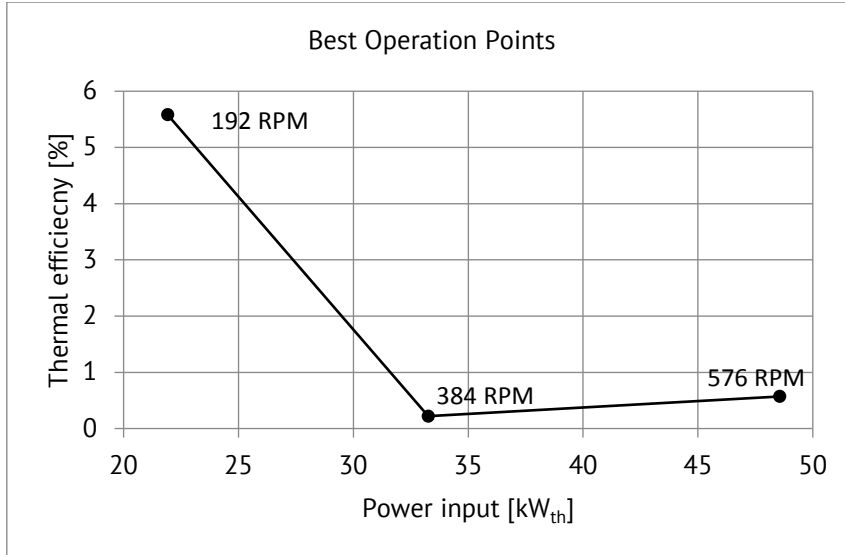


Figure 5.2 Total efficiency for the best operation points for each pump rotational speed, as a function of the total power input, 70°C.

In Figure 5.2 the efficiency at 192 RPM pump rotational speed is around 5.6%, while for lower pump rotational speed the efficiency decreases to 0.5%. However, for the one operational point at 23 kW_{th} power input, the operation is considered efficient, since the thermal efficiency reaches more than half of the design expected engine efficiency. For other pump rotational speeds, the efficiency resulted low or negative, since the power consumed by the pump is more than the power produced by the expander (negative net power production).

The thermal power production increases almost linearly with the increase of the pump rotational speed, as observed in Figure 5.3 below:

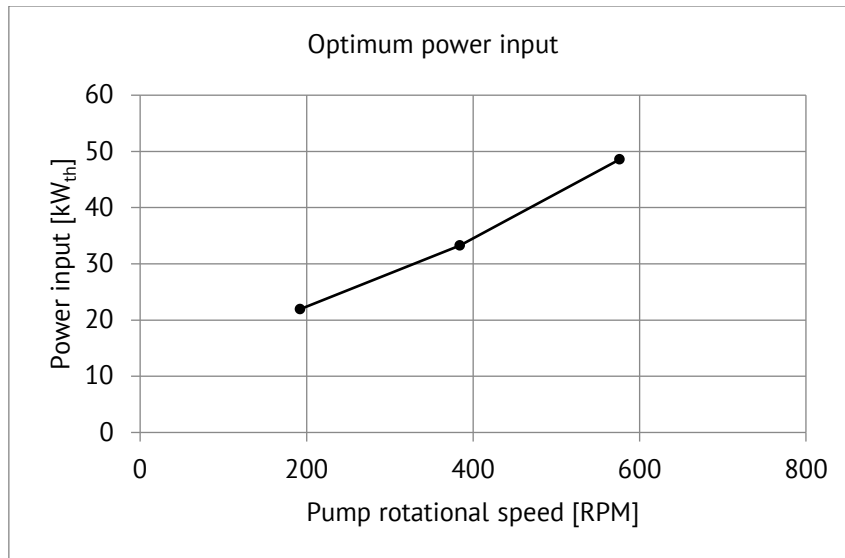


Figure 5.3 Relation of the best power input points with the pump rotational speed at 70°C

The maximum thermal power input is noticed at around 50 kW_{th} for a pump rotational speed at 576 RPM. For higher pump rotational speed, the engine does not produce net power, therefore higher operation points are not examined. For the same reason the two- stage operation at 70 °C is not presented in the current

test. However, even at low load operation where the system operates only at single stage, it presents sufficient efficiency based on the maximum design value.

5.2.1.2 ORC engine evaluation for operation at 85°C with water on the heat source cycle- single & two- stage operation

For the next experiment, the temperature of the heat source rises to 85°C, while the working fluid on the heat source cycle side remains water. The engine is tested for single and two- stage operation and the same properties are investigated in both operational conditions. At first, the **single stage operation** is presented.

In Figure 5.4, the total power production of the engine is presented. In this chart, once again, the best operational points for each pump rotational speed are presented throughout the whole power input range.

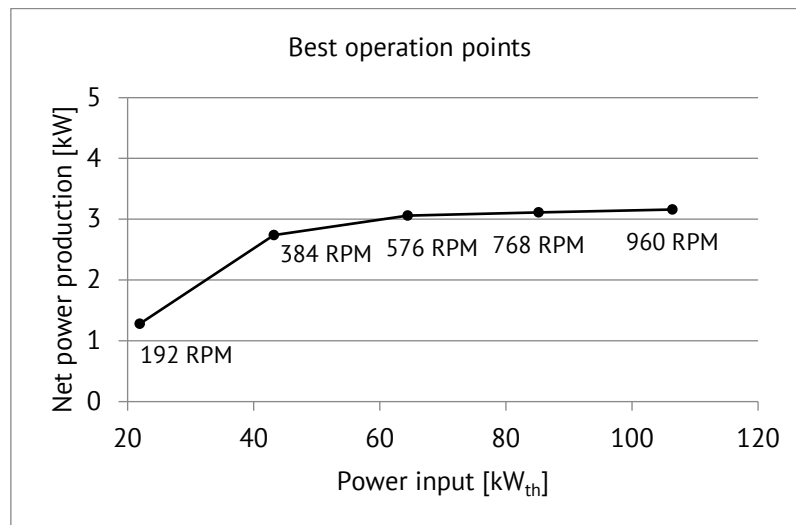


Figure 5.4 Total power production of the expander overview for the best operation points of the ORC engine, single- stage operation at 85°C

In the current experiment and for single- stage operation the thermal power input varies between wider limits starting from around 20 kW_{th} and reaching up to 107 kW_{th}. The maximum power production as clearly presented in Figure 5.4 is noticed at the high pump's rotational speed of 960 RPM and reached the value of 3.16 kW which is a sufficient production for such a low operating temperature – compared to the design one- and for single stage operation. As presented in Figure 5.4, the power production increases with the increase of the thermal power input and the pump's rotational speed increase. As the pump's rotational speed increases the thermal power input increases, since the mass flow rate of the fluid, available to transfer the thermal energy, increases. The engine's production depends on the enthalpy difference at the expander's inlet and outlet and also on the fluid mass flow rate. As the mass flow rate increases with the increase in the pump's rotational speed, the engine's power production increases as well.

The total thermal efficiency for the optimum operation points as a function to the thermal power input is presented in Figure 5.5:

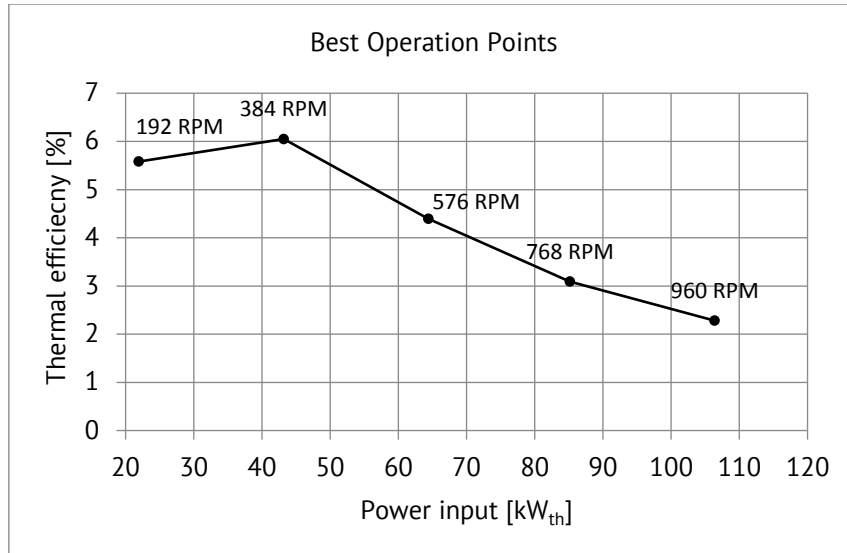


Figure 5.5 Total efficiency for the best operation points for each pump rotational speed, as a function of the total power input, single- stage operation at 85°C

As noticed in Figure 5.5, the best thermal efficiency is observed at 384 RPM of pump rotational speed and around 43 kW_{th} power input. The maximum thermal efficiency is about 6% which is sufficient for the current operational conditions, especially in comparison to the design conditions. For higher pump's rotational speed, the thermal efficiency decreases, since the total power production remains around the same value (see Figure 5.4) but the thermal power input increases (with the increase of the mass flow rate due to the increase of the pump's rotational speed). Therefore, the denominator of the efficiency ratio increases and the efficiency decreases.

Finally, concerning the single- stage operation, in Figure 5.6 the total thermal power is presented in comparison to the total thermal power of the two- stage operation at 85°C:

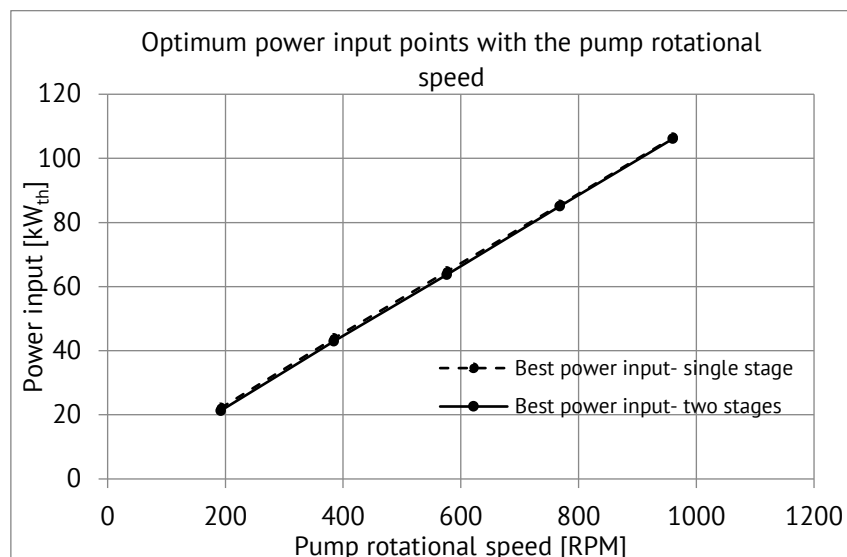


Figure 5.6 Relation of the best power input points with the pump rotational speed, single and two- stage operation at 85°C

In Figure 5.6 the single stage operation curve almost coincides with the curve of the two- stage operation, which was expected, since the pump

operation is the same for single and two- stage operation of the ORC engine. The thermal power input varies from 20 up to 107 kW_{th} and the maximum value is presented for pump operation at 960 RPM. The correlation of the power input and the pump rotational speed is once again proportional to the pump rotational speed, since it depends on the mass flow rate which changes in proportion to the pump rotational speed change.

After the single- stage operation experimental investigation, the system operated at two- stage mode by opening the electro vane that isolates the first expander. The **two- stage operation evaluation** is presented below; however, it should be noted that the operating temperature of 85 °C is still low, especially for the two- stage operation, in comparison to the design temperature of 120-130°C.

In Figure 5.7, the total power production for two- stage operation at the best operation points for each pump rotational speed is presented as a function of the thermal power input:

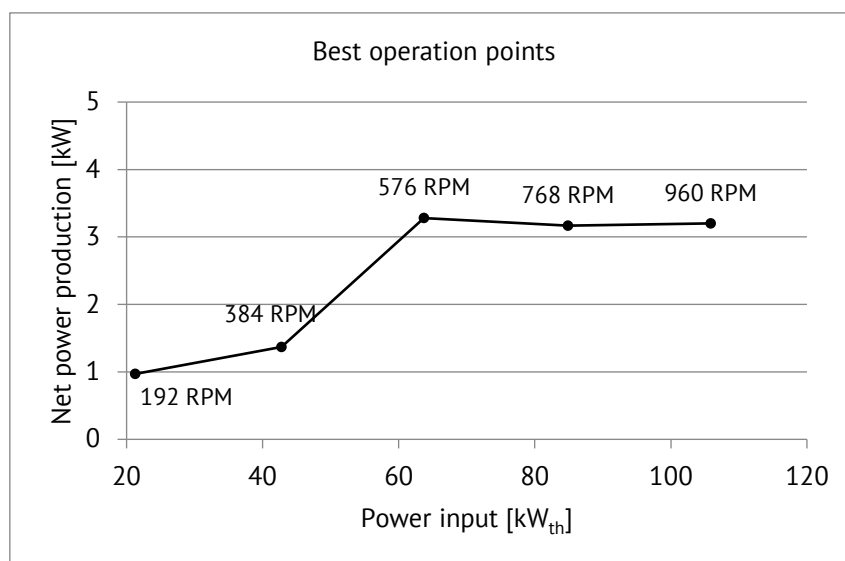


Figure 5.7 Total power production of the expander overview for the best operation points of the ORC engine, two- stage operation at 85°C

In two- stage operation, the total power production of the two expanders reaches a slightly higher value of 3.28 kW, for power input 63.6 kW_{th} and rotational speed 576 RPM. The further pump rotational speed increase provokes an increase of the pump power consumption and this could cause a slight decrease at the net power production of the engine. The total power production of the two- stage system is comparable to the single- stage operation; however, the temperature operation is still low. In Figure 5.8 the total thermal efficiency of the two- stage system is presented:

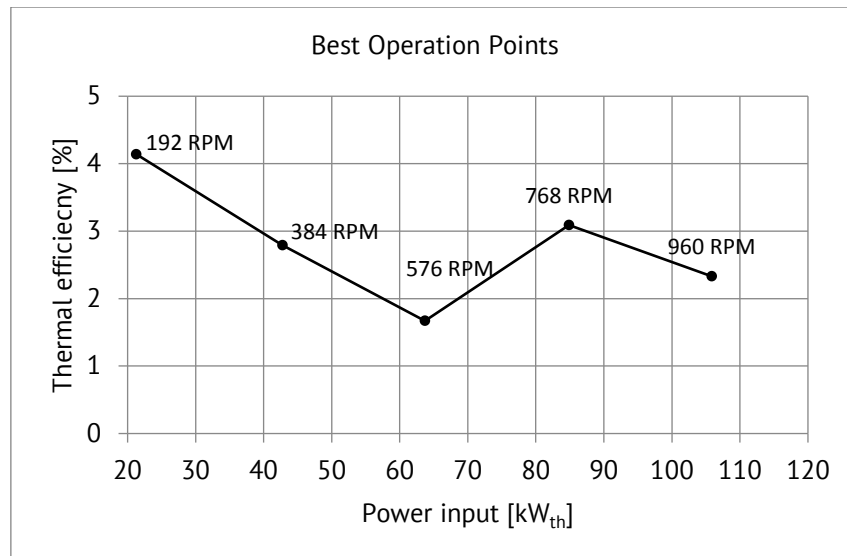


Figure 5.8 Total efficiency for the best operation points for each pump rotational speed, as a function of the total power input, two- stage operation at 85°C

The maximum thermal efficiency is noticed in Figure 5.8 for pump rotational speed at 192 RPM and thermal power input at 22 kW_{th}. The maximum thermal efficiency is around 4.2 % which is low compared to the expected from the design, however reasonable, considering the low operating temperature of 85°C. In comparison to the single- stage operation, the efficiency of the two- stage operation is slightly lower since the difference of the expanders' power production to the pump power consumption has not reached high values. Even though it could be mentioned that the single- stage operation at 85 °C was slightly more efficient than the two- stage system, however the thermal efficiency of the two- stage system reaches almost the half of the expected from the design at full operation. Moreover, in Figure 5.8, the total thermal efficiency presents a decrease for 576 RPM pump rotational speed because the power produced by the expanders remains almost the same as in 384 RPM but the power input is higher, therefore the efficiency decreases. For higher pump rotational speed, the power production from the expanders is significantly higher and the efficiency increases.

A straight comparison of the single and two- stage operation is presented in Figures 5.9 and 5.10, concerning the total power production and efficiency accordingly.

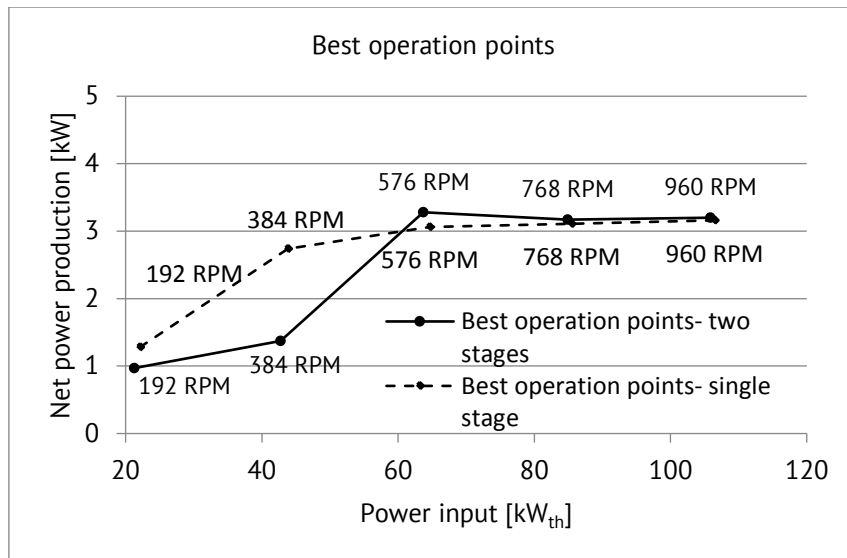


Figure 5.9 Total power production of the expander overview for the best operation points of the ORC engine, single and two- stage operation comparison at 85°C

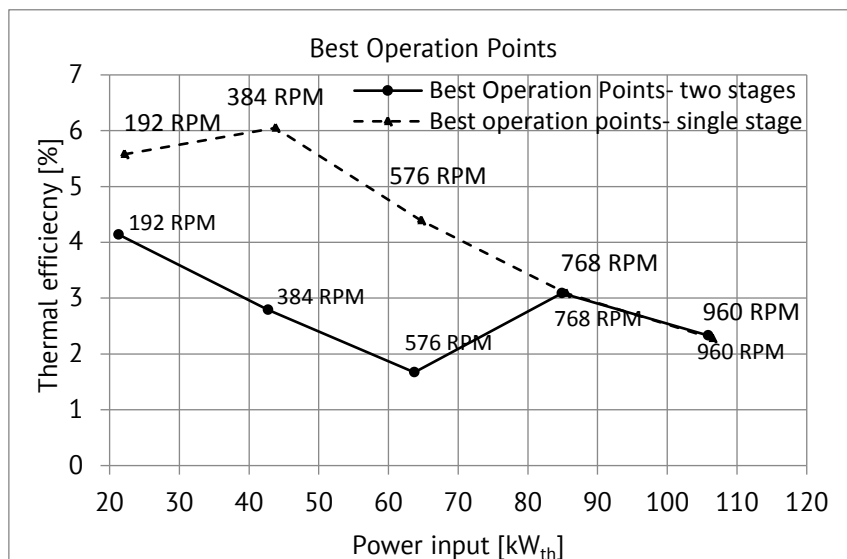


Figure 5.10 Total efficiency for the best operation points for each pump rotational speed, as a function of the total power input, single and two- stage operation comparison at 85°C

Additionally, to previous comments on the single and two- stage operation comparison, the interesting fact that derives from the Figures 5.9 and 5.10 is that for high pump rotational speed, the engine performance is identical (the curves coincide).

The evaluation of the ORC engine for single and two- stage operation at 85°C has shown that the engine operates efficiently for such a low temperature (compared to the design one), however without important differences which would prove the superiority of the two- stage configuration. This was expected, since the engine has been designed for operation at a much higher temperature of 120-130°C.

5.2.1.3 ORC engine evaluation for operation at 95°C with water on the heat source cycle- single & two- stage operation

The next experimental step is the increase of the operating temperature to 95°C, while the working fluid on the heat source cycle side remains water. The engine is tested once again for single and two- stage operation and the same properties are investigated in both operational conditions. The **single stage operation** is presented first. In Figure 5.11, the total power production of the ORC engine is presented. In this chart, the best operational points for each pump rotational speed are presented throughout the whole power input range.

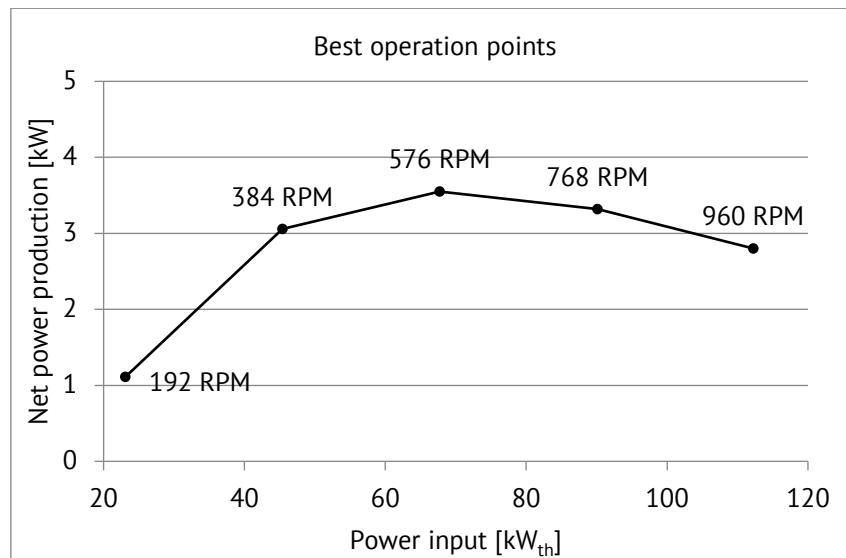


Figure 5.11 Total power production of the expander overview for the best operation points of the ORC engine, single- stage operation at 95°C

The maximum power production of 3.55 kW is noticed at 576 RPM pump's rotational speed and for around 67 kW_{th} thermal power input. Apart from the operation at 192 RPM of pump's rotational speed where the power production is low, in all other operation points the power production varies around 3 kW which is sufficient for one stage operation and at 95 °C, a temperature lower than the design one, with water on the heat source cycle.

Concerning the efficiency, throughout the whole thermal load, in Figure 5.12 a general preview of the best operation points for each pump's rotational speed is presented:

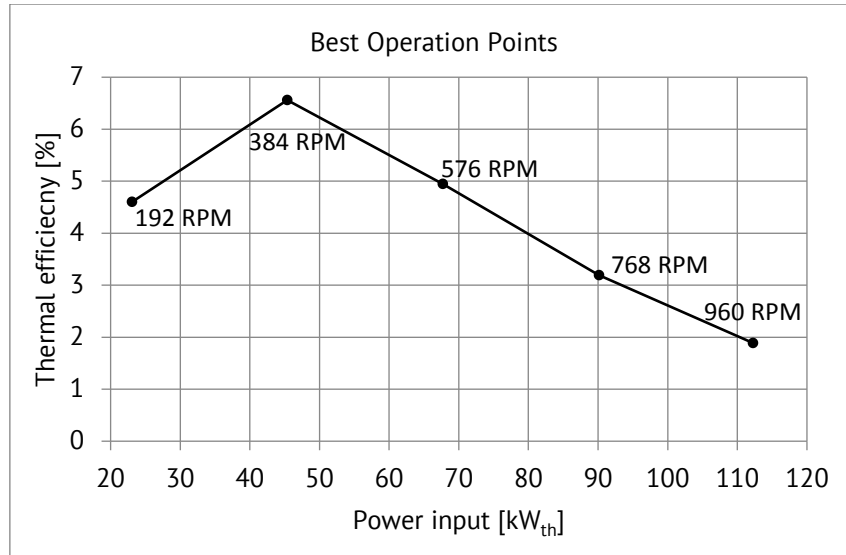


Figure 5.12 Total efficiency for the best operation points for each pump rotational speed, as a function of the total power input, single- stage operation at 95°C

At single- stage operation at 95 °C the best efficiency is observed at 6.6% for 384 RPM pump's rotational speed. The thermal power input at that point is around 45 kW_{th}. However, in most load range the efficiency is around 3 to 5 % which is good considering the operational conditions. The thermal power input in relation to the pump's rotational speed for single and two- stage operation is presented in Figure 5.13:

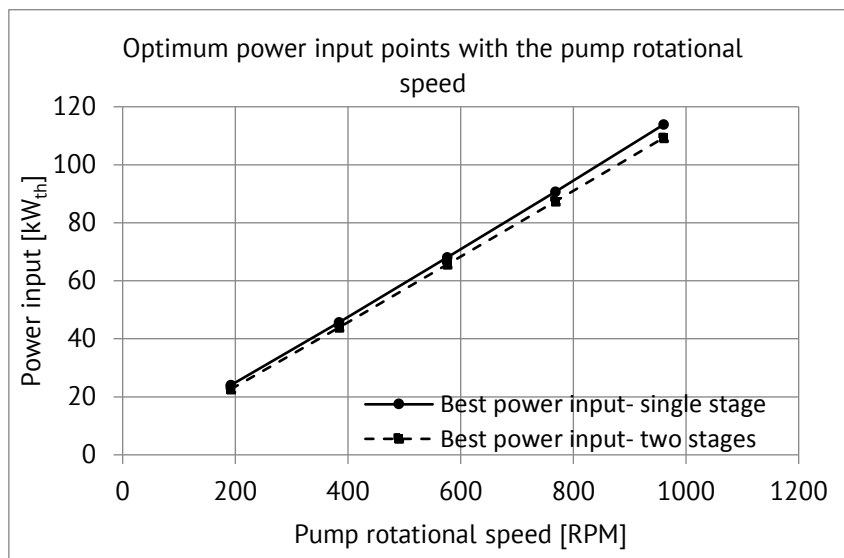


Figure 5.13 Relation of the optimum power input points with the pump rotational speed, single and two- stage operation at 95°C

The two curves in Figure 5.13 are very close, however the single stage operation reaches a slightly higher maximum thermal power input for the same pump's rotational speed, reaching 114 kW_{th} than the maximum of 109 kW_{th} for the two stages operation. The thermal power input depends on the enthalpy difference at the evaporator's inlet and outlet and the mass flow rate from the pump. For the same pump rotational speed, the mass flow rate is the same, thus the slight divergence between the two curves is due to the different pressure at the

evaporator's outlet for the two- stage system which influences the outlet enthalpy at the evaporator and consequently the enthalpy difference and thermal input of the two- stage system.

The total power production for the best operation points of the ORC engine **at two- stage operation at 95 °C** is presented in Figure 5.14:

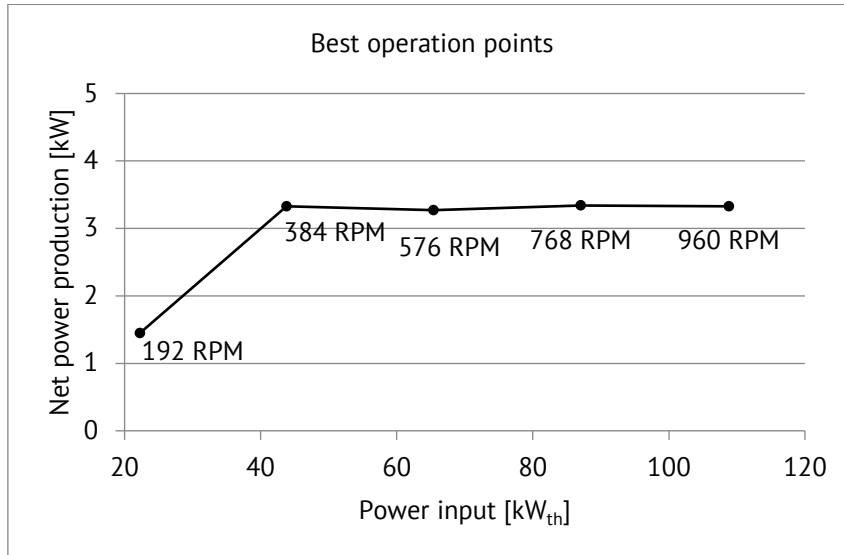


Figure 5.14 Total power production of the expander overview for the best operation points of the ORC engine, two- stage operation at 95°C

As observed in Figure 5.14, the maximum power production for the two- stage operation is noticed at 3.3 kW for medium and high pump's rotational speed. Although the maximum power production for the two- stage system is slightly lower than that of the single- stage system (of the class of 0.2 kW), however the power production remains high and around the maximum value of 3.3 kW for most of the pump's operation points, which is sufficient for the current operational conditions.

A general preview of the efficiency throughout the whole thermal load best operation points for each pump's rotational speed is presented in Figure 5.15:

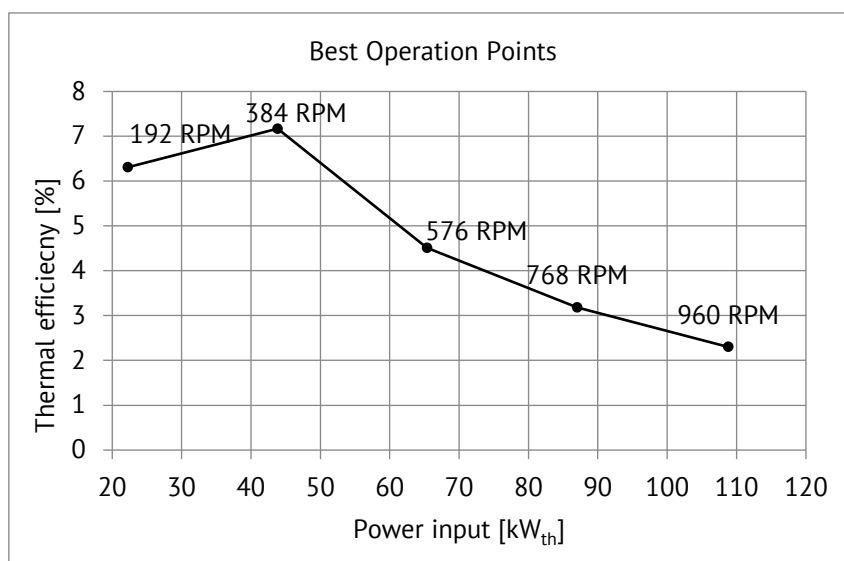


Figure 5.15 Total efficiency for the best operation points for each pump rotational speed, as a function of the total power input, two- stage operation at 95°C

The maximum thermal efficiency for the two- stage system is observed at 7.2 % for 44 kW_{th} power thermal input and 384 RPM pump's rotational speed. As the pump's rotational speed increases, the pump's consumption increases as well, reducing the net power production (power produced by the expanders minus the pump's consumption). The maximum expected thermal efficiency for operation at 120~ 130 °C of the two- stage system, according to the design, is around 10 %, therefore the maximum of 7.2 % for operation at 95 °C is evaluated as sufficient operation of the ORC engine.

A straight comparison of the single and two- stage operation is presented in Figures 5.16 and 5.17, concerning the total power production and efficiency accordingly.

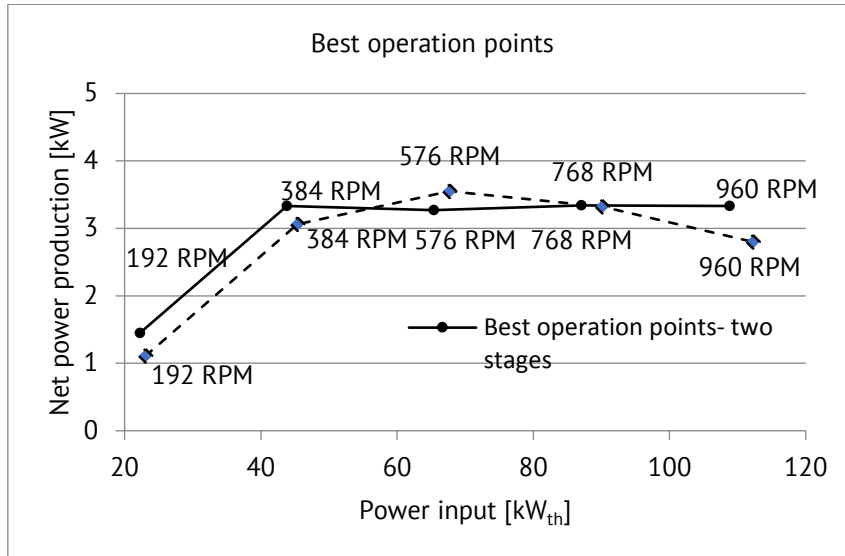


Figure 5.16 Total power production of the expander overview for the best operation points of the ORC engine, single and two- stage operation comparison at 95°C

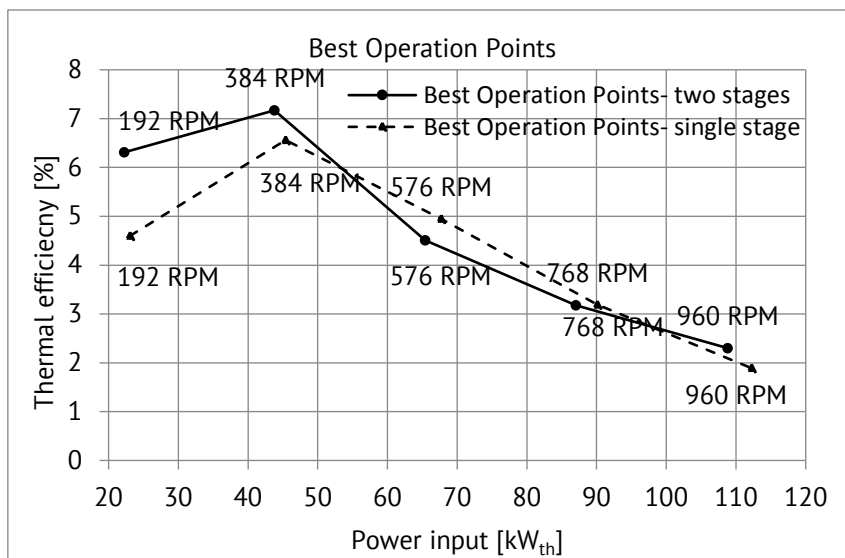


Figure 5.17 Total efficiency for the best operation points for each pump rotational speed, as a function of the total power input, single and two- stage operation comparison at 95°C

The next experimental step is the replacement of the heat cycle working fluid. In order to proceed to higher operating temperatures, as analyzed in Chapter 2, the water must be replaced with the mono- ethylene glycol (MEG) which is safer and more efficient. Once the heat cycle working fluid is replaced, the ORC engine is tested for 95 °C in order to compare the operation at the same temperature with different working fluid on the heat cycle. However, as Figure 5.18 presents, the replacement with MEG on the heat cycle leads to almost the same power input to the ORC engine, therefore the analysis of the experimental results for this test are not presented, since they almost coincide to the operation points with water at 95 °C.

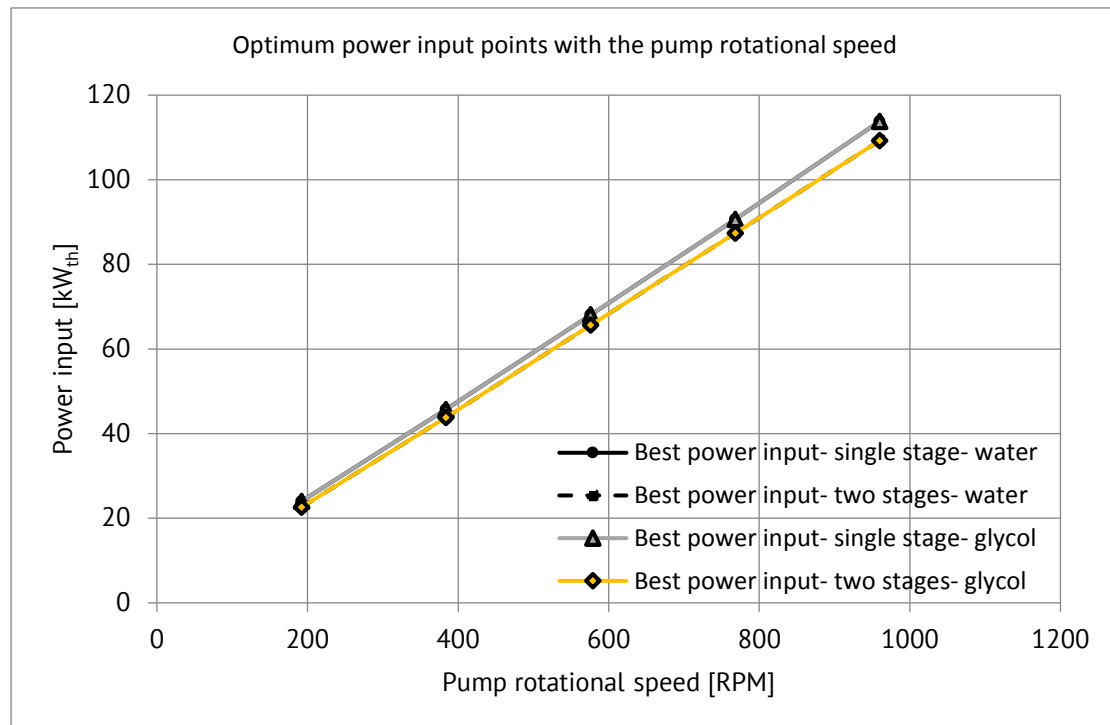


Figure 5.18 Relation of the optimum power input points with the pump rotational speed, single and two- stage operation at 95°C, for water and MEG on the heat cycle

5.2.1.4 ORC engine evaluation for operation at 110°C with glycol on the heat source cycle- single & two- stage operation

The operating temperature was next increased to 110°C, while the working fluid on the heat source cycle side shifted to glycol (MEG). The engine is tested for single and two- stage operation and the same properties are investigated in both operational conditions. The **single stage operation** is presented. In Figure 5.19, the total power production of the ORC engine for the best operational points for each pump rotational speed throughout the whole power input range is presented.

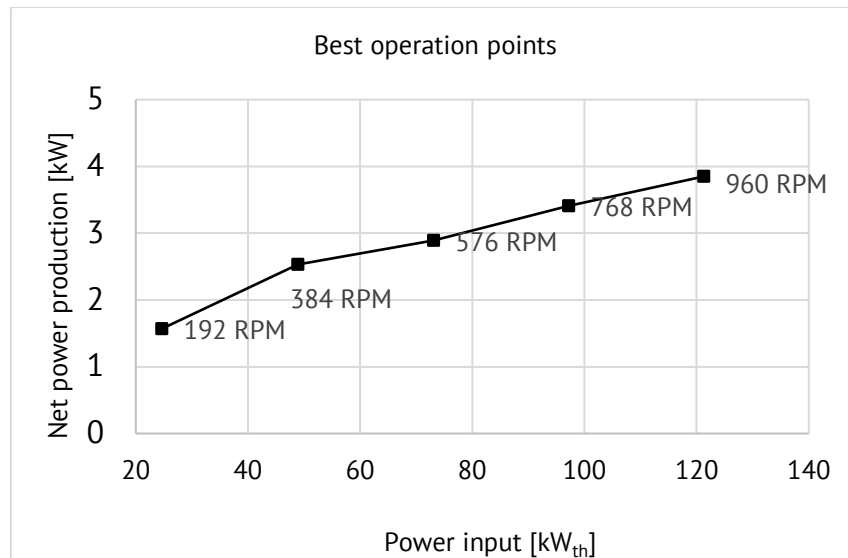


Figure 5.19 Total power production of the expander overview for the best operation points of the ORC engine, single- stage operation at 110°C

As observed in Figure 5.19, the maximum power production of 3.85 kW is noticed at 960 RPM pump's rotational speed and for around 121 kW_{th} thermal power input. The total power production increases smoothly with the rotational speed increase and almost linearly with the power input. The operating temperature increase among with the glycol (MEG) replacement on the heat source cycle led to operation conditions closer to the design conditions, therefore even at single stage operation, the ORC engine presents a sufficient operation.

Concerning the efficiency, throughout the whole thermal load, in Figure 5.20 a general preview of the best operation points for each pump's rotational speed for single stage operation is presented:

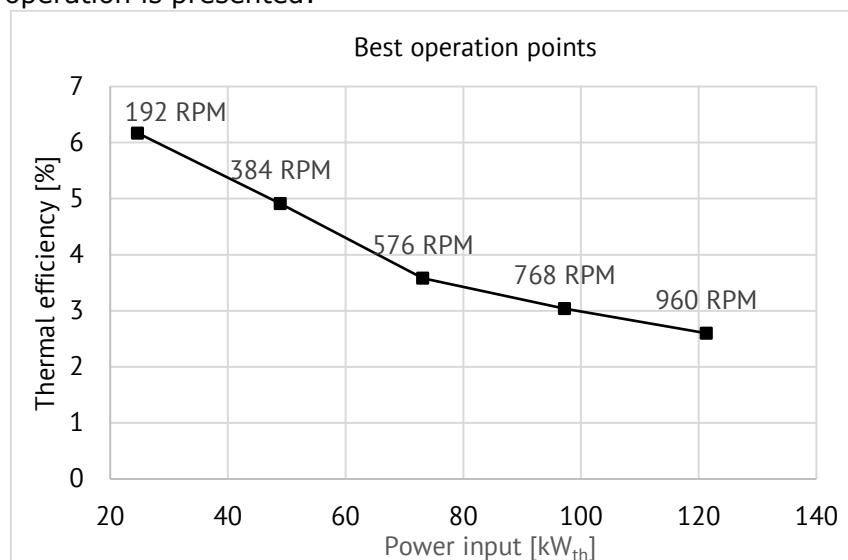


Figure 5.20 Total efficiency for the best operation points for each pump rotational speed, as a function of the total power input, single- stage operation at 110°C

At single- stage operation at 110 °C the best efficiency is observed at 6.2% for 192 RPM pump's rotational speed. The thermal power input at that point is around 25 kW_{th}. Once again as at 95°C, it is noticed that in most load range the

efficiency is around 3 to 5 % which is good considering the operational conditions, however it is interesting that the total efficiency profile is similar to this for single stage operation at 95°C, which is expected considering the fact that the engine is designed for two- stage operation and moreover the increase from 95 to 110 °C is not that great.

The thermal power input in relation to the pump's rotational speed for single and two- stage operation is presented in Figure 5.21:

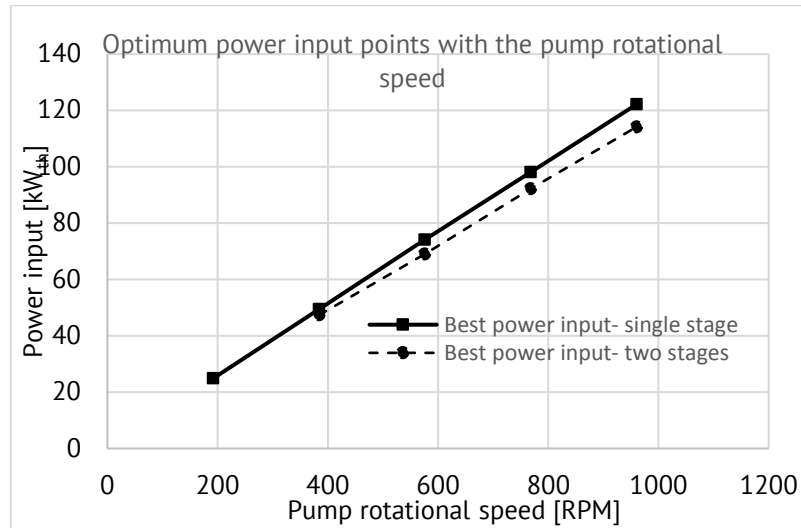


Figure 5.21 Relation of the optimum power input points with the pump rotational speed, single and two- stage operation at 110°C

The two curves in thermal curves are close but for single- stage operation the pump rotational speed operation range is wider since the ORC engine operated effectively for low pump rotational speed (192 RPM) and also the single- stage curve reaches a slightly higher maximum thermal power input for the same pump's rotational speed, reaching 122 kW_{th} than the maximum of 114 kW_{th} for the two-stage operation. As explained previously for 95 °C, for the same pump rotational speed, the mass flow rate is the same, thus the slight divergence between the two curves is due to the different pressure at the evaporator's outlet for the two- stage system which influences the outlet enthalpy at the evaporator and consequently the enthalpy difference and thermal input of the two- stage system.

The total power production for the best operation points of the ORC engine **at two- stage operation at 110 °C** is presented in Figure 5.22:

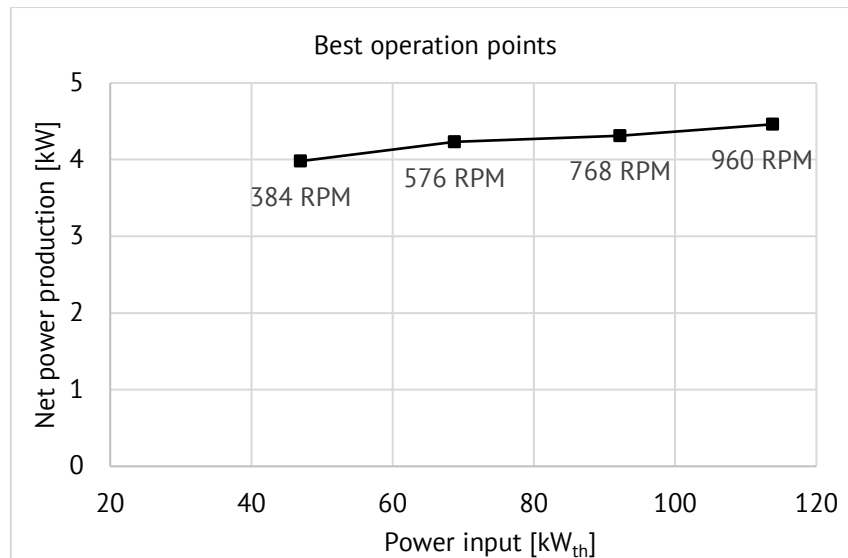


Figure 5.22 Total power production of the expander overview for the best operation points of the ORC engine, two- stage operation at 110°C

The maximum power production for the two- stage operation is noticed at 4.5 kW for high pump's rotational speed, at 115 kW_{th}. Although the power production for the two- stage system starts at 384 RPM pump's rotational speed (when in single- stage operation it starts from 192 RPM), the power production is significantly high throughout the whole power input range and remains over 4 kW. A better operation at 110 °C two- stage system with MEG on the heat source cycle is already observed.

The efficiency throughout the whole thermal load best operation points for each pump's rotational speed is presented in Figure 5.23:

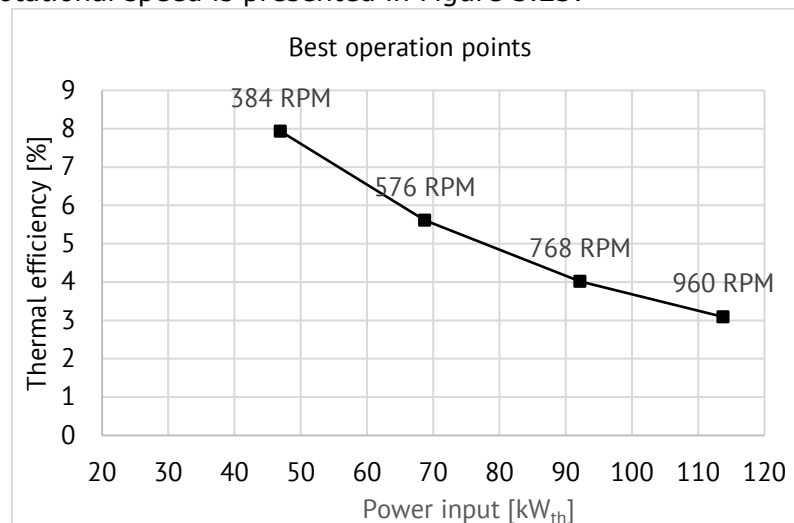


Figure 5.23 Total efficiency for the best operation points for each pump rotational speed, as a function of the total power input, two- stage operation at 110°C

The maximum thermal efficiency for two- stage operation is observed at 7.93 % for 47 kW_{th} power thermal input and 384 RPM pump's rotational speed. As explained previously, with the pump's rotational speed increase, the pump's consumption increases as well, reducing the net power production and compared to the maximum expected efficiency based on the design of 10% (at 120~ 130°C),

the resulted efficiency of $\sim 8\%$ at 110°C is evaluated as very sufficient operation of the ORC engine.

Figures 5.24 and 5.25 present a straight comparison of the single and two- stage operation concerning the total power production and efficiency accordingly. Both total power production and ORC thermal efficiency present higher values for two- stage operation as expected throughout the whole power input range, however for a narrower pump rotational speed range than the single- stage operation.

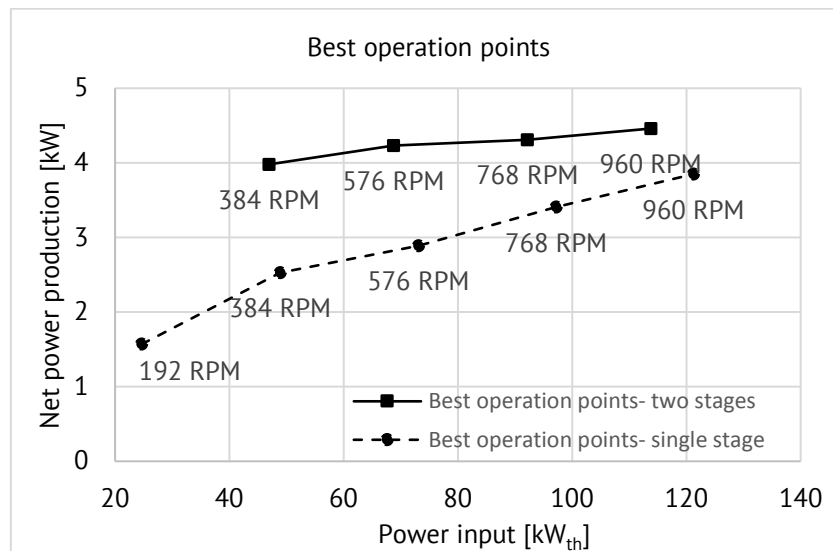


Figure 5.24 Total power production of the expander overview for the best operation points of the ORC engine, single and two- stage operation comparison at 110°C

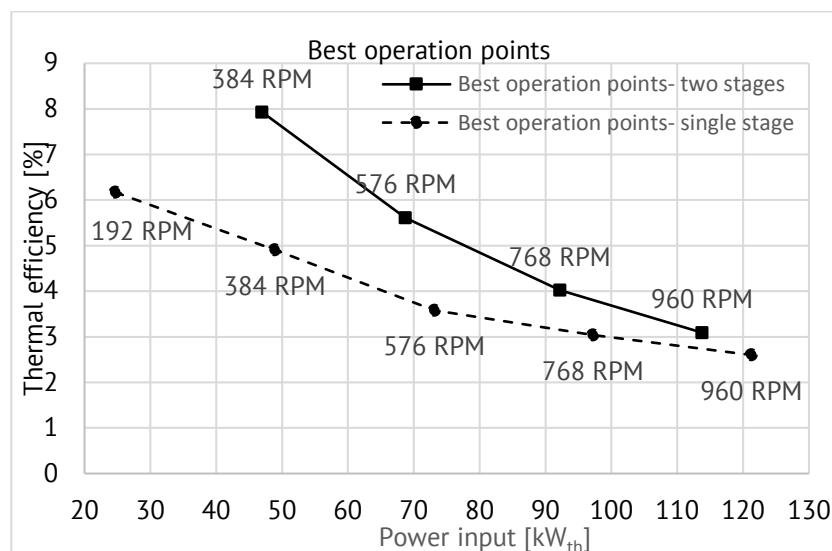


Figure 5.25 Total efficiency for the best operation points for each pump rotational speed, as a function of the total power input, single and two- stage operation comparison at 110°C

5.2.1.5 ORC engine evaluation for operation at 120°C with glycol on the heat source cycle- single & two- stage operation

The next step is the increase of the operating temperature to 120°C (working fluid on the heat source cycle side remains glycol (MEG) for the rest of the experimental steps). The engine is once again tested for single and two- stage operation and the same properties are investigated in both operational conditions. The total power production of the ORC engine for the best operational points for each pump rotational speed throughout the whole power input range for **single stage operation** is presented in Figure 5.26.

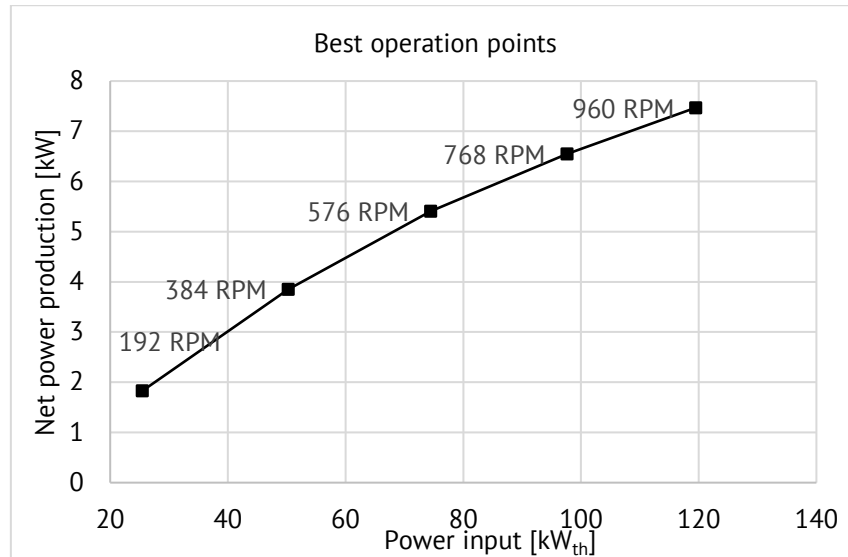


Figure 5.26 Total power production of the expander overview for the best operation points of the ORC engine, single- stage operation at 120°C

The maximum power production of 7.47 kW is noticed at 960 RPM pump's rotational speed and for around 120 kW_{th} thermal power input. The total power production is significantly increased for operating temperature of 120°C, since it is almost doubled than at 110°C. The operating temperature increase leads to a higher enthalpy on the expander's inlet therefore a higher power production (see Table 5.2).

Figure 5.27 gives a general preview of the best operation points for each pump's rotational speed for single stage operation concerning the efficiency, throughout the whole thermal load:

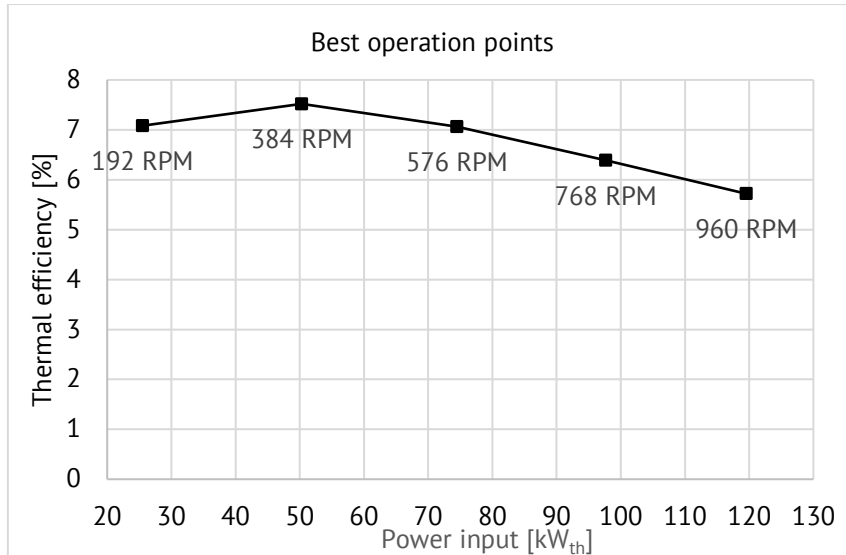


Figure 5.27 Total efficiency for the best operation points for each pump rotational speed, as a function of the total power input, single- stage operation at 120°C

At single- stage operation at 120 °C the best efficiency already reaches a value of 7.52% for 384 RPM pump's rotational speed. The thermal power input at that point is around 50 kW_{th}. At 120°C, in most of the load range the efficiency is around 6 to 7 % which is significantly higher than in previous experimental operating temperatures. This is expected, since the temperature increase effects the enthalpy at the evaporator's inlet, thus the evaporator's thermal load decreases (enthalpy drop decreases) and the thermal efficiency increases.

The thermal power input in relation to the pump's rotational speed for single and two- stage operation is presented in Figure 5.28:

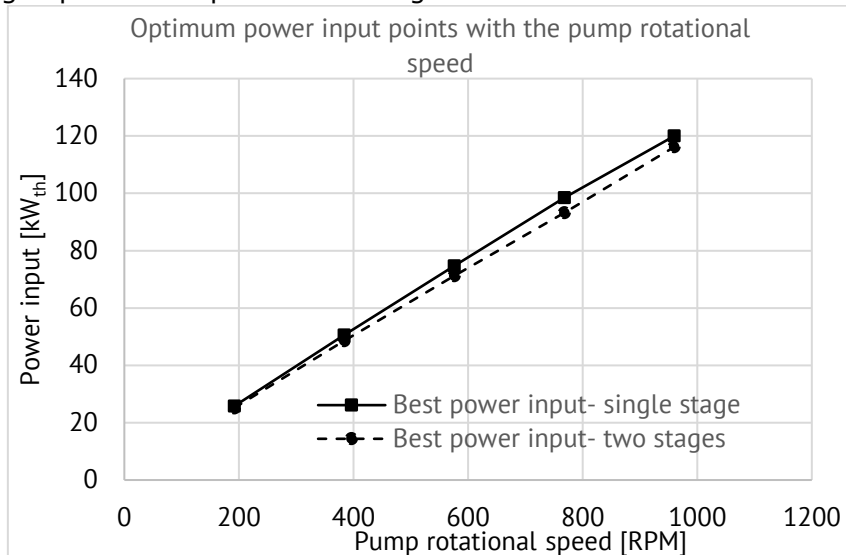


Figure 5.28 Relation of the optimum power input points with the pump rotational speed, single and two- stage operation at 120°C

For single- stage operation, the thermal curve reaches a slightly higher maximum thermal power input for the same pump's rotational speed, reaching 120 kW_{th} than the maximum of 116 kW_{th} for the two-stage operation. An interesting observation is that for 110 and 120°C operating temperature, the thermal curves

profiles for single and two- stage operation are similar due to small temperature difference and operation close to design conditions.

The total power production for the best operation points of the ORC engine **at two- stage operation at 120 °C** is presented in Figure 5.29:

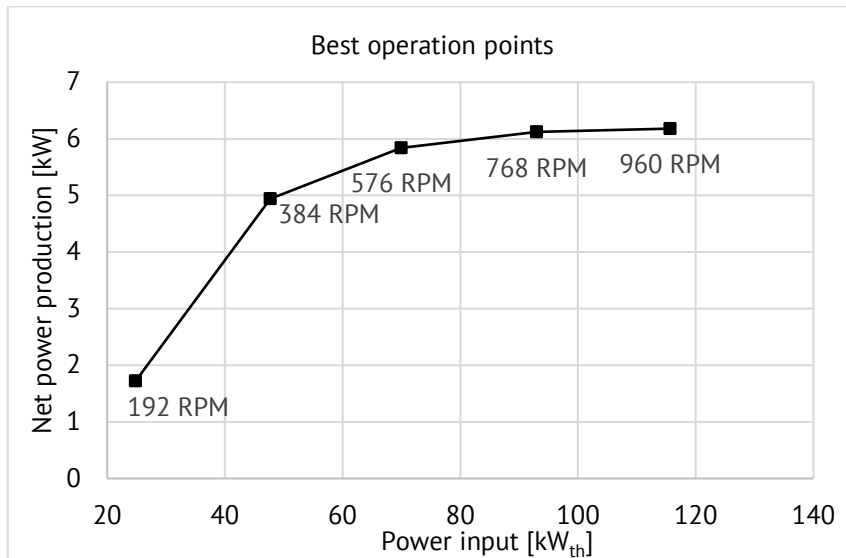


Figure 5.29 Total power production of the expander overview for the best operation points of the ORC engine, two- stage operation at 120°C

The maximum power production for the two- stage operation is noticed at 6.18 kW for high pump's rotational speed, at 116 kW_{th} . The power production is again significantly high throughout the most of power input range fluctuating around 5 and 6 kW.

The efficiency throughout the whole thermal load best operation points for each pump's rotational speed is presented in Figure 5.30:

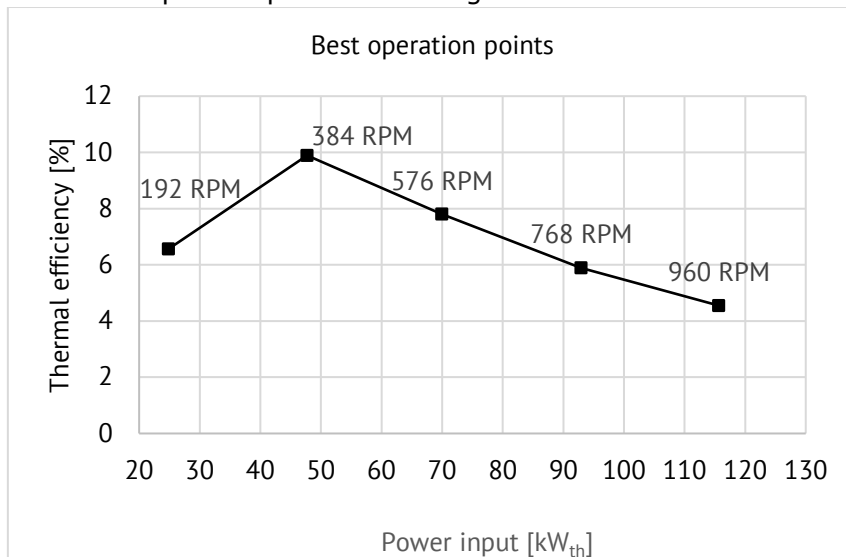


Figure 5.30 Total efficiency for the best operation points for each pump rotational speed, as a function of the total power input, two- stage operation at 120°C

The maximum thermal efficiency for two- stage operation is observed at 9.89 % for 48 kW_{th} power thermal input and 384 RPM pump's rotational speed. The resulted thermal efficiency for two- stage operation at this operation point is very close to the design one (10%) while in the rest of the power input range, the

efficiency remains over 4.5%. The operation of the ORC engine is once again very sufficient compared to the design.

Figures 5.31 and 5.32 present a straight comparison of the single and two-stage operation concerning the total power production and efficiency accordingly.

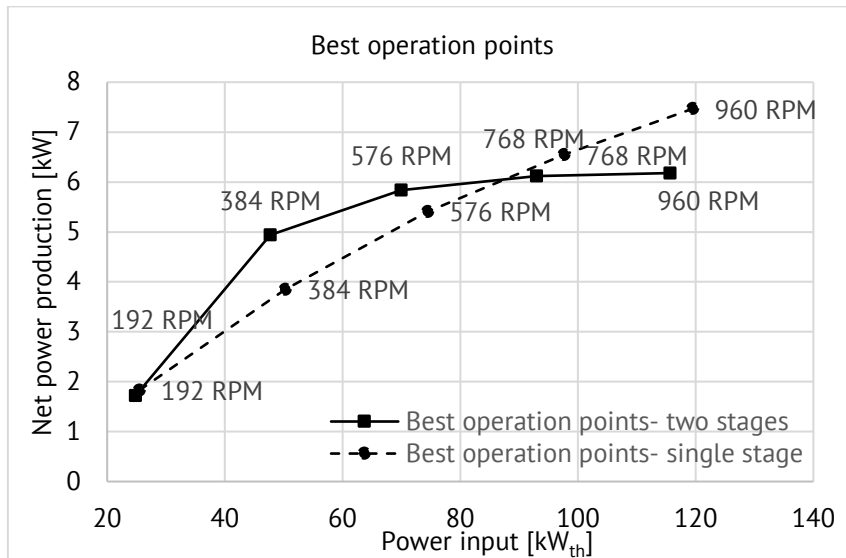


Figure 5.31 Total power production of the expander overview for the best operation points of the ORC engine, single and two- stage operation comparison at 120°C

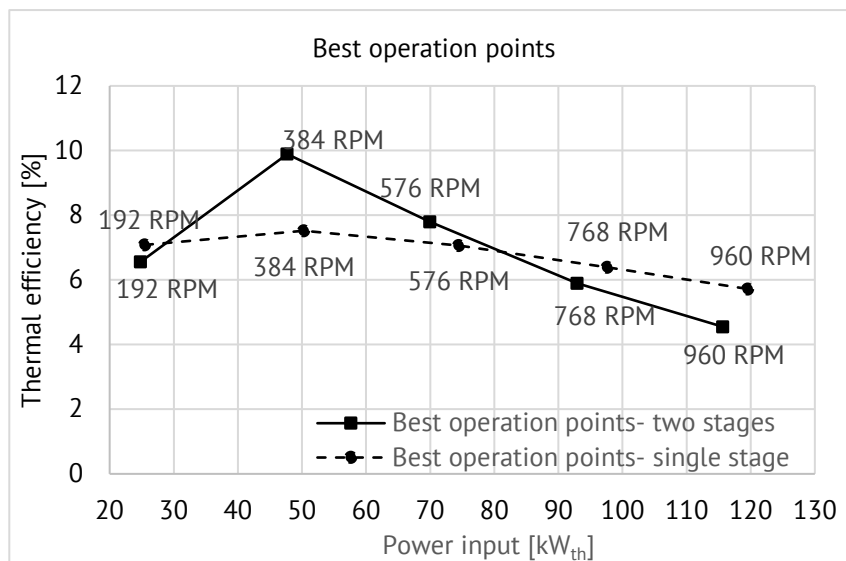


Figure 5.32 Total efficiency for the best operation points for each pump rotational speed, as a function of the total power input, single and two- stage operation comparison at 120°C

5.2.1.6 ORC engine evaluation for operation at 130°C with glycol on the heat source cycle- single & two- stage operation

The final experimental step is the increase of the maximum operating temperature of 130°C. The engine is once again tested for single and two- stage operation and the same properties are investigated in both operational conditions. The total power production of the ORC engine for the best operational points for

each pump rotational speed throughout the whole power input range for **single stage operation** is presented in Figure 5.33.

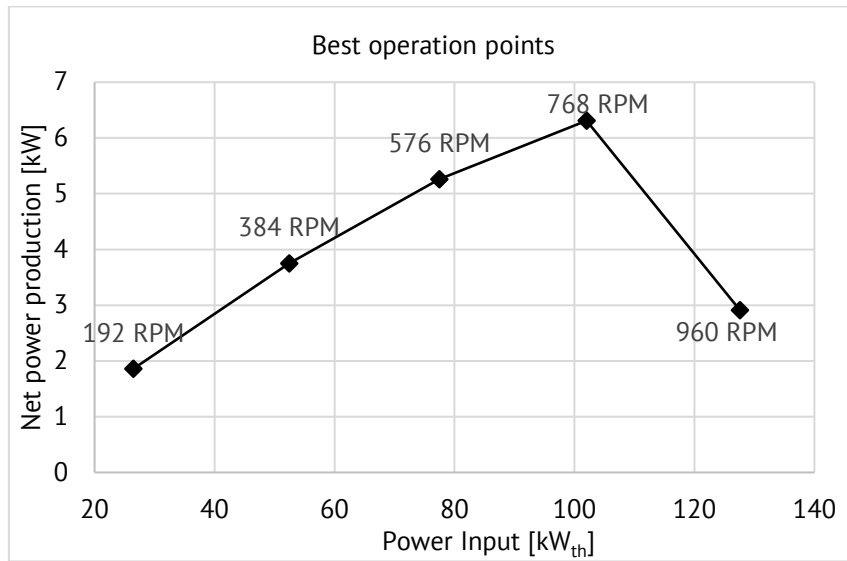


Figure 5.33 Total power production of the expander overview for the best operation points of the ORC engine, single- stage operation at 130°C

The maximum power production of 6.31 kW is noticed at 768 RPM pump's rotational speed and for around 102 kW_{th} thermal power input, while for higher rotational speed the total power production falls deeply. The single- stage production is high throughout the whole power input range, even if it is lower compared to the single-stage production of 120°C.

Figure 5.34 gives a general preview of the best operation points for each pump's rotational speed for single stage operation concerning the efficiency, throughout the whole thermal load:

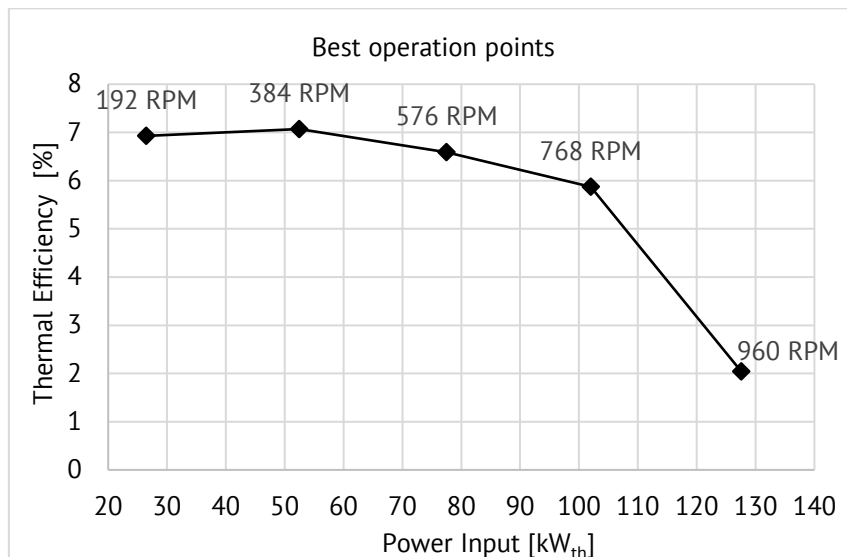


Figure 5.34 Total efficiency for the best operation points for each pump rotational speed, as a function of the total power input, single- stage operation at 130°C

At single- stage operation at 130 °C the best efficiency is around 7% for 384 RPM pump's rotational speed, similar to 120°C. The thermal power input at that point is around 53 kW_{th} . Once again, throughout the most of the load range

the efficiency is around 6 to 7 % which is high for single stage operation. However, for high pump rotational speed (960 RPM) the efficiency significantly drops to 2%, due to the expander’s incapacity of producing power.

The thermal power input in relation to the pump's rotational speed for single and two- stage operation is presented in Figure 5.35:

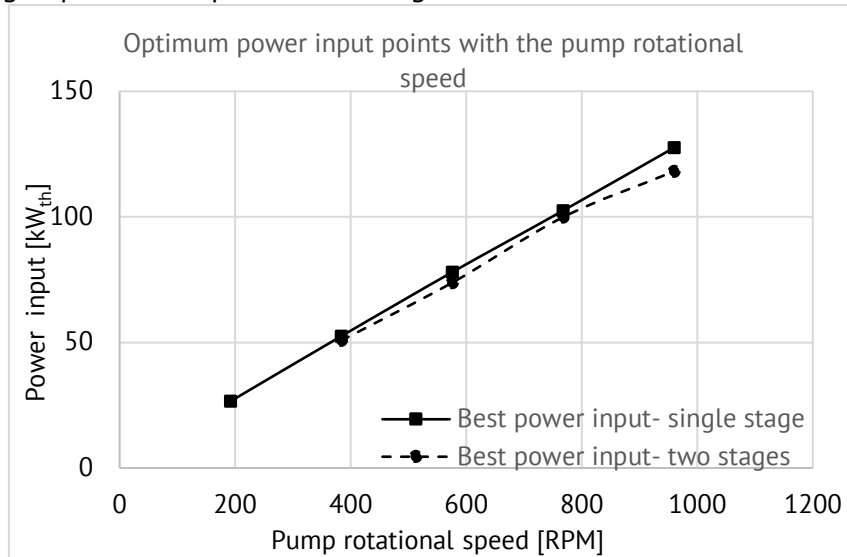


Figure 5.35 Relation of the optimum power input points with the pump rotational speed, single and two- stage operation at 130°C

For single- stage operation, the thermal curve reaches a slightly higher maximum thermal power input for the same pump's rotational speed, reaching 127.6 kW_{th} than the maximum of 118 kW_{th} for the two-stage operation. Moreover, the single- stage curve expands to a wider pump rotational speed range as the engine operated for 192RPM.

The total power production for the best operation points of the ORC engine **at two- stage operation at 130 °C** is presented in Figure 5.36:

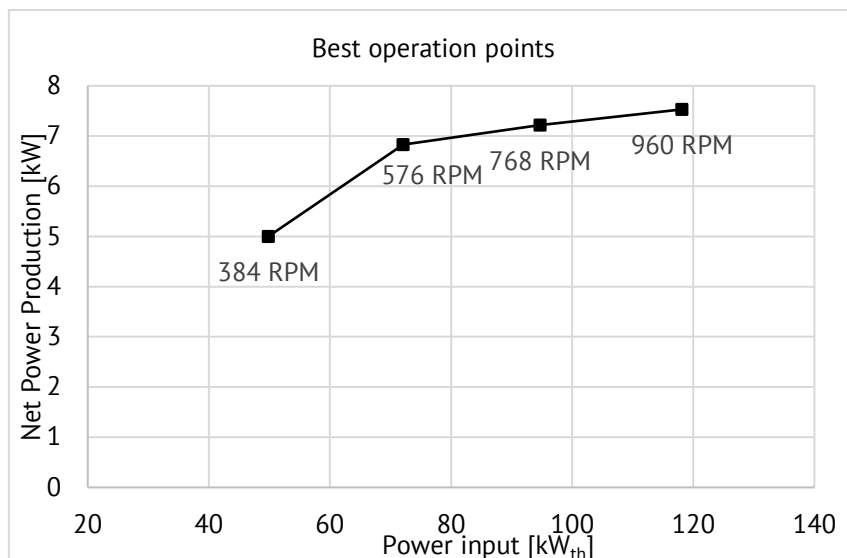


Figure 5.36 Total power production of the expander overview for the best operation points of the ORC engine, two- stage operation at 130°C

The maximum power production for the two- stage operation is noticed at 7.53 kW for high pump's rotational speed, at 118 kW_{th} and it is the highest value

for two- stage operation throughout all experimental operating temperatures. Considering that the ORC two- stage engine has been designed for a maximum power production of 10 kW, the maximum produced power of 7.53 kW shows a deviation of around 15%. The power production is again significantly high throughout the most of power input range fluctuating around 5 and 7.5 kW.

The efficiency throughout the whole thermal load best operation points for each pump's rotational speed is presented in Figure 5.37:

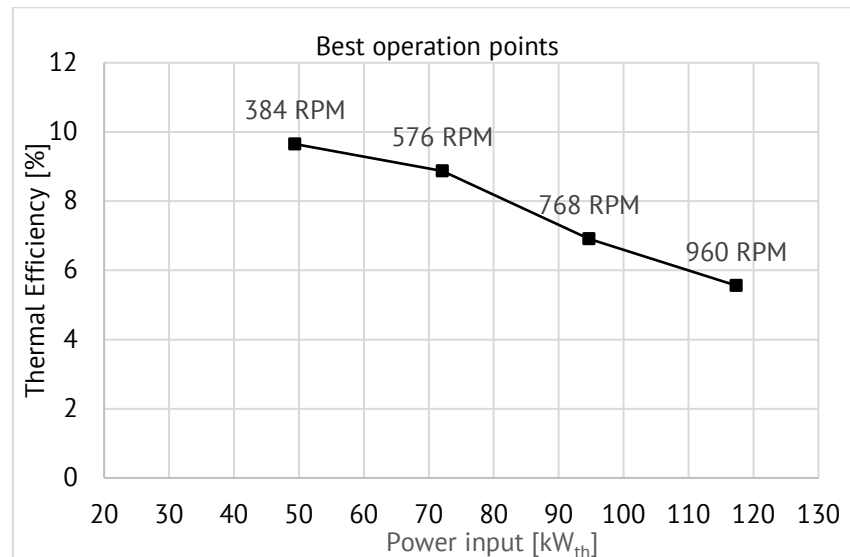


Figure 5.37 Total efficiency for the best operation points for each pump rotational speed, as a function of the total power input, two- stage operation at 130°C

The maximum thermal efficiency for two- stage operation is observed at 9.65 % for 49 kW_{th} power thermal input and 384 RPM pump's rotational speed. The resulted thermal efficiency for two- stage operation at this operation point is once again very close to the design one (10%) while in the rest of the power input range, the efficiency remains over 5.6%. The operation of the ORC engine is once again very sufficient compared to the design.

Figures 5.38 and 5.39 present a straight comparison of the single and two- stage operation concerning the total power production and efficiency accordingly.

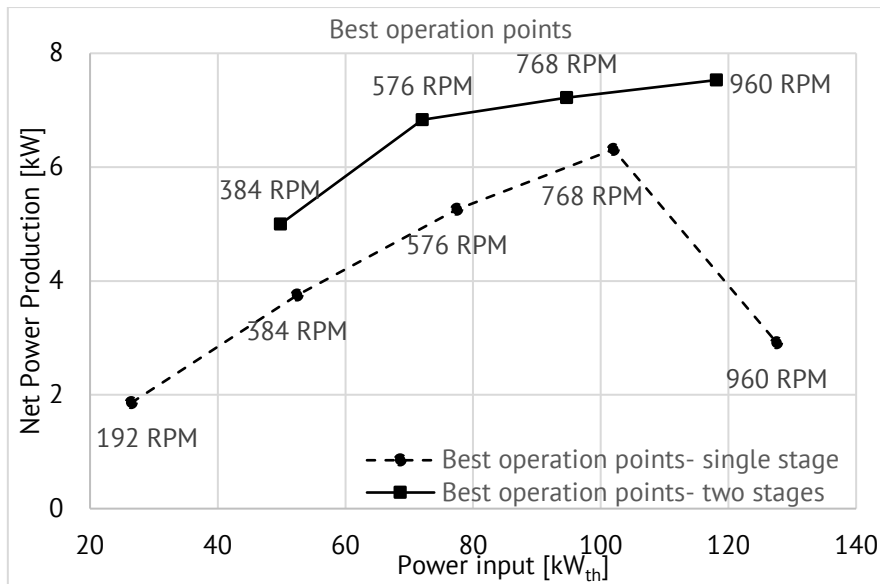


Figure 5.38 Total power production of the expander overview for the best operation points of the ORC engine, single and two-stage operation comparison at 130°C

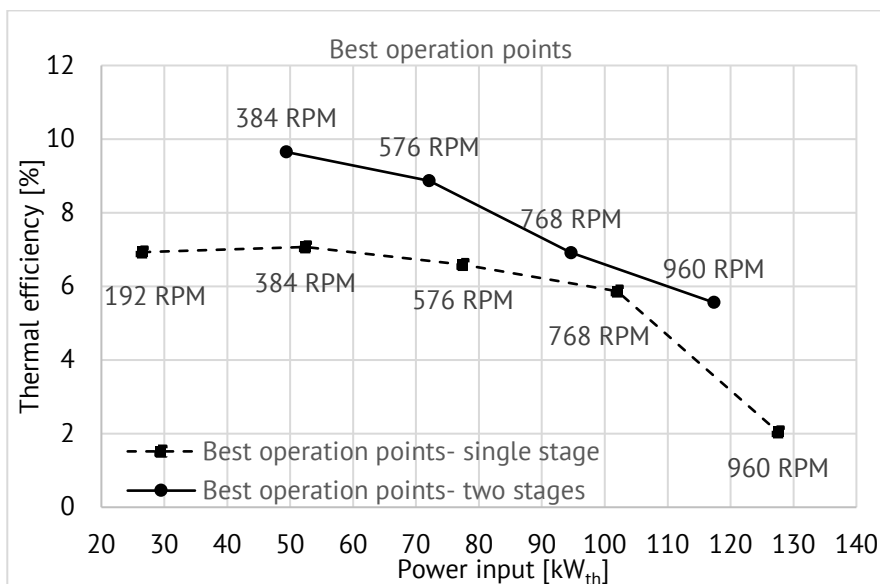


Figure 5.39 Total efficiency for the best operation points for each pump rotational speed, as a function of the total power input, single and two-stage operation comparison at 130°C

In order to provide an overview of the operation at all temperatures, Figures 5.40 and 5.41 below present the maximum power production and thermal efficiency of the two-stage system for different operation temperatures.

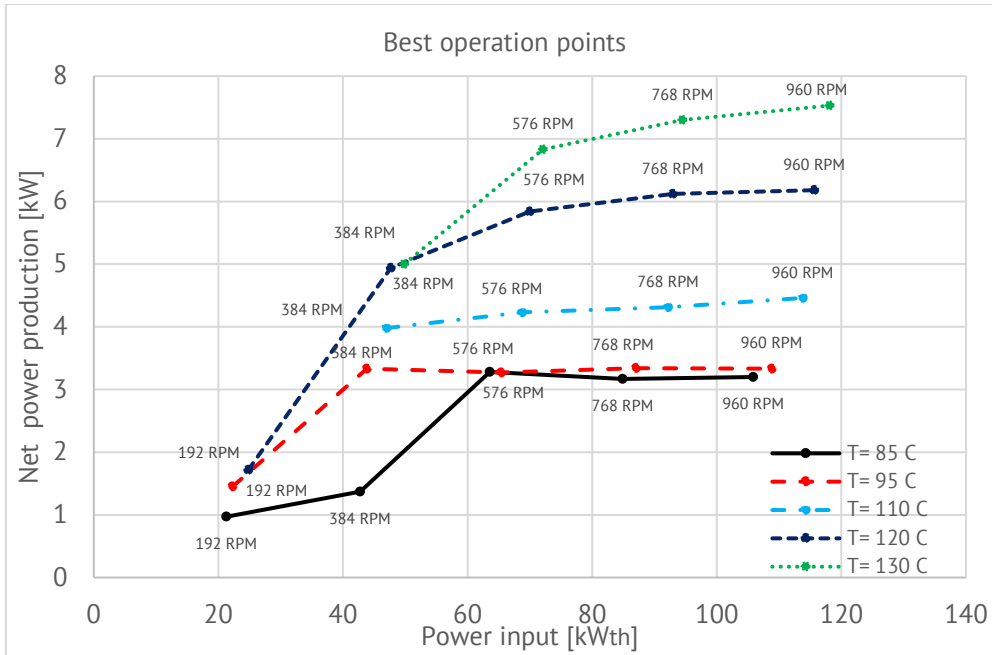


Figure 5.40 Total power production of the expander overview for the best operation points of the ORC engine, two-stage operation comparison for all tested operating temperatures

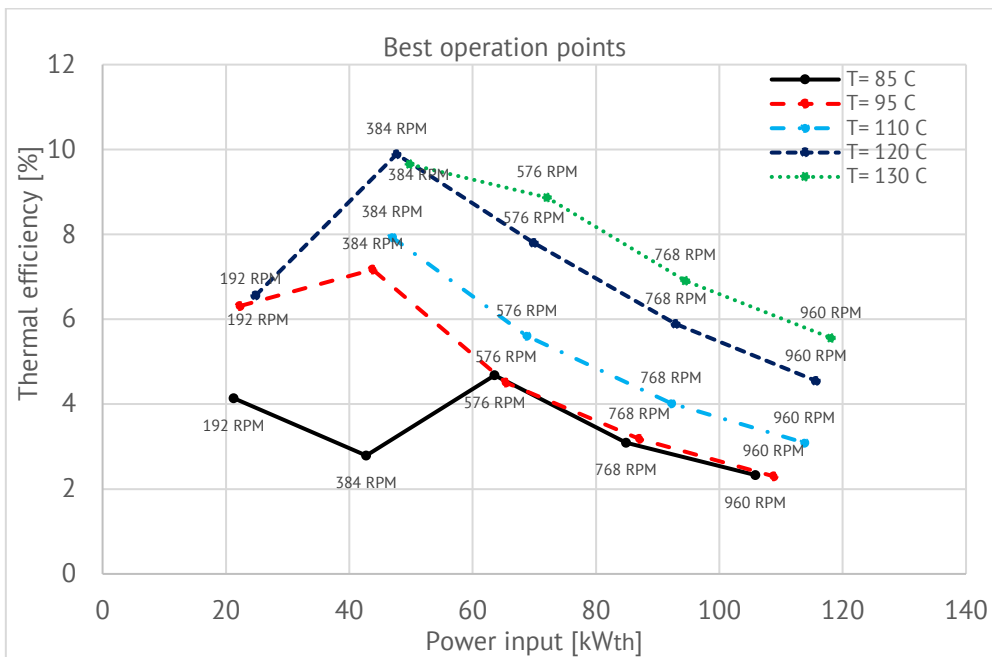


Figure 5.41 Total thermal efficiency for the best operation points for each pump rotational speed, as a function of the total power input, two-stage operation comparison for all tested operating temperatures

As it is observed from the previous analysis and Figure 5.40, the power production increases as the operating temperature increases which was expected since the evaporator enthalpy drop becomes higher. The maximum power production achieved was 7.53 kW for 130°C operating temperature which is close to the design value of 10 kW. As expected, the net power production of the two-stage system increases as the operation temperature gets closer to the design temperature of 130 °C. However, even at low operation temperature of 85 °C, the

system produces around 3.5 kW for high pump rotational speed. For high heat input the net power production at 85 and 95 °C is almost the same and the net power production at 110 °C is almost constant throughout the whole heat input range. Moreover, for 110 and 130 °C the system does not produce power until almost 45 kW_{th} at the inlet, thus for low pump's rotational speed the expansion of the working fluid is inefficient.

Following the net power production, the thermal efficiency increases with the operation temperature increase, reaching a maximum of 9.89% at 120 °C, very close to the design value of 10%. In almost all cases, the highest thermal efficiency is for a heat input of around 45 to 50 kW_{th}, since for higher heat input -thus for higher pump rotational speed- the expansion efficiency decreases resulting in an efficiency decrease. The next paragraph will focus on the expanders' performance investigation and this result will be explained.

An important result extracted from Figures 5.40 and 5.41 is that even though the net power production and the thermal efficiency reach higher values for operation at 130 °C, the two-stage system performs better at 120 °C, as the relevant curve in both Figures clearly indicates, since the system operates efficiently for a wider thermal input range and rotational speeds. The slightly less efficient operation for a wider thermal input range though at 120°C may be due to an undersized expander in comparison to the designed one. Therefore, for high temperature (130 °C) and low pump rotational speed the expansion of the working fluid is not efficient and the system does not produce electric power until almost 45 kW_{th} of thermal input.

For operation at 120°C and in order to present a clearer picture of the ORC engine performance in two-stage operation, the thermal efficiency as a function of the expanders' rotational speed for three different pump rotational speeds is given in Figures 5.42 to 5.44, further investigating the efficient performance of the ORC engine.

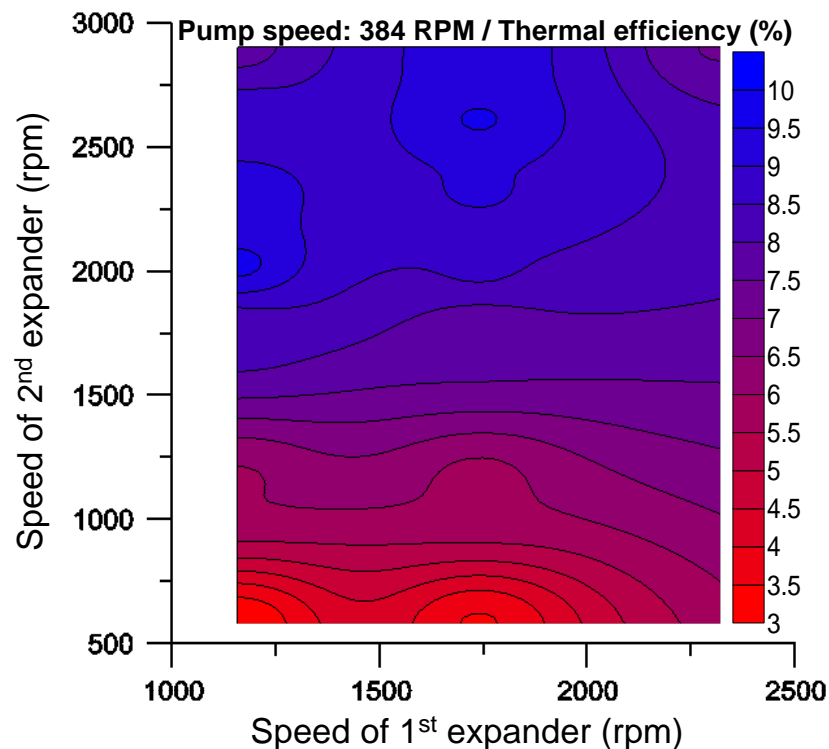


Figure 5.42 ORC two-stage operation efficiency for each expanders' rotational speed, Pump speed: 384 RPM, T=120°C

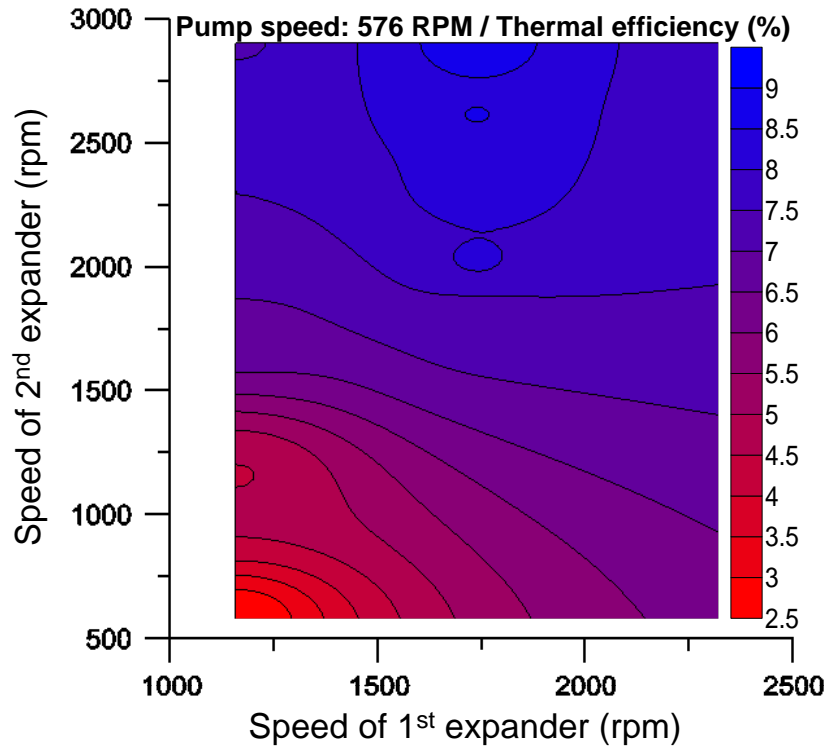


Figure 5.43. ORC two-stage operation efficiency for each expanders' rotational speed, Pump speed: 576 RPM, $T=120^{\circ}\text{C}$

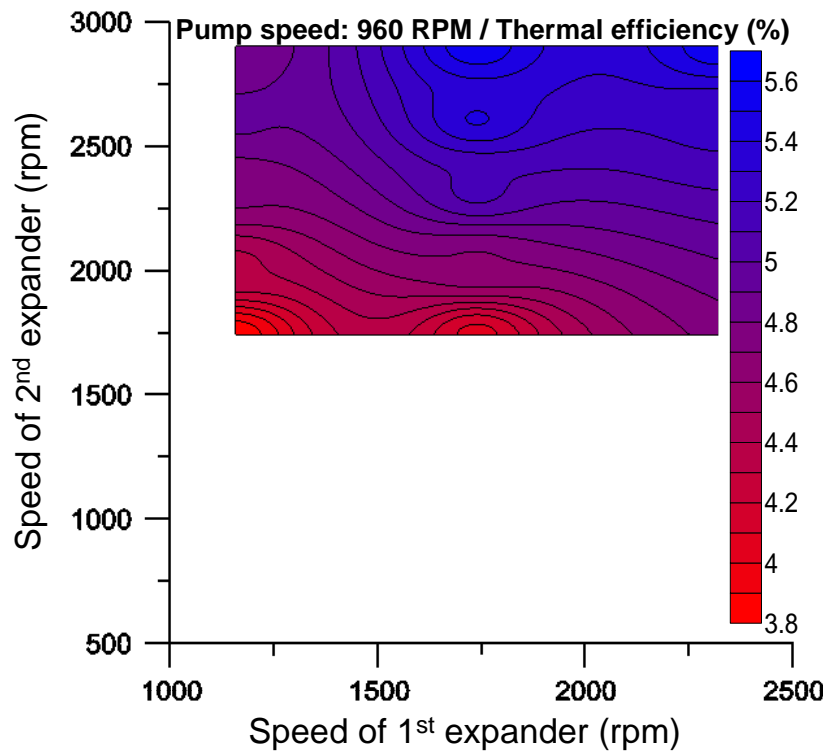


Figure 5.44. ORC two-stage operation efficiency for each expanders' rotational speed, Pump speed: 960 RPM, $T=120^{\circ}\text{C}$

As observed in Figures 5.42- 5.44, for low pump rotational speed, many expanders' rotational speed combinations result in an efficiency ranging from 8 to

~10% and even more above 5%. However, as the pump rotational speed increases the ORC thermal efficiency decreases reaching maximum values of around 6%, as discussed previously.

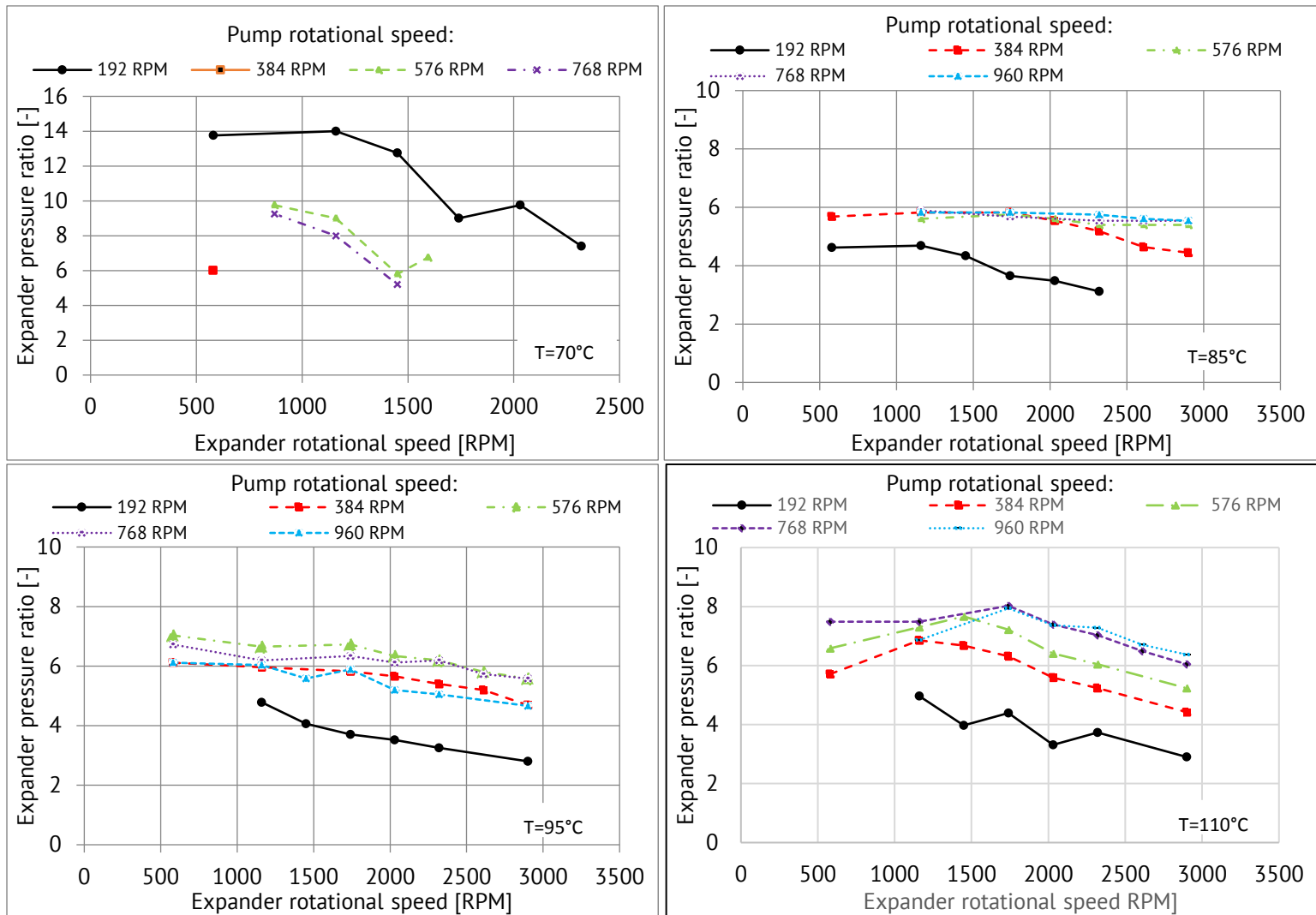
5.2.2 Scroll expanders operation evaluation at single and two- stage operation

The components of the ORC engine that is necessary to be evaluated are the scroll expanders, since they are the result of market available scroll compressors as explained in Chapter 3. Their performance investigation and the plotting of their operation curves are necessary for their operation evaluation.

Next, the test results of the expanders' operation investigation at single and two-stage operation are presented, for all operation temperatures.

Single stage operation

One of the most important parameters under investigation concerning the expander operation is its pressure ratio. The pressure ratio (inlet pressure to outlet pressure) indicates the capacity of the expander to expand the refrigerant. In Figure 5.45, the pressure ratio of the low pressure (second) expander as a function of the pump and expander rotational speed for single stage operation is presented.



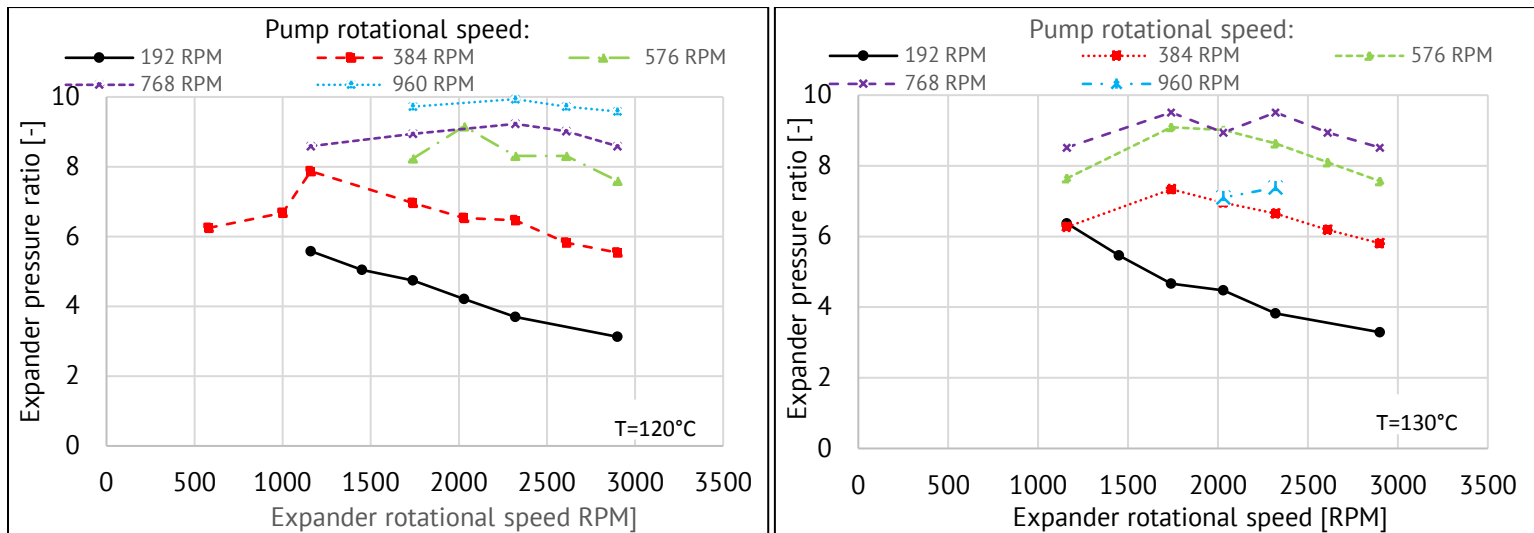


Figure 5.45 Expander's pressure ratio as a function of its rotational speed, at several pump rotational speeds - single stage operation, for all temperature range

At single-stage operation, as observed in Figure 5.45, for most operation temperatures the pressure ratio of the expander generally increases as the pump rotational speed increases, reaching values of around 9.5 which are very high for the selected type of expander. This is the reason that for very high pump's rotational speed the pressure ratio suddenly drops, since the expander can no longer efficiently expand the refrigerant. Moreover, at high pump speed, the heat supply is large and the condenser might not be able to reject all this heat. This would lead to an increase of condensation temperature and pressure which would also contribute in the pressure ratio reduction. The pressure ratio for constant pump rotational speed decreases with the increase of the expander rotational speed, since the inlet pressure decreases as well. Concerning the pressure ratio, the best performance is noticed for a temperature range between 85 and 120 °C, since for 70°C the pressure ratio reaches excessive values and only for low pump rotational speed and for 130°C for high pump rotational speed the pressure ratio intensively drops. In all cases however, the expander is over- expanding the working fluid since it is designed with a pressure ratio of around 3~4 and according to Figure 5.45 it reaches much higher values in single- stage operation.

A main variable to be considered is the expansion efficiency (Table 5.2). The expansion efficiency expresses the real power produced by the expander in comparison to the theoretical power production, if the process was isentropic. In Figure 5.46, the expander's efficiency as a function of the expander's rotational speed at several pump's rotational speeds is given for single stage operation and for the same conditions as in Figure 5.45.

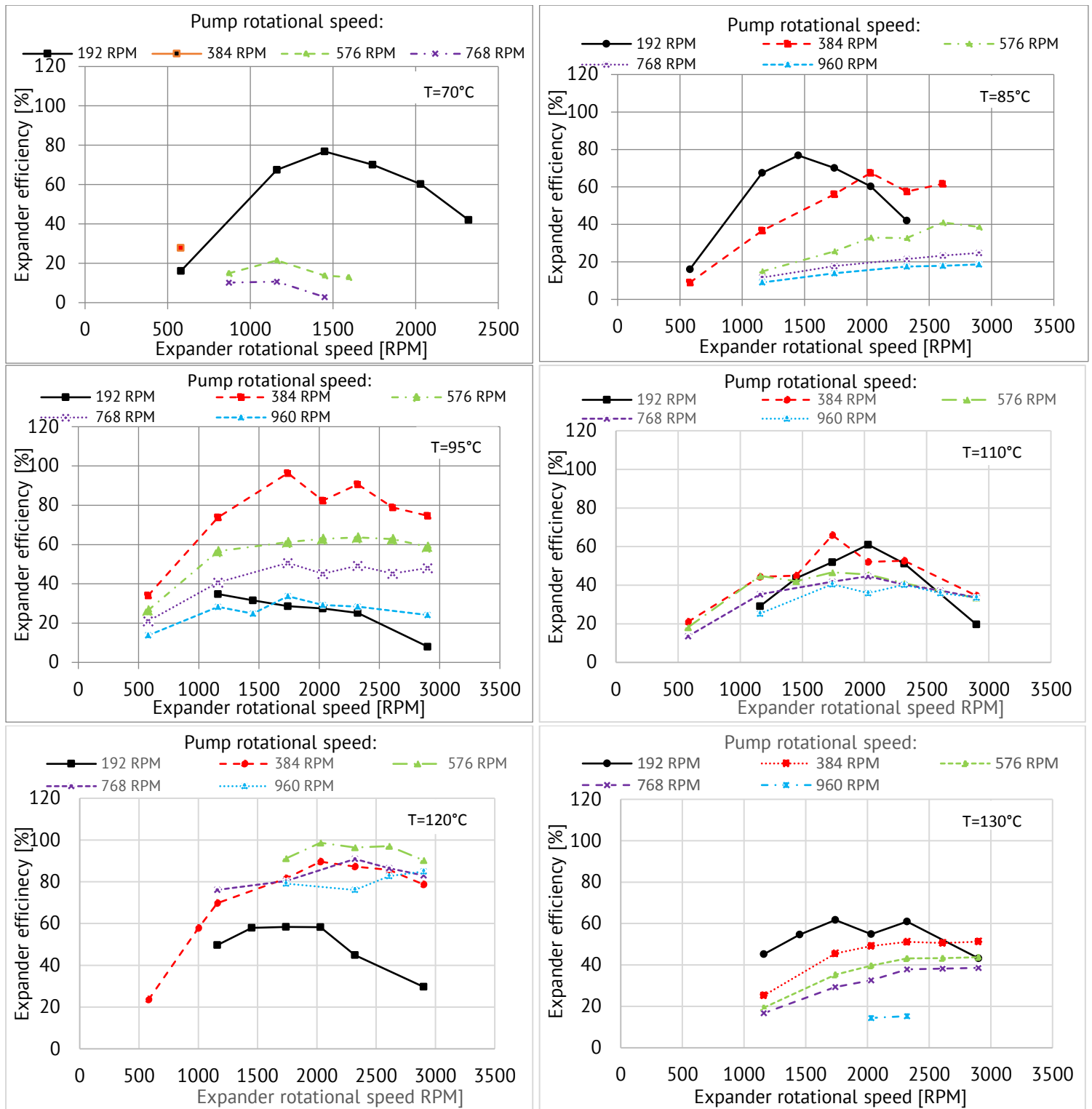


Figure 5.46 Expander's efficiency as a function of its rotational speed, at several pump rotational speeds -single stage operation, for all temperature range

Figure 5.46 demonstrates that for low (70-85°C) and very high (130°C) temperature, the expander's efficiency decreases with the pump rotational speed increase. The efficiency for high pump rotational speed is considerably low due to the incapability of the expander to efficiently expand the refrigerant at such high pump rotational speed (high refrigerant flow). However, for 95° and 120°C the expander's efficiency reaches high values of ~90% for medium pump rotational speed and the best performance is noticed at 120°C. Moreover,

the expander's efficiency in most cases increases with the expander's rotational speed increase reaching a maximum value at 1500- 2500 RPM and then deeply drops for higher rotational speed. In general, since the ORC engine is designed for two- stage operation, the result of Figures 5.45 and 5.46 for the mediocre operation of one expander is justified.

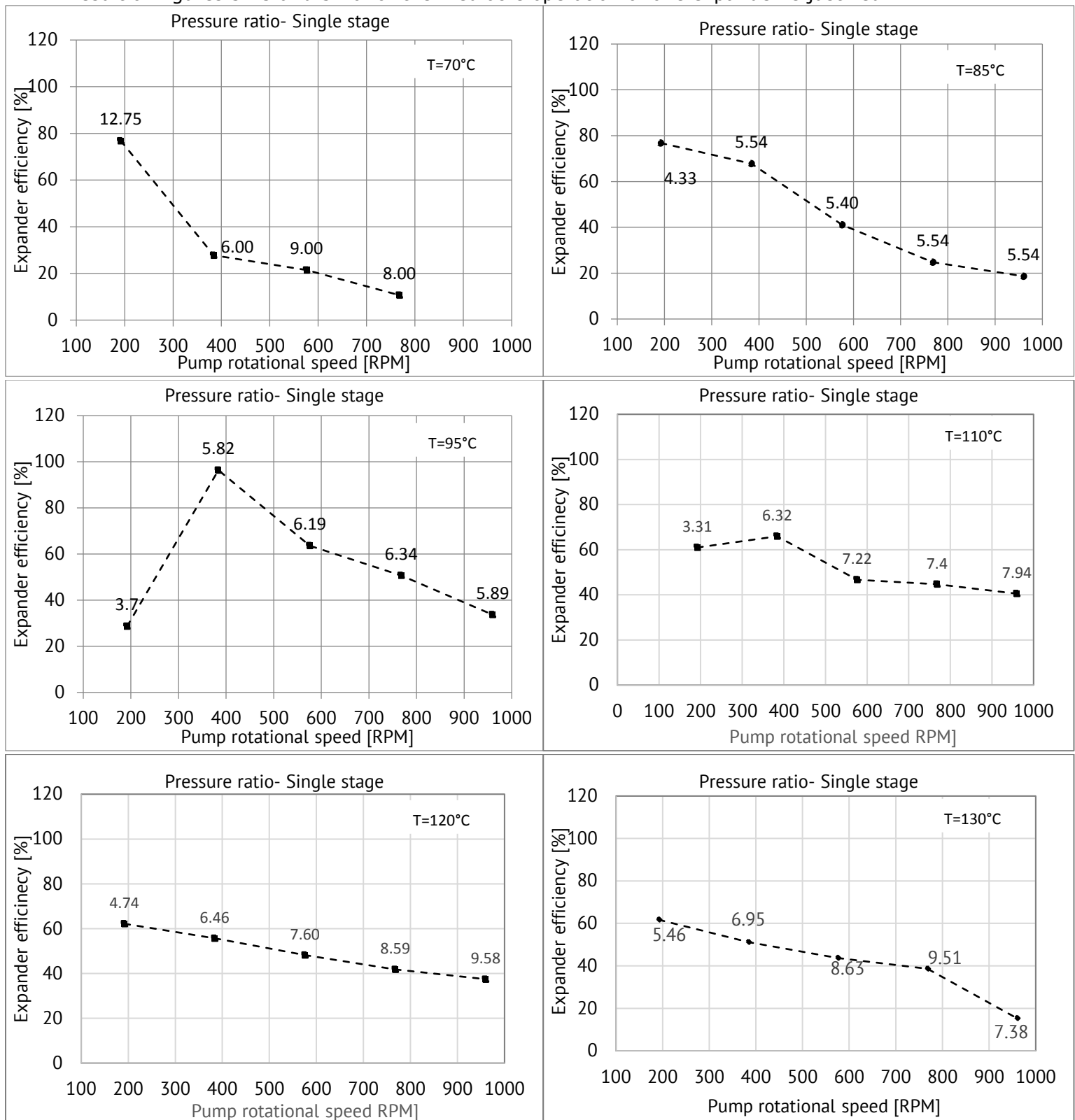


Figure 5.47 Expander's efficiency as a function of the pump rotational speed at several pressure ratios, at single-stage operation, for all temperature range

Figure 5.47 illustrates the expander's efficiency as a function of the pump rotational speed, related to the pressure ratio for single stage operation. As the pump's rotational speed increases in most cases, the pressure ratio of the expander gradually increases while the expander's efficiency decreases. For high pump's rotational speed, the expander can no longer efficiently expand the refrigerant, leading to a steep efficiency and pressure ratio drop. The efficiency decrease of the expander for single stage operation can be justified by the fact that the ORC engine is designed for two-stage efficient operation at 120- 130 °C. An interesting observation is that for single- stage operation the best expander efficiency is noticed at 95°C for 586 RPM pump rotational speed and a pressure ratio of 5.82.

Two- stage operation

The same properties for the two- stage expanders' performance, are investigated so as to get a detailed picture of their operation. In order to avoid confusion, the operation at each operation temperature is evaluated separately. Since the ORC engine did not operate in two- stage mode at 70 °C, the investigation starts at T= 85°C.

Operation Temperature: 85°C

The expanders' pressure ratios are investigated for each pump rotational speed in two- stage operation of the ORC engine. The pressure ratio as a function of the expander rotational speed for high pressure (1) and low pressure (2) expander is presented in Figure 5.48.

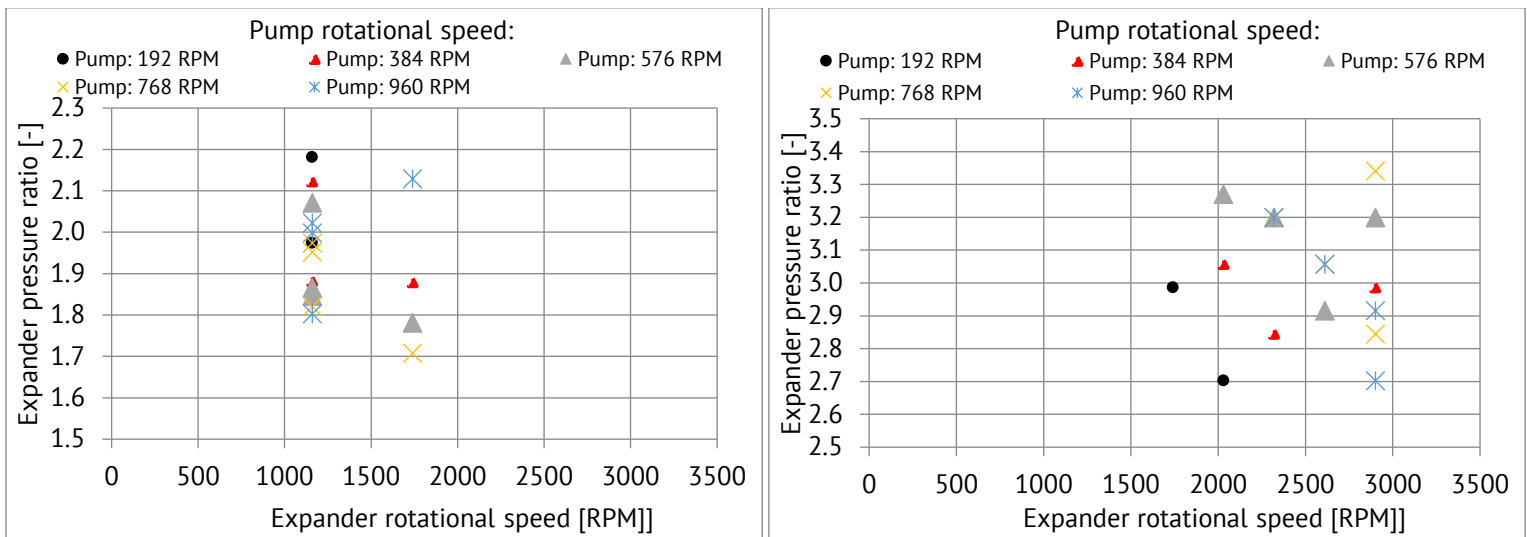


Figure 5.48 Expander's pressure ratio for the high pressure (left) and low-pressure expander (right) as a function of its rotational speed, at several pump rotational speeds -two stage operation, T=85°C.

As observed in Figure 5.48, the pressure ratio of the high pressure (HP) expander varies between 1.7 and 2.15, when the pressure ratio of the low pressure (LP) expander varies between 2.7 and 3.35 accordingly. Even though the LP expander presents a pressure ratio within the design values, the HP expander presents a much lower pressure ratio, when it was expected to be similar to the HP expander's pressure ratio. However, the operation temperature is much lower than the design one, therefore the HP expander's under- expansion could be justified.

The expanders' efficiency as a function of their rotational speed for each pump rotational speed is given in Figure 5.49.

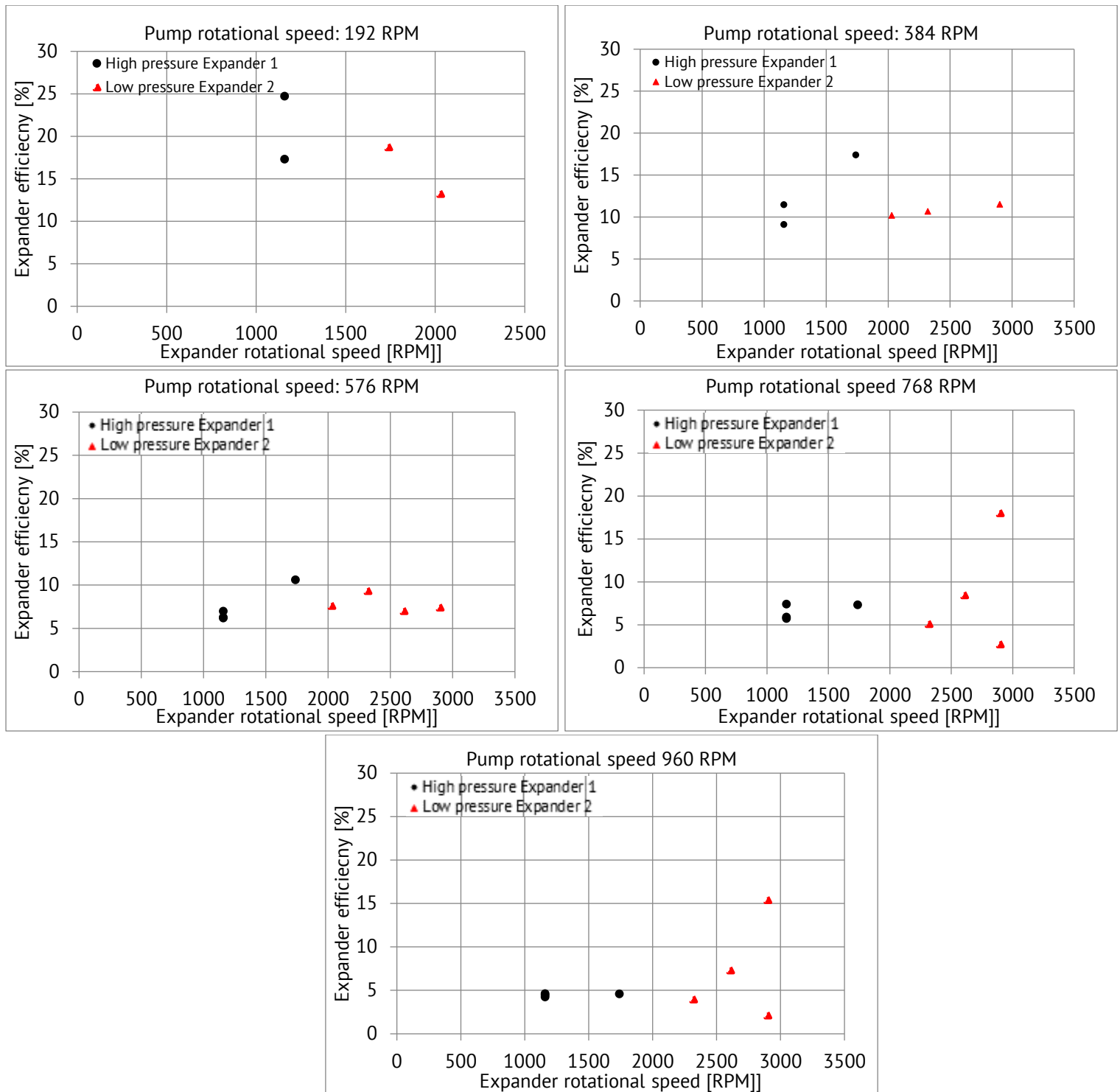


Figure 5.49 Expanders' efficiency as a function of its rotational speed, at several pump rotational speeds-two stage operation, $T=85^{\circ}\text{C}$

For low pump rotational speed, the efficiency of both expanders is between 13 and 25%. It can be observed in Figure 5.49 that the increase of the pump rotational speed results in a decrease of the expanders' efficiency. This is due to the fact that the mass flow rate increases with the increase of the pump rotational speed while the enthalpy difference between the inlet and the isentropic condition and the expander's power production remains almost the same, therefore the ratio of the expander efficiency decreases (see Table 5.2).

Operation Temperature: 95°C

The same properties are investigated for 95°C. The expanders' pressure ratios for each pump rotational speed in two-stage operation as a function of the expander rotational speed for high pressure (1) and low pressure (2) expander are presented in Figure 5.50.

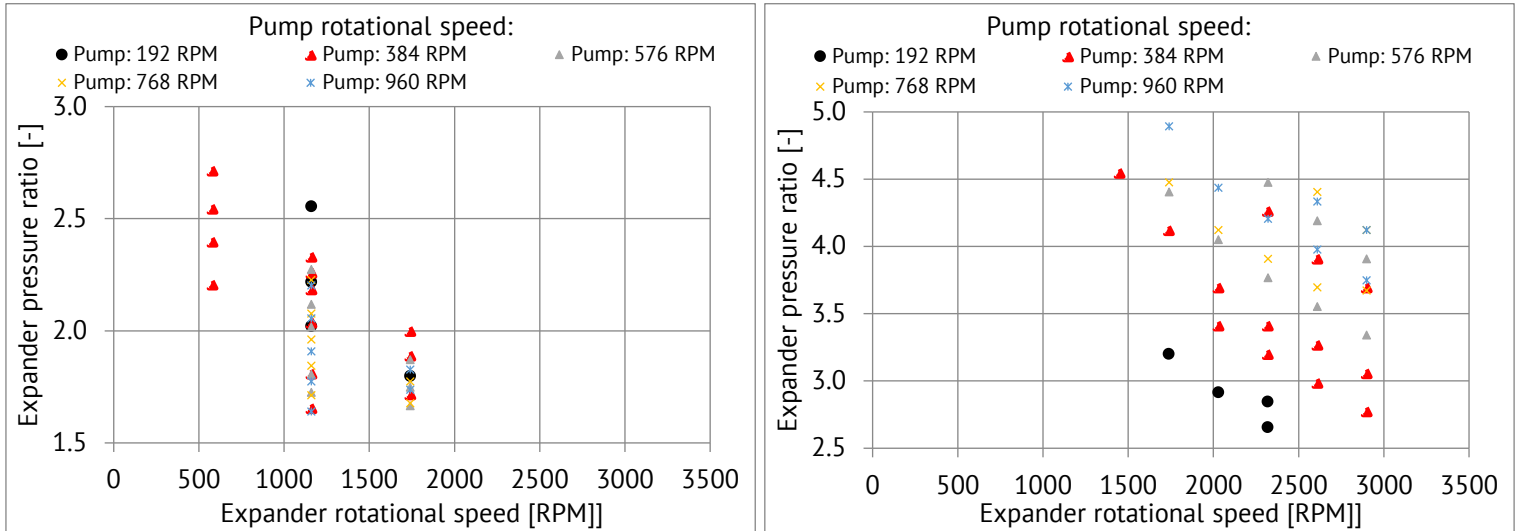
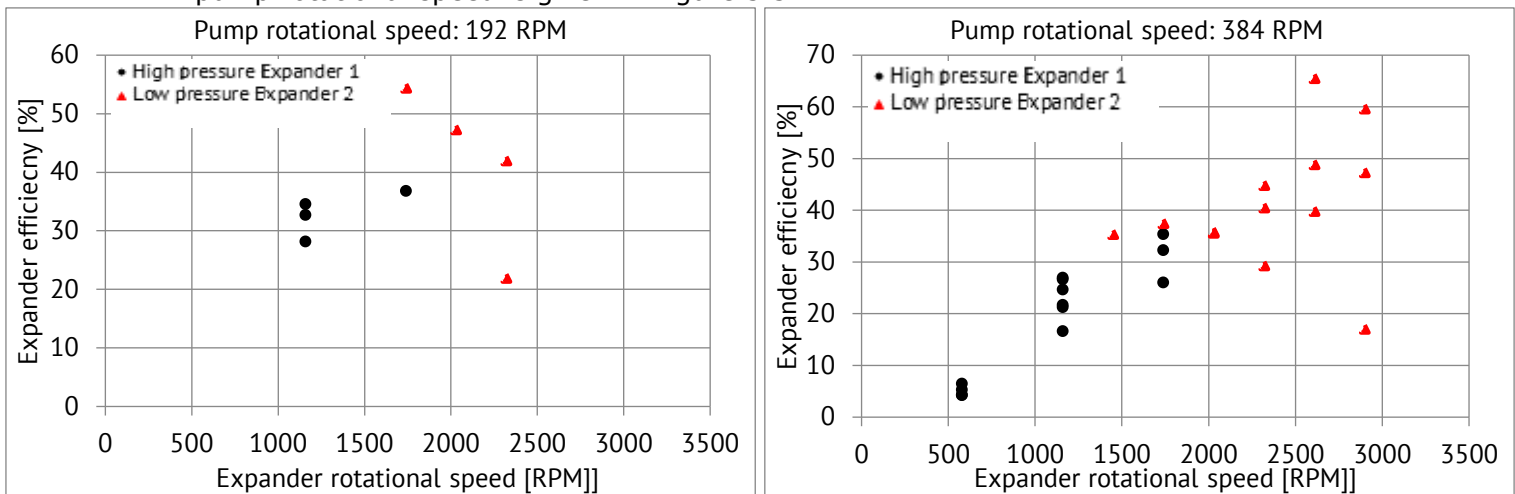


Figure 5.50 Expander's pressure ratio for the high pressure (left) and low-pressure expander (right) as a function of its rotational speed, at several pump rotational speeds -two stage operation, T=95°C.

As observed in Figure 5.50, the pressure ratio of the high pressure (HP) expander varies between 1.7 and 2.7 and the pressure ratio of the low pressure (LP) expander varies between 2.7 and 4.90 accordingly. Once again, the LP expander presents a pressure ratio within the design values, however the HP expander presents a much lower pressure ratio, when it was expected to be similar to the HP expander's pressure ratio. The operation temperature is again lower than the design one, therefore the HP expander's under-expansion could be justified.

The expanders' efficiency as a function of their rotational speed for each pump rotational speed is given in Figure 5.51.



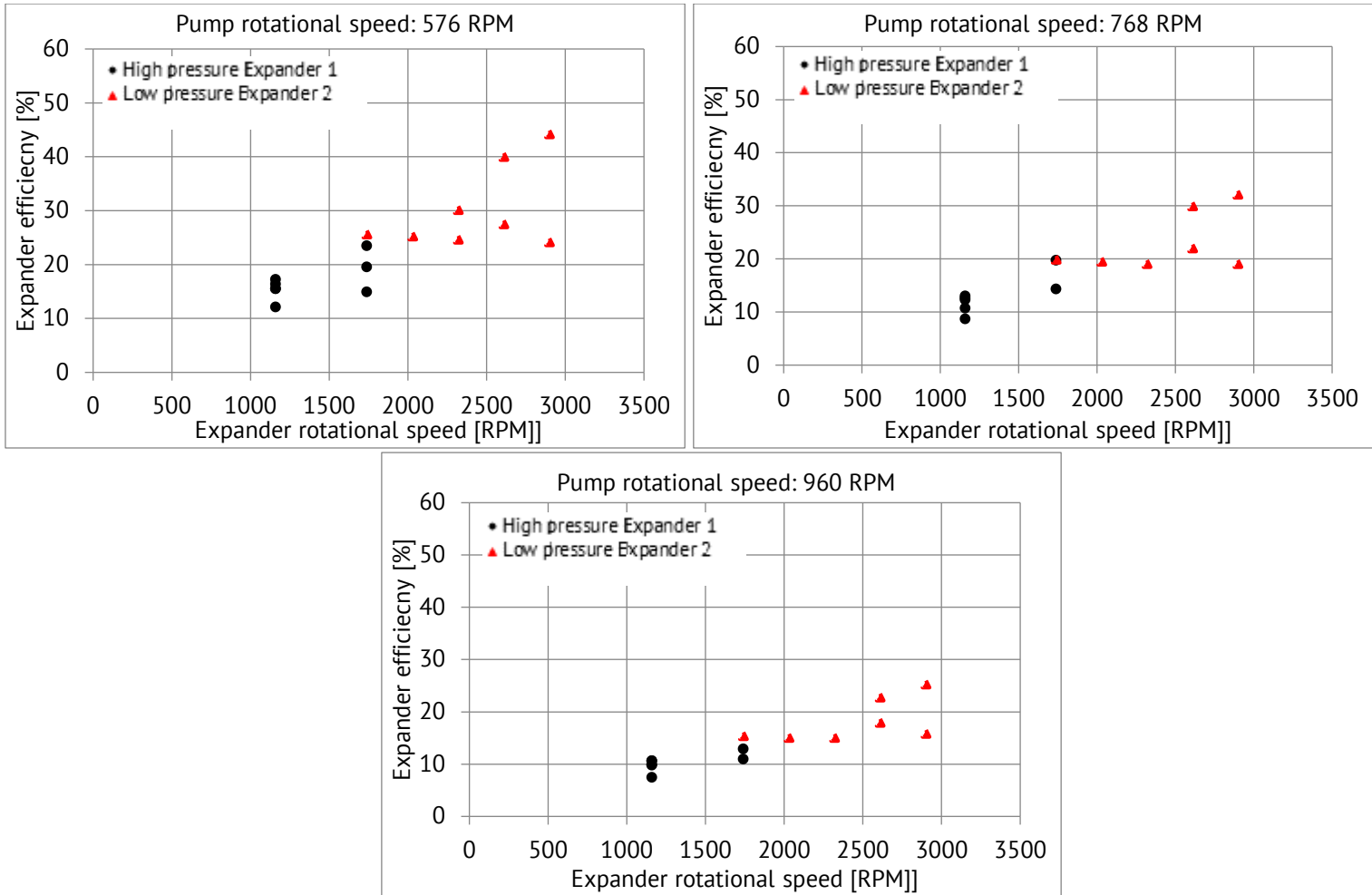


Figure 5.51 Expanders' efficiency as a function of its rotational speed, at several pump rotational speeds-two stage operation, $T=95^{\circ}\text{C}$

At 95°C , the efficiency of the HP expander varies between 5 and 35%, when the LP expander presents an efficiency between 15 and 65%. For higher pump rotational speed, the efficiency of the HP expander is around 12% and of the LP around 20%. Once again, the decrease of the expanders' efficiency with the increase of the pump rotational speed is due to the fact that the mass flow rate increases with the increase of the pump rotational speed while the enthalpy difference between the inlet and the isentropic condition and the expander's power production remains almost the same, therefore the ratio of the expander efficiency decreases.

Operation Temperature: 110°C

The next step is the operation investigation at 110°C . The expanders' pressure ratios for each pump rotational speed in two-stage operation as a function of the expander rotational speed are presented in Figure 5.52.

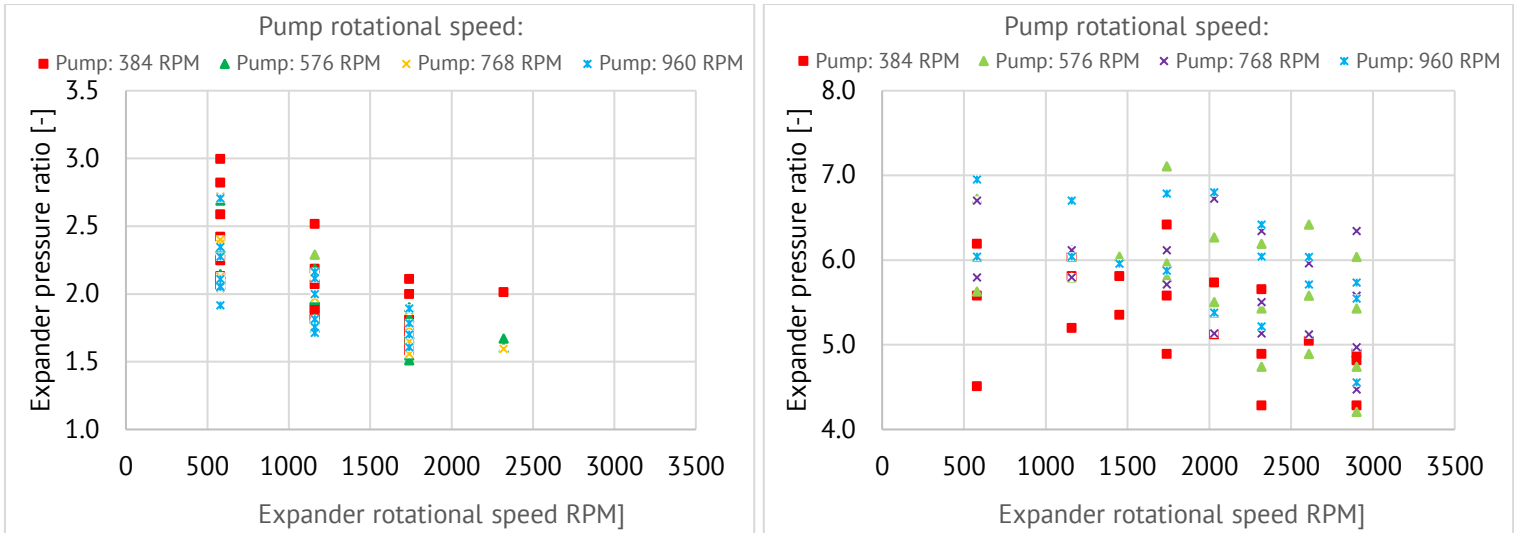
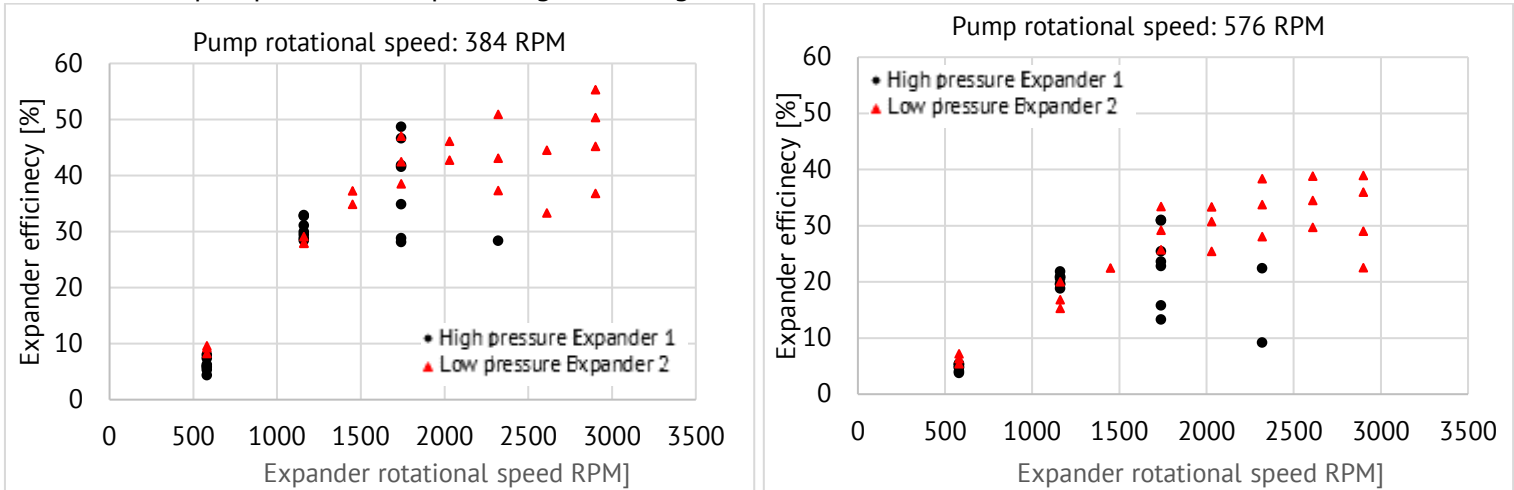


Figure 5.52 Expander's pressure ratio for the high pressure (left) and low-pressure expander (right) as a function of its rotational speed, at several pump rotational speeds -two stage operation, $T=110^{\circ}\text{C}$.

In Figure 5.52, the pressure ratio of HP expander varies between 1.5 and 3.0, roughly close to the design one and the pressure ratio of the LP expander has increased and varies between 4.5 and 7.1. The LP expander's pressure ratio increased with the temperature increase and presents a pressure ratio within the design values; however, the LP expander presents a much higher-pressure ratio than the design one for a wide operation range, revealing an overexpansion of the working fluid.

The expanders' efficiency as a function of their rotational speed for each pump rotational speed is given in Figure 5.53.



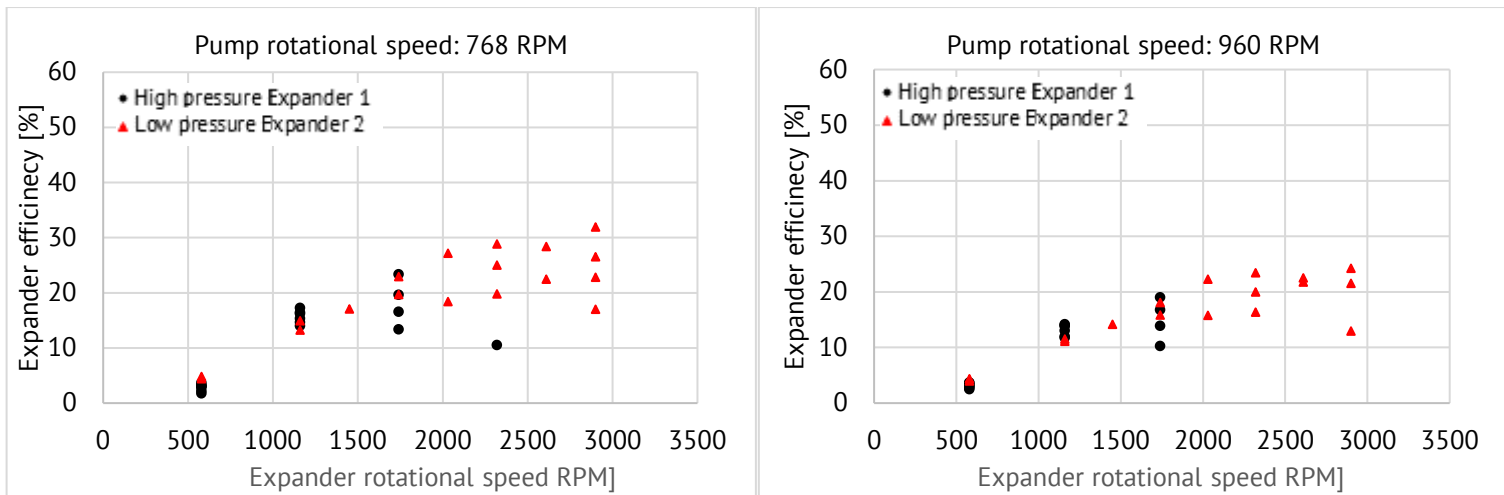


Figure 5.53 Expanders' efficiency as a function of its rotational speed, at several pump rotational speeds-two stage operation, $T=110^{\circ}\text{C}$

For low pump rotational speed, the efficiency of the HP expander varies between 5 and 50%, when the LP expander presents an efficiency between 5 and 55%. For higher pump rotational speed, the efficiency of both expanders varies between 5 and 35%. At 110°C the operation points (combination of expanders' rotational speed) are more than those of lower temperature, as the operation temperature increases, getting closer to the design temperature and the efficiency of both expanders is higher for a wider operation range.

Operation Temperature: 120°C

The operation investigation at 120°C concerning the expanders' pressure ratios for each pump rotational speed in two- stage operation as a function of the expander rotational speed is presented in Figure 5.54.

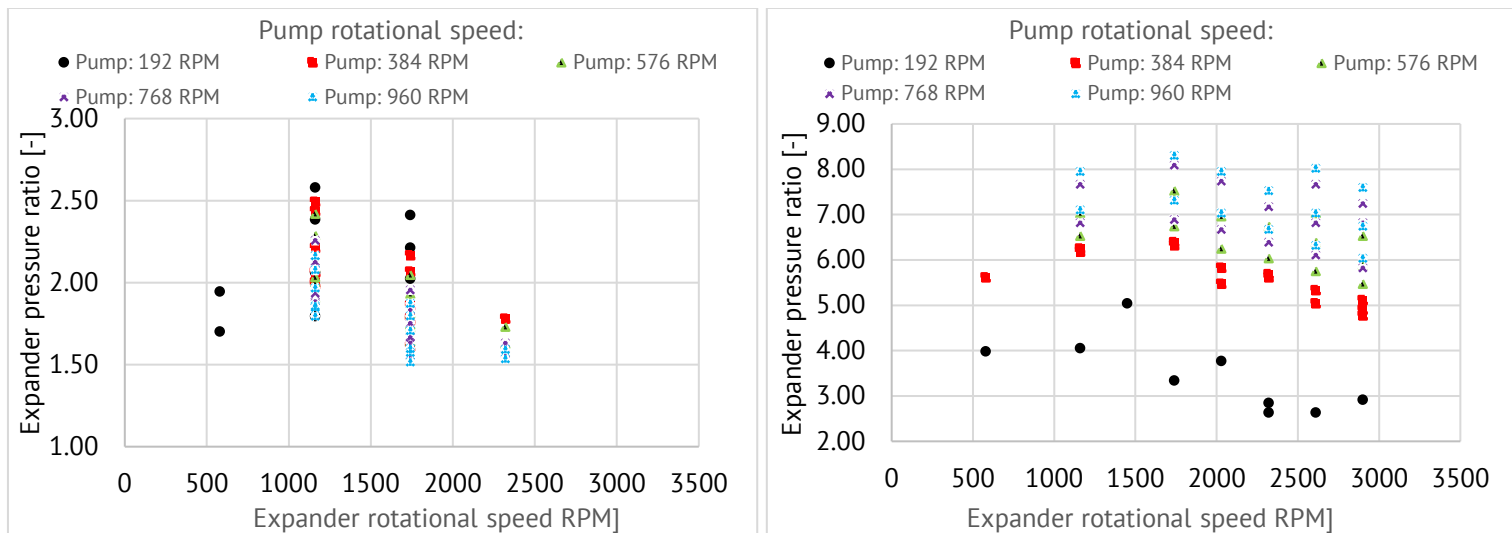


Figure 5.54 Expander's pressure ratio for the high pressure (left) and low-pressure expander (right) as a function of its rotational speed, at several pump rotational speeds -two stage operation, $T=120^{\circ}\text{C}$.

The pressure ratio of the HP expander varies between 1.5 and 2.7, under the limit of the design pressure ratio. The pressure ratio of LP expander varies between 2.5 and 8.3. The LP expander's pressure ratio increased even more with the

temperature increase and presents a pressure ratio within the design values. The HP expander's pressure ratio remains almost the same as at 110°C but the LP expander presents a much higher-pressure ratio for high pump rotational speed than the design one for a wide operation range, revealing again an overexpansion of the working fluid.

The expanders' efficiency as a function of their rotational speed for each pump rotational speed is given in Figure 5.55.

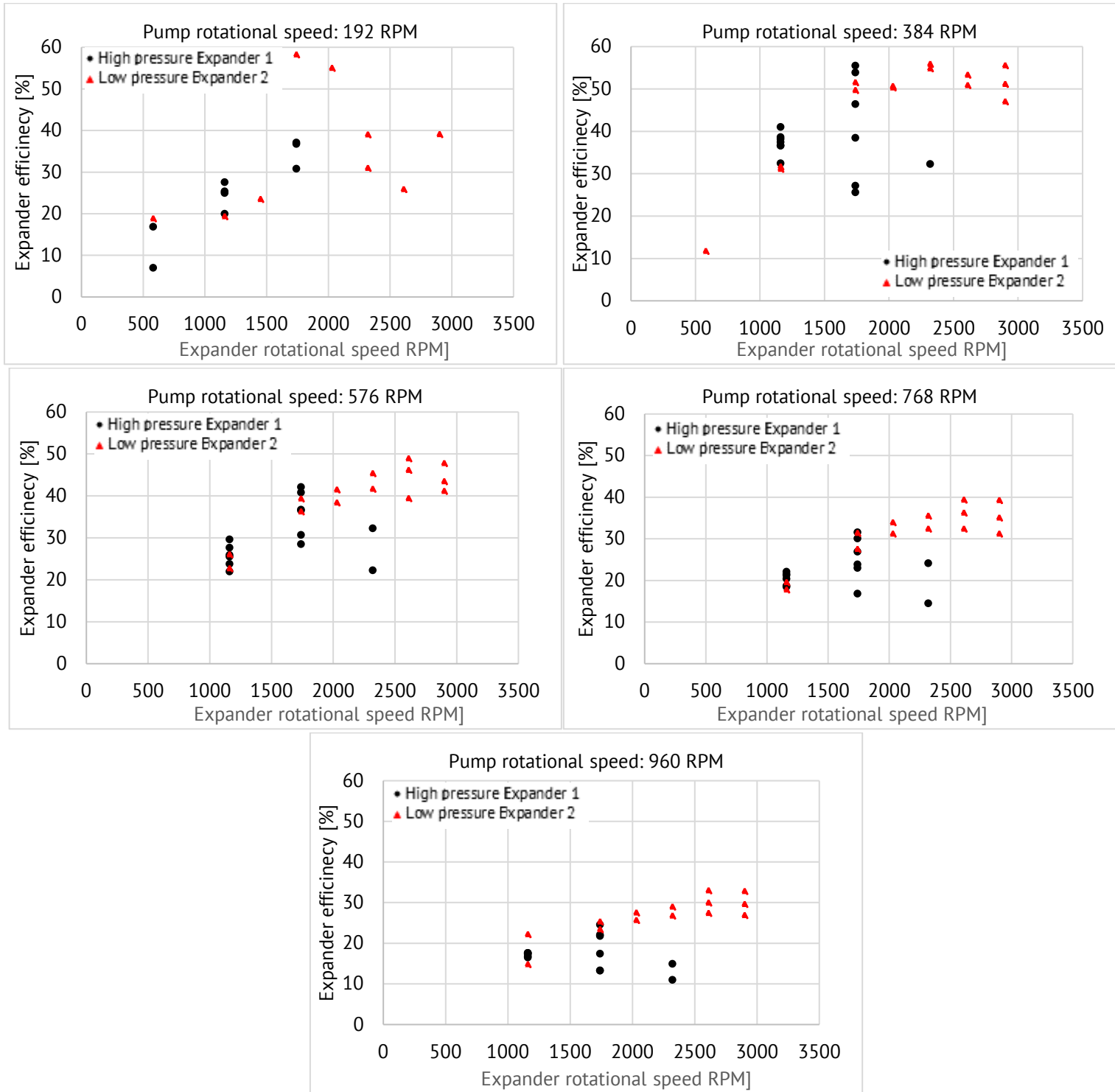


Figure 5.55 Expanders' efficiency as a function of its rotational speed, at several pump rotational speeds-two stage operation, $T=120^{\circ}\text{C}$

For low pump rotational speed, the efficiency of the two expanders reaches values of 60% when for high pump rotational speed, the efficiency of both expanders varies between 10 and 30%. The expanders' efficiency is very similar to the one at 110°C and their operation seems to stabilize.

Operation Temperature: 130°C

Finally, the operation investigation at 130 °C concerning the expanders' pressure ratios for each pump rotational speed in two- stage operation as a function of the expander rotational speed is presented in Figure 5.56.

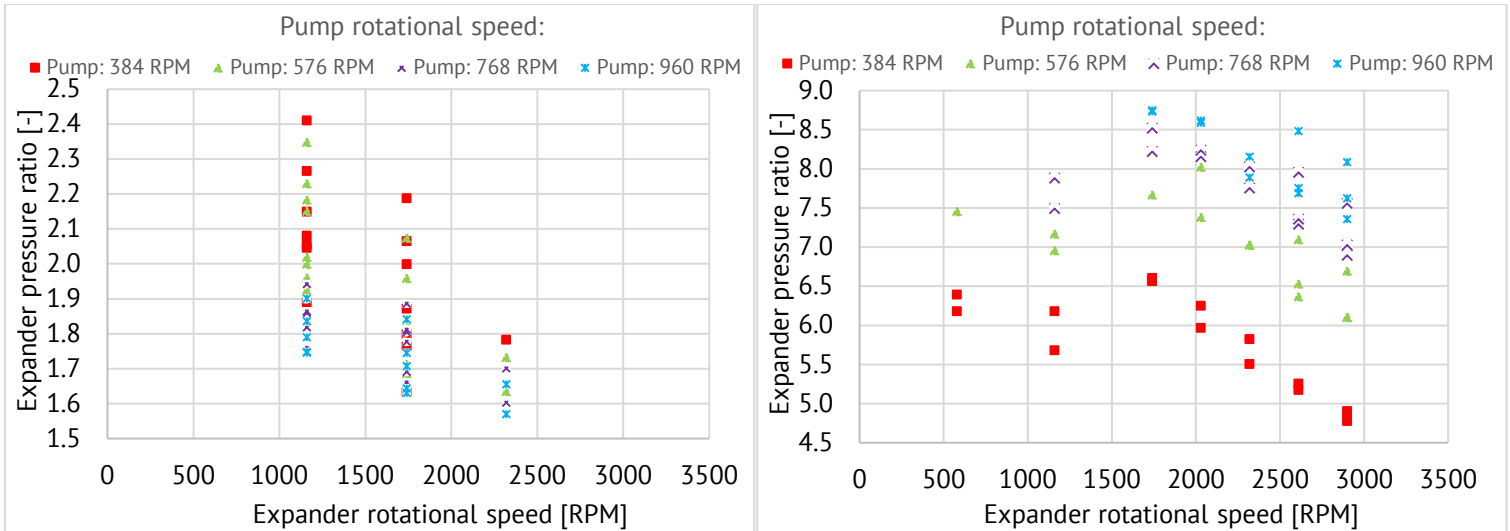


Figure 5.56 Expander's pressure ratio for the high pressure (left) and low-pressure expander (right) as a function of its rotational speed, at several pump rotational speeds -two stage operation, $T=130^{\circ}\text{C}$.

At 130°C, the expanders operated efficiently for a narrower pump rotational speed range. In Figure 5.56, the pressure ratio of the HP expander varies between 1.55 and 2.4 and the pressure ratio of the LP expander varies between 4.7 and 8.7. The LP expander's pressure ratio increased with the temperature increase and for low pump rotational speed it presents a pressure ratio within the design values; however, for higher pump rotational speed the pressure ratio is much higher than the design one for a wide operation range, revealing an overexpansion of the working fluid. On the contrary, the HP expander's pressure ratio starts to decrease at 130°C.

The expanders' efficiency as a function of their rotational speed for each pump rotational speed is given in Figure 5.57.

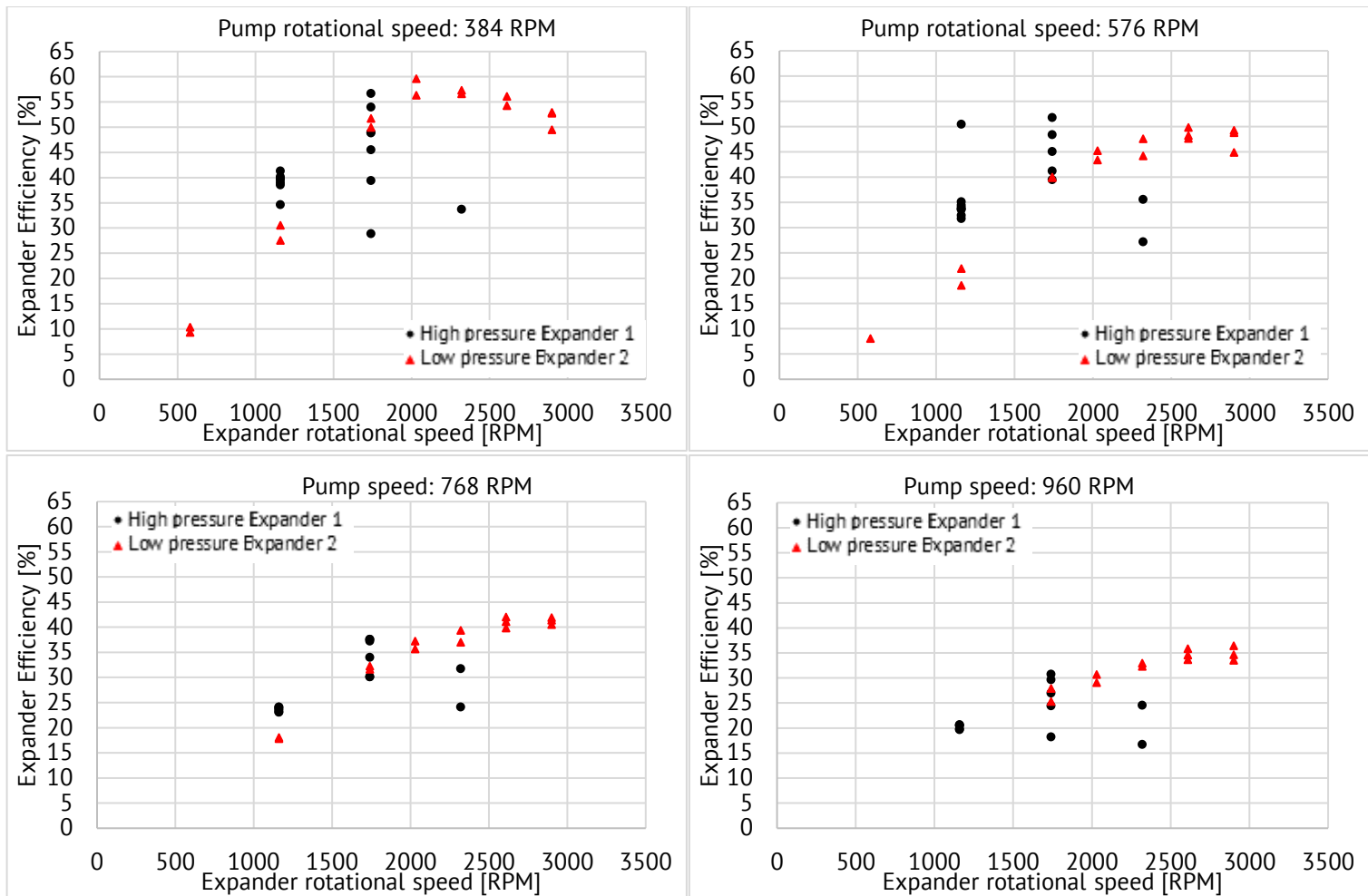


Figure 5.57 Expanders' efficiency as a function of its rotational speed, at several pump rotational speeds-two stage operation, $T=130^{\circ}\text{C}$

For low pump rotational speed, the efficiency of both expanders varies between 10 and 60%, while for higher pump rotational speed, the efficiency of both expanders varies between 15 and 40%.

As derived from the above figures, the expanders best operation is noticed at operating temperature of 120- 130°C, as was expected per design. However, in all cases the HP expander presents a considerably low-pressure ratio compared to the design one and compared to the LP expander.

A comparison of the volume flow rate at the inlet of each expander when operating at the same rotational speeds and constant pump rotational speed will help understanding their operation, therefore the operation at the highest temperature of 130 °C is chosen and the indicative diagram is presented in Figure 5.58.

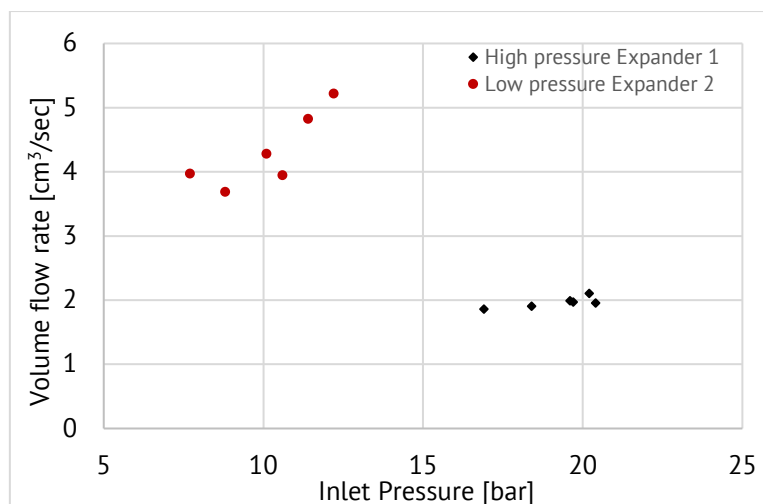


Figure 5.58 Volume flow rate at the HP and LP expander inlet respectively as a function of the inlet pressure, for each pump rotational speed and for the same expanders' rotational speed - two stage operation.

It can be observed that the volume flow rate of the HP expander is roughly half of the LP expander for the same expander rotational speed (for a pre-defined pump rotational speed). Therefore, the argument that the HP expander is of smaller capacity is confirmed, since the volume flow rate is much lower and the inlet pressure relatively higher in comparison to the LP expander.

5.3 Conclusions

The experimental results of the two-stage ORC engine tested at the laboratory for both single and two-stage operation at a wide operating temperature range have been presented, revealing its performance capability. The HTF used was water for low operating temperature (70, 85 and 95 °C) and MEG for high operating temperature (110, 120 and 130 °C) with variable heat input. This heat is provided by an electric heater and is controlled with the speed variation of the organic fluid pump, as explained in Chapter 3.

The ORC engine evaluation for single and two-stage operation showed that the best operation is noticed at 120 ~ 130 °C, where the net power production reaches values of 7.5 kW and the engine efficiency is around 9.9%, which is very close to the design value of 10%. Moreover, it has been proven that the ORC engine presents an efficient and sufficient operation both in single stage mode and in lower operating temperatures, since the net power production in these cases is more than half the maximum value and the efficiency remains around 6~7 %, which is very sufficient for such far from design operating conditions. Especially the two-stage net power production and thermal efficiency investigation for operation at lower HTF temperatures showed that even at these conditions the two-stage system keeps a sufficiently high performance.

The two modified hermetic scroll expanders (compressors in reverse operation) that are used for power production require a separate performance evaluation, presented in the current chapter. Various parameters have been examined, when regulating the expanders and pump speed, exhibiting the heat-to power conversion efficiency of such engine. Moreover, the expansion efficiency investigation has shown an average of 62% at single stage operation and an average of 61% for two-stage operation. The low-pressure expander presented an efficiency increase with the increase of its rotational speed, while the efficiency of

the high-pressure expander decreased for high rotational speed, due to the fact that it could no longer manage efficiently the volume flowrate. The pressure ratio of the HP expander was constantly low revealing an under- expansion, when the pressure ratio of the LP expander was significantly high presenting an overexpansion. Additionally, the LP expander was characterized by a wider range of operation (proven by the availability of much more operational points) for each predefined pump rotational speed. As resulted from the tests and especially for two-stage operation, the high-pressure (first) expander was proven to be slightly smaller than designed.

The evaluation of the ORC engine resulted in an efficient performance concerning the power production and the cycle's efficiency, close to the design. However, most importantly, the two-stage system presented a remarkable flexibility, since even at low thermal input with the by-pass of the low-pressure expander, the system operated with an acceptable power output. In the present chapter, the real test data are presented and the advantages and potential of such technology are identified. Also, concrete proof is provided, whether a two-stage ORC system can be indeed more efficient than a single stage one, and if the theoretical assumptions can be verified. The system tested shows that the two stages expansion offers flexibility and these results deploy the potential of this technology, which appears to be promising possibly in combination with renewable energy heat sources.

References:

- 5.1 Manolakos D, Kosmadakis G, Kyritsis S, Papadakis G. Identification of behaviour and evaluation of performance of small scale, low-temperature Organic Rankine Cycle system coupled with a RO desalination unit. *Energy* 2009;34(6):767–74.
- 5.2 Manolakos D, Kosmadakis G, Kyritsis S, Papadakis G. On site experimental evaluation of a low-temperature solar organic Rankine cycle system for RO desalination. *Solar Energy* 2009;83(5):646–56.

CHAPTER 6 – Theoretical investigation and evaluation of the integrated system

6.1 Introduction

In Chapters 4 and 5, the two sub- systems of the RO unit and the ORC engine have been thoroughly investigated and evaluated in several operation conditions. Both systems have been installed and tested in the National Technical University of Athens Laboratory of Hydraulic Turbomachines, however in a different timetable. Due to the fact that the ORC engine was built by scratch, therefore its installation was delayed in comparison to the RO unit installation and due to some other time schedule issues of the European program within which this experimental evaluation took place, the connection of the two systems and the experimental evaluation of the integrated system were made impossible.

However, the data that derived for each system's operation are more than enough for a theoretical evaluation of the integrated system, meaning the integrated system's performance in case they were electrically connected. In the current chapter, two cases of operation at 120 and 130 °C (design point) of the ORC engine both in single and two- stage mode are presented where the net power produced by the expander(s) would be driven to the RO unit. The RO unit is considered to operate for the desalination of high water salinity, since this is the design point of the specific set- up. As the experimental investigation of the RO unit has resulted in fresh water production of a good quality within the potable water limits for the whole operation range, the fresh water quality is not examined in the current Chapter, as it is considered acceptable and good throughout the whole operation range of the integrated system.

This theoretical evaluation will help to the examination of the flexibility of such a system to operate at variable conditions, thus with several different renewable energy heat sources. For simplicity reasons and for the current analysis, the electric loss from the electric connection between the expanders' output and the RO electric panel is neglected, meaning that all the net power production from the expanders is directed entirely to the RO units' electric panel with no conversion losses.

6.2 Operation at 120°C: Single and two- stage operation, high water salinity

In Chapter 5, the net power production of the ORC engine for single and two- stage operation derived as per Figure 5.31 which is reminded in Figure 6.1.

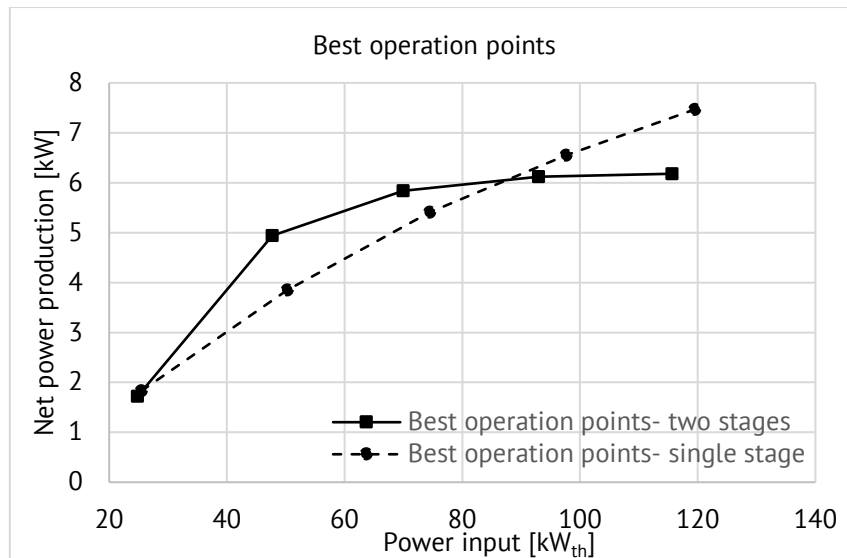


Figure 6.1 Total power production of the expander overview for the best operation points of the ORC engine, single and two- stage operation comparison at 120°C

In case that the three sub- units where electrically connected to the ORC engine, the net power production would be exploited for their operation. The experimental investigation of the RO unit revealed the operation at different power input as per Figure 4.22, reminded in Figure 6.2

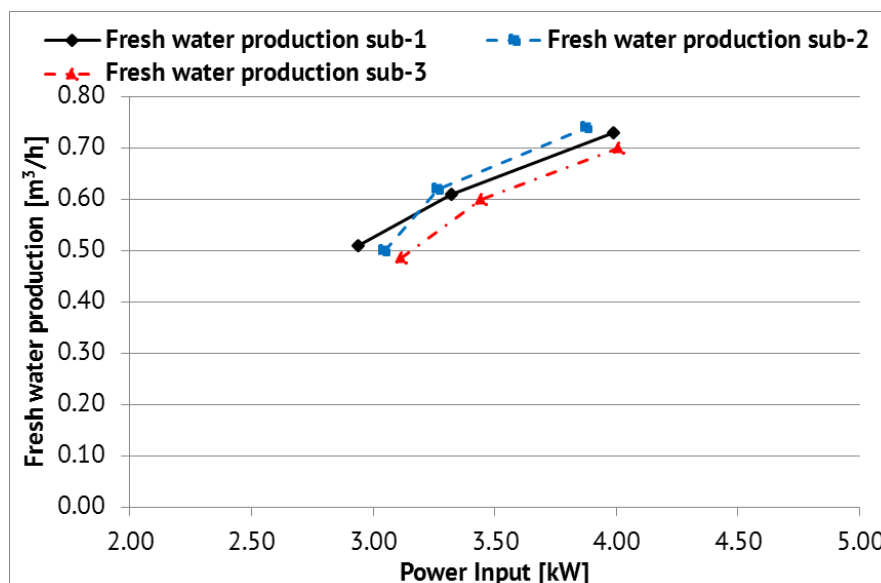


Figure 6.2 Fresh water production as a function of the power input for the three sub- units (high water salinity)

Moreover, the fresh water production as a function of the power input for the whole RO unit is presented in Figure 6.3, where the fresh water production starts from 0.50 m³/h for operation of only the first sub- unit and reaches a maximum of ~2.3 m³/h for full operation of all three sub- units.

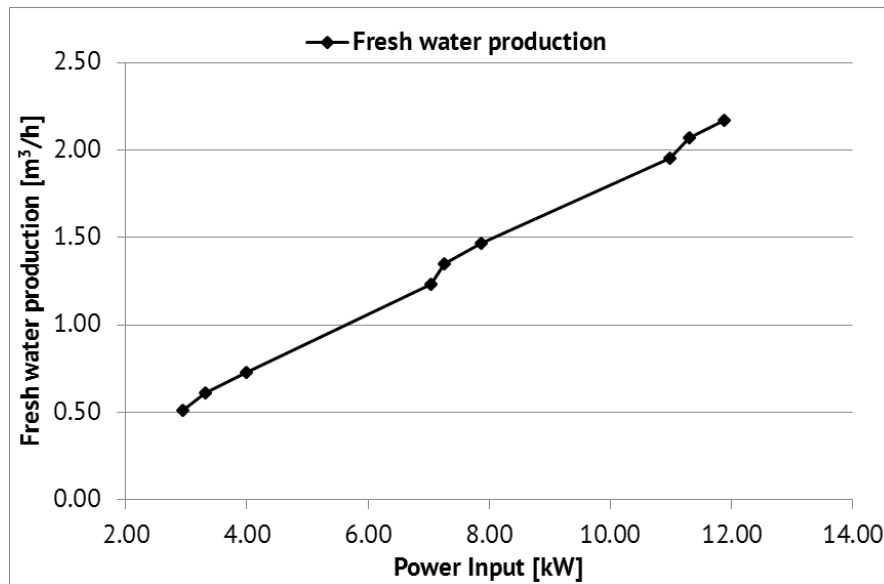


Figure 6.3 Fresh water production as a function of the total power input for the whole RO unit

Based on the aforementioned results, the RO unit operation and fresh water production for the whole operation range of the ORC engine can derive.

In Figure 6.4, the operation profile concerning the fresh water production for each sub- unit with electricity from the ORC engine for **single- stage operation**, throughout the whole operation range is presented.

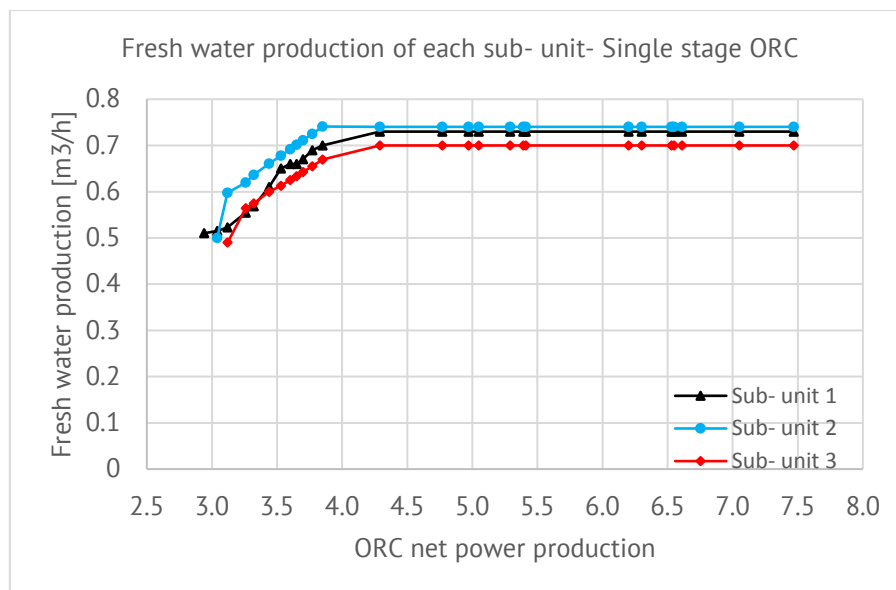


Figure 6.4 Fresh water production from each sub- unit as a function of the total power input from the ORC engine at single- stage operation, $T=120\text{ }^{\circ}\text{C}$

As presented in Figure 6.4, all three sub- units operate for the most of the operation range of the ORC engine producing the maximum fresh water quantities according to their design. For the first sub- unit, the fresh water production starts at 2.9 kW from the ORC engine and has a value of 0.5 m³/h. The second sub- unit starts operating at 3.1 kW producing ~0.5 m³/h and the third sub- unit starts operating at 3.2 kW producing ~0.49 m³/h. From ~4 kW all three sub- units operate producing their maximum capacity of 0.7 to 0.72 m³/h.

The operation of the whole RO unit powered by the ORC engine at single stage operation is presented in Figure 6.5.

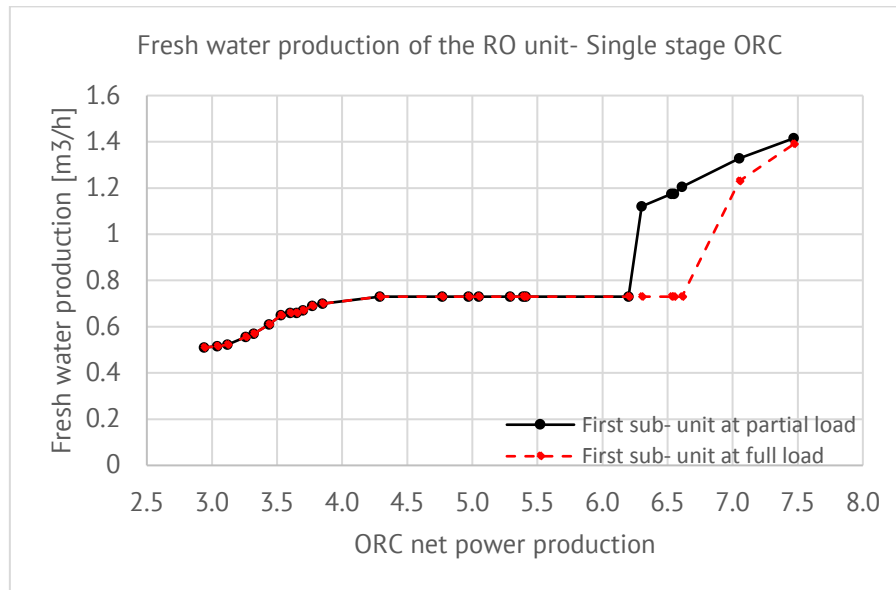


Figure 6.5 Fresh water production from the whole RO unit as a function of the total power input from the ORC engine at single- stage operation, $T=120\text{ }^{\circ}\text{C}$

The fresh water production starts from $0.50\text{ m}^3/\text{h}$ for operation of only the first sub- unit and reaches a maximum of $1.47\text{ m}^3/\text{h}$ for full operation the two sub- units. According to Figure 6.3, the second sub- unit starts operating at 7 kW input and the third at 10.9 kW input, therefore, considering that each sub- unit starts operating when the previous has reached its maximum capacity, the third sub- unit does not operate up to 10.9 kW offered by the ORC engine. The dotted line of Figure 6.5 shows exactly this case where the second sub- unit starts to operate when the first sub- unit has reached its maximum capacity and continuous to operate at maximum capacity. Then, the second sub- unit starts operating adding some $0.5\text{ m}^3/\text{h}$ to the maximum production of $0.73\text{ m}^3/\text{h}$ of the first sub- unit.

The continuous line of Figure 6.5 presents the case where at $\sim 6.2\text{ kW}$ the second sub- unit starts operating, but both the first and the second sub- unit operate at a lower pump rotational speed (partial load operation) consuming $\sim 3.1\text{ kW}$ each. In this case, the SEC of each sub- unit is lower and as presented in Figure 6.5, the resulted fresh water production for a power input between 6.2 and 7.5 is slightly higher than in the previous case.

The same theoretical investigation for the operation of the integrated system for **two- stage ORC operation** is presented in Figures 6.6. and 6.7.

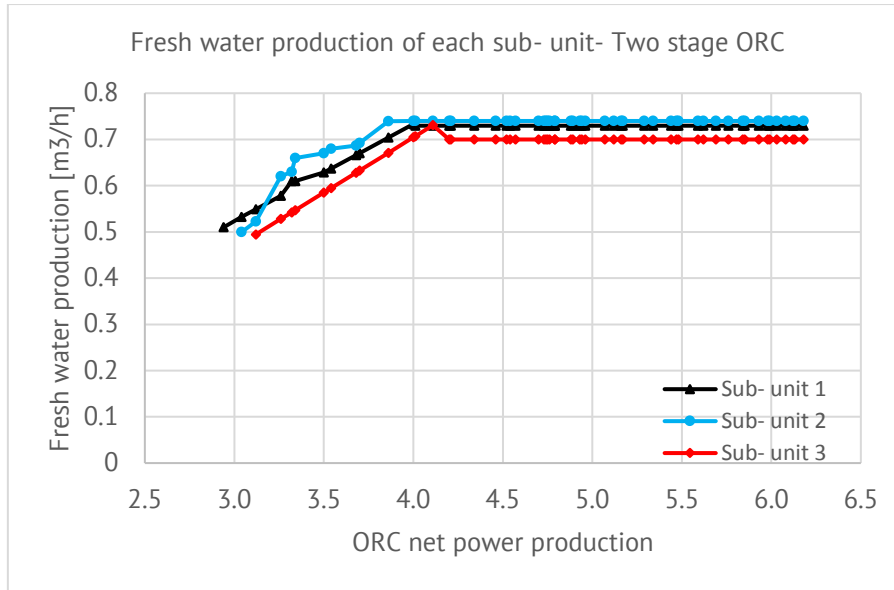


Figure 6.6 Fresh water production from each sub- unit as a function of the total power input from the ORC engine at two- stage operation, $T=120\text{ }^{\circ}\text{C}$

In Figure 6.6, the operation profile concerning the fresh water production for each sub- unit with electricity from the ORC engine for two- stage operation, throughout the whole operation range is presented. The results are similar to the single- stage ORC operation, however, the power production of the ORC engine in this case reaches a maximum of 6.1 kW. According to the aforementioned analysis of Figure 6.5, where it was mentioned that the second sub- unit would start to operate either at $\sim 7\text{ kW}$ (with the first sub- unit operating at full load) or at $\sim 6.2\text{ kW}$ (where both sub- units would operate at partial load consuming $\sim 3.1\text{ kW}$ each), it is expected that only the first sub- unit would operate in two- stage ORC mode, as presented in Figure 6.7.

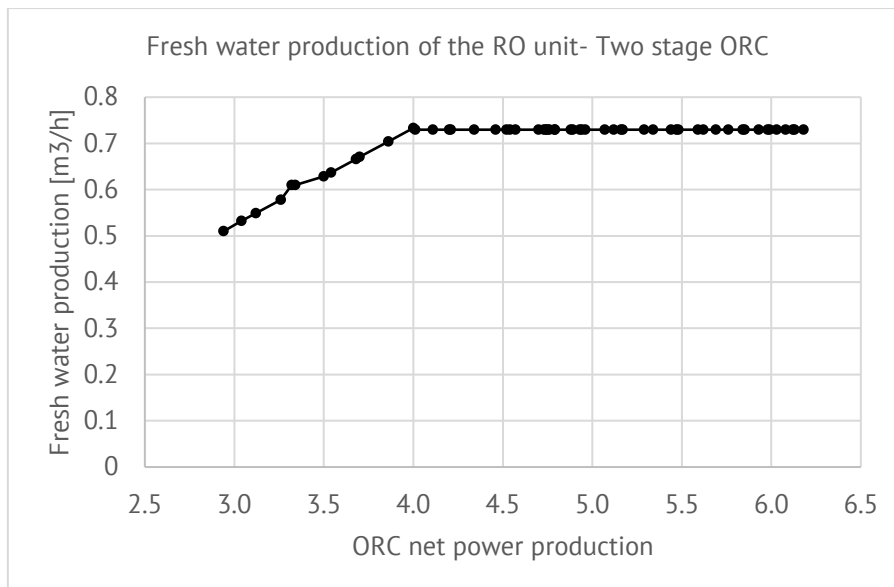


Figure 6.7 Fresh water production from the whole RO unit as a function of the total power input from the ORC engine at two- stage operation, $T=120\text{ }^{\circ}\text{C}$

A very interesting fact that derives from the above analysis is that for ORC operation temperature of $120\text{ }^{\circ}\text{C}$, the single stage operation shows a slightly better

performance with a higher net power production, leading to a better overall performance of the integrated system with two of the three RO sub- units operating.

One more case of ORC operation temperature at 130 °C is presented next, in order to get a clearer picture of the integrated system operation at the design point.

6.3 Operation at 130°C: Single and two- stage operation, high water salinity

In Chapter 5, the net power production of the ORC engine for single and two-stage operation derived as per Figure 5.38 which is reminded in Figure 6.8.

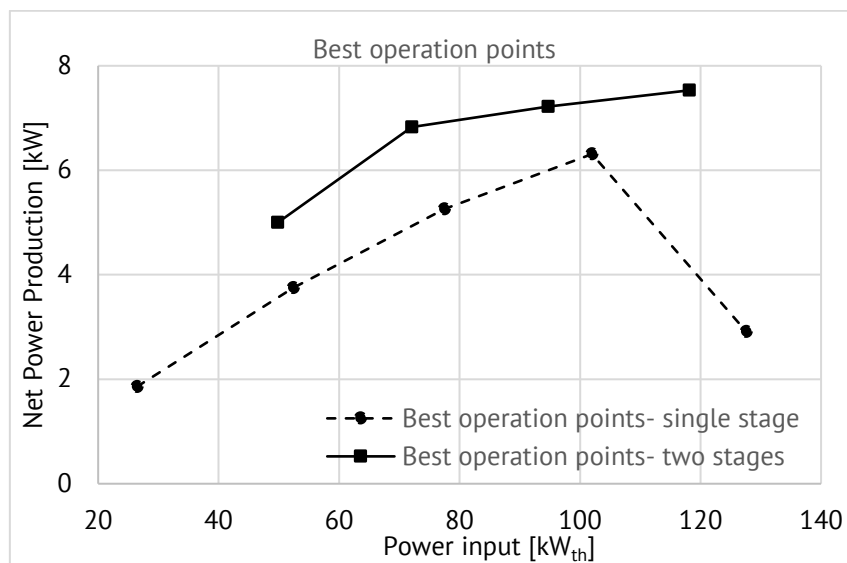


Figure 6.8 Total power production of the expander overview for the best operation points of the ORC engine, single and two- stage operation comparison at 130°C

Taking again into consideration the RO unit operation of Figures 6.2 and 6.3, the integrated system operation at 130 °C can be evaluated. In Figure 6.9, the operation profile concerning the fresh water production for each sub- unit with electricity from the ORC engine for **single- stage operation**, throughout the whole operation range is shown.

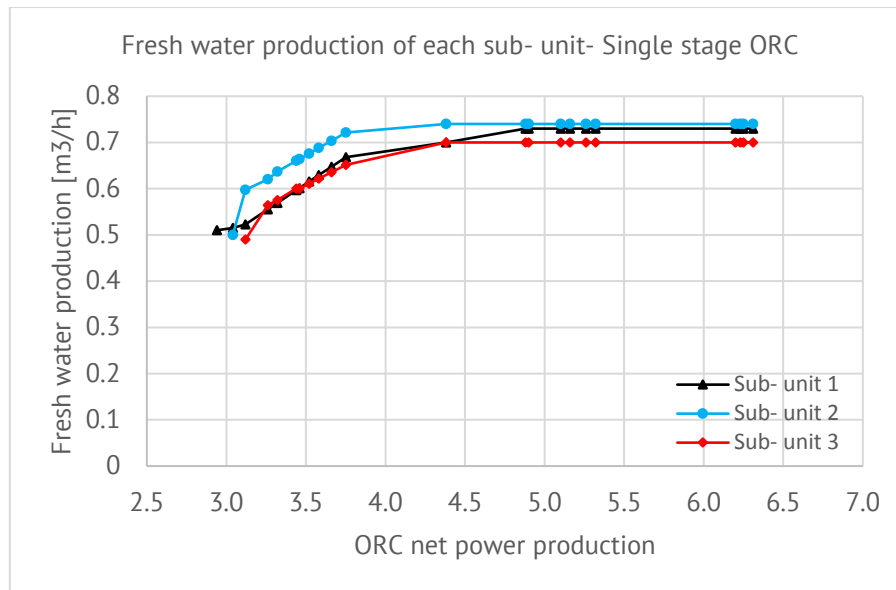


Figure 6.9 Fresh water production from each sub-unit as a function of the total power input from the ORC engine at single-stage operation, $T=130\text{ }^{\circ}\text{C}$

Once again, all three sub-units operate for the most of the operation range of the ORC engine producing the maximum fresh water quantities according to their design. For the first sub-unit, the fresh water production starts at 2.9 kW from the ORC engine and has a value of $0.5\text{ m}^3/\text{h}$, for the second sub-unit at 3.1 kW producing $\sim 0.5\text{ m}^3/\text{h}$ and the third sub-unit at 3.2 kW producing $\sim 0.49\text{ m}^3/\text{h}$. From $\sim 4\text{ kW}$ all three sub-units operate producing their maximum capacity of 0.7 to $0.72\text{ m}^3/\text{h}$.

The operation of the whole RO unit powered by the ORC engine at single stage operation is presented in Figure 6.10.

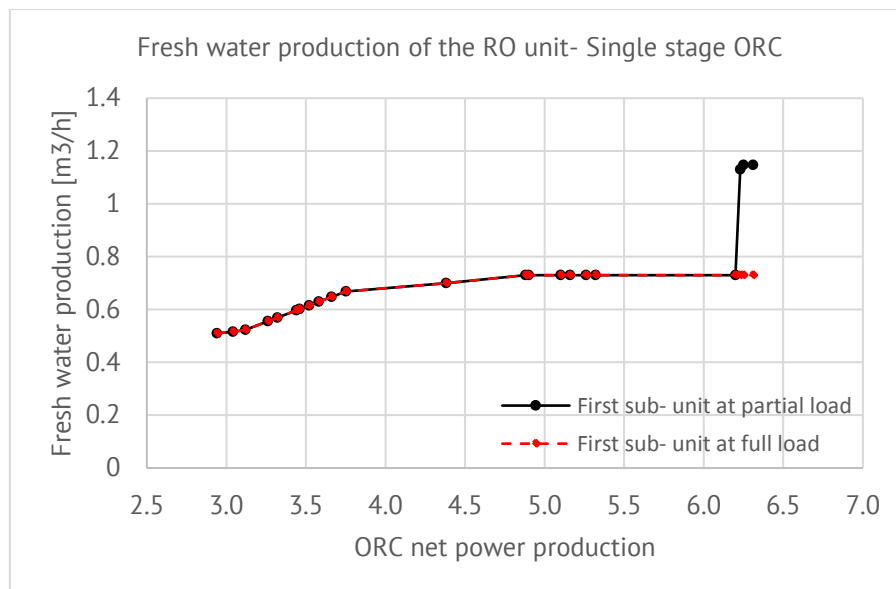


Figure 6.10 Fresh water production from the whole RO unit as a function of the total power input from the ORC engine at single-stage operation, $T=130\text{ }^{\circ}\text{C}$

The fresh water production starts from $0.50\text{ m}^3/\text{h}$ for operation of only the first sub-unit. The dotted line of Figure 6.10 shows the case where only the first sub-unit operates at its maximum capacity and the power production from the

ORC cannot start any other sub- unit. The maximum fresh water production in this case is $\sim 0.7 \text{ m}^3/\text{h}$.

The continuous line of Figure 6.10 presents the case where at $\sim 6.2 \text{ kW}$ the second sub- unit starts operating, but both the first and the second sub- unit operate at a lower pump rotational speed (partial load operation). In this case, the SEC of each sub- unit is lower and as presented in Figure 6.10, the resulted fresh water production for a power input between 6.2 and 6.3 is much higher than in the previous case, reaching a maximum of $1.14 \text{ m}^3/\text{h}$.

In Figure 6.11, the operation profile concerning the fresh water production with electricity from the ORC engine for **two- stage operation**, throughout the whole operation range is presented.

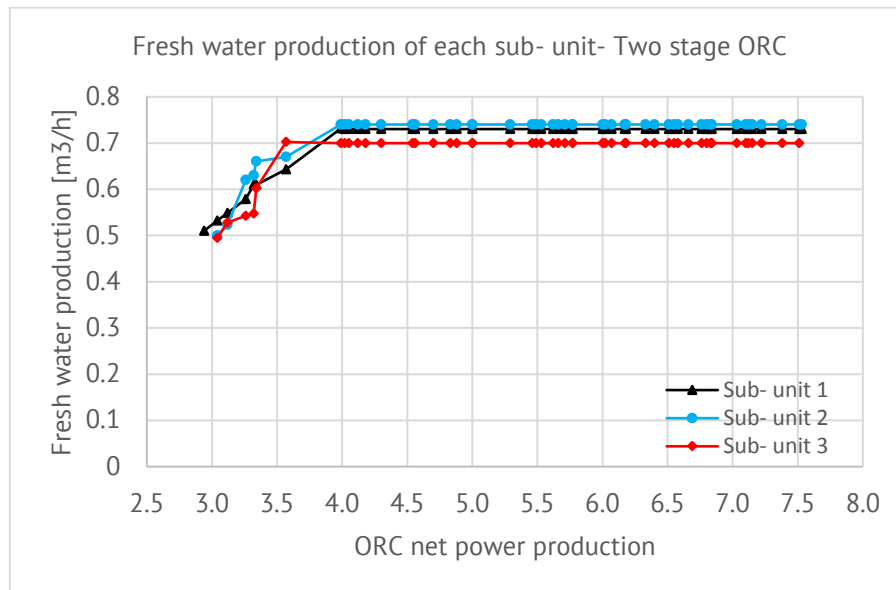


Figure 6.11 Fresh water production from each sub- unit as a function of the total power input from the ORC engine at two- stage operation, $T=130 \text{ }^\circ\text{C}$

The results are similar to the single- stage ORC operation, however, the power production of the ORC engine in this case reaches a maximum of 7.5 kW , which is the maximum net power production from the ORC engine, as resulted from the experimental investigation of Chapter 5. In Figure 6.12, the operation of the whole RO unit in two- stage ORC operation at $130 \text{ }^\circ\text{C}$ is presented, both for full and partial load operation of the first sub- unit.

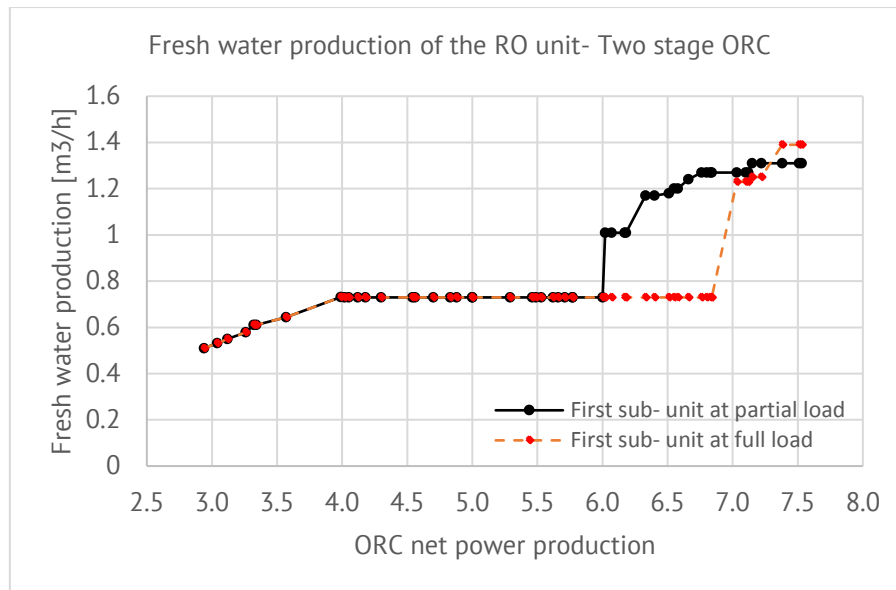


Figure 6.12 Fresh water production from the whole RO unit as a function of the total power input from the ORC engine at two- stage operation, $T=130\text{ }^{\circ}\text{C}$

A very interesting fact that derives from Figure 6.12 is that for the case of the full load operation of the first sub- unit, where the first sub- unit operates producing the maximum capacity of $0.73\text{ m}^3/\text{h}$ until at $\sim 7\text{ kW}$ the second sub- unit starts operating, adding to the fresh water production, the maximum fresh water production reaches a value of $\sim 1.4\text{ m}^3/\text{h}$. On the other hand, the case where the first and second sub- units operate at partial load ($\sim 3\text{ kW}$ each) the total maximum fresh water production is $\sim 1.3\text{ m}^3/\text{h}$. Even if the maximum fresh water production value is slightly lower in the second case, the fresh water production is higher for a wider power range (6 to 7.2 kW), the SEC of each sub- unit is lower and the operation of the integrated system much smoother.

6.4 Conclusions

In the current chapter, a theoretical investigation of the integrated system operation based on the experimental results of the sub- systems has been presented. The net power production of the ORC engine both in single and two- stage operation at 120 and 130 $^{\circ}\text{C}$ (design point) has been driven to the RO unit in order to examine the fresh water production and the sub- units' operation. In Chapter 4, the experimental investigation of the RO unit had shown that the unit had been a little oversized for the specific designed and constructed ORC engine, since the operation of all three sub- units required a power input higher than 10 kW which is the production limit of this ORC engine. With the current theoretical investigation this has been verified, since the third sub- unit has not operated at all. The maximum net power production of the ORC engine was noticed at 130 $^{\circ}\text{C}$, two- stage operation with a value of 7.58 kW, capable to operate only two of the three sub- units. However, the fresh water production of a good quality and quantity has been noticed throughout the whole operation range both for 120 and 130 $^{\circ}\text{C}$ and the maximum production has reached $\sim 1.4\text{ m}^3/\text{h}$, not that much lower than the design of $2.1\text{ m}^3/\text{h}$. Moreover, the flexibility of the system has been noticed with the operation of more than one sub- unit and the comparison of the one sub- unit operation at full load with the operation of two sub- units at partial load has

shown that the partial load operation leads to a higher fresh water production for a wider load range and a much smoother operation of the whole system. In addition, at 130 °C, the better performance at the two- stage ORC engine operation is obvious.

A general overview of the integrated system, even if a slight sub- operation of the RO unit has been noticed compared to the theoretical design of the unit, results that the integrated system operation has been sufficient and efficient throughout the whole operation range.

CHAPTER 7 – Thesis appraisal- Future work suggestions

7.1 Synopsis

In the current thesis, a hybrid energy desalination system based on the reverse osmosis method which operates with electricity from a two- stage organic Rankine cycle engine has been evaluated. More specifically, the current thesis focused on the below subjects:

- Numerical simulation, design, selection of equipment and installation at the laboratory of a RO desalination unit, consisting of three identical sub-units for operation at variable power input.
- Investigation on a case study of a multi- skid RO system connected to a Photovoltaic (PV) field of several capacities in comparison to one conventional RO unit for a typical winter and a typical summer day, in order to ensure the flexibility of the selected asset for the current research. Comparison of operation in three different places (Greece, Spain and UAE).
- Numerical simulation, design, construction and installation at the laboratory of a two- stage ORC engine for operation and power production at variable thermal load input, in order to investigate the operation in a wide load range up to 130 °C and the efficiency improvement in comparison to the single- stage one. Sizing of the engine and selection of the appropriate consisting components (i.e. the pressure pump, the expanders, the evaporator, the condenser etc.)
- Selection of the appropriate organic fluid for the best ORC engine performance under the design conditions.
- Design and modification of the two scroll expanders from market available scroll compressors in order to fulfill the research requirements, and separate evaluation of their performance.
- Experimental investigation of the RO unit in variable power input for different feed water salinities and in different feed water temperatures.
- Experimental investigation of the ORC engine for single and two- stage operation for several operating temperatures (from 70 to 130 °C) and with different heat transfer fluid on the power cycle (water for low temperature and MEG for high temperature).
- Theoretical evaluation of the integrated system for high feed water salinity, for single and two- stage ORC engine operation at 120 and 130 °C.

The main scope of the developed system was the evaluation of the flexibility of such a system to operate efficiently in variable power input coming from renewable energy sources. At the laboratory, the heat cycle representing the heat source of variable load was simulated with the help of an electric heater.

7.2 Overall conclusions

Following a detailed analysis of the simulation model development, both for the ORC engine and the RO unit, the resulted outline was presented and the organic fluid selection resulted in R245fa, extensively justified as well as the chosen two-stage ORC configuration with two scroll expanders in series. All the components of the ORC engine have then been outlined in order to specify their properties and conclude to a specific design and the RO unit with its three sub- units were carefully designed, based on the power available from the ORC engine that would feed this system. Both ORC and RO systems were tested as per their design in partial and full load operation, where full load was the barrier set as the maximum heat power input to the system from a low temperature heat source (equal to 100 kW_{th}).

Based on the detailed design, the next step was the selection of the components that would be combined to construct the prototype of the thesis, in order to be experimentally evaluated and to validate or cancel the accuracy of the design. The prototype design and construction were developed and all measurement instrumentation and measurement locations on the system were selected. The heat source cycle setting was defined and all the ORC components' selection was justified and presented in detail. Special care was given to the explanation of the scroll expanders' modification, presenting step- by- step the scroll compressors' transformation into expanders. The reason for this modification was that there were no market available scroll expanders for the current application but there were market available scroll compressors accordingly. The RO unit and each sub- unit were also presented in detail. Finally, the ORC assembly and the RO unit assembly were installed in the laboratory, resulting in the integrated prototype test- rig.

7.2.1 Conclusions on the RO unit operation

The RO unit implemented to operate in a wide load range at the laboratory with variable power input was first investigated. All three sub- units of the system were examined in switchable operation according to the available load and for three different feed water salinities. Each sub- unit operation as well as the whole RO unit investigation showed that such a system is able to produce fresh water of good quality throughout the whole available power input range, due to the fact that it consists of three identical sub- units. The specific energy consumption has been kept low, even though for high salinity it reached a slightly higher value due to the fact that the sub- units' HP pumps operated at lower rotational speed than the nominal one, so the power needed for the production of a cubic meter of fresh water was higher. It was also noticed that for high feed water salinities (>30.000 ppm) the total power demand exceeded the available power of 10 kW, expected to be fed from the ORC engine that was to be electrically connected to the RO unit. This led to the assumption that the RO unit operated in slightly different test conditions (i.e. feed water quality, temperatures etc.) in comparison to the design that preceded or that it might resulted to be a little oversized. Membranes' and HP pump's operation for all three sub- units was proven to be efficient and the slight differences that occurred were due to some measurement instrumentation uncertainty. However, these differences laid within acceptable limits throughout the whole operation. The fresh water production slightly exceeded the maximum value of 2.1 m³/h and for lower HP pumps' rotational speed than the nominal one, as well as the power demand exceeded the expected of 10 kW in comparison to the design.

The next step of investigation was the temperature effect on the RO unit operation for a constant feed water salinity of 37500 ppm. At low temperature the RO unit operation resulted to be relatively steady. At high temperature of 23 °C the SEC and the fresh water salinity of the RO unit resulted to be slightly poorer, however, the RO unit investigation has shown that such a system is able to produce fresh water of acceptable quality throughout the whole available power input range. The membranes operation, as well as the HP pump operation, were proven to be efficient at any water temperature.

Case- studies of the operation of the RO desalination unit consisting of several sub- units, powered by a PV system in different locations for different installed capacity were also examined. The results of these studies verified the offered flexibility of such a system. In addition, the comparison on the fresh water production to a conventional RO unit of similar capacity showed that the multi- skid system operated within a larger load range, producing more fresh water in some cases than the conventional unit system.

The configuration tested, undoubtedly offers flexibility and can secure an acceptable fresh water quality at all operating conditions from very low load up to the maximum one. These results are remarkable in order to further improve such integrated systems with increased performance, while at the same time they show promising improvement for future commercialized systems, powered by renewable energy sources.

7.2.2 Conclusions on the ORC engine operation

The experimental results of the two-stage ORC engine tested at the laboratory for both single and two-stage operation at a wide operating temperature range were presented, revealing its performance capability.

The ORC engine evaluation for single and two- stage operation showed that the best operation was noticed at 120 ~ 130 °C, where the net power production reached values of 7.5 kW and the engine efficiency was around 9.9%, almost the design value of 10%. In addition, it was proven that the ORC engine presents an efficient and sufficient operation both in single stage mode and in lower operating temperatures, since the net power production in these cases was more than half the maximum value and the efficiency remained around 6~7 %, which was very sufficient for such far from design operating conditions. Especially the two-stage net power production and thermal efficiency investigation for operation at lower HTF temperatures showed that even at these conditions the two-stage system kept a sufficiently high performance.

The two modified hermetic scroll expanders that are used for power production required a separate performance evaluation. Various parameters have been examined, when regulating the expanders and pump speed, exhibiting the heat-to power conversion efficiency of such engine. The expansion efficiency investigation showed an average of 62% at single stage operation and an average of 61% for two-stage operation. The low-pressure expander presented an efficiency increase with the increase of its rotational speed, while the efficiency of the high-pressure expander decreased for high rotational speed, due to the fact that it could no longer manage efficiently the volume flowrate. The pressure ratio of the HP expander was constantly low revealing an under- expansion, when the pressure ratio of the LP expander was significantly high presenting an overexpansion. Additionally, the LP expander was characterized by a wider range of operation for each predefined pump rotational speed. As resulted from the tests and especially for two-stage operation, the high-pressure (first) expander was proven to be slightly smaller than designed.

The evaluation of the ORC engine resulted in an efficient performance concerning the power production and the cycle's efficiency, close to the design. However, most importantly, the two-stage system presented a remarkable flexibility, since even at low thermal input with the by-pass of the low-pressure expander, the system operated with an acceptable power output. Moreover, concrete proof was provided, whether a two-stage ORC system can be indeed more efficient than a single stage one, and that the theoretical assumptions could be verified. The system tested showed that the two stages expansion offers flexibility and these results deploy the potential of this technology, which appears to be promising, possibly in combination with renewable energy heat sources.

7.2.3 Conclusions on the integrated system theoretical operation evaluation

A theoretical investigation of the integrated system operation based on the experimental results of the sub- systems was also presented. The net power production of the ORC engine both in single and two- stage operation at 120 and 130 °C (design point) was driven to the RO unit in order to examine the fresh water production and the sub- units' operation. As mentioned before, the experimental investigation of the RO unit had shown that the unit was a little oversized for the specific designed and constructed ORC engine, since the operation of all three sub- units required a power input higher than 10 kW which is the production limit of this ORC engine. With the current theoretical investigation this was verified, since the third sub- unit did not operate at all. The maximum net power production of the ORC engine was noticed at 130 °C, two- stage operation with a value of 7.58 kW, capable to operate only two of the three sub- units. However, the fresh water production of a good quality and quantity was noticed throughout the whole operation range both for 120 and 130 °C and the maximum production reached $\sim 1.4 \text{ m}^3/\text{h}$, close to the design of $2.1 \text{ m}^3/\text{h}$. In addition, the flexibility of the system was noticed with the operation of more than one sub- unit and the comparison of the one sub- unit operation at full load with the operation of two sub- units at partial load showed that the partial load operation leads to a higher fresh water production for a wider load range and a much smoother operation of the whole system. At 130 °C, the better performance at the two- stage ORC engine operation was also obvious.

A general overview of the integrated system, even if a slight sub- operation of the RO unit was noticed compared to the theoretical design of the unit, resulted that the integrated system operation was sufficient and efficient throughout the whole operation range.

7.3 Innovative elements

The innovation of the current thesis is summarized in:

- The two- stage ORC construction for operation at a temperature range of 120 to 130 °C. The present work is the sequel of another research of the design and experimental investigation of an autonomous RO desalination system with solar single stage ORC engine operating at a temperature range of 60 to 80°C (see Chapter 1 for reference). The present system intended to bring the research a step forward by increasing the operation temperature range up to 130°C, using a two-

stage ORC engine, in order to investigate the efficiency amelioration and with the use of three RO desalination units, in order to operate at a wide load range and produce fresh water even at low power input.

- The scroll expanders modification from market available scroll compressors (in reverse operation). These expanders were not market available for the capacities needed in the current test- rig, therefore their modification in the machine shop was an innovative experience of its own.
- The combination of a multi- skid RO unit to variable power input sources in order to increase the operation range and offer flexibility.
- Testing of each sub- system in several operating conditions simulated in the Laboratory (different operating temperatures, different salinities, single and two- stage operation of the ORC etc.), which can be a very good reference for further operation prediction with extrapolation of the results.

Overall, the system developed has been a very promising prototype which presented a sufficient and efficient operation under most of the operation conditions it was exposed to, and it is certainly an excellent springboard for further research in the field of water desalination through renewable energy sources.

7.4 Future work suggestions

The present thesis highlights all the aspects of the design, construction and operation of the hybrid RO -ORC system, therefore it can stand as a solid groundwork for further investigations associated with the system constituents, aiming at the improvement of their individual performance that could result to a more efficient system as well. With the gained experience as a bow in the quiver, the following research topics that are regarded as being of importance for obtaining further valuable know- how on RO and ORC applications, are proposed for further investigation.

First and foremost, the RO unit which resulted to be slightly oversized could be reconsidered and the sub- units could be replaced by more adequate ones. Other refrigerant candidates could also replace the used R245fa and the ORC engine could be examined again, in order to compare several organic fluids performance. A preheater that did not offer much in the current investigation and was not used, could be helpful with the use of other working fluids and could be investigated. In addition, the high- pressure expander that resulted to be slightly undersized could be replaced with an adequate one in order to meet the exact design parameters. Finally, the integrated system could be actually connected to some kind of renewable source (PV, concentrated solar panels, wind generators etc.) and be further investigated under real thermal conditions in the field.

Concerning the ORC technology, the two- stage ORC configuration can be further investigated for operation at different temperatures, higher than 130 °C. The ORC technology is very promising in the field of heat-to-power conversion engines and the multiple- stage configuration should be further examined. The investigation of supercritical and trans- critical Organic Rankine Engines has already started being investigated and this is also another field of interest for the current technology, where the two- stage system could also be examined.

As far as the RO desalination technology is concerned, the multi- skid configuration could expand to several sub- systems for wider power input ranges and fresh water productions. Moreover, since the RO technology is currently the most well- known and used desalination technology, the combination with renewable energy sources is mandatory. Their connection to larger heat-to-power engines could also be checked and several configurations with sub- units of different capacities for the increase of flexibility seem to be a promising application.

7.5 Epilogue

There is a rumor (if not a prediction) that the biggest problem humanity will come across in the near future is water scarcity. Many countries already face fatal problems, living under conditions of water shortage or water of very bad quality. Moreover, nowadays the need of renewable energy sources usage and “green technologies” is more than ever needed. Such prototypes that can replace the conventional power sources with the combination of different technologies are mandatory and any kind of environmentally friendly technology that can help towards the water solution is highly appreciated. Therefore, the scientific community shall keep on working hard towards this path, leading soon to more market available technologies, widely applied for the wellbeing of humanity.

7.6 Publications- Acknowledgement

The most important subjects investigated in the present thesis and the main conclusions have resulted in certain publications in acclaimed scientific journals in the fields of energy and water desalination and in the proceedings of relevant conferences:

Journal Publications

- [1] Erika Ntavou, George Kosmadakis, Dimitris Manolacos, George Papadakis, Dimitris Papantonis. Experimental evaluation of a multi- skid reverse osmosis unit operating at fluctuating power input. *Desalination* 398 (2016) 77-86.
- [2] Erika Ntavou, George Kosmadakis, Dimitris Manolacos, George Papadakis, Dimitris Papantonis. Experimental testing of a small- scale two stage Organic Rankine Cycle engine operating at low temperature. *Energy* 141 (2017) 869- 879.
- [3] George Kosmadakis, Dimitris Manolacos, Erika Ntavou, George Papadakis. Multiple Reverse Osmosis sub-units supplied by unsteady power sources for seawater desalination. *Desalination and Water Treatment* 55 (11) (2015) 3111-3119

Participation in conferences

- [1] Erika Ntavou, George Kosmadakis, Dimitris Manolacos, George Papadakis, Dimitris Papantonis. Experimental investigation of a multi- skid reverse osmosis (RO) unit, operating at a wide load range, powered by a small- scale Organic

Rankine Cycle (ORC) Engine. Desalination for the Environment: Clean Water and Energy, European Desalination Society (EDS), Limassol, Cyprus, 11-15 May 2014.

[2] Erika Ntavou, George Kosmadakis, Dimitris Manolakos, George Papadakis, Dimitris Papantonis. Experimental investigation of a small- scale two- stage Organic Rankine Cycle Engine operating at low temperature. 3rd International Seminar on ORC Power Systems (ASME), October 12-14, 2015, Brussels, Belgium.

[3] Erika Ntavou, George Kosmadakis, Dimitris Manolakos, George Papadakis, Dimitris Papantonis. Experimental investigation of a multi- skid RO unit, powered by a small- scale Organic Rankine Cycle Engine. The International Desalination Association (IDA) World Congress on Desalination and Water Reuse 2015/San Diego, CA, USA.

[4] George Kosmadakis, Dimitris Manolakos, Erika Ntavou, George Papadakis. Multiple Reverse Osmosis sub-units supplied by unsteady power sources for seawater desalination. Desalination for the Environment: Clean Water and Energy, European Desalination Society (EDS), Limassol, Cyprus, 11-15 May 2014.

[5] George Kosmadakis, Dimitris Manolakos, Erika Ntavou, George Papadakis. Implementation of a two- stage Organic Rankine Cycle using scroll expanders operating at variable heat input. 2nd International Seminar on ORC Power Systems (ASME), October 07 - 08, 2013, Rotterdam, The Netherlands.

[6] George Kosmadakis, Dimitris Manolakos, Erika Ntavou, George Papadakis. Design and implementation of a two-stage Organic Rankine cycle, operating under variable heat input. Industrial Technologies 2014, Megaron, The Athens Concert Hall. (Poster)

[7] George Kosmadakis, Dimitris Manolakos, Erika Ntavou, George Papadakis. Integrated system based on low-concentration PV/thermal units and a low-temperature supercritical Organic Rankine cycle.

[8] George Kosmadakis, Dimitris Manolakos, Olle Olsson, Erika Ntavou, Joakim Bystrom, George Papadakis. Design and implementation of a hybrid low-concentration PV/thermal system, including a bottoming supercritical ORC engine. EU PVSEC 2014, 29th European PV Solar Energy Conference and Exhibition, September 22-26, Amsterdam, The Netherlands.

Acknowledgment

The present work was conducted within the framework of the project with contract No. 09SYN-32-982, partly funded by the Greek General Secretary of Research and Technology (GSRT).

APPENDIX I- RO unit design

DOW Filmtec S.A. software ROSA 9.0 has been used for the RO unit design. In the current software, the input is the feed water analysis under treatment, along with the desired permeate flow rate. The output is the system design according to some limitations such as the HPP pressure occurred and the permeate water quality. The design takes place for a temperature range between 18 and 25 °C (typical Mediterranean Sea- water temperature) and for two different fouling factors ("ff", indicating the membranes' age): ff= 1 (for the first year of operation) and ff= 0.85 (for the third year of operation). This check offers a good prediction for the unit life operation. The four different reports that occurred for the current test representing the final design are presented right after:

Case 1: T= 18°C, ff=0.85

Reverse Osmosis System Analysis for FILMTEC™ Membranes													ROSA 9.0.0 ConfigDB u399339_282	
Project: My thesis											Case: 1			
Project Information:														
Case-specific:														
System Details														
Feed Flow to Stage 1	2.19 m³/h	Pass 1 Permeate Flow	0.70 m³/h	Osmotic Pressure:										
Raw Water Flow to System	2.19 m³/h	Pass 1 Recovery	32.00 %	Feed	27.34 bar									
Feed Pressure	61.68 bar	Feed Temperature	18.0 C	Concentrate	40.85 bar									
Flow Factor	0.85	Feed TDS	39457.02 mg/l	Average	34.09 bar									
Chem. Dose	None	Number of Elements	4	Average NDP	26.92 bar									
Total Active Area	29.36 M²	Average Pass 1 Flux	23.84 lmh	Power	4.69 kW									
Water Classification: Surface Supply SDI < 3				Specific Energy	6.69 kWh/m³									
Stage	Element	#PV	#Ele	Feed Flow (m³/h)	Feed Press (bar)	Recirc Flow (m³/h)	Conc Flow (m³/h)	Conc Press (bar)	Perm Flow (m³/h)	Avg Flux (lmh)	Perm Press (bar)	Boost Press (bar)	Perm TDS (mg/l)	
1	SW30-4040	1	2	2.19	61.33	0.00	1.77	60.98	0.41	28.17	0.00	0.00	113.40	
2	SW30-4040	1	2	1.77	60.63	0.00	1.49	60.37	0.29	19.52	0.00	0.00	188.05	
Pass Streams (mg/l as Ion)														
Name	Feed	Adjusted Feed	Concentrate		Permeate									
			Stage 1	Stage 2	Stage 1	Stage 2	Total							
NH4+ + NH3	0.00	0.00	0.00	0.00	0.00	0.00	0.00	0.00	0.00					
K	415.00	415.00	511.26	609.13	1.94	3.25	2.48							
Na	12000.06	12000.06	14787.74	17624.34	38.16	63.52	48.54							
Mg	1480.00	1480.00	1824.49	2175.41	1.81	2.95	2.27							
Ca	560.00	560.00	690.35	823.14	0.66	1.09	0.84							
Sr	8.00	8.00	9.86	11.76	0.01	0.02	0.01							
Ba	0.01	0.01	0.01	0.01	0.00	0.00	0.00							
CO3	3.28	3.28	4.80	6.51	0.00	0.00	0.00							
HCO3	156.00	156.00	190.42	224.99	1.61	2.52	1.98							
NO3	2.10	2.10	2.58	3.05	0.06	0.09	0.07							
Cl	22102.71	22104.00	27240.02	32466.83	65.42	108.75	83.15							
F	0.50	0.50	0.62	0.73	0.00	0.00	0.00							
SO4	2700.00	2700.00	3328.99	3970.00	1.01	1.63	1.26							
SiO2	3.00	3.00	3.69	4.40	0.02	0.03	0.02							
Boron	4.38	4.38	5.30	6.18	0.47	0.74	0.58							
CO2	4.47	4.47	5.04	5.64	4.49	5.06	4.72							
TDS	39455.72	39457.02	48625.12	57955.61	113.40	188.05	143.96							
pH	7.30	7.30	7.34	7.38	5.77	5.90	5.83							

APPENDIX I- RO unit design

Reverse Osmosis System Analysis for FILMTEC™ Membranes							ROSA 9.0.0 ConfigDB u399339_282	
Project: My thesis							Case: 1	
Design Warnings								
-None-								
Solubility Warnings								
Langelier Saturation Index > 0								
Antiscalants may be required. Consult your antiscalant manufacturer for dosing and maximum allowable system recovery.								
Stage Details								
Stage	Element	Recovery	Perm Flow (m ³ /h)	Perm TDS (mg/l)	Feed Flow (m ³ /h)	Feed TDS (mg/l)	Feed Press (bar)	
Stage 1	1	0.10	0.22	100.92	2.19	39457.02	61.33	
	2	0.10	0.19	128.00	1.96	43921.78	61.14	
Stage 2	Element	Recovery	Perm Flow (m ³ /h)	Perm TDS (mg/l)	Feed Flow (m ³ /h)	Feed TDS (mg/l)	Feed Press (bar)	
Stage 2	1	0.09	0.16	165.79	1.77	48625.12	60.63	
	2	0.08	0.13	215.25	1.62	53349.58	60.49	
<p>Permeate Flux reported by ROSA is calculated based on ACTIVE membrane area. DISCLAIMER: NO WARRANTY, EXPRESSED OR IMPLIED, AND NO WARRANTY OF MERCHANTABILITY OR FITNESS FOR A PARTICULAR PURPOSE, IS GIVEN. Neither FilmTec Corporation nor The Dow Chemical Company assume any obligation or liability for results obtained or damages incurred from the application of this information. Because use conditions and applicable laws may differ from one location to another and may change with time, customer is responsible for determining whether products are appropriate for customer's use. FilmTec Corporation and The Dow Chemical Company assume no liability, if, as a result of customer's use of the ROSA membrane design software, the customer should be sued for alleged infringement of any patent not owned or controlled by the FilmTec Corporation nor The Dow Chemical Company.</p>								
Scaling Calculations								
			Raw Water	Adjusted Feed	Concentrate			
pH			7.30	7.30	7.38			
Langelier Saturation Index			0.38	0.38	0.78			
Stiff & Davis Stability Index			-0.62	-0.62	-0.40			
Ionic Strength (Molal)			0.82	0.82	1.23			
TDS (mg/l)			39455.72	39457.02	57955.61			
HCO ₃			156.00	156.00	224.99			
CO ₂			4.47	4.47	5.64			
CO ₃			3.28	3.28	6.51			
CaSO ₄ (% Saturation)			24.38	24.38	39.05			
BaSO ₄ (% Saturation)			30.07	30.07	48.01			
SrSO ₄ (% Saturation)			13.79	13.79	23.77			
CaF ₂ (% Saturation)			18.61	18.61	58.94			
SiO ₂ (% Saturation)			2.70	2.40	3.96			
Mg(OH) ₂ (% Saturation)			0.02	0.02	0.04			
To balance: 1.30 mg/l Cl added to feed.								

APPENDIX I- RO unit design

Case 2: T= 25°C, ff=0.85

Reverse Osmosis System Analysis for FILMTEC™ Membranes										ROSA 9.0.0 ConfigDB u399339_282			
Project: My thesis										Case: 1			
Project Information:													
Case-specific:													
System Details													
Feed Flow to Stage 1	2.19 m³/h	Pass 1 Permeate Flow	0.70 m³/h	Osmotic Pressure:									
Raw Water Flow to System	2.19 m³/h	Pass 1 Recovery	32.00 %	Feed	28.08 bar								
Feed Pressure	58.43 bar	Feed Temperature	25.0 C	Concentrate	42.01 bar								
Flow Factor	0.85	Feed TDS	39456.78 mg/l	Average	35.04 bar								
Chem. Dose	None	Number of Elements	4	Average NDP	22.70 bar								
Total Active Area	29.36 M²	Average Pass 1 Flux	23.84 lmh	Power	4.44 kW								
Water Classification: Surface Supply SDI < 3				Specific Energy	6.34 kWh/m³								
Stage	Element	#PV	#Ele	Feed Flow (m³/h)	Feed Press (bar)	Recirc Flow (m³/h)	Conc Flow (m³/h)	Conc Press (bar)	Perm Flow (m³/h)	Avg Flux (lmh)	Perm Press (bar)	Boost Press (bar)	Perm TDS (mg/l)
1	SW30-4040	1	2	2.19	58.09	0.00	1.76	57.77	0.43	28.99	0.00	0.00	162.73
2	SW30-4040	1	2	1.76	57.42	0.00	1.49	57.18	0.27	18.70	0.00	0.00	286.04
Pass Streams (mg/l as Ion)													
Name	Feed	Adjusted Feed	Concentrate		Permeate								
			Stage 1	Stage 2	Stage 1	Stage 2	Total						
NH4+ + NH3	0.00	0.00	0.00	0.00	0.00	0.00	0.00	0.00	0.00				
K	415.00	415.00	514.53	608.58	2.80	4.95	3.64						
Na	12000.06	12000.06	14884.46	17613.65	54.75	96.70	71.20						
Mg	1480.00	1480.00	1836.74	2174.91	2.60	4.47	3.33						
Ca	560.00	560.00	694.99	822.95	0.95	1.65	1.23						
Sr	8.00	8.00	9.93	11.76	0.01	0.02	0.02						
Ba	0.01	0.01	0.01	0.01	0.00	0.00	0.00						
CO3	4.33	4.33	6.25	8.19	0.00	0.00	0.00						
HCO3	156.00	156.00	191.37	224.35	2.26	3.78	2.85						
NO3	2.10	2.10	2.59	3.04	0.08	0.14	0.10						
Cl	22102.71	22102.71	27417.12	32446.62	93.85	165.51	121.96						
F	0.50	0.50	0.62	0.73	0.00	0.01	0.00						
SO4	2700.00	2700.00	3351.61	3969.72	1.45	2.47	1.85						
SiO2	3.00	3.00	3.72	4.40	0.03	0.05	0.04						
Boron	4.38	4.38	5.28	6.05	0.69	1.10	0.85						
CO2	3.85	3.85	4.47	5.08	3.88	4.47	4.11						
TDS	39456.78	39456.78	48944.12	57923.49	162.73	286.04	211.09						
pH	7.30	7.30	7.32	7.36	5.92	6.07	5.99						

APPENDIX I- RO unit design

Reverse Osmosis System Analysis for FILMTEC™ Membranes							ROSA 9.0.0 ConfigDB u399339_282	
Project: My thesis							Case: 1	
Design Warnings								
-None-								
Solubility Warnings								
Langelier Saturation Index > 0								
Antiscalants may be required. Consult your antiscalant manufacturer for dosing and maximum allowable system recovery.								
Stage Details								
Stage	Element	Recovery	Perm Flow (m ³ /h)	Perm TDS (mg/l)	Feed Flow (m ³ /h)	Feed TDS (mg/l)	Feed Press (bar)	
Stage 1	1	0.11	0.23	142.87	2.19	39456.78	58.09	
	2	0.10	0.19	186.78	1.95	44143.77	57.91	
Stage 2	1	0.09	0.15	249.57	1.76	48944.12	57.42	
	2	0.08	0.12	332.09	1.61	53580.48	57.29	
<p>Permeate Flux reported by ROSA is calculated based on ACTIVE membrane area. DISCLAIMER: NO WARRANTY, EXPRESSED OR IMPLIED, AND NO WARRANTY OF MERCHANTABILITY OR FITNESS FOR A PARTICULAR PURPOSE, IS GIVEN. Neither FilmTec Corporation nor The Dow Chemical Company assume any obligation or liability for results obtained or damages incurred from the application of this information. Because use conditions and applicable laws may differ from one location to another and may change with time, customer is responsible for determining whether products are appropriate for customer's use. FilmTec Corporation and The Dow Chemical Company assume no liability, if, as a result of customer's use of the ROSA membrane design software, the customer should be sued for alleged infringement of any patent not owned or controlled by the FilmTec Corporation nor The Dow Chemical Company.</p>								
Scaling Calculations								
			Raw Water		Adjusted Feed		Concentrate	
pH			7.30		7.30		7.36	
Langelier Saturation Index			0.54		0.54		0.92	
Stiff & Davis Stability Index			-0.49		-0.49		-0.29	
Ionic Strength (Molal)			0.82		0.82		1.22	
TDS (mg/l)			39456.78		39456.78		57923.49	
HCO ₃			156.00		156.00		224.35	
CO ₂			3.85		3.85		5.08	
CO ₃			4.33		4.33		8.19	
CaSO ₄ (% Saturation)			24.38		24.38		39.05	
BaSO ₄ (% Saturation)			30.07		30.07		48.01	
SrSO ₄ (% Saturation)			13.79		13.79		23.77	
CaF ₂ (% Saturation)			18.61		18.61		58.82	
SiO ₂ (% Saturation)			2.40		2.40		3.52	
Mg(OH) ₂ (% Saturation)			0.02		0.02		0.04	
To balance: 0.00 mg/l Cl added to feed.								

APPENDIX I- RO unit design

Case 3: T= 18°C, ff=1

Reverse Osmosis System Analysis for FILMTEC™ Membranes													ROSA 9.0.0 ConfigDB u399339_282	
Project: My thesis													Case: 1	
Project Information:														
Case-specific:														
System Details														
Feed Flow to Stage 1	2.19 m³/h	Pass 1 Permeate Flow	0.70 m³/h	Osmotic Pressure:										
Raw Water Flow to System	2.19 m³/h	Pass 1 Recovery	32.00 %	Feed	27.34 bar									
Feed Pressure	58.52 bar	Feed Temperature	18.0 C	Concentrate	40.85 bar									
Flow Factor	1.00	Feed TDS	39457.02 mg/l	Average	34.09 bar									
Chem. Dose	None	Number of Elements	4	Average NDP	23.69 bar									
Total Active Area	29.36 M²	Average Pass 1 Flux	23.84 lmh	Power	4.45 kW									
Water Classification: Surface Supply SDI < 3				Specific Energy	6.35 kWh/m³									
Stage	Element	#PV	#Ele	Feed Flow (m³/h)	Feed Press (bar)	Recirc Flow (m³/h)	Conc Flow (m³/h)	Conc Press (bar)	Perm Flow (m³/h)	Avg Flux (lmh)	Perm Press (bar)	Boost Press (bar)	Perm TDS (mg/l)	
1	SW30-4040	1	2	2.19	58.18	0.00	1.77	57.83	0.42	28.73	0.00	0.00	112.02	
2	SW30-4040	1	2	1.77	57.48	0.00	1.49	57.22	0.28	18.96	0.00	0.00	193.24	
Pass Streams (mg/l as Ion)														
Name	Feed	Adjusted Feed	Concentrate		Permeate									
			Stage 1	Stage 2	Stage 1	Stage 2	Total							
NH4+ + NH3	0.00	0.00	0.00	0.00	0.00	0.00	0.00	0.00						
K	415.00	415.00	513.64	609.11	1.92	3.34	2.48							
Na	12000.06	12000.06	14856.53	17623.71	37.69	65.29	48.66							
Mg	1480.00	1480.00	1832.98	2175.33	1.79	3.02	2.28							
Ca	560.00	560.00	693.56	823.11	0.66	1.12	0.84							
Sr	8.00	8.00	9.91	11.76	0.01	0.02	0.01							
Ba	0.01	0.01	0.01	0.01	0.00	0.00	0.00							
CO3	3.28	3.28	4.84	6.51	0.00	0.00	0.00							
HCO3	156.00	156.00	191.27	224.98	1.60	2.58	1.99							
NO3	2.10	2.10	2.59	3.05	0.06	0.10	0.07							
Cl	22102.71	22104.00	27366.75	32465.67	64.61	111.76	83.36							
F	0.50	0.50	0.62	0.73	0.00	0.00	0.00							
SO4	2700.00	2700.00	3344.49	3969.87	1.00	1.67	1.27							
SiO2	3.00	3.00	3.71	4.40	0.02	0.03	0.02							
Boron	4.38	4.38	5.32	6.17	0.47	0.75	0.58							
CO2	4.47	4.47	5.05	5.64	4.49	5.07	4.72							
TDS	39455.72	39457.02	48851.32	57953.55	112.02	193.24	144.31							
pH	7.30	7.30	7.34	7.38	5.76	5.90	5.83							

APPENDIX I- RO unit design

Reverse Osmosis System Analysis for FILMTEC™ Membranes							ROSA 9.0.0 ConfigDB u399339_282	
Project: My thesis							Case: 1	
Design Warnings								
-None-								
Solubility Warnings								
Langelier Saturation Index > 0								
Antiscalants may be required. Consult your antiscalant manufacturer for dosing and maximum allowable system recovery.								
Stage Details								
Stage	Element	Recovery	Perm Flow (m ³ /h)	Perm TDS (mg/l)	Feed Flow (m ³ /h)	Feed TDS (mg/l)	Feed Press (bar)	
Stage 1	1	0.11	0.23	98.81	2.19	39457.02	58.18	
	2	0.10	0.19	127.83	1.96	44074.59	57.99	
Stage 2	Element	Recovery	Perm Flow (m ³ /h)	Perm TDS (mg/l)	Feed Flow (m ³ /h)	Feed TDS (mg/l)	Feed Press (bar)	
Stage 2	1	0.09	0.15	169.07	1.77	48851.32	57.48	
	2	0.08	0.12	223.49	1.61	53525.15	57.34	
<p>Permeate Flux reported by ROSA is calculated based on ACTIVE membrane area. DISCLAIMER: NO WARRANTY, EXPRESSED OR IMPLIED, AND NO WARRANTY OF MERCHANTABILITY OR FITNESS FOR A PARTICULAR PURPOSE, IS GIVEN. Neither FilmTec Corporation nor The Dow Chemical Company assume any obligation or liability for results obtained or damages incurred from the application of this information. Because use conditions and applicable laws may differ from one location to another and may change with time, customer is responsible for determining whether products are appropriate for customer's use. FilmTec Corporation and The Dow Chemical Company assume no liability, if, as a result of customer's use of the ROSA membrane design software, the customer should be sued for alleged infringement of any patent not owned or controlled by the FilmTec Corporation nor The Dow Chemical Company.</p>								
Scaling Calculations								
			Raw Water	Adjusted Feed	Concentrate			
pH			7.30	7.30	7.38			
Langelier Saturation Index			0.38	0.38	0.78			
Stiff & Davis Stability Index			-0.62	-0.62	-0.40			
Ionic Strength (Molal)			0.82	0.82	1.23			
TDS (mg/l)			39455.72	39457.02	57953.55			
HCO ₃			156.00	156.00	224.98			
CO ₂			4.47	4.47	5.64			
CO ₃			3.28	3.28	6.51			
CaSO ₄ (% Saturation)			24.38	24.38	39.05			
BaSO ₄ (% Saturation)			30.07	30.07	48.01			
SrSO ₄ (% Saturation)			13.79	13.79	23.77			
CaF ₂ (% Saturation)			18.61	18.61	58.93			
SiO ₂ (% Saturation)			2.70	2.40	3.96			
Mg(OH) ₂ (% Saturation)			0.02	0.02	0.04			
To balance: 1.30 mg/l Cl added to feed.								

APPENDIX I- RO unit design

Case 4: T= 25°C, ff=1

Reverse Osmosis System Analysis for FILMTEC™ Membranes										ROSA 9.0.0 ConfigDB u399339_282			
Project: My thesis										Case: 1			
Project Information:													
Case-specific:													
System Details													
Feed Flow to Stage 1	2.19 m³/h	Pass 1 Permeate Flow	0.70 m³/h	Osmotic Pressure:									
Raw Water Flow to System	2.19 m³/h	Pass 1 Recovery	32.00 %	Feed	28.08 bar								
Feed Pressure	56.06 bar	Feed Temperature	25.0 C	Concentrate	42.01 bar								
Flow Factor	1.00	Feed TDS	39456.78 mg/l	Average	35.04 bar								
Chem. Dose	None	Number of Elements	4	Average NDP	20.23 bar								
Total Active Area	29.36 M²	Average Pass 1 Flux	23.84 lmh	Power	4.26 kW								
Water Classification: Surface Supply SDI < 3				Specific Energy	6.08 kWh/m³								
Stage	Element	#PV	#Ele	Feed Flow (m³/h)	Feed Press (bar)	Recirc Flow (m³/h)	Conc Flow (m³/h)	Conc Press (bar)	Perm Flow (m³/h)	Avg Flux (lmh)	Perm Press (bar)	Boost Press (bar)	Perm TDS (mg/l)
1	SW30-4040	1	2	2.19	55.72	0.00	1.75	55.39	0.43	29.60	0.00	0.00	160.66
2	SW30-4040	1	2	1.75	55.05	0.00	1.49	54.81	0.27	18.09	0.00	0.00	295.08
Pass Streams (mg/l as Ion)													
Name	Feed	Adjusted Feed	Concentrate		Permeate								
			Stage 1	Stage 2	Stage 1	Stage 2	Total						
NH4+ + NH3	0.00	0.00	0.00	0.00	0.00	0.00	0.00						
K	415.00	415.00	517.17	608.57	2.76	5.11	3.65						
Na	12000.06	12000.06	14960.69	17613.53	54.04	99.79	71.40						
Mg	1480.00	1480.00	1846.16	2174.90	2.57	4.60	3.34						
Ca	560.00	560.00	698.55	822.95	0.94	1.71	1.23						
Sr	8.00	8.00	9.98	11.76	0.01	0.02	0.02						
Ba	0.01	0.01	0.01	0.01	0.00	0.00	0.00						
CO3	4.33	4.33	6.30	8.19	0.00	0.00	0.00						
HCO3	156.00	156.00	192.31	224.34	2.23	3.89	2.86						
NO3	2.10	2.10	2.60	3.04	0.08	0.15	0.10						
Cl	22102.71	22102.71	27557.55	32446.40	92.65	170.78	122.29						
F	0.50	0.50	0.62	0.73	0.00	0.01	0.00						
SO4	2700.00	2700.00	3368.80	3969.71	1.43	2.54	1.85						
SiO2	3.00	3.00	3.74	4.40	0.03	0.05	0.04						
Boron	4.38	4.38	5.30	6.05	0.68	1.13	0.85						
CO2	3.85	3.85	4.49	5.08	3.88	4.48	4.11						
TDS	39456.78	39456.78	49194.79	57923.12	160.66	295.08	211.65						
pH	7.30	7.30	7.33	7.36	5.92	6.08	5.99						

APPENDIX I- RO unit design

Reverse Osmosis System Analysis for FILMTEC™ Membranes							ROSA 9.0.0 ConfigDB u399339_282	
Project: My thesis							Case: 1	
Design Warnings								
-None-								
Solubility Warnings								
Langelier Saturation Index > 0								
Antiscalants may be required. Consult your antiscalant manufacturer for dosing and maximum allowable system recovery.								
Stage Details								
Stage	Element	Recovery	Perm Flow (m ³ /h)	Perm TDS (mg/l)	Feed Flow (m ³ /h)	Feed TDS (mg/l)	Feed Press (bar)	
Stage 1	1	0.11	0.24	139.75	2.19	39456.78	55.72	
	2	0.10	0.19	186.60	1.95	44314.97	55.54	
Stage 2	Element	Recovery	Perm Flow (m ³ /h)	Perm TDS (mg/l)	Feed Flow (m ³ /h)	Feed TDS (mg/l)	Feed Press (bar)	
Stage 2	1	0.09	0.15	255.11	1.75	49194.79	55.05	
	2	0.07	0.12	347.00	1.60	53774.65	54.92	
<p>Permeate Flux reported by ROSA is calculated based on ACTIVE membrane area. DISCLAIMER: NO WARRANTY, EXPRESSED OR IMPLIED, AND NO WARRANTY OF MERCHANTABILITY OR FITNESS FOR A PARTICULAR PURPOSE, IS GIVEN. Neither FilmTec Corporation nor The Dow Chemical Company assume any obligation or liability for results obtained or damages incurred from the application of this information. Because use conditions and applicable laws may differ from one location to another and may change with time, customer is responsible for determining whether products are appropriate for customer's use. FilmTec Corporation and The Dow Chemical Company assume no liability, if, as a result of customer's use of the ROSA membrane design software, the customer should be sued for alleged infringement of any patent not owned or controlled by the FilmTec Corporation nor The Dow Chemical Company.</p>								
Scaling Calculations								
		Raw Water	Adjusted Feed	Concentrate				
pH		7.30	7.30	7.36				
Langelier Saturation Index		0.54	0.54	0.92				
Stiff & Davis Stability Index		-0.49	-0.49	-0.29				
Ionic Strength (Molal)		0.82	0.82	1.22				
TDS (mg/l)		39456.78	39456.78	57923.12				
HCO ₃		156.00	156.00	224.34				
CO ₂		3.85	3.85	5.08				
CO ₃		4.33	4.33	8.19				
CaSO ₄ (% Saturation)		24.38	24.38	39.05				
BaSO ₄ (% Saturation)		30.07	30.07	48.01				
SrSO ₄ (% Saturation)		13.79	13.79	23.77				
CaF ₂ (% Saturation)		18.61	18.61	58.82				
SiO ₂ (% Saturation)		2.40	2.40	3.52				
Mg(OH) ₂ (% Saturation)		0.02	0.02	0.04				
To balance: 0.00 mg/l Cl added to feed.								

It should be noted that the above analysis concerns each one of the three identical RO sub- units of the current test- rig. The design resulted in a system of two membrane vessels with two membranes in each (four membranes total for each sub- unit) of the type of SW30-4040. The high pressure of the system for the worst case (low temperature of 18°C at the third year of operation ff= 0.85) does not exceed the value of 62 bar which is an acceptable value for a sea- water RO unit. The permeate water for each case lays within acceptable limits for human use and consumption, however, it should also be noted that if the produced water was to really be consumed, a post treatment in order to enrich it with calcium and magnesium would be recommended.

APPENDIX II- Experimental uncertainty analysis

An uncertainty analysis based on errors propagation, as described in [1,2] has been conducted in order to determine the uncertainty of the calculated quantities due to the error associated with the direct measurement of primary quantities. Assuming that a quantity R is calculated from a combination of measured quantities x_i , $R = R(x_1, x_2, x_3, \dots, x_i)$, then the uncertainty in the calculated value is equal to:

$$U_R = [\sum_{i=1}^N ((\frac{\partial R}{\partial x_i}) U_{x_i})^2]^{1/2} \quad (1)$$

where U_{x_i} is the uncertainty associated with the measurement of the values x_i . Equation (II.1) is valid whether the measurement uncertainty is given in absolute or relative values. The uncertainty in the measured values required for the system determination are given for a confidence level equal to 95% and presented in Table 1 for the ORC engine and Table 2 for the RO unit. Since the instrument accuracy acc is available the typical uncertainty of the measurement was calculated as $U_{x_i} = 1.645 \frac{acc}{\sqrt{3}}$.

Moreover, it must be noted that the error in the electrical signals directly measured by the data loggers was considered negligible.

Table 1. ORC engine measured properties

Temperature sensor Pt 100		Measurement range	Accuracy (%)
1	After the pump	0-80 °C	±0.05
2	After the evaporator	0-200 °C	±0.05
3	Between the scroll expanders	0-200 °C	±0.05
4	After the second expander	0-150 °C	±0.05
5	After the condenser	0-80 °C	±0.05
Pressure sensors			
1	After the pump	0-35 bar	±1.6
2	After the evaporator	0-35 bar	±1.6
3	Between the scroll expanders	0-35 bar	±1.6
4	After the second expander	0-35 bar	±1.6
5	After the condenser	0-35 bar	±1.6
Power production			
Multimeter		-	±0.02
Frequency inverters			
1	Pump	-	±5
2	Expanders	-	±1

APPENDIX II- Experimental uncertainty analysis

Measured Property	Symbol	Uncertainty
Electric heater inlet temperature	$T_{hot_{in}} [^{\circ}\text{C}]$	0.047
Electric heater outlet temperature	$T_{hot_{out}} [^{\circ}\text{C}]$	0.047
Pump's frequency	$f_{ORC_p} [\text{Hz}]$	4.7%
Pump's inlet temperature	$T_{ORC_{P_{in}}} [^{\circ}\text{C}]$	0.047
Pump's outlet temperature	$T_{ORC_{P_{out}}} [^{\circ}\text{C}]$	0.047
Pump's inlet pressure	$p_{ORC_{P_{in}}} [\text{bar}]$	1.51%
Pump's outlet pressure	$p_{ORC_{P_{out}}} [\text{bar}]$	1.51%
Evaporator's inlet temperature	$T_{ORC_{EV_{in}}} [^{\circ}\text{C}]$	0.047
Evaporator's outlet temperature	$T_{ORC_{EV_{out}}} [^{\circ}\text{C}]$	0.047
Evaporator's inlet pressure	$p_{ORC_{EV_{in}}} [\text{bar}]$	1.51%
Evaporator's outlet pressure	$p_{ORC_{EV_{out}}} [\text{bar}]$	1.51%
First expander's frequency	$f_{ORC_{e1}} [\text{Hz}]$	0.95%
First expander's inlet temperature	$T_{ORC_{e1_{in}}} [^{\circ}\text{C}]$	0.047
First expander's outlet temperature	$T_{ORC_{e1_{out}}} [^{\circ}\text{C}]$	0.047
First expander's inlet pressure	$p_{ORC_{e1_{in}}} [\text{bar}]$	1.51%
First expander's outlet pressure	$p_{ORC_{e1_{out}}} [\text{bar}]$	1.51%
First expander's power production	$P_{ORC_{e1_{meas}}} [\text{kW}]$	0.019
Second expander's frequency	$f_{ORC_{e2}} [\text{Hz}]$	0.95%
Second expander's inlet temperature	$T_{ORC_{e2_{in}}} [^{\circ}\text{C}]$	0.047
Second expander's outlet temperature	$T_{ORC_{e2_{out}}} [^{\circ}\text{C}]$	0.047
Second expander's inlet pressure	$p_{ORC_{e2_{in}}} [\text{bar}]$	1.51%
Second expander's outlet pressure	$p_{ORC_{e2_{out}}} [\text{bar}]$	1.51%

APPENDIX II- Experimental uncertainty analysis

Second expander's power production	$P_{ORC_{e1}meas}$ [kW]	0.019
Condenser's inlet temperature	$T_{ORCCON_{in}}$ [°C]	0.047
Condenser's outlet temperature	$T_{ORCCON_{out}}$ [°C]	0.047
Condenser's inlet pressure	$p_{ORCCON_{in}}$ [bar]	1.51%
Condenser's outlet pressure	$p_{ORCCON_{out}}$ [bar]	1.51%

APPENDIX II- Experimental uncertainty analysis
Table 2. RO sub-unit instrumentation and measurement range

Temperature thermometers		Measurement range	Accuracy (%)	Uncertainty U
1	After the membranes	0-60 °C	±0.15	0.14
Pressure gauges				
1	After the feed pump and before the filters	0-10 bar	±0.1	0.095
2	Between the two filters	0-10 bar	±0.1	0.095
3	After the filters and before the high-pressure pump	0-10 bar	±0.1	0.095
4	After the high-pressure pump and before the membranes	0-100 bar	±1.0	0.95
5	At the brine's membranes outlet	0-100 bar	±1.0	0.95
Pressure switches				
1	Low- pressure switch after the filters and before the high-pressure pump (protects the high-pressure pump from no water operation)	2 bar	≤ ±1.0 % of span ± 1 digit	0.95
2	High-pressure switch after the high-pressure pump and before the membranes (protects the membranes and membrane vessels under high pressure)	70 bar	≤ ±1.0 % of span ± 1 digit	0.95
Water flow rate (mechanical flow meter)				
1	At the membranes' outlet on the fresh water side (on each sub-unit)	0.1 – 1 m ³ /h	±0.05	0.047
2	At membranes' outlet on the brine's side	0.25 – 2.5 m ³ /h	±0.125	0.119
Water conductivity				
1	At the membranes' outlet on the fresh water side (digital indication)	0-2000 mS/cm	±2	1.90

The uncertainty associated with quantities deriving from the directly measured ones was calculated with the use of equation (1) and are presented in Tables 3 and 4.

APPENDIX II- Experimental uncertainty analysis

Table3. ORC engine calculated properties that derive directly from the measured ones

Calculated property	Equation	Unit	Uncertainty U
Pump's rotational speed	$RPM_{ORCP} = \frac{f_{ORCP}}{50} * 960$	RPM	0.34%
Pump isentropic efficiency	$n_{OPCPis} = \frac{h_{ORCPoutis} - h_{ORCPin}}{h_{ORCPout} - h_{ORCPin}} * 100$	%	2%
Pump power consumption	$P_{ORCP} = (h_{ORCPout} - h_{ORCPin}) * m_{ORCP}$	kW	2.6%
Evaporator thermal load	$Q_{ORCEV} = (h_{ORCEVout} - h_{ORCEVin}) * m_{ORCP}$	kW _{th}	2.6%
First expander's rotational speed	$RPM_{ORCe1} = \frac{f_{ORCe1}}{50} * 2900$	RPM	0.55%
First expander isentropic efficiency	$n_{OPCe1is} = \frac{h_{ORCe1out} - h_{ORCe1in}}{h_{ORCe1outis} - h_{ORCe1in}} * 100$	%	2%
First expander actual efficiency	$n_{OPCe1} = \frac{P_{ORCe1meas}}{m_{ORCP} * (h_{ORCe1in} - h_{ORCe1outis})} * 100$	%	0.97%
Second expander's rotational speed	$RPM_{ORCe2} = \frac{f_{ORCe2}}{50} * 2900$	RPM	0.55%
Second expander isentropic efficiency	$n_{OPCe2is} = \frac{h_{ORCe2out} - h_{ORCe2in}}{h_{ORCe2outis} - h_{ORCe2in}} * 100$	%	2%
Second expander actual efficiency	$n_{OPCe2} = \frac{P_{ORCe2meas}}{m_{ORCP} * (h_{ORCe2in} - h_{ORCe2outis})} * 100$	%	0.97%
Condenser thermal load	$Q_{ORCCON} = (h_{ORCCONout} - h_{ORCCONin}) * m_{ORCP}$	kW _{th}	2.6%
ORC engine's thermal efficiency	$n_{ORCth} = \frac{P_{ORCe} - P_{ORCP}}{Q_{ORCEV}} * 100$	%	1.16%

APPENDIX II- Experimental uncertainty analysis

Table 4. Equations governing the RO unit calculated properties

Calculated Property	Equation	Unit	Uncertainty U
Feed water flow rate	$Q_f = Q_{fr} + Q_{br}$	m^3/h	0.10%
Recovery rate	$recovery = \frac{Q_{fr}}{Q_f}$	%	0.10%
Specific energy consumption	$SEC = \frac{P}{Q_{fr}}$	kWh/m^3	0.43%
Fresh water salinity	$salinity = 0.627 * 1.00114 * con$	mg/l	1.19%
Total fresh water salinity	$salinity_{tot} = 0.627 * \frac{(con_1 * Q_{fr_1} + con_2 * Q_{fr_2} + con_3 * Q_{fr_3})}{(Q_{fr_1} + Q_{fr_2} + Q_{fr_3})}$	ppm	2.29%
Total specific energy consumption	$SEC_{tot} = \frac{P_1 + P_2 + P_3}{Q_{fr_1} + Q_{fr_2} + Q_{fr_3}}$	kWh/m^3	0.67%

References:

1. R.J. Moffat, Describing the uncertainties in experimental results, Exp. Therm, Fluid. Sci.1(1988) 3-17.
2. M.E. Mathioulakis, Measurement, quality of measurement and uncertainty, Hellas Lab publications, Athens, 2004.

APPENDIX III – PV- RO Case study design

In order to prove the flexibility offered by the use of a multi- skid RO desalination unit in combination to renewable energy sources, different case studies of RO desalination powered by a photovoltaic field have been presented in Chapter 4. For this analysis, it is assumed that the solar-powered reverse osmosis system does not incorporate any energy storage and would only operate when the solar power is available. Three different locations have been selected where the system could be installed; Athens- Greece, Palma- Spain and Abu Dhabi- United Arab Emirates (UAE). For all cases, the mono-crystalline silicon photovoltaic (PV) technology has been chosen. The orientation has been determined to be South and the slope degree has been set at 32° for Greece, 37° for Spain and 22° for UAE [4.11, 4.12]. The PV panels have been chosen to apply fixed mounting position. Three different cases of installed peak PV power are being observed for each case with the help of the appropriate software [4.12]; 10 kWp, 15 kWp and 20 kWp. The scenarios examined are for a typical summer day (July 21st) and a typical winter day (December 21st). Based on the daily solar irradiance profile for the 21st of July and with the use of the appropriate software [4.13], the PV daily power production occurs, presented in Figure 4.30, and the values are hereby presented in table;

Table 1. PV power production for different capacity for the three locations (Athens- Greece, Palma- Spain and Abu Dhabi- United Arab Emirates), July 21st & December 21st

ATHENS- GREECE							
JULY 21st	10 kW	15 kW	20 kW	DECEMBER 21st	10 kW	15 kW	20 kW
0:00	0	0.00	0	0:00	0	0	0
1:00	0	0.00	0	1:00	0	0	0
2:00	0	0.00	0	2:00	0	0	0
3:00	0	0.00	0	3:00	0	0	0
4:00	0	0.00	0	4:00	0	0	0
5:00	0.01	0.02	0.02	5:00	0	0	0
6:00	0.47	0.70	0.94	6:00	0	0	0
7:00	1.65	2.47	3.29	7:00	0	0	0
8:00	3.39	5.09	6.79	8:00	0.56	0.84	1.13
9:00	4.97	7.46	9.95	9:00	1.81	2.71	3.61
10:00	6.36	9.54	12.71	10:00	2.45	3.67	4.90
11:00	6.75	10.12	13.49	11:00	4.25	6.38	8.51
12:00	6.50	9.75	13.00	12:00	5.34	8.01	10.68
13:00	5.31	7.97	10.62	13:00	5.70	8.56	11.41
14:00	5.60	8.40	11.20	14:00	3.72	5.58	7.45

APPENDIX III – PV- RO Case study design

15:00	4.96	7.43	9.91	15:00	1.62	2.43	3.24
16:00	3.49	5.24	6.99	16:00	0.15	0.23	0.31
17:00	1.71	2.57	3.42	17:00	0	0	0
18:00	0.51	0.76	1.02	18:00	0	0	0
19:00	0.02	0.03	0.04	19:00	0	0	0
20:00	0	0.00	0	20:00	0	0	0
21:00	0	0.00	0	21:00	0	0	0
22:00	0	0.00	0	22:00	0	0	0
23:00	0	0.00	0	23:00	0	0	0
0:00	0	0.00	0	0:00	0	0	0
PALMA- SPAIN							
JULY 21st	10 kW	15 kW	20 kW	DECEMBER 21st	10 kW	15 kW	20 kW
0:00	0	0.00	0	0:00	0	0.00	0
1:00	0	0.00	0	1:00	0	0.00	0
2:00	0	0.00	0	2:00	0	0.00	0
3:00	0	0.00	0	3:00	0	0.00	0
4:00	0	0.00	0	4:00	0	0.00	0
5:00	0	0.00	0	5:00	0	0.00	0
6:00	0.27	0.41	0.55	6:00	0	0.00	0
7:00	0.97	1.45	1.93	7:00	0	0.00	0
8:00	2.38	3.58	4.77	8:00	0.44	0.66	0.89
9:00	4.11	6.16	8.22	9:00	2.64	3.96	5.28
10:00	5.53	8.29	11.06	10:00	4.89	7.33	9.78
11:00	6.51	9.77	13.03	11:00	5.79	8.69	11.58
12:00	6.90	10.35	13.80	12:00	5.06	7.58	10.11
13:00	7.07	10.61	14.14	13:00	6.32	9.48	12.64
14:00	6.49	9.73	12.97	14:00	5.73	8.60	11.46
15:00	5.39	8.09	10.78	15:00	3.20	4.81	6.41
16:00	3.99	5.99	7.98	16:00	0.91	1.36	1.82
17:00	2.22	3.33	4.44	17:00	0	0.00	0
18:00	0.81	1.22	1.62	18:00	0	0.00	0

APPENDIX III – PV- RO Case study design

19:00	0.19	0.29	0.38	19:00	0	0.00	0
20:00	0	0.00	0	20:00	0	0.00	0
21:00	0	0.00	0	21:00	0	0.00	0
22:00	0	0.00	0	22:00	0	0.00	0
23:00	0	0.00	0	23:00	0	0.00	0
0:00	0	0.00	0	0:00	0	0.00	0

ABU DHABI- UAE							
JULY 21 st	10 kW	15 kW	20 kW	DECEMBER 21 st	10 kW	15 kW	20 kW
0:00	0	0	0	0:00	0	0	0
1:00	0	0	0	1:00	0	0	0
2:00	0	0	0	2:00	0	0	0
3:00	0	0	0	3:00	0	0	0
4:00	0	0	0	4:00	0	0	0
5:00	0.00	0.00	0.00	5:00	0	0	0
6:00	0.29	0.44	0.59	6:00	0	0	0
7:00	1.41	2.12	2.82	7:00	0.48	0.73	0.97
8:00	3.10	4.66	6.21	8:00	2.61	3.91	5.21
9:00	4.64	6.95	9.27	9:00	4.65	6.97	9.29
10:00	5.62	8.43	11.24	10:00	6.03	9.05	12.06
11:00	6.15	9.23	12.31	11:00	6.77	10.16	13.54
12:00	6.88	10.32	13.76	12:00	6.90	10.35	13.79
13:00	6.62	9.93	13.24	13:00	6.56	9.84	13.11
14:00	5.79	8.69	11.58	14:00	5.63	8.45	11.27
15:00	4.54	6.81	9.07	15:00	4.11	6.17	8.23
16:00	2.94	4.41	5.88	16:00	1.97	2.96	3.95
17:00	1.30	1.95	2.60	17:00	0.06	0.10	0.13
18:00	0.26	0.39	0.52	18:00	0	0	0
19:00	0.00	0.00	0.00	19:00	0	0	0
20:00	0	0	0	20:00	0	0	0
21:00	0	0	0	21:00	0	0	0
22:00	0	0	0	22:00	0	0	0
23:00	0	0	0	23:00	0	0	0
0:00	0	0	0	0:00	0	0	0

Based on Figure 4.29, where a RO sub- unit requires at least 3.085 kW to operate, the number of units operating occur by simply dividing the produced kW_e from the PV panels to the minimum necessary power for a unit to operate: $number\ of\ units = \frac{PV\ kW_e}{3.085}$ The results for all areas and all PV systems for July and December are presented in the next table.

Table 2. Number of operating sub- units throughout the day of July 21st and December 21st for different PV capacity.

ATHENS- GREECE		PALMA- SPAIN		ABU DHABI- UAE		
10 kW PV system						
TIME	JULY 21st	DECEMBER 21st	JULY 21st	DECEMBER 21st	JULY 21st	DECEMBER 21st
0:00	0	0	0	0	0	0
1:00	0	0	0	0	0	0
2:00	0	0	0	0	0	0
3:00	0	0	0	0	0	0
4:00	0	0	0	0	0	0
5:00	0	0	0	0	0	0
6:00	0	0	0	0	0	0
7:00	0	0	0	0	0	0
8:00	1	0	0	0	1	0
9:00	1	0	1	0	1	1
10:00	2	0	1	1	1	2
11:00	2	1	2	1	1	2
12:00	2	1	2	1	2	2
13:00	1	1	2	2	2	2
14:00	1	1	2	1	1	1
15:00	1	0	1	1	1	1
16:00	1	0	1	0	0	0
17:00	0	0	0	0	0	0
18:00	0	0	0	0	0	0
19:00	0	0	0	0	0	0
20:00	0	0	0	0	0	0
21:00	0	0	0	0	0	0
22:00	0	0	0	0	0	0
23:00	0	0	0	0	0	0
0:00	0	0	0	0	0	0

APPENDIX III – PV- RO Case study design

15 kW PV system						
TIME	JULY 21st	DECEMBER 21st	JULY 21st	DECEMBER 21st	JULY 21st	DECEMBER 21st
0:00	0	0	0	0	0	0
1:00	0	0	0	0	0	0
2:00	0	0	0	0	0	0
3:00	0	0	0	0	0	0
4:00	0	0	0	0	0	0
5:00	0	0	0	0	0	0
6:00	0	0	0	0	0	0
7:00	0	0	0	0	0	0
8:00	1	0	1	0	1	1
9:00	2	0	1	1	2	2
10:00	3	1	2	2	2	3
11:00	3	2	3	2	2	3
12:00	3	2	3	2	3	3
13:00	2	2	3	3	3	3
14:00	2	1	3	2	2	2
15:00	2	0	2	1	2	2
16:00	1	0	1	0	1	0
17:00	0	0	1	0	0	0
18:00	0	0	0	0	0	0
19:00	0	0	0	0	0	0
20:00	0	0	0	0	0	0
21:00	0	0	0	0	0	0
22:00	0	0	0	0	0	0
23:00	0	0	0	0	0	0
0:00	0	0	0	0	0	0

20 kW PV system						
TIME	JULY 21st	DECEMBER 21st	JULY 21st	DECEMBER 21st	JULY 21st	DECEMBER 21st
0:00	0	0	0	0	0	0
1:00	0	0	0	0	0	0
2:00	0	0	0	0	0	0
3:00	0	0	0	0	0	0
4:00	0	0	0	0	0	0
5:00	0	0	0	0	0	0
6:00	0	0	0	0	0	0
7:00	1	0	0	0	0	0
8:00	2	0	1	0	2	1
9:00	3	1	2	1	3	3
10:00	4	1	3	3	3	4
11:00	4	2	4	3	3	4
12:00	4	3	4	3	4	4
13:00	3	3	4	4	4	4
14:00	3	2	4	3	3	3
15:00	3	1	3	2	2	2
16:00	2	0	2	0	1	1
17:00	1	0	1	0	0	0
18:00	0	0	0	0	0	0
19:00	0	0	0	0	0	0
20:00	0	0	0	0	0	0
21:00	0	0	0	0	0	0
22:00	0	0	0	0	0	0
23:00	0	0	0	0	0	0
0:00	0	0	0	0	0	0

The comparison to only one big (conventional) RO unit is necessary in order to prove that the multi-skid system operates at a wider load range than one single unit, since at low power load, one sub-unit can operate producing power. In order to better realize the benefit of the multi-skid RO system, the fresh water production

of the previously examined systems for each examined day and location is presented and compared to the operation of a large conventional unit instead. According to the maximum power input from the PV system, in each case a conventional RO unit of the appropriate capacity has been chosen for the comparison:

- For the PV system of 10 kWp, for all areas, a conventional unit of 7 kW has been chosen.
- For the system of 15 kWp for Greece a unit of 10 kW - when for Spain and UAE one of 11 kW, have been chosen.
- For the system of 20 kWp for Greece and UAE a unit of 14 kW and for Spain one of 15 kW have been chosen.

Based on the maximum fresh water production of the previously tested RO unit and taking into account that the conventional unit stops operating for power load below 50% of its capacity, for the multi-skid RO system, the fresh water production for each case occurs knowing the SEC and the power production of the experimental results and with linear interpolation (since the SEC is the ratio of the power consumption to the freshwater production, as mentioned before).

Table 3. Daily fresh water production for the different case studies for multi- skid system

	Resulted SEC [kWh/m³]	Corresponding Power from experiment [kW]	PV Power [kW_e]	SEC resulted from linear interpolation for PV power [kWh/m³]	Produced fresh water [m³]
Athens July 21st 10 kWe	6.110098	3.0856	3.39392	5.821011	0.583046
	5.693467	3.52995	4.97415	5.306303	0.937404
	5.147306	3.86048	6.35678	5.503699	1.155001
	5.599426	7.02728	6.74599	5.559266	1.213468
	5.331797	7.35788	6.49852	5.523935	1.176429
	5.156939	7.68384	5.31009	5.354265	0.99175
	5.578545	11.04552	5.59799	5.395368	1.037555
	5.508057	11.51184	4.95638	5.303766	0.934502
	5.301649	11.63712	3.49333	5.094888	0.685654
TOTAL FRESH WATER PRODUCED					8.71
Athens December 21st 10 kWe	6.110098	3.0856	4.25334	5.203394	0.817416
	5.693467	3.52995	5.34096	5.358672	0.996695
	5.147306	3.86048	5.70469	5.410601	1.054354
	5.599426	7.02728	3.72315	5.1277	0.726086
TOTAL FRESH WATER PRODUCED					3.59

Athens July 21st 15 kWe	6.110098	3.0856	5.09088	5.322969	0.956399
	5.693467	3.52995	7.46122	5.276361	1.414084
	5.147306	3.86048	9.53517	5.389124	1.769336
	5.599426	7.02728	10.119	5.462345	1.852501
	5.331797	7.35788	9.74779	5.41579	1.799883
	5.156939	7.68384	7.96514	5.192219	1.534053
	5.578545	11.04552	8.39698	5.246378	1.600529
	5.508057	11.51184	7.43457	5.125677	1.450456
	5.301649	11.63712	5.24	5.344258	0.980492
TOTAL FRESH WATER PRODUCED					13.36
Athens December 21st 15 kWe	6.110098	3.0856	3.67223	5.12043	0.717172
	5.693467	3.52995	6.38001	5.507016	1.158524
	5.147306	3.86048	8.01144	5.198025	1.541247
	5.599426	7.02728	8.55704	5.266452	1.624821
	5.331797	7.35788	5.58472	5.393473	1.035459
TOTAL FRESH WATER PRODUCED					6.07
Athens July 21st 20 kWe	6.110098	3.0856	3.29128	5.066042	0.649675
	5.693467	3.52995	6.78784	5.565241	1.219685
	5.147306	3.86048	9.95	5.44115	1.828657
	5.599426	7.02728	12.7136	5.24	2.42626
	5.331797	7.35788	13.492	5.202105	2.593565
	5.156939	7.68384	12.997	5.228421	2.485837
	5.578545	11.04552	10.6202	5.525204	1.922137
	5.508057	11.51184	11.196	5.555799	2.015192
	5.301649	11.63712	9.91276	5.43648	1.823378
			6.98666	5.069502	1.378175
			3.42419	5.085017	0.673388
TOTAL FRESH WATER PRODUCED					19.02
Athens December 21st 20 kWe	6.110098	3.0856	3.61067	5.111641	0.706362
	5.693467	3.52995	4.89631	5.29519	0.924671
	5.147306	3.86048	8.50667	5.260135	1.617196
	5.599426	7.02728	10.6819	5.532942	1.930601

APPENDIX III – PV- RO Case study design

	5.331797	7.35788	11.4094	5.523542	2.065595
	5.156939	7.68384	7.44629	5.28437	1.409116
	5.578545	11.04552	3.24	5.965329	0.543138
TOTAL FRESH WATER PRODUCED					9.19

APPENDIX III – PV- RO Case study design

	Resulted SEC [kWh/m ³]	Corresponding Power from experiment [kW]	PV Power [kW _e]	SEC resulted from linear interpolation for PV power [kWh/m ³]	Produced fresh water [m ³]
Palma July 21st 10 kWe	6.110098	3.0856	4.10871	5.182745	0.792767
	5.693467	3.52995	5.52879	5.385488	1.026609
	5.147306	3.86048	6.51356	5.526083	1.178694
	5.599426	7.02728	6.8997	5.581211	1.236237
	5.331797	7.35788	7.07191	5.563297	1.271173
	5.156939	7.68384	6.48702	5.522294	1.174697
	5.578545	11.04552	5.3912	5.365845	1.004725
	5.508057	11.51184	3.99146	5.166006	0.772639
TOTAL FRESH WATER PRODUCED					8.46
Palma December 21st 10 kWe	6.110098	3.0856	4.88975	5.294254	0.923596
	5.693467	3.52995	5.79132	5.422969	1.067924
	5.147306	3.86048	5.05586	5.317969	0.950713
	5.599426	7.02728	6.3177	5.49812	1.149065
	5.331797	7.35788	5.73223	5.414533	1.058675
	5.156939	7.68384	3.20483	5.0537	0.634155
TOTAL FRESH WATER PRODUCED					5.78
Palma July 21st 15 kWe	6.110098	3.0856	3.57674	5.106797	0.700388
	5.693467	3.52995	6.16306	5.476042	1.125459
	5.147306	3.86048	8.29318	5.23336	1.584676
	5.599426	7.02728	9.77034	5.418618	1.803105
	5.331797	7.35788	10.3496	5.491266	1.884738
	5.156939	7.68384	10.6079	5.523661	1.920447
	5.578545	11.04552	9.73054	5.413627	1.797416
	5.508057	11.51184	8.08681	5.207478	1.552923
	5.301649	11.63712	5.9872	5.450935	1.09838
		3.33051	5.880466	0.566368	
TOTAL FRESH WATER PRODUCED					14.03
	6.110098	3.0856	3.95881	5.161344	0.767011
	5.693467	3.52995	7.33462	5.350626	1.370797

APPENDIX III – PV- RO Case study design

Palma December 21st 15 kWe	5.147306	3.86048	8.68699	5.28275	1.644407
	5.599426	7.02728	7.5838	5.210605	1.455455
	5.331797	7.35788	9.47655	5.381772	1.76086
	5.156939	7.68384	8.59835	5.271633	1.63106
	5.578545	11.04552	4.80724	5.282474	0.910036
TOTAL FRESH WATER PRODUCED					9.54
Palma July 21st 20 kWe	6.110098	3.0856	4.76899	5.277013	0.903729
	5.693467	3.52995	8.21741	5.223857	1.573054
	5.147306	3.86048	11.0576	5.576719	1.982815
	5.599426	7.02728	13.0271	5.224889	2.493278
	5.331797	7.35788	13.7994	5.184242	2.661797
	5.156939	7.68384	14.1438	5.166116	2.737802
	5.578545	11.04552	12.974	5.227684	2.481787
	5.508057	11.51184	10.7824	5.545546	1.944335
	5.301649	11.63712	7.98293	5.19445	1.536819
			4.44067	5.230139	0.849054
TOTAL FRESH WATER PRODUCED					19.16
Palma December 21st 20 kWe	6.110098	3.0856	5.27841	5.349742	0.986666
	5.693467	3.52995	9.7795	5.419767	1.804413
	5.147306	3.86048	11.5826	5.391475	2.148318
	5.599426	7.02728	10.1117	5.46143	1.851475
	5.331797	7.35788	12.6354	5.245505	2.408805
	5.156939	7.68384	11.4645	5.515213	2.078705
	5.578545	11.04552	6.40966	5.511249	1.163014
TOTAL FRESH WATER PRODUCED					12.44

APPENDIX III – PV- RO Case study design

	Resulted SEC [kWh/m ³]	Corresponding Power from experiment [kW]	PV Power [kW _e]	SEC resulted from linear interpolation for PV power [kWh/m ³]	Produced fresh water [m ³]
Abu Dhabi July 21st 10 kWe	6.110098	3.0856	3.10484	6.092058	0.509654
	5.693467	3.52995	4.63523	5.257916	0.881572
	5.147306	3.86048	5.61894	5.398359	1.040861
	5.599426	7.02728	6.15416	5.474772	1.124094
	5.331797	7.35788	6.87791	5.5781	1.23302
	5.156939	7.68384	6.6216	5.541507	1.19491
	5.578545	11.04552	5.79079	5.422894	1.067841
	5.508057	11.51184	4.53716	5.243915	0.865224
TOTAL FRESH WATER PRODUCED					7.92
Abu Dhabi December 21st 10 kWe	6.110098	3.0856	4.64539	5.259367	0.88326
	5.693467	3.52995	6.03011	5.457061	1.105011
	5.147306	3.86048	6.77207	5.56299	1.217344
	5.599426	7.02728	6.89747	5.580893	1.235908
	5.331797	7.35788	6.55734	5.532333	1.185276
	5.156939	7.68384	5.63338	5.400421	1.043137
	5.578545	11.04552	4.11264	5.183307	0.793439
TOTAL FRESH WATER PRODUCED					7.46
Abu Dhabi July 21st 15 kWe	6.110098	3.0856	4.65726	5.261061	0.885232
	5.693467	3.52995	6.95284	5.588798	1.244067
	5.147306	3.86048	8.42841	5.25032	1.605314
	5.599426	7.02728	9.23124	5.351007	1.725141
	5.331797	7.35788	10.3169	5.487165	1.880188
	5.156939	7.68384	9.9324	5.438943	1.826164
	5.578545	11.04552	8.68618	5.282648	1.644285
	5.508057	11.51184	6.80574	5.567797	1.22234
	5.301649	11.63712	4.40756	5.225412	0.843486
TOTAL FRESH WATER PRODUCED					12.88
	6.110098	3.0856	3.90791	5.154077	0.758217
	5.693467	3.52995	6.96808	5.590974	1.246309

APPENDIX III – PV- RO Case study design

Abu Dhabi December 21st 15 kWe	5.147306	3.86048	9.04516	5.32767	1.69777
	5.599426	7.02728	10.1581	5.467249	1.857991
	5.331797	7.35788	10.3462	5.49084	1.884266
	5.156939	7.68384	9.836	5.426853	1.812469
	5.578545	11.04552	8.45008	5.253037	1.608608
	5.508057	11.51184	6.16896	5.476885	1.126363
TOTAL FRESH WATER PRODUCED					11.99
Abu Dhabi July 21st 20 kWe	6.110098	3.0856	6.20968	5.482698	1.132596
	5.693467	3.52995	9.27045	5.355924	1.730878
	5.147306	3.86048	11.2379	5.549465	2.025042
	5.599426	7.02728	12.3083	5.262721	2.338771
	5.331797	7.35788	13.7558	5.186537	2.652213
	5.156939	7.68384	13.2432	5.213516	2.540167
	5.578545	11.04552	11.5816	5.393122	2.147476
	5.508057	11.51184	9.07432	5.331327	1.702075
	5.301649	11.63712	5.87675	5.435166	1.081246
	TOTAL FRESH WATER PRODUCED				
Abu Dhabi December 21st 20 kWe	6.110098	3.0856	5.21055	5.340054	0.975749
	5.693467	3.52995	9.29078	5.358474	1.733848
	5.147306	3.86048	12.0602	5.275779	2.285956
	5.599426	7.02728	13.5441	5.197679	2.605798
	5.331797	7.35788	13.7949	5.184479	2.660807
	5.156939	7.68384	13.1147	5.220279	2.51226
	5.578545	11.04552	11.2668	5.545097	2.031849
	5.508057	11.51184	8.22527	5.224843	1.574262
	5.301649	11.63712	3.94833	5.159848	0.765203
	TOTAL FRESH WATER PRODUCED				

As a reminder, linear interpolation is a method of curve fitting using linear polynomials to construct new data points within the range of a discrete set of known data points. If the two known points are given by the coordinates (x_0, y_0) , the linear interpolant is the straight line between these points. For a value x in the interval (x_0, x_1) , the value y along the straight line is given from the equation of slopes:

$$\frac{y - y_0}{x - x_0} = \frac{y_1 - y_0}{x_1 - x_0}$$

$$\rightarrow y = y_0 + (x - x_0) \frac{y_1 - y_0}{x_1 - x_0}$$

For the conventional unit, a similar way for the freshwater production calculation occurs, taking into account that the conventional unit will stop operating when the power input falls below 50% of each capacity and assuming that the SEC at 100% of the capacity is 5 kWh and at 50% of the capacity is 6 kWh. In other words, for the PV system of 10 kW_e, where a 7 kW conventional unit has been considered, the SEC for 100% of its capacity (i.e. 7 kW) is assumed 5 kWh/m³ and the SEC for 50% of its capacity (i.e. 3.5 kW) is assumed 6 kWh/m³. Therefore, in order to calculate any SEC value (y) between 3.5 and 7 kW power, the linear interpolation will give:

$$\frac{y - 5}{6 - 5} = \frac{x - 7}{3.5 - 7}$$

where x is the power produced each time of the day from the PV system. In the exact same way, all SEC values are calculated in the same way. The produced water can be then calculated as the ratio of power produced by the PV system to the corresponding SEC. The results are presented in the table below.

Table 4. Daily fresh water production for the different case studies for a conventional unit

	PV Power [kW_e]	SEC resulted from linear interpolation for PV power [kWh/m³]	Produced fresh water [m³]		PV Power [kW_e]	SEC resulted from linear interpolation for PV power [kWh/m³]	Produced fresh water [m³]
Athens July 21st 10 kWe	4.97	5.654409	0.879694	Athens December 21st 10 kWe	4.25	5.673767	0.74965
	6.36	5.617275	1.131648		5.34	5.644557	0.946214
	6.75	5.606822	1.203175		5.70	5.634788	1.012405
	6.50	5.613468	1.157666		3.72	5.688007	0.654561
	5.31	5.645386	0.940607				
	5.60	5.637654	0.992964				
	4.96	5.654886	0.876477				
TOTAL FRESH WATER PRODUCED			7.18	TOTAL FRESH WATER PRODUCED			3.36
Athens July 21st 15 kWe		SEC resulted from linear interpolation for PV power [kWh/m³]	Produced fresh water [m³]	Athens December 21st 15 kWe	PV Power [kW_e]	SEC resulted from linear interpolation for PV power [kWh/m³]	Produced fresh water [m³]
	5.09	5.981824	0.851058		3.67	5.861999	1.088368
	7.46	5.507756	1.354675		6.38	5.698856	1.405798
	9.54	5.092966	1.872223		8.01	5.644296	1.516051
	10.12	4.9762	2.033479		8.56	5.941528	0.939947

APPENDIX III – PV- RO Case study design

	9.75	5.050442	1.930087				
	7.97	5.406972	1.473124				
	8.40	5.320604	1.578201				
	7.43	5.513086	1.348531				
	5.24	5.952	0.880376				
TOTAL FRESH WATER PRODUCED			13.32	TOTAL FRESH WATER PRODUCED			4.95
Athens July 21st 20 kWe	PV Power [kW_e]	SEC resulted from linear interpolation for PV power [kWh/m³]	Produced fresh water [m³]	Athens December 21st 20 kWe	PV Power [kW_e]	SEC resulted from linear interpolation for PV power [kWh/m³]	Produced fresh water [m³]
	9.95	5.578571	1.783610755		8.51	5.784761	1.470531
	12.71	5.183771	2.452577274		10.68	5.474014	1.951383
	13.49	5.072571	2.659794976		11.41	5.370086	2.124622
	13.00	5.143286	2.526983862		7.45	5.936244	1.254377
	10.62	5.482829	1.936992897				
	11.20	5.400571	2.073113956				
	9.91	5.583891	1.775242253				
TOTAL FRESH WATER PRODUCED			15.21	TOTAL FRESH WATER PRODUCED			6.80

Palma July 21st 10 kWe	PV Power [kW_e]	SEC resulted from linear interpolation for PV power [kWh/m³]	Produced fresh water [m³]	Palma December 21st 10 kWe	PV Power [kW_e]	SEC resulted from linear interpolation for PV power [kWh/m³]	Produced fresh water [m³]
	4.11	5.677652	0.723664		4.89	5.656675	0.864421
	5.53	5.639512	0.980367		5.79	5.632462	1.028204
	6.51	5.613064	1.160429		5.06	5.652214	0.894492
	6.90	5.602694	1.231497		6.32	5.618325	1.124481
	7.07	5.598069	1.263277		5.73	5.634049	1.017426
	6.49	5.613777	1.155554				
	5.39	5.643208	0.955343				

APPENDIX III – PV- RO Case study design

	3.99	5.680801	0.702623				
TOTAL FRESH WATER PRODUCED			8.17	TOTAL FRESH WATER PRODUCED			4.93
Palma July 21st 15 kWe		SEC resulted from linear interpolation for PV power [kWh/m³]	Produced fresh water [m³]	Palma December 21st 15 kWe		SEC resulted from linear interpolation for PV power [kWh/m³]	Produced fresh water [m³]
	6.16	5.879444	1.048239		7.33	5.6664327	1.294398
	8.29	5.492149	1.510006		8.69	5.4205473	1.602604
	9.77	5.223575	1.870432		7.58	5.6211273	1.34916
	10.35	5.118255	2.022096		7.58	5.2769909	1.795825
	10.61	5.071291	2.091755		9.48	5.4366636	1.581549
	9.73	5.230811	1.860235				
	8.09	5.529671	1.46244				
	5.99	5.911418	1.01282				
TOTAL FRESH WATER PRODUCED			12.88	TOTAL FRESH WATER PRODUCED			7.62
Palma July 21st 20 kWe		SEC resulted from linear interpolation for PV power [kWh/m³]	Produced fresh water [m³]	Palma December 21st 20 kWe		SEC resulted from linear interpolation for PV power [kWh/m³]	Produced fresh water [m³]
	8.22	5.904345	1.3917563 31		9.78	5.696067	1.716887
	11.06	5.525653	2.0011389 3		11.58	5.455653	2.123045
	13.03	5.263053	2.4751981 74		10.11	5.651773	1.78912
	13.80	5.16008	2.6742608 64		12.64	5.31528	2.377184
	14.14	5.11416	2.7656154 68		11.46	5.4714	2.09535
	12.97	5.270133	2.4617972 98				

APPENDIX III – PV- RO Case study design

	10.78	5.562347	1.9384624 24				
	7.98	5.935609	1.3449217 35				
TOTAL FRESH WATER PRODUCED			17.05	TOTAL FRESH WATER PRODUCED			10.10
Abu Dhabi July 21st 10 kWe		SEC resulted from linear interpolation for PV power [kWh/m³]	Produced fresh water [m³]	Abu Dhabi December 21st 10 kWe		SEC resulted from linear interpolation for PV power [kWh/m³]	Produced fresh water [m³]
	4.64	5.663511	0.818438		4.65	5.663238	0.820271
	5.62	5.637091	0.99678		6.03	5.626048	1.07182
	6.15	5.622717	1.094517		6.77	5.606122	1.207978
	6.88	5.603279	1.227479		6.90	5.602754	1.231086
	6.62	5.610163	1.180287		6.56	5.611889	1.168473
	5.79	5.632476	1.028107		5.63	5.636704	0.99941
	4.54	5.666145	0.800749		4.11	5.677546	0.724369
TOTAL FRESH WATER PRODUCED			7.15	TOTAL FRESH WATER PRODUCED			7.22
Abu Dhabi July 21st 15 kWe		SEC resulted from linear interpolation for PV power [kWh/m³]	Produced fresh water [m³]	Abu Dhabi December 21st 15 kWe		SEC resulted from linear interpolation for PV power [kWh/m³]	Produced fresh water [m³]
	6.95	5.735847	1.212173		6.97	5.733076	1.2154173
	8.43	5.467562	1.54153		9.05	5.355425	1.6889713
	9.23	5.321593	1.734676		10.16	5.153073	1.9712705
	10.32	5.1242	2.013368		10.35	5.118873	2.0211872
	9.93	5.194109	1.912243		9.84	5.211636	1.8873151
	8.69	5.420695	1.602411		8.45	5.463622	1.5466078

APPENDIX III – PV- RO Case study design

	6.81	5.762593	1.18102		6.17	5.878371	1.0494336
TOTAL FRESH WATER PRODUCED			11.19	TOTAL FRESH WATER PRODUCED			11.38
Abu Dhabi July 21st 20 kWe	PV Power [kW_e]	SEC resulted from linear interpolation for PV power [kWh/m³]	Produced fresh water [m³]	Abu Dhabi December 21st 20 kWe	PV Power [kW_e]	SEC resulted from linear interpolation for PV power [kWh/m³]	Produced fresh water [m³]
	9.27	5.67565	1.6333723 89		9.29	5.672746	1.637792
	11.24	5.394586	2.0831812 85		12.06	5.277114	2.285378
	12.31	5.241671	2.3481632 09		13.54	5.065129	2.673989
	13.76	5.034886	2.7320977 64		13.79	5.0293	2.742907
	13.24	5.108114	2.5925809 92		13.11	5.126471	2.558231
	11.58	5.345486	2.1666132 17		11.27	5.390457	2.090138
	9.07	5.703669	1.5909620 07		8.23	5.824961	1.412073
TOTAL FRESH WATER PRODUCED			15.15	TOTAL FRESH WATER PRODUCED			15.40

APPENDIX IV- ORC simulation in EES

Engineering Equation Solver software has been used for the ORC unit design. The input data are the heat source temperature, the organic fluid selected, the condensation temperature, the expanders' and pump's efficiencies as per literature and manufacturers, the MEG properties and the intermediate expansion pressure. The design is presented below;

EES Ver. 10.451:

```

1: {given}
2: p[2]=p[3]                                     "Pressure drop in evaporator neglected"
3: p[5]=p[1]                                     "Pressure drop in condenser neglected"
4: p[4]=SQRT(p[3]*p[5])                         "Intermediate pressure at the expanders"
5: n_exm=0.85
6: n_exis=0.85
7: n_pm=0.75
8: n_pis=0.85
9: T_ev=115
10: T[3]=T_ev+5 [C]                             "Superheating at the evaporator"
11: T_cond=40
12: T[1]=T_cond-5 [C]                           "Subcooling at the pump"
13:
14: mass_coll=(v_coll*rho)                       "Heat cycle working fluid mass"
15: v_coll=0.00194                              "Heat cycle working fluid volume"
16: rho=density(EG,T=T_mean,C=60[%])           "Heat cycle working fluid density"
17: T_mean=(T_1coll+T_2coll)/2
    "Mean temperature at the heat cycle"
18: cp_coll=Cp(EG,T=T_2coll,C=60[%])           "MEG cp"
19: T_2coll=125                                  "Output temperature"
20: T_1coll=110
    "Inlet temperature"
21:
22:
23: R$='R245fa'
24:
25: $UnitSystem SI C kPa
26:
27: "PUMP (R$,h[1],h[2],T[1],T[2],p[1],p[2],T_ev,h2is,s[1],n_pis,mass_orc,Q_p)"
28: h[1]=Enthalpy(R$,T=T[1],p=p[1])
29: s[1]=Entropy(R$,T=T[1],p=p[1])
30: p[2]=Pressure(R$,T=T_ev,x=1)
31: h2is=Enthalpy(R$,p=p[2],s=s[1])
32: h[2]=h[1]+n_pis*(h2is-h[1])
33: s[2]=Entropy(R$,h=h[2],p=p[2])
34: T[2]=Temperature(R$,h=h[2],p=p[2])
35:
36: Q_p=(mass_orc*(h[2]-h[1]))/n_pm
37:
38: "EVAPORATOR (R$,h[3],T[3],p[3],Q_ev,mass_orc)"
39: h[3]=Enthalpy(R$,T=T[3],p=p[3])
40: s[3]=Entropy(R$,T=T[3],p=p[3])
41: Q_ev=mass_orc*(h[3]-h[2])
42:
43:
44: "EX1 (R$,T[4],p[4],h[4],h[3],h4is,s[3],x[4],n_exm,mass_orc,Q_ex1)"
45: h4is=Enthalpy(R$,P=P[4],s=s[3])
46: h[4]=h[3]-n_exis*(h[3]-h4is)
47: x[4]=Quality(R$,h=h[4],p=p[4])
48: s[4]=Entropy(R$,h=h[4],p=p[4])
49: T[4]=Temperature(R$,h=h[4],p=p[4])
50: Q_ex1=mass_orc*(h[3]-h[4])*n_exm
51:
52: "EX2 (R$,T[5],p[5],s[4],h[5],h[4],x[5],n_exm,mass_orc,Q_ex2)"
53: h5is=Enthalpy(R$,p=p[5],s=s[4])
54: h[5]=h[4]-n_exis*(h[4]-h5is)
55: s[5]=Entropy(R$,h=h[5],p=p[5])
56: x[5]=Quality(R$,h=h[5],p=p[5])
57: T[5]=Temperature(R$,h=h[5],p=p[5])
58: Q_ex2=mass_orc*(h[4]-h[5])*n_exm

```

EES Ver. 10.451:

```

60: "CONDENSER (R$, T[4], T[5], p[4], p[5], h[4], h[5], mass_orc, Q_cond)"
61: P[5]=Pressure(R$, T=T_cond, x=1)
62: Q_cond=mass_orc*(h[5]-h[1])
63:
64: "PREHEATER"
65: Q_ev1=mass_orc*(h[3]-h2a)
66: Q_out1=mass_orc*(h5a-h[1])
67: n_IHE=0.6
68: n_IHE=Q_ev1/Q_cond
69:
70: n_th=((Q_ex1+Q_ex2-Q_p)/Q_ev)*100
71: n_thpre=((Q_ex1+Q_ex2-Q_p)/Q_ev1)*100
72:
73: mass_orc=(mass_coll*cp_coll*(T_2coll-T_1coll))/(h[3]-h[2])
74:
75: v[5]=Volume(R$, T=T[5], p=p[5])
76: v[3]=Volume(R$, T=T[3], p=p[3])
77: v_ratio=v[5]/v[3]
    
```

$p_2 = p_3$ Pressure drop in evaporator neglected

$p_5 = p_1$ Pressure drop in condenser neglected

$p_4 = \sqrt{p_3 \cdot p_5}$ Intermediate pressure at the expanders

$n_{exm} = 0.85$

$n_{exts} = 0.85$

$n_{pm} = 0.75$

$n_{pls} = 0.85$

$T_{ev} = 115$

$T_3 = T_{ev} + 5$ [C] Superheating at the evaporator

$T_{cond} = 40$

$T_1 = T_{cond} - 5$ [C] Subcooling at the pump

$mass_{coll} = V_{coll} \cdot \rho$ Heat cycle working fluid mass

$V_{coll} = 0.00194$ Heat cycle working fluid volume

$\rho = \rho(EG, T = T_{mean}, C = 60 \text{ [\%]})$ Heat cycle working fluid density

$T_{mean} = \frac{T_{1coll} + T_{2coll}}{2}$ Mean temperature at the heat cycle

$cp_{coll} = Cp(EG, T = T_{2coll}, C = 60 \text{ [\%]})$ MEG cp

$T_{2coll} = 125$ Output temperature

$T_{1coll} = 110$ Inlet temperature

$R\$ = 'R600'$

PUMP (R\$, h₁, h₂, T₁, T₂, p₁, p₂, T_{ev}, h2[s], s, 1, n_{pls}, mass_orc, Q, p)

EES Ver. 10.451:

$$h_1 = h(R\$, T = T_1, P = p_1)$$

$$s_1 = s(R\$, T = T_1, P = p_1)$$

$$p_2 = P(R\$, T = T_{ev}, X = 1)$$

$$h_{2is} = h(R\$, P = p_2, s = s_1)$$

$$h_2 = h_1 + n_{pis} \cdot (h_{2is} - h_1)$$

$$s_2 = s(R\$, h = h_2, P = p_2)$$

$$T_2 = T(R\$, h = h_2, P = p_2)$$

$$Q_p = \frac{mass_{orc} \cdot (h_2 - h_1)}{n_{pm}}$$

EVAPORATOR (R\$,h3,T3,p3,Qev,mass,orc)

$$h_3 = h(R\$, T = T_3, P = p_3)$$

$$s_3 = s(R\$, T = T_3, P = p_3)$$

$$Q_{ev} = mass_{orc} \cdot (h_3 - h_2)$$

EX1 (R\$,T4,p4,h4,h3,h4is,s3,x4,nex,m,mass,orc,Q,ex1)

$$h_{4is} = h(R\$, P = p_4, s = s_3)$$

$$h_4 = h_3 - n_{ex1s} \cdot (h_3 - h_{4is})$$

$$x_4 = x(R\$, h = h_4, P = p_4)$$

$$s_4 = s(R\$, h = h_4, P = p_4)$$

$$T_4 = T(R\$, h = h_4, P = p_4)$$

$$Q_{ex1} = mass_{orc} \cdot (h_3 - h_4) \cdot n_{exm}$$

EX2 (R\$,T5,p5,s4,h5,h4,x5,nex,m,mass,orc,Q,ex2)

$$h_{5is} = h(R\$, P = p_5, s = s_4)$$

$$h_5 = h_4 - n_{ex2s} \cdot (h_4 - h_{5is})$$

$$s_5 = s(R\$, h = h_5, P = p_5)$$

$$x_5 = x(R\$, h = h_5, P = p_5)$$

$$T_5 = T(R\$, h = h_5, P = p_5)$$

$$Q_{ex2} = mass_{orc} \cdot (h_4 - h_5) \cdot n_{exm}$$

CONDENSER (R\$,T4,T5,p4,p5,h4,h5,mass,orc,Q,cond)

$$p_5 = P(R\$, T = T_{cond}, X = 1)$$

$$Q_{cond} = mass_{orc} \cdot (h_5 - h_1)$$

PREHEATER

EES Ver. 10.451:

$$Q_{ev1} = \text{mass}_{orc} \cdot (h_3 - h_{2a})$$

$$Q_{out1} = \text{mass}_{orc} \cdot (h_{5a} - h_1)$$

$$\eta_{HE} = 0.6$$

$$\eta_{HE} = \frac{Q_{ev1}}{Q_{cond}}$$

$$\eta_{th} = \left[\frac{Q_{ex1} + Q_{ex2} - Q_p}{Q_{ev}} \right] \cdot 100$$

$$\eta_{sppt} = \left[\frac{Q_{ex1} + Q_{ex2} - Q_p}{Q_{ev1}} \right] \cdot 100$$

$$\text{mass}_{orc} = \frac{\text{mass}_{coll} \cdot \text{cp}_{coll} \cdot (T_{2coll} - T_{1coll})}{h_3 - h_2}$$

$$v_5 = v(RS, T = T_5, P = p_5)$$

$$v_3 = v(RS, T = T_3, P = p_3)$$

$$v_{ratio} = \frac{v_5}{v_3}$$

Arrays Table: Main

	p_i [kPa]	T_i [C]	h_i [kJ/kg]	s_i [kJ/kg-K]	v_i [m ³ /kg]	x_i
1	379.2	35	283.9	1.287		
2	2022	35.6	286.4	1.286		
3	2022	120	751.2	2.548	0.0191	
4	875.7	88.74	721.7	2.562		100
5	379.2	65.06	690.2	2.579	0.1177	100

Parametric Table: Table 1

	mass_{orc} [kg/s]	v_{ratio}	η_{th}
Run 1	0.4256	7.929	10.5
Run 2	0.4256	7.929	10.5
Run 3	0.4256	7.929	10.5
Run 4	0.4256	7.929	10.5
Run 5	0.4256	7.929	10.5
Run 6	0.4256	7.929	10.5
Run 7	0.4256	7.929	10.5
Run 8	0.4256	7.929	10.5
Run 9	0.4256	7.929	10.5
Run 10	0.4256	7.929	10.5

EES Ver. 10.451:

